SYNTHESIS, CHARACTERISATION AND STUDIES ON S, N, O DONOR LIGANDS AND THEIR METAL COMPLEXES

Thesis Submitted to the
University of Calicut in Partial Fulfilment of
the Requirements for the Award of the degree of

DOCTOR OF PHILOSOPHY IN CHEMISTRY

By
SANGEETHA K. G., M.Sc., B.Ed

DEPARTMENT OF CHEMISTRY
UNIVERSITY OF CALICUT
KERALA 673635
INDIA
March 2018

Dedicated To

The Fond Memory of My Beloved Father, Ammamma
And also to my Mother, Brothers, Husband, Kids and in-laws
For their incomparable love and support

Dr. K. K. Aravindakshan
Professor (Retired)
Department of Chemistry
University of Calicut.

Dr. Renuka N. K.
Associate Professor
Department of Chemistry
University of Calicut.

CERTIFICATE

This is to certify that the thesis entitled **"Synthesis, characterisation and studies on S, N, O donor ligands and their metal complexes"** is an authentic record of the research work carried out by Mrs. **SANGEETHA K. G.,** in the Department of Chemistry, University of Calicut under our supervision in partial fulfilment of the requirements for the Degree of **Doctor of Philosophy in Chemistry**, under the Faculty of Science of the University of Calicut. This work has not been presented earlier for any other degree/diploma of any University/Institute and has undergone plagiarism check using URKUND software at CHMK library, University of Calicut.

Calicut University
Date :

Dr. K. K. Aravindakshan
(Guide)

Dr. Renuka. N. K.
(Co-guide)

DECLARATION

I, **Sangeetha K. G.,** hereby declare that this thesis entitled **"Synthesis, characterisation and studies on S, N, O donor ligands and their metal complexes"** is a bonafide record of the original research work carried out by me for the award of the degree of **Doctor of Philosophy in Chemistry,** under the supervision of Dr. K. K. Aravindakshan, Professor (Rtd.) of Chemistry, University of Calicut and Dr. Renuka N. K., Associate Professor of Chemistry, University of Calicut.

I further declare that no part of this thesis has previously formed the basis for the award of any degree or diploma of any University/Institute.

Calicut University
Date: SANGEETHA. K. G.

ACKNOWLEDGEMENT

It is a pleasure to express my sincere thanks to all those who helped me to successfully complete this study and made it an unforgettable experience. It has been a great privilege for me to work under the guidance of Prof. Dr. K. K. Aravindakshan, Department of Chemistry, University of Calicut. Words are insufficient to appreciate my teacher for his whole-hearted involvement, timely help, constant encouragement and valuable suggestions throughout the course of the work. I am immensely thankful to him for the freedom I could enjoy in the pursuit of this research work. His kindness, expertise and vision have guided me through the past years of study and research.

I express my profound gratitude to my co-guide Dr. Renuka. N. K., Associate Professor, Department of Chemistry, University of Calicut for her timely help and constant encouragement.

I express my profound gratitude to Dr. P. Raveendran, Head of Department of Chemistry, University of Calicut, for his continued support. I am immensely grateful to the former Heads of the Department of Chemistry, Dr. Gangadevi, Dr. V. M. Abdul Mujeeb and Dr. K. Muraleedharan for providing the necessary facilities to carry out the research work successfully.

I also express my sincere thanks to Mr Mohanan, Librarian, Department of Chemistry, University of Calicut.

I gratefully remember Mr Satheesh, Technician, Department of chemistry for carrying out the measurement during my initial stages.

I express my sincere thanks to Dr. Mohamed Shahin Thayyil, Department of Physics and Central Sophisticated Instrumentation Facility (CSIF), University of Calicut, for providing the facility for computational studies. I owe my gratitude to Dr. Anu Augustine, Head of the Department of Biotechnology and Microbiology, School of Life sciences, Kannur University, Kerala, for providing software for molecular docking studies and for providing laboratory facility to do antibacterial studies. I would like to thank Dr. Rajan. P. P., Head of the Department of Botany, the Zamorin's Guruvayurappan College, Calicut for providing laboratory facility to carry out antifungal studies. I would like to thank Dr. A. Sindhu, Head of the Department of Zoology, for her assistance in evaluating biological studies. I express my sincere thanks to Dr. K. Sreeranjini for her support and encouragement.

A special note of thanks to Dr. D. K. Babu, Head of the Department of Chemistry and Prof. T. M. Gokulachandran Head, the Zamorin's Guruvayurappan college, for their support and prayers. I am grateful to the Management, Principal, staff and students of the Zamorin's Guruvayurappan College, Calicut, especially to all the faculty members of the Department of Chemistry and Zoology, for their support and encouragement.

A special note of thanks to Mr. Arun, research scholar, Department of Biotechnology and Microbiology, School of Life sciences, Kannur University for the helpful interactions. A special note of thanks to Safna Hussain, Vijisha K. Rajan and Shameera Ahammed, research scholars, University of Calicut, for the helpful interactions. I take this opportunity to thank all the teachers and non-teaching staff of the Department of Chemistry, University of Calicut for their support during this period. I would like to extend my gratitude to my group members, Dr. Priya, Priya Varma, Subin, Soufeena and Nibila.

A special thanks to Binu Noufal, Shahanas Beegum, Kavitha. A. P., Subair. N., for their company, support and providing a pleasant atmosphere during my research period. Other research scholars of this department are also have to be mentioned in this context for the pleasant experience over the past years.

My thanks are due to SAIF, STIC Cochin, SAIF, IIT Chennai, NIT Calicut, for providing necessary facilities for NMR and TG/DTG data. Thanks are due to SAIF, IIT Chennai, SAIF, STIC, Cochin and Department of Physics, M. G. University for single crystal XRD data. Thanks are also due to KFRI, Peechi for providing C, H, N, S analyses.

At this juncture, I also remember my much loved teachers during my studies with great gratitude.

My parents deserve a special mention for their invaluable support and prayers. I dedicate this thesis before the fond memories of my father who may be watching me through the stars. My mother, Geetha, deserves a special mention for her unconditional support and prayers. With great pleasure, I would like to give special thanks to Anishettan, my husband, for his love, patience and encouragement. It is only with a heart brimming with love that I can remember Gouri and Gourav who sacrificed their yearning moments with their amma for realising her dreams. I would like to thank my brothers, Maheshettan, Sangeesh and Sandeep for their love, support, encouragement and understanding. I can never forget the love, support, care, understanding and encouragement provided by my grandparents, uncles, aunts, cousins and in-laws without which the completion of my dream would have been impossible.

I am indebted to University Grants Commission, New Delhi for granting me the Teacher Fellowship under the Faculty Development Programme to complete my research work.

I thank diacritech technologies, Chennai for the neat processing of my thesis.

Last but the most, the blessings bestowed by the Almighty is to be gratefully memorised and I render everything before the feet of Almighty GOD.

SANGEETHA K. G.

PREFACE

Over the past few decades, researches in inorganic chemistry are widely centred on Schiff's base metal complexes. This thesis is the beginning of our endeavour to evaluate the coordination behaviour of some interesting compounds. A great deal of attention has been focused on the complexes of Schiff's bases from the thiourea family due to their versatile physicochemical properties. The main objective of this study is the synthesis and characterisation of the novel ligands and complexes with ONS or NNS donor atoms. In addition to this, computational approach for the screening of ligands for their non-linear optical property and anticancer activity became another objective of the study.

The entire thesis is divided into ten Chapters. Chapter I gives a brief outline on history, importance, applications of nitrogen, sulphur, and oxygen Schiff's base ligands followed by a description of their recent developments in various fields. The objective and scope of this investigation is also included in this chapter. Chapter II portrays the procedure adopted for the synthesis of precursor of ligands, principle, procedure and instrumentation of the physico-chemical techniques employed for the structure elucidation of the ligands and the complexes. In addition to this, the procedures adopted for DFT, molecular docking studies and evaluation of biological activities of the compounds are described briefly. Chapters III–VII deal with the synthesis and characterisation of the novel ligands, derived from N(4)-methyl-N(4)-phenylthiosemicarbazide and 1-phenyl-3-methyl-4-benzoyl-5-pyrazolone (PMBP-MPTSC), benzophenone (B-MPTSC and BP-MPTSC), 3-formylchromone (FC-MPTSC), 3-methoxy-4-hydroxy-benzaldehyde (vanillin) (V-MPTSC), 3,4- dimethoxybenzaldehyde (MV-MPTSC) and their transition metal complexes. We could isolate single crystals of some compounds and their structures have been established by single-crystal X-ray diffraction studies. Chapters VIII–X deal with the in-silico screening of all ligands for their non-linear optical property using DFT studies, in-silico screening for their anticancer activity using molecular docking studies and *in vitro* antimicrobial screening of selected ligands and complexes, respectively.

The references cited in the thesis are arranged in serial order at the end of each chapter.

The research work presented in this thesis has partly been published/is under publication as indicated below and are attached at the end of the thesis.

- **K. G. Sangeetha**, K. K. Aravindakshan, Synthesis, structural and spectroscopic studies of 1-phenyl-3-methyl-4-benzoyl-5-pyrazolone N(4)-methyl-N(4)-phenyl thiosemicarbazone and its cadmium(II) complex, Inorganica Chimica Acta 469 (2018) 25–31.
- **K. G. Sangeetha**, K. K. Aravindakshan, K. P. Safna Hussan, Insight into the theoretical and experimental studies of 1-phenyl-3-methyl-4-benzoyl-5-pyrazolone N(4)-methyl-N(4)-phenylthiosemicarbazone – A potential NLO material, Journal of Molecular Structure 1150 (2017) 135–145.
- **K. G. Sangeetha**, K. K. Aravindakshan, Exploring the coordination capabilities, thermal and antimicrobial studies of 1-phenyl-3-methyl-4-benzoyl-5-pyrazolone N (4)-methyl- N(4)-phenylthiosemicarbazone and its transition metal ions, World journal of pharmaceutical and medical research 3(9) (2017) 238–245.

- **K. G. Sangeetha**, K. K. Aravindakshan, Novel ligands, benzophenone N(4)-methyl-N(4)-phenylthiosemicarbazone, 1-(amino-N-methylphenylmethanethio) (diphenylmethylene)thiocarbonohydrazide and the transition metal complexes of the latter, Inorganica Chimica Acta 469 (2018) 387–396.
- **K. G. Sangeetha**, K. K. Aravindakshan, Synthesis, structural, spectral and antimicrobial studies of 2-[2-(Diphenylmethylidene)hydrazine]-N-methyl-N-phenylhydrazine-1-carbothioamide and its transition metal complexes (Communicated).

CONTENTS

CHAPTER I

A BRIEF OUTLINE ON NITROGEN, SULPHUR, OXYGEN DONOR LIGANDS AND THEIR METAL COMPLEXES

1. Introduction

Schiff's bases, also termed as anils, imines or azomethines, comprise an important class of nitrogen donor ligands since their discovery by Hugo Schiff in 1864.[1] They are the reaction products of primary amines and carbonyl compounds. A Schiff's base or azomethine has a functional group that contains a carbon–nitrogen double bond with the nitrogen atom connected to an aryl- or alkyl group, but not to hydrogen. It can be represented as $R_1R_2C{=}N{-}R_3$, where R_1, R_2 and R_3 are aryl or alkyl groups.

The first azomethine complex was prepared in 1840 by Ettling[2] by the reaction of cupric acetate, salicylaldehyde and aqueous ammonia. After an *era* of relative inactivity, systematic studies of azomethine complexes were initiated by Pfeiffer *et al*.[3] in 1931. They studied diverse aspects such as synthesis, ligand replacement, stereochemistry and esterification of Schiff's base metal complexes. After that, a variety of methods for the synthesis of imines have been described. The classical method involves azeotropic distillation of any primary amine with an aldehyde or a ketone under specific conditions. An *in situ* method for water elimination was developed in the 1990s using dehydrating solvents such as tetramethyl orthosilicate.

$NH_2{-}NH_2$ is the simplest compound that contains N–N bond. In 1863, Hoffman effectively converted azobenzene to hydrazobenzene[4] which was the first of hydrazine derivative. After that, in 1877 Emil Fischer synthesized phenylhydrazine.[4] N, N disubstituted ethylenediamine, $RH_2CHNCH{-}CHNHCH_2R^1$, in which R and R^1 groups containing at least one additional donor atom like N, O or S became the most common chelating nitrogen donor ligands.

Semicarbazones and thiosemicarbazones constitute N, O and N, S donor ligands, respectively. They are principally Schiff's bases obtained by the condensation of an aldehyde or a ketone with semicarbazide and thiosemicarbazide, respectively.

Reaction of semicarbazide with aldehydes:

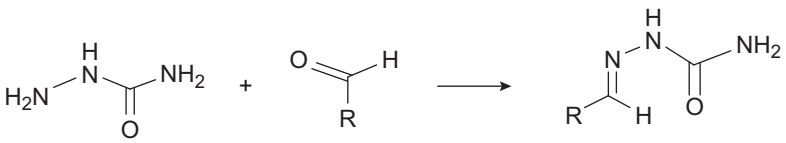

Reaction of semicarbazide with ketones:

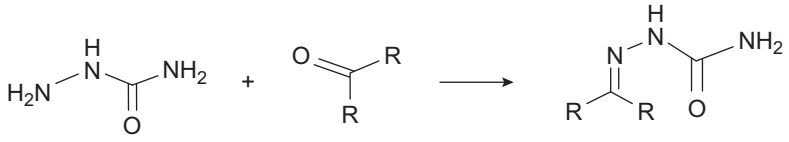

Reaction of thiosemicarbazide with aldehydes:

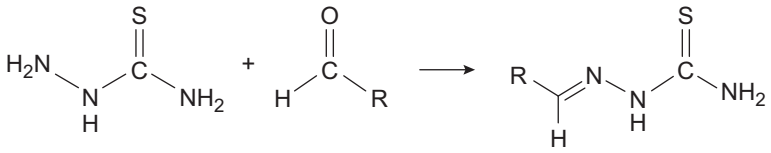

Reaction of thiosemicarbazide with ketones:

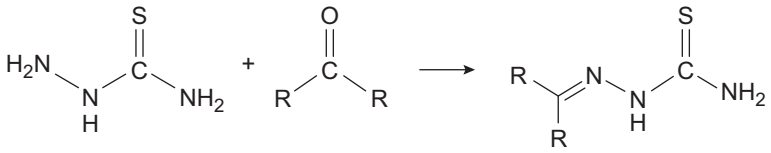

Thiosemicarbazones are broadly classified as mono-thiosemicarbazones and *bis*-thiosemicarbazones. Mono-thiosemicarbazones are the compounds in which one (C=O) group from an aldehyde/ketone and one NH_2 group from thiosemicarbazide condense forming a (C=N) linkage with the elimination of a water molecule. *Bis*-thiosemicarbazones are the compounds in which two (C=O) groups from two aldehyde/ketone molecules and two NH_2 groups from two thiosemicarbazide molecules condense forming two (C=N) linkages by the elimination of two water molecules.

Akbar Ali and Livingstone in 1974 first reviewed the chemistry of thiosemicarbazones along with other N, S donor ligands,[5] followed by a review by Campbell in 1975.[6] The subsequent developments in metal-thiosemicarbazone chemistry were reviewed by Padhye and Kauffman in 1985,[7] West *et al*.[8,9] in 1991–1993, Casas *et al*.[10,11] in 1999–2000 and then by Lobana *et al*.[12] In some cases, thiosemicarbazones act as bidentate and in a few cases they behave as a mono-dentate neutral S donor ligands.[13,14] These reviews describe several aspects of thiosemicarbazones such as synthesis of metal complexes, spectroscopic properties, crystal structures and biological applications.

The researches on thiosemicarbazone complexes diverge mainly into three paths:

1. Structure and bonding of the complexes
2. Biological applications of the complexes
3. Analytical applications such as ion sensors, metal ion extractants, and so on

1.1. Structure and bonding of the complexes

During the 1970s, studies on structural details of thiosemicarbazone complexes were one of the main subjects in the literature. In 1969, the crystal structure determination of thiosemicarbazones was reported in literature. A mesmerizing feature of thiosemicarbazones

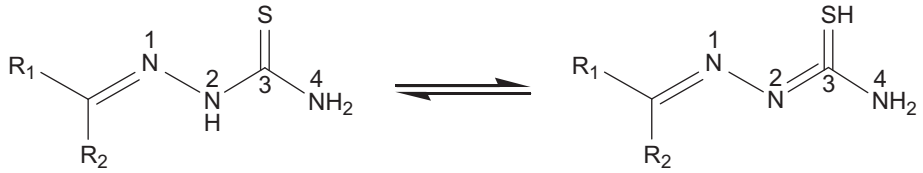

is that in the solid state they generally exist in the thio-keto form, whereas in solution state they display a thio-keto–thio-enol tautomerism. In thio-keto form, they act as a neutral bidentate ligands and the thio-enol form, they undergo deprotonation and act as mono-anionic bidentate ligands in metal complexes.

A number of bonding modes have been observed for the thiosemicarbazones in their neutral or anionic forms. Thus, they are handy ligands in both neutral and anionic forms. Aromatic substituents on the thiosemicarbazone skeleton can further boost the delocalization of electron charge density. The delocalization is further enhanced on complexation through the metal chelate rings. Normally, in thione form they cannot cause any spin pairing in metal complexes[15] but in thiol forms they can lead to low-spin complexes of Co(II) and Ni(II).[16] However, in Fe(III) complexes, they are not capable of causing spin pairing. When an extra coordination functionality is present near the donating centres, they coordinate in a tridentate manner.

Thiosemicarbazones can exist in *E*-form (*trans*-) and *Z*-form (*cis*-).[17] In *trans*- form, they act as mono-dentate ligands by coordinating through sulphur alone.[18] If sulphur centre is substituted, the bonding may occur through the hydrazine nitrogen and the amide nitrogen.[19] During complexation, the compound exists in *Z*-form because of the extra stability allied with the electron delocalization in the chelated complexes.

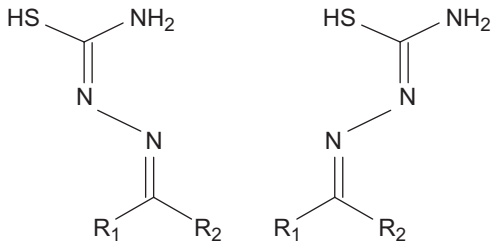

Current reports on transition metal complexes of heterocyclic thiosemicarbazones imply that stereochemistries adopted by these complexes often depend upon the anion of the metal salt used and the nature of the substituent at N(4).[20,21] Studies on N(4)-substituted thiosemicarbazones have indicated that an additional potential bonding site together with the presence of bulky groups at the N(4) position enhance their biological activity.[22,23]

Stereochemistry of metal complexes of thiosemicarbazones depends very much on the oxidation state of the metal which in turn is related to its softness.[24] The degree of softness and hardness plays an important part in determining the stability of a thiosemicarbazone metal complex. Stereochemistry of thiosemicarbazones is decided by steric effect of substituents on the thiosemicarbazone moiety.[25] The stability of thiosemicarbazones is enhanced by intramolecular hydrogen bonding in *E* (*trans*-) conformation. This mode of

hydrogen bonding and conformation is reported for 2-formylpyridine thiosemicarbazone[26] and for many heterocyclic mono-substituted thiosemicarbazones.[27]

Benzaldehyde thiosemicarbazone is normally found to act as a neutral bidentate ligand depending upon the pH of the medium, yielding complexes of the type $[ML_2X_2]$ (where M = Co(II), Ni(II), Cu(II) or Fe(II); L = the ligand in the thione form; and X = a mono-anionic ligand). However, salicylaldehyde thiosemicarbazone is found to act as a tridentate uninegative ligand, yielding complexes of the type, ML_2 which may be spin-free or spin-paired.[28] In addition, it is also possible to synthesize complexes containing two non-equivalent ligands – one protonated and the other deprotonated within the same coordination sphere.

Aravindakshan and Nair[29] have isolated complexes of vanillin thiosemicarbazone (3-methoxy-4-hydroxy-benzaldehydethiosemicarbazone) (VTSCH) with several divalent metal ions. Structures have been assigned to these complexes based on electrical conductivity and magnetic susceptibility measurements and by spectral studies. Lobana *et al*.[30] have reported the bonding patterns, geometry and fluorescence properties of some Ni(II) complexes of salicylaldehyde-based thiosemicarbazones by invoking the effects of substituents at the C-2 and N-1 atoms of the thio ligand and by using bipyridines/phenanthrolines as auxiliary ligand.

Klayman and Lin[31] described the preparation of a variety of N(4)-mono- and N(4)-disubstituted thiosemicarbazones. Three NNS donor ligands such as pyridine-2-carbaldehyde N(4)-p-methoxyphenylthiosemicarbazone, pyridine-2-carbaldehyde N(4)-(methyl)-N(4)-(phenyl)thiosemicarbazone and pyridine-2-carbaldehyde N(4)-2-phenethylthiosemicarbazone were synthesized and characterised by Rapheal *et al*.[32] Ten copper complexes of these ligands were prepared and the crystal structure of a binuclear copper complex of pyridine-2-carbaldehyde N(4)-methyl-N(4)-phenylthiosemicarbazone was determined by single crystal X-ray diffraction studies.[33]

Peng *et al*.[33] reported photochromic thiosemicarbazones derived from 4-acylpyrazolone.[34,35] They found that their photochromic properties are due to intermolecular proton transfer. They also found out that the absorption and emission characteristics of such chromophoric species may be tuned by adjusting the pH value.

The crystal structures of salicylaldehyde N(4)-phenylthiosemicarbazone and its Zn(II) complex were studied by Seena *et al*.[36] The monomeric complex belongs to orthorhombic system with a space group, *P21cn*. The Zn(II) complex is five coordinate and have an approximately trigonal bi-pyramidal geometry. The crystal structure of a Co(III) complex of *N*-[phenyl(pyridin-2-yl)methylene]aniline with azide as co-ligand was reported by Sasi *et al*.[37]

Sithambaresan[38] studied transition metal complexes of some N(4)-phenylsemicarbazones of 2-benzoylpyridine, 3-ethoxysalicylaldehyde and 2-formylpyridine. Single-crystal XRD studies of 3-ethoxysalicylaldehyde N(4)-phenylsemicarbazone and Ni(II), Zn(II), Cu(II) and Cd(II) complexes of 2-benzoylpyridine N(4)-phenylsemicarbazone were also reported.

Philip[39] synthesized di-2-pyridylketone N(4)-methyl-N(4)-phenylthiosemicarbazone and di-2-pyridylketone 3-tetramethyleneiminylthiosemicarbazone. Structural and spectral investigations of transition metal complexes of these thiosemicarbazones were done. Crystal structures of copper bromide and copper azide complexes of di-2-pyridylketone N(4)-methyl-N(4)-phenylthiosemicarbazone were reported. With Cu(II) sulphate, di-2-pyridylketone

3-tetramethyleneiminylthiosemicarbazone yielded a complex with an empirical formula, $[Cu_2L_2(SO_4)]$ but with di-2-pyridylketone N(4)-methyl-N(4)-phenylthiosemicarbazone, a complex having an empirical formula, $[CuL(SH)\cdot H_2O]$ was yielded. The crystal structures of these complexes were also reported.

Sivakumar[40] studied structural, spectral, biological and electrochemical behaviours of some N(4)-substituted thiosemicarbazones and their transition metal complexes. Single-crystal X-ray diffraction study of vanadium complex of 2-acetylpyridine N(4)-morpholinethiosemicarbazone, $[VO_2(L4M)]$ was reported by them.[38] Single-crystal X-ray diffraction study Ni(II) complex of 2-acetylpyridine N(4)–hexahydroazepinethiosemicarbazone, $[Ni(HL_4A)_2](ClO_4)_2\ H_2O$ was also reported.[38]

Kurup and Joseph[41] reported the transition metal complexes of furan-2-aldehyde thiosemicarbazone. The infrared (IR) spectra suggested the coordination of thiosemicarbazone to metal through azomethine nitrogen and thiolate sulphur atoms. The Co(II) complexes of 1-salicylaldehyde thiosemicarbazone having trigonal bipyramidal geometry were reported by El-Shazly *et al*.[42] Crystal structure of N′-[(*E*)-3,5-dichloro-2-hydroxybenzylidene]-4-nitro-benzohydrazide dimethylformamide mono-solvate was reported by Joseph *et al*. in 2015.[43] The hydrazone molecule adopted an *E* conformation with respect to azomethine bond. The dihedral angle between the two aromatic rings [8.96 (11)] showed that they were almost coplanar and stabilized by the intramolecular O–H···N hydrogen bond.

1.2. Biological applications of the complexes

Thiosemicarbazones are considered as one of the most vital scaffolds and are embedded in many biologically active compounds. Nowadays, the areas in which thiosemicarbazones are receiving more attention are antitumour, antiprotozoal, antibacterial and antiviral studies. In all these cases, their action has been shown to involve interaction with metal ions.[44,45] They stand as milestones in this promising *era* for the specific treatment of viral diseases. These compounds are the first one to be effective in humans and to be found in clinical medicine for viral diseases. Thiosemicarbazones are the only compound which is able to block the genetic expression of a wide variety of viruses.

Durham *et al*.[46] reported that the anti-smallpox activity of the metal complexes of thiosemicarbazones depends on the group at N(4) position. The first report on the medical application of thiosemicarbazones appeared in the 1950s as drugs against tuberculosis[47] and leprosy.[48] In the 1960s, their antiviral properties were discovered and a huge amount of research was carried out which led to the commercialization of methisazone, Marboran®, to treat smallpox.[49] Isatin-β-thiosemicarbazone and methylisatin-β-thiosemicarbazone (methisazone) prevent the multiplication of smallpox virus and the latter has also been used in the treatment of smallpox.[50] Thiosemicarbazones were also found effective against human immunodeficiency virus (HIV).[51]

Antimalarial activity of thiosemicarbazones was first reported by Klayman *et al*.[52]

N-(salicylidene)-2-hydroxyaniline showed activity against *Mycobacterium tuberculosis* $H_{37}Rv$.[53] In the 1960s, one of the first reports on antitumour activity was published.[54] Brockman *et al*.[55] reported that 2-formylpyridine thiosemicarbazone possesses antileukemic activity in mice. In recent times, Triapine® (3-aminopyridine-2-carboxaldehyde

thiosemicarbazone) has been developed as an anticancer drug and has reached the clinical phase II on several cancer types.[56,57]

Research was conducted on the outcomes of Pt(II) and Pd(II) complexes of 2-acetylpyridine thiosemicarbazone (AcTsc) on sister chromatid exchange (SCE) rates, kinetics of human lymphocyte proliferation and leukemia P388. The compounds, $[Pt(AcTsc)_2H_2O]$ and [Pd(AcTsc] were found to be most efficient in producing antitumour and cytogenetic effects.[58]

Schiff's base complexes derived from 4-hydroxysalicylaldehyde and amines have strong anticancer activity against Ehrlich ascites carcinoma (EAC).[59] Thomas and Parameswaran[60] reported the antitumour activities of Mn^{2+}, Co^{2+}, Ni^{2+} and Cu^{2+} complexes of anthracene-9-carboxaldehyde thiosemicarbazone. They have also reported the cytotoxic activity of phenylglyoxal bis(thiosemicarbazone) against EAC cells.

Synthesis, characterisation and antitumour studies of metal chelates of thiosemicarbazones of β-diketoesters were reported by Aravindakshan and Jayasree.[61] Activity of quinoline-2-carboxaldehyde thiosemicarbazone and its Cu(II) complex as proteasome inhibitors in human prostate cancer cell lines, PC-3 and LNCaP was reported by Adsule *et al*.[62] Presently, the main known effects related to their anticancer activity are in the order of discovery, ribonucleotide reductase (RR) inhibition[63], reactive oxygen species (ROS) production,[64] topoisomerase-II inhibition,[65] mitochondria disruption,[66] and more recently, multi-drug resistance protein (MDRI) inhibition.[67,68]

The antitumour activities of Zn(II) complexes of thiosemicarbazones against MCF-7 and T24 human cancer cell lines were studied by Demertzi.[69] In the past few decades, Ni(II) thiosemicarbazone complexes had gained great importance in chemotherapy because of the versatility of coordination geometry (square–planar, octahedral, tetrahedral), the formation of monomeric and dimeric complexes and their ability to imitate Pt(II) complexes to some extent.[70] Ni(II) complexes of salicylaldehyde thiosemicarbazone exhibit cytotoxicity under identical conditions on human lung cancer cells (A549) and liver cancer cells (HepG2) as compared to *cis*-diamminedichloridoplatinum(II).[71] Cytotoxic and antitumour studies of acetoacetanilide N(4)-methyl-N(4)-phenylthiosemicarbazone and its copper complex on Dalton's lymphoma ascites (DLA) cell lines were reported by Priya *et al*.[72]

The effect of the pyrazolone thiosemicarbazone ligand and its metal complexes on the proliferation of HL-60 cells was tested by Pahontu[73] and Braña *et al*.[74] Pyrazolone complexes were scrutinized for their property as cytotoxic agents by brine shrimp lethality bioassay by Ahasan and Islam.[75] Manganese complexes of N-(1-phenyl-3-methyl-4-benzoyl-5-pyrazolone)-2-thiophenecarboxylic acid hydrazide and N-(1-phenyl-3-methyl-4-propenylidene-5-pyrazolone)-2-thiophenecarboxylic acid hydrazide have been synthesized, characterised and studied the biological activities by Li *et al*.[76] The inhibitory effects of the complexes on the cell population growth of the human oesophageal cancer *Eca-109 cells* and the cervical cancer *HeLa cells* were determined by MTT assay. They significantly inhibited the growth of *Eca-109* and *HeLa cells*. The inhibitory activity of former complex was found to be stronger than that of latter.

In mammalian cells, heterocyclic thiosemicarbazones inhibit ribonucleotide reductase, a key enzyme in the synthesis of DNA precursors.[77] The Cu(II) complex (1:1) of 2-formylpyridine thiosemicarbazone has been shown to inhibit the RNA-dependent DNA

polymerases.[78] The copper complex has significant inhibitory activity than the free ligand and has lower IC_{50} value against tumour cells than the other reported topoisomerase-II inhibitors.[79]

Novel Ni(II) thiosemicarbazone complexes were characterised by various spectral and analytical techniques and their efficacy to interact with calf thymus (CT)–DNA/bovine serum albumin (BSA) was explored by Kalaivani *et al.*[80] From the binding studies, it was inferred that one of the complexes [Ni(Msal–ptsc)(PPh_3)] was more active than the other complexes and the complexes bind with CT–DNA in an intercalation mode. The complexes were also tested for their *in vitro* cytotoxicity against human lung adenocarcinoma (A549) cell line.

Synthesis and characterisation of Cu(II) complexes of thiosemicarbazone derivative of anthracene, their DNA and protein-binding ability and DNA-cleavage properties were reported by Kate *et al.*[81] Their cellular uptake was monitored by fluorescence microscopy. Their anticancer efficacy on cervical cancer cells (*HeLa cells*) was correlated with their redox potentials.

Synthesis and chemical characterisation of a series of vanadium(IV) complexes of thiosemicarbazones were reported by Lewis *et al.*[82] Potentiality of these compounds as chemotherapeutic candidates was evaluated by studies on colorectal cancer cell lines. The coordination chemistry of vanadium attracts increasing interest because of the use of many vanadium complexes as models for the biological functions, such as haloperoxidation, phosphorylation, insulin mimicking,[83,84] nitrogen fixation,[85] tumour growth inhibition and prophylaxis against carcinogenesis.[86] The insulin-mimetic potential of vanadyl dithiocarbamates[87] has increased the interest on sulphur coordinated vanadium complexes.

Preparation and structural characterisation of some oxovanadium(IV) and the *cis*-dioxidovanadium(V) complexes with 2-acetylpyridine thiosemicarbazone (Haptsc), 2-acetylpyridine N(4)-methylthiosemicarbazone (Hapmtsc) and 2-acetylpyridine N(4)-phenylthiosemicarbazone (Happtsc), both in solution and in the solid state were reported by Thompson *et al.*[83] The activities of these complexes, free ligands and common vanadium salts against *M. tuberculosis* H*37*Rv (ATCC 27294) were evaluated. The vanadium compounds showed comparable or higher anti-*M. tuberculosis* activities than the free thiosemicarbazone ligands, with the MIC values in the range of 62.5–1.56 (μg/mL).[88]

Zn(II) complexes, [Zn(AcPipPheF)$_2$] and [Zn(OAc)(AcPipPheF)]$_2$ of 2-acetyl-pyridine 1-(4-fluorophenyl)-piperazinylthiosemicarbazone (HAcPipPheF) were synthesized and characterised by Stanojkovic *et al.*[89] These compounds were tested for their *in vitro* antiproliferative activity against four human cancer cell lines: *HeLa* (cervix adenocarcinoma cell line), *K562* (chronic myelogenous leukaemia), *MDA-MB-361* and *MDA-MB-453* (breast cancer cell lines). Zinc complexes of 2-formyl- and 2-acetyl thiosemicarbazones have been evaluated for their *in vitro* antiproliferative activity against, *MCF-7* (human breast cancer cell line), *T24* (human bladder cancer cell line) and *L-929* (mouse fibroblast). The results showed that the zinc complexes displayed IC_{50} values in the μM range better than the usual reference, *cis*-platin.[90] Later, the acetyl derivative was modified by substituting an ethyl group on the terminal nitrogen and its Pt and Pd complexes with empirical formulae, [PtL_2] and [PdL_2] were synthesized. These complexes were tested on human tumour cell lines of different origins (breast, colon and ovary cancers).[91]

The literature reports many studies on the antifungal activity of thiosemicarbazones and their metal complexes. In the early 1960s, 40 thiosemicarbazones derived from aliphatic and aromatic aldehydes and ketones together with many of their metal complexes

were examined for toxicity against *Chaetomium globosum*. Antifungal, antibacterial and antifertility activities of heterocyclic thiosemicarbazones and their coordination compounds with the dimethylsilicon moiety have been explained.[92]

Metal complexes of p-anisaldehyde thiosemicarbazones have been screened for antifungal activity on *Allernarai* sp., *Paecilomyces* sp. and *Pestalotia* sp. In some cases, the complexes were more active than the free ligands.[93] The thiosemicarbazones and their complexes showed growth inhibitory activity against the human pathogenic bacteria, *Salmonella typhi*, *Shigella dysenteriae*, *Staphylococcus*, *Photobacterium* sp. and *Staphylococcus aureus* and the complexes against plant pathogenic fungi. An increase in the coordination number from 4 to 5 of the complexes led to higher activity, probably due to the increase in lipophilicity.[94]

Sheikhy *et al.*[95] have reported the antibacterial activities of 1-(2,4-dimethylthiazole-5-carboxyl)-N(4)-ethylthiosemicarbazide, 1-(4-fluorobenzoyl)-N(4)-ethylthiosemicarbazide, 2-pyridinealdehyde N(4)-methylthiosemicarbazone, and 2-acetylpyridine N(4)-N(4)-dimethylthiosemicarbazone. It was observed that all the four compounds were exhibiting inhibitory effect against *Escherichia coli* at 0.4–0.5 μM concentration.

Umadevi *et al.*[96] reported the antibacterial activities of 2-(4-chlorophenyl) (2-hydroxyphenyl) methylthiosemicarbazide and 2-(2-hydroxyphenyl)(4-hydroxyphenyl) methylthiosemicarbazide against Gram-positive *Bacillus subtilis* and *S. aureus* and Gram-negative *S. typhi* and *S. dysenteriae*. Synthesis and antimicrobial activity of a series of Schiff's bases derived from the condensation of 5-chloro-salicylaldehyde and primary amines were reported.[97] Schiff's base derived from 4-aminoantipyrine (4-amino-1, 5-dimethyl-2-phenylpyrazole-3-one) and benzaldehyde derivative was tested for its anti-inflammatory effect. The results showed promising activity which could be beneficial for the treatment of inflammatory diseases.[98]

1.3. Analytical and anticorrosion applications

Thiosemicarbazones have been widely used as analytical reagents in the spectrophotometric determination of metals.[99] Diaz *et al.*[100] established the analytical use of thiosemicarbazone for the determination of iron in olive oil. The determination was made by spectrophotometry based on the formation of a 5,5-dimethylcyclohexane 1,2,3-trione-1,2-dioxine-3-thiosemicarbazone (DCDT)-Fe(II) complex in a strongly acidic medium. The solution of the complex was violet in colour. For the spectrophotometric determination of Cu(II), use of pyridoxal-4-phenyl-3-thiosemicarbazone (PPT) was reported by Sarma *et al.*[101] Pavon *et al.*[102] reported the use of 4-phenyl-3-thiosemicarbazone of biacetylmonoxime for the selective spectrophotometric determination of manganese by means of extraction in amyl alcohol at pH l0, where the interference of Fe(III) was eliminated by masking with tartrate. Fluorescent complexes of 2-hydroxy-5-methoxybenzaldehyde thiosemicarbazone and 2-hydroxy-5-chlorobenzaldehyde thiosemicarbazone with gallium were synthesized by Morisige and are suggested as selective reagents for gallium.[103]

Corrosion inhibition properties of thiosemicarbazones have reported by Ebenso *et al.*[104] The inhibition of corrosion of aluminium in HCl solution by some derivatives of thiosemicarbazones has been studied using weight loss and hydrogen evolution techniques. The inhibition efficiency of thiosemicarbazone derivatives such as 2-acetylpyridine

4-phenylthiosemicarbazone, 2-acetylpyridine4-phenylisomethylthiosemicarbazone and 2-acetylpyridine 4-phenylisoethyl thiosemicarbazone were studied. It was established that the inhibition efficiency depended on concentration of the compound.[97]

Complexes of N(4)-methyl-N(4)-phenylthiosemicarbazones of anisoin, benzoin and furoin with various divalent transition metal ions were reported by Jeevana.[105] Interaction of these thiosemicarbazones with mild steel in HCl solution were studied by using weight loss method, electrochemical analysis, adsorption studies and SEM analysis. Furoin thiosemicarbazone was found to be better corrosion inhibitor compared to the other two. Complexes of N(4)-methyl-N(4)-phenylthiosemicarbazones of acetylacetone, benzoylacetone, acetoacetanilide, ω-bromoacetoacetanilide and N-ethylacetoacetanilide with divalent transition metal ions were synthesized and characterised using various physicochemical methods. The corrosion inhibition efficiency of acetylacetone N(4)-methyl-N(4)-phenylthiosemicarbazone was evaluated using weight loss, electrochemical impedance spectroscopic and potentiodynamic polarization methods, absorption studies and SEM analysis. The adsorption of inhibitor was found to obey Langmuir adsorption isotherm model. It was found to be a mixed-type inhibitor, that is, it affects both anodic and cathodic processes.[106]

1.4. Catalytic applications

Schiff's base complexes have been found to catalyze hydrolysis, carboxylation, decarboxylation, elimination, aldol condensation and redox reactions.[107,108] Datta *et al.*[109] have reported the synthesis, characterisation and catalytic activity of nickel complexes of thiosemicarbazones of salicylaldehyde, 2-hydroxyacetophenone and 2-hydroxynaphthaldehyde. The complexes were found to show efficient catalytic activity for Suzuki cross-coupling reactions. Several Cu(II) complexes of Schiff's bases are found to act as catalysts for the oxidative coupling of phenols, oxidation of phenols to quinines, and so on. These complexes usually form adducts with oxygen molecules. A lot of such complexes which can bind reversibly with dioxygen are presented in the review by Basolo *et al.*[110] Parrey and Hashmi[111] studied the catalytic oxidation of alcohols using polystyrene EDTA Cu(II) complex and the catalytic oxidation of phenols using l-histidine Cu(II) complex. Various alkenes can be converted efficiently and selectively to their corresponding epoxides in the presence of catalytic amount of vanadyl Schiff's base complexes.[112]

The catalytic property of polystyrene supported transition metal complexes of thiosemicarbazones has been reported by Cherriar and Sreekumar.[113] The physical and spectral properties of Co(II), Ni(II) and Cu(II) complexes of 1-methyl-isatin N(4)-methyl-thiosemicarbazone and N(4)-dimethylthiosemicarbazone were reported by West *et al.*[114] Several nickel complexes of thiosemicarbazones were reported to function as efficient homogeneous catalysts for the alcoholysis of silanes[115] and for the reduction of imines to primary and secondary amines.[116]

1.5. Miscellaneous

Thiosemicarbazone derivatives were also reported to show second-harmonic generation (SHG) abilities. Zinc halide complexes of 4-methoxybenzaldehyde thiosemicarbazone were found to possess non-linear optical (NLO) properties.[117] Likewise, theoretical and

experimental second-order optical non-linearity studies on cadmium halide complexes of bis-2-chlorobenzaldehyde thiosemicarbazone were also reported.[118]

In 2017, Zeyrek *et al.*[119] reported spectroscopic, quantum mechanical and molecular docking studies of a benzoxazole derivative with oxidoreductase enzyme which catalyzes the transfer of electrons from one molecule to another. Experimental, theoretical and docking studies of compounds derived from 2-amino-4-chlorobenzenethiol were reported by Kusmariya in 2015.[120] Dimeric complexes of Zn(II), Cu(II) and Ni(II) with 2-hydroxy-5-methyl benzaldehyde 2-aminothiophenol were synthesized and studied by Shafaatian in 2016.[121] Feng *et al.*[122] reported the crystal structure, density functional theory (DFT) calculation and photophysical studies of a Schiff's base. Synthesis, crystal structures, spectral and DFT studies of Cu(II) and Ni(II) complexes with N′-(pyridin-2-ylmethylene) acetohydrazide have been carried out by Patel.[123]

2. Objectives and scope of the investigation

The motivation behind this research is the relevance of O, N, S donor ligands in pharmacology, analytical chemistry and NLO applications. In modern technology, crystals are the unappreciated pillars in electronic, photonic, computer industries and fiber-optic communications. Growth of single crystals and their characterisation toward device fabrication have assumed great thrust due to their importance for both academic as well as applied research. Obviously, it is more difficult to prepare single crystals rather than polycrystalline materials. The additional attempt for isolating single crystals is justified by their outstanding advantages.[124] Many physical properties of solids are obscured or complicated by the effect of grain boundaries, and, therefore growing of single crystals is very significant. The chief benefits of single crystals are the anisotropy, uniformity of composition and the absence of boundaries between individual grains. The production of single crystals first in the laboratory and then extending it to commercial production, characterisation and utilization of these crystals in devices are the major stages involved in recent research in material science.

NLO crystals are very important for laser frequency conversion.[125] In recent years, there has been considerable progress in the development of coherent ultraviolet sources based on NLO processes. To enable a material to be potentially useful for NLO applications, it should be available in the form of a bulk single crystal.[126] The exploration for new materials has identified novel semi-organic systems of considerable potential and high performance. The scope of semi-organic single crystals in the abovementioned fields lead us to prepare good quality single crystals as one of the objectives of the study. Keeping all these in mind, using DFT method, we have computed the first-order hyper-polarizability, linear polarizability and the dipole moment, which determine the NLO properties of compounds.

Cancer remains a threat to human health as it causes mortality and morbidity. Inhibition of histone deacetylase-, ribonucleotide reductase- and DNA methyl transferase enzymes are emerging as an innovative and significant approach for the treatment of cancer. Currently, the use of computers to predict the binding of small molecules to known target structures is a vital factor in the drug discovery process. Hence it is interesting to conduct molecular docking to investigate the biological behaviour through the determination of

the probable binding mode by inserting the compounds into the active sites of the protein targets. These investigations can further be validated in wet lab studies.

The major objectives of our study include

I. To synthesize and characterise the novel ligands derived from N(4)-methyl-N(4)-phenylthiosemicarbazide and 1-phenyl-3-methyl-4-benzoyl-5-pyrazolone (PMBP-MPTSC), benzophenone (B-MPTSC and BP-MPTSC), 3-formylchromone (FC-MPTSC), 3-methoxy-4-hydroxy-benzaldehyde (vanillin) (V-MPTSC), 3,4 dimethoxybenzaldehyde (MV-MPTSC) and their transition metal complexes. However, we have noticed that during the synthesis of the ligands, BP-MPTSC, V-MPTSC and MV-MPTSC in the presence of glacial acetic acid and chilling of the resultant refluxed solution, thiosemicarbazide moiety has undergone dimerization by deamination followed by condensation forming versatile new ligands.

II. To accomplish single-crystal X-ray diffraction studies of some of the ligands and complexes.

III. To carry out in-silico screening, using DFT studies, of all the ligands for ascertaining their NLO property.

IV. To perform in-silico screening, using molecular docking studies, of all the ligands for evaluating their anticancer activity.

V. To perform *in vitro* antimicrobial screening of the selected ligands and complexes.

References

1. H. Schiff, Ann., 131 (1864) 188.
2. C. Ettling, Ann., 35 (1840) 241.
3. P. Pfeiffer, E. Bucholz, O. Barren, J. Prakt, Chem., 129 (1931) 63.
4. R. L. Shell, PhD thesis, Graduate Faculty of Texas Technological College, 1959.
5. M. Akbar Ali, S. E. Livingstone, Coord. Chem. Rev., 13 (1974) 115.
6. M. J. M. Campbell, Coord. Chem. Rev., 15 (1975) 279.
7. S. Padhye, G. B. Kauffman, Coord. Chem. Rev., 63 (1985) 127.
8. D. X. West, S. Padhye, P. B. Sonawane, Struct. Bond. (Berlin, Ger.), 76 (1991) 4.
9. D. X. West, A. E. Liberta, S. Padhye, R. C. Chilkate, P. B. Sonawane, A. S. Kumbhar, R. G. Yerande, Coord. Chem. Rev., 123 (1993) 49.
10. J. S. Casas, M. S. Garcia-Tasende, J. Sordo, Coord. Chem. Rev., 209 (2000) 197.
11. J. S. Casas, M. S. Garcia-Tasende, J. Sordo, Coord. Chem. Rev., 283 (1999) 193.
12. T. S. Lobana, R. Sharma, G. Bawa, S. Khanna, Coord. Chem. Rev., 253 (2009) 977.
13. T. S. Lobana, R. Rekha, R. J. Butcher, A. Castineiras, E. Bermejo, P. V. Bharatam, Inorg. Chem., 45 (2006) 1535.
14. K. Liebermeister, B. Naturforsch, 5 (1950) 79.
15. N. A. Ryabova, V. I. Ponomarev, L. O. Atomayan, V. V. Ze1entzov, V. I. Shipi1ov, J. Struct. Chem. U. S. S. R., 2 (1981) 234.
16. K. S. Siddiqui, Synth. React. Inorg. Met. Org. Chem., 20 (1990) 133.
17. D. X. West, G. A. Bain, R. J. Butcher, J. P. Jasinki, Y. Li, R. Y. Pozdniakiv, J. Valdez-Martinez, R. A. Toscano, S. H. Ortega, Polyhedron, 15 (1996) 665.
18. P. Domiano, G. G. Fava, M. Nardelli, P. Sagarabotto, Acta Crystallogr., B25 (1969) 343; G. D. Andreetti, G. Fava, M. Nardelli, P. Sagarabotto, Acta Crystallogr., B26 (1970) 1005.
19. N. V. Gebeleu, M. D. Revenko, V. M. Leovats, Russ. J. Inorg. Chem., 22 (1977) 1009.
20. D. X. West, M. A. Lockwood, H. Gebremedhin, A. Castineiras, A. E. Liberta, Polyhedron, 12 (1993) 1887; D. X. West, S. L. Dietrich, I. Thientanavanich, C. A. Brown, A. E. Liberta, Transition Met. Chem., 19 (1994) 195.
21. S. B. Padhye, P. B. Sonawane, R. C. Chikate, D. X. West, Asian J. Chem. Rev., 2 (1980) 125.
22. S. K. Jain, B. S. Garg, Y. K. Bhoon, Spectrochim. Acta A., 42 (1986) 959; M. E. Hossain, M. N. Alam, J. Begum, M. A. Ali, M. Nazimudhin, F. E. Smith, R. C. Hynes, Inorg. Chim. Acta, 249 (1996) 207.
23. W. Hu, W. Zhou, C. Xia, X. Wen, Bioorg. Med. Chem. Lett., 16(8) (2006) 2213.
24. F. A. Cotton, R. G. Wilkinson, Advanced Inorganic Chemistry, 5th ed., Wiley Eastern Company, New Delhi, 1973.
25. I. Cogi, A. M. M. Lanfredi, A. Tiripicchipo, J. Chem. Soc. Perkin Trans., 2 (1976) 1808.
26. V. N. Byushkin, Y. M. Chumakov, N. M. Samus, I. O. Baka, Zh. Strukt. Khim., 28 (1987) 140.
27. D. X. West, G. A. Bain, R. J. Butcher, J. P. Jasinski, Y. Li, R. Y. Pozdnikav, J. Valdies Martinez, R. A. Toscano, S. Hemandez-Ortega, Polyhedron, 15 (1996) 665.
28. N. A. Ryabova, V. I. Ponomarev, L. O. Atomayan, V. V. Zelentzov, V. I. Shipilov, Sov. J. Coord. Chem., 4 (1976) 95.
29. K. K. Aravindakshan, C. G. Nair, Proc. Indian Acad. Sci. (Chem. Sci.), 93 (1984) 111.
30. T. S. Lobana, P. Kumari, A. Castineiras, R. J. Butcher, Eur. J. Inorg. Chem., 2013 (2013) 3557.
31. D. L. Klayman, A. J. Lin, Org. Prep. Proc. Int., 16 (1981) 79.

32. P. F. Rapheal, E. Manoj, M. R. P. Kurup, Polyhedron, 26 (2007) 818.
33. B. -H. Peng, G. -F. Liu, L. Liu, D. -Z. Jia, K. -B. Yu, J. Photochem. Photobiol. A Chem., 171 (2005) 243.
34. X. C. Tang, D. Z. Jia, K. Liang, X. G. Zhang, X. Xia, Z. Y. Zhou, J. Photochem. Photobiol. A Chem., 134 (2000) 23.
35. L. Liu, D. Z. Jia, Y. L. Ji, K. B. Yu, J. Photochem. Photobiol. A Chem. 154 (2003) 117.
36. E. B. Seena, M. R. P. Kurup, E. Suresh, J. Chem. Crystallogr., 38 (2008) 93.
37. S. Sasi, M. R. P. Kurup, E. Suresh, J. Chem. Crystallogr., 37 (2007). doi:10.1007/s10870-006-9087-3.
38. M. Sithambaresan, PhD thesis, Department of Applied Chemistry, Cochin University of Science and Technology, 2012.
39. V. Philip, PhD thesis, Department of Applied Chemistry, Cochin University of Science and Technology, 2004.
40. S. Sivakumar, PhD thesis, Department of Applied Chemistry, Cochin University of Science and Technology, 2003.
41. M. R. P. Kurup, M. Joseph, Synth. React. Inorg. Met. Org. Chem., 33 (2003) 1275.
42. R. M. El-Shazly, G. A. A. Al-Hazmi, S. E. Ghazy, M. S. El-Shahawi, A. A. El-Asmy, J. Coord. Chem., 59 (2006) 845.
43. B. Joseph, N. R. Sajitha, M. Sithambaresan, E. B. Seena, M. R. P. Kurup, Acta Cryst., E71 (2015) o826–o827.
44. R. A. Finch, M. C. Liu, A. H. Cory, J. G. Cory, A. C. Sartorelli, Adv. Enzyme Regul., 39 (1999) 3.
45. W. Antholine, J. Knight, H. Whelan, D. H. Petering, Mol. Pharmacol., 13 (1977) 89.
46. N. N. Durham, R. W. Chesnut, D. F. Haslam, K. D. Berlin, N. N. Durham, D. E. Kiser, Mol. Pathol. Disease, 4 (1974) 77.
47. E. M. Bavin, R. J. Rees, J. M. Robson, M. Seiler, D. E. Seymour, D. Suddaby, J. Pharm. Pharmacol., 2(11) (1950) 764.
48. O. Koch, G. Stuttgen, N. Schmiedebergs, Arch. Exp. Pathol. Pharmacol., 210 (4–5) (1950) 409.
49. G. A. Kune, Br. Med. J., 2 (1964) 621.
50. D. Ronen, L. Sherman, S. Nar-Nun, Y. Teitz, Antimicrob. Agents Chemother., 31 (1987) 1798.
51. J. C. Logan, M. P. Fox, J. H. Morgan, A. M. Makohon, C. J. Pfau, J. Gen. Virol., 28 (1975) 271.
52. D. L. Klayman, J. F. Bartosevich, I. S. Griffin, C. J. Mason, J. P. Scovill, *J. Med Chem.,* 22 (1979) 855.
53. A. O. De Souza, F. C. S. Galetti, C. L. Silva, B. Bicalho, M. M. Parma, S. F. Fonseca, A. J. Marsaioli, Trindade, A. C. L. B. R. P. Freitas-Gil, F. S. Bezerra, Quim. Nova., 30 (2007) 1563.
54. A. C. Sartorelli, B. A. Booth, Cancer Res., 27 (1967) 1614.
55. R. W. Brockman, J. R. Thomson, M. J. Bell, H. E. Skipper, Cancer Res., 16 (1956) 167.
56. C. M. Nutting, C. M. L. van Herpen, A. B. Miah, Ann. Oncol., 20 (2009) 1275.
57. B. Ma, B. C. Goh, E. H. Tan, Invest. New Drugs, 26 (2008) 169.
58. Z. Iakovidou, A. Papageorgiou, M. A. Demertzis, E. Mioglou, D. Mourelatos, A. Kotsis, P. N. Yadav, D. K. Demertzi, Anticancer Drugs, 12 (2001) 65.
59. Z. S. Wu, Z. P. Lu, Z. H. Yen, Trans. Met. Chem., 18 (1993) 291.
60. J. Thomas, G. Parameswaran, Asian J. Chem., 14 (2002) 1354.
61. K. K. Aravindakshan, S. Jayasree, Polyhedron, 12 (1993) 1187.
62. S. Adsule, V. Barve, D. Chen, J. Med. Chem., 49 (2006) 7242.
63. R. W. Brockman, R. W. Sidwell, G. Arnett, S. Shaddix. Proc. Soc. Exp. Biol. Med., 133 (1970) 609.
64. J. Shao, B. Zhou, A. J. Di Bilio, Mol. Cancer Ther., 5 (2006) 586.

65. I. H. Hall, C. B. Lackey, T. D. Kistler, R. W. Durham, Jr., E. M. Jouad, M. Khan, X. D. Thanh, S. Djebbar-Sid, O. Benali-Baitich, G. M. Bouet, Pharmazie, 55(12) (2000) 937.
66. J. Yuan, D. B. Lovejoy, D. R. Richardson, Blood, 104 (2004) 1450.
67. J. A. Ludwig, G. Szakács, S. E. Martin, Cancer Res., 66 (2006) 4808.
68. C. Wu, S. Shukla, A. M. Calcagno, M. D. Hall, M. M. Gottesman, S. V. Ambudkar, Mol. Cancer Ther., 6 (2007) 3287.
69. D. K. Demertzi, A. Alexandratos, A. Papageorgiou, P. N. Yadav, P. Dalezis, M. A. Demertzis, Polyhedron, 27 (2008) 2731.
70. R. Prabhakaran, P. Kalaivoni, R. Huang, P. Poornima, V. V. Padma, F. Dallemer, K. Natarajan, J. Biol. Inorg. Chem., 18 (2013) 233; E. Pahontu, V. Fala, A. Gulea, D. Poier, V. Tapcov, T. Rosu, Molecules, 18 (2013) 8812; S. Datta, D. K. Seth, S. Gangopadhyay, P. Karmakar, S. Bhattacharya, Inorg. Chim. Acta, 392 (2012) 118; E. Ramchandran, D. S. Raja, N. S. P. Bhuvanesh, K. Natarajan, Eur. J. Med. Chem., 64 (2013) 179; E. Ramchandran, D. S. Raja, J. L. Mike, T. R. Wagner, M. Zeller, K. Natarajan, RSC Adv., 2 (2012) 8515; A. Basu, D. Thiyagarajan, C. Kar, A. Ramesh, G. Das, RSC Adv., 3 (2013) 14088.
71. R. Prabhakaran, P. Kalaivani, P. Poorima, F. Dallemer, G. Paramaguru, V. Padma, R. Renganathan, R. Huang, K. Natarajan, Dalton Trans., 41 (2012) 9323.
72. N. P. Priya, A. P. Firdous, R. Jeevana, K. K. Aravindakshan, Indian J. Pharm. Sci., 77(6) (2015) 655.
73. E. Pahontu, J. Cell. Mol. Med., 19 (2015) 865.
74. M. F. Braña, A. Gradillas, A. G. Ovalles, B. López, N. Acero, F. Llinares, D. Muñoz Mingarro, Bioorg. Med. Chem., 14 (2006) 9.
75. N. B. Ahasan, R. Islam, Bangladesh J. Pharmacol., 2 (2007) 81.
76. Y. Li, J. Zhao, C. -C. He, L. Zhang, S. -R. Sun, G. -C. Xu, J. Inorg. Biochem., 150 (2015) 28.
77. F. A. French, E. J. Blanz, Jr., J. R. Do Amaral, D. A. French, J. Med. Chem., 13 (1970) 1117.
78. W. Antholine, J. Knight, II., H. Whelan, D. H. Petering, Mol. Pharmacol., 13 (1977) 89.
79. J. Easmon, G. Pürstinger, G. Heinisch, J. Med Chem., 44 (2001) 2164.
80. P. Kalaivani, S. Saranya, P. Poornima, R. Prabhakaran, F. Dallemer, V. Padma, K. Natarajan, Eur. J. Med. Chem., 82 (2014) 584.
81. A. N. Kate, A. A Kumbhar, A. A. Khan, P. V. Joshi, V. G. Puranik, Bioconjugate Chem., 25 (2014) 102.
82. N. A. Lewis, F. Liu, L. Seymour, A. Magnusen, T. R. Erves, J. F. Arca, F. A. Beckford, R. Venkatraman, A. G. Sarrías, F. R. Fronczek, D. G. VanDerveer, N. P.Seeram, A. Liu, W. L. Jarrett, A. A. Holder, Eur. J. Inorg. Chem., 4 (2012) 664.
83. K. H. Thompson, B. D. Liboiron, Y. Sun, K. D. D. Bellman, V. Karunaratne, G. Rawji, J. Wheeler, K. Sutton, S. Bhanot, S. B. C. Cassidy, J. H. McNeill, V. G. Yuen, C. Orvig, J. Biol. Inorg. Chem., 8 (2003) 66; K. H. Thompson, J. H. McNeill, C. Orvig, Chem. Rev., 99 (1999) 2561; Y. Shechter, I. Goldwaser, M. Mironchik, M. Fridkin, D. Gefel, Coord. Chem. Rev., 237 (2003) 3.
84. H. Yasui, Y. Adachi, A. Katoh, H. J. Sakurai, Biol. Inorg. Chem., 12 (2007) 843.
85. R. R. Eady, Coord. Chem. Rev., 237 (2003) 23.
86. P. K. Sasmal, A. K. Patra, A. R. Chakravarty, J. Inorg. Biochem., 102 (2008) 1463.
87. H. Sakurai, H. Watanabe, H. Tamura, H. Yasui, R. Matsushita, J. Takada, Inorg. Chim. Acta, 283 (1998) 175.
88. P. I. da, S. Maia, F. R. Pavan, C. Q. F. Leite, S. S. Lemos, G. F. de Sousa, A. A. Batista, O. R. Nascimento, J. Ellena, E. E. Castellano, E. Niquet, V. M. Deflon, Polyhedron, 28 (2009) 398.
89. T. P. Stanojkovic, D. K. Demertzi, A. Primikyri, I. G. Santos, A. Castineiras, Z. Juranic, M. A. Demertzis, J. Inorg. Biochem., 104 (2010) 467.

90. D. Kovala-Demertzi, P. N. Yadav, J. Wiecek, S. Skoulika, T. Varadinova, M. A. Demertzis, J. Inorg. Biochem., 100 (2006) 1558.
91. D. Kovala-Demertzi, A. Boccarelli, M. A. Demertzis, M. Coluccia, Chemotherapy, 53 (2007) 148.
92. D. Singh, R. V. Singh, R. B. Goyal, Appl. Organomet. Chem., 5 (2004) 45.
93. B. G. Benns, B. A. Gingras, C. H. Bayley, Appl. Microbiol., 8 (1960) 353.
94. P. Bindu, M. R. P. Kurup, T. R. Satyakeerthy, Polyhedron, 18 (1999) 321.
95. M. Sheikhy, A. R. Jalilian, A. Novinrooz, F. J. Motamedi-Sedeh. J. Biomed. Sci. Eng., 5 (2012) 39.
96. P. Umadevi, K. Deepti, I. Srinath, G. Vijayalakshmi, M. Tarakaramji, Int. J. Pharm. Sci., 4(3) (2012) 379.
97. L. Shi, H. M. Ge, S. Tan, H. Q. Li, Y. C. Song, H. L. Zhu, Eur. J. Med. Chem., 42(4) (2007) 558.
98. M. S. Alam, J. H. Choi, D. U. Lee, Bioorg. Med. Chem., 20 (2012) 4103.
99. A. M. A. Khader, K. S. Prasad, Turk. J. Chem., 20 (1996) 222.
100. G. Diaz, A. Guiberteau Lopez, M. D. Soto, J. M. Ortiz, J. Agric. Food Chem., 51 (2003) 3743.
101. S. Sarma, J. Rajesh Kumar, K. Janardhan Reddy, A. Varada Reddy, J. Agric. Food Chem., 53 (2005) 5492.
102. J. N. C. Pavon, J. C. J. Sanchez, F. Pino, Anal. Chim. Acta, 75 (1975) 335.
103. K. Morisige, Anal. Chim. Acta, 72 (1974) 295.
104. E. E. Ebenso, U. J. Ekpe, B. I. Ita, O. E. Offiong, U. J. Ibok, Mat. Chem. Phys., 60 (1999) 79.
105. R. Jeevana, PhD thesis, Department of Chemistry, University of Calicut, 2012.
106. N. P. Priya, PhD thesis, Department of Chemistry, University of Calicut, 2015.
107. D. Hall, H. J. Morgan, T. N. Waters, J. Chem. Soc. A, 677 (1966); N. Kitajima, H. Fukui, Y. Moro-oka, J. Chem. Soc. Chem. Commun., 485 (1988) 677.
108. J. C. Bailer, Catal. Rev. Sci. Eng., 10 (1974) 17; M. M. Taqui Khan, A. E. Martell, Homogeneous Catalysis by Metal Complexes, Academic Press, New York City, New York, 1981.
109. S. Datta, D. K. Seth, R. J. Butcher, S. Bhattacharya, Inorg. Chim. Acta, 377 (2011) 120.
110. F. Basolo, B. M. Hoffman, J. A. Ibers, Acc. Chem. Res., 8 (1975) 384.
111. I. R. Parrey, A. A. Hashmi, Mor. J. Chem., 3 N°1 (2015) 147.
112. G. Grivani, A. D. Khalaji, V. Tahmasebi, K. Gotoh, H. Ishida, Polyhedron, 31 (2012) 265.
113. K. S. Cherriar, K. Sreekumar, Polym. Int., 48(6) (1999) 455.
114. D. X. West, A. K. El-Sawaf, G. A. Bain, Trans. Met. Chem., 23 (1998) 1.
115. D. E. Barber, Z. Lu, T. Richardson, R. H. Crabtree, Inorg. Chem., 3 (1992) 4709.
116. A. H. Vetter, A. Berkessel, Synthesis, (1995) 419.
117. Y. P. Tian, W. T. Yu, C. Y. Zhao, M. H. Jiang, Z. G. Cai, H. K. Fun, Polyhedron, 2 (2002) 1217.
118. Y. P. Tian, C. Y. Duan, C. Y. Zhao, X. Z. You, T. C. W. Mak, Z. Y. Zhang, Inorg. Chem., 36 (1997) 1247.
119. C. T. Zeyrek, B. Boyacioglu, Ö. Temiz-Arpaci, H. Ünver, A. Elmali, J. Mol. Struct., 1136 (2017) 112.
120. B. S. Kusmariya, A. P. Mishra, J. Mol. Struct., 1101 (2015) 176.
121. B. Shafaatian, S. Sedighe Mousavi, S. Afshari, J. Mol. Struct., 1123 (2016) 191.
122. J. Feng, Z. Wen-Xuan, P. Cheng-Yu, S. Lin, M. Hui, L. Rong-Bao, T. Dong-Liang, Chinese J. Struct. Chem., 35 (2016) 679.
123. R. N. Patel, Y. P. Singh, Y. Singh, R. J. Butcher, M. Zeller, R. K. Bhubon Singh, O. U-wang, J. Mol. Struct., 1136 (2017) 157.
124. R. A. Laudise, The Growth of Single Crystals', Prentice-Hall, Englewood Cliffs, New Jersey, 1970.
125. S. K. Kurtz, T. T. Perry, J. Appl. Phys., 39 (1968) 3798.
126. B. Bailey, J. F. Owens, Phys. Rev. D47 (1993) 2735.

CHAPTER II

MATERIALS AND METHODS

This chapter portrays the procedure adopted for the synthesis of precursor of ligands, principle, procedure and instrumentation of the physico-chemical techniques employed for the structure elucidation of the ligands and the complexes. In addition to this, the procedures adopted for computational (density functional theory [DFT]) and molecular docking studies and evaluation of biological activities of the compounds are described briefly.

1. Reagents

Carbondisulphide (Merck), N-methylaniline (SRL), hydrazine hydrate 98% (Glaxo fine Chemicals), sodium chloroacetate, ethylacetoacetate (Merck), phenylhydrazine, benzoyl chloride (Merck) and so on, were used as received**.** The metal salts used for the synthesis of the complexes were vanadyl sulphate, chromium chloride, chromium nitrate, manganese acetate, ferric nitrate, cobalt acetate, cobalt chloride, cobalt nitrate, nickel acetate, nickel chloride, nickel nitrate, copper acetate, copper chloride, copper nitrate, copper sulphate, zinc acetate, zinc nitrate, zinc sulphate and cadmium acetate. All of them were of Analar grade. The commercial grade solvents, methanol and ethanol were purified and dried by using standard procedures. DMSO, DMF, $CHCl_3$ and $C_2H_2Cl_2$ used for re-crystallization were used as received.

2. Ligands

The names of the ligand synthesized and used in this investigation are given in Chapter I. Of the five carbonyl compounds used for the synthesis of ligands, four, that is, benzophenone, 3-formylchromone, 4-hydroxy-3-methoxybenzaldehyde, 3,4-dimethoxybenzaldehyde, were purchased and used. However, the other two ligand precursors, 1-phenyl-3-methyl-4-benzoyl-5-pyrazolone and N(4)-methyl-N(4)-phenylthiosemicarbazide, were synthesized in our laboratory. The details of the synthesis of the ligands will be given in the respective chapters.

2.1. Synthesis of ligand precursors

(A) Synthesis of 1-phenyl-3-methyl-4-benzoyl-5-pyrazolone

1-Phenyl-3-methyl-4-benzoyl-5-pyrazolone (PMBP) was prepared by using Jenson's method.[1,2] It involves two steps.

(a) Synthesis of 1-phenyl-3-methyl-5-pyrazolone

Ethylacetoacetate (49 mL, 0.384 mol) and phenylhydrazine (36.5 mL, 0.37 mol) were mixed together in a large china dish. The mixture was heated on a boiling water bath in a fume cupboard for about 2 hours and stirred from time to time with a glass rod. The heavy reddish syrup was allowed to cool, about 100 mL of ether added and the mixture stirred vigorously.

The syrup which was insoluble in ether, solidified within 15 minutes. The solid was filtered with a pump and washed thoroughly with ether to remove the coloured impurities. On re-crystallization from hot water, obtained colourless crystals of pyrazolone (m.p. 132°C).

(b) Synthesis of PMBP

1-phenyl-3-methyl-5-pyrazolone, 15 g (0.082 mol), was placed in a flask equipped with a reflux condenser and a magnetic stirrer and dissolved in 60–80 mL of freshly distilled ethanol by heating. $Ca(OH)_2$, 12 g, was added followed by 9.9 mL of benzoyl chloride drops within one minute. The reaction mixture got converted to a thick paste and the temperature was raised during the first few minutes. The mixture was refluxed for 30 minutes. The calcium complex in the flask was decomposed by pouring the mixture to 2N HCl (200 mL). The cream-coloured crystals separated were collected on a Buchner funnel. The product was re-crystallized from ethanol–water mixture which was slightly acidified to destroy any undecomposed calcium complex (m.p. 98°C).

(B) Synthesis of N(4)-methyl-N(4)-phenylthiosemicarbazide

N(4)-methyl-N(4)-phenylthiosemicarbazide was prepared by using a modified procedure reported by Scovill *et al*.[3] It involves two steps

(a) Synthesis of carboxymethyl-(N-methyl-N-phenyl)dithiocarbamate

A mixture consisting of 12 mL CS_2 (15.2 g, 0.2 mol) and 21.6 mL (21.2 g, 0.2 mol) of N-methylaniline was stirred with a solution of 8.4 g (0.21 mol) of NaOH in 250 mL water for 4 hours. After the disappearance of the organic layer, the straw-coloured solution was treated with 23.2 g of sodium chloroacetate and allowed to stand overnight (17 hours). The solution was acidified with conc. HCI (25 mL) and the solid that separated was filtered, washed with water and dried. This afforded 39.7 g (82%) of the pale buff-coloured carboxymethyl-(N-methyl-N-phenyl) dithiocarbamate (m.p. 197°C–198°C).

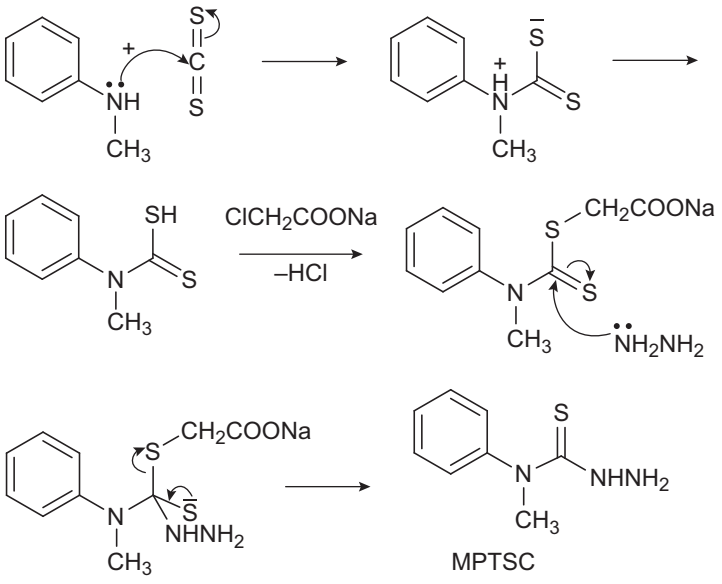

Scheme 1. Reaction pathway of the formation of N(4)-methyl-N(4)-phenylthiosemicarbazide.

(b) Synthesis of N(4)-methyl-N(4)-phenylthiosemicarbazide (MPTSC)

A mixture of 17.8 g of carboxymethyl-(N-methyl-N-phenyl) dithiocarbamate, 20 mL of hydrazine hydrate and 10 mL of water was heated on the rings of a water bath for 25 minutes. The compound separated was filtered, washed with water, dried and re-crystallized from 2:1 alcohol. The yield was 78% and m.p. 124°C–125°C. The reaction pathway of the formation of the precursor is shown in **Scheme 1.**

3. Experimental techniques

3.1. Elemental analyses

Elemental (CHNS) analyses of the ligands and the complexes were performed on a Vario EL III CHNS elemental analyzer at the SAIF, Cochin University of Science and Technology, Kochi 22, India and on Euro Vector CHNS analyser Model No: EA 3000 KFRI Peechi, Thrissur. The percentages of metals present in the complexes were determined by reported methods[4].

3.2. Magnetic measurements

Magnetic susceptibility values for the complexes at room temperature were measured using Sherwood Scientific Magnetic Susceptibility Balance. $HgCo(SCN)_4$ was used as the calibrant.

The mass magnetic susceptibility (χ_g in cm^3g^{-1}) and the molar magnetic susceptibility (χ_m in $cm^3\,mol^{-1}$) are defined as follows:

$$\chi_m = M\,\chi_g$$

If χ is positive, then $(1 + \chi) > 1$ and the material is called paramagnetic. In this case, the magnetic field is strengthened by the presence of the material. Alternatively, if χ is negative, then $(1 + \chi) < 1$, and the material is diamagnetic. In this case, the magnetic field is weakened in the presence of the material.

The susceptibility value calculated from magnetic measurements is the sum of paramagnetic and diamagnetic susceptibilities. The value of diamagnetic susceptibility is subtracted from the calculated susceptibility to find the exact paramagnetic susceptibility.[5] Diamagnetic corrections were made using Pascal's constants for all atoms and bonds, when structural formula of the complexes is correctly known.

$$\chi_{M\text{corrected}} = \chi_M - \text{Diamagnetic corrections}$$

The magnetic moment is calculated using the relation,

$$\mu_{\text{eff}} = 2.828\sqrt{\chi_{M\text{corrected}}}\,T$$

where χ_M is the molar susceptibility.

3.3. Electronic spectra

The electronic spectra in solid state were recorded on a JascoV-550 model UV–VIS spectrometer.

3.4. Infrared (IR) spectra

Infrared (IR) spectra were recorded on a Jasco-FT-IR-4100 model spectrometer using KBr pellets with a scanning range of 400–4000 cm^{-1}.

3.5. Raman spectra

Raman spectra of the ligands were recorded on MultiRAM spectrometer, range 3600 to 50 cm^{-1} with a laser excitation wavelength 1064 nm.

3.6. NMR spectra

^{1}H NMR spectra of the ligands and the zinc complexes were recorded on a model 400 MHz Bruker Avance III FT NMR at SAIF, Cochin and IIT Chennai.

3.7. Electron spin resonance spectra

The ESR spectra were recorded on a FA200 model ESR instrument at SAIF, IIT, Chennai.

3.8. X-ray crystallography

Single crystal X-ray crystallographic data were collected on a Bruker Model Kappa Apex II diffractometer at SAIF, Cochin, School of Pure and Applied Physics, M G University, Kottayam, SAIF, IIT Chennai, with graphite monochromatic M_o $K\alpha$ (λ = 0.71073 Å) radiation. Direct methods were used to solve the structure and refined by least-square on F^2 using SHELXL-97[6]/SHELXL-2014/7[7]. All non-hydrogen atoms were refined anisotropically. All hydrogen atoms, except those attached to nitrogen, were geometrically fixed at calculated positions. Those on nitrogen atoms were refined from Fourier maps. The crystallographic tools, PLATON[8], ORTEP[9], DIAMOND[10] and MERCURY[11] were used for structure analysis and presentation of the results.

3.9. Thermogravimetry

For thermogravimetric studies, TG/DTG were recorded on TGA Q50 V20.13 Build 39 model thermogravimetric analyzer fitted with a thermal analysis controller in nitrogen atmosphere with a heating rate of 10°C/min at NIT, Calicut.

4. DFT studies

DFT studies of ligands were performed at the Department of Physics and Department of Chemistry, University of Calicut. For computational studies, the molecules are optimized by using DFT (B3LYP) method with the 6–31+G (d,p) basis sets, using the Gaussian 09[12] program. Details of the studies are discussed in Chapter VIII.

5. Molecular docking studies

Molecular docking studies of ligands were performed at the Department of Biotechnology, School of life sciences, Thalassery campus, Kannur University. Molecular docking studies were performed using the Glide program integrated in Schrodinger molecular modelling software. The Maestro (version 10.4) was used as graphical user interface. The ligands under study were docked into the binding site of the selected proteins. Details of the studies are discussed in Chapter IX.

6. Biological studies

Antifungal studies were performed at the Department of Botany, The Zamorin's Guruvayurappan College, Calicut. Antibacterial studies were performed at the Department of Biotechnology, School of life sciences, Thalassery campus, Kannur University.

The antifungal activities of the ligand and complexes were tested for their effect on the growth of microbial cultures and studied their interaction with *Alternaria alternata*, *Aspergillus niger*, *Colletotrichum gloeosporioides, Sclerotium rolfsii* using potato dextrose agar medium.[13] The diametrical growth of the fungus was recorded in each petri plate and average growth of the fungal colony was calculated after 72 hours. The percentage inhibition was calculated by the equation,

$$\text{Percentage inhibition} = C - T/C \times 100$$

where C and T are the diameters of the fungal colony in the control and the test plates, respectively.

The synthesized compounds were tested *in vitro* for their antibacterial activity against Gram-positive and Gram-negative organisms by Kirby–Bauer agar diffusion method.[14] Mueller–Hinton agar medium was used in this method. The bacterial strains used were *Staphylococcus aureus*, *Enterococcus faecalis, Bacillus subtili*, *Escherichia coli*, *Pseudomonas aeruginosa* and *Klebsiella pneumoniae*. Details of the studies are discussed in Chapter X.

References

1. B. S. Jensen, Acta Chem. Scand., 13 (1959) 1668.
2. B. A. Uzoukwu, Synth. React. Inorg. Met. Org. Chem., 23 (1993) 1087.
3. J. P. Scovill, D. L. Klayman, C. F. Franchino, J. Med. Chem., 25 (1982) 1261.
4. A. I. Vogel, A text book of Quantitative Inorganic Analysis, ELBS, London, 1978.
5. J. E. Huheey, E. A. Keiter, R. L. Keiter, Inorganic Chemistry, 4th ed., Addison Wesley publishing company, India, 1993.
6. G. H. Sheldrick, SHELXL 97, Program for Crystal Structure Refinement, University of Göttingen, Göttingen, Germany, 1997.
7. G. M. Sheldrick, SHELXL-2014/7: Program for the Solution of Crystal Structures, University of Göttingen, Göttingen, Germany, 2014.
8. A. L. Spek, J. Appl. Cryst., 36 (2003) 7.
9. L. J. Farrugia, J. Appl. Cryst., 45 (2012) 849.
10. Diamond-Crystal and Molecular Structure Visualization Crystal Impact – Dr. H. Putz, Dr. K. Brandenburg GbR, Kreuzherrenstr. 102, 53227 Bonn, Germany.
11. C. F Macrae, P. R Edington, P. McCabe, E. Pidcock, G. P. Sheilds, R. Taylor, M. Towler, J. Van de Streek, J. Appl. Cryst., 39 (2006) 453.
12. M. J. Frisch, G. W. Trucks, H. B. Schlegel, G. E. Scuseria, M. A. Robb, J. R.Cheeseman, G. Scalmani, V. Barone, B. Mennucci, G. A. Petersson, H.Nakatsuji, M. Caricato, X. Li, H. P. Hratchian, A. F. Izmaylov, J. Bloino, G.Zheng, J. L. Sonnenberg, M. Hada, M. Ehara, K. Toyota, R. Fukuda, J.Hasegawa, M. Ishida, T. Nakajima, Y. Honda, O. Kitao, H. Nakai, T. Vreven,J. A. Montgomery Jr., J. E. Peralta, F. Ogliaro, M. Bearpark, J. J. Heyd, E.Brothers, K. N. Kudin, V. N. Staroverov, R. Kobayashi, J. Normand, K.Raghavachari, A. Rendell, J. C. Burant, S. S. Iyengar, J. Tomasi, M.Cossi, N. Rega, J. M. Millam, M. Klene, J. E. Knox, J. B. Cross, V. Bakken, C. Adamo, J. Jaramillo, R. Gomperts, R. E. Stratmann, O. Yazyev, A. J. Austin,R. Cammi, C. Pomelli, J. W. Ochterski, R. L. Martin, K. Morokuma, V. G.Zakrzewski, G. A. Voth, P. Salvador, J. J. Dannenberg, S. Dapprich, A. D.Daniels, Ö. Farkas, J. B. Foresman, J. V. Ortiz, J. Cioslowski, D. J. Fox,Gaussian 09, Revision A.1, Gaussian, Inc., Wallingford, Connecticut, 2009.
13. H. L. Singh. Inorg. Chem. Indian J., 2 (2007) 135.
14. A. W Bauer, W. M. Kirby, J. C. Sherries, M. Tuck, Am. J. Clin. Pathol., 45 (1966) 493.

CHAPTER III

NOVEL LIGAND, 1-PHENYL-3-METHYL-4-BENZOYL-5-PYRAZOLONE N(4)-METHYL-N(4)-PHENYLTHIOSEMICARBAZONE AND ITS TRANSITION METAL COMPLEXES

1. Introduction

In 1883, Knorr[1,2] carried out the reaction of ethylacetoacetate with phenylhydrazine which yielded 1-phenyl-3-methyl-5-pyrazolone. The original synthesis of an acylpyrazolone appeared at the end of the 19th century. However, it was only in 1959 Jensen reported a convenient method of preparation of 1-phenyl-3-methyl-4-acyl-pyrazol-5-ones[3] (Fig. 1).

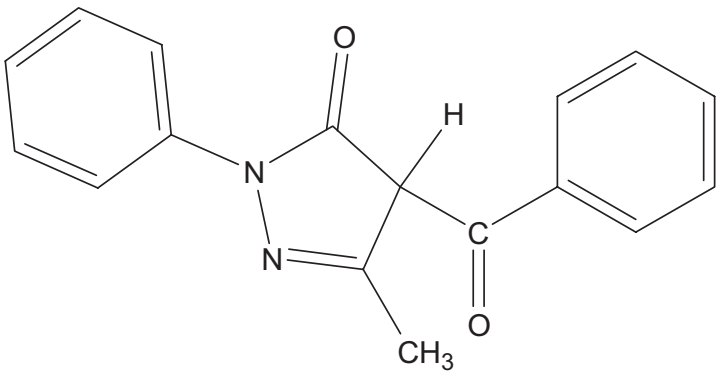

Fig. 1. 1-Phenyl-3-methyl-4-benzoyl-pyrazol-5-one.

Acyl-5-pyrazolones are an interesting class of β-diketones containing a pyrazolone ring fused to a chelating wing. They find applications as laser materials,[4] as ^{1}H NMR shift reagents,[5] in chromatographic study and in the petrochemical industry. The nature of the substituent at the fourth position of the pyrazolone ring causes significant variations in the electronic, steric and chemical parameters as a ligand, thereby affecting complexation and extraction of metal ions.

This chapter portrays the synthesis and characterisation of 1-phenyl-3-methyl-4-benzoyl-5-pyrazolone N(4)-methyl-N(4)-phenylthiosemicarbazone (PMBP-MPTSC), (H_2L) and its several transition metal complexes. The structure of the ligand was drawn using Chem Draw ultra (Fig. 2).

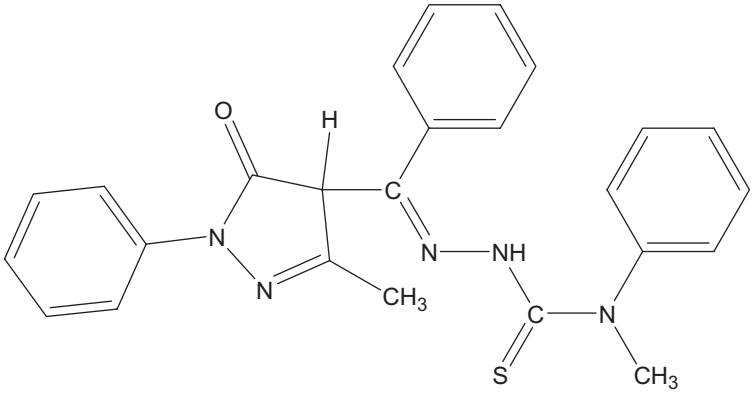

Fig. 2. 1-Phenyl-3-methyl-4-benzoyl-5-pyrazolone N(4)-methyl-N(4)-phenylthiosemicarbazone (PMBP-MPTSC), (H_2L).

*IUPAC name of the compound.

*N-methyl-2-((3-methyl-5-oxo-1-phenyl-4,5-dihydro-1H-pyrazol-4-yl)(phenyl) methylene)-N-phenylhydrazinecarbothioamide.

2. Experimental

2.1. Materials and methods

Carbon disulphide (Merck), N-methylaniline (SRL), hydrazine hydrate 98% (Glaxo fine Chemicals), ethylacetoacetate (Merck), phenylhydrazine, benzoyl chloride and so on were used as received. Commercially available metal salts were used without further purification. The solvents were purified and dried by standard procedure. The ligand was characterised by using partial elemental analyses, FT-IR, FT-Raman, electronic and ^{1}H NMR spectra, TG, DSC and single-crystal X-ray diffraction. The complexes were characterised by partial elemental analyses, FT-IR and electronic spectra. The zinc(II) complexes were characterised by ^{1}H NMR spectra. EPR spectrum of the copper(II) complex was also recorded. Thermal stabilities of the complexes were also ascertained. The melting points of the ligand and the complexes were determined in one side open capillary on a melting point apparatus. The details regarding these techniques are given in Chapter II.

2.2. Synthesis

2.2.1. 1-Phenyl-3-methyl-4-benzoyl-5-pyrazolone N(4)-methyl-N(4)-phenylthiosemicarbazone (H_2L)

It involves five steps of which two each for the synthesis of the precursors 1-phenyl-3-methyl-4-benzoyl-5-pyrazolone (PMBP) and N(4)-methyl-N(4)-phenylthiosemicarbazide (MPTSC) and one for the synthesis of ligand, 1-phenyl-3-methyl-4-benzoyl-5-pyrazolone N(4)-methyl-N(4)-phenylthiosemicarbazone (H_2L). The details regarding the syntheses of the precursors are explained in Chapter II.

The ligand was prepared by stirring the hot methanolic solution of PMBP (750 mg, 2.76 mmol) and MPTSC (500 mg, 2.76 mmol) on a magnetic stirrer. The solution was then refluxed

at 60°C–80°C for 30 minutes. The compound obtained was filtered, washed with methanol and dried over anhydrous $CaCl_2$. Its melting point and solubility in different solvents were noted.

2.2.2. Metal complexes

Ligand (H_2L) (1 mmol) was dissolved in two or three drops of chloroform and excess of hot methanol. To this solution, metal salt (1 mmol) dissolved in hot water/hot methanol was added dropwise and refluxed for 3–4 hours. The precipitate obtained was cooled and filtered. It was then washed with water, methanol and finally with ether. The product was dried over $CaCl_2$ in a desiccator.

3. Results and discussion

3.1. Characterisation of the ligand

One of the starting compounds PMBP used for the preparation of the ligand can undergo keto–enol tautomerism in solution (I and II). During the synthesis of the ligand, it may be the enolic form of PMBP (II) that reacts with N(4)-methyl-N(4)-phenylthiosemicarbazide (MPTSC) (III) forming the product. As a result, the ligand formed can be a mixture of keto–imine/enol–imine tautomer (IV and V) in solution. On crystallization, as a result of delocalization of electrons due to extended conjugation, the compound undergoes rearrangement and tends to exist as the stable conformer (VI). However, during complexation, in the presence of metal ions in solution, the ligand can exist in enol–imine tautomer (IV) and coordinates through enolic oxygen after deprotonation. The possibility of thione–thiol tautomerism and coordination of the ligand through S^- is ruled out because of the presence of NH–C=S bond in the crystal structure of the Cd(II) complex discussed elsewhere in this chapter.

The reaction pathway in the formation of the ligand 1-phenyl-3-methyl-4-benzoyl-5-pyrazolone N(4)-methyl-N(4)-phenylthiosemicarbazone (H_2L) can be represented as follows (Scheme 1):

3.1.1. Microanalytical data

The suggested formula for the ligand is $C_{25}H_{23}N_5OS$. CHNS percentages are in agreement with the suggested molecular formula (Table 1). The compound is yellow in colour and melted at 163°C. It is non-hygroscopic and stable at normal atmospheric conditions. It is soluble in $CHCl_3$ but partially soluble in DMF, DMSO, ethanol and methanol.

3.1.2. Single-crystal XRD studies of ligand (H_2L)

Single crystals of H_2L suitable for X-ray analysis were obtained from its solution in 1:1 (v/v) mixture of methanol and DMSO. A crystal with dimensions 0.35 × 0.30 × 0.30 mm^3 was selected for collecting the data. H_2L crystallizes with one molecule per asymmetric unit into a triclinic crystal system with a space group of *P–1*. The title compound has C_1 point group symmetry.

X-ray crystallographic data were collected at 296(2) K on a Bruker Model Kappa Apex II diffractometer with graphite monochromated Mo *Kα* (λ = 0.71073 Å) radiation. Direct methods were used to solve the structure and refined by least square on F^2 using

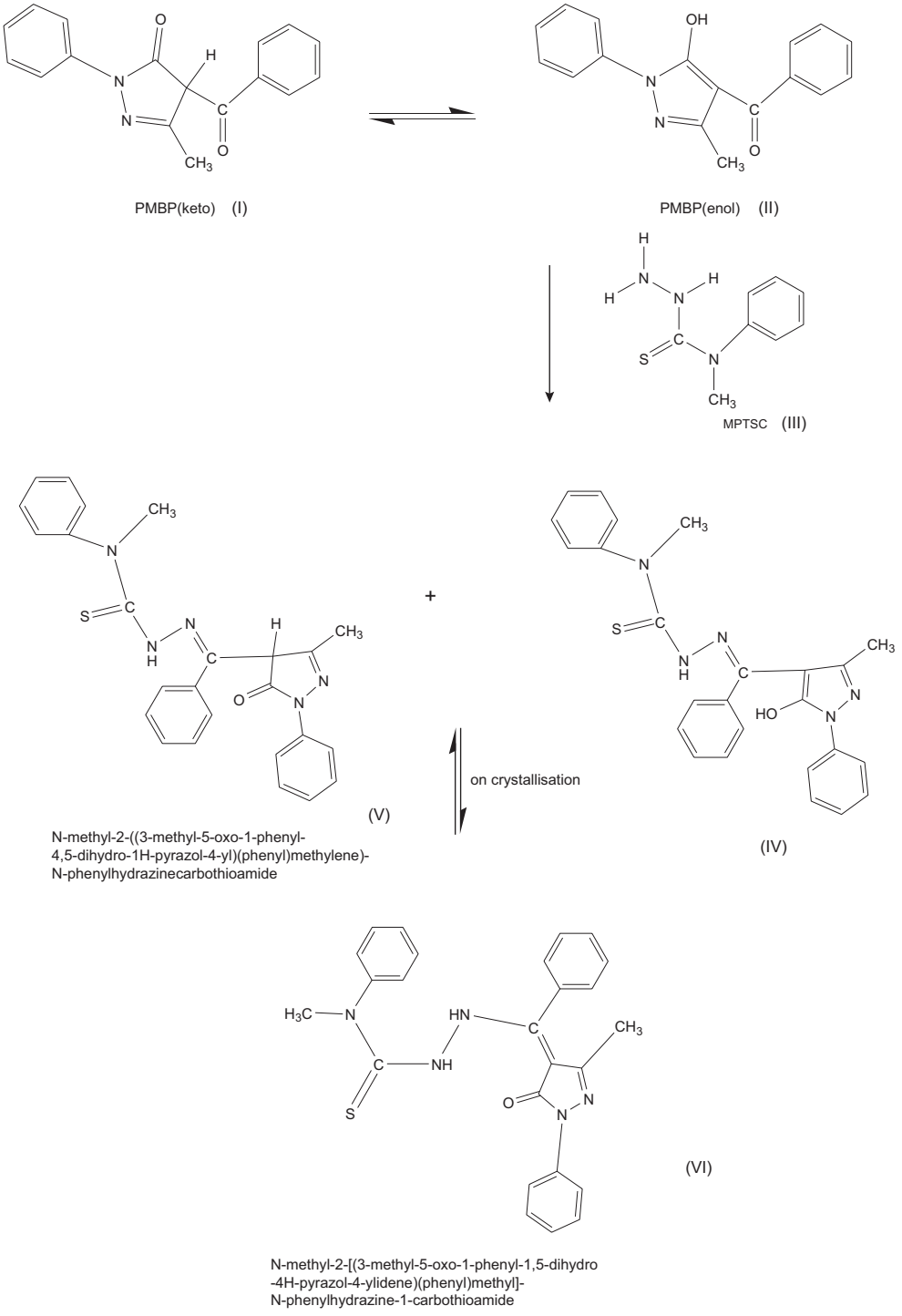

Scheme 1. The reaction pathway of 1-phenyl-3-methyl-4-benzoyl-5-pyrazolone N(4)-methyl-N(4)-phenylthiosemicarbazone (H_2L).

Table 1. Analytical data of the ligand

SI. no	Compound	Molecular Weight	Melting Point	Colour	Yield	Elemental Analysis Found (Calculated)			
						C	H	N	S
1	$C_{25}H_{23}N_5OS$ (H_2L)	441.54	163	Yellow	80	68.2 (68.0)	5.0 (5.2)	15.9 (15.9)	7.2 (7.2)

SHELXL-97.[6] All non-hydrogen atoms were refined anisotropically. All hydrogen atoms except those attached to nitrogen were geometrically fixed at calculated positions. The crystallographic tools PLATON,[7] ORTEP,[8] DIAMOND3.2d[9] and MERCURY3.5.1[10] for windows were used for structure analysis and presentation of the results. The structure was finally refined to the conventional *R*-value of 0.0540.

Crystal data and structure refinement parametres are given in Table 2. PLATON diagram of H_2L with the atom numbering scheme is shown in Fig. 3. Selected bond lengths and bond angles are listed in Table 3. Table 4 shows hydrogen bonding interaction parameters of H_2L.

Table 2. Crystal data and structure refinement for H_2L

Identification code	H_2L		
Empirical formula	$C_{25}\ H_{23}\ N_5\ O\ S$	ρ (calculated) (mg/m^3)	1.306
Formula weight	441.54	Absorption coefficient (mm^{-1})	0.172
Temperature (K)	296(2)	F(000)	464
Wavelength (Å)	0.71073	Crystal size (mm^3)	0.350 × 0.300 × 0.300
Crystal system	Triclinic	Theta range for data collection	1.60°–28.31°
Space group	*P–1*	Index ranges	$-10 \le h \le 10$, $-14 \le k =\le 14$, $-11 \le l \le 17$
Unit cell dimensions		Reflections collected	8957
a(Å)	7.8930(4)	Independent reflections	5465 [*R*(int) = 0.0174]
b(Å)	11.2019(5)	Completeness to theta	28.31° 97.6%
c(Å)	13.0211(7)	Refinement method	Full-matrix least squares on F^2
α(°)	96.175(3)	Data/restraints/parameters	5465/0/299
β(°)	100.922(3)	Goodness-of-fit on F^2	0.981
γ(°)	91.005(3)	Final *R* indices [$I > 2$sigma(I)]	$R_1 = 0.0540$, w$R_2 = 0.1461$
Volume (Å^3)	1123.02(10)	*R* indices (all data)	$R_1 = 0.0828$, w$R_2 = 0.1790$
Z	2	Largest diff. peak and hole (e.A^{-3})	0.381 and −0.365

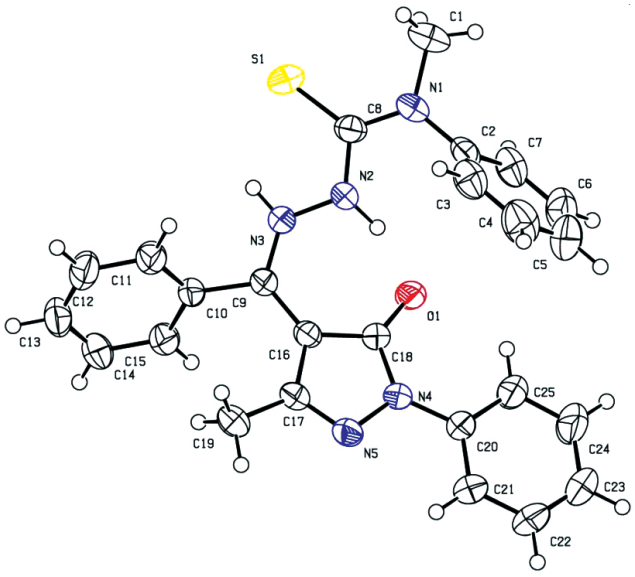

Fig. 3. The molecular structure of the compound H_2L with atom numbering scheme.

Table 3. Selected bond lengths (Å), bond angles and torsion angles (°) of H_2L

Bond Length (Å)		**Bond Length (Å)**		**Bond Angle (°)**		**Torsion Angles (°)**	
C(1)–N(1)	1.469(3)	C(10)–C(11)	1.378(3)	N(1)–C(8)–S(1)	124.60(2)	N(3)–C(9)–C(10)–C(11)	−56.1(3)
C(1)–H(1A)	0.9300	C(10)–C(15)	1.391(3)	N(2)–C(8)–S(1)	121.90(1)	N(3)–C(9)–C(10)–C(15)	126.4(2)
C(2)–C(3)	1.374(3)	C(11)–C(12)	1.383(3)	C(11)–C(10)–C(9)	120.40(2)	N(3)–C(9)–C(16)–C(18)	−21.5(3)
C(2)–C(7)	1.377(3)	C(12)–C(13)	1.375(3)	C(10)–C(11)–C(12)	120.0	N(2)–C(8)–N(1)–C(2)	178.3(2)
C(2)–N(1)	1.435(3)	C(13)–C(14)	1.373(3)	O(1)–C(18)–N(4)	125.2(17)	S(1)–C(8)–N(1)–C(2)	175.82(16)
C(3)–C(4)	1.370(4)	C(14)–C(15)	1.377(3)	O(1)–C(18)–C(16)	129.75(17)	N(2)–C(8)–N(1)–C(1)	178.3(2)
C(3)–H(3)	0.9300	C(16)–C(17)	1.436(3)	C(8)–N(1)–C(2)	122.02(17)	S(1)–C(8)–N(1)–C(1)	−2.6(3)
C(4)–C(5)	1.374(4)	C(16)–C(18)	1.437(2)	C(8)–N(1)–C(1)	121.3(2)	C(7)–C(2)–N(1)–C(8)	104.4(2)
C(5)–C(6)	1.370(4)	C(17)–N(5)	1.304(2)	C(2)–N(1)–C(1)	116.5(2)	C(3)–C(2)–N(1)–C(1)	102.2(3)
C(6)–C(7)	1.370(4)	C(17)–C(19)	1.491(3)	C(8)–N(2)–N(3)	115.5(16)	N(1)–C(8)–N(2)–N(3)	−179.16(18)
C(8)–N(1)	1.349(3)	C(18)–O(1)	1.258(2)	C(9)–N(3)–N(2)	124.21(16)	S(1)–C(8)–N(2)–N(3)	1.7(3)
C(8)–N(2)	1.368(3)	C(18)–N(4)	1.367(2)	C(16)–C(9)–N(3)	124.68(16)	C(16)–C(9)–N(3)–N(2)	−12.9(3)
C(8)–S(1)	1.671(2)	C(20)–N(4)	1.422(2)			C(10)–C(9)–N(3)–N(2)	166.61(17)
C(9)–N(3)	1.327(2)	N(2)–N(3)	1.384(2)			C(8)–N(2)–N(3)–C(9)	−168.70(18)
C(9)–C(16)	1.401(3)	N(2)–H(2N)	0.98(3)			O(1)–C(18)–N(4)–N(5)	−178.01(18)
C(9)–C(10)	1.483(3)	N(4)–N(5)	1.398(2)			O(1)–C(18)–N(4)–C(20)	−1.4(3)

Table 4. Hydrogen bonding interaction parameters of H_2L in [Å and °]

D–H···A	d(D–H)	d(H···A)	d(D···A)	<(DHA)
N(3)–H(3N)···.S(1)	0.89(2)	2.29(2)	2.8517(18)	121.20(19)
N(2)–H(2N)···O(1)	0.98(2)	1.61(2)	2.558(2)	162(2)
C(7)–H(7)···O(1)[a]	0.93	2.42	3.324(3)	163
C(21)–H(21)···N(5)	0.93	2.42	2.767(3)	102
C(25)–H(25)···O(1)	0.93	2.24	2.873(3)	125

[a]Symmetry transformations used to generate equivalent atoms: 1−*x*, 1−*y*, −*z*.

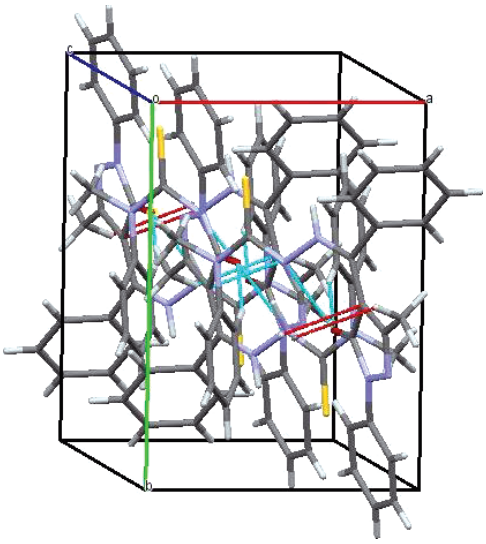

Fig. 4. Intermolecular bond interaction of H_2L along *c**-axis.

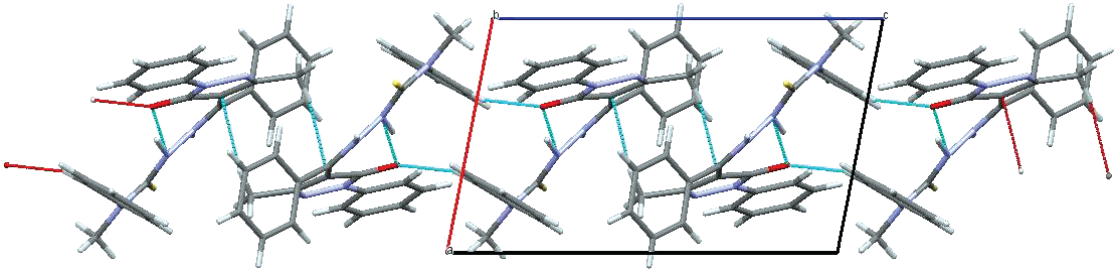

Fig. 5. Supramolecular chain mediated by C–H···O interaction along *b*-axis.

It is found that the molecules in a unit cell are arranged in inverted face-to-face manner, which are the repeating units of the packing in the crystal lattice. An interesting attribute of the crystal packing is the formation of a supramolecular chain mediated by intermolecular C–H···O and H···C interactions. Fig. 4 shows intermolecular bond interaction of H_2L along *c**-axis. Fig. 5 shows supramolecular chain mediated by C–H···O interaction along *b*-axis.

The bond distances C(9)–N(3), C(8)–N(1), C(8)–N(2) and N(2)–N(3) are 1.327(2) Å, 1.349(3) Å, 1.368(2) Å and 1.384(2) Å, respectively. They are found to be at the midway between the analogous single [C–N, 1.47 Å; N–N, 1.45 Å] and double bonds [C=N, 1.28 Å; N=N, 1.25 Å].[11,12] The C(8)–S(1) bond length, 1.671(2) Å, is closer to C=S bond length [1.61 Å] than to C–S bond length [1.81 Å].[13] Therefore, the ligand exists in the thione form.

The bond length of C(18)–O(1) is 1.258(2) Å, which is in accordance with the double bond (C=O), indicating that the ligand is in the keto-form in the crystalline state. All the bond lengths possess bond equalization due to partial double bond and single bond characteristics. This indicates that there is significant electron delocalization around the pyrazolone ring and the thiosemicarbazide moiety.[14]

A torsion angle value of −5.1(4) corresponding to S(1)–C(8)–N(2)–N(3) moiety confirms the syn-periplanar configuration of the S(1) atom with respect to azomethine nitrogen atom, N(3). The terminal nitrogen atoms N(1) and N(3) of the thiosemicarbazide fragment are in an anti-periplanar conformation with respect to the C(8)–N(2) with a torsion angle of −179.16(18)°. Similarly, the nitrogen atoms N(1) and N(3) of the thiosemicarbazide fragment are in an anti-periplanar conformation with respect to C(8)–N(2), with a torsion angle −179.16(18). The bond angles of C(16)–C(9)–N(3), C(8)–N(3)–N(2) and C(9)–N(3)–N(2) are 124.68(16)°, 115.50(16)° and 124.21(16)°, respectively. It is an evidence for the deviation of the co-planarity of thiosemicarbazide and pyrazolone moieties.

3.1.3. Spectroscopic analysis

(a) Electronic spectrum

The electronic absorption spectra of the ligand in solid state and in chloroform were recorded in the range 200–900 nm. The compound registered three C–T bands at 259, 321 and 425 br nm in solid state. In chloroform, these bands observed at 256, 318 and 362–415 nm with a shoulder at 379 nm (Fig. 6). Since the keto form is more polar than the enol form, the later form must be dominant in non-polar solvents.[15] In the present scenario, enol–imine tautomeric form is present in solution, whereas keto–imine form is present in the solid state. The first two bands can be attributed, respectively, to the $\pi-\pi^*$ and $n-\pi^*$ transitions of the azomethine chromophore and the benzene ring. A broad band between 400 and 440 nm may be due to the strong intramolecular hydrogen bonding in the compound.

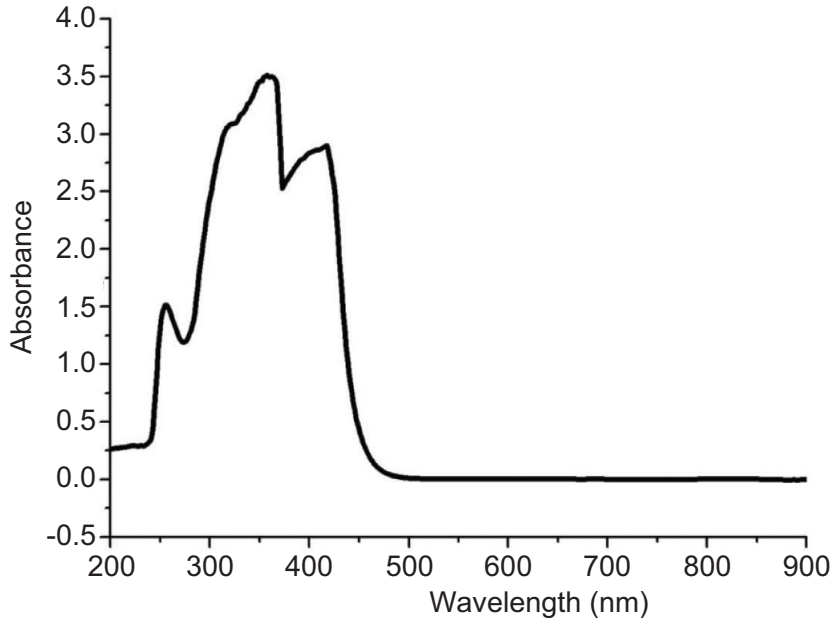

Fig. 6. Electronic spectrum of H_2L in chloroform.

(b) Vibrational spectra

The FT-IR and FT-Raman spectra of the ligand are shown in Figs. 7 and 8, respectively. The vibrations due to N–H stretching usually absorb in the region 3450–3250 cm^{-1}.[16] In the FT-IR and FT-Raman spectra, weak broad bands were observed at 3426 cm^{-1}.[17] It indicates the presence of hydrogen bonded tautomeric keto–imine or imine–ol form (=O···H–N or the O–H···N) of the compound in the solid state. Based on the information obtained from single-crystal XRD studies, the presence of hydrogen bonded imine–ol form (O–H···N) of the compound is ruled out.

The band for ν(C=O) of pyrazol-5-one moiety was seen at 1626 and 1629 cm^{-1}, respectively, in FT-IR and FT-Raman spectra. This is at a lower wave number than that usually found for carbonyls and indicates its involvement in hydrogen bonding with N–H of the thiosemicarbazide moiety. The ligand does not show any band between 2000 and 2500 cm^{-1} suggesting that in the solid state it is in the thione form. Moreover, we observed the C=S stretching mode at 1362, 1250 and 766 cm^{-1} in FT-IR and at 1247 and 1367 cm^{-1} in FT-Raman spectra.

The C–N stretching vibration is moderately to strongly active in the range 1220–1330 cm^{-1}. The sharp peaks at 1316 and 1313 cm^{-1} in FT-IR and FT-Raman, respectively, are assigned to C–N stretching vibration. In the present case, the bands observed at 1024 and 1106 cm^{-1} in FT-IR and at 1167 and 1147 cm^{-1} in FT-Raman spectrum are assigned to N–N stretching vibrations.

The aromatic and aliphatic C–H vibrations generally absorb in the region 2850–3100 cm^{-1}.[18,19] In the present investigation, the aromatic and aliphatic C–H stretching bands appear at 2924–3150 cm^{-1} in FT-IR and at 2926–3057 cm^{-1} in FT-Raman spectra as weak bands.

In aromatic compounds, the C–H in-plane and out-of-plane bending vibrations appear in the range of 1000–1300 cm^{-1} and 750–1000 cm^{-1}, respectively.[20] In this study, several bands in the range 695–1283 cm^{-1} in FT-IR and FT-Raman spectra are assigned to C–H in-plane and out-of-plane bending vibrations.

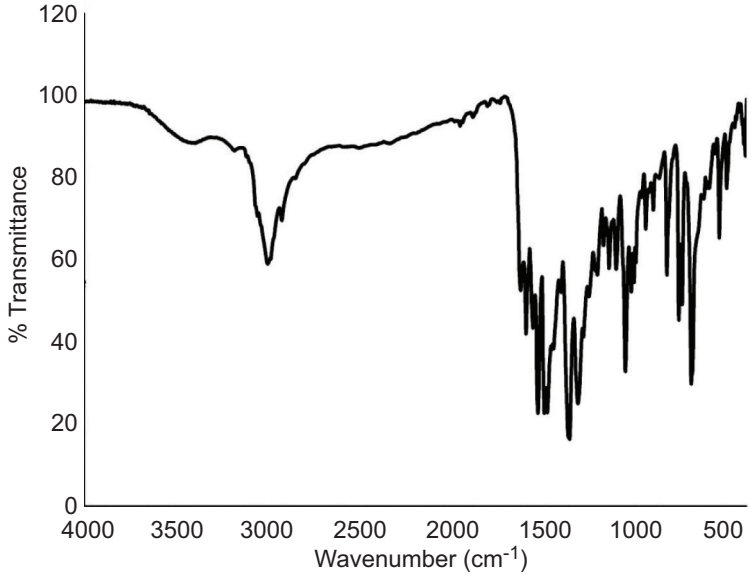

Fig. 7. FT-IR spectrum of H_2L.

Normally, the ring carbon–carbon stretching vibrations occur in the range of 1650–1347 cm^{-1}.[21] The identification of vibrations in this range is very difficult because of its mixing with C=N band which is usually observed in this range. In this work, the very strong bands observed at 1478 and 1534 cm^{-1} in the FT-IR and 1482 and 1532 cm^{-1} in FT-Raman are assigned to the C–C stretching vibrations.

(c) ^{1}H NMR spectrum

The ^{1}H NMR spectrum of the ligand was recorded in $CDCl_3$ (Fig. 9). A sharp singlet, which integrates as one hydrogen at 14.479 ppm in the ligand spectrum may be due to

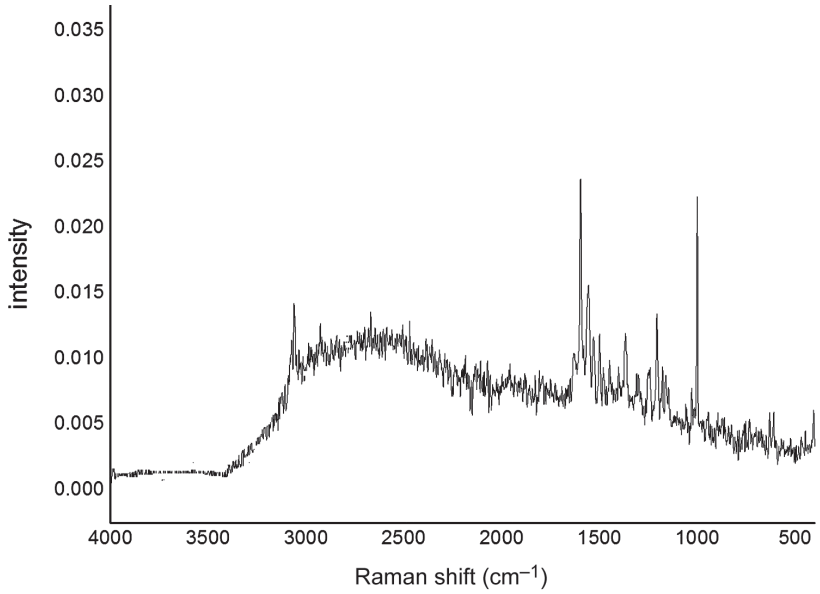

Fig. 8. FT-Raman spectrum of H_2L.

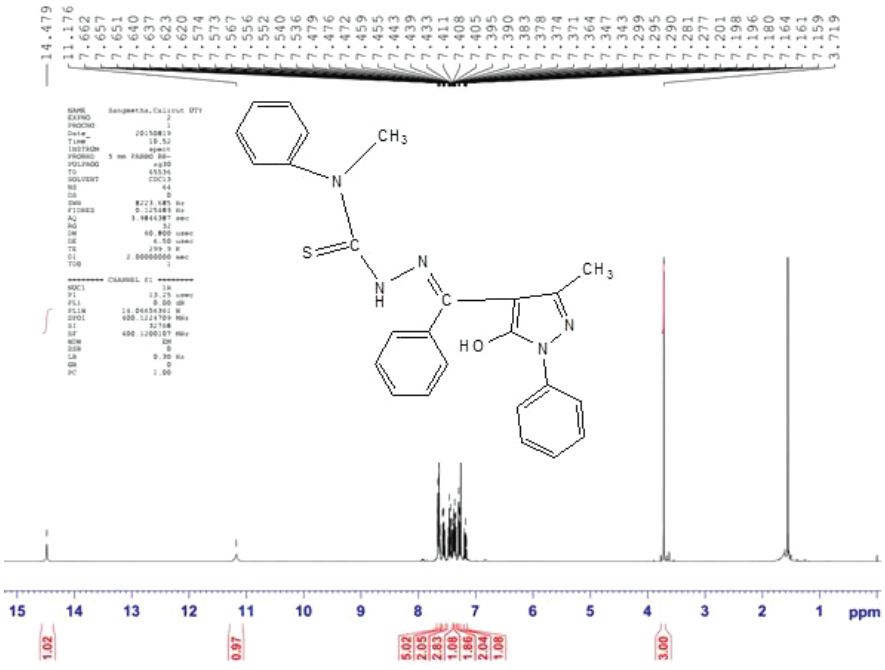

Fig. 9. NMR spectrum of H_2L.

the NH proton. In the spectrum of H_2L, a sharp singlet at 11.176 ppm corresponds to OH proton. The downfield shift of NH and OH proton signals is assigned to intramolecular hydrogen bonding interactions. As a result of decrease in the electron density around the proton, the OH and NH protons absorb at downfield. Absence of a singlet corresponding to –CH proton substantiates the existence of imine–ol tautomer of the ligand in solution. However, in the solid state, the compound is in its keto–imine form. Aromatic protons give peaks in the region 7.159–7.662 ppm. The peak observed at 3.179 ppm may be due to N–CH_3 protons. Methyl protons of the substituted pyrazolone show a singlet at 1.5 ppm.

3.2. Characterisation of the complexes

3.2.1. Formulae and general properties of the complexes

All the complexes were found to be stable at room temperature. The colours of all the complexes indicate the presence of sulphur-to-metal charge-transfer bands, which dominate their visible spectra and also substantiate that the colour is not due to the gegenions present but due to thiosemicarbazones.[22] Partial elemental analytical data complexes are in agreement with the suggested molecular formulae. In the complexes, the ligand was found to be coordinated to metal ions either in mono-anionic $(HL^-)^-$ or in neutral (H_2L) form. Molecular formulae, colours, partial elemental analyses and magnetic moments of the complexes are given in Table 5.

3.2.2. Electronic spectra and magnetic moments

The electronic spectra of complexes were recorded in solid state and their probable assignments are given in Table 6.

Cr(III) ion has a d^3 configuration (t_{2g}^3). Three spin-allowed transitions are observed for a high-spin chromium(III) complex. They are $^4A_{2g}(F) \rightarrow {}^4T_{2g}(F)$ (ν_1), $^4A_{2g}(F) \rightarrow {}^4T_{1g}(F)$ (ν_2) and $^4A_{2g}(F) \rightarrow {}^4T_{1g}(P)$ (ν_3). The highest energy band observed at 314 nm is assigned to the $^4A_{2g} \rightarrow {}^4T_{2g}$ transition. Two broad bands with maxima at 369 and 445 nm are assigned to $^4A_{2g}(F) \rightarrow {}^4T_{1g}(F)$ and $^4A_{2g}(F) \rightarrow {}^4T_{1g}(P)$ transitions. The positions of the bands in the electronic spectrum of $[Cr(HL)_2]NO_3$ point out a 6-coordinate octahedral geometry.[23] Its magnetic moment 3.8 BM is consistent with an octahedral geometry.[24]

The Mn(II) complex belongs to the d^5 system. In the high-spin, octahedrally coordinated Mn(II) complex, the lowest configuration $(t_{2g})^3 (e_g)^2$ gives rise to a ground state, $^6A_{1g}$. In such complexes, electronic transitions are both spin forbidden and Laporte-forbidden[25,26] and therefore, their intensities are very low. However, some forbidden transitions can occur to the quartet excited states and they are $^6A_{1g} \rightarrow {}^4A_{1g}(G)$, $^6A_{1g} \rightarrow {}^4E_g(G)$, $^6A_{1g} \rightarrow {}^4E_g(D)$, $^6A_{1g} \rightarrow {}^4A_{1g}(G)$, $^6A_{1g} \rightarrow {}^4T_{1g}(G)$ and $^6A_{1g} \rightarrow {}^4T_{2g}(G)$.

In this study, the electronic spectrum of Mn(II) complex exhibited four very low intense bands. They are one broad band at 390 nm due to $^6A_{1g} \rightarrow {}^4A_{1g}(G)$ and $^6A_{1g} \rightarrow {}^4E_g$ (G), another one at 577 nm due to $^6A_{1g} \rightarrow {}^4A_{1g}(G)$, third one at 700 nm due to $^6A_{1g} \rightarrow {}^4T_{1g}(G)$ and fourth one at 860 nm are $^6A_{1g} \rightarrow {}^4T_{2g}(G)$ transitions. These are in accordance with the octahedral environment around Mn(II) ion.

Table 5. Molecular formulae, colours, partial elemental analyses and magnetic moments of the complexes

Complex No	Compound	Molecular Weight	Melting Point	Colour	Yield	Elemental Analysis Found (Calculated)					μ in BM
						C	H	N	S	M	
	$C_{25}H_{23}N_5OS$ ($\mathbf{H_2L}$)	442	163	Yellow	80	68.2 (68.0)	5.0 (5.2)	15.9 (15.9)	7.2 (7.2)	_	_
1	$[Cr(HL)_2]NO_3$	996	174	Brown	75	61.0 (60.2)	4.7 (4.4)	14.6 (14.1)	6.5 (6.4)	5.6 (5.2)	3.8
2	$[Mn(HL)_2]2H_2O$	974	213	Brownish black	70	62.0 (61.6)	5.2 (4.9)	14.8 (14.3)	6.9 (6.5)	5.69 (5.6)	4.9
3	$[Fe(HL)_2]NO_3$	1001	130	Black	80	60.4 (59.9)	4.8 (4.4)	14.3 14.0	6.8 (6.4)	5.5 (5.5)	4.3
4	$[Co(HL)_2]CH_3COO$	1032	260	Coffee brown	80	58.9 (58.1)	4.7 (4.6)	13.8 (13.5)	6.5 (6.2)	6.6 (5.7)	D
5	$[Co(HL)_2]Cl$	977	230	Brown	80	61.0 (61.4)	4.5 (4.5)	14.3 (14.3)	6.7 (6.6)	5.7 (6.0)	D
6	$[Co(HL)_2]NO_3$	1005	>280	Greenish brown	80	57.3 (59.7)	4.2 (4.4)	14.0 (13.9)	7.3 (6.4)	5.8 (5.9)	D
7	$[Ni(HL)CH_3COO]$	559	225	Brown	70	53.5 (53.6)	4.0 (4.2)	12.5 (12.5)	6.0 (5.7)	10.3 (10.5)	D
8	$[Ni(HL)_2]H_2O$	960	204	Light green	70	62.4 (62.5)	4.8 (4.6)	14.8 (14.6)	7.0 (6.7)	5.8 (5.8)	2.7
9	$[Ni(H_2L)_2] (NO_3)_2 2H_2O$	1106	200	Yellowish green	70	55 (54.3)	4.0 (4.5)	13 (12.7)	6.0 (5.8)	5.5 (5.3)	3.1
10	$[Ni(H_2L)_2]SO_4$	1039	221	Leaf green	70	58.1 (57.8)	4.2 (4.4)	13.6 (13.4)	9.4 (9.2)	5.8 (5.7)	2.9
11	$[Cu(HL)_2]H_2O$	965	203	Green	80	62.2 (62.2)	4.6 (4.8)	14.5 (14.5)	6.8 (6.6)	6.8 (6.6)	2.1
12	[Cu(HL)Cl]	541	230	Dark green	80	55.7 (55.5)	3.7 (4.0)	12.8 (12.9)	5.8 (5.9)	11.9 (11.7)	1.7
13	$[Cu(HL)NO_3]$	568	215	Green	80	52.8 (52.8)	3.7 (3.9)	12.0 (12.3)	5.8 (5.6)	10.9 (11.1)	1.7
14	$[(CuHL)_2(OH)_2] 5H_2O$	1135	195	Green	70	53.0 (52.7)	4.7 (4.9)	12.1 (12.3)	5.8 (5.6)	10.9 (11.1)	D
15	$[Zn(HL)_2]$	948	190	Yellow	80	63.3 (63.4)	4.6 (4.6)	14.6 (14.8)	7.0 (6.8)	6.9 (6.9)	D
16	$[(ZnHL)_2(NO_3)_2 2H_2O$	1174	130	Yellow	80	51.0 (51.1)	4.0 (4.0)	14.0 (14.3)	5.3 (5.4)	11.2 (11.1)	D
17	$[(ZnHL)_2(OH)_2] 2H_2O$	1138	178	Yellow	70	52.7 (52.7)	4.6 (4.9)	12.2 (12.3)	5.7 (5.6)	11.4 (11.5)	D
18	$[Cd(HL)_2]$	996	230	Golden	70	60.3 (60.3)	4.5 (4.42)	14.2 (14.06)	6.5 (6.43)	11.6 (11.2)	D

Normally, magnetic moment values of Schiff's base complexes of Mn(II) are found to be significantly lower than the expected spin only value and it ranges from 4.70 to 5.50 BM at room temperature.[27,28] In the current investigation, the observed value was 4.90 BM.

Table 6. Electronic spectral band and their assignments

Complex No:	Compound	Bands in nm	Bands in cm^{-1}	Assignments
	$C_{25}H_{23}N_5OS$ (H_2L)	259	38610	$\pi \rightarrow \pi^*$
		321, 425br	31152, 23529	$n–\pi^*$
1	$[Cr(HL)_2]NO_3$	255	39216	$\pi \rightarrow \pi^*$
		323	30960	$^4A_{2g}(F) \rightarrow {}^4T_{2g}(F)$
		409	24450	$^4A_{2g}(F) \rightarrow {}^4T_{1g}(F)$
		424	23585	$^4A_{2g}(F) \rightarrow {}^4T_{1g}(P)$
2	$[Mn(HL)_2]2H_2O$	250	40000	$\pi \rightarrow \pi^*$
		311, 338	32154, 29585	$n–\pi^*$
		390	25602	$^6A_{1g} \rightarrow {}^4A_{1g}(G)$
		577	17331	$^6A_{1g} \rightarrow {}^4A_{1g}(G)$
		700	14285	$^6A_{1g} \rightarrow {}^4T_{1g}(G)$
		860	11627	$^6A_{1g} \rightarrow {}^4T_{2g}(G)$
3	$[Fe(HL)_2]NO_3$	246	40650	$\pi \rightarrow \pi^*$
		409	24450	$^6A_{1g} \rightarrow {}^4A_{1g}(G)$
		424	23585	$^6A_{1g} \rightarrow {}^4E_g(G)$,
		588	17007	$^6A_{1g} \rightarrow {}^4T_{2g}(G)$
		695	14388	$^6A_{1g} \rightarrow {}^4T_{1g}(G)$
4	$[Co(HL)_2]CH_3COO$	254	39370	$\pi \rightarrow \pi^*$
		323, 358	30959, 27932	$n–\pi^*$
		594-630 br,606sh	16835–15873	$^1A_{1g} \rightarrow {}^1T_{2g}$, $^1A_{1g} \rightarrow {}^1T_{1g}$
5	$[Co(HL)_2]Cl$	266	37593	$\pi \rightarrow \pi^*$
		321	31152	$n–\pi^*$
		367-530br,442sh	27247–18867	$^1A_{1g} \rightarrow {}^1T_{2g}$, $^1A_{1g} \rightarrow {}^1T_{1g}$
6	$[Co(HL)_2]NO_3$	263	38023	$\pi \rightarrow \pi^*$
		366	27322	$n–\pi^*$
		646br	15479	$^1A_{1g} \rightarrow {}^1T_{2g}$, $^1A_{1g} \rightarrow {}^1T_{1g}$
7	$[Ni(HL)CH_3COO]$	254	39370	$\pi \rightarrow \pi^*$
		338	29586	$n–\pi^*$
		509	19646	$^1A_{1g} \rightarrow {}^1B_{1g}$
8	$[Ni(HL)_2]H_2O$	283	35336	$\pi \rightarrow \pi^*$
		340	29412	$^3A_{2g}(F) \rightarrow {}^3T_{1g}(P)$
		590	16949	$^3A_{2g}(F) \rightarrow {}^3T_{1g}(F)$
		873	11455	$^3A_{2g}(F) \rightarrow {}^3T_{2g}(F)$

Complex No:	Compound	Bands in nm	Bands in cm^{-1}	Assignments
9	$[Ni(H_2L)_2(NO_3)_2]2H_2O$	254	39370	$\pi \rightarrow \pi^*$
		366	27322	$n–\pi^*$
		406	24631	$^3A_{2g}(F) \rightarrow {}^3T_{1g}(P)$
		596	16779	$^3A_{2g}(F) \rightarrow {}^3T_{1g}(F)$
		873	11455	$^3A_{2g}(F) \rightarrow {}^3T_{2g}(F)$
10	$[Ni(H_2L)_2]SO_4$	252	39683	$\pi \rightarrow \pi^*$
		323	30960	$n–\pi^*$
		409	24450	C–T
		418	23923	$^3A_{2g}(F) \rightarrow {}^3T_{1g}(P)$
		604	16556	$^3A_{2g}(F) \rightarrow {}^3T_{1g}(F)$
		887	11273	$^3A_{2g}(F) \rightarrow {}^3T_{2g}(F)$
11	$[Cu(HL)_2]H_2O$	260	38462	$\pi \rightarrow \pi^*$
		343	29411	$n–\pi^*$
		386	25906	C–T
		532	18796	$^2E_g \rightarrow {}^2T_{2g}$
12	[Cu(HL)Cl]	259, 302	38610, 32894	$\pi \rightarrow \pi^*$
		334, 353	30211, 28329	$n - \pi^*$
		489	20450	C–T and $^2B_{1g} \rightarrow {}^2E_g$
		646	15480	$^2B_{1g} \rightarrow {}^2A_{1g}$
13	$[Cu(HL)NO_3]$	260	38462	$\pi \rightarrow \pi^*$
		328	30488	$n–\pi^*$
		419	23866	C–T
		600	16667	$^2B_{1g} \rightarrow {}^2E_g$
		889	11249	$^2B_{1g} \rightarrow {}^2A_{1g}$
14	$[(CuHL)_2(OH)_2]5H_2O$	252	39682	$\pi \rightarrow \pi^*$
		305, 327	32786, 30581	$n \rightarrow \pi^*$
		431	23201	C–T
		598	16722	$^2B_1 \rightarrow {}^2A_1$
15	$[Zn(HL)_2]$	259	38610	$\pi \rightarrow \pi^*$
		352	28409	$n \rightarrow \pi^*$
		409	24450	C–T
16	$[(ZnHL)_2(NO_3)_2]2H_2O$	263	38023	$\pi \rightarrow \pi^*$
		354	28248	$n \rightarrow \pi^*$
		463	21598	C–T
17	$[(ZnHL)_2(OH)_2]2H_2O$	263	38023	$\pi \rightarrow \pi^*$
		409	24449	$n \rightarrow \pi^*$
18	$[Cd(HL)_2]$	252	39682	$\pi \rightarrow \pi^*$
		399	25062	$n \rightarrow \pi^*$
		703	14224	C–T

Fe(III) complexes having d^5 configuration gives Russell Saunders term ^6S in an octahedral geometry in their ground state leading to the notation $^6A_{1g}$. As there is no excited state with spin multiplicity 6, all electronic transitions are spin forbidden. Since the system is octahedral, the transitions are also Laporte-forbidden. Subsequently, the intensities of transitions of octahedral high-spin Fe(III) complexes have extremely low molar extinction coefficient values and therefore, it is very difficult to locate the bands. However, some forbidden transitions can occur to the quartet excited states. They are $^6A_{1g} \rightarrow {}^4A_{1g}(G)$, $^6A_{1g} \rightarrow {}^4E_g(G)$, $^6A_{1g} \rightarrow {}^4A_{1g}(G)$, $^6A_{1g} \rightarrow {}^4T_{1g}(G)$ and $^6A_{1g} \rightarrow {}^4T_{2g}(G)$.

The electronic spectrum of the Fe(III) complex exhibited four very low intense bands. The band at 409 nm may be due to $^6A_{1g} \rightarrow {}^4A_{1g}(G)$ transition. The band at 424 nm may be due to $^6A_{1g} \rightarrow {}^4E_g(G)$ and another at 588 nm due to $^6A_{1g} \rightarrow {}^4T_{2g}(G)$ transitions. The weak band observed at 695 nm may be due to $^6A_{1g} \rightarrow {}^4T_{1g}(G)$ transition.[29]

Fe(III) is isoelectronic with Mn(II) and has five 3d electrons. Fe(III) is known to exist in three spectroscopic states with $S = 5/2$ ($^6A_1$, $\mu = 5.92$ BM), 3/2 ($^4A_2$, $\mu = 4.00$ BM) and 1/2 ($^2T_2$, $\mu = 2.6$ BM). The dithiocarbamate complexes of Fe(III) are widely known to exhibit all the three states while varying the temperature.[30] In the current case, the observed magnetic moment value was 4.3 BM and is an evidence for high spin centre in the complex.[31] The lower magnetic moment value than the expected one may be due to the effective quenching of orbital angular momentum.

Co(III) has a d^6 configuration, giving the electronic arrangement $(t_{2g})^6$ $(e_g)^0$ and the ground state is $^1A_{1g}$. This arrangement has very large crystal field stabilization energy and is found to be diamagnetic. Excitation of an electron to the e_g orbital yields the configuration $(t_{2g})^5 (e_g)^1$ which spans the states $^3T_{1g} + {}^3T_{2g} + {}^1T_{1g} + {}^1T_{2g}$ with the triplet states lying lower in energy than the singlet states. It exhibits two spin-allowed transitions at relatively low energy $^1A_{1g} \rightarrow {}^1T_{1g}$ and $^1A_{1g} \rightarrow {}^1T_{2g}$. Two spin forbidden bands corresponding to $^1A_{1g} \rightarrow {}^3T_{1g}$ and $^1A_{1g} \rightarrow {}^3T_{2g}$ are observed at higher energies than the spin-allowed transitions.[32] These are usually difficult to interpret by the overlap of intra-ligand and charge-transfer transitions.

In the present scenario, all Co(III) complexes exhibited one broad band due to d–d transition. In $[Co(HL)_2]CH_3COO$, a broad band in the region 594–630 nm with a shoulder at 606 nm was observed. In $[Co(HL)_2]Cl$, a broad band in the region 367–530 nm with a shoulder at 442 nm was observed. In $[Co(HL)_2]NO_3$, a broad band at 646 nm was observed. All these Co(III) complexes are diamagnetic indicating their low-spin octahedral geometry.[33]

$[Ni(HL)CH_3COO]$ showed a single broad band at 509 nm which can be assigned to $^1A_{1g} \rightarrow {}^1B_{1g}$ transition. The complex was found to be diamagnetic. These observations are consistent with low-spin square-planar geometry.[34] Since, thiols can cause spin pairing than thioethers, coordination occurs through the thiolato sulphur atom.[35]

Octahedral Ni(II) ion with d^8 configuration has $^3A_{2g}$ ground state. The three spin-allowed transitions are $^3A_{2g}(F) \rightarrow {}^3T_{2g}(F)$, $^3A_{2g}(F) \rightarrow {}^3T_{1g}(F)$ and $^3A_{2g}(F) \rightarrow {}^3T_{1g}(P)$ in the range 1250–909, 666–526 and 400–345 nm, respectively.[36]

In this study, broad bands at 340, 590 and 873 nm may be assigned to $^3A_{2g}(F) \rightarrow {}^3T_{1g}(P)$, $^3A_{2g}(F) \rightarrow {}^3T_{1g}(F)$ and $^3A_{2g}(F) \rightarrow {}^3T_{2g}(F)$, transitions for $[Ni(HL)_2]H_2O$. In $[Ni(H_2L)_2](NO_3)_2 2H_2O$, bands at 406, 596, 873 nm correspond to $^3A_{2g}(F) \rightarrow {}^3T_{1g}(P)$, $^3A_{2g}(F) \rightarrow {}^3T_{1g}(F)$ and

$^3A_{2g}(F) \rightarrow {}^3T_{2g}(F)$ transitions, respectively. In $[Ni(H_2L)_2]SO_4$, bands at 418, 604 and 887 nm correspond to $^3A_{2g}(F) \rightarrow {}^3T_{1g}(P)$, $^3A_{2g}(F) \rightarrow {}^3T_{1g}(F)$ and $^3A_{2g}(F) \rightarrow {}^3T_{2g}(F)$ transitions, respectively. These observations support an octahedral structure for the complexes.[37] All the three Ni(II) complexes registered magnetic moments in the range 2.72–3.10 BM confirming their octahedral geometries.[38]

The spectroscopic ground state term of copper(II) is ^2D. It gets split up in an octahedral field into two levels $^2T_{2g}$ and ^2E_g. When the symmetry of copper(II) complex lowers to D_{4h} or C_{4v}, the energy levels again split and give more transitions.[39] As a result, electronic spectrum of a Cu(II) complex becomes a bit more complicated. For the square planar complexes with D_{4h} point group, three vibronically induced transitions, such as $^2B_{1g} \rightarrow {}^2A_{1g}$, $^2B_{1g} \rightarrow {}^2B_{2g}$ and $^2B_{1g} \rightarrow {}^2E_g$, are predicted. A single absorption band is usually found, since the four lower orbitals are so close in energy that individual transitions will not be prominent.

The broad band observed at 532 nm in the electronic spectrum of $[Cu(HL)_2]H_2O$ may be assigned to $^2E_g \rightarrow {}^2T_{2g}$ transition. This is in agreement with an octahedral geometry of the complex. A magnetic moment value 2.1 BM supports its distorted octahedral structure.

In this study, the coordinated gegenions, X–Cu(II) charge-transfer was observed at 400–500 nm. For [Cu(HL)Cl], the Cl–Cu(II) charge-transfer band was found at 489 nm and in $[Cu(HL)NO_3]$, the O–Cu(II) charge-transfer band was observed at 419 nm. These complexes also showed a broad *d–d* combination band in the range 588–666 nm and appear as a shoulder on the intra-ligand and charge transfer bands. Such an attribute is expected for a square planar complex in accordance with previous information. The magnetic moment values of these complexes were found to be 1.7 BM, which support their square planar structures.

Five coordinated Cu(II) complex of polyfunctional pyridyl phthalazines having a magnetic moment of 0.70 BM was reported by Bullock *et al*.[40] Jeevana *et al*.[41] reported five coordinated Cu(II) complex of benzoin N(4)-methyl(phenyl)thiosemicarbazone having a magnetic moment of 0.81 BM. The solid-state electronic spectrum of this compound showed band at 15313 cm^{-1} (653 nm).[42,43] However, in the present case, $[(CuHL)_2(OH)_2]5H_2O$ is diamagnetic and showed a band at 16722 cm^{-1} (598 nm), indicating a 5-coordinate trigonal bi-pyramidal geometry for it. This strongly supports its existence as a dimer in the solid state with spins of electrons ordered antiparallel with strong antiferromagnetic interaction of copper(II) centres.[44]

As expected, zinc(II) and cadmium(II) complexes showed bands almost similar to the ligand and were found to be diamagnetic. A weak band observed at 703 nm in cadmium(II) complex could be due to the ligand to metal charge-transfer transition. Representative spectra of the complexes **(6)**, **(7)**, **(8)** and **(11)** are presented in Fig. 10.

3.2.3. Vibrational spectra

The IR spectral assignments of the compounds are depicted in Table 7.

The band due to ν(C=O) at 1626 cm^{-1} in the ligand spectrum shifts to higher wave number on coordination with metal ions. In the spectra of complexes **(1), (3), (7)** and **(11)**, this band is observed at 1722 cm^{-1}. This band is absent in the spectra of the other complexes, suggesting the enolization of the –C=O of the pyrazolone group. The stretching band corresponding to –C=N group is observed in the spectra of complexes in the range 1535–1572 cm^{-1}.

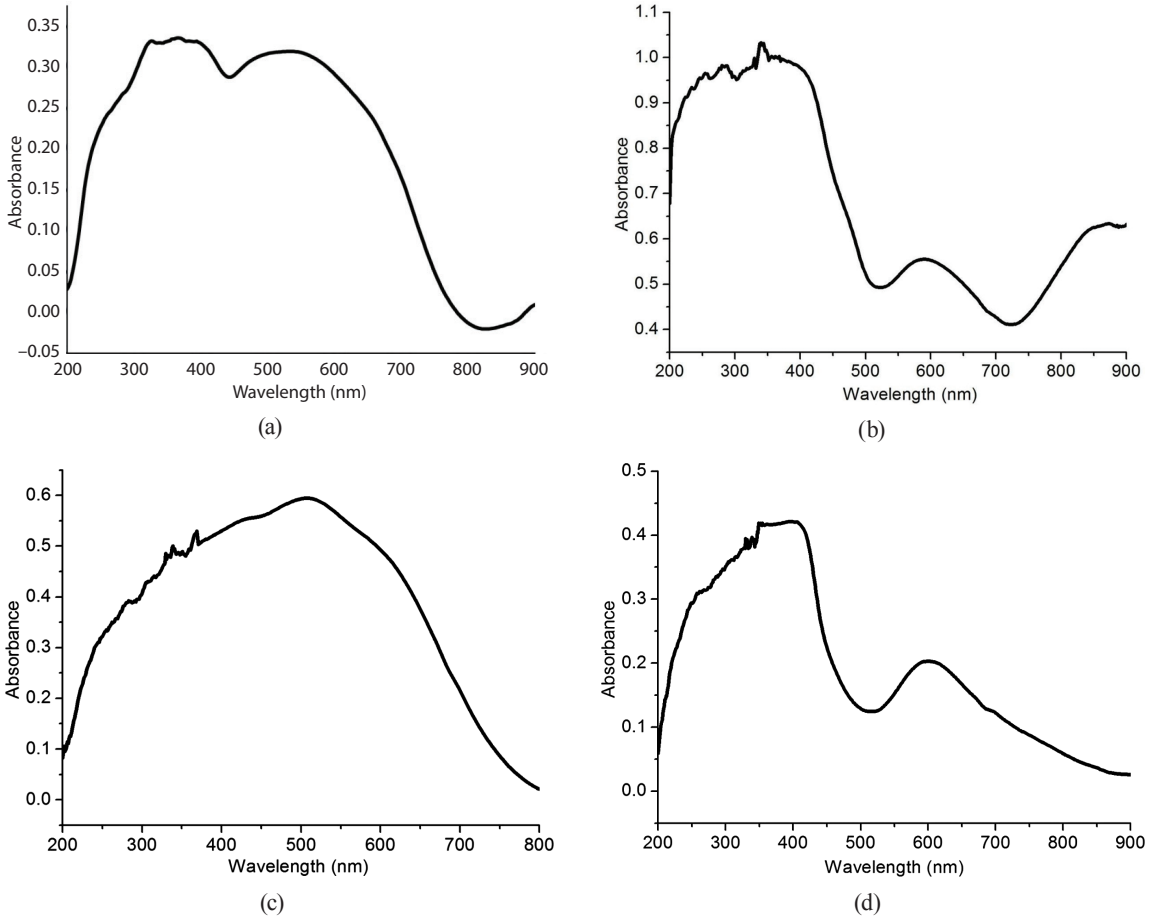

Fig. 10. Electronic spectra of the compounds (a) $[Co(HL)_2NO_3]$ **(6)**, (b) $[Ni(HL)CH_3COO]$ **(7)**, (c) $[Ni(HL)_2]2H_2O$ **(8)** and (d) $[Cu(HL)_2]H_2O$ **(11)**.

The shift in the wave number of C=S stretching frequencies to lower wave number in the spectra of certain complexes indicates the involvement of thione sulphur in coordination. The ν(N–N) band at 1106 cm^{-1} in the spectrum of the ligand undergoes a shift to higher wave number in the spectra of the complexes substantiating the coordination of azomethine nitrogen.[45] This blue shift is due to the decrease in the repulsion between the lone pairs on the two nitrogen atoms. The ν(M–N) bands are observed around 440–485 cm^{-1} in the spectra of complexes. The shift of the centres of the broad band at 3428 cm^{-1}, due to NH···O stretching present in the ligand, to higher wave number in the spectra of the complexes may be due to the removal of intramolecular hydrogen bonding. It may also be due to the involvement of azomethine nitrogen in the complex formation. All these confirm the participation of azomethine nitrogen in coordination.

The broad absorption bands centred at 3400 cm^{-1} in the IR spectra of the certain metal complexes may be assigned to lattice water molecules.[46,47]

The spectrum of the complex $[Co(HL)_2]CH_3COO$ displays relatively strong bands at 1567 and 1406 cm^{-1} due to ν_{as}(COO) and ν_s(COO), indicating the ionic nature of the acetate group in this compound.[48] The spectrum of the complex $[Co(HL)_2]NO_3$ shows two medium bands at 1406 and 1381 cm^{-1} corresponding to ν_1 and ν_4 of the nitrato group. The absence of a combination band at 1740 cm^{-1} assignable to $\nu_1 + \nu_4$ indicates the ionic nature of

Table 7. IR spectral assignments

Complex No:	Compound	ν((N–H)/ ν(O–H)	C=O	C=N (cyclic)	C=N	C–O	C=S	N–N	M–O	M–N
	$C_{25}H_{23}N_5OS$ (H_2L)	3428	1626	1597	–	–	766	1106	–	–
1	$[Cr(HL)_2]NO_3$	3438	1722	1595	1551	–	689	1156	658	473
2	$[Mn(HL)_2]2H_2O$	3438	–	1595	1535	1438	760	1127	658	459
3	$[Fe(HL)_2]NO_3$	3438	1722	1593	1548	–	695	1121	658	477
4	$[Co(HL)_2]CH_3COO$	3438	–	1590	1571	1361	755	1125	638	448
5	$[Co(HL)_2]Cl$	3414	–	1602	1560	1362	756	1129	639	443
6	$[Co(HL)_2]NO_3$	3438	–	1620	1569	1354	758	1126	636	448
7	$[Ni(HL)CH_3COO]$	3426	1722	1596	1569	–	694	1117	643	433
8	$[Ni(HL)_2]H_2O$	3401	–	1603	1571	1437	760	1107	660	472
9	$[Ni(H_2L)_2(NO_3)_2]$ $2H_2O$	3438		1603	1569	1434	758	1109	661	435
10	$[Ni(H_2L)_2]SO_4$	3437		1603	1572	1434	754	1111	659	482
11	$[Cu(HL)_2]H_2O$	3435	1722	1599	1559	–	693	1128	661	462
12	[Cu(HL)Cl]	3438	–	1592	1558	1416	760	1129	663	441
13	$[Cu(HL)NO_3]$	3438	–	1592		1419	756	1129	662	448
14	$[(CuL)_2(OH)_2$ $(H_2O)]5H_2O$	3450		1603	1565	–	689	1128	661	453
15	$[Zn(HL)_2]$	3438		1602	1552	1434	761	1126	659	433
16	$(ZnHL)_2(NO_3)_2$ $2H_2O$	3438	–	1599	1569	1437	760	1129	–	445
17	$[(ZnHL)_2(OH)_2]$ $2H_2O$	3425	–	1602	1568	1437	754	1108	659	444
18	$[Cd(HL)_2]$	3439	–	1597	1543	1437	762	1126	659	465

the group.[49] In all the cobalt complexes, the ligand acts as mono-anionic tridentate one and coordinates through ketonic oxygen, azomethine nitrogen and thiol sulphur after deprotonation.

The spectrum of the complex $[Ni(HL)CH_3COO]$ shows bands at 1596 and 1430 cm^{-1} which may be due to ν_{as}(COO) and ν_s(COO) of the coordinated acetate group. Since the separation is greater than 144 cm^{-1}, the acetate group may be acting as unidentate ligand. Since only thiols can cause spin pairing, coordination might have occurred through the thiolato sulphur atom by deprotonation. For this complex, the ligand acts as mono-anionic tridentate one and coordinated through ketonic oxygen, azomethine nitrogen and deprotonated thiol sulphur.

The spectrum of the complex $[Ni(H_2L)_2(NO_3)_2]2H_2O$ shows two medium bands at 1437 and 1384 cm^{-1} corresponding to ν_1 and ν_4 of the nitrato group. The absence of a combination band at 1740 cm^{-1}, assignable to $\nu_1 + \nu_4$, indicates the ionic nature of the group. In this complex, the ligand acts as neutral tridentate one and coordinates through ketonic oxygen, azomethine nitrogen and thione sulphur.

The spectrum of $[Cu(HL)NO_3]$ has strong bands at 1440, 1350 and 1022 cm^{-1} due to $\nu_{as}(NO_2)$, $\nu_s(NO_2)$ and $\nu(NO)$, respectively, indicating the unidentate coordination of the nitrate ion. The separation of the two highest frequency bands was 90 cm^{-1}. However, the combination band was not observed in the spectrum of complex.

The spectrum of $[(ZnHL)_2(NO_3)_2]2H_2O$ has strong bands at 1437, 1308 and 1001 cm^{-1} indicating the unidentate coordination of the nitrate ion. The separation of the two highest bands was found to be 127 cm^{-1}. In addition to this, a weak combination band was observed at 1725 cm^{-1}.

IR spectra of the complexes **(6)**, **(8)**, **(11)** and **(18)** are presented in Fig. 11.

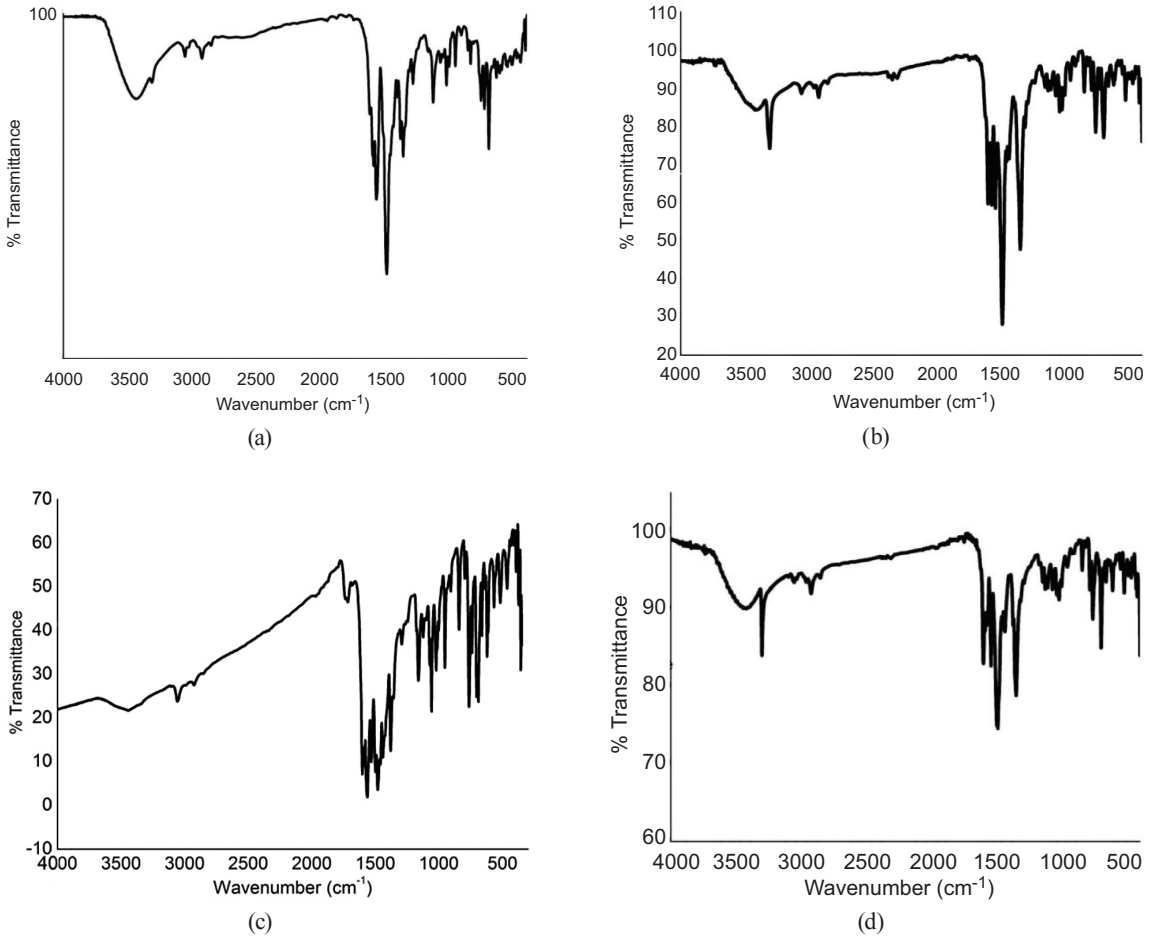

Fig. 11. IR spectra of the compounds (a) $[Co(HL)_2NO_3]$ (**6**), (b) $[Ni(HL)_2H_2O]$ (**8**), (c) $[Cu(HL)_2H_2O]$ (**11**) and (d) $[Cd(HL)_2]$ (**18**).

3.2.4. ^{1}HNMR spectra

The ^{1}H NMR spectra of the Zn(II) complexes were recorded in $CDCl_3$.

(a) $[Zn(HL)_2]$ (16)

The prominent feature of this spectrum compared to that of the ligand is the absence of a singlet at 14.476 ppm (^{2}NH proton) and the presence of a new singlet at 6.675 ppm. The absence of a peak at 11.176 ppm (OH proton) in the complex spectrum is an indication of the deprotonation of O–H during complexation. Aromatic protons exhibit multiplet signals

in the range 6.760–8.130 ppm. N–CH_3 protons in the complex show peaks at 3.409–3.646 ppm. Singlets at 1.230–1.292 ppm in the complex correspond to the methyl protons of the substituted pyrazolone. Both CHNS and ^{1}H NMR data are in agreement with the formula $Zn(HL)_2$ for zinc complex (**15)** (Fig. 12).

(b) $[(ZnHL)_2(NO_3)_2]$ $2H_2O$ (16)

Aromatic protons exhibit multiplet signals in the range 6.787–8.128 ppm. Singlets at 6.710 and 6.768 ppm could be attributed to NH protons. N–CH_3 protons in the complex show peaks at 3.487–3.720 ppm. Singlet peaks at 1.244–1.34 ppm in the complex correspond to the methyl protons of the substituted pyrazolone. Broad peak at 1.655 ppm may be attributed to water molecules. Both CHNS and ^{1}HNMR data are in agreement with the formula $[(ZnHL)_2(NO_3)_2]$ $2H_2O$ for zinc complex **(16)** (Fig. 13).

(c) $[(ZnHL)_2(OH)_2]$ $2H_2O$ (17)

Aromatic protons exhibit multiplet signals in the range 6.765–7.975 ppm. NH protons show signals at 6.676 and 6.696 ppm. N–CH_3 protons in the complex show peaks at 3.487–3.719 ppm. Singlet peaks at 3.441 may be due to coordinated water molecules. Singlet peaks at 2.04 and 2.06 ppm may be due to OH protons. Singlet peaks at 1.23–1.30 ppm in the complex correspond to the methyl protons in the substituted pyrazolone.

In addition, the spectrum of the complex shows a broad peak centred at 1.577 ppm due to water molecules. Fig. 14 shows the spectrum of $[(ZnHL)_2(OH)_2]$ $2H_2O$ **(17)**.

3.2.5. ESR spectrum

The ESR spectrum of the copper(II) complex was recorded in frozen DMF solution at 77 K in the X-band with 100 kHz field modulation (Fig. 15). The Cu(II) ion has an effective spin of $S = 3/2$ and is associated with a spin angular momentum, $m_s = \pm 1/2$, leading to a doubly

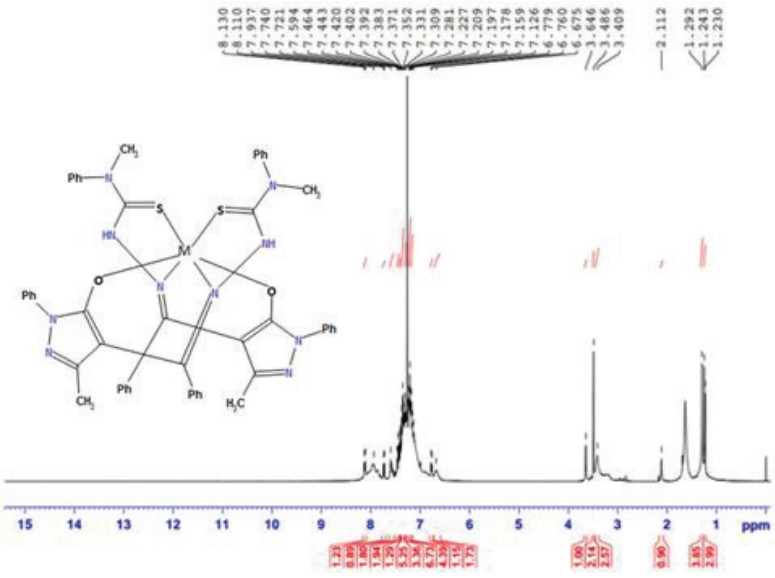

Fig. 12. ^{1}H NMR spectrum of $Zn(HL)_2$.

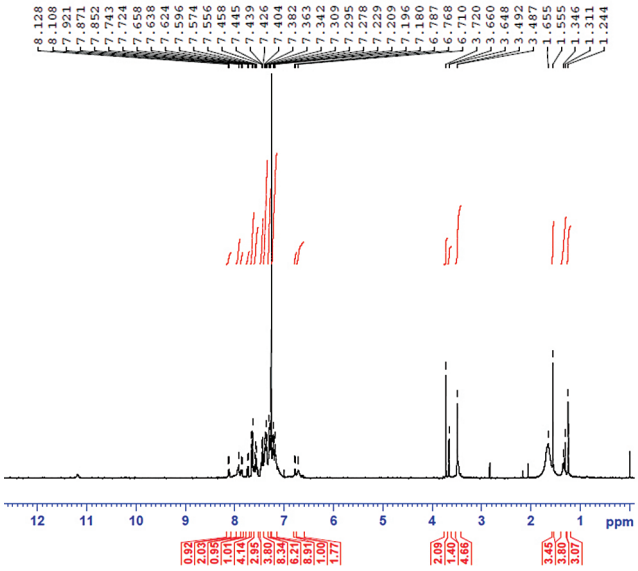

Fig. 13. ^{1}H NMR spectrum of $[(ZnHL)_2(NO_3)_2]$ $2H_2O$ (**16**).

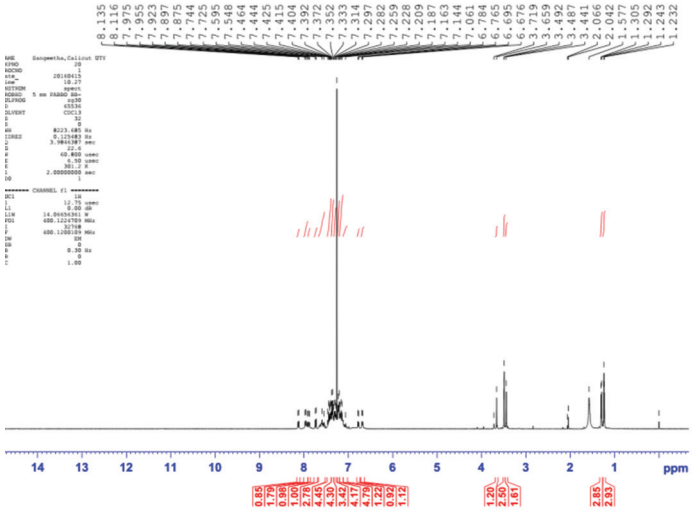

Fig. 14. ^{1}H NMR spectrum of $[(ZnHL)_2(OH)_2]$ $2H_2O$ (**17**).

degenerate spin state in the absence of magnetic field. In a magnetic field, the degeneracy is lifted between these states and the energy difference between them is given by $E = hv = g\beta B$, where h is the Planck's constant, v is the frequency, g is the Lande's splitting factor, equals to 2.0023 (for a free electron), β is the Bohr magneton and B is the magnetic field. The solution spectrum of the complex **(11)** at 77 K in DMF is axial and shows four hyperfine lines characteristic of a monomeric Cu(II) complex. They corresponds to −3/2, −1/2, 1/2 and 3/2 which arise from the coupling of the odd electron with copper nuclei (I = 3/2). The spectrum also gives three superhyperfine lines in the perpendicular region which arise from the coupling of the electron spin with nuclear spin of nitrogen atom which is co-planar. This indicates that in this complex, azomethine nitrogen atom has coordinated to the metal centre. The absence of half-field signal in the spectrum confirms the monomeric nature of the complex **(11)**.

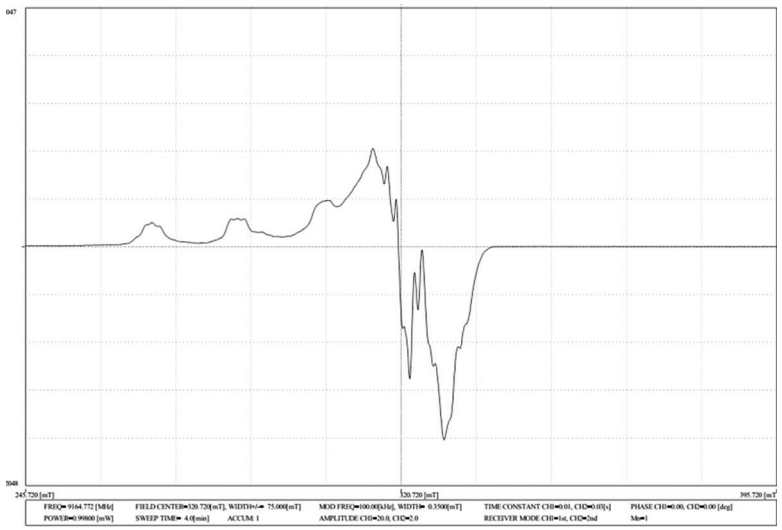

Fig. 15. ESR spectrum of $[Cu(HL)_2H_2O]$ **(11)**.

3.2.6. Thermal studies

Thermo gravimetric analysis of the ligand and complexes were used to acquire ideas about the thermal stability and to fix the nature of the water molecules (if present), is inside or outside the coordination sphere, that is, coordinated or not. For the ligand, H_2L, two stages of decomposition were observed and are evident from DTG peaks at 163°C and 273°C. The first stage of decomposition of the ligand occurred at 140°C–170°C and second stage occurred at 170°C–750°C due to its complete decomposition (Fig. 16). The differential scanning calorimetry (DSC) plot supports the thermogravimetric-derivative thermogravimetric (TG-DTG) analysis giving temperature maxima at 163°C and 273°C (Fig. 17). A sharp endothermic peak in DSC plot of the ligand indicates its melting point. Comparing the TG and DSC curves, it is evident that the mass loss process starts after the melting, that is, in its liquid state. The TG/DTG/DSC studies reveal the purity of the compound.

The complex, $[Co(HL)_2]CH_3COO$, showed two stages of decomposition between 268°C and 359°C. It is clear from the DTG peaks at 272°C and 283°C. Here, the decomposition starts at 272°C after the melting point. The residual mass left behind at 745°C was 24% which may be due to the formation of Co_3O_4 (calc. 23.4%).

The complex, $[Co(HL)_2]Cl$, showed three stages of decomposition as is evident from the DTG peaks at 225°C, 262°C and 295°C. The complex, registered the first stage of decomposition between 213°C and 231°C with a weight loss of 1.2% which may be due to moisture. The second stage of decomposition is in between 240°C and 571°C. The residual mass left behind at 745°C was 26% which may be due to the formation of Co_3O_4 (calc. 25%).

The complex $[Co(HL)_2]NO_3$ showed three stages of decomposition between 246°C and 615°C and demonstrates a weight loss of 61.3%. It is evident from the DTG peaks at 227°C, 274°C and 281°C. The residual mass left behind at 745°C was 20.9% which may be due to the formation of two molecules of CoS (calc. 20.3%).

In $[Ni(HL)CH_3COO]$, four decomposition stages are observed. It is evident from the DTG peaks with temperature maxima at 225°C, 302°C, 310°C and 321°C. Here, the decomposition

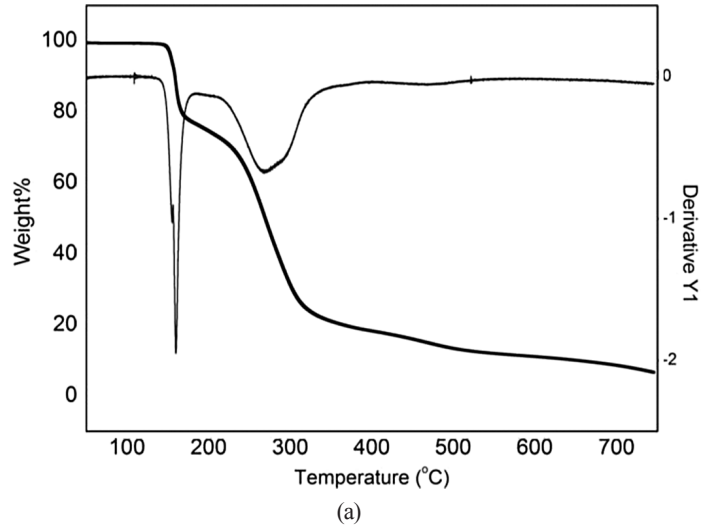

(a)

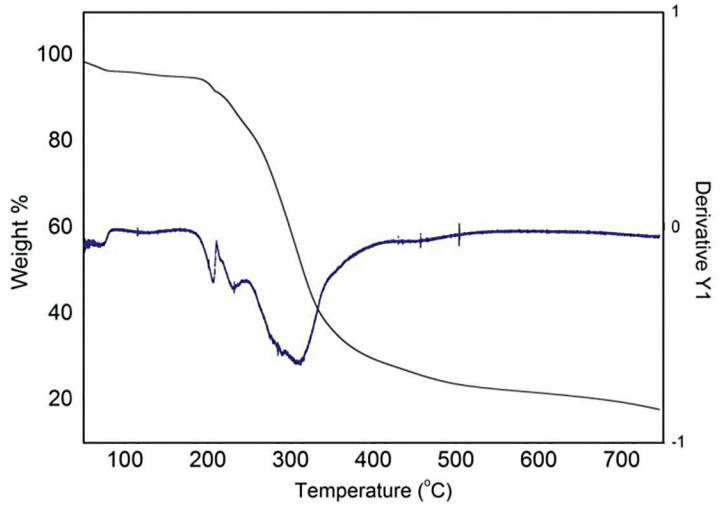

(b)

Fig. 16. TG-DTG plot of (a) ligand and (b) $[Ni(HL)_2]\ H_2O$.

starts after the melting of the compound at 225°C. The residual mass left behind at 745°C was 55.35% which may be due to the formation of a mixture of nickel oxide and nickel sulphide.

For $[Ni(HL)_2]\ H_2O$, four decomposition stages are observed. It is evident from the DTG peaks at 71°C, 204°C, 231°C and 309°C. Initial mass loss corresponds to loss of one lattice water molecule. Here also the decomposition starts after the melting of the compound at 204°C. The first stage is at 184°C–210°C and demonstrates a mass loss of 3.3%. The second stage occurs at 254°C–649°C with a mass loss of 70.5%. A residual mass of 17.7% was left which may be due to the formation of a mixture of nickel oxide and nickel sulphide.

For $[Ni(H_2L)](NO_3)_2$, four decomposition stages are observed. It is evident from the DTG peaks at 47°C, 116°C, 199°C and 313°C. A residual mass of 8.5% was left which may be due to the formation of nickel sulphide (calc. 8.2%).

Three decomposition stages are observed for $[Ni(H_2L)_2]SO_4$. It is evident from the DTG peaks at 302°C, 310°C and 321°C. The absence of any thermal change before 302°C

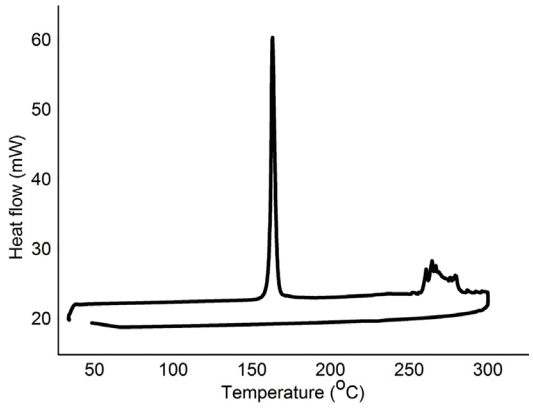

Fig. 17. DSC plot of ligand.

demonstrates its high thermal stability. A residual mass of 16.55% was left which may be due to the formation of a mixture of nickel oxide and nickel sulphide (calc. 16%).

For $[Cu(HL)_2]H_2O$, initial mass loss of 2% corresponds to loss of one water molecule in temperature range 150°C–170°C. The next step of decomposition occurs in the temperature range 180°C–250°C and 230°C–350°C. It is evident from the DTG peaks at 161°C, 203°C and 307°C. A residual mass of 25% was left which may be due to the formation of a mixture of copper oxide and copper sulphide (calc. 24.7%).

For [Cu(HL)Cl] complex, two stages of decomposition are observed and is evident from the DTG peaks at 231°C and 300°C. The first stage is at 220°C–240°C and the second stage occurs at 245°C–500°C with a mass loss of 56.9%. The residual mass left behind at 745°C was 28.6%. This may be due to the formation of Cu_2S (29.4%).

For $[Cu(HL)NO_3]$, two stages of decomposition occurred and is evident from the DTG peaks at 214°C and 297°C. The first stage was at 190°C–223°C and the second stage at 240°C–550°C. The residual mass of 27.5% was observed at 750°C which may be due to the formation of copper sulphide (calc. 28%).

For $[(CuHL)_2(OH)_2]5H_2O$, DTG peaks are observed at 196°C and 302°C indicating a two-step decomposition. The first stage is at 183°C–216°C and the second stage was observed at 240°C–467°C. The residual mass of 34.81% was observed at 750°C which may be due to the formation of $2Cu_2S$ and CuO (calc. 34.9%).

DTG analysis showed seven peaks at 46°C, 83°C, 158°C, 250°C, 296°C, 380°C and 448°C for $Zn(HL)_2$. The residual mass of 9.1% was observed at 750°C which may be due to the formation of ZnO (calc. 8.6%). DTG analysis showed four peaks at 39°C, 143°C, 288°C and 487°C for zinc(II) nitrate complex. The residual mass of 15.1% was observed at 750°C which may be due to the formation of the mixture of ZnO and ZnS (calc. 15.2%).

For the cadmium(II) complex, DTG peaks are observed at 144°C, 220°C and 298°C. The slight weight loss (<2%) observed at around 144°C could be attributed to the presence of entrapped water or solvent molecule. The absence of any thermal change before this temperature demonstrates their high thermal stability. The horizontal thermal curve observed above 745°C corresponds to metal oxysulphate residue. This probably has formed due to the oxidation of the sulphide.

3.2.7. Single-crystal XRD studies of [Cd(HL)$_2$]

Single crystals of cadmium(II) complex were grown from its chloroform solution. A crystal with approximate dimensions 0.300 × 0.250 × 0.200 mm^3 was selected for collecting the data. The compound crystallized with one molecule per asymmetric unit into monoclinic crystal system with space group $P2_1/c$.

X-ray crystallographic data for the Cd(II) complex were collected at 293(2) K on a Bruker Model Kappa Apex II diffractometer. Direct methods were performed to solve the structures and refined by least square on F^2 using SHELXL-2014/7.[50] All non-hydrogen atoms were refined anisotropically. All hydrogen atoms, except those attached to nitrogen were geometrically fixed at calculated positions. The crystallographic tools PLATON for Windows, DIAMOND 3.2d and MERCURY 3.5.1 were used for structure analysis and presentation of the results. The structure was finally refined to the conventional *R*-value, $R_1 = 0.0308$.

The molecular structure of the cadmium complex with atom numbering scheme is depicted in Fig. 18. Crystal data and structure refinement parameters of the complex are given in Table 8. Selected bond lengths and bond angles are summarized in Table 9.

An interesting attribute of the crystal packing of the complex is the formation of a supramolecular chain mediated by intermolecular C–H…O hydrogen bond. The crystal structure is further stabilized by intermolecular C–H…S interactions. In the unit cell, molecules are arranged in a face-to-face manner, which are the repeating units of the packing in the crystal lattice. Fig. 19 represents the packing diagram showing hydrogen bond interaction along *b*-axis. The important hydrogen bonding interaction parameters are listed in Table 10.

On complex formation, significant changes occur in the geometrical parameters of the ligand. It is clear from Table 9 that the bond length, C(9)–N(3) in the complex is compressed to 1.306(3) Å from 1.327(2) Å. Coordination lengthens the C(9)–C(16) bond from 1.399(2) to 1.429(3) Å in the complex. It is also found that the C(8)–N(2) bond in the complex is compressed to 1.333(3) from 1.368(2) Å. This supports the extensive π delocalization along the thiosemicarbazone chain and the involvement of azomethine nitrogen in coordination. It is also confirmed by the existence of S(1) and N(3) in *Z* configuration with respect to C(8)–N(2) bond with a torsion angle of −5.1(4) Å.

Coordination lengthens the C(8)–S(1) bond from 1.671(2) Å to 1.692(3) Å. It is intermediate between double bond (C=S) [1.60 Å] and single bond (C–S) bond length [1.81 Å]. The bond lengths Cd–S(1) 2.6029(8) Å and Cd–S(2) 2.573(9) Å corroborate the coordination of the thione sulphur (C=S).

From the above observations, we confirmed that the ligand is coordinated through the azomethine nitrogen [Cd–N(3) = 2.369(2) Å], [Cd–N(8) = 2.384(2) Å], thione sulphur [Cd–S(1) = 2.6029(8) Å], [Cd–S(2) = 2.573(9) Å] and pyrazolone oxygen [Cd–O(1) = 2.297(2)

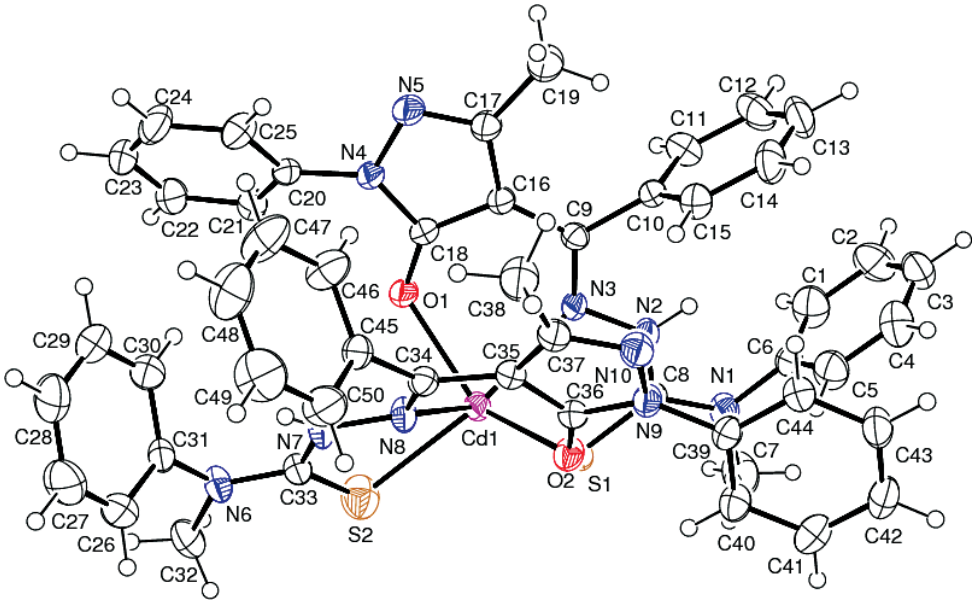

Fig. 18. ORTEP diagram of $Cd(HL)_2$ with 40% probability.

Å], [Cd–O(2) = 2.368(2) Å]. These bond lengths are comparable to those reported for similar cadmium(II) complexes.[51]

The coordination results in the formation of two five-membered [Cd–N(3)–N(2)–S(1–C(8)], [Cd–N(7)–N(8)–C(33)–S(2)] and two six-membered [Cd–O(1)–C(18)–C(16)–C(9)–N(3)], [Cd–O(2)–C(36)–C(35)–C(34)–N(8)] metallocycles in the complex. Ring puckering analyses and least-square plane calculations showed that the five-membered ring comprising of Cd(1), N(3), N(2), C(8) and S(1) atoms adopts an envelope conformation on Cd(l). The mean plane deviation calculations gave evidence for planarity of the five-membered Cd–N(3)–N(2)–C(8)–S(1) metallocycle with a maximum mean plane deviation of 0.0007 Å at S1 and 0.0003 Å at Cd.

The least square planes comprising of [Cd, N(3), N(2), S(1), C(8)] (plane 1) and [Cd, N(7), N(8), S(2), C(33)] (plane 2) with a dihedral angle of 38.206(64)° show a *Z* conformation between these planes. The least square planes involving [Cd, O(1), C(18), C(16), C(9), N(3)] (plane 3), [Cd, O(2), C(36), C(35), C(34), N(8)] (plane 4) with a dihedral angle 81.185 (43)° show a puckered arrangement. The dihedral angles formed by the least square (plane 1) and (plane 4), (plane 2) and (plane 4), (plane 2) and (plane 3) and (plane 1) and (plane 3) are 64.830(44)°, 36.820(81)°, 72.323(54)° and 39.130(4)°, respectively. These evidences suggested a distorted octahedral coordination geometry for the complex, with the Cd atom lying in an approximate plane with the O(1)–O(2)–N(1)–N(8)–S(1)–S(2) atoms.

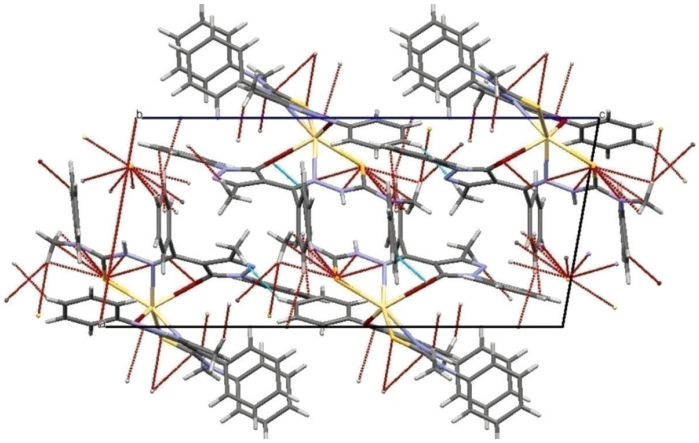

Fig. 19. Hydrogen bond interaction of $Cd(HL)_2$ along *b*-axis.

Table 8. Crystal data and structure refinement parameters of $Cd(HL)_2$

Identification code	$Cd(HL)_2$		
Empirical formula	$C_{50}H_{44}CdN_{10}O_2S_2$	Theta range for data collection	2.055–24.999°
Formula weight	993.47	Index ranges	$-11 \le h \le 11$, $-26 \le k =\le 26$, $-25 \le l \le 25$
Temperature	293(2) K	Reflections collected	66073
Wavelength	0.71073 Å	Independent reflections	8034[*R*(int) = 0.0346]
Crystal system	Monoclinic	Completeness to theta	24.99° 100%
Space group	$P\ 2_1/c$	Refinement method	Full-matrix least-squares on F^2
Unit cell dimensions	*a*(Å) = 9.6939(5) *α*(°)= 90	Data/restraints/ parameters	8034/10/604
	b(Å)=22.5183(11) *β*(°)= 99.680(4).	Goodness-of-fit on F^2	1.084
	c(Å) = 21.2054(10) *γ*(°)= 90°	Final *R* indices [$I > 2$ sigma (I)]	R_1 = 0.0308, wR_2 = 0.0748
Volume (Å^3)	4559.2(4)	*R* indices (all data)	R_1 = 0.0411, wR_2 = 0.0829
Z	4	Largest diff. peak and hole	0.445 and −0.390
ρ (calculated) (mg/m^3)	1.447		
Absorption coefficient (mm^{-1})	0.624		
F(000)	2040		
Crystal size (mm^3)	0.300 × 0.250 × 0.200		

Table 9. Selected bond length (Å), bond angle (°) and torsion angles (°) of $Cd(HL)_2$

Bond Length (Å)		**Bond Angle (°)**		**Torsion Angle (°)**	
C(8)–N(1)	1.349(3)	N(1)–C(8)–S(1)	121.5(2)	S(1)–C(8)–N(2)–N(3)	−5.1(4)
C(8)–N(2)	1.333(3)	N(2)–C(8)–S(1)	123.6(2)	C(8)–N(2)–N(3)–C(9)	−172.5(3)
C(33)–N(7)	1.340(4)	N(3)–C(9)–C(16)	119.2(2)	N(2)–N(3)–C(9)–C(16)	−177.4(2)
C(8)–S(1)	1.692(3)	C(8)–N(2)–N(3)	122.1(2)	C(35)–C(36)–O(2)–Cd(1)	37.4(4)
C(33)–S(2)	1.70(1)	C(9)–N(3)–N(2)	115.3(2)	C(16)–C(18)–O(1)–Cd(1)	33.0(4)
C(9)–N(3)	1.306(3)	O(1)–C(18)–C(16)	132.1(2)	N(4)–C(18)–O(1)–Cd(1)	−147.3(2)
C(34)–N(8)	1.300(3)	O(1)–C(18)–N(4)	123.5(2)	N(9)–C(36)–O(2)–Cd(1)	−142.9(2)
C(9)–C(16)	1.429(3)	C(10)–C(9)–N(3)	120.3(2)	N(1)–C(8)–S(1)–Cd(1)	166.5(2)
C(34)–C(35)	1.434(4)	O(1)–Cd(1)–O(2)	130.69(6)	N(6)–C(33)–S(2)–Cd(1)	161.7(2)
C(9)–C(10)	1.494(3)	O(1)–Cd(1)–S(2)	94.1(3)	N(7)–C(33)–S(2)–Cd(1)	−16.4(9)
C(17)–N(5)	1.308(3)	O(1)–Cd(1)–N(3)	76.90(7)	N(2)–C(8)–S(1)–Cd(1)	−16.2(3)
C(17)–C(19)	1.492(4)	O(2)–Cd(1)–N(3)	79.92(7)		
C(18)–O(1)	1.254(3)	O(1)–Cd(1)–N(8)	79.11(7)		
C(36)–O(2)	1.261(3)	O(2)–Cd(1)–N(8)	72.55(7)		
C(18)–N(4)	1.378(3)	C(18)–O(1)–Cd(1)	119.73(16)		
C(20)–N(4)	1.411(3)	C(36)–O(2)–Cd(1)	119.73(16)		
N(2)–N(3)	1.385(3)				
N(7)–N(8)	1.384(3)				
N(4)–N(5)	1.391(3)				
N(3)–Cd(1)	2.369(2)				
N(2)–H(2N)	0.88(2)				
N(7)–H(7)	0.88(2)				
N(8)–Cd(1)	2.384(2)				
N(3)–Cd(1)	2.369(2)				
O(1)–Cd(1)	2.297(2)				
O(2)–Cd(1)	2.368(2)				
S(1)–Cd(1)	2.6029(8)				
Cd(1)–S(2)	2.573(9)				
C(7)–N(1)	1.456(4)				
N(9)–N(10)	1.395(3)				

Table 10. Hydrogen bonding interaction parameters in $Cd(HL)_2$

D–H···A	d(D–H)	d(H···A)	d(D···A)	<(DHA)
C(21)–H(21)···O(1)	0.93	2.47	2.982(3)	115.2
C(26)–H(26)···O(^{2})^{1}a	0.93	2.52	3.354(4)	150
C(32)–H(32B)···S(^{1})^{2}b	0.96	2.92	3.648(4)	133.4
C(40)–H(40)···O(2)	0.93	2.32	2.902(3)	120

[a]Symmetry transformations used to generate equivalent atoms: $-x + 1, -y, -z + 2$.

[b]Symmetry transformations used to generate equivalent atoms: $-x, -y, -z + 2$.

4. Conclusions

In the present investigation, we were able to obtain single crystals of 1-phenyl-3-methyl-4-benzoyl-5-pyrazolone-N(4)-methyl-N(4)-phenylthiosemicarbazone and its Cd(II) complex. From the study, coordination capabilities of thiosemicarbazone are found to be unpredictable and are very interesting. We observed that with different salts of same metal, this ligand has coordinated in different modes and can act as tridentate ligand with N, S, O donor atoms. In complexes, the ligand was in mono-anionic (HL^-) or neutral (H_2L) form. Based on elemental analyses, spectral, magnetic, structural and thermal studies, the following geometries are assigned to the complexes (Figs. 20–23).

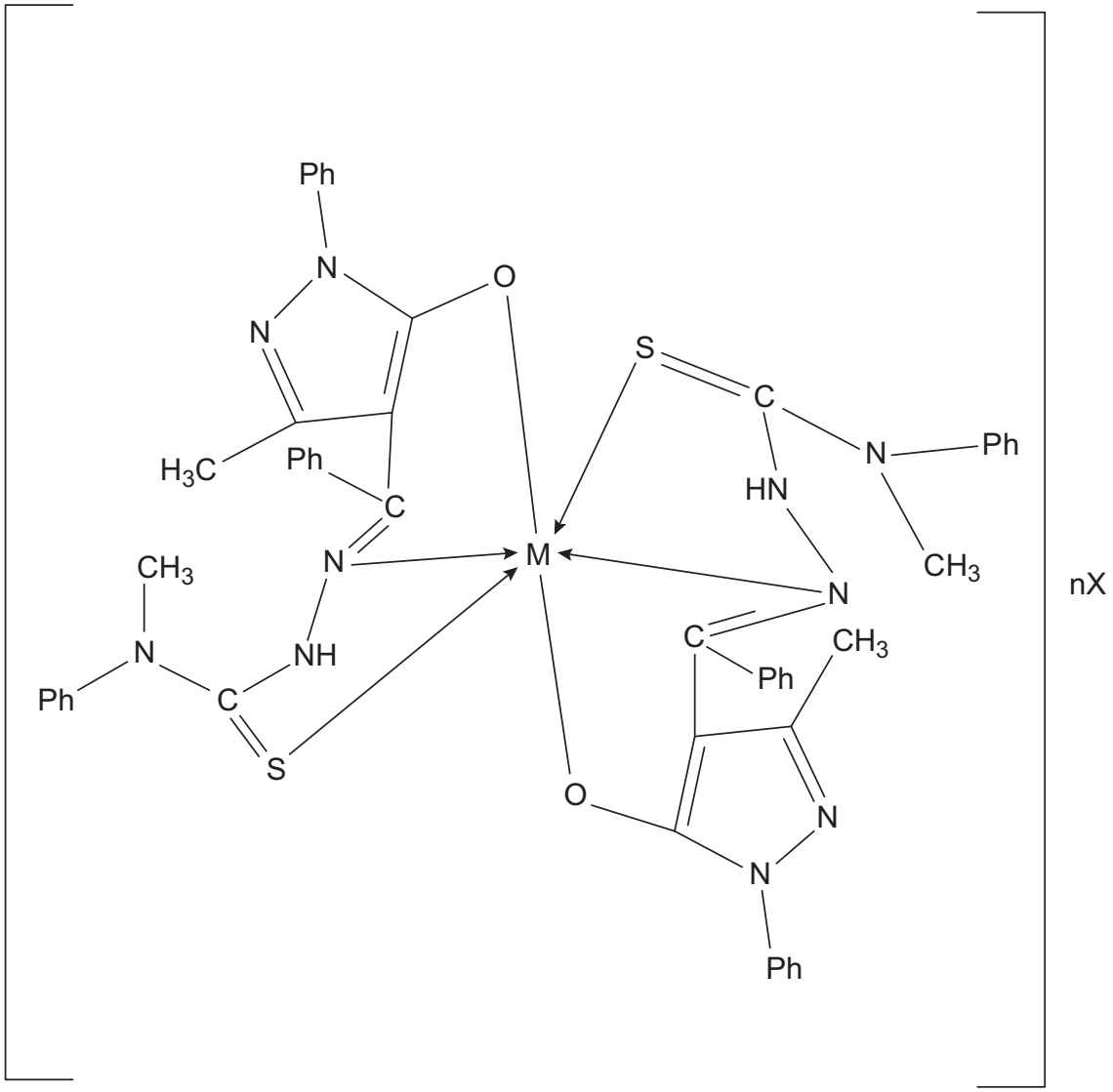

Fig. 20. Proposed structure of complexes $[M(HL)_2]$ *n*X, where M = Cr(III), Mn(II), Fe(II), Co(III), Ni(II), Cu(II), Zn(II), Cd(II); X = H_2O, NO_3^-, CH_3COO^-, Cl^-; *n* = 0, 1, 2, 3…**(1)**, **(2)**, **(3)**, **(4)**, **(5)**, **(6)**, **(8)**, **(9)**, **(10)**, **(11)**, **(15)**, **(18)**.

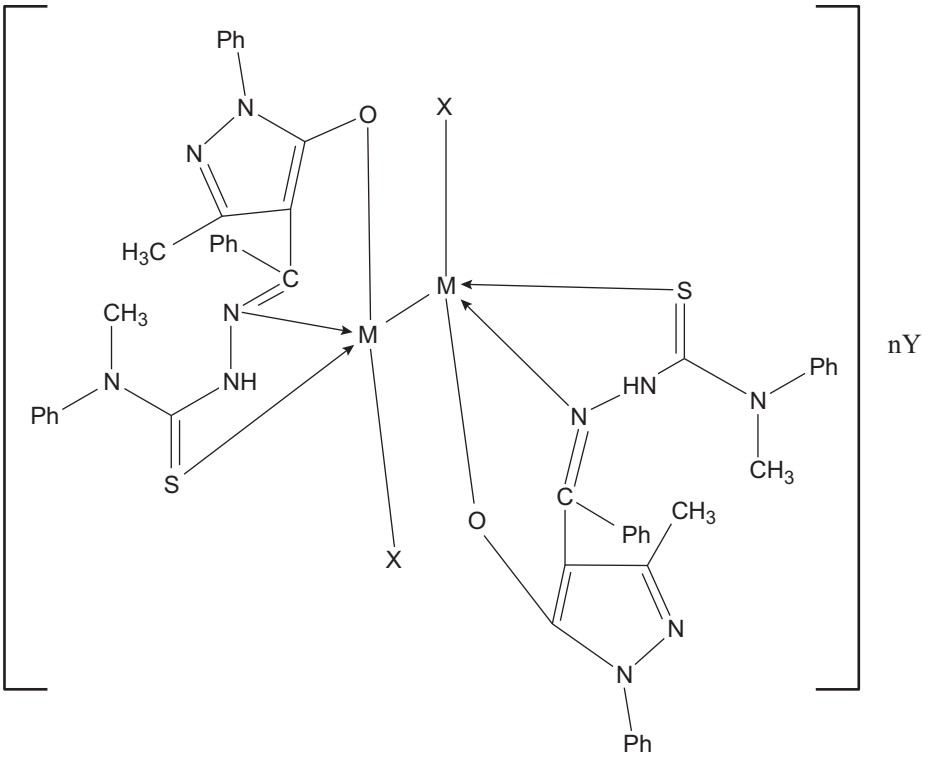

Fig. 21. Proposed structure of complexes $[(MHL)_2X_2]$ nH_2O, where M = Cu(II), Zn(II); X = OH^-, NO_3^-; **(14)**, **(16)** and **(17).**

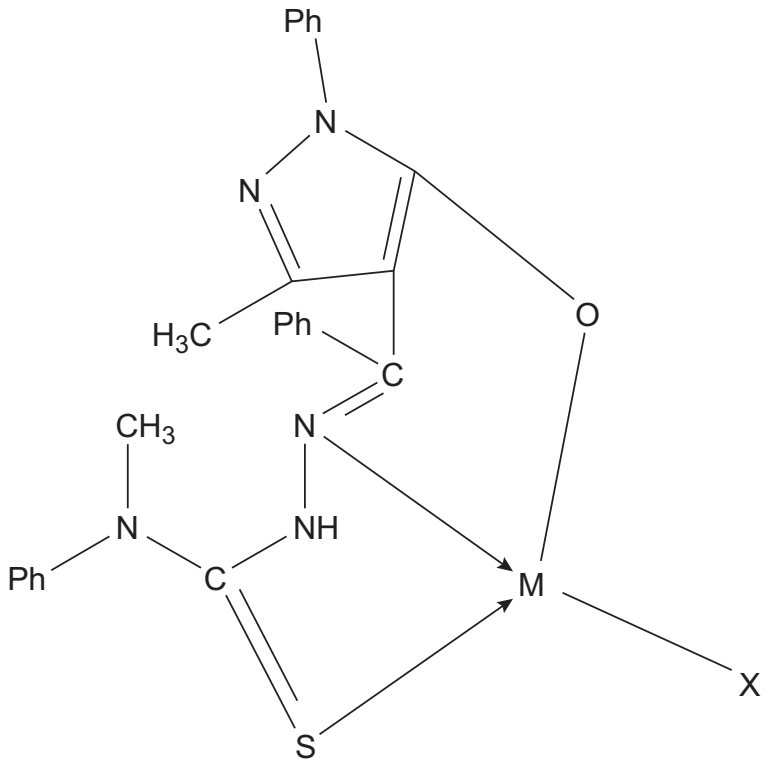

Fig. 22. Proposed structure of complexes [M(HL)X], where M = Cu(II); X = Cl^-, NO_3^- **(12)** and **(13)**.

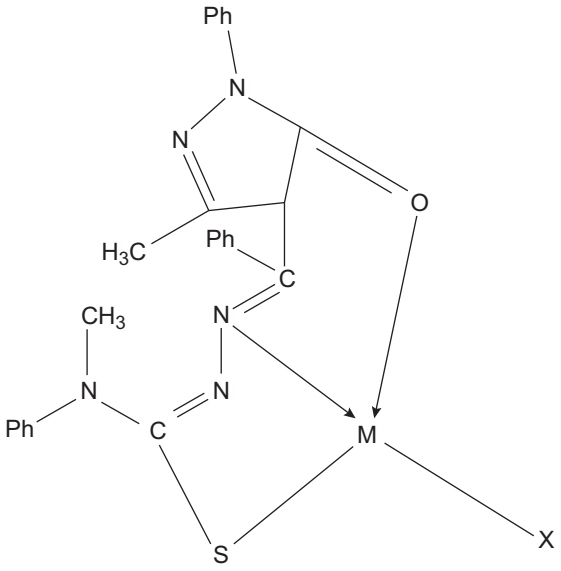

Fig. 23. Proposed structure of complex [M(HL)X], where M = Ni(II); X = CH_3COO^- **(7)**.

References

1. Knorr, Ger. Pat., 26 (1883) 429.
2. Knorr, Blank, Ber., 16 (1887) 2597; Knorr, Blank, Ber., 18 (1885) 311.
3. B. S. Jensen, Acta Chem. Scand., 13 (1959) 1668.
4. R. G. Charles, E. P. Riedel, J. Inorg. Nucl. Chem., 28 (1966) 3005.
5. H. Samelson, A. Lempicki, J. Chem. Phys., 39 (1963) 110.
6. G. H. Sheldrick, SHELXL 97. Program for Crystal Structure Refinement, University of Göttingen, Göttingen, Germany, 1997.
7. A. L. Spek, PLATON, A Multipurpose Crystallographic Tool, Utrecht University, Utrecht, The Netherlands, 1999.
8. L. J. Farrugia, J. Appl. Crys., 45 (2012) 849.
9. Diamond-Crystal and Molecular Structure Visualization Crystal Impact – Dr. H. Putz and Dr. K. Brandenburg GbR, Kreuzherrenstr. 102, 53227 Bonn, Germany.
10. C. Macrae, P. R. Edington, P. McCabe, E. Pidcock, G. P. Shields, R. Taylor, M. Towler, J. Van de Streek, J. Appl. Cryst., 39 (2006) 453.
11. G. J. Palenik, D. F. Rendle, W. S. Cruler, Acta Cryst. B, 30 (1974) 2390.
12. K. O. Ferraz, S. M. S. V. Wardell., J. L. Wardell, S. R. W. Louro, H. Beraldo, Spectrochim Acta A, 73 (2009) 140; H. Arslan, U. Florke, N. Kulcu, G. Binzet, Spectrochim Acta A, 68 (2007) 1347.
13. V. Suni, M. R. P. Kurup, M. Nethaji, Spectrochim. Acta, 63A (2006) 174.
14. E. M. Jouad, M. Allain, M. A. Khan, G. M. Bouet, J. Mol. Struct., 604 (2002) 205.
15. K. Meyer, Ann., 380 (1911) 220.
16. R. M. Silverstein, G. C. Bassler, C. Morril, Spectroscopic Identification of Organic Compounds, 4th ed., John Wiley, New York City, New York, 1981.
17. D. X. West, N. M. Kozub, G. Bain, Transition Met. Chem., 21 (1996) 52.
18. Y. Sun, Y. Wang, Z. Liu, C. Huang, C. Yu, Spectrochim. Acta A, 96 (2012) 42.
19. S. Subashchandrabose, H. Saleem, O. Erdogdu, V. Dereli, V. Thanikachalam, J. Jayabharathi, Spectrochim. Acta A, 86 (2012) 231.
20. G. Varsányi, Assignment for Vibrational Spectra of Seven Hundred Benzene Derivatives, Vol. 1–2, Akadémiai Kiadó, Budapest, 1974.
21. J. Chowdhury, M. Ghosh, T. N. Misra, J. Colloid Interf. Sci., 228 (2000) 372.
22. P. F. Rapheal, E. Manoj, M. R. P. Kurup, Polyhedron, 26 (2007) 818.
23. U. Kumar, S. Chandra, J. Saudi Chem. Soc., 15 (2011) 187.
24. J. E. Huheey, E. A. Keiter, R. L. Keiter, Inorganic Chemistry, Principles of Structure and Reactivity, 4th ed., Harper Collins College Publishers, New York City, New York, 1993.
25. W. Linert, F. Renz, R. Boca, J. Coord. Chem., 40 (1996) 293.
26. S. Chandra, L. K. Gupta, Spectrochim. Acta Part A, 61 (2005) 2549.
27. A. K. Mukherjee, P. Ray, Indian Chem. Soc., 32 (1955) 633.
28. L. Sacconi, R. Cini, Ann. Chim. (Italy), 42 (1952) 723.
29. D. N. Sathyanarayana, Electronic Absorption Spectroscopy and Related Techniques Universities Press, India limited (2001).
30. S. Sreekumar, PhD thesis, Cochin University of Science and Technology, 2003.
31. S. Vasudevan, H. N. Vasan, C. N. R. Rao, Chem. Phys. Lett., 65 (1979) 444.
32. R. P. John, A. Sreekanth, M. R. P. Kurup, S. M. Mobin, Polyhedron, 21 (2002) 2515.

33. D. J. Radanovic, M. I. Djuran. Inorg. Chim. Acta, 207 (1993) 111.
34. B. Gray, C. J. Ballhausen, J. Am. Chem. Soc., 85 (1963) 260.
35. R. Bindu, PhD thesis, Cochin University of Science and Technology, 1997.
36. C. K. Jorgenson, Acta Chem. Scand., 10 (1956) 887.
37. A. B. P. Lever, Inorganic Electronic Spectroscopy, 2nd ed., Elsevier, Amsterdam (1984) Coordination Compounds, Springer verlag, NY, Vol II-11 (1981).
38. L. Sacconi, Transition Met. Chem., Ed. R. L. Carlin, 4 (1968) 199.
39. G. L. Miessler, D. A. Tarr, Inorganic Chemistry, 2nd ed., Prentice Hall, Upper Saddle River, New Jersey, 1999.
40. G. Bullock, F. W. Hartstock, L. K. Thompson, Can. J. Chem., 61 (1983) 57.
41. R. Jeevana, PhD thesis, University of Calicut, 2012.
42. L. Sacconi, G. Speroni, J. Amer, Chem. Soc., 87 (1965) 3102.
43. M. E. Khalifa, A. A. El-Asmy, K. M. Ibrahim, M. M. Mostafa, Synth. React. Inorg. Met. Org. Chem., 16 (1986) 1319.
44. D. Sutton, Electronic Spectra of Transition Metal Complexes, McGraw Hill, London, 1968.
45. S. Renjusha, M. R. P. Kurup, Polyhedron, 27 (2008) 3294.
46. R. M. Issa, A. M. Khedr, H. F. Rizk, Spectrochim. Acta A., 62 (2005) 621.
47. M. H. Habibi, M. Montazerozohori, A. Lalegani, R. W. Harrington, W. J. Clegg, Fluor. Chem. 127 (2006) 769.
48. K. Nakamoto, Infrared and Raman Spectra of Inorganic and Coordination Compounds, 5th ed., Wiley, New York City, New York, 1997.
49. I. Nakagwa, J. L. Walter, J. Chem. Phys., 51 (1969) 1389.
50. G. M. Sheldrick, SHELXL-2014/7: Program for the Solution of Crystal Structures, University of Göttingen, Göttingen, Germany, 2014.
51. Z. -F. Chen, Y. -Z Tang, H. Liang, H. -K. Fun, K. -B. Yu, J. Coord. Chem., 59 (2006) 207.

CHAPTER IV

NOVEL LIGANDS, BENZOPHENONE N(4)-METHYL-N(4)-PHENYLTHIOSEMICARBAZONE, 2-[2-(DIPHENYLMETHYLIDENE) HYDRAZINE]-N-METHYL-N-PHENYLHYDRAZINE-1-CARBOTHIOAMIDE AND TRANSITION METAL COMPLEXES OF THE LATTER

1. Introduction

Benzophenone derivatives are very important due to their versatile properties such as electrochemical, spectroscopic, metal complexation, adsorptive and crystallographic properties.[1,2] They have the ability to absorb a broad range of UV radiation (200–350 nm). The benzophenone derivatives like, 2-hydroxy-4-methoxybenzophenone are used as raw materials in the manufacture of sunscreen cream or lotions.[3] These creams are useful in various medical treatments to shun photosensitization, phototoxicity or allergic reactions of patients.[4]

Topical studies have shown that benzophenone thiosemicarbazone exhibits inhibitory effects on parasites including *Trypanosoma brucei* and *Plasmodium falciparum*.[5] Schiff's bases derived from benzophenone have been extensively studied for their cytotoxic activities against human oral squamous carcinoma cells (HSC-2) and normal human gingival fibroblasts (HGF). Antibiotic activities of these compounds against methicillin-resistant *Staphylococcus aureus,* vancomycin-resistant *Enterococcus faecium* and protein kinase C inhibitor have been studied.[6] Benzophenone thiosemicarbazone containing a π-electron conjugation system can act as one of the potential semi-organic optical materials.

This chapter portrays the synthesis and characterisation of two ligands derived from benzophenone and N(4)-methyl-N(4)-phenylthiosemicarbazide. One is benzophenone N(4)-methyl-N(4)-phenylthiosemicarbazone (BMPTSC) (**HL)** (Fig. 1) and the other is 2-[2-(diphenylmethylidene)hydrazine]-N-methyl-N-phenylhydrazine-1-carbothioamide (BP-MPTSC), ($\mathbf{H_2L'}$) (Fig. 2) Several transition metal complexes of the latter ligand (H_2L') were synthesized and characterised. The structures of the ligands were drawn using ChemDraw Ultra.

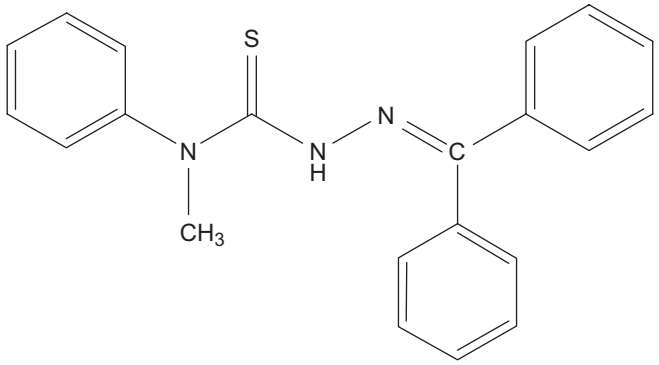

Fig. 1. Benzophenone N(4)-methyl-N(4)-phenylthiosemicarbazone (BMPTSC),(HL)

*2-(diphenylmethylene)-N-methyl-N-phenylhydrazinecarbothioamide.

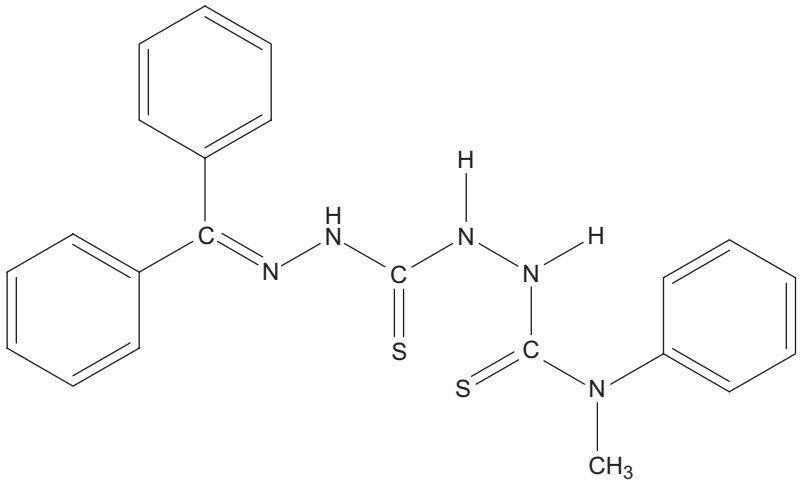

Fig. 2. 2-[2-(diphenylmethylidene)hydrazine]-N-methyl-N-phenylhydrazine-1-carbothioamide (BP-MPTSC), (H_2L').

*IUPAC name of the compound

2. Experimental

2.1. Materials and methods

All the chemicals used in this study are of AR grade. Benzophenone, glacial acetic acid and sodium acetate trihydrate were used as received. Commercially available metal salts were used without further purification. The solvents were purified and dried by using standard procedure. The melting points of the ligands and complexes were recorded on a melting point apparatus. The ligand and complexes were characterised by partial elemental analyses, magnetic susceptibility measurements, Fourier-transform infrared spectroscopy (FT-IR) and electronic spectra. The ligand HL was characterised by single-crystal X-ray diffraction (XRD) studies and H_2L' by powder XRD studies. FT-Raman spectra of the ligands were recorded. The ligands and Zn(II) complexes were also characterised by ^{1}H nuclear magnetic resonance (NMR) spectra. EPR spectrum of Mn(II) complex was also recorded. Thermal stabilities of complexes were also ascertained. Details regarding these techniques are explained in Chapter II.

2.2. Synthesis

Synthesis of the precursor, N(4)-methyl-N(4)-phenylthiosemicarbazide (MPTSC) is discussed in Chapter II.

2.2.1. 2-(Diphenylmethylene)-N-methyl-N-phenylhydrazinecarbothioamide (HL)

HL was prepared by dropwise addition of a hot methanolic solution of benzophenone (0.345 g, 1 mmol) to a boiling methanolic solution of N(4)-methyl-N(4)-phenylthiosemicarbazide (MPTSC) (0.182 g, 1 mmol) taken in a round bottom flask. The reaction mixture was refluxed for 2 hours. The volume of the solution was reduced and kept overnight. The ligand obtained was filtered, washed with methanol and water and dried. Cream-coloured crystals were formed on slow evaporation of the washings. They were filtered and dried at room temperature. The formation of the ligand, HL, is demonstrated in Scheme 1 shown below.

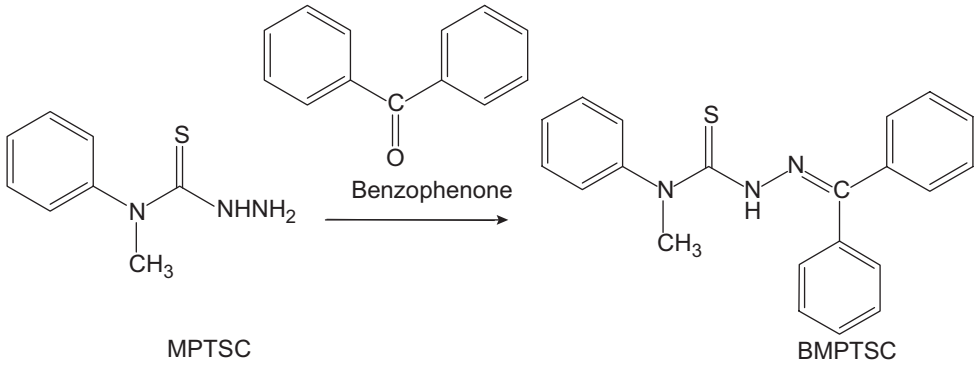

Scheme 1. The formation of ligand BMPTSC (**HL**).

2.2.2. 2-[2-(diphenylmethylidene)hydrazine]-N-methyl-N-phenylhydrazine-1-carbothioamide (H_2L')

H_2L' was prepared by dropwise addition of a hot methanolic solution of benzophenone (0.345 g,1 mmol) to a boiling methanolic solution of MPTSC (0.364 g, 2 mmol) taken in a round bottom flask. Two drops of glacial acetic acid was added to the reaction mixture and refluxed at 60°C–80°C for 30 minutes. The solution was chilled and kept overnight. The cream-coloured precipitate obtained was filtered, washed with methanol and dried. The melting point and solubility of the compound in different solvents were noted. The formation of ligand, H_2L' is demonstrated in Scheme 2.

2.2.2.1 Metal complexes of H_2L'

A hot methanolic solution of H_2L' was added dropwise to hot methanolic/water solution of metal acetate/sulphate/chloride/nitrate in a 1:1 molar ratio. The resulting mixture containing the ligand and the metal salt was then refluxed for 3 hours and then cooled to room temperature. The precipitate formed was filtered, washed with water followed by methanol and dried. Yields and melting points of the complexes were noted.

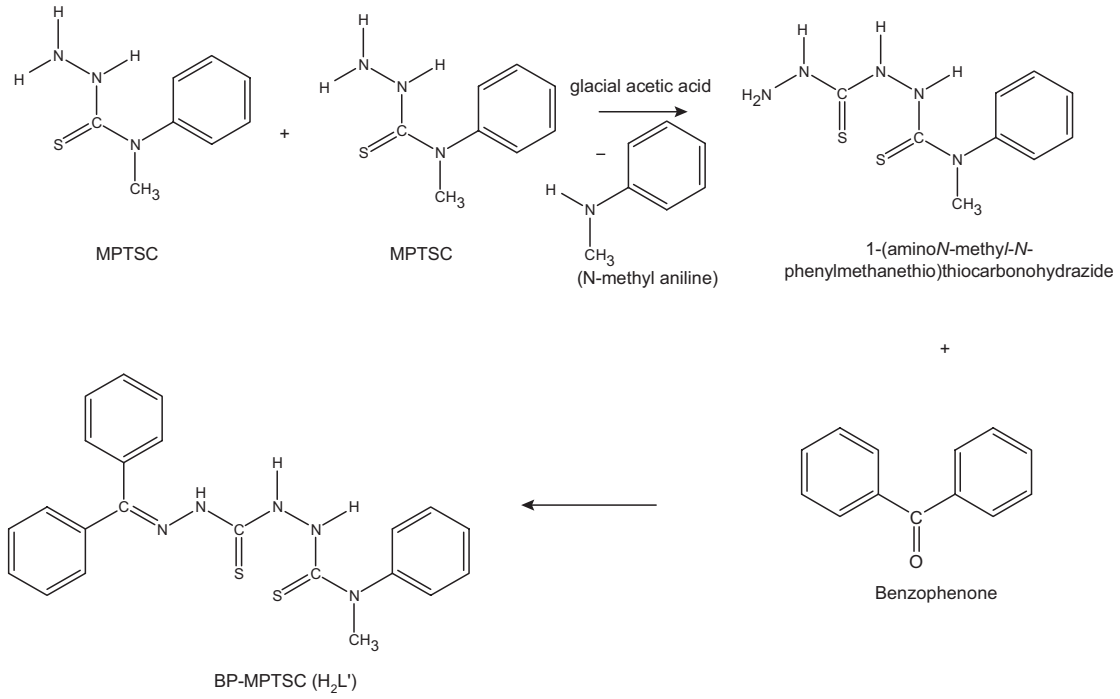

Scheme 2. The formation of ligand BP-MPTSC (**H_2L'**).

3. Results and discussion

In this investigation, we were able to obtain single crystals of benzophenone N(4)-methyl-N(4)-phenylthiosemicarbazone [IUPAC name: (2-(diphenylmethylene)-N-methyl-N-phenylhydrazinecarbothioamide)] (HL) by refluxing equimolar quantities of benzophenone and N(4)-methyl-N(4)-phenyl thiosemicarbazide. However, the yield of the product was low. Therefore, for increasing the yield and also to enhance the speed of the reaction, we decided to modify the procedure. In the modified procedure, we added two drops of glacial acetic acid to the reaction mixture and chilled the resultant solution. Moreover, we used 2 mmol of N(4)-methyl-N(4)-phenyl thiosemicarbazide and 1 mmol of benzophenone. We were able to obtain a faster reaction rate and a better yield. Anticipating that the ligand thus obtained was benzophenone N(4)-methyl-N(4)-phenylthiosemicarbazone (HL), we prepared its complexes. However, the elemental analytical and ^{1}H NMR spectral data of the ligand (H_2L') and its complexes were not in agreement with the crystal data of the expected ligand (HL). We were able to synthesize and study the single crystals of Mn(II) and Ni(II)complexes of the ligand (H_2L'). This prompted us to investigate more about the unexpected structure of H_2L'. Further, data obtained from elemental analysis and ^{1}H NMR spectrum helped us to confirm the ligand structure. The formation of H_2L' might have taken place through the above hidden steps (Scheme 2). As N-methyl aniline is a better leaving group, its substitution with other group has been already reported.[7] To the best of our knowledge, the structure of the ligand (H_2L') obtained has not been reported so far.

3.1. Characterisation of the ligands (HL and H_2L')

3.1.1. Microanalytical data

The suggested formula for the compound, (HL) is $C_{21}H_{19}N_3S$. CHNS percentages of ligands were in agreement with the suggested molecular formula (Table 1). It is cream in colour and melts at 153°C. The suggested formula for the ligand (H_2L') is $C_{22}H_{21}N_5S_2$. It is cream in colour and melts at 160°C. The ligands are soluble in organic solvents like DMF, DMSO, $CHCl_3$, methanol, ethanol, and so on.

Table 1. Analytical data of the ligands (HL and H_2L')

Compound	Molecular Weight	Colour	Yield	Melting Point	Elemental Analysis Found(calculated)			
					C	H	N	S
$C_{21}H_{19}N_3S$	345	Shining cream crystals	60	153	73.5 (73.0)	5.3 (5.5)	12.1 (12.2)	9.2 (9.3)
$C_{22}H_{21}N_5S_2$	419	Cream	85	160	62.8 (63.0)	5.2 (5.0)	16.5 (16.7)	15.0 (15.2)

3.1.2. Single-crystal XRD studies of HL ($C_{21}H_{19}N_3S$)

Single crystals of HL fit for X-ray analysis were obtained by the slow evaporation of its solution (1:1 methanol and water). A crystal with dimensions, 0.35 × 0.30 × 0.20 mm^3 was selected for collecting the data. HL crystallizes with two molecules per asymmetric unit into a triclinic crystal system with a space group of *P*−1.

X-ray crystallographic data were collected at 296(2) K. Direct methods were performed to solve the structure and it was refined by least-square on F^2 using SHELXL-97.[8] All non-hydrogen atoms were refined anisotropically. All hydrogen atoms, except those attached to nitrogen were geometrically fixed at calculated positions. The crystallographic tools, PLATON for Windows[9], DIAMOND 3.2d[10] and MERCURY 3.5.1[11] were used for structure analysis and presentation of the results. The structure was finally refined to the conventional *R*-value, 0.0611.

The molecular structure of the compound with the atom numbering scheme is given in Fig. 3. Crystal data and structure refinement for HL are given in Table 2. Selected bond lengths and bond angles are listed in Table 3. Hydrogen bonding interaction parameters are shown in Table 4. Packing diagram, showing intermolecular interactions along *b*-axis is shown in Fig. 4. Packing diagram along *a*-axis is shown in Fig. 5.

The bond lengths, C(9)–N(3), C(8)–N(1), C(8)–N(2) and N(3)–N(2) are 1.285(3) Å, 1.339(4), 1.388(4) and 1.371(3), respectively. They are found to be midway between the analogous single [C–N, 1.47 Å; N–N, 1.45 Å] and double bonds [C N, 1.28 Å; N=N, 1.25 Å].[12,13] The C(9)–N(3) bond length, 1.285(3) Å is close to C=N bond length. This confirms the presence of azomethine bond in the ligand which is evident from the IR data.[12]C(8)–S(1) bond length is found to be 1.655(2) Å, which is close to C=S bond length of 1.61 Å than C–S single bond of 1.81 Å.[14] This substantiates the existence of HL in thione form in solid state.

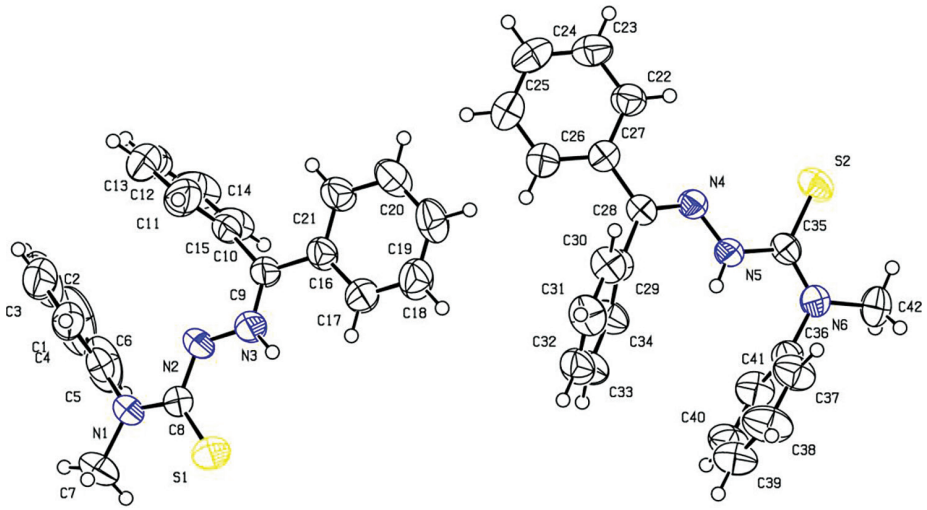

Fig. 3. The molecular structure of HL with the atom numbering scheme.

Table 2. Crystal data and structure refinement for HL

Parameters			
Empirical formula	C_{21} H_{19} N_3 S	Theta range for data collection (°)	1.09 to 28.37.
Formula weight	345.45	Limiting indices	$-13 \le h \le 13$, $-8 \le k \le 13$, $-25 \le l \le 23$
Temperature (K)	296(2)	Reflections collected/ unique	15549/9040 [R(int) = 0.0252]
Wavelength (Å)	0.71073	Completeness to theta = 28.37	96.7 %
Crystal system	Triclinic	Absorption correction	Semi-empirical from equivalents
Space group	$P-1$		
Unit cell dimensions	a (Å) = 10.0166(6) α (°) = 103.794(3)	Max. and min. transmission	0.9648 and 0.9395
	b (Å) = 10.0685(5) β (°) = 90.656(2)	Refinement method	Full-matrix least-squares on F^2
	c (Å) = 19.2274(11) γ (°) = 96.566(3)		
Volume (A^3)	1869.34(18)	Data/restraints/ parameters	9040/0/453
Z	4	Goodness-of-fit on F^2	1.022
$\rho_{Calculated}$ (mg/m^3)	1.227	Final R indices [$I >$ 2sigma(I)]	R_1 = 0.0611, wR_2 = 0.1543
Absorption coefficient (mm^{-1})	0.181	R indices (all data)	R_1 = 0.1360, wR_2 = 0.1954
F(000)	728	Largest diff. peak and hole ($e.A^{-3}$)	0.388 and −0.389
Crystal size (mm^3)	0.35 × 0.30 × 0.20		

Table 3. Selected bond lengths (Å), bond angles and torsion angles (°) of HL

Bond length (Å)		Bond angles (°)		Torsion angles(°)	
C(8)–N(1)	1.339(4)	N(1)–C(8)–S(1)	124.50(3)	C(9)–N(3)–N(2)–C(8)	177.0(3)
C(8)–N(2)	1.388(4)	N(2)–C(8)–S(1)	123.30(3)	N(1)–C(8)–N(2)–N(3)	177.1(3)
C(8)–S(1)	1.655(4)	N(1)–C(8)–N(2)	112.20(3)	S(1)–C(8)–N(2)-N(3)	3.7(5)
C(9)–N(3)	1.285(3)	C(9)–N(3)–N(2)	116.80(2)	N(2)–C(8)–N(1)–C(6)	0.5(5)
N(3)–N(2)	1.371(3)	C(9)–N(3)–H(3N)	121.60	S(1)–C(8)–N(1)–C(6)	179.7(3)
N(3)–H(3N)	0.86	N(2)–N(3)–H(3N)	121.60	N(2)–C(8)–N(1)–C(7)	179.2(4)
				S(1)–C(8)–N(1)–C(7)	0.0(5)

Table 4. Hydrogen bonding interactions of HL [Å and °]

D–H···A	d(D–H)	d(H···A)	d(D···A)	<(DHA)
N(3)–H(3N)···S(1)	0.86	2.66	3.004(2)	105
C(39)–H(39)···S(2)[a]	0.93	2.87	3.644(3)	141
C(25)–H(25)···S(1)[b]	0.93	2.83	3.569(3)	138
C(34)–H(34)···S(2)[c]	0.93	2.73	3.657(3)	172
C(42)–H(42A)···S(2)	0.96	2.54	3.051	114

[a]Symmetry transformations used to generate equivalent atoms: $-1 + x, y, z$.
[b]Symmetry transformations used to generate equivalent atoms: $1 + x, y, z$.
[c]Symmetry transformations used to generate equivalent atoms: $1 - x, 1 - y, 2 - z$.

A torsion angle of 3.7(5)° corresponding to S(1)–C(8)–N(2)–N(3) moiety confirms the *syn* or *Z* configuration of the S(1) atom with respect to azomethine nitrogen atom, N(3). Atom N(1) lies *trans* to N(3) in the unit, N(1)–C(8)–N(2)–N(3) with a torsion angle of −177.0(3)°. Atom, C(9) lies *trans* to C(8) in C(9)–N(3)–N(2)–C(8) with a torsion angle of 177.0(2)°.

The mean plane of the phenyl rings [C(1), C(2), C(3), C(4), C(5), C(6)] and [C(10), C(11), C(12), C(13), C(14), C(15)] forms a dihedral angle of 17.60(115)°. This indicates a *Z* conformation between these planes. The mean plane of these phenyl rings [C(10), C(11), C(12),

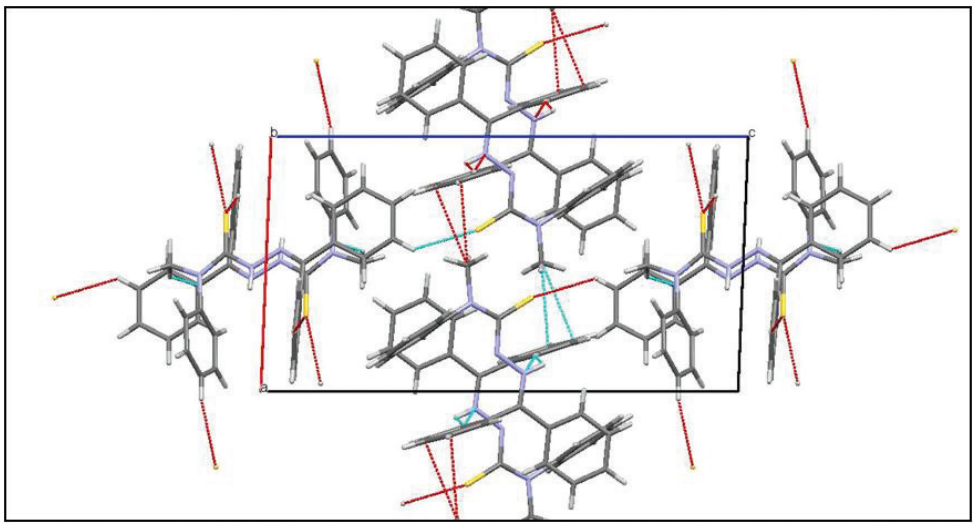

Fig. 4. Packing diagram of HL along the *b*-axis showing intermolecular interaction.

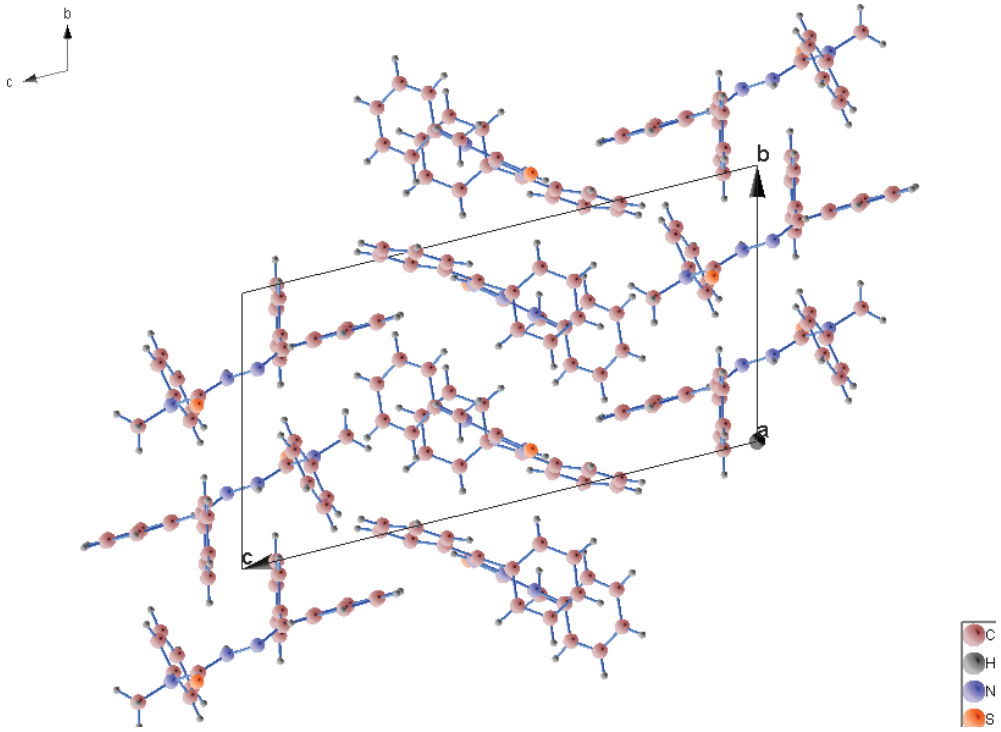

Fig. 5. Packing diagram along the a-axis of HL.

C(13), C(14), C(15)] and [C(16), C(17), C(18), C(19), C(20), C(21)] of benzophenone moiety assumes a dihedral angle, 76.177(138)°. It indicates that these phenyl rings of benzophenone moiety are substantially out of plane with each other. The mean plane deviation calculation shows that the central thiosemicarbazone bridge C(9)–N(3)–N(2)–C(8)–S(1) itself is nearly planar with a maximum mean plane deviation of 0.0045 Å for S(1) and C(9)–N(3)–N(2)–C(8)–(N1) shows a maximum deviation of 0.0158 Å for N(1). In the crystal lattice, two-dimensional packing of the molecules is stabilized by non-conventional intermolecular hydrogen bonding interactions.

For the second asymmetric unit, the bond lengths, C(28)–N(4), C(35)–N(5), C(35)–N(6) and N(4)–N(5) are 1.294(3), 1.367(3), 1.348(3) and 1.361(3), respectively. C(35)–S(2) bond length is found to be 1.664(3)Å, which is close to C=S bond length of 1.61 Å than C–S single bond of 1.81 Å.[13] The torsion angles for, S(2)–C(35)–N(5)–N(4), N(6)–C(35)–N(5)–N(4), C(28)–N(4)–N(5)–C(35) and N(5)–C(35)–N(6)–C(36) are 5.2(3)°,−176.83(19)°, −174.0(2)° and 1.3(3)°, respectively. Considering the above data, the two molecules in an asymmetric unit are found to exist in the *E* isomeric form with respect to C=N bond.

3.1.3. Spectroscopic analysis of HL

(a) Electronic spectrum

The electronic absorption spectrum of the ligand, HL in $CHCl_3$ was recorded in the range, 200–900 nm and is presented in Fig. 6. It registered bands at 257, 319, 352 and 419 nm, which are attributed to $\pi\rightarrow\pi^*$ and $n\rightarrow\pi^*$ transitions. The absorption bands observed below 360 nm are attributed to $\pi\rightarrow\pi^*$ and $n\rightarrow\pi^*$ transitions of the azomethine chromophore and benzene rings. The weak band at 414 nm may be due to the presence of the thiol form of

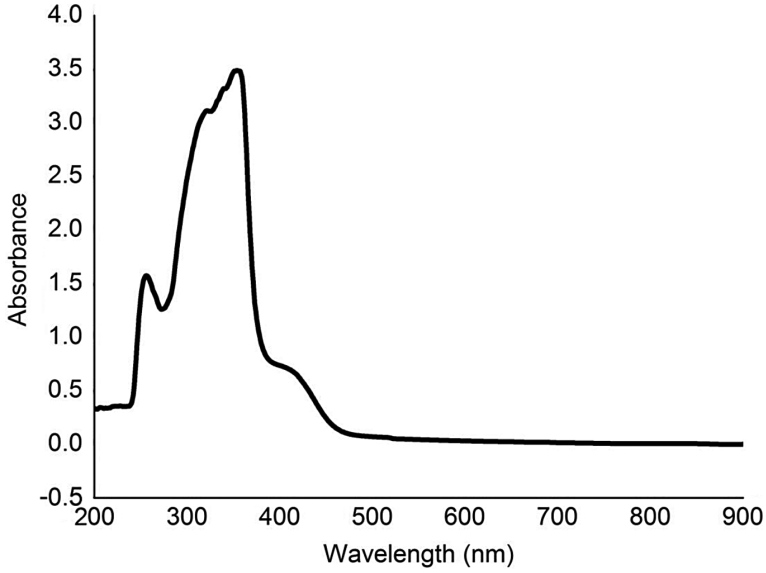

Fig. 6. Electronic spectrum of HL.

the compound in the nonpolar solvent. P. N. Prasad reported that the essential requirement for a material to be useful for photonic and optoelectronic applications is that it should be transparent in the region 450–1200 nm.[15] From the UV–Vis spectrum, it is clear that the crystal is transparent in the region between 420 and 900 nm.

(b) Vibrational spectra

The FT-IR spectrum of the compound was recorded in the region 4000–400 cm^{-1} and is presented in Fig. 7. It showed split bands at 3255–3169 cm^{-1} due to N–H stretching vibration. The Davydov splitting of the band observed between 3255 and 3169 cm^{-1} may be due to the interacting molecules in the unit cell. A split band at 1561–1594 cm^{-1} in the ligand is assigned to ν(C=N) stretching. ν(S–H) band at 2560 cm^{-1} is absent, indicating the existence

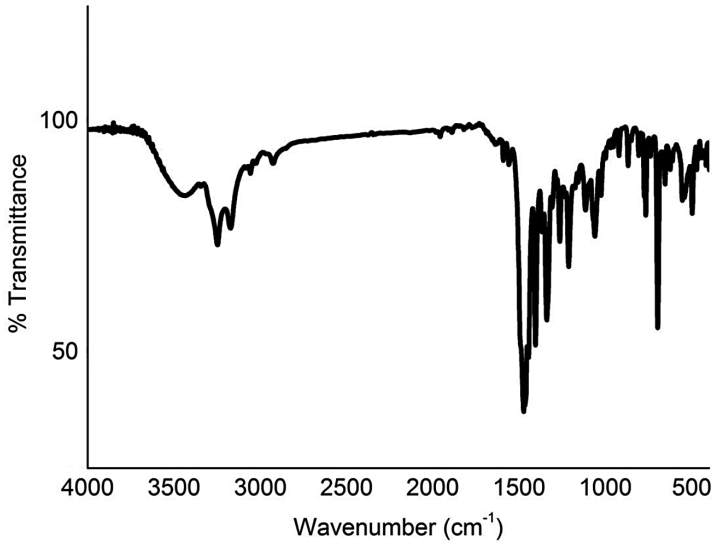

Fig. 7. FT-IR spectrum of HL.

of thione tautomer in the solid state.[16] The bands at 1332 and 770 cm^{-1} may be assigned to ν(NH–C=S) and *ν*(C=S), respectively. The bands observed at 1063 and 1111 cm^{-1} in the spectrum are assigned to N–N stretching vibrations. The ring carbon–carbon stretching vibrations are observed at 1480 cm^{-1}. The bands in the range 770–878 cm^{-1} and 1150–1222 cm^{-1} are assigned to C–H in-plane and out-of-plane bending vibrations, respectively.

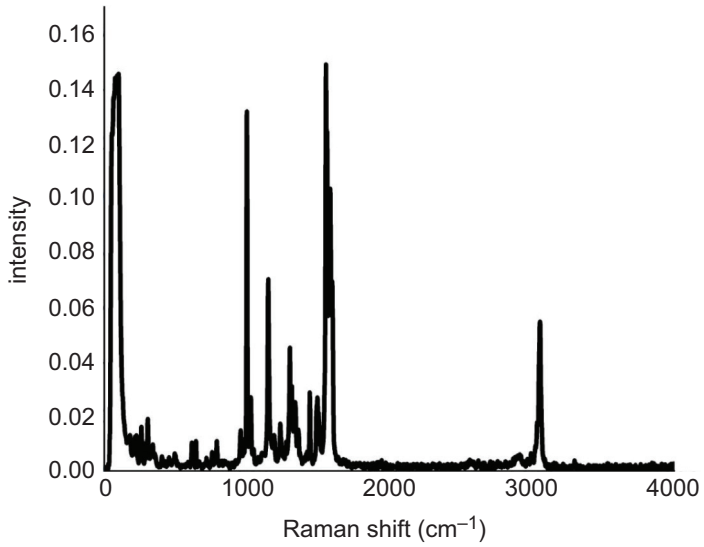

Fig. 8. FT-Raman spectrum of HL.

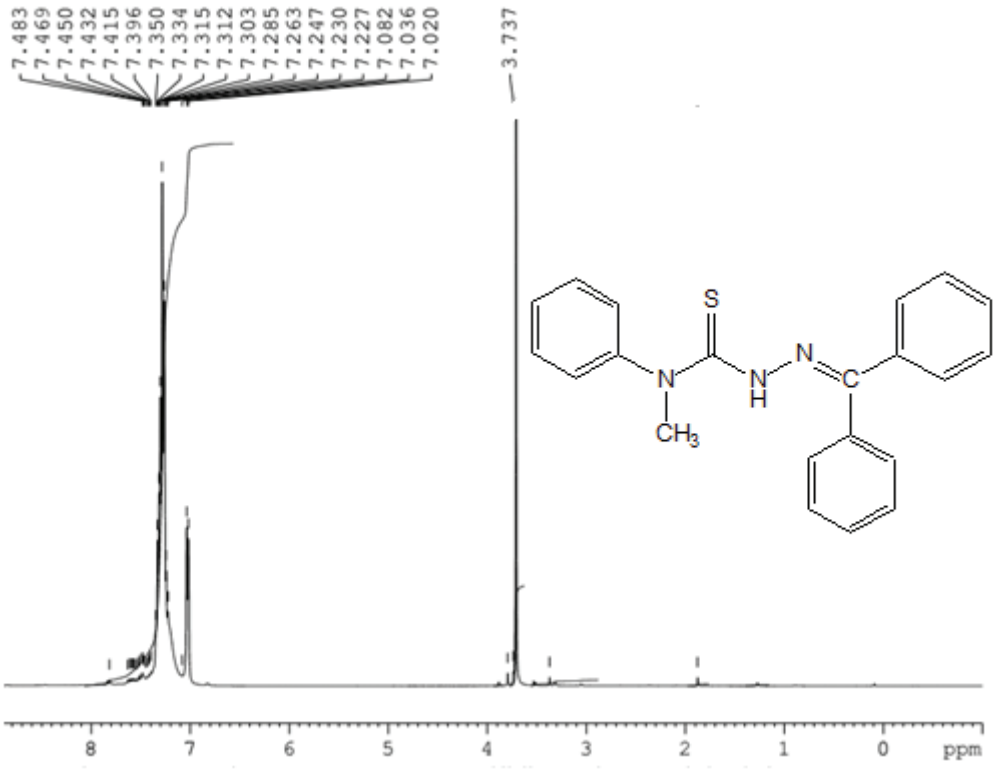

Fig. 9. NMR spectrum of HL.

The FT-Raman spectrum of the compound, HL, was recorded in the region 4000–400 cm^{-1} and is presented in Fig. 8. The sharp band at 3064 cm^{-1} may be assigned to NH stretching vibration. The C=N stretching vibration band is observed at 1583 cm^{-1}. The bands observed at 1559 and 1492 cm^{-1} may be due to the ring C–C stretching vibrations. The bands due to C=S stretching vibrations are observed at 1334 and 1143 cm^{-1}.

(c) ^{1}H NMR spectrum

The ^{1}H NMR spectrum of HL was recorded in $CDCl_3$ and is presented in Fig. 9. The multiplet at 7.036–7.48 ppm is assigned to aromatic protons. Peaks observed at 3.71–3.79 ppm correspond to N–CH_3 protons. A singlet observed at 7.02 ppm may be due to NH proton.

3.1.4. Powder XRD of ligand H_2L'

Since we couldn't obtain the single crystals of H_2L' we recorded its powder XRD pattern. It revealed the crystallinity of the compound. Matching the peaks using MATCH software, it is found that the crystal belongs to monoclinic system (Fig. 10).

3.1.5. Spectroscopic analysis of H_2L'

(a) Electronic spectrum

The solid state electronic spectrum of the ligand, H_2L' was recorded in the range, 200–900 nm and is presented in Fig. 11. It registered bands at 254 and 344, which are attributed to $\pi \rightarrow \pi^*$ and $n \rightarrow \pi^*$ transitions.

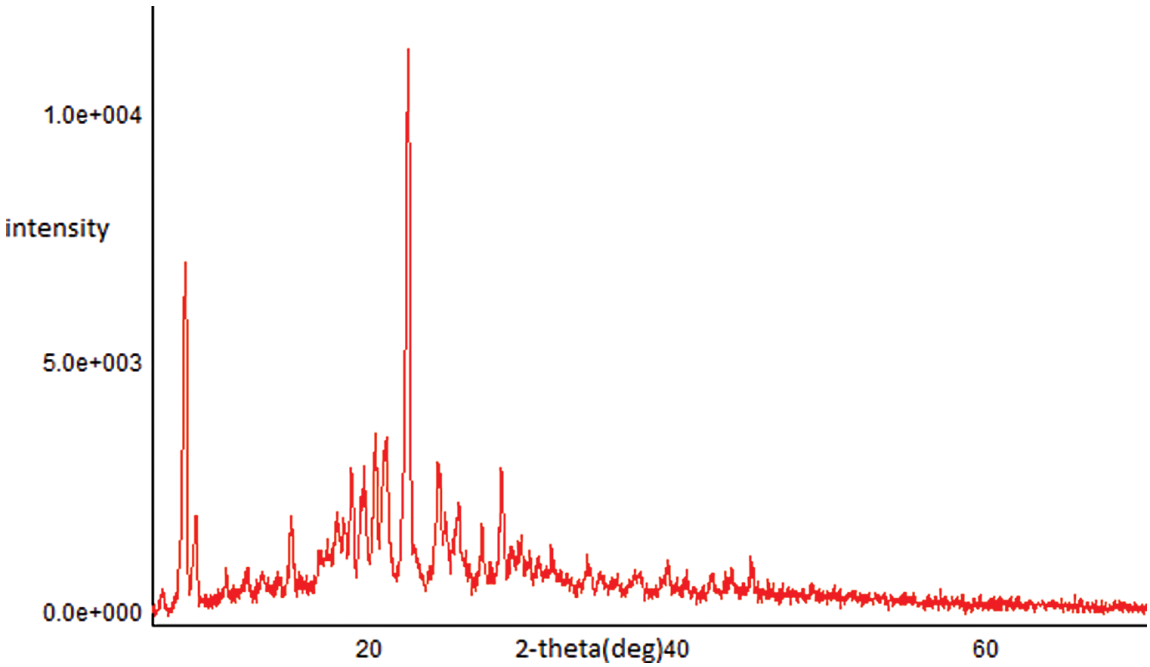

Fig. 10. Powder XRD pattern of H_2L'.

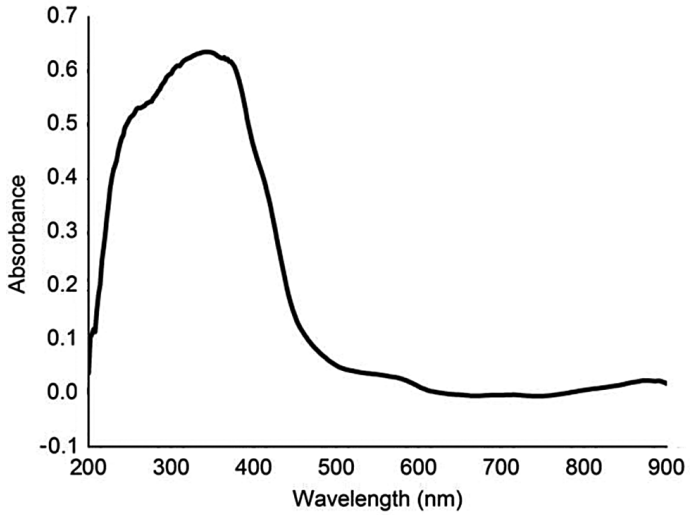

Fig. 11. Electronic spectrum of H_2L'.

(b) Vibrational spectra

The FT-IR spectrum of H_2L' is presented in Fig. 12 and FT-Raman spectrum in Fig. 13. The ligand, H_2L' showed a deep broad band at 3250–3153 cm^{-1} due to N–H stretching. The band at 1583 cm^{-1} in the ligand is assigned to ν(C=N) stretching. No band is observed at 2560 cm^{-1} which indicates the presence of thione tautomer in the solid state.[17,18] The bands near 1323 and 771 cm^{-1} in the ligand may be assigned to ν(NH–C=S) and *ν*(C=S), respectively.

A sharp band is observed at 3071 cm^{-1} in the FT-Raman spectrum and may be due to N–H stretching vibration. The sharp peak at 1589 cm^{-1} may be assinged to ν(C=N) stretching vibration. The C=S stretching vibrations are observed at 1296 and 1111 cm^{-1}.

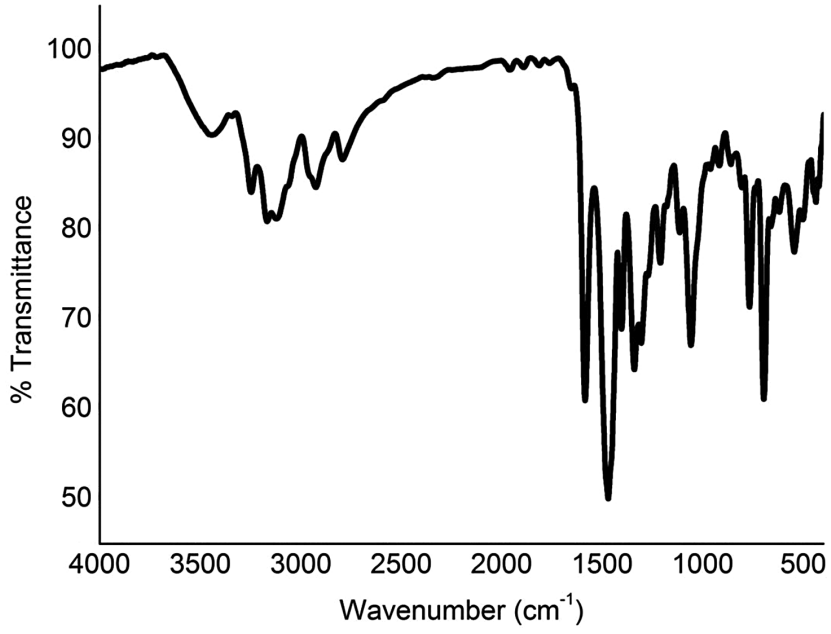

Fig. 12. FT-IR spectrum of H_2L'.

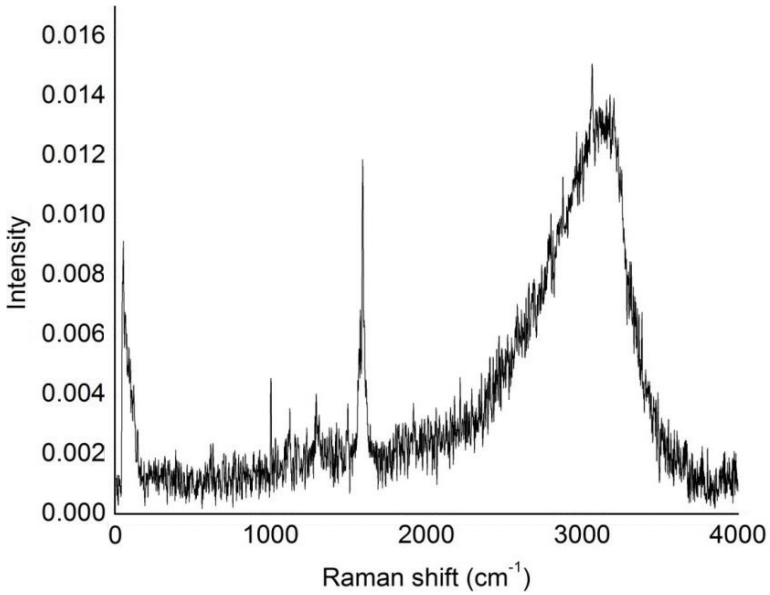

Fig. 13. FT-Raman spectrum of H_2L'.

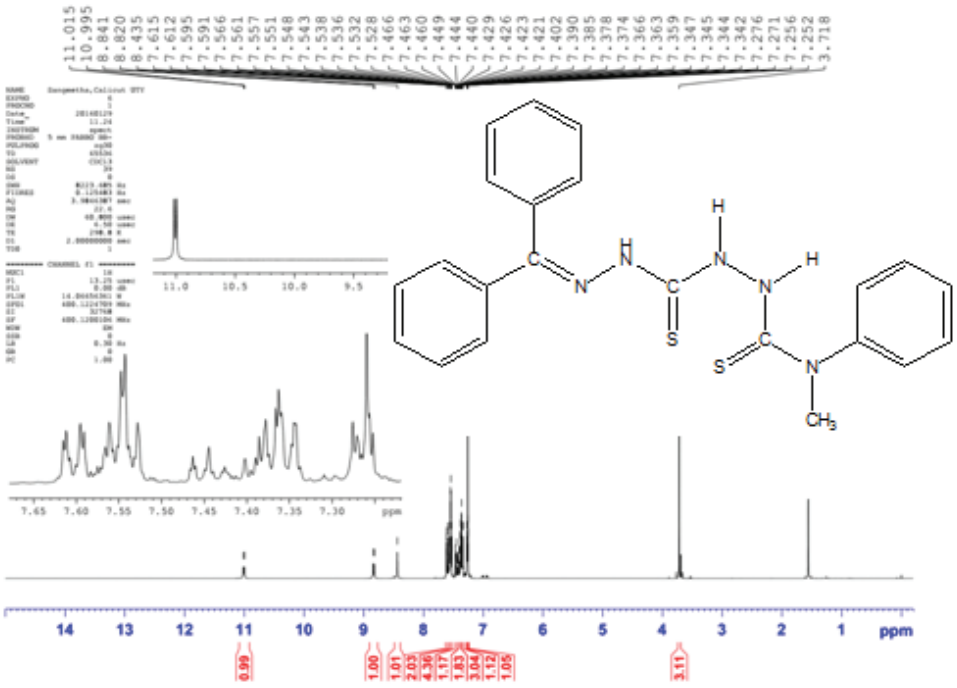

Fig. 14. NMR spectrum of H_2L'.

(c) ^{1}H NMR spectrum

The ^{1}H NMR spectrum of the ligand H_2L' was recorded in $CDCl_3$ (Fig. 14). A sharp singlet observed at 3.718 ppm corresponds to N–CH_3 protons. The multiplet at 7.615–7.252 ppm is assigned to aromatic protons. A singlet at 8.44 ppm may be due to the NH proton adjacent to azomethine group. The NH proton adjacent to NH group gives doublet at 8.82–8.84 ppm. The doublet at 10.96–11.02 ppm has been assigned to NH proton.

3.2. Characterisation of the metal complexes of H_2L'

3.2.1. Formulae and general properties of the complexes

On the basis of elemental analyses and spectral studies, the complexes were assigned empirical formulae as presented in the Table 5. In the complexes **(1), (6), (8), (9), (10), (11)** and **(13)**, the ligand acted as mono-anionic tridentate (HL'^{-}) whereas in complexes **(2), (3), (4), (5), (7)** and **(12)**, it acted as neutral bidendate (H_2L').

3.2.2. Electronic spectra and magnetic moments

The electronic spectra of the complexes were recorded in solid state and their probable assignments are given in Table 6.

Mn(II) belongs to d^5 system. The ground state of high-spin octahedral Mn(II) complex is $^6A_{1g}$. In such cases, electronic transitions are both Laporte and spin forbidden.[19,20] However, some forbidden transitions occur and consequently, they have extremely low molar extinction coefficient values. In this case, a broad band at 435 nm may be due to $^6A_{1g} \rightarrow {}^4T_{2g}(G)$ transition. The magnetic moment observed for the complex **(1)** is 5.5 BM.

The ground state in tetrahedral Co(II) is $^4A_2$. The possible transitions are $^4A_2 \rightarrow {}^4T_2$, $^4A_2 \rightarrow {}^4T_1$ (F) and $^4A_2 \rightarrow {}^4T_1$ (P). The first transition, $^4A_2 \rightarrow {}^4T_2$ is not usually observed since it occurs in the region, 3000–5000 cm^{-1}. $^4A_2 \rightarrow {}^4T_1$ (P) transition appears as an intense broad band in the visible region. Co(II) ions in a tetrahedral geometry show an intense $^4A_2 \rightarrow {}^4T_1$ (P) absorption band at 666 nm with fine splitting due to spin-orbit coupling.[21] This band is useful in differentiating tetrahedral and octahedral geometries of Co(II) ions.

In this study, Co(II) complexes **(2)**, **(3)** and **(4)** show bands in the region 635–687 nm due to $^4A_2 \rightarrow {}^4T_1$ (P) transition. However, the other bands are not observed as they may be out of the range of the spectrophotometer used.

Tetrahedral Co(II) complexes show magnetic moments around 3.9 BM corresponding to the spin only value for three unpaired electrons. In this investigation, the observed magnetic moment of the Co(II) complexes **(2)**, **(3)** and **(4)** are between 3.7 and 4.1 BM which indicate their tetrahedral geometry.

The ground state for regular tetrahedral Ni(II) ion is $^3T_1(F)$. Tetrahedral Ni(II) complexes show two broad bands in the visible region. One at 666 nm due to $^3T_1(F) \rightarrow {}^3T_1(P)$ transition and another one at 1250 nm due to $^3T_1(F) \rightarrow {}^3A_2(F)$ transition. In this study, the complex **(5)** showed a band at 751 nm and the complex **(7)** showed a band at 678 nm due to $^3T_1(F) \rightarrow {}^3T_1(P)$ transition. However, the other transition is not observed as it is out of the range of the used spectrophotometer. Tetrahedral complexes are expected to have orbital contribution to the magnetic moment. The spin-orbit coupling also allows the $^3T_2(F)$ term to mix with the ground state. Normally, they show magnetic moments in the range 3.6–4.10 BM In certain cases, effective magnetic moment is found to be as low as 3.20 BM. This may be due to the distortions and inequalities in the field of coordinated ligands which give only small orbital contribution. In this case, the complex **(5)** showed a magnetic moment 2.07 BM whereas the magnetic moment of complex **(7)** was 3.20 BM.

Octahedral Ni(II) ion with d^8 configuration has $^3A_{2g}$ ground state. The three, spin-allowed transitions are, $^3A_{2g}(F) \rightarrow {}^3T_{2g}(F)$, $^3A_{2g}(F) \rightarrow {}^3T_{1g}(F)$ and $^3A_{2g}(F) \rightarrow {}^3T_{1g}(P)$ which absorb in

Table 5. Molecular formulae, colours, partial elemental analyses data and magnetic moments of the complexes

Compound No.	Compound	Molecular Weight	Melting point	Colour	Yield	Elemental Analysis Found(calculated)					μ in BM
						C	H	N	S	M	
H_2L'	$C_{22}H_{21}N_5S_2$	419	160	Cream	85	63.4 (63.0)	5.2 (5.0)	16.5 (16.7)	15.0 (15.2)	–	D
1	$[Mn(HL')_2]\ H_2O$	911	182	Orange crystals	75	57.9 (57.9)	4.1 (4.2)	15.6 (15.4)	14.0 (14.1)	6.0 (6.0)	5.5
2	$[Co(H_2L')(CH_3COO)_2]\ 2H_2O$	631.9	225	Green	80	49.3 (49.4)	4.6 (4.7)	11.2 (11.1)	10.2 (10.1)	9.1 (9.3)	3.7
3	$[Co(H_2L')_2]Cl_2$	968	230	Reddish orange	80	54.6 (54.6)	4.4 (4.5)	14.5 (14.5)	13.0 (13.2)	6.1 (6.1)	3.7
4	$[Co(H_2L')_2](NO_3)_2$	1021	215	Magenta	80	51.8 (51.7)	4.2 (4.1)	16.4 (16.4)	12.6 (12.5)	5.8 (5.8)	4.1
5	$[Ni(H_2L')(CH_3COO)_2]$	596	180	Green	75	52.1 (52.3)	4.4 (4.5)	12.0 (11.8)	10.9 (10.7)	10.1 (9.9)	2.1
6	$[Ni(H_2L')_2]\ 1.5H_2O$	923	220	Brown crystals	65	56.6 (56.8)	4.4 (4.6)	15.1 (15.2)	13.6 (13.8)	6.4 (6.4)	3.0
7	$[Ni(H_2L')_2]SO_4$	993	200	Brown	65	53.5 (53.5)	4.1 (4.2)	14.1 (14.1)	15.9 (16.1)	6.1 (5.9)	3.2
8	$[Cu(HL')]_2$	965	220	Black	80	54.7 (54.7)	3.8 (3.9)	14.6 (14.5)	13.4 (13.3)	13.0 (13.1)	1.5
9	$[Cu(HL')Cl]_2\ 4H_2O$	1180	160	Green	80	44.9 (44.7)	3.9 (4.1)	12.1 (11.8)	10.7 (10.8)	10.5 (10.7)	D
10	$[Cu(HL')NO_3]_2\ 2H_2O$	1143	199	orange	80	46.0 (46.1)	3.9 (3.8)	14.5 (14.6)	11.2 (11.3)	10.9 (11.1)	D
11	$[(Cu(HL')H_2O)_2SO_4]$	1079	170	Green	80	48.0 (48.1)	3.7 (4.0)	12.9 (12.7)	14.6 (14.5)	11.8 (11.5)	D
12	$[Zn(H_2L')(CH_3COO)_2]\ 2H_2O$	638	>280	Yellow	70	48.8 (48.9)	4.8 (4.9)	11.1 (10.9)	10.4 (10.3)	10.5 (10.4)	D
13	$[Zn(HL')_2]$	903	199	Light yellow	70	58.8 (58.5)	4.6 (4.7)	15.6 (15.5)	14.2 (14.2)	7.4 (7.2)	D

Table 6. Electronic spectral band and their assignments

Compound No.	Compound	λ nm	λ cm^{-1}	Assignments
H_2L'	$C_{22}H_{21}N_5S_2$	254	39370	$\pi\rightarrow\pi^*$
		344	29070	$n\rightarrow\pi^*$
1	$[Mn(HL')_2\ H_2O$	247	40486	$n\rightarrow\pi^*$
		321	31153	$n\rightarrow\pi^*$
		435br	22989	$^6A_{1g}\rightarrow{}^4T_{2g}(G)$
2	$[Co(H_2L')(CH_3COO)_2]\ 2H_2O$	423br	23641	C–T
		634br	15773	$^4A_2\rightarrow{}^4T_1(P)$
3	$[Co(H_2L')_2]\ Cl_2$	240	41667	$\pi\rightarrow\pi^*$
		311	32154	$n\rightarrow\pi^*$
		471	21231	C–T
		685	14598	$^4A_2\rightarrow{}^4T_1(P)$
4	$[Co(H_2L')_2]\ (NO_3)_2$	249	40161	$\pi\rightarrow\pi^*$
		321	31153	$n\rightarrow\pi^*$
		497	20121	C–T
		687	14556	$^4A_2\rightarrow{}^4T_1(P)$
5	$[Ni(H_2L')(CH_3COO)_2]$	316	31647	$\pi\rightarrow\pi^*$
		356	28090	$n\rightarrow\pi^*$
		399	25063	$^3A_{2g}(F)\rightarrow{}^3T_{1g}(P)$
		751br	13316	$^3A_{2g}(F)\rightarrow{}^3T_{2g}(F)$
6	$[Ni(HL')_2]\ 1.5H_2O$	416	24038	$^3A_{2g}(F)\rightarrow{}^3T_{1g}(P)$
		687br	14556	$^3A_{2g}(F)\rightarrow{}^3T_{2g}(F)$
7	$[Ni(H_2L')_2]\ SO_4$	308	32468	$n\rightarrow\pi^*$
		678	14749	$^3T_1(F)\rightarrow{}^3T_1(P)$
8	$[Cu(HL')]_2$	252	39683	$\pi\rightarrow\pi^*$
		311	32154	$\pi\rightarrow\pi^*$
		349	28653	$n\rightarrow\pi^*$
		428	23364	C–T
9	$[Cu(HL')Cl]_2\ 4H_2O$	261	38315	$\pi\rightarrow\pi^*$
		328	30488	$n\rightarrow\pi^*$
		402	24875	C–T
10	$[Cu(HL')NO_3]_2\ 2H_2O$	306	32680	$\pi\rightarrow\pi^*$
		449	222721	C–T
11	$[(Cu(HL')H_2O)_2SO_4]$	256	39063	$\pi\rightarrow\pi^*$
		313	31949	$n\rightarrow\pi^*$
		425	23529	$^2B_{1g}\rightarrow{}^2E_g$
		878	11389	$^2B_{1g}\rightarrow{}^2A_{1g}$
12	$[Zn(H_2L')(CH_3COO)_2]\ H_2O$	249	40161	$\pi\rightarrow\pi^*$
		302	33153	$n\rightarrow\pi^*$
		382	26178	C–T
13	$[Zn(HL')_2]$	250	40000	$\pi\rightarrow\pi^*$
		308	32467	$n\rightarrow\pi^*$

Broad = br

the range 8000–11000, 15000–19000 and 25000–29000 cm^{-1}, respectively. The broad bands observed at 687 and 416 nm in the spectrum of the complex **(6)** are due to $^3A_{2g}(F) \rightarrow {}^3T_{1g}(F)$ and $^3A_{2g}(F) \rightarrow {}^3T_{1g}(P)$ transitions, respectively. The magnetic moments of octahedral Ni(II) complexes fall in the range 2.90–3.30 BM. which is due to spin-orbit coupling or higher states mixing with the ground states[22]. In this investigation, the observed magnetic moment of the Ni(II) complex **(6)** is 3.0 BM which indicates octahedral geometry.

The tetrahedral and pseudo-tetrahedral Cu(II) complexes usually show transitions in the range 1400–1000 nm and the energy of these bands are very low compared to square planar or distorted octahedral complexes. Square planar or distorted octahedral complexes normally show absorptions in the region 1000–500 nm. If this region is blank, we can infer a tetrahedral geometry to such Cu(II) complexes. In this investigation, no bands are observed in the region mentioned above for the Cu(II) complexes **(8), (9)** and **(10)** which confirms their tetrahedral geometry. The complex, **(11)** showed a band at 878 nm, which indicates its octahedral or square planar geometry.

The compound **(8)** shows a magnetic moment 1.5 BM. The compounds **(9)**, **(10)** and **(11)** are diamagnetic. The low magnetic moment values as well as diamagnetic nature of the Cu(II) complexes may be due to anti-ferromagnetic interactions between neighbouring copper ions.[23] These observations pinpoint the dimeric nature of the Cu(II) complexes.[24]

As expected, no characteristic absorption bands are observed in the visible region of the Zn(II) complexes and are diamagnetic in nature. Representative spectra of the complexes **(3), (6)** and **(8)** are presented in Fig. 15.

3.2.3. Vibrational spectra

The IR spectral assignments are depicted in the Table 7. In the spectra of the complexes, N–H bands show a slight shift to lower frequencies. The band at 1583 cm^{-1} in the spectrum of the free ligand is assigned to ν(C=N). However, in the spectra of the complexes this band is shifted to higher (2–27 cm^{-1}) or lower (5 cm^{-1}) wave numbers indicating the participation of azomethine nitrogen in coordination.[25] The new bands in the spectra of the complexes in the region 440–478 cm^{-1} are assigned to (M–N) stretching vibration.[26,27] The bands appearing in the regions, 1490–1440, 1100–1064 and 805–740 cm^{-1} are usual modes of phenyl ring vibrations.[28] The ligand can exhibit thione–thiol tautomerism since it contains two thioamido –NH–C=S functional groups. ν(S–H) band (at 2560 cm^{-1}) is absent in the IR spectrum of ligand,[29] but *ν*(N–H) band is present at 3260–3057 cm^{-1}, indicating that in solid state, the ligand remains as the thione tautomer.[30,31] The appearance of broad bands around 3400 cm^{-1} in the spectra of the complexes may be due to ν(OH) of the water molecules.[32,33] The bands near 1340 and 771 cm^{-1} in the spectrum of the free ligand may be assigned to ν(NH–C=S) and *ν*(C=S). These bands are seen to be shifted to lower or higher wave numbers in the spectra of the complexes, indicating the involvement of sulphur in coordination. We can thus conclude that the ligand can act as bidentate/tridentate/tetradentate one coordinating through azomethine nitrogens and two thione/thiolato sulphur. According to Stefov *et al*[34], coordinated water should exhibit bands at 825, 575 and 500 cm^{-1}.

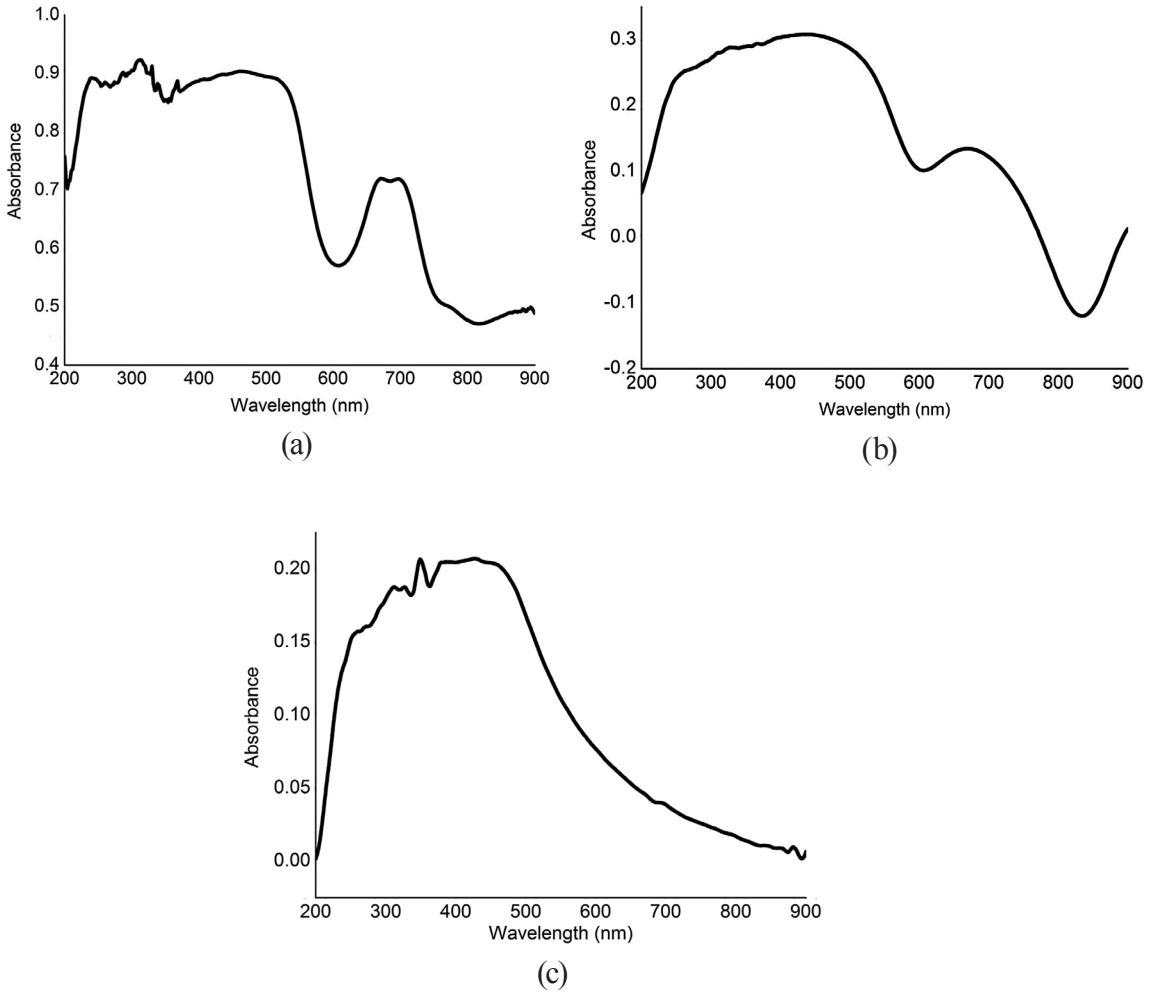

Fig. 15. Electronic spectra of the complexes (a) $[Co(H_2L')_2]Cl_2$ (**3**), (b) $[Ni(HL')_2]$ $1.5H_2O$ (**6**) and (c) $[Cu(HL')]_2$ (**8**).

3.2.3.1. Coordination of anions

The $\nu_{as}(COO^-)$ and $\nu_s(COO^-)$ of the free acetate ions are observed at 1560 and 1416 cm^{-1}, respectively.[35] For the coordinated acetate ion, $\nu_{as}(COO^-)$ occurs in the range 1650–1500 cm^{-1} and $\nu_s(COO^-)$ is seen above 1400 cm^{-1}. In unidendate complexes, the energy of separation between these two bands is generally greater than 144 cm^{-1}.[36] The $\nu_{as}(COO^-)$ and $\nu_s(COO^-)$ are at 1632 and 1440 cm^{-1} for the complex **(2)** and at 1551 and 1441 cm^{-1} for the complex **(5)**.[37] For the complex **(12)** $\nu_{as}(COO^-)$ and $\nu_s(COO^-)$ are at 1655 and 1441 cm^{-1}. These bands indicate unidentate coordination of acetate group in complexes. IR spectra of the complexes **(3)**, **(6)** and **(8)** are presented in Fig. 16.

Table 7. IR spectral assignments

Complex No:	Compound	ν(N–H)/OH	ν(C–H)	ν(C=N)	ν(Phenyl/CN–NH)	ν(NH–CS)	ν(C=S)	ν(N–N)	νC=S	ν(M–N)
	$C_{22}H_{21}N_5S_2$	3444 3249	3165 2920	1583	1468	1332	1269	1060	770	–
1	$[Mn(HL')_2]\ H_2O$	3313 3125	3057 2940	1590	1486	1354	1215	1056	770	472
2	$[Co(HL')CH_3COO)_2]\ 2H_2O$	3414	3046 2924	1599	1492	1405	1231	1045	764	478
3	$[Co(H_2L')_2]Cl_2$	3426	3134 2924	1590	1489	1383	1215	1059	768	475
4	$[Co(H_2L')_2](NO_3)_2$	3401 3131	3059 2920	1591	1486	1357	1214	1058	766	475
5	$[Ni(HL')(CH_3COO)_2]$	3426	3059 2924	1599	1494	1328	1226	1072	770	483
6	$[Ni(HL')_2]\ 1.5H_2O$	3363 3133	3057 2920	1555	1488	1361	1223	1065	770	469
7	$[Ni(H_2L')]\ _2SO_4$	3438 3138	3059 2920	1586	1492	1352	1230	1060	770	468
8	$[Cu(HL')_2]_2$	3430	3057 2923	1596	1492	1386	1277	1051	755	473
9	$[Cu(HL')Cl]_2\ 4H_2O$	3439 3260	3057 2924	1552	1489	1381	1277	1071	770	440
10	$[Cu(HL')NO_3]_2\ 2H_2O$	3438 3231	2923	1596	1494	1356	1273	1039	770	453
11	$[(Cu(HL')H_2O)_2SO_4]$	3437 3205	2924	1596	1492	1359	1265	1045	770	472
12	$[Zn(H_2L')(CH_3COO)_2]\ 2H_2O$	3438 3353	3059 2920	1591 1542	1482	1333	1216	1031	770	462
13	$[Zn(HL')_2]$	3413 3317	3057 2924	1586 1545	1489	1368	1218	1058	770	445

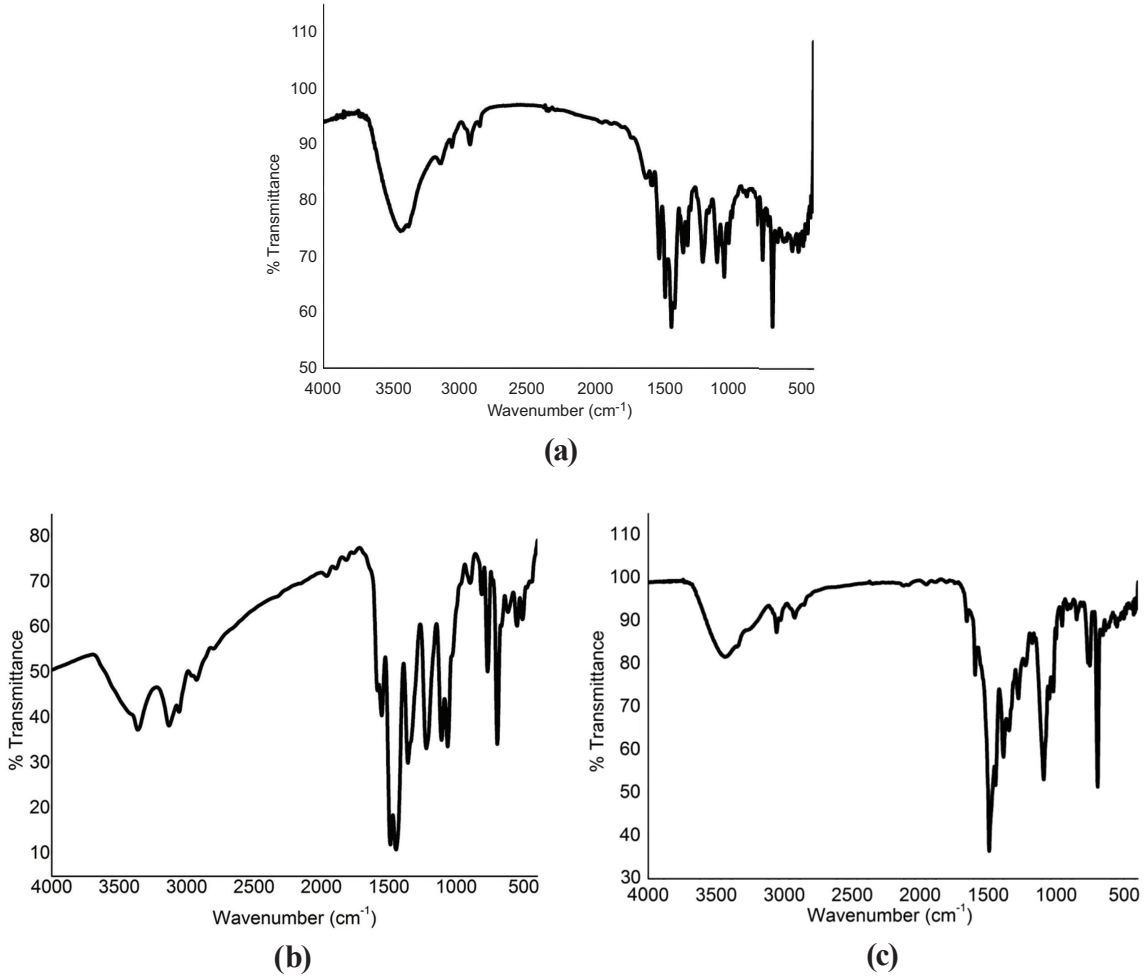

Fig. 16. IR spectra of the complexes (a) $[Co(H_2L')_2]$ Cl_2 (**3**), (b) $[Ni(HL')_2]$ H_2O (**6**), (c) $[Cu(HL')_2]$ (**8**).

3.2.4. ^{1}H NMR spectra

The ^{1}H NMR spectra of Zn(II) complexes were recorded in DMSO.

(a) NMR Spectrum of $[Zn(H_2L')(CH_3COO)_2]2H_2O$ (12)

Doublets at 10.11 and 9.9 ppm correspond to NH protons. A singlet at 9.73 ppm is attributed to N–H proton adjacent to azomethine group. Aromatic protons show multiplet signals in the range 6.92–7.76 ppm. Sharp singlets observed at 2.75–3.11 ppm correspond to N–CH_3 protons. Singlet observed at 2.2–2.42 ppm may be due to CH_3 protons of acetate group. Singlet at 2.5 ppm is attributed to DMSO protons. Slight difference in the peak position of protons in comparison with the ligand may be due to the difference in the solvent used for recording the ^{1}H NMR spectrum of the complex. Fig. 17 presents the ^{1}H NMR spectrum of $[Zn(H_2L')(CH_3COO)_2]2H_2O$ **(12)**.

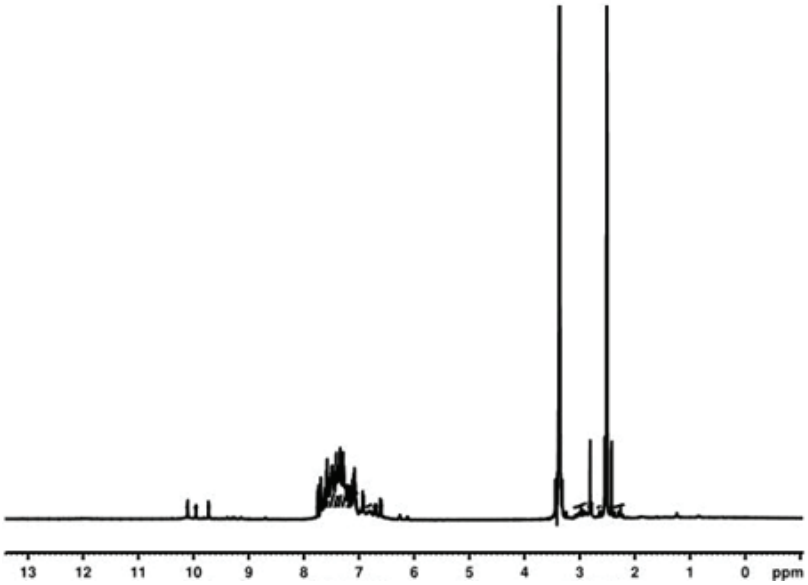

Fig. 17. ^{1}H NMR Spectrum of $Zn(H_2L')(CH_3COO)_2 2H_2O$ **(12)**.

(b) ^{1}H NMR Spectrum of $[Zn(HL')_2]$ (13)

A singlet at 9.567 ppm is attributed to N–H proton. Singlet peak at 8.597 ppm may be assigned to N–H proton adjacent to azomethine group. Aromatic protons show multiplets in the range 7.04–7.61 ppm. Singlet peak in the range 3.34–3.55 ppm is attributed to $N–CH_3$ protons. Singlet peak at 2.499 ppm is attributed DMSO protons. Fig. 18 represents the ^{1}H NMR spectrum of $[Zn(HL')_2]$ (**13)**.

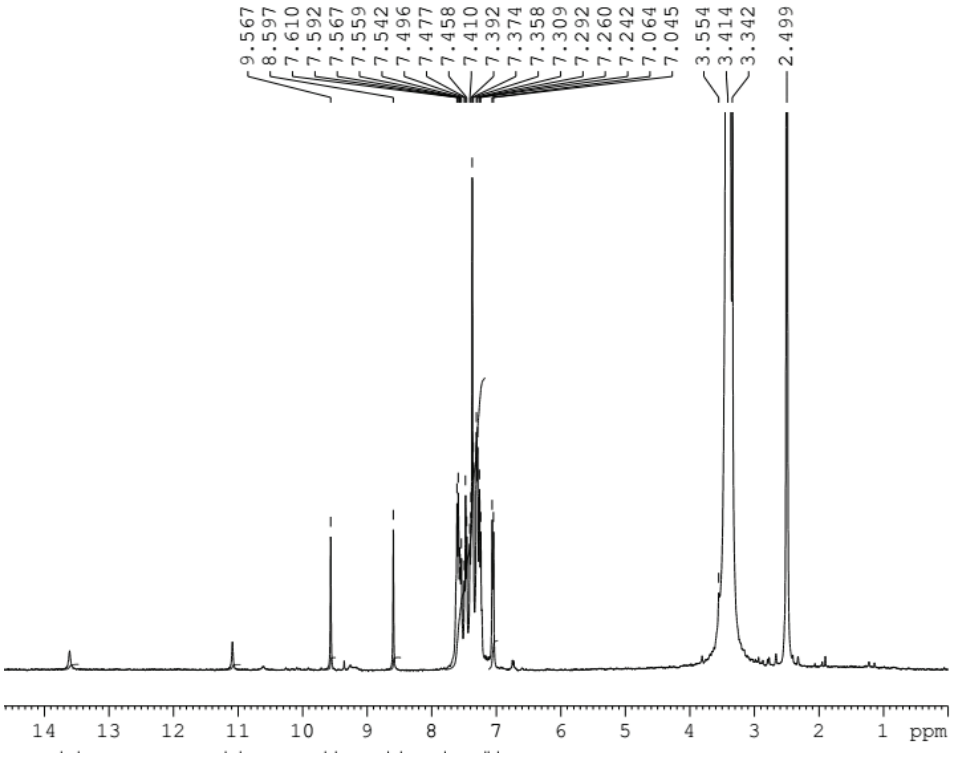

Fig. 18. ^{1}H NMR Spectrum of $[Zn(HL')_2]$ **(13)**.

3.2.5. ESR spectrum

The X band ESR spectrum was recorded in dimethylformamide at 77K (Fig. 19). Mn^{2+} (d^5) being an odd electron system, the zero-field splitting produces three doubly degenerate spin states, *Ms* = 5/2, 3/2, 1/2 (Kramers' degeneracy). Each of them splits into two singlets by the applied field, producing six levels. Therefore, the spectrum of the complex exhibits a six line hyperfine pattern centred at $g = 2.001$ which is expected for an odd unpaired electron system ($S = \pm 5/2$), $Ms = \pm 5/2, \pm 3/2, \pm 1/2$ and $I = 5/2$, $MI = \pm 5/2, \pm 3/2, \pm 1/2$, with *g* and *A* tensors isotropic, resulting from allowed transitions. The spectrum also gives three super-hyperfine lines which arise from the coupling of the electron spin with nuclear spin of nitrogen atom which is coplanar. This indicates that in this complex azomethine nitrogen atom has coordinated to the Mn^{2+}.

3.3. Thermal studies

For $[Mn(HL')_2]H_2O$, the decomposition occurred in four stages and is evident from the derivative thermogravimetry (TG-DTG) peaks at 194, 205, 256 and 281°C. TG-DTG curve of $Mn(HL')_2H_2O$ is shown in Fig. 20. The first stage is at 97.5°C–100°C and demonstrates a mass loss of 2.2%, corresponding to the loss of H_2O (calc. 2%). The second stage occurred at 237°C–198°C, with a mass loss of 21.1%. The next stage decomposition occurred at 237°C–490°C, with a mass loss of 69.9%. The residual mass of 7.8 % was observed at 540°C and may be due to the formation of manganese oxide (calc. 7.76%).

For $[Ni(HL')_2]1.5H_2O$, two stages of decomposition occurred and are evident from the DTG peaks at 200°C and 290°C. The first stage is at 150°C–230°C and demonstrates a

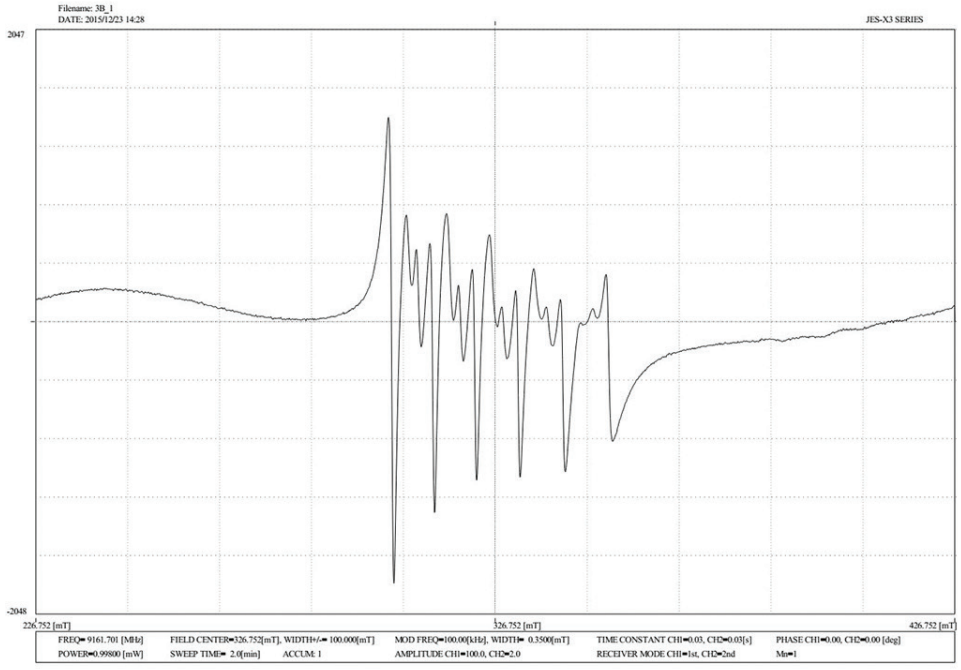

Fig. 19. The X band ESR spectrum of $[Mn(HL')_2H_2O]$ in DMF at 77K.

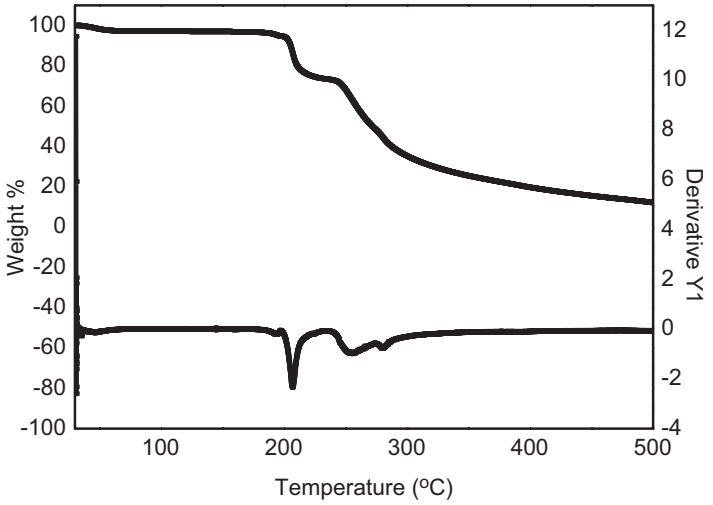

Fig. 20. TG-DTG curve of $[Mn(HL')_2H_2O]$ **(1).**

mass loss of 2%, corresponding to the loss of H_2O (calc. 1.96%). The second stage occurred at 250°C–600°C, with a mass loss of 81%. The residual mass of 11.8% was observed at 750°C and may be due to the formation of nickel sulphide (calc. 11.6%).

For $[(CuHL')_2]$, two-stage decomposition occurs in the temperature range 260°C–590°C which may be due to the partial decomposition of the ligand moiety. The residual mass of 15% was observed at 750°C which may be due to the formation of Cu_2S (calc. 14.8%). For $[Zn(HL')_2]$, three stages of decomposition occurred in the temperature range 240°C–610°C which may be due to the decomposition of the ligand moiety. The residual mass of 9.3% was observed at 750°C which may be due to the formation of ZnO (calc. 9.0%).

3.4. X-ray crystal structure studies

X-ray crystallographic data were collected at 273(2) K for $[Mn(HL)_2]H_2O$ and $Ni(HL')_2$ $1.5H_2O$ on a Bruker Model Kappa Apex II diffractometer with graphite monochromatic *Mo Kα* (λ = 0.71073 Å) radiation. Direct methods were performed to solve the structure and refined by least-square on F^2 using SHELXL-2014/7.[38] All non-hydrogen atoms were refined anisotropically. All hydrogen atoms, except those attached to nitrogen were geometrically fixed at calculated positions. The crystallographic tools, PLATON for Windows,[9] DIAMOND 3.2d,[10] and MERCURY 3.5.1[11] were used for structure analysis and presentation of the results. The structures were finally refined to the conventional *R*-value 0.1676 for Mn(II) and 0.0641 for Ni(II) complex.

3.4.1. Single-crystal XRD studies of Mn(II) complex

Single crystals of $Mn(HL')_2H_2O$ suitable for X-ray analysis were obtained from its solution in 1:1 (v/v) mixture of methanol and DMF. A crystal with dimension, 0.600 × 0.510 × 0.420 mm^3 was selected for collecting the data. $Mn(HL')_2H_2O$ crystallizes with two molecules per asymmetric unit into triclinic crystal system with a space group of *P*−1.

The molecular structure of the Mn(II) complex with atom numbering scheme is depicted in Fig. 21. Crystal data and structure refinement parameters of the complex are given in Table 8. Selected bond lengths and bond angles are summarized in Table 9. The important hydrogen bonding interaction parameters are listed in Table 10. Fig. 22 shows the packing diagram of $Mn(HL')_2H_2O$ along the *b*-axis showing intermolecular interactions. Fig. 23 shows supramolecular chain interlinked with water molecule along *c*-axis.

The X-ray structural analysis of the compound reveals that the Mn(II) ion isoctahedrally bonded to N(3), N(1), S(2), N(6), N(8) and S(4) atoms belonging to the two units of the deprotonated ligand. One half of the molecule of the complex is related to the other half by a two-fold axis passing through Mn atom. It is coordinated through the azomethine N, hydrazine N and the thione S atom of the two deprotonated ligands in a meridonal fashion. The metal center is shared by four fused five-membered chelate rings. An interesting attribute of the crystal packing is the formation of a supramolecular chain interlinked by water molecule. In the crystal, the molecules are interconnected by N–H···S, N–H···O and C–H–S interactions, forming a three-dimensional network. It is clear from the Table 10 that coordination shortens the C(7)–N(1) to 1.292(16) and C(14)–N(3) 1.305(18) Å when compared to C–N bonds which is not involved in coordination. Relatively larger bond lengths Mn(1)–N(8) 2.090(11); Mn(1)–N(3) 2.101(10); Mn(1)–N(1) 2.422(12); Mn(1)–N(6) 2.465(12); Mn(1)–S(4) 2.571(5) and Mn(1)–S(2), 2.587(5) Å indicates weak coordination of the ligand with Mn(II). The bond angles, N(6)–Mn(1)–S(4) 148.2(3); N(8)–Mn(1)–S(2) 106.6(3); N(3)–Mn(1)–S(2) 77.7(3); N(6)–Mn(1)–S(2) 85.4(3); S(4)–Mn(1)–S(2) 102.44(17);

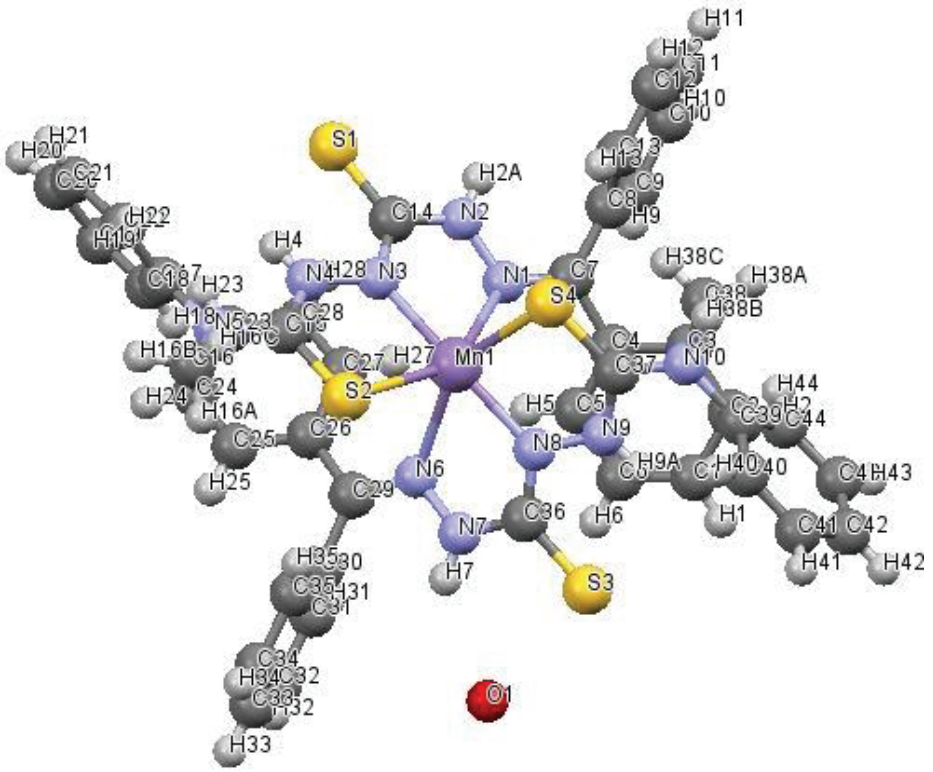

Fig. 21. The molecular structure of the $[Mn(HL')_2]H_2O$ with atom numbering scheme.

Table 8. Crystal data and structure refinement for $[Mn(HL')_2]H_2O$

Identification code	$[Mn(HL')_2]H_2O$		
Empirical formula	$C_{44}\ H_{38}\ Mn\ N_{10}\ O\ S_4$	Index ranges	$-13 \le h \le 13$, $-16 \le k \le 16$, $-18 \le l \le 18$
Formula weight	906.02	Reflections collected	76164
Temperature (K)	273(2)	Independent reflections	8040 [R(int) = 0.1674]
Wavelength (Å)	0.71073	Completeness to theta = 25.242°	97.40%
Crystal system	Triclinic	Absorption correction	Semi-empirical from equivalents
Space group	$P-1$	Max. and min. Transmission	0.80 and 0.71
Unit cell dimensions	a (Å) = 11.4002(9)	Refinement method	Full-matrix least-squares on F^2
	a(°) = 75.840(4)		
	b (Å) = 13.5853(12)	Data/restraints/ parameters	8040/4/490
	b(°) = 73.614(4).		
	c (Å) = 15.8787(15)	Goodness-of-fit on F^2	1.108
	g(°) = 82.609(4)		
Volume (Å^3)	2282.9(4)	Final R indices [$I > 2$ sigma(I)]	$R1$ = 0.1676,
			w$R2$ = 0.4279
Z	2	R indices (all data)	$R1$ = 0.2185,
			w$R2$ = 0.4550
ρ (calculated) mg/m^3	1.318	Extinction coefficient	0.009(2)
Absorption coefficient (mm^{-1})	0.517	Largest diff. peak and hole (e.Å^{-3})	2.028 and −0.774
F(000)	938		
Crystal size (mm^3)	0.600 × 0.510 × 0.420		
Theta range for data collection	1.830°–25.000°.		

Table 9. Selected bond lengths (Å) and bond angles and torsion angles (°)

Bond lengths (Å)		**Continuation of Bond angles (°)**		**Continuation of Torsion angles (°)**	
C(7)–N(1)	1.292(16)	C(7)–N(1)–Mn(1)	129.3(10)	S(3)–C(36)–N(8)–N(9)	0(2)
C(14)–N(3)	1.305(18)	N(2)–N(1)–Mn(1)	106.7(8)	N(10)–C(37)–N(9)–N(8)	178(1)
C(14)–N(2)	1.363(17)	N(1)–N(2)–C(14)	121.2(12)	N(9)–C(37)–S(4)–Mn(1)	−8(1)
C(14)–S(1)	1.693(14)	N(1)–N(2)–H(2A)	119.4	N(10)–C(37)–S(4)–Mn(1)	173(1)
C(15)–N(5)	1.340(16)	C(14)–N(2)–H(2A)	119.4	N(3)–Mn(1)–N(1)–C(7)	166(1)
C(15)–N(4)	1.344(17)	C(14)–N(3)–N(4)	113.5(10)	N(3)–Mn(1)–N(1)–N(2)	14.4(9)
C(15)–S(2)	1.694(13)	C(14)–N(3)–Mn(1)	125.2(9)	N(6)–Mn(1)–N(1)–C(7)	−89(1)
C(16)–N(5)	1.45(2)	N(4)–N(3)–Mn(1)	121.3(8)	N(6)–Mn(1)–N(1)–N(2)	119.5(9)
C(17)–N(5)	1.440(19)	C(15)–N(4)–N(3)	122.2(11)	N(8)–Mn(1)–N(1)–C(7)	−16(1)
C(29)–N(6)	1.316(17)	C(15)–N(5)–C(17)	120.3(12)	N(8)–Mn(1)–N(1)–N(2)	−167.9(9)
C(36)–N(8)	1.298(17)	C(15)–N(5)–C(16)	120.2(13)	S(2)–Mn(1)–N(1)–C(7)	168(1)
C(36)–N(7)	1.370(18)	C(17)–N(5)–C(16)	118.8(12)	N(8)–Mn(1)–S(2)–C(15)	−170.8(6)

C(36)–S(3)	1.702(13)	C(29)–N(6)–N(7)	116.7(12)	S(4)–Mn(1)–S(2)–C(15)	107.9(5)
C(37)–N(9)	1.325(18)	C(29)–N(6)–Mn(1)	131.8(9)	N(1)–Mn(1)–S(4)–C(37)	–97.8(6)
C(37)–N(10)	1.357(17)	N(7)–N(6)–Mn(1)	105.5(8)	N(3)–Mn(1)–S(4)–C(37)	–166.1(6)
C(37)-S(4)	1.708(14)	N(6)–N(7)–C(36)	120.6(12)	N(6)–Mn(1)–S(4)–C(37)	12.3(8)
C(38)–N(10)	1.44(2)	C(36)–N(8)–N(9)	114.1(10)	N(8)–Mn(1)–S(4)–C(37)	9.1(6)
C(39)–N(10)	1.424(18)	C(36)–N(8)–Mn(1)	125.3(9)	S(2)–Mn(1)–S(4)–C(37)	113.8(5)
Mn(1)–N(8)	2.090(11)	N(9)–N(8)–Mn(1)	120.6(8)	C(7)–N(1)–N(2)–C(14)	–176(1)
Mn(1)–N(3)	2.101(10)	C(37)–N(9)–N(8)	121.6(11)	Mn(1)–N(1)–N(2)–C(14)	–20(2)
Mn(1)–N(1)	2.422(12)	C(37)–N(10)–C(39)	121.5(12)	C(14)–N(1)–N(3)–N(4)–C(15)	–172(1)
Mn(1)–N(6)	2.465(12)	C(37)–N(10)–C(38)	121.9(13)	Mn(1)–N(3)–N(4)–C(15)	9(2)
Mn(1)–S(4)	2.571(5)	C(39)–N(10)–C(38)	116.4(12)	Mn(1)–N(6)–N(7)–C(36)	–20(2)
Mn(1)–S(2)	2.587(5)	C(15)–S(2)–Mn(1)	97.0(5)	Mn(1)–N(8)–N(9)–C(37)	12(2)
N(1)–N(2)	1.356(16)	C(37)–S(4)–Mn(1)	96.0(5)	N(1)–Mn(1)–N(8)–N(9)	71(1)
N(2)–H(2A)	0.86	**Torsion angles (°)**		N(3)–Mn(1)–N(8)–C(36)	–85(6)
N(3)–N(4)	1.379(14)	N(8)–Mn(1)–N(6)–N(7)	15.6(9)	N(3)–Mn(1)–N(8)–N(9)	97(6)
N(4)–H(4)	0.86	S(2)–Mn(1)–N(6)–C(29)	57(1)	N(6)–Mn(1)–N(8)–C(36)	–12(1)
N(6)–N(7)	1.368(16)	S(2)–Mn(1)–N(6)–N(7)	–94.0(9)	N(6)–Mn(1)–N(8)–N(9)	170(1)
N(7)–H(7)	0.86	S(4)–Mn(1)–N(6)–C(29)	163(1)	S(2)–Mn(1–N(8)–C(36)	66(1)
N(8)-N(9)	1.391(15)	S(4)–Mn(1)–N(6)–N(7)	12(1)	S(2)–Mn(1)–N(8)–C(36)	–111.8(9)
N(9)–H(9A)	0.86	N(1)–Mn(1)–N(8)–C(36)	–111(1)	S(4)–Mn(1)–N(8)–C(36)	166(1)
Bond angles (°)		N(1)–Mn(1)–N(6)–N(7)	117.7(9)	S(4)–Mn(1)–N(8)–N(9)	–12.2(9)
N(1)–C(7)–C(8)	123.9(13)	N(3)–Mn(1)–N(6)–C(29)	–19(1)	N(1)–Mn(1)–S(2)–C(15)	5.0(8)
N(1)–C(7)–C(4)	117.5(13)	N(3)–Mn(1)–N(6)–N(7)	–169.3(9)	N(3)–Mn(1)–S(2–C(15)	6.8(6)
N(3)–C(14)–N(2)	113.6(12)	S(3)–C(36)–N(8)–Mn(1)	–178.1(8)	N(6)–Mn(1)–S(2)–C(15)	–103.4(6)
N(3)–C(14)–S(1)	126.3(10)	C(4)–C(7)–N(1)–N(2)	–170(1)	S(2)–C(15)–N(4)–N(5)	0(2)
N(2)–C(14)–S(1)	120.2(11)	C(8)–C(7)–N(1)–Mn(1)	–138(1)	N(4)–C(15)–N(5)–C(16)	–161(1)
N(5)–C(15)–N(4)	117.0(12)	C(8)–C(7)–N(1)–N(2)	11(2)	N(4)–C(15)–N(5)–C(17)	8(2)
N(5)–C(15)–S(2)	122.0(11)	S(1)–C(14)–N(2)–N(1)	–167(1)	S(2)–C(15)–N(5)–C(16)	21(2)
N(4)–C(15)–S(2)	121.0(9)	N(2)–C(14)–N(3)–Mn(1)	2(2)	S(2)–C(15)–N(5)–C(17)	–169(1)
N(8)–Mn(1)–N(3)	175.1(5)	N(2)–C(14)–N(3)–N(4)	–178(1)	N(4)–C(15)–S(2)–Mn(1)	–6(1)
N(8)–Mn(1)–N(1)	105.8(4)	S(1)–C(14)–N(3)–Mn(1)	–176.2(8)	N(5)–C(15)–S(2)–Mn(1)	172(1)
N(3)–Mn(1)–N(1)	69.9(4)	S(1)–C(14)–N(3)–N(4)	4(2)	C(26)–C(29)–N(6)–Mn(1)	41(2)
N(8)–Mn(1)–N(6)	69.9(4)	N(5)–C(15)–N(4)–N(3)	–178(1)	C(26)–C(29)–N(6)–N(7)	–171(1)
N(3)–Mn(1)–N(6)	108.6(4)	N(8)–Mn(1)–N(3)–N(4)	143(5)	C(30)–C(29)–N(6)–Mn(1)	–138(1)
N(1)–Mn(1)–N(6)	103.7(4)	S(2)–Mn(1)–N(3)-C(14)	171(1)	C(30)–C(29)-N(6)–N(7)	10(2)
N(8)–Mn(1)–S(4)	78.3(3)	S(2)–Mn(1)–N(3)–N(4)	–8.9(9)	N(8)–C(36)–N(7)–N(6)	13(2)
N(3)–Mn(1)–S(4)	103.3(3)	N(6)–Mn(1)–N(3)–N(4)	72(1)	S(3)–C(36)–N(7)–N(6)	–164(1)
N(1)–Mn(1)–S(4)	86.2(3)	N(8)–Mn(1)–N(3)–C(14)	–37(6)	N(7)–C(36)–N(8)–Mn(1)	6(2)
N(6)–Mn(1)–S(4)	148.2(3)	N(1)–Mn(1)–N(3)–C(14)	–10(1)	N(7)–C(36)–N(8)–N(9)	–176(1)
N(8)–Mn(1)–S(2)	106.6(3)	N(1)–Mn(1)–N(3)–N(4)	170(1)	S(4)–Mn(1)–N(3)–C(14)	71(1)
N(3)–Mn(1)–S(2)	77.7(3)	N(6)–Mn(1)–N(3)–C(14)	–108(1)	S(4)–Mn(1)–N(3)–N(4)	–109(1)
N(1)–Mn(1)–S(2)	147.5(3)	N(1)–Mn(1)–N(6)–C(29)	–92(1)		
N(6)–Mn(1)–S(2)	85.4(3)	S(2)–Mn(1)–N(1)–N(2)	16(1)		
S(4)–Mn(1)–S(2)	102.44(17)	S(4)–Mn(1)–N(1)–C(7)	60(1)		
C(7)–N(1)–N(2)	118.0(12)	S(4)–Mn(1)–N(1)–N(2)	–91.2(9)		

Table 10. Hydrogen bonding interaction parameters [Å and °]

D–H···A	d(D–H)	d(H···A)	d(D···A)	<(DHA)
N(4)–H(4A) ··S(1)	0.84(4)	2.47(4)	2.9(5)	113(3)
N(7)–H(7A) ··O(1)	0.85(3)	2.47(3)	3.32(7)	150(3)
N(9)–H(9A) ··S(3)	0.85(4)	2.39(4)	2.896(4)	119(3)
C(38)–H(38a) ··S(4)	0.96	2.68	3.05 (6)	103
C(43)–H(43) ··S(2)	0.93	2.82	3.49(7)	130

N(3)–Mn(1)–N(1) 69.9(4) and N(8)–Mn(1)–N(6) 69.9(4)° indicate a distorted octahedral geometry.

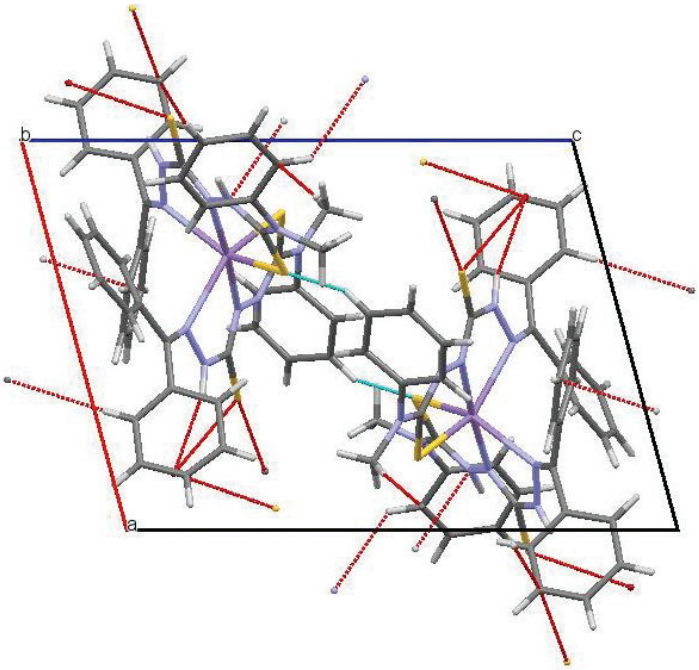

Fig. 22. Packing diagram of $[Mn(HL')_2]H_2O$ along the *b*-axis showing intermolecular interaction.

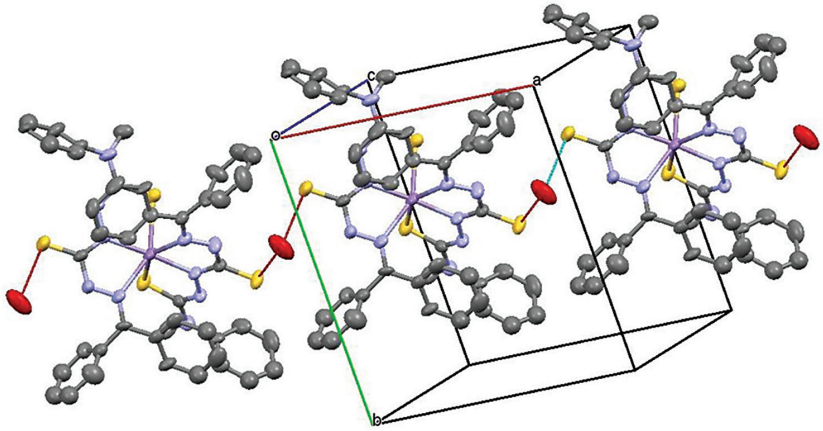

Fig. 23. Supramolecular chain interlinked with water molecule along *c*-axis (omitting H atoms).

3.4.2. Single-crystal XRD studies of Ni(II) complex

Single crystals of $Ni(HL')_2 1.5H_2O$ suitable for X-ray analysis were obtained from its solution in 1:1 (v/v) mixture of methanol and DMF. A crystal with dimension, 0.630 × 0.560 × 0.510 mm^3 was selected for collecting the data. It crystallized with two molecules per asymmetric unit into triclinic crystal system with a space group of *P*–1.

The molecular structure with atom numbering scheme is depicted in Fig. 24. Crystal data and structure refinement parameters of the complex are given in Table 11. Selected bond lengths and bond angles are summarized in Table.12. The important hydrogen bonding interaction parameters are listed in Table 13.

The single-crystal X- ray diffraction studies disclose the occurrence of six coordinated Ni complex with distorted octahedral geometry. One half of the molecule of the complex is related to the other half by a two-fold axis passing through Ni(II) ion. It is coordinated through the azomethine N–, hydrazine N– and the thione S atoms of the two deprotonated ligands in a meridonal fashion. The metal center is shared by four fused five-membered chelate rings.

The adjacent molecules are arranged in an offset manner within the unit cell when viewed along the *c*-axis. An interesting attribute of the crystal packing is the formation of a supramolecular chain linked by water molecule. Fig. 25 shows the packing diagram of $Ni(HL')_2 1.5H_2O$ along the *a*-axis showing intermolecular interactions. Fig. 26 shows supramolecular chain interlinked with water molecule along the *c*-axis. In the crystal,

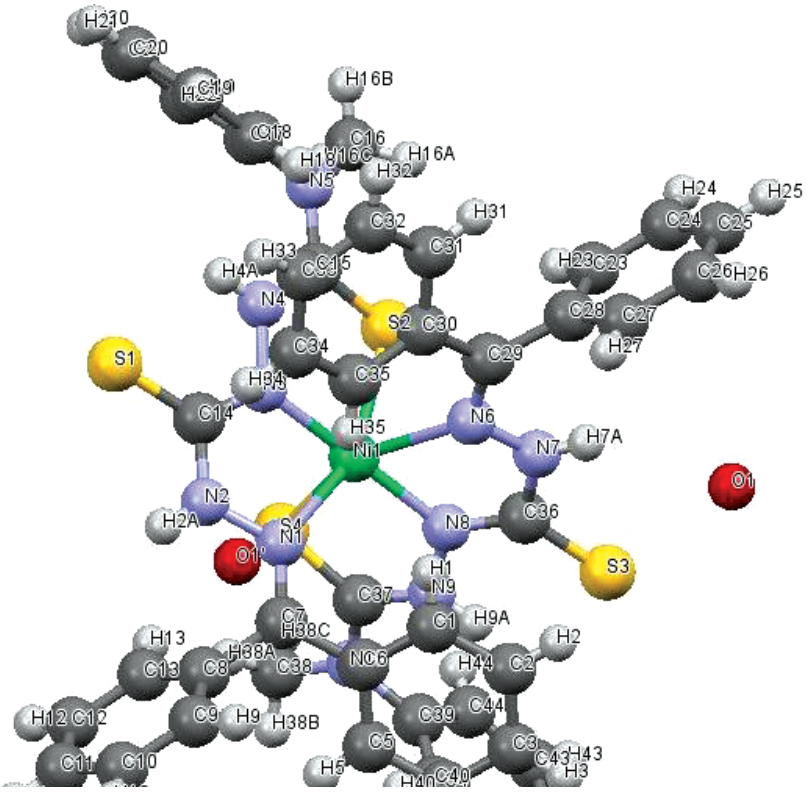

Fig. 24. The molecular structure of the Ni(II) complex with atom numbering scheme.

Table 11. Crystal data and structure refinement parameters for $Ni(HL')_2 1.5\ H_2O$

Parameters		**Parameters**	
Empirical formula	$C_{44}\ H_{36}\ C_{10}\ N_{10}\ Ni\ O\ S_4$	Index ranges	$-13 \le h \le 13, -14 \le k \le 15, -19 \le l \le 19$
Formula weight	907.78	Reflections collected	13992
Temperature (K)	273(2)	Independent reflections	7315 [R(int) = 0.0582]
Wavelength (Å)	0.71073	Completeness to theta = 24.999°	95.50%
Crystal system	Triclinic	Absorption correction	Semi-empirical from equivalents
Space group	$P\bar{1}$	Max. and min. Transmission	0.71 and 0.62
Unit cell dimensions	a Å = 11.0784(9) α° = 75.823(2)	Refinement method	Full-matrix least-squares on F^2
	b Å = 13.3220(7) β° =74.2340(10)		
	c Å = 16.3160(9) γ° = 84.270(2)		
Volume (Å^3)	2245.4(3)	Data/restraints/parameters	7315/0/544
Z	2	Goodness-of-fit on F^2	0.963
ρ(calculated) mg/m^3	1.343	Final R indices [I > 2sigma(I)]	R_1 = 0.0641, wR_2 = 0.1511
Absorption coefficient (mm^{-1})	0.664	R indices (all data)	$R1$ = 0.1192, w$R2$ = 0.1794
F(000)	940	Extinction coefficient	0.0036(7)
Crystal size (mm^3)	0.630 × 0.560 × 0.510	Largest diff. peak and hole (e.Å^{-3})	1.296 and −0.270
Theta range for data collection	1.818°–24.999°		

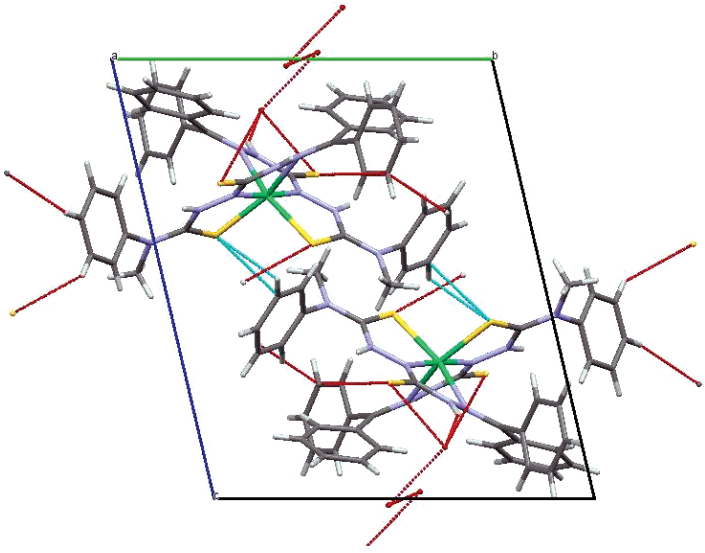

Fig. 25. Packing diagram of $Ni(HL')_2 1.5H_2O$ along the a-axis showing intermolecular interactions.

the molecule are interconnected by N–H···S and N–H···O interactions, forming a three-dimensional network.

The bond lengths, C(14)–N(3) and C(29)–N(6) (1.312(7) and 1.297(7) Å) are shorter, when compared to C–N bonds which is not involved in coordination. Comparatively shorter bond lengths, N(3)–Ni(1) 1.959; N(6)–Ni(1) 2.394; N(8)–Ni(1) 1.948; Ni(1)–S(4) 2.4194 and N(8)–Ni(1) 1.948 Å indicate strong coordination of the ligand with Ni(II) ion.

Table 12. Selected bond lengths (Å), bond angles and torsion angles (°)

Bond lengths (Å)		**Torsion angles (°)**			
C(14)–N(3)	1.312(7)	N(3)–C(14)–N(2)–N(1)	12.6(6)	Ni(1–N(8–N(9–H(9A	–173(3)
C(14)–N(2)	1.371(7)	S(1)–C(14)–N(2)–N(1)	–166.8(3)	C(36)–N(8)–Ni(1)–N(1)	–110.4(3)
C(14)–S(1)	1.696(5)	N(2)–C(14)–N(3)–Ni(1)	6.1(6)	C(36–N(8)–Ni(1)–N(3)	–63(2)
C(15)–N(4)	1.339(7)	S(1)–C(14)–N(3)–N(4)	2.4(6)	C(36)–N(8)–Ni(1)–N(6)	–13.2(3)
C(15)–N(5)	1.343(7)	S(1)–C(14)–N(3)–Ni(1)	–174.6(2)	C(36)–N(8)–Ni(1)–S(2)	66.5(3)
C(15)–S(2)	1.704(5)	S(2)–C(15)–N(4)–N(3)	0.9(6)	C(36)–N(8)–Ni(1)–S(4)	166.1(3)
C(36)–N(8)	1.302(6)	S(2)–C(15)–N(4)–H(4A)	–174(3)	N(9)–N(8)–Ni(1)–N(1)	73.1(3)
C(36)–N(7)	1.393(7)	N(4)–C(15)–S(2)–Ni(1)	–6.0(4)	N(9)–N(8)–Ni(1)–N(3)	120(2)
C(36)–S(3)	1.694(5)	N(5)–C(15)–S(2)–Ni(1)	174.2(4)	N(9)–N(8)–Ni(1)–N(6)	170.2(3)
C(37)–N(9)	1.335(6)	Ni(1)–N(1)–N(2)–C(14)	–20.5(5)	N(9)–N(8)–Ni(1)–S(2)	–110.0(3)
C(37)–N(10)	1.352(6)	C(7)–N(1)–Ni(1)–N(3)	167.3(4)	N(9)–N(8)–Ni(1)–S(4)	–10.5(3)
C(37)–S(4)	1.707(5)	C(7)–N(1)–Ni(1)–N(6)	–91.0(4)	C(15)–S(2)–Ni(1)–N(1)	2.5(3)
N(1)–N(2	1.394(6)	C(7)–N(1)–Ni(1)–N(8)	–16.0(4)	C(15)–S(2)–Ni(1)–N(3)	6.7(2)
N(1)–Ni(1)	2.328(5)	C(7)–N(1)–Ni(1)–S(2)	171.6(3)	C(15)–S(2)–Ni(1)–N(6)	–98.5(2)
N(3)–N(4)	1.375(6)	C(7)–N(1)–Ni(1)–S(4)	65.4(4)	C(15)–S(2)–Ni(1)–N(8)	–170.0(2)
N(3)–Ni(1)	1.959(4)	N(2)–N(1)–Ni(1)–N(3)	16.5(3)	C(15)–S(2)–Ni(1)–S(4)	105.5(2)
N(6)–N(7)	1.378(6)	N(2)–N(1)–Ni(1)–N(6)	118.3(3)	C(37)–S(4)–Ni(1)-N(1)	–96.0(2)
N(6)–Ni(1)	2.394(4)	N(2)–N(1)–Ni(1)–N(8)	–166.7(3)	C(37)–S(4)–Ni(1)–N(3)	–169.1(2)
N(8)–N(9)	1.390(6)	N(2)–N(1)–Ni(1)–S(2)	20.8(4)	C(37)–S(4)–Ni(1)–N(6)	9.3(3)
N(8)–Ni(1)	1.948(4)	N(2)–N(1)–Ni(1)–S(4)	–85.3(3)	C(37)–S(4)–Ni(1)–N(8)	7.7(2)
Ni(1)–S(4)	2.4194(17)	Ni(1)–N(3)–N(4)–C(15)	7.1(6)	C(37)–S(4)–Ni(1)–S(2)	107.3(2)
Ni(1)–S(2)	2.4318(17)	C(14)–N(3)–Ni(1)–N(1)	–13.2(3)		
C(29)–N(6)	1.297(7)	C(14)–N(3)–Ni(1)–N(6)	–110.3(4)		
Bond lengths (°)		C(14)–N(3)–Ni(1)–N(8)	–61(2)		
N(1)–Ni(1)–N(6)	100.44(16)	C(14)–N(3)–Ni(1)–S(2)	168.5(4)		
N(8)–Ni(1)–S(4)	82.67(13)	C(14)–N(3)–Ni(1)–S(4)	69.1(4)		
N(3)–Ni(1)–S(4)	100.08(15)	N(14)–N(3)–Ni(1)–N(1)	169.9(4)		
N(1)–Ni(1)–S(4)	85.54(12)	C(29)–N(6)–Ni(1)–S(2)	61.7(4)		
N(6)–Ni(1)–S(4)	155.83(11)	C(29)–N(6)–Ni(1)–S(4)	163.4(3)		
N(8)–Ni(1)–S(2)	100.75(14)	N(7)–N(6)–Ni(1)–N(1)	117.7(3)		
N(3)–Ni(1)–S(2)	81.84(14)	N(7)–N(6)–Ni(1)–N(3)	–166.2(3)		
N(1)–Ni(1)–S(2)	155.92(12)	N(7)–N(6)–Ni(1)–N(8)	17.2(3)		
N(6)–Ni(1)–S(2)	83.45(12)	N(7)–N(6)–Ni(1)–S(2)	–86.2(3)		
S(4)–Ni(1)–S(2)	100.67(6)	N(7)–N(6)–Ni(1)–S(2)	15.4(4)		
C(15)–S(2)–Ni(1)	95.5(2)	N(1)–N(8)–Ni(9)–C(37)	10.3(5)		
C(37)–S(4)–Ni(1)	95.27(19)				

Table 13. Hydrogen bonding interaction parameters [Å and °]

D–H···A	d(D–H)	d(H···A)	d(D···A)	<(DHA)
N(4)–H(4A) ··S(1)	0.84(4)	2.47(4)	2.9(5)	113(3)
N(7)–H(7A) ··O(1)	0.85(3)	2.47(3)	3.32(7)	150(3)
N(9)–H(9A) ··S(3)	0.85(4)	2.39(4)	2.896(4)	119(3)
C(38)–H(38a) ··S(4)	0.96	2.68	3.05 (6)	103
C(43)–H(43) ··S(2) [a]	0.93	2.82	3.49(7)	130

[a]Symmetry transformations used to generate equivalent atoms: $1 - x$, $1 - y$, $1 - z$

The bite angles, N(6)–Ni(1)–S(4) (155.83°), N(1)–Ni(1)–S(2) (155.92°), N(8)–Ni(1)–S(4) (82.67°), N(6)–Ni(1)–S(2) 83.45(12), N(8)–Ni(1)–S(2) (100.75°), S(4)–Ni(1)–S(2) (100.67°) and N(3)–Ni(1)–S(2) (81.84°) are somewhat far from a perfect octahedron indicating significant distortion in the geometry.

4. Conclusions

In this investigation, we synthesized two ligands derived from benzophenone and N(4)-methyl-N(4)-phenyl thiosemicarbazide (HL and H_2L'). We were able to obtain single crystals of benzophenone N(4)-methyl-N(4)-phenyl thiosemicarbazone (HL) by refluxing equimolar quantities of benzophenone and N(4)-methyl-N(4)-phenyl thiosemicarbazide. We were also able to synthesize single crystals of Ni(II) and Mn(II) complexes of the ligand, H_2L'. To the best of our knowledge, the structures of the ligands and the complexes of H_2L' are not been reported so far. Based on the elemental analyses, spectral, magnetic and thermal investigations, following tentative structures were assigned for the complexes (Figs. 27–32).

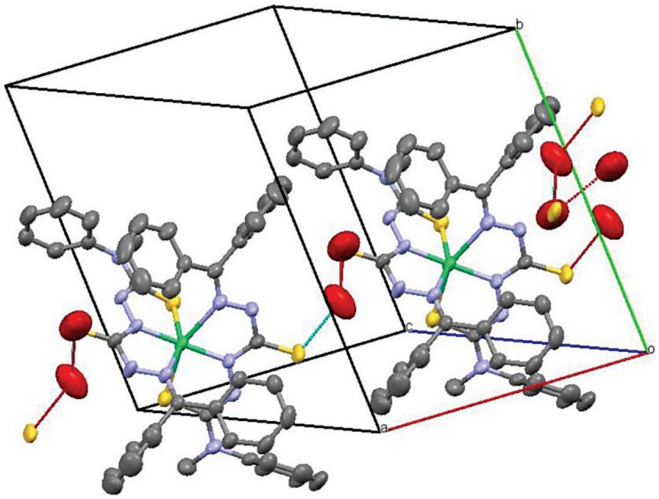

Fig. 26. Supramolecular chain of $Ni(HL')_2 1.5H_2O$ interlinked with water molecule (omitting H atoms).

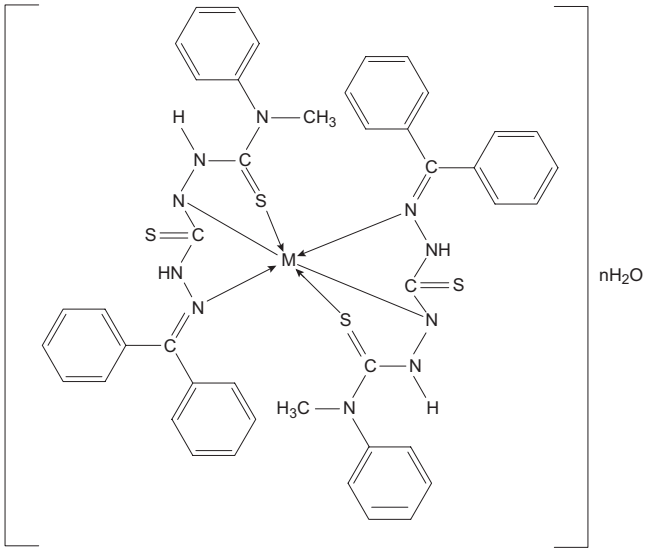

Fig. 27. Proposed structure of complexes $[M(HL')_2]$ nH_2O, where M = Ni(II), Mn(II), Zn(II); n = 0, 1, 2... **(1)**, **(6)** and **(13).**

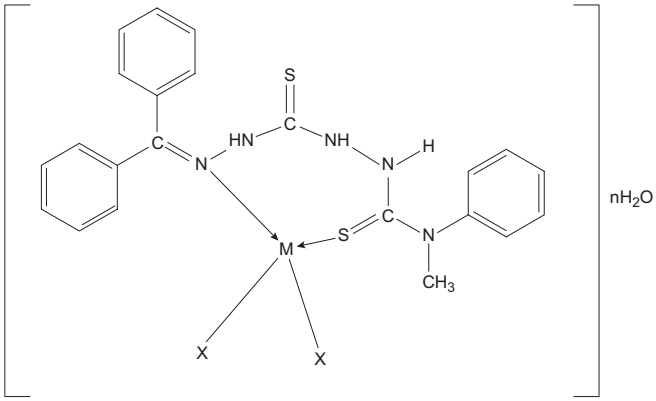

Fig. 28. Proposed structure of complexes $[MH_2L'X_2]$ nH_2O, where M = Co(II), Ni(II), Zn(II); X = CH_3COO^-; n = 0, 1 ,2...(**2), (5)** and **(12**).

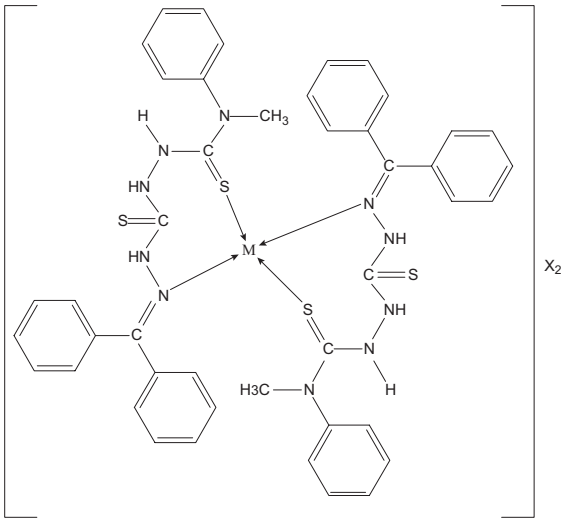

Fig. 29. Proposed structure of complexes $[M(H_2L')_2]X_2$, where M = Co(II); X = Cl^-, NO_3^- **(3)** and **(4)**.

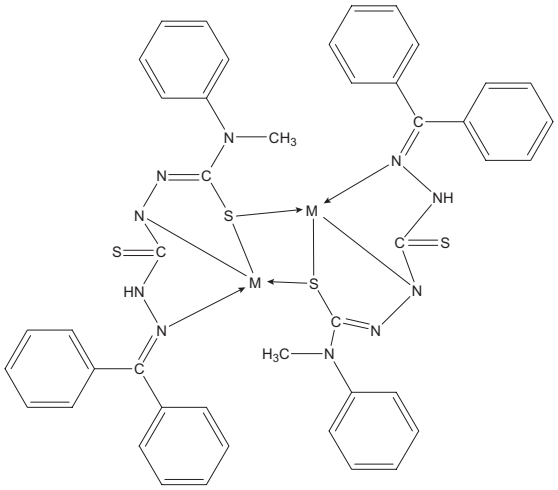

Fig. 30. Proposed structure of complexes $[M(HL')]_2$ **(8),** where M = Cu(II).

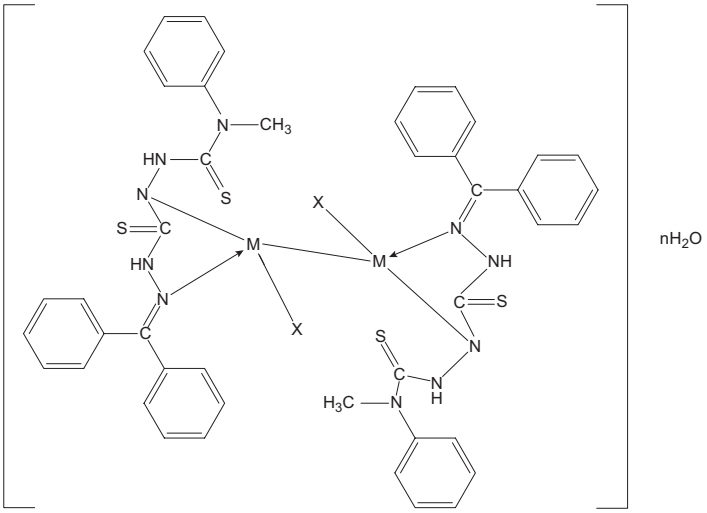

Fig. 31. Proposed structure of complex $[MHL'X]_2nH_2O$, where M = Cu(II); X = Cl^-, NO_3^-; *n* = 1, 2, 3... **(9), (10)**.

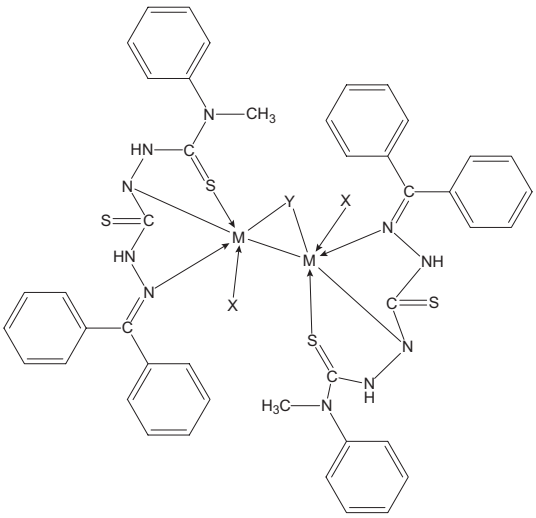

Fig. 32. Proposed structure of complex $[MHL'X]_2Y$, where M = Cu(II); X = H_2O; Y = SO_4^{2-} **(11)**.

References

1. S. E. Blanco, J. J. Silber, F. H. Ferretti, J. Mol. Struct. (Theochem), 582 (2002) 91.
2. A. A. Osowole, R. Kempe, R. Schobert, Int. Res. J. Pure Appl. Chem., 2 (2) (2012) 105.
3. P. Jandera, M. Skavrada, L. Andel, D. Komers, G. Guiochon, J. Chromatogr. A, 908 (2001) 3.
4. A. K. Kadry, C. S. Okereke, M. S. Abdel-Rahman, M. A. Friedman, R. A. Davis, J. Appl. Toxicol., 15 (1995) 97.
5. R. Siles, S. Chen, M. Zhou, K. G. Pinney, M. L. Trawick, Bioorg. Med. Chem. Lett., 16 (16) (2006) 4405.
6. A. A. Jarrahpour, M. Zarei, Molbank, M374 (2004) 243.
7. J. P. Scovill, Phosphrous Sulfur Silicon., 60 (1991) 25.
8. G. H. Sheldrick, SHELXL 97. Program for Crystal Structure Refinement, University of Göttingen, Göttingen, Germany, 1997.
9. A. L. Spek, PLATON, A Multipurpose Crystallographic Tool, Utrecht University, Utrecht, the Netherlands, 1999.
10. Diamond-Crystal and Molecular Structure Visualization, Crystal Impact – Dr. H. Putz, Dr. K. Brandenburg GbR, Kreuzherrenstr. 102, 53227 Bonn, Germany.
11. C. F. Macrae, P. R. Edington, P. McCabe, E. Pidcock, G. P. Sheilds, R. Taylor, M. Towler, J. Van de Streek, J. Appl. Crystallogr., 39 (2006) 453.
12. G. J. Palenik, D. F. Rcndle, W. S. Cru1er, Acta Cryst., 830 (1974) 2390.; K. O. Ferraz, S. M. S. V. Wardell, J. L. Wardell, S. R. W. Louro, H. Beraldo, Spectrochim. Acta A., 73 (2009) 140.
13. H. Arslan, U. Florke, N. Kulcu, G. Binzet, Spectrochim. Acta A., 68 (2007) 1347.
14. V. Suni, M. R. P. Kurup, M. Nethaji, Spectrochim. Acta A., 63 (2006) 174
15. P. N. Prasad, Springer Ser. Wave-Phenon., 9 (1989) 305.
16. R. M. Silverstein, G. C. Bassler, C. Morril, Spectroscopic Identification of Organic Compounds, 4th ed., John Wiley, New York City, New York, 1981.
17. A. H. Al-Amiery, K. Al-Majedy, H. A. Razzaq, J. Al-Nahrain University, 14(1) (2011) 7.
18. B. P. Singh, Int. Pharmaceut. Res. Development, 4(3) (2012) 51–57.
19. J. E. Huheey, E. A. Keiter, R. L. Keiter, Inorganic Chemistry, Principles of Structure and Reactivity, 4th ed., Harper Collins College Publishers, New York City, New York, 1993.
20. W. Linert, F. Renz, R. Boca, J. Coord. Chem., 40 (1996) 293; S. Purohit, A. P. Koley, L. S. Prasad, P. T. Manoharan, S. Ghosh, Inorg. Chem., 28 (1989) 375.
21. A. B. P. Lever, Inorganic Electronic Spectroscopy, 2nd ed., Elsevier, Amsterdam (1984).
22. L. Sacconi, Transition Metal Chemistry, ed., R. L. Carlin Marcel Dekker, New York City, New York, vol. 4, 1968, 199.
23. D. Sutton, Electronic Spectra of Transition Metal Complexes, McGraw Hill, London, 1968.
24. O. Maddock, A. Sharpe, R. L. Martin, Proc. Roy. Austral. Chem. Inst., 38 (1971) 33.
25. G. G. Mohamed, M. M. Omar, A. M. M. Hindy, Spectrochim. Acta A., 62 (2005) 1140.
26. M. M. Omar, G. G. Mohamed, A. M. M. Hindy, J. Therm. Anal. Calorim., 86 (2006) 315.
27. G. G. Mohamed, M. M. Omar, A. M. Hindy, Turk. J. Chem., 30 (2006) 3
28. Mohammad Shakira, Ambreen Abbasia, Asad U. Khanb, Shahper N. Khan, Spectrochim. Acta A., 78 (2011) 29.
29. R. M. Silverstein, G. C. Bassler, C. Morril, Spectroscopic Identification of Organic Compounds, 4th ed., John Wiley, New York City, New York, 1981.
30. A. H. Al-Amiery, K. Al-Majedy, H. A. Razzaq, J. Al-Nahrain University, 14(1) (2011) 7.

31. B. P. Singh, Int. Pharmaceut. Res. Development, 4(3) (2012) 51.
32. K. Krishnankutty, M. B. Ummathur D. K. Babu, J. Serb. Chem. Soc., 75(5) (2010) 639; R. M. Issa, A. M. Khedr, H. F. Rizk, Spectrochim. Acta A., 62 (2005) 621; M. H. Moustafa, A. A. Elnaeem O. A. Abbas, Ass. Univ. Bull. Environ. Res., 14(2) (2011) 27.
33. M. H. Moustafa, A. A. Elnaeem O. A. Abbas, Ass. Univ. Bull. Environ. Res., 14(2) (2011) 27; M. H. Habibi, M. Montazerozohori, A. Lalegani, R. W. Harrington, W. Clegg, J. Fluor. Chem. 127 (2006) 769; A. P. Mishra and D. K. Mishra, Int. J. Pharma. Bio. Sci., 2 (2011) B-430.
34. V. Stefov, V. M. Petrusevski, B. Soptrajanov, J. Mol. Struct., 293 (1993) 97.
35. J. Kuncheria., PhD thesis, University of Calicut, 1992.
36. K. Nakamoto, Infrared and Raman Spectra of Inorganic and Coordination Compounds, 3rd ed., John Wiley and Sons, New York City, New York, 1978.
37. N. F. Curtis, J. Chem. Soc. (A), 1968 (1968) 1579.
38. G. M. Sheldrick, SHELXL-2014/7: Program for the Solution of Crystal Structures, University of Göttingen, Göttingen, Germany, 2014.

CHAPTER V

NOVEL LIGAND, 3-FORMYL CHROMONE N(4)-METHYL-N(4)-PHENYLTHIOSEMICARBAZONE AND ITS TRANSITION METAL COMPLEXES

1. Introduction

The chromone ring system, 1-benzopyran-4-one, is the nucleus in several flavonoids, such as flavones, flavonols and isoflavones.[1] Chromonenes are compounds which contain γ-pyrone nucleus fused to benzene ring. Molecules which contain chromone ring in their structure are being paid more attention in the recent past because of their interesting biological properties.

3-Formylchromone (Fig. 1) has emerged as a valuable synthon for the incorporation of chromone moiety into a number of molecular frameworks. Schiff's bases of 3-formylchromone and its complexes have antimycobacterial, antifungal, anticonvulsant and mushroom tyrosinase inhibition activities and have extensive applications in biological, clinical and pharmacological areas.[2,3] It acts as a potent topoisomerase inhibitor which is an anticancer agent. These compounds also serve as intermediates in the synthesis of many pharmaceuticals, agrochemicals and dye-stuffs. Chromone hydrazones and their metal complexes often possess diverse biological and pharmaceutical activities, such as antimicrobial, tuberculostatic, anticancer and antioxidant properties.[4]

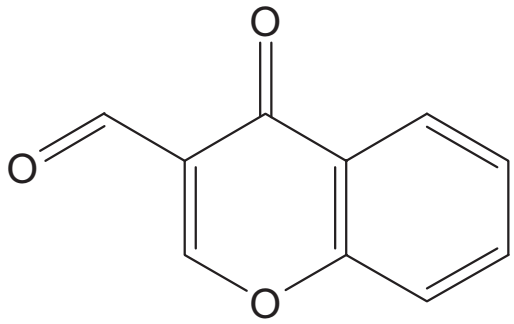

Fig. 1. 3-Formylchromone.

Khan *et al.*[5] conducted that *in vitro* and *in vivo* studies of butanohydrazide derivative of 3-formylchromone and reported their anti-inflammatory activities. Li *et al.*[6] synthesized and characterised 3-carbaldehyde chromone semicarbazone and its transition metal

complexes. They conducted *in vitro* antioxidant screening of Ni(II), Cu(II) and Zn(II) complexes of 3-carbaldehydechromone semicarbazone. These complexes possessed significant antioxidant activity against superoxide and hydroxyl radicals. The scavenging effects of Cu(II) complex are stronger than Zn(II), Ni(II) complexes and some standard antioxidants, such as mannitol and Vitamin C. They also synthesized and studied the crystal structures, biological activities and fluorescence properties of transition metal complexes of 3-carbaldehydechromone thiosemicarbazone.[7]

DNA-binding property of the La(III) and Eu(III) complexes with 6-hydroxy chromone-3-carbaldehyde-(2′-hydroxy) benzoylhydrazone was reported by Wang *et al*.[8] The experimental results showed that La(III) and Eu(III) complexes are effective inhibitors of superoxide and hydroxyl radicals than mannitol.

Cu(II), Fe(III), Co(II) and Co(III), Ni(II), Cr(III), Pd(II), Pt(IV) and Zn(II) complexes of 2-methyl-7-hydroxy-5-methoxy-6-formylchromone thiosemicarbazone and 2-methyl-5, 7-dimethoxy-6-formylchromone thiosemicarbazone were synthesized and characterised by Nabil Youssef *et al*.[9] Al-Saeedi *et al*.[10] reported the synthesis, spectroscopic characterisation and electrochemical studies of Girard's T chromone complexes. Pd(II) complexes of chromone-based Schiff's bases were synthesized, characterised and their biological activities were studied by Kavitha and Laxma Reddy.[11]

This chapter portrays the synthesis and characterisation of a novel ligand, 3-formyl chromone N(4)-methyl-N(4)-phenylthiosemicarbazone (HL) (Fig. 2) and its complexes.

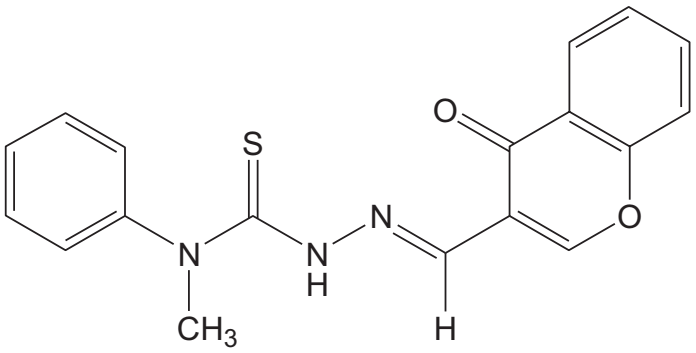

Fig. 2. 3-Formylchromone N(4)-methyl-N(4)-phenylthiosemicarbazone (HL).

2. Experimental

2.1. Materials and methods

3-Formylchromone (Sigma Aldrich) and commercially available metal salts were used without further purification. The solvents were purified and dried by standard procedure. The melting points of the ligand and complexes were recorded on a melting point apparatus. The ligand and complexes were further characterised by using partial elemental analyses, FT-IR, FT-Raman, electronic and ^{1}H NMR spectra. The Zn(II) and Ni(II) complexes were

characterised by ^{1}H NMR spectra. EPR spectrum of Cu(II) complex was also recorded. Magnetic susceptibilities of the complexes at room temperature were measured. Thermal stabilities of complexes were also ascertained. Details regarding the techniques used for the characterisation of the ligand and the complexes are explained in Chapter II.

2.2. Synthesis

Synthesis of the precursor, N(4)-methyl-N(4)-phenylthiosemicarbazide (MPTSC) is discussed in Chapter II.

2.2.1. 3-Formylchromone N(4)-methyl-N(4)-phenylthiosemicarbazone (HL)

HL was synthesized by the dropwise addition of hot methanolic solution of 3-formyl chromone (0.174 g, 1 mmol) with constant stirring to a boiling methanolic solution of N(4)-methyl-N(4)-phenylthiosemicarbazide (0.182 g, 1 mmol). The mixture was stirred on a magnetic stirrer at room temperature for 30 minutes. The compound obtained as yellow solid was filtered, washed with methanol, dried and kept in a desiccator.

2.2.2. Metal complexes

To the hot methanolic solution of HL (0.34 g, 1 mmol), a hot methanolic solution of the metal salt (1 mmol) was added dropwise. The reaction mixture was stirred and refluxed for 60 minutes. The complex separated out was filtered, washed several times with water and methanol. It was then dried and kept in a desiccator.

3. Results and discussion

3.1. Characterisation of the ligand (HL)

3.1.1. Microanalytical data

The suggested formula for the ligand is $C_{18}H_{15}N_3O_2S$. CHNS percentages of ligand were in agreement with the suggested molecular formulae (Table 1). It is yellow in colour and melted at 170°C. It is non-hygroscopic and stable at normal atmospheric conditions. It is soluble in common solvents like methanol, ethanol, DMF, DMSO and so on.

Table 1. Analytical data of the ligand

Compound	Molecular Weight	Melting Point	Colour	Yield	Elemental Analysis Found (Calculated)			
					C	H	N	S
$C_{18}H_{15}N_3O_2S$ (HL)	337	170	Yellow powder	70	64.2 (64.1)	4.3 (4.4)	12.4 (12.5)	9.6 (9.5)

The reaction pathway of the ligand can be represented by the following Scheme 1:

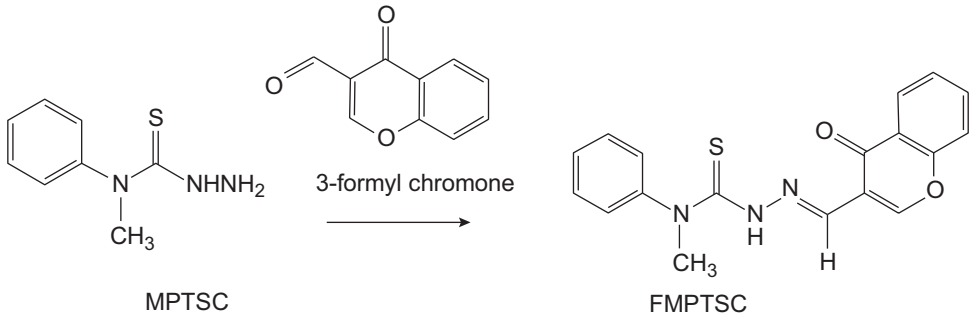

Scheme 1. Formation of 3-formylchromone N(4)-methyl-N(4)-phenylthiosemicarbazone (FMPTSC) (**HL)**.

3.1.2. Powder XRD studies

Since we could not obtain the single crystals of H_2L, we recorded its powder XRD pattern. It revealed the crystallinity of the compound. Matching the peaks using MATCH software, it is found that the crystal belongs to triclinic system (Fig. 3).

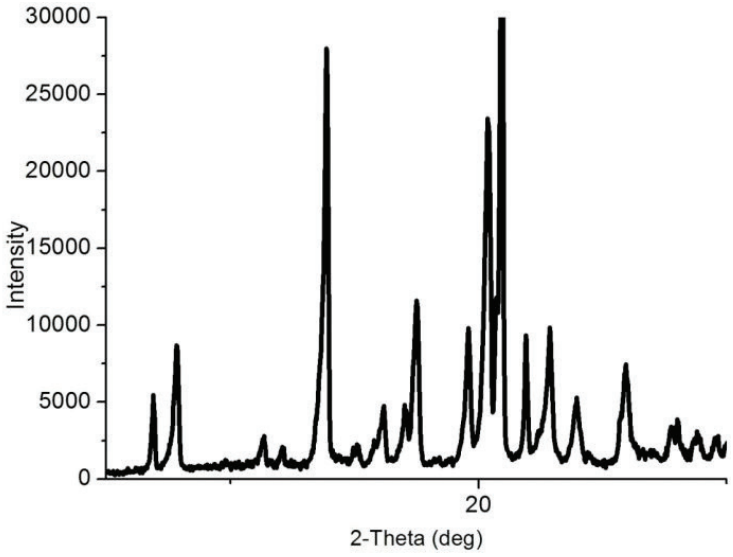

Fig. 3. Powder XRD of HL.

3.1.3. Spectroscopic analysis

(a) Electronic spectrum

The electronic absorption spectrum of the ligand in solid state was recorded in the range 200–900 nm (Fig. 4). The compound registered bands at 259, 321 and 385 nm. The two former bands may be attributed to the π–π* transitions of the azomethine chromophore and the benzene ring (intra-ligand charge transfer) and the latter one may be due to the n–π* transition.

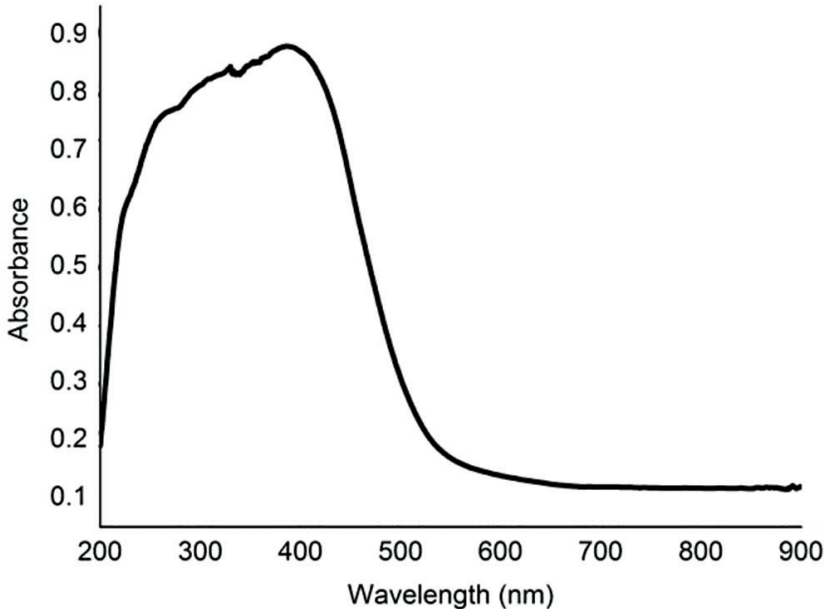

Fig. 4. Electronic spectrum of the ligand.

(b) Vibrational spectrum

The FT-IR spectrum of the compound was recorded in the region 4000–400 cm^{-1} and is presented in Fig. 5. A broad band observed at 3447 cm^{-1} can be assigned as N–H stretching vibration. The absence of any bands at 2500–2580 cm^{-1} due to ν(SH) shows that the ligand exists in thione form[12] in the solid state. The band observed at 1642 cm^{-1} may be due to ν(C=O). The band observed at 1572 cm^{-1} may be due to ν(C=N). The band observed at 794 cm^{-1} can be assigned to ν(C=S).

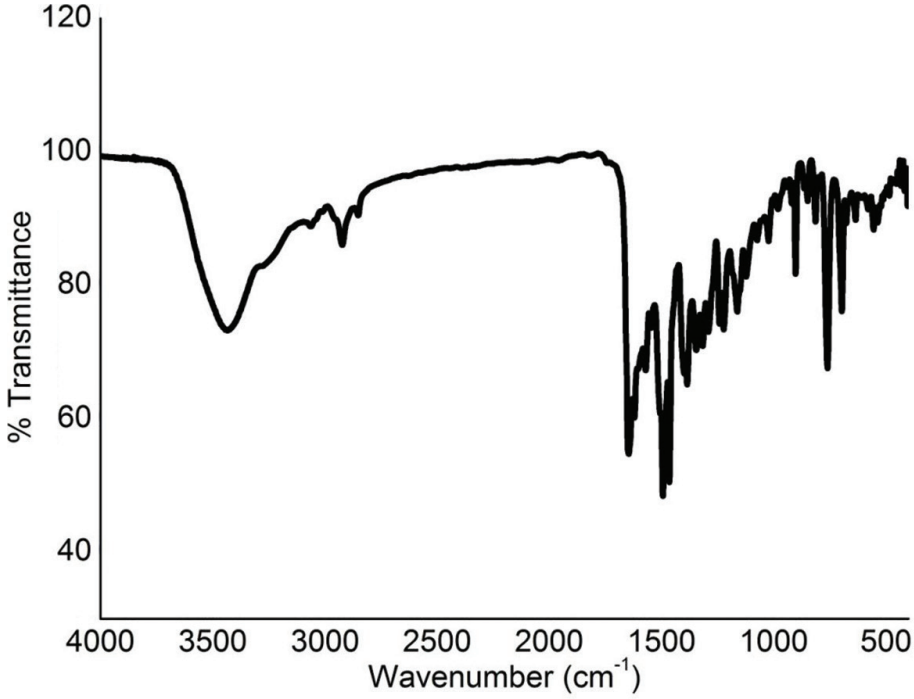

Fig. 5. FT-IR spectrum of the ligand.

(c) ^{1}H NMR spectrum

The ^{1}H NMR spectrum of the ligand was recorded in DMSO and is presented in Fig. 6. The peak observed at 11.423 ppm is assigned to SH/NH proton. A singlet observed at 8.054 ppm can be assigned to azomethine proton. Aromatic protons show a multiplet peak in the region 7.209–8.043 ppm. N–CH_3 protons absorb at 3.612 ppm in the ^{1}H NMR spectrum.

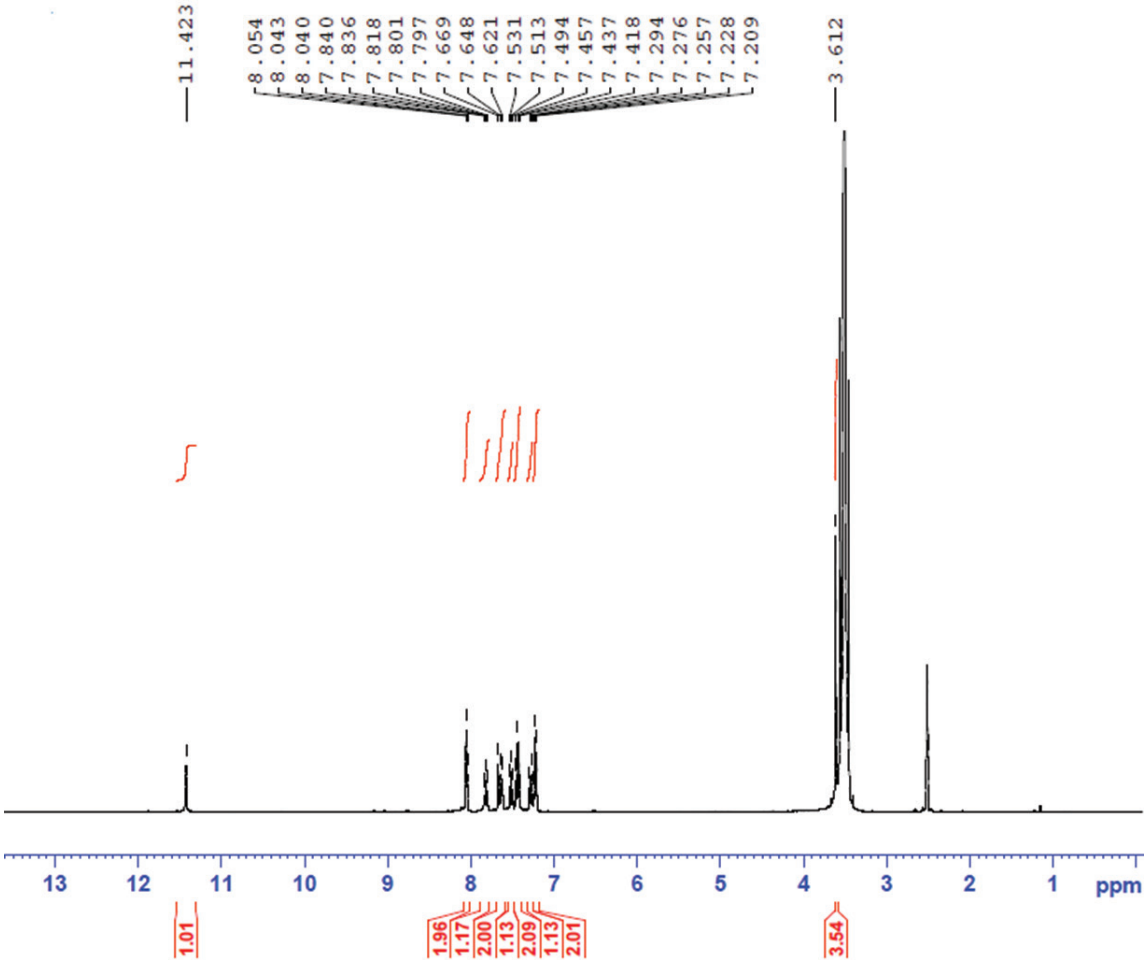

Fig. 6. NMR spectrum of HL.

3.2. Characterisation of the metal complexes

3.2.1. Formulae and general properties of the complexes

All the complexes were found to be stable at room temperature. Partial elemental analytical data of the complexes were in agreement with the suggested molecular formulae. In the complexes, the ligand was coordinated either as mono-anionic (L^-) or as neutral (HL). Based on partial elemental analyses, spectral, magnetic and thermal data, we have assigned the formulae for the complexes and are presented in Table 2.

Table 2. Molecular formulae, colours, partial elemental analyses data and magnetic moments of the complexes

Compound No.	Compound	Molecular Weight	Melting Point	Colour	Yield	Elemental Analysis Found (Calculated)					μ in BM
						C	H	N	S	M	
H_2L	$C_{18}H_{15}N_3O_2S$	337	170	Yellow	80	64.2 (64.1)	4.3 (4.4)	12.4 (12.5)	9.6 (9.5)	–	–
1	$[Mn(L)_2]$	727	240	Brownish black	70	59.2 (59.4)	4.0 (3.9)	11.6 (11.6)	8.6 (8.8)	7.6 (7.5)	4.8
2	$[Co(L)OH]4H_2O$	485	>260	Brown	80	44.2 (44.4)	4.5 (4.7)	8.5 (8.7)	6.3 (6.6)	11.9 (12.1)	2.6
3	$[Co(L)_2]Cl$	766	240	Brown	80	56.2 (56.4)	3.8 (3.7)	10.7 (10.9)	8.2 (8.4)	7.8 (7.7)	D
4	$[NiLCH_3COO]2H_2O$	490	210	Yellow	70	48.7 (48.9)	4.1 (4.3)	8.8 (8.6)	6.8 (6.5)	11.4 (11.9)	3.1
5	$[Ni(HL)Cl_2]$	467	180	Light green	70	46.4 (46.2)	3.1 (3.2)	9.2 (9.0)	7.0 (6.9)	12.7 (12.6)	D
6	$[Cu(L)_2]$	738	200	Green	80	58.4 (58.6)	4.0 (3.8)	11.5 (11.3)	8.9 (8.7)	8.8 (8.6)	1.7
7	$[Cu(L)Cl]H_2O$	456	220	Green	80	47.7 (47.5)	3.5 (3.7)	9.8 (9.6)	7.5 (7.3)	14.2 (14.0)	1.2
8	$[Zn(L)CH_3COO]2H_2O$	496	>250	Yellow	80	47.5 (48.3)	4.4 (4.2)	8.7 (8.5)	6.6 (6.5)	12.9 (13.1)	D
9	$[Zn(L)(NO_3)]2H_2O$	499	230	Yellow	80	43.0 (43.2)	3.5 (3.6)	(8.5) (8.4)	(6.2) (6.4)	13.0 (13.1)	D
10	[Cd(L)Cl]	483	235	Golden	70	44.6 (44.7)	3.0 (2.9)	8.5 (8.7)	6.3 (6.6)	23.0 (23.1)	D

3.2.3. Electronic spectra and magnetic moments

The electronic spectra of the complexes were recorded in solid state and their probable assignments are given in Tables 3. In the spectra of all these complexes, the bands observed below 350 nm can be assigned to $\pi \rightarrow \pi^*$ and $n \rightarrow \pi^*$ transitions.

The Mn(II) complex belongs to d^5 system. For high-spin octahedral complexes, electronic transitions are both Laporte and spin forbidden.[13,14] However, some forbidden transitions occur to the quartet excited states and they are $^6A_{1g} \rightarrow {}^4A_{1g}(G)$, $^6A_{1g} \rightarrow {}^4E_g(G)$, $^6A_{1g} \rightarrow {}^4E_g(D)$, $^6A_{1g} \rightarrow {}^4A_{1g}(G)$, $^6A_{1g} \rightarrow {}^4T_{1g}(G)$ and $^6A_{1g} \rightarrow {}^4T_{2g}(G)$. In this case, the Mn(II) complex exhibited two very low intense bands. One broad band at 406 nm due to $^6A_{1g} \rightarrow {}^4A_{1g}(G)$ and $^6A_{1g} \rightarrow {}^4E_g(G)$ transitions and another at 687 nm due to $^6A_{1g} \rightarrow {}^4T_{1g}(G)$ transition. This is in accordance with an octahedral geometry.

The Mn(II) complexes may be high-spin (S = 5/2) or low-spin (S = 1/2). High-spin Mn(II) complexes in octahedral and tetrahedral geometries have a spin-only value of 5.92 BM at room temperature. But low-spin complexes show magnetic moment values close to 2.5 BM. Normally, magnetic moment values of Schiff's base complexes of high-spin Mn(II) are found to be significantly lower than the expected spin-only value and they ranges from 4.7 to 5.5 BM at room temperature.[15,16] In this investigation, the magnetic moment of the complex **(1)** was 4.8 BM.

Usually, Co(II) complexes exist in octahedral, tetrahedral and square-planar geometries. If the ligands have several donor atoms, five coordinate geometry is also possible for Co(II) complexes. The electronic spectrum of a square-planar complex of Co(II) is similar to that of low-spin five coordinated complexes. It gives rise to two absorption bands due to $^2A_1 \rightarrow {}^2E$ at higher energy and $^2A_1 \rightarrow {}^2B_1$ at lower energy region. In the case of Co(II) complexes, the dark colour together with some weak and broad bands in their spectra in the region 1000–1200 nm are characteristic of square-planar geometry.[17]

In this study, the Co(II) complex **(2)** showed a broad band at 404 nm. This can be assigned to $^2A_1 \rightarrow {}^2E$ transition and is characteristic of square-planar geometry. However, the bands due to the other transitions are not observed as they may be out of the range of the spectrophotometer used.

The magnetic moment values for Co(II) complexes generally pinpoint the coordination geometries. Octahedral Co(II) complexes usually show magnetic moments in the range 4.8–5.6 BM. Tetrahedral and high-spin octahedral Co(II) complexes possess three unpaired electrons and may be distinguished by the magnitude of the deviation of effective magnetic moments from the spin-only value. Since the tetrahedral high-spin Co(II) complex with ground term ($^4A_2$) has no orbital contribution, the expected magnetic moment is 3.88 BM. However, the magnetic moments of Co(II) complexes get increased above the spin-only value *via* contribution from higher orbitally degenerate terms and occur in the range 4.2–4.7 BM.[18] Square-planar Co(II) complexes are of low-spin type and they show magnetic moments in the range 2.20–2.90.[19,20] The magnetic moment of the complex **(2)** reported here is 2.58 BM. This shows that it is in low-spin square-planar configuration with one unpaired electron.

Co(III) has a d^6 configuration with an electronic arrangement of $(t_{2g})^6$ $(e_g)^0$ and the ground state is $^1A_{1g.}$ This arrangement has very large crystal field stabilization energy

and is found to be diamagnetic. It exhibits two spin-allowed transitions at relatively low energy, $^1A_{1g} \rightarrow {}^1T_{1g}$ and $^1A_{1g} \rightarrow {}^1T_{2g}$ and two spin-forbidden bands corresponding to $^1A_{1g} \rightarrow {}^3T_{1g}$ and $^1A_{1g} \rightarrow {}^3T_{2g}$ at higher energies.[21] These are usually difficult to interpret due to the overlap of intra-ligand and charge-transfer transitions. A broad band at 488 nm in the spectrum of the complex **(3)** may be due to $^1A_{1g} \rightarrow {}^1T_{2g}$ and $^1A_{1g} \rightarrow {}^1T_{1g}$ transitions. Here, cobalt is in +III oxidation state showing a diamagnetic behaviour. These observations are characteristic of octahedral geometry.

The ground state for regular tetrahedral Ni(II) ion is $^3T_1(F)$. Tetrahedral Ni(II) complexes show two broad bands in the visible region, one at 666 nm due to $^3T_1(F) \rightarrow {}^3T_1(P)$ transition and another one at 1250 nm due to $^3T_1(F) \rightarrow {}^3A_2(F)$ transition. In this study, the complex **(4)** showed a band at 593 nm due to $^3T_1(F) \rightarrow {}^3T_1(P)$ transition. However, the other transition is not observed as it may be out of the range of the spectrophotometer used.

Ni(II) ions exhibit magnetic moments higher than the spin-only value expected for two unpaired electrons in octahedral (2.8–3.2 BM) and tetrahedral (3.4–4.2 BM) geometries. This increase in the magnetic moment values from the spin-only value may be due to some 'mixing in' of upper states *via* spin-orbit coupling. Here, the magnetic moment of the complex **(4)** is 3.02 BM, consistent with a tetrahedral geometry. In the complex **(5**), a band at 617 nm may be assigned to $^1A_{1g} \rightarrow {}^1B_{1g}$ transition which is consistent with low-spin square-planar geometry.[22] Since thiols can cause spin-pairing than thioethers, coordination might have occurred through the thiolato sulphur atom after deprotonation.[23] This Ni(II) complex was found to diamagnetic confirming its square-planar geometry.

The spectroscopic ground state term of Cu(II) is ^2D. It gets split up by an octahedral field into two levels, $^2T_{2g}$ and ^2E_g. When the symmetry of the Cu(II) complex lowers to D_{4h} or C_{4v}, the energy levels again split and give more transitions.[24] For square-planar copper complexes with a $d_{x^2-y^2}$ ground state, three spin-allowed transitions are expected.[25] [$^2B_{1g} \rightarrow {}^2A_{2g}$ ($d_{x^2-y^2} \rightarrow d_{z^2}$), $^2B_{1g} \rightarrow {}^2B_{2g}$ ($d_{x^2-y^2} \rightarrow d_{xy}$) and $^2B_{1g} \rightarrow {}^2E_g$ ($d_{x^2-y^2} \rightarrow d_{xz;yz}$)]. It is quite difficult to resolve these bands as they are very close in energy.

Tetrahedral and pseudotetrahedral Cu(II) complexes usually show transitions in the range 7000–10000 cm^{-1}.[26] Square-planar or distorted octahedral complexes normally absorb in the region 10000–20000 cm^{-1}.[26] In the spectrum of the complex **(6)**, this region is blank and therefore, it may have tetrahedral geometry. The complex **(7)** showed two bands, one at 596 nm and another at 704 nm. These can be assigned to $^2B_{1g} \rightarrow {}^2E_g$, $^2B_{1g} \rightarrow {}^2A_{1g}$ transitions. Therefore, we propose a square-planar geometry for the complex.

The magnetic moment values of Cu(II) complexes usually do not provide any indication to their stereochemistries. The room temperature magnetic moments of the mononuclear Cu(II) complexes are in the range 1.79–1.81 BM which are very close to the spin-only value of 1.73 BM for d^9 Cu(II) system. The magnetic moment of complex **(6)** was found to be 1.74 BM. The complex **(7)** showed a magnetic moment of 1.23 BM. The low magnetic moment of the latter complex (**7)** may be ascribed to the strong antiferromagnetic interaction between the neighbouring Cu(II) ion centres.[27,28]

Cadmium and zinc complexes showed charge-transfer transitions in the range 399–420 nm. As expected, these complexes are diamagnetic. Electronic spectra of the complexes **(3)**, **(5)**, **(7)** and **(8)** are presented in Fig. 7.

Table 3. Electronic spectral bands and their assignments

	Compound	Band (nm)	(cm^{-1})	Assignments
1	$[Mn(L)_2]$	254	39370	$\pi \rightarrow \pi^*$
		292	34306	$n \rightarrow \pi^*$
		337	29673	$^6A_{1g} \rightarrow {}^4A_{1g}(G)$,
		406	24630	$^6A_{1g} \rightarrow {}^4E_g(G)$
		687	14556	$^6A_{1g} \rightarrow {}^4T_{1g}(G)$
2	$[Co(L)OH]4H_2O$	252	39682	$\pi \rightarrow \pi^*$
		299, 325	33444, 30769	$n \rightarrow \pi^*$
		404	24752	$^2A_1 \rightarrow {}^2E$
3	$[Co(L)_2]Cl$	295	33898	$\pi \rightarrow \pi^*$
		488	20492	$^1A_{1g} \rightarrow {}^1T_{2g}$, $^1A_{1g} \rightarrow {}^1T_{1g}$
4	$[NiLCH_3COO]2H_2O$	253	39525	$\pi \rightarrow \pi^*$
		441	22676	*C–T*
		593	16863	$^3T_1(F) \rightarrow {}^3T_1(P)$
5	$[NiLCl_2]$	262	38168	$\pi \rightarrow \pi^*$
		319	31347	$n \rightarrow \pi^*$
		412	24272	*C–T*
		617	16207	$^1A_{1g} \rightarrow {}^1B_{1g}$
6	$[Cu(L)_2]$	262	38178	$\pi \rightarrow \pi^*$
		400	25000	*C–T*
7	$[CuLCl]H_2O$	271	36900	$\pi \rightarrow \pi^*$
		312	32051	$n \rightarrow \pi^*$
		362	27624	$n \rightarrow \pi^*$
		426	23474	*C–T*
		596	16778	$^2B_{1g} \rightarrow {}^2E_g$
		704	142045	$^2B_{1g} \rightarrow {}^2A_{1g}$
8	$[Zn(L)CH_3COO]2H_2O$	323	30959	$n \rightarrow \pi^*$
		399	25062	*C–T*
9	$[Zn(L)(NO_3)]2H_2O$	258	38759	$n \rightarrow \pi^*$
		319	31347	$n \rightarrow \pi^*$
		418	23923	*C–T*
10	[Cd(L)Cl]	254	39370	$\pi \rightarrow \pi^*$
		312	32051	$n \rightarrow \pi^*$
		404	24752	*C–T*

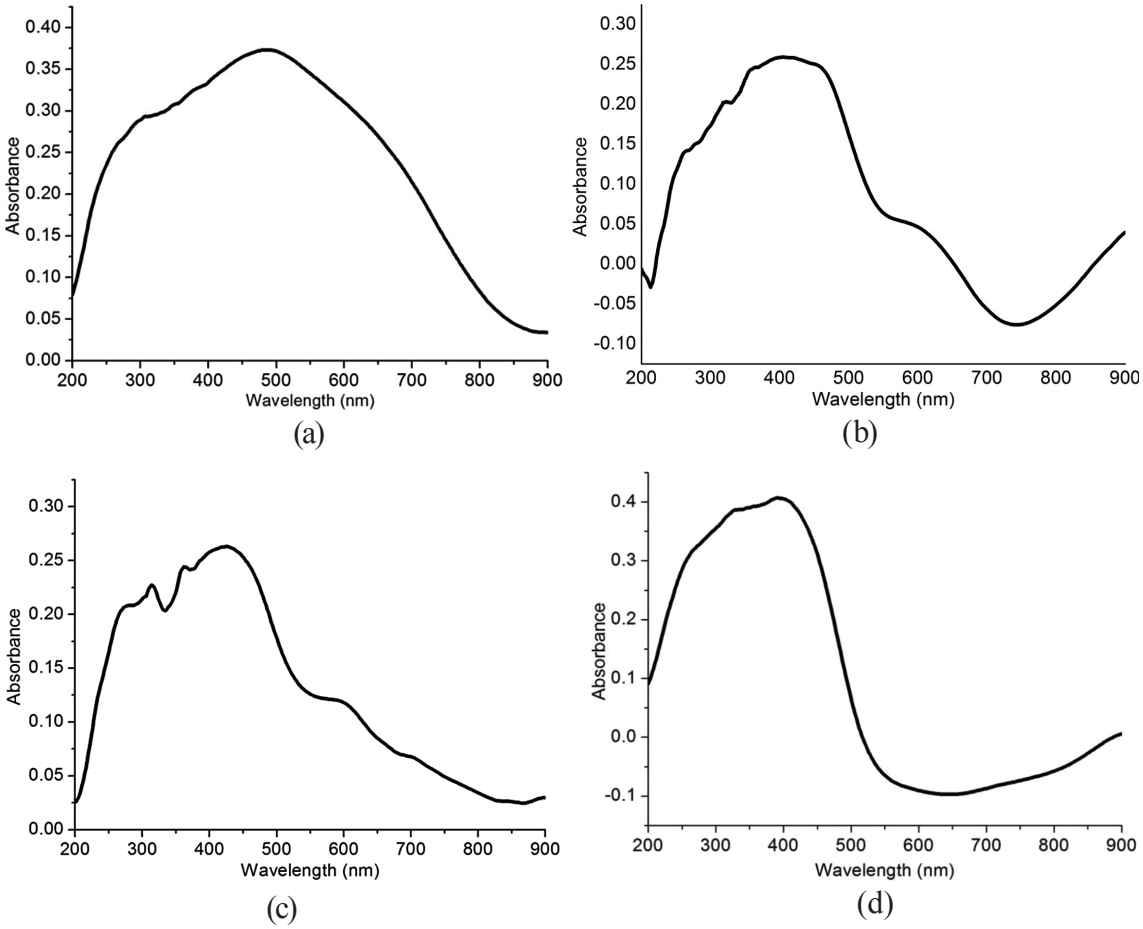

Fig. 7. Electronic spectra of complexes (a) $[Co(L)_2]Cl$ **(3)**, (b) $[Ni(L)Cl_2]$ **(5)**, (c) $[CuLClH_2O]$ **(7)** and (d) $[Zn(L)CH_3COO]2H_2O$ **(8)**.

3.2.2. Vibrational spectra

The IR spectral asssignments of the compounds are depicted in Table 4. The spectra of all of the complexes under this study showed broad bands in the range 3426–3487 cm^{-1}. They may be assigned to ν(N–H) and ν(OH) of water molecules.[29,30] The ν(C=O) band observed at 1642 cm^{-1} in the ligand spectrum is shifted to lower wavenumbers on coordination with the metal ions.[31,32] The shift of C=N stretching frequencies to lower wavenumber in the spectra of the complexes indicates the involvement of azomethine nitrogen in coordination. The peak at 794 cm^{-1}, due to C=S stretching vibration, is not observed in the spectra of the complexes. This indicates the involvement of thiol sulphur in coordination with the metal ions. The spectra of the complexes show new bands around 430 cm^{-1} and 520–568 cm^{-1} and are assigned to the νM–N and νM–O, respectively.[33] IR spectra of the complexes **(1)**, **(2)**, **(5)** and **(8)** are presented in Fig. 8.

Table 4 IR spectral assignments							
Compound No:	**Compound**	**NH/OH**	**C=O**	**C=N**	**N–N**	**C=S**	**C–S**
H_2L	$C_{18}H_{15}N_3O_2S$	3434	1642	1572	1161	794	–
1	$[Mn(L)_2]$	3438	1615	1544	1161	–	760
2	$[Co(L)OH]4H_2O$	3434	1621	1544	1152	–	759
3	$[Co(L)_2]Cl$	3426	1618	1544	1181	–	759
4	$[NiLCH_3COO]2H_2O$	3422	1615	1595	1184	–	760
5	$[Ni(HL)Cl_2]$	3414	1621	1538	1153	–	–
6	$[Cu(L)_2]$	3438	1615	1553	1179	–	763
7	$[Cu(L)Cl]H_2O$	3471	1612	1535	1133	–	759
8	$[Zn(L)CH_3COO]2H_2O$	3440	1621	1520	1152	–	759
9	$[Zn(L)(NO_3)]2H_2O$	3450	1615	1553	1179	–	759
10	[Cd(L)Cl]	3450	1613	1553	1171	–	760

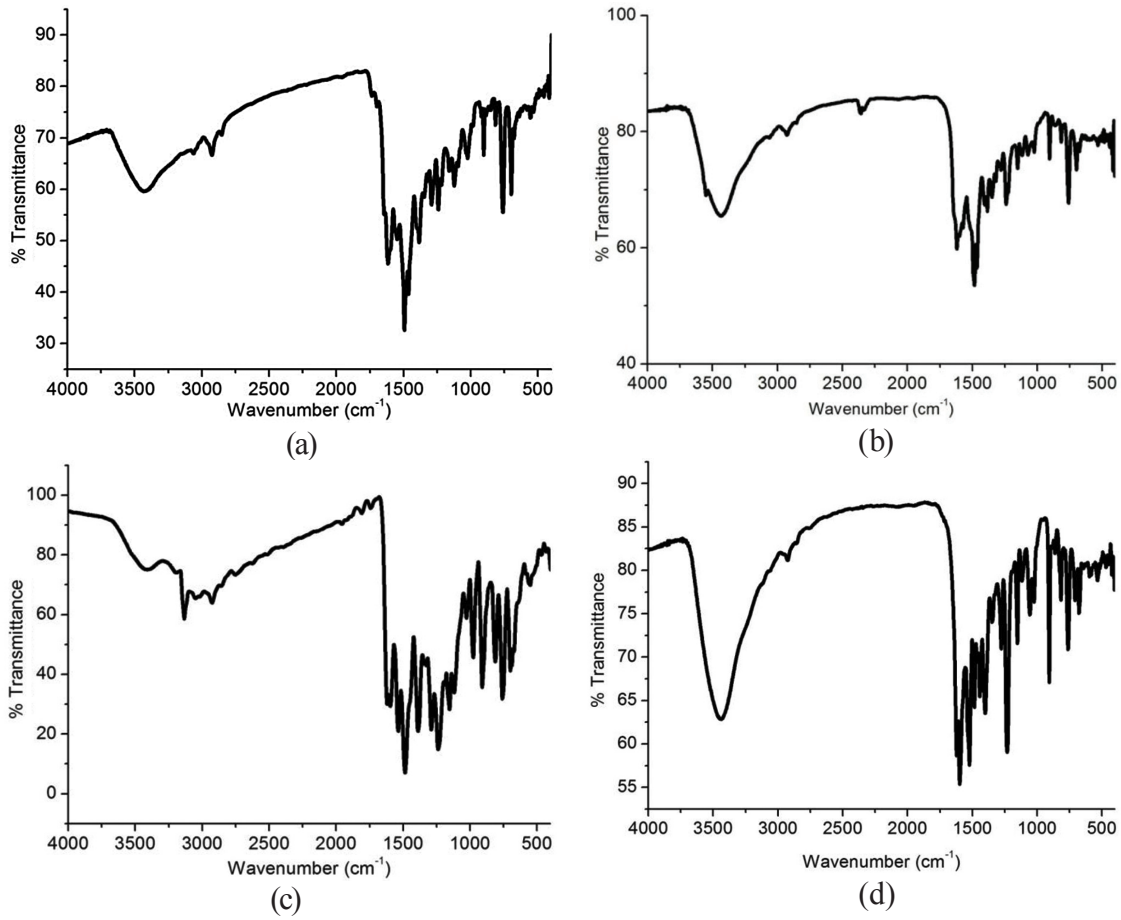

Fig. 8. IR spectra of the complexes(a) $[Mn(L)_2]$ **(1)**, (b) $[Co(L)OH]\ 4H_2O$ **(2)**, (c) $[Ni(L)Cl_2]$ **(5)** and (d) $[Zn(L)CH_3COO]\ 2H_2O$ **(8)**.

3.2.4. ^{1}H NMR spectrum

The ^{1}H NMR spectrum of the Ni(II) complex **(5)** was recorded in acetone at room temperature (Fig. 9). A peak observed at 11.423 ppm in the ligand spectrum due to NH proton was shifted to 11.834 ppm in the complex. This slight shift in the peak position may be due to the difference in the solvent used. A singlet observed at 8.763 ppm can be assigned to azomethine proton. N–CH_3 protons absorb in the region 3.888 ppm. Aromatic protons show a multiplet peak in the region 6.977–7.827 ppm. The peak observed in the region 1.980–2.089 ppm may be due to the solvent (acetone).

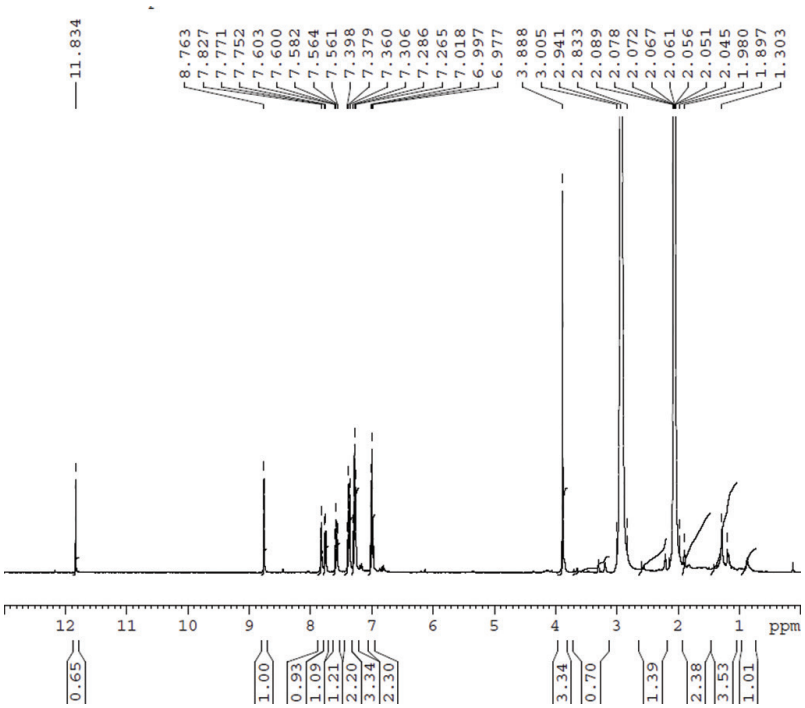

Fig. 9. ^{1}H NMR spectrum of the Ni(II)complex.

3.2.5. ESR spectrum

The ESR spectrum of Cu(II) complex **(6)** at 77 K in DMF was recorded in the X-band with 100 kHz field modulation (Fig. 10). The Cu(II) ion has an effective spin of $S = 3/2$ and is associated with a spin angular momentum, $m_s = \pm 1/2$, leading to a doubly degenerate spin state in the absence of magnetic field. In a magnetic field, the degeneracy between these states is lifted and the energy difference between them is given by $E = h\nu = g\beta B$, where h is the Planck's constant, ν is the frequency, g is the Lande's splitting factor equals to 2.0023 (for a free electron), β is the Bohr magneton and B is the magnetic field strength. The solution spectrum of the Cu(II) complex at 77 K in DMF shows four hyperfine lines. It is characteristic of monomeric Cu(II) complex corresponding to −3/2, −1/2, 1/2 and 3/2 which arise from the coupling of the odd electron with the copper nuclei ($I = 3/2$). The spectrum also gives three superhyperfine lines in the perpendicular region which arise from the coupling of the electron spin with nuclear spin of nitrogen atom which is co-planar. It indicates that in this complex azomethine nitrogen atom has coordinated to the metal

centre. Since there is no half-field signal in the ESR spectrum, we can confirm the monomeric nature of the complex.

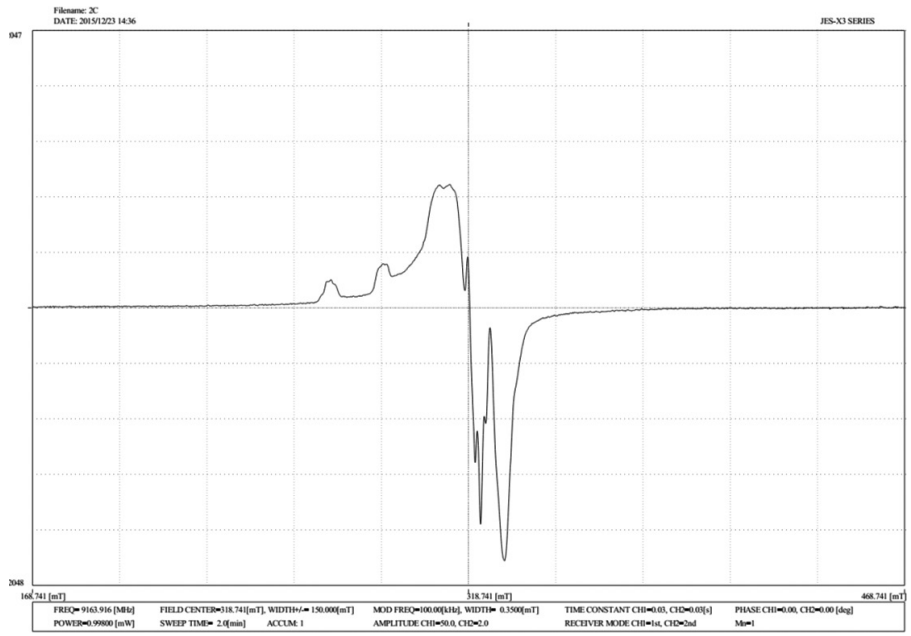

Fig. 10. ESR spectrum of Cu(II) complex (**6)** at 77 K in DMF.

3.2.6. Thermal studies

Thermo gravimetric analysis of the Schiff's base complexes are used to acquire ideas about their thermal stabilities, to fix whether the water molecules (if present) are coordinated or not to the central metal ion. It can propose a general scheme for thermal decomposition of metal complexes.

The $[Ni(HL)Cl_2]$ complex showed two stages of decomposition and is evident from the DTG peaks at 150°C and 260°C. A residual mass of 20% was left which may be due to the formation of NiS (calc. 19.4%).

The complex, $[Cu(L)_2]$, registered the first stage of decomposition between 95.5°C and 97.5°C with a weight loss of 1.2% which may be due to moisture. The next step of decomposition occurred in the temperature range 180°C–550°C with a mass loss 76%. This may be due to the complete decomposition of the ligand moiety. It is evident from the DTG peaks with temperature maxima at 163°C and 266°C. A residual mass of 22.3% was left which may be due to the formation of CuS (calc. 22.8%).

The complex, $[Cu(L)Cl]H_2O$, registered a first stage of decomposition between 100°C and 250°C with a weight loss of 4% which may be due to the elimination of one water molecule in the lattice. The next step of decomposition occurred in the temperature range 180°C–450°C with a mass loss 75% due to the decomposition of the ligand moiety. It is evident from the DTG peaks with temperature maxima at 145°C and 283°C. A residual mass of 20.6% was left which may be due to the formation of CuS (calc. 20.1%).

The Cd(II) complex **(10)** showed two stages of decomposition. DTG analysis showed two peaks at 153°C and 298°C due to the decomposition of the ligand moiety. TG-DTG

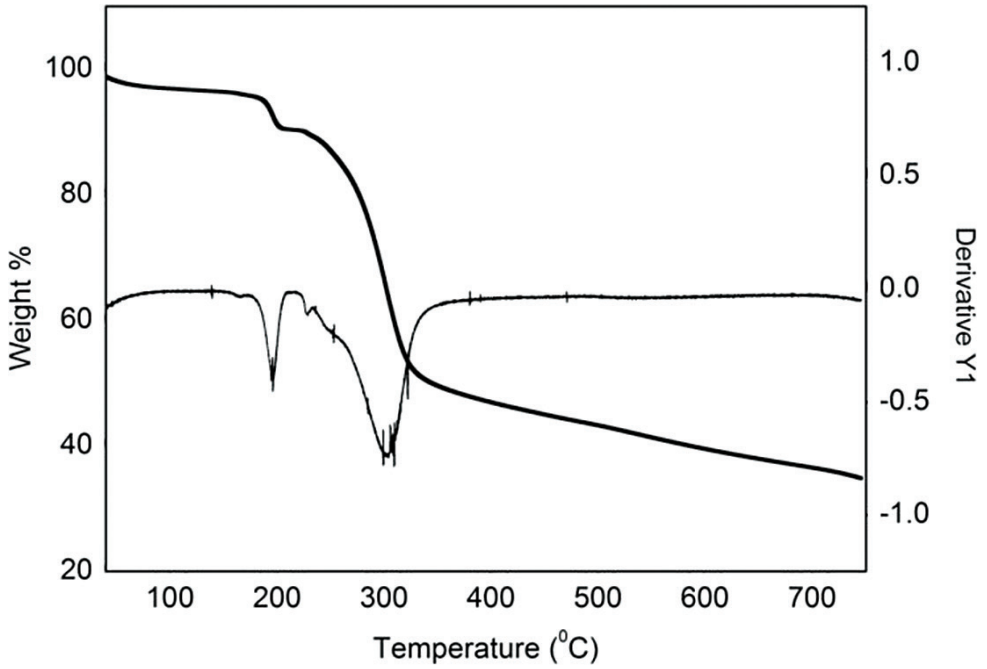

Fig. 11. TG-DTG curve of [Cd(L)Cl]**(10)**.

curve of [Cd(L)Cl] **(10)** is shown in Fig.11. A residual mass of 25% was left which may be due to the formation of CdO (calc. 24.6%).

4. Conclusions

Since the attempts to grow the single crystals of 3-formylchromone N(4)-methyl-N(4)-phenylthiosemicarbazone and its metal complexes were failed, the structures of the compounds were proposed based on elemental analyses, spectral and thermal studies. Following tentative structures are assigned for the complexes (Figs 12–16).

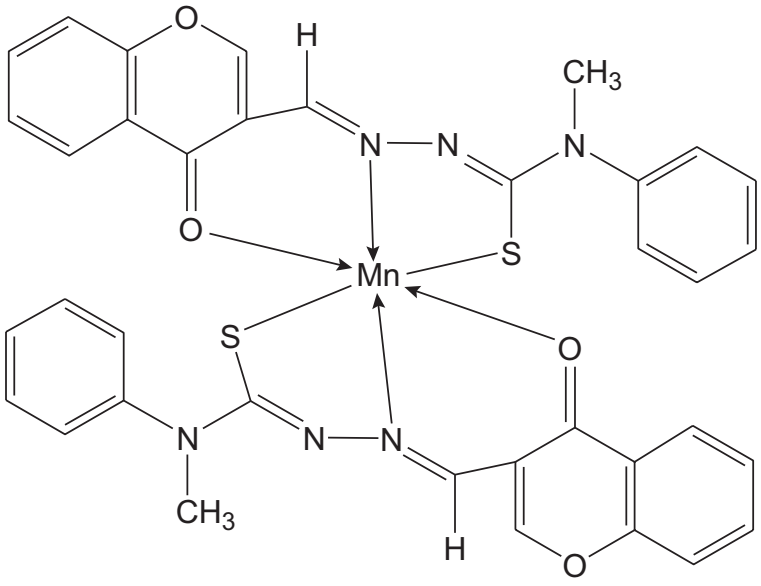

Fig. 12. Proposed structure of complex $[Mn(L)_2]$ **(1)**.

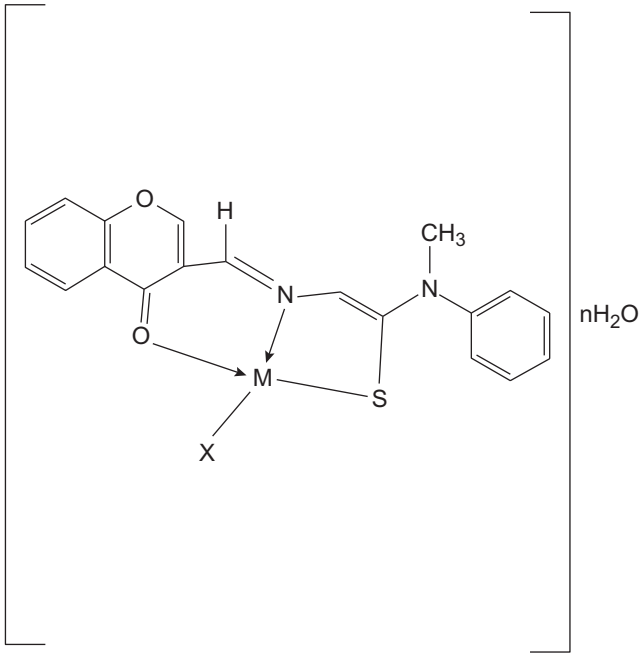

Fig. 13. Proposed structure of complexes [MLX]nH_2O, where M = Co(III), Ni(II),Cu(II), Zn(II), Cd(II); X = OH, Cl^-, CH_3COO^- **(2, 4, 7, 8, 9, 10)**.

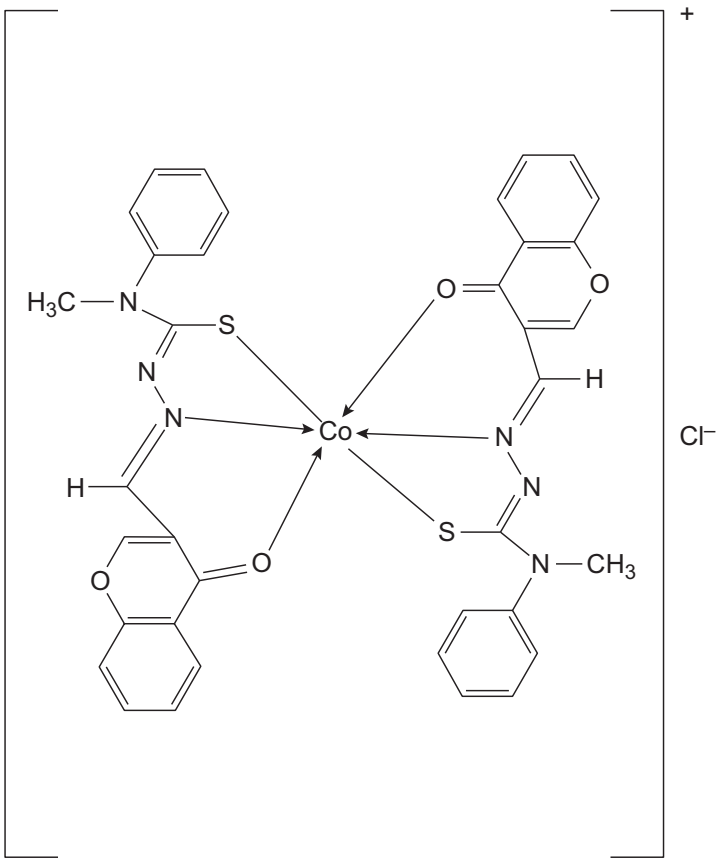

Fig. 14. Proposed structure of complex [CoL_2]Cl (3).

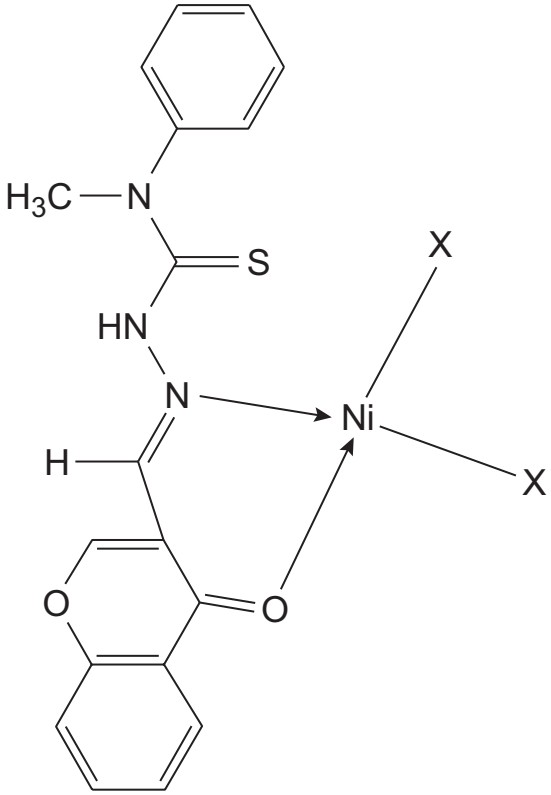

Fig. 15. Proposed structure of complex $[NiLX_2]$**(5)**, where X = Cl^-.

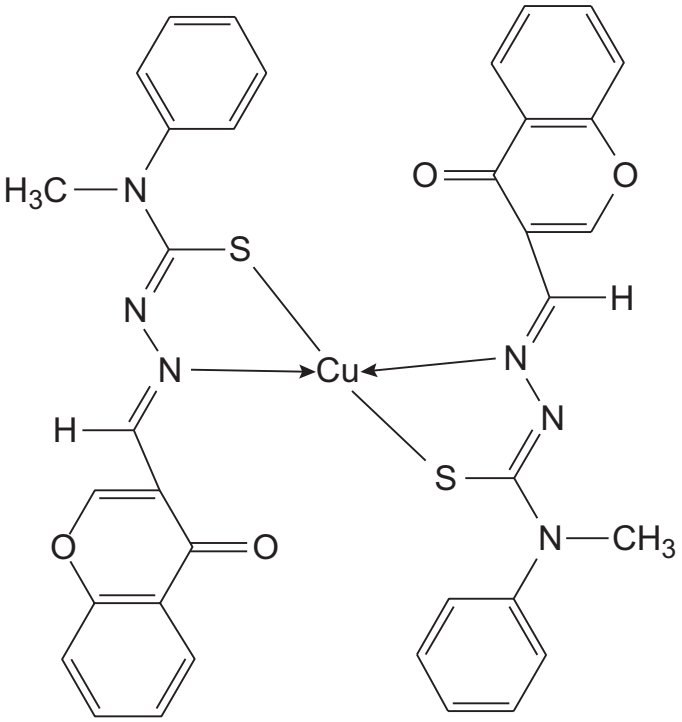

Fig. 16. Proposed structure of complex $[ML_2]$, where M = Cu(II) **(6).**

References

1. L. Rackova, S. Firakova, D. Kostalova, M. Stefek, E. Sturdik, M. Majekova, Bioorg. Med. Chem., 13 (2005) 6477.
2. B. K. Kaymakcioglu, S. Rollas, Farmaco, 57 (2002) 595.
3. S. R. Zhang, A. D. Sherry, J. Solid State Chem., 171 (2003) 38; W. Huang, M. -Z. Liu, Y. Li, Y. Tan, G. -F. Yamg, Bioorg. Med. Chem., 15 (2007) 5191.
4. S. Küçükgüzel, S. Rollas, I. Küçükgüzel, M. Kiraz, Eur. J. Med. Chem., 34 (1999) 1093.
5. K. M. Khan, N. Ambreen, U. R. Mughal, S. Jalil, S. Perveen, M. I. Choudhary, Eur. J. Med. Chem., 45 (2010) 4058.
6. Y. Li, Z. -Y. Yang, Z. -C. Liao, Z. -C. Han, Z. -C. Liu, Inorg. Chem. Commun., 13 (2010) 1213.
7. Y. Li, Z. -Y. Yang, J. -C. Wu, Eur. J. Med. Chem., 45 (2010) 5692.
8. B. D. Wang, Z. Y. Yang, T. Li, Bioorg. Med. Chem., 14 (2006) 6012.
9. S. Nabil Youssef, K. H. Hegab, A. E. Eid, Synth. React. Inorg. Met. Org. Chem., 33 (2003) 1647.
10. S. I. Al-Saeedi, A. -N. M. A. Alaghaz, R. A. Ammar, J. Mol. Struct., 1111 (2016) 201.
11. P. Kavitha, K. Laxma Reddy, Arabian J. Chem., 9 (2016) 640.
12. M. Belicchi Ferrari, S. Capacchi, G. Pelosi, G. Reffo, P. Tarasconi, R. Albertini, S. Pinelli, P. Lunghi, Inorg. Chim. Acta, 286 (1999) 134.
13. W. Linert, F. Renz, R. Boca, Coord. Chem., 40 (1996) 293.
14. S. Chandra, L. K. Gupta, Spectrochim. Acta A, 61 (2005) 2549.
15. A. K. Mukherjee, P. Ray, Indian Chem. Soc., 32 (1955) 633.
16. L. Sacconi, R. Cini, Ann. Chim. (Italy), 42 (1952) 723.
17. H. Nishikawa, S. Yamado, Bull. Chem. Soc. Japan, 8 (1964) 37.
18. B. N. Figgs, Introduction to Ligand Field, Wiley, New York City, New York, 1966.
19. K. P. Deepa, PhD thesis, University of Calicut, 1998.
20. N. L. Mary, PhD thesis, University of Calicut, 1992.
21. R. P. John, A. Sreekanth, M. R. P. Kurup, S. M. Mobin, Polyhedron, 21 (2002) 2515.
22. B. Gray, C. J. Ballhausen, J. Am. Chem. Soc., 85 (1963) 260.
23. R. Bindu, PhD thesis, Cochin University of Science and Technology, 1997.
24. G. L. Miessler, D. A. Tarr, Inorg. Chem., 2nd ed., Prentice Hall, Upper Saddle River, New Jersey, 1999.
25. B. Harikumar, M. R. P. Kurup, T. N. Jayaprakash, Trans. Met. Chem., 22 (1997) 507; P. Bindu, M. R. P. Kurup, Trans. Met. Chem., 22 (1997) 578.
26. J. Kuncheria, PhD thesis, University of Calicut, 1992.
27. D. Matoga, J. Szklarzewicz, R. Grybos, K. Kurpiewska, W. Nitek, Inorg. Chem., 50 (2011) 3501.
28. S. Bootwala, M. Tariq, S. Somasundaran, K. Aruna, Int. J. Pharm. Bio. Sci., 3 (2013) 345.
29. M. H. Moustafa, A. A. Elnaeem, O. A. Abbas, Ass. Univ. Bull. Environ. Res., 14 (2) (2011) 27; A. P. Mishra, D. K. Mishra, Int. J. Pharma. Bio. Sci., 2 (2011) B-430.
30. R. M. Issa, A. M. Khedr, H. F. Rizk, Spectrochim. Acta A, 62 (2005) 621; M. H. Habibi, M. Montazerozohori, A. Lalegani, R. W. Harrington, W. J. Clegg, Fluor. Chem., 127 (2006) 769.
31. O. A. El-Gammal, G. A. El-Reash, S. F. Ahmed, J. Mol. Struct., 1007 (2012) 1.
32. B. D. Wang, Z. Y. Yang, M. H. Lu, J. Hai, Q. Wang, Z. N. Chen, J. Organomet. Chem., 694 (2009) 4069.
33. K. Ramakrishna Reddy, K. Madhusudhan Reddy, K. N. Mahendra, Indian J. Chem., 45A (2006) 347.

CHAPTER VI

NOVEL LIGAND DERIVED FROM 4-HYDROXY 3-METHOXYBENZALDEHYDE AND N(4)-METHYL-N(4)-PHENYLTHIOSEMICARBAZIDE AND ITS TRANSITION METAL COMPLEXES

1. Introduction

Vanillin (Fig. 1) is familiar as the main flavour and fragrance compound in vanilla. It is used in perfumes, to mask unpleasant odours or tastes in medicines, livestock fodder and cleaning products. It is also used in the flavour industry, especially creamy profiles such as cream soda.

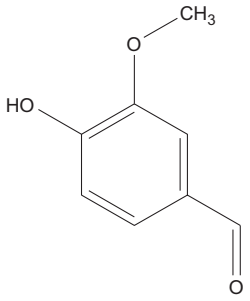

Fig. 1. Vanillin.

This chapter portrays the synthesis and characterisation of a novel ligand derived from 4-hydroxy-3-methoxybenzaldehyde and N(4)-methyl-N(4)-phenylthiosemicarbazide and its complexes. The structure of the ligand, 2-{2-[(4-hydroxy-3-methoxyphenyl)methylidene] hydrazinecarbonothioyl}-N-methyl-N-phenylhydrazine-1-carbothioamide, (H_2L) is shown as Fig. 2.

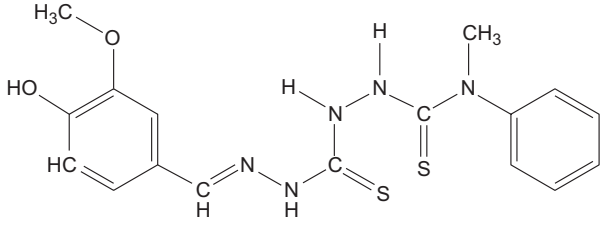

Fig. 2. 2-{2-[(4-hydroxy-3-methoxyphenyl)methylidene]hydrazinecarbonothioyl}-N-methyl-N-phenylhydrazine-1-carbothioamide. (IUPAC name of the compound.)

2. Experimental

2.1. Materials and methods

Vanillin (Merck), glacial acetic acid and commercially available metal salts were used without further purification. The solvents were purified and dried by standard procedure. The melting points of the ligand and complexes were recorded on a melting point apparatus. The ligand was characterised by partial elemental analyses, powder X-ray diffraction (XRD), Fourier-transform infrared spectroscopy (FT-IR), FT-Raman, electronic and ^{1}H nuclear magnetic resonance (NMR) spectra. The complexes were characterised by partial elemental analyses, magnetic susceptibility measurements, FTIR, electronic and ^{1}H NMR spectra. The details regarding these techniques are given in Chapter II.

2.2. Synthesis

Synthesis of the precursor N(4)-methyl-N(4)-phenylthiosemicarbazide (MPTSC) is discussed in Chapter II.

2.2.1. 2-{2-[(4-hydroxy-3-methoxyphenyl)methylidene]hydrazinecarbonothioyl}-N-methyl-N-phenylhydrazine-1-carbothioamide (H_2L)

H_2L was prepared by dropwise addition of a hot 70% ethanolic solution of vanillin (0.152 g, 1 mmol) to a boiling 70% ethanolic solution of MPTSC (0.364 g, 2 mmol) taken in a flat-bottomed flask, added two drops of glacial acetic acid, refluxed, stirred at 60°C–80°C for 1 hour and chilled. A light yellow coloured precipitate obtained was filtered and washed with water, followed by ethanol and dried. The melting point of the compound and its solubility in different solvents were noted. The reaction pathway of the ligand can be represented as Scheme 1:

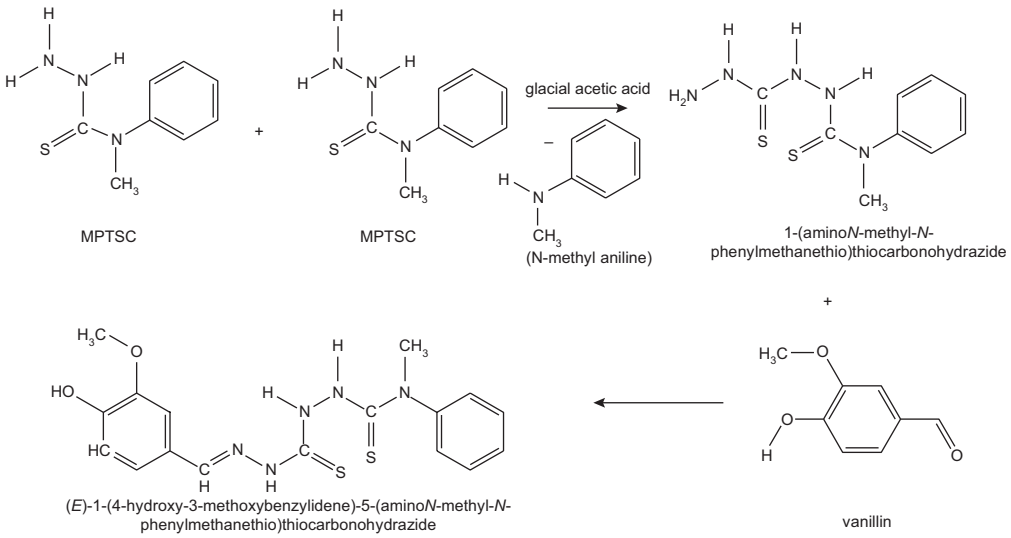

Scheme 1. Formation of H_2L.

2.2.2. Metal complexes

A hot ethanolic solution of H_2L was added dropwise to a hot ethanolic solution of metal acetate/chloride/nitrate in 1:1 molar ratio and refluxed for 3 hours. Then it was cooled to room temperature and the solid separated was collected. It was washed with water, followed by ethanol and dried.

3. Results and discussion

3.1. Characterisation of the ligand

3.1.1. Microanalytical data

The ligand H_2L was light yellow in colour having a melting point of 180°C. The suggested formula for the ligand is $C_{17}H_{19}N_5O_2S_2$ (Table 1). The partial elemental analysis of the ligand was in agreement with the suggested molecular formula. The ligand was soluble in polar solvents like methanol and ethanol.

Table 1. Analytical data of the ligand

Compound	Molecular Weight	Melting Point	Colour	Yield	Elemental Analysis Found(calculated)			
					C	H	N	S
$C_{17}H_{19}N_5O_2S_2$. (H_2L)	389	240	Light yellow	80	52.2 (52.4)	4.7 (4.9)	17.9 (17.9)	16.8 (16.4)

3.1.2. Powder XRD of the ligand, H_2L

Since we couldn't obtain a single crystal of H_2L, we recorded its powder XRD pattern. It revealed the crystallinity of the compound. Using MATCH software, it was found that the compound belongs to monoclinic crystal system. (Fig. 3).

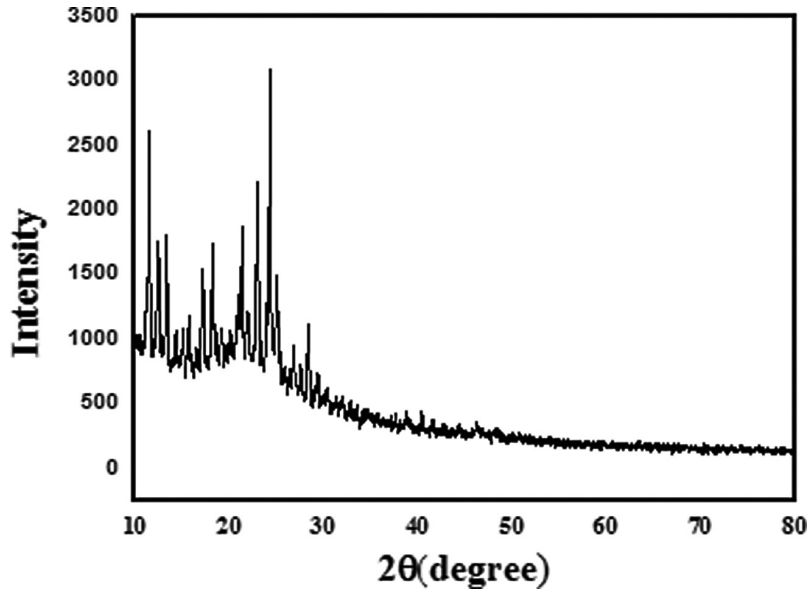

Fig. 3. Powder XRD of the ligand.

3.1.3. Spectroscopic analysis of H_2L

(a) Electronic spectrum

The electronic absorption spectrum of the ligand was recorded in solid state in the range of 200–900 nm (Fig. 4). The compound registered charge-transfer bands at 260, 318 and 410 nm. The absorption band observed at 260 nm may be attributed to the π–π^* transition of the azomethine chromophore and the benzene ring (intra-ligand charge-transfer transition). The band at 318 nm may be due to the n–π^* transition. The weak band observed at 410 nm could be due to the charge-transfer transition.

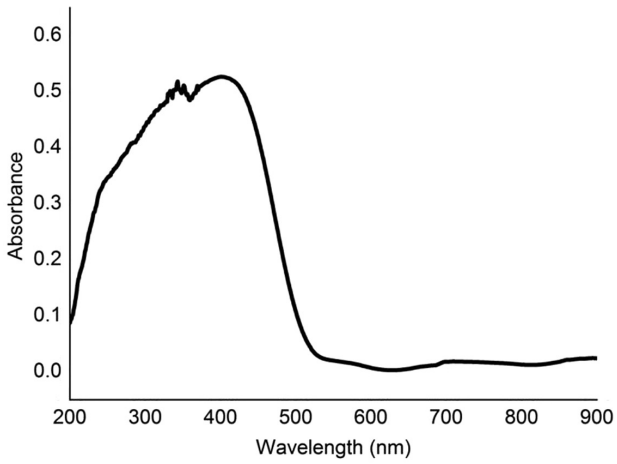

Fig. 4. Electronic spectrum of the ligand.

(b) Vibrational spectra

The FT-IR spectrum of the compound was recorded in the region 4000–400 cm^{-1} and is presented as Fig. 5. The ligand H_2L showed a broad band at 3455–3255 cm^{-1} due to OH stretching vibration. Sharp bands at 3157 and 3010 cm^{-1} may be due to NH stretching vibrations. A sharp band at 1603 cm^{-1} in the ligand spectrum was assigned to ν(C=N). The ν(S–H) band at 2560 cm^{-1} was absent in the IR spectrum, indicating the existence of the thione tautomer in the solid state. The bands at 1125 and 763 cm^{-1} in the ligand spectrum may be assigned to ν(NH–C=S) and ν(C=S), respectively.

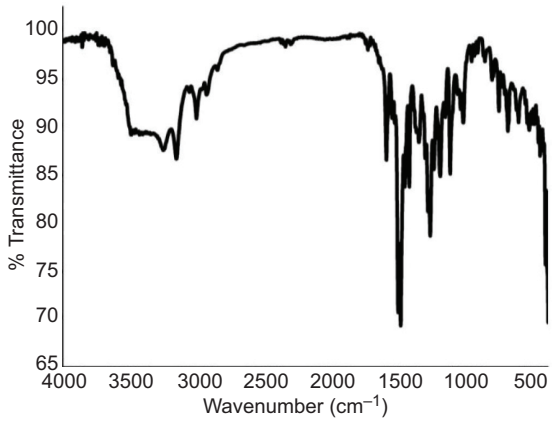

Fig. 5. FT-IR spectrum of the ligand.

The FT-Raman spectrum of the compound was recorded in the region 4000–400 cm^{-1} and is presented as Fig. 6. In the Raman spectrum, the ligand H_2L showed a doublet at 3076 cm^{-1} due to N–H stretching vibration. The band observed at 1593 cm^{-1} is assigned to ν(C=N). The bands at 1277 and 797 cm^{-1} in the ligand may be assigned to ν(NH–C=S) and ν(C=S), respectively.

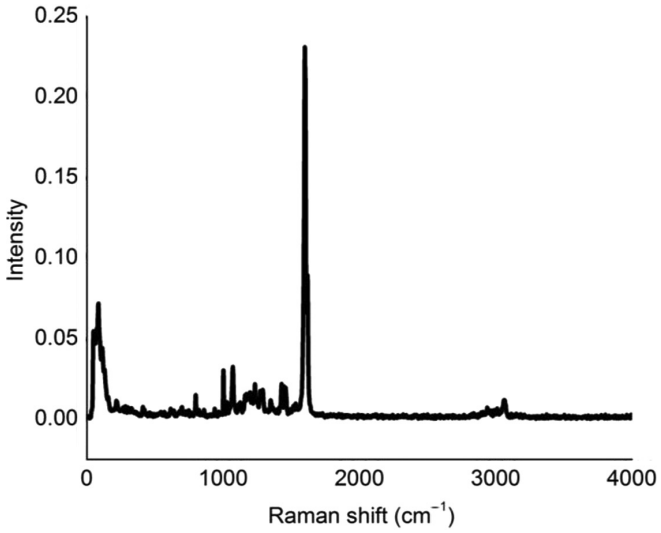

Fig. 6. Raman spectrum of the ligand.

(c) ^{1}H NMR spectrum

The ^{1}H NMR spectrum of the ligand was recorded in $CDCl_3$ and is presented as Fig. 7. The two doublets at 10.874–10.894 and 8.851–8.871 ppm are assigned to NH protons. A singlet at 8.629 ppm may be assigned to N–H proton adjacent to azomethine group. A singlet at 7.626 ppm can be assigned to O–H proton. Aromatic protons registered multiplet peaks in the region 6.777–7.580 ppm. Singlet at 3.983 ppm is assigned to methoxy protons. ^{4}N–CH_3 protons absorb at 3.702 ppm.

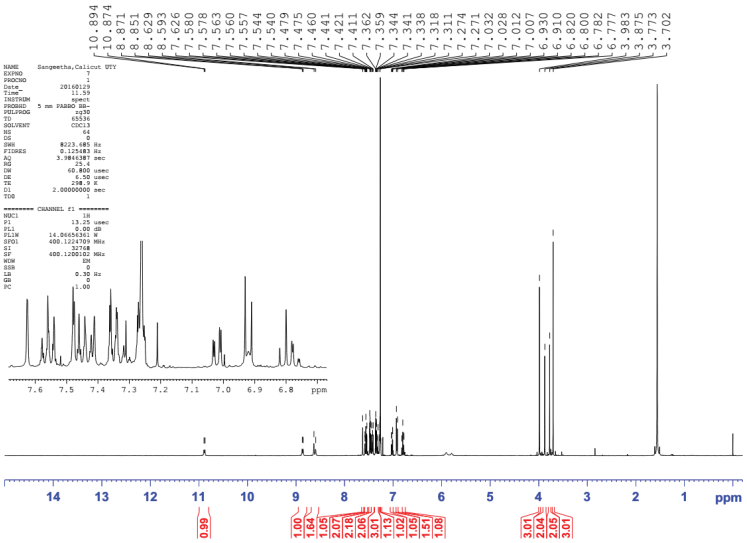

Fig. 7. NMR spectrum of the ligand.

3.2. Characterisation of the metal complexes

3.2.1. Formulae and general properties of the complexes

From the elemental analysis and spectral studies, the compounds were assigned the empirical formula as presented in the Table 2. The ligand, H_2L acted as mono-anionic tridentate (HL^-) in all the complexes.

Table 2. Molecular formula, colour, partial elemental analyses and magnetic moments of the complexes

Complex No.	Compound	Molecular Weight	Melting Point	Colour	Yield	Elemental Analysis Found (calculated)					μ in BM
						C	H	N	S	M	
	$C_{17}H_{19}N_5O_2S_2$ (H_2L)	389	240	Light yellow	80	52.2 (52.4)	4.7 (4.9)	17.9 (17.9)	16.8 (16.4)	–	–
1	$[Mn(HL)_2]$	833	260	Green	80	49.3 (49.0)	3.9 (4.3)	16.0 (16.8)	15.0 (15.3)	7.2 (6.6)	6.0
2	$[Co(HL)CH_3COO]$	507	>300	Green	70	45.4 (45.0)	3.7 (4.1)	14.3 (13.8)	13.0 (12.6)	11.9 (11.6)	4.1
3	$[Ni(HL)CH_3COO]_2$	1013	255	Greenish yellow	70	45.3 (45.0)	3.8 (4.1)	13.5 (13.8)	13.2 (12.6)	11.5 (11.6)	1.6
4	$[Ni(HL)_2]$	837	280	Brown	80	49.0 (48.8)	4.0 (4.3)	16.9 (16.7)	15.5 (15.2)	6.8 (7.0)	3.6
5	$[Cu_2(HL)(CH_3COO)_3]$	693	270	Black	70	40.0 (39.8)	3.3 (3.9)	10.5 (10.1)	9.5 (9.2)	18.6 (18.3)	1.2
6	$[Cu_2(HL)Cl_3]$	623	260	Black	75	32.3 (32.7)	2.5 (2.9)	11.6 (11.2)	10.6 (10.3)	20.2 (20.3)	D
7	$[Zn(HL)CH_3COO]$	513	220	Yellow	80	39.6 (39.8)	3.8 (4.1)	13.4 (13.6)	12.4 (12.4)	12.2 (12.7)	D
8	$[Cd(HL)CH_3COO]$	560	250	Yellow	80	37.0 (36.4)	3.6 (3.8)	12.7 (12.5)	11.7 (11.4)	20.1 (20.0)	D

3.2.2. Electronic spectra and magnetic moments

The electronic spectra of complexes were recorded in solid state and their probable assignments are given in Table 3.

Table 3. Electronic spectral bands and their assignments

Complex No.	Compound	Band in nm	Band in cm^{-1}	Assignments
	$C_{17}H_{19}N_5S_2O_2$ (H_2L)	260	38461	$\pi \rightarrow \pi^*$
		318	31446	$n-\pi^*$
		410	24390	C–*T*
1	$[Mn(HL)_2]$	254	39370	$\pi \rightarrow \pi^*$
		306	32679	$n-\pi^*$
		368	27173	$^6A_{1g} \rightarrow {}^4A_{1g}(G)$
		730	13698	$^6A_{1g} \rightarrow {}^4T_{1g}(G)$

2	[Co(HL)CH_3COO]	268	37313	$\pi \rightarrow \pi^*$
		306	32679	$n-\pi^*$
		420	23809	*C–T*
		699	14306	$^4A_2 \rightarrow {}^4T_1(P)$
3	[$(Ni(HL)CH_3COO)_2$]	277	36101	$\pi \rightarrow \pi^*$
		335	298507	$n-\pi^*$
		408	24509	*C–T*
		880	11363	$^3A_{2g}(F) \rightarrow {}^3T_{2g}(F)$
4	[$Ni(HL)_2$]	263	38022	$\pi \rightarrow \pi^*$
		330	30303	$n-\pi^*$
		380	26315	$^3A_{2g}(F) \rightarrow {}^3T_{1g}(P)$
		590	16949	$^3A_{2g}(F) \rightarrow {}^3T_{1g}(F)$
		873	11454	$^3A_{2g}(F) \rightarrow {}^3T_{2g}(F)$
5	[$Cu_2(HL)(CH_3COO)_3$]	259 290	38610, 34487	$\pi \rightarrow \pi^*$
		311 361	32154, 27700	$n-\pi^*$
		402	24875	*C–T*
		444	22522	*C–T*
		699	14306	$^2B_{1g} \rightarrow {}^2E_g$
		844	11848	$^2B_{1g} \rightarrow {}^2A_{1g}$
6	[$Cu_2(HL)Cl_3$]	273	36630	$\pi \rightarrow \pi^*$
		304	32894	$n-\pi^*$
		341	29325	*C–T*
		377	26525	*C–T*
		583	17152	$^2B_{1g} \rightarrow {}^2E_g$
7	[Zn(HL)CH_3COO]	338	29585	$n-\pi^*$
		400	25000	*C*–T
		705	14184	*C–T*
8	[Cd(HL)CH_3COO]	267	37453	$\pi \rightarrow \pi^*$
		313	319	$n-\pi^*$
		405	24691	*C–T*
		711	14064	*C–T*

In the electronic spectra of all the complexes, the $\pi \rightarrow \pi^*$ and the $n \rightarrow \pi^*$ bands were observed around 250 and 320 nm, respectively. The band around 340–440 nm is assignable to S → M charge-transfer transition.

In this study, the electronic spectrum of Mn(II) complex exhibited two broad bands of very low intensities, one at 368 and another at 730 nm. They may be assigned to $^6A_{1g} \rightarrow {}^4A_{1g}(G)$ and $^6A_{1g} \rightarrow {}^4T_{1g}(G)$ transitions, respectively. The magnetic moment value of the Mn(II) complex was found to be 6.0 BM which is in accordance with an octahedral geometry.

The ground state in a tetrahedral Co^{2+} ion is $^4A_2$. The possible transitions are $^4A_2 \rightarrow {}^4T_2$, $^4A_2 \rightarrow {}^4T_1$ (F) and $^4A_2 \rightarrow {}^4T_1$ (P). The first transition, $^4A_2 \rightarrow {}^4T_2$ is not usually observed in the spectrum, since it occurs in the region 3000–5000 cm^{-1}. $^4A_2 \rightarrow {}^4T_1$(P) transition appears as intense broad band in the visible region. In this study, Co(II) complex showed band in the region 699 nm due to $^4A_2 \rightarrow {}^4T_1$ (P) transition. However, the other transitions were not observed as they absorb out of the range of the spectrophotometer used in this study.

The observed values of magnetic moment for Co(II) complexes are generally diagnostic of the coordination geometry about the metal ion.[1] Tetrahedral and octahedral Co(II) complexes can be distinguished by the extent of deviation of the effective magnetic moment value (μ_{eff}) from the spin-only value even though they have same number of unpaired electrons. The tetrahedral Co(II) complexes have magnetic moments in the range 3.8–4.7 BM, while octahedral complexes have in the range 4.8–5.6 BM. This is due to large contribution from its $^4T_{1g}$ ground term.[2] The low-spin square-planar Co(II) complexes have magnetic moments in the range 2.1–2.9 BM at room temperature. The observed magnetic moment value was 4.1 BM which excludes the possibility of octahedral and square-planar geometry to the complex. The green colour and the magnetic moment value (4.1 BM) of the Co(II) complex reported here indicate its tetrahedral geometry.

Octahedral Ni(II) complexes with d^8 configuration have a ground state $^3A_{2g.}$ The three spin-allowed transitions are $^3A_{2g}$ (F) $\rightarrow {}^3T_{2g}$ (F), $^3A_{2g}$ (F) $\rightarrow {}^3T_{1g}$ (F) and $^3A_{2g}$ (F) $\rightarrow {}^3T_{1g}$ (P). They are observed in the range 8000–11000, 15000–19000 and 25000–29000 cm^{-1}, respectively. However, in the case of the complex **(3)**, only a broad band in the region 880 nm was observed which is assigned to $^3A_{2g}$ (F) $\rightarrow {}^3T_{2g}$ (F) transition. For octahedral Ni(II) complexes, magnetic moments are found to be in the range 2.94–3.04 BM. The magnetic moment of the complex **(3)** was 1.6 BM, which is very low for an octahedral complex. This may be because of the distortion and inequalities in the field of coordinated ligands or due to the antiferromagnetic interactions between two metal centres. The greenish-yellow colour of the complex and its electronic spectrum indicate an octahedral geometry.

In the electronic spectrum of the Ni(II) complex **(4)**, three transitions were observed. They are at 380, 590 and 873 nm due to $^3A_{2g}$(F) $\rightarrow {}^3T_{1g}$(P), $^3A_{2g}$ (F) $\rightarrow {}^3T_{1g}$ (F) and $^3A_{2g}$ (F) $\rightarrow {}^3T_{2g}$ (F) transitions, respectively. Its magnetic moment was 3.6 BM, which is higher than that found for octahedral complexes.

The Cu(II) complex **(5)** showed bands at 699 and 844 nm which may be due to $^2B_{1g} \rightarrow {}^2E_g$ and $^2B_{1g} \rightarrow {}^2A_{1g}$ transitions, respectively. This is in accordance with a square-planar geometry. It registered a very low magnetic moment value of 1.20 BM and may be due to antiferromagnetic interactions between two Cu(II) ions.[3] The compound **(6)** was diamagnetic and strongly supported its existence as a dimer in the solid state.[4] No characteristic d–d transitions were observed for Zn(II) and Cd(II) complexes. However, they showed charge-transfer bands in the visible range. Representative spectra of the complexes **(2), (3)** and **(6)** are presented in Fig. 8.

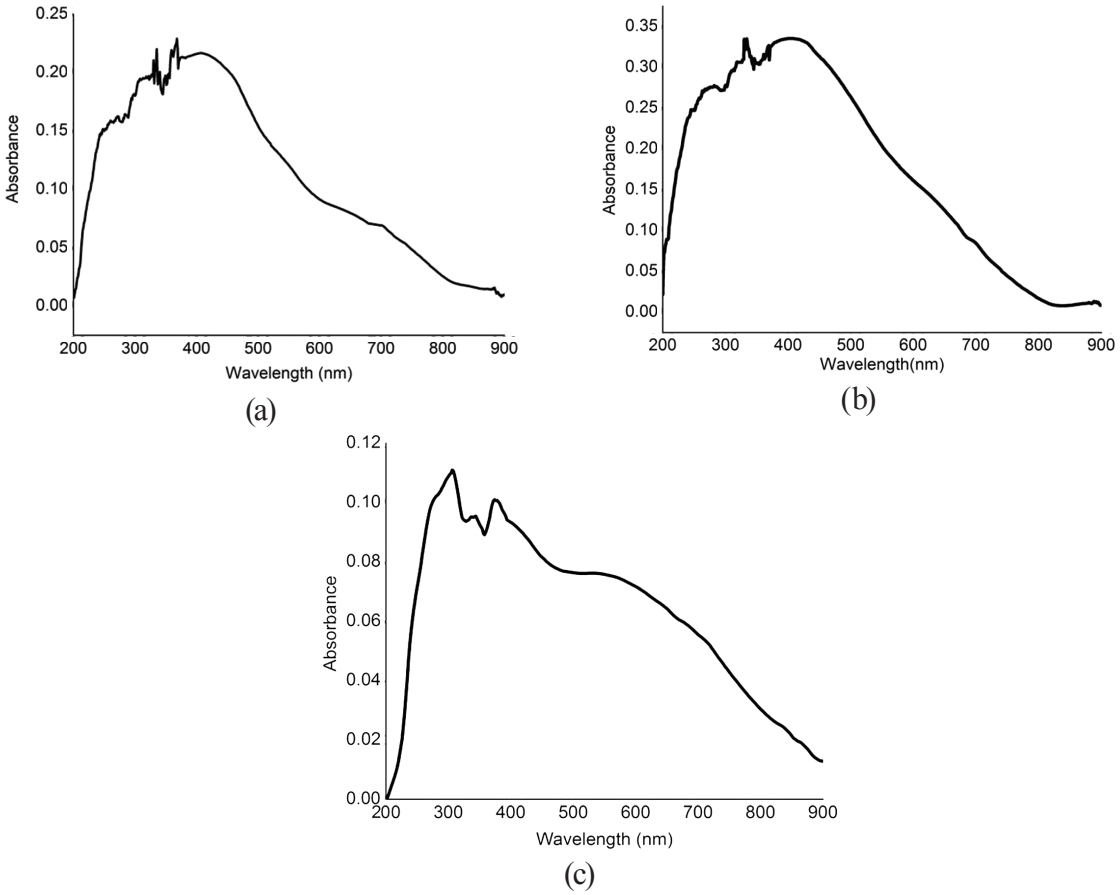

Fig. 8. Electronic spectra of the compounds (a) $[Co(HL)CH_3COO]$ **(2)**, (b) $[Ni(HL)CH_3COO]_2$ **(3)** and **(c)** $[Cu_2(HL)Cl_3]$ **(6)**.

3.2.3. Vibrational spectra

The IR spectra of the ligand and the metal complexes were compared to assign the mode of coordination. The IR spectral assignments are depicted in the Table 4. The broad band present in the region 3450 cm^{-1} is assigned to the ν(OH). The bands at 3255, 3157 and 3010 cm^{-1} are assigned to n(NH). A sharp band at 1603 cm^{-1} for the ligand is found to be shifted to lower wavenumbers in the spectra of the complexes. The IR spectra of all the complexes showed new bands at 400–480 and 520–620 cm^{-1}, assigned to ν(M–N) and ν(M–O), respectively. The M–O band may be either due to coordinated acetate$^-$, nitrate$^-$ or hydroxyl anion or coordinated water molecule.

3.2.3.1. Coordination of anions

The $\nu_{as}(COO^-)$ and $\nu_s(COO^-)$ of the free acetate ions are observed at 1560 and 1416 cm^{-1}, respectively.[5] For the coordinate acetate ion, $\nu_{as}(COO^-)$ occurs in the range 1650–1500 cm^{-1} and for $\nu_s(COO^-)$ is seen above 1400 cm^{-1}. In unidendate complexes, the energy of separation between these two is generally greater than 144 cm^{-1}.[6]

For the complex $[Co(HL)CH_3COO]$, the $\nu_{as}(COO^-)$ and $\nu_s(COO^-)$ of acetate ion are observed at 1599 and 1384 cm^{-1}, respectively. In $[(Ni(HL)CH_3COO)_2]$, the $\nu_{as}(COO^-)$ and $\nu_s(COO^-)$ of acetate ion are observed at 1593 and 1353 cm^{-1}, respectively. In the case of $[Cu_2(HL)(CH_3COO)_3]$, two types of acetate coordination was observed. One is bridging

Table 4. IR spectral assignments

Complex No.	Compound	ν(OH)/ ν(NH)	ν(C=N)	ν(N–N)	ν(C=S)	ν(M–N)
	H_2L	3455	1603	1125	763	–
1	$[Mn(HL)_2]$	3414	1591	1123	759	407
2	$[Co(HL)CH_3COO]$	3414	1563	1120	751	416
3	$[(NiHLCH_3COO)_2]$	3426	1571	1126	757	408
4	$[Ni(HL)_2]$	3450	1595	1128	755	422
5	$[Cu_2L(CH_3COO)_3]$	3355	1591	1123	763	418
6	$[Cu_2(HL)Cl_3]$	3426	1592	1127	763	410
7	$[Zn(HL)CH_3COO]$	3424	1590	1130	763	418
8	$[Cd(HL)CH_3COO]$	3438	1592	1111	753	419

bidentate and other is unidentate. The $\nu_{as}(COO^-)$ and $\nu_s(COO^-)$ of bridging acetate ion are observed at 1669 and 1513 cm^{-1}, respectively. The $\nu_{as}(COO^-)$ and $\nu_s(COO^-)$ of unidentate acetate ion are observed at 1591 and 1426 cm^{-1}, respectively. In $[Zn(HL)CH_3COO]$, the $\nu_{as}(COO^-)$ and $\nu_s(COO^-)$ of acetate ion are observed at 1591 and 1389 cm^{-1}, respectively. In $[Cd(HL)CH_3COO]$, the $\nu_{as}(COO^-)$ and $\nu_s(COO^-)$ of acetate ion are observed at 1595 and 1369 cm^{-1}, respectively. Representative spectra of the complexes **(2)**, **(4)** and **(6)** are presented in Fig. 9.

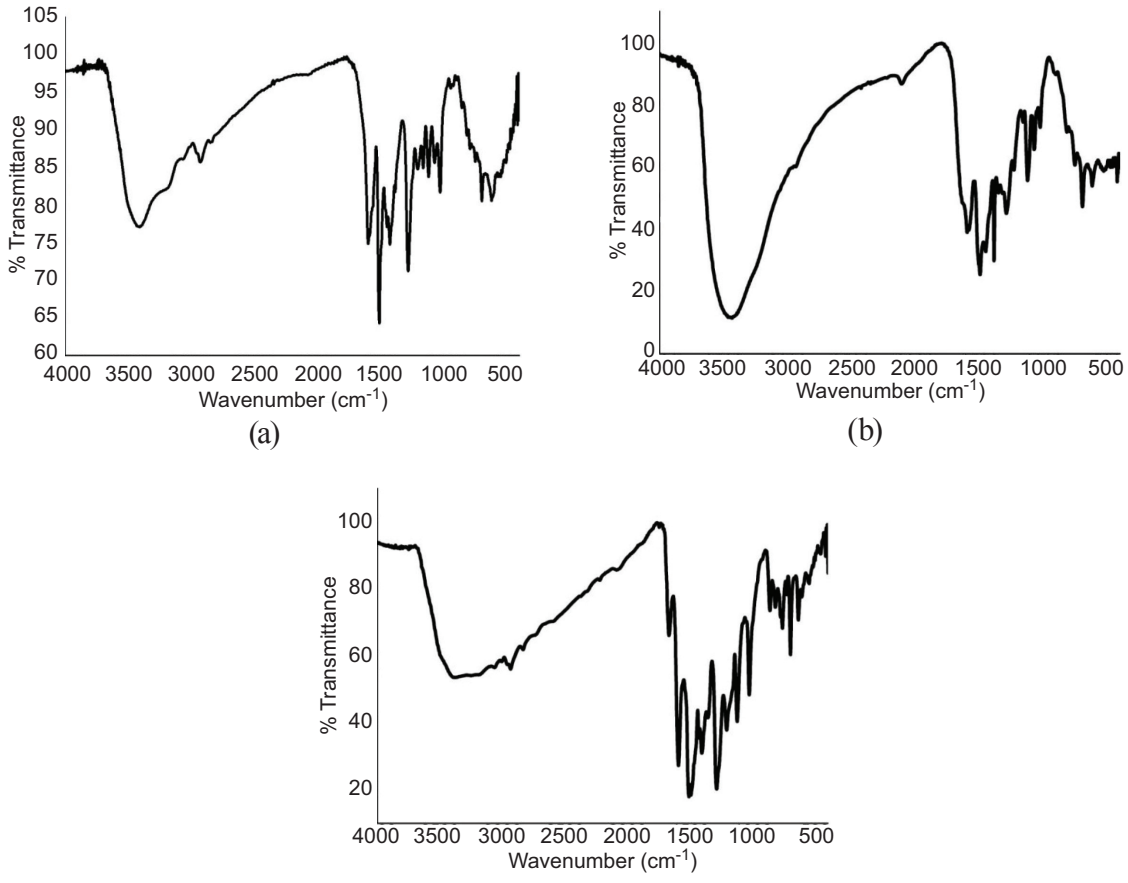

Fig. 9. IR spectra of the compounds (a) $[CoHLCH_3COO]$ **(2)**, (b) $[Ni(HL)_2]$ **(4)** and (c) $[Cu_2(HL)Cl_3]$ **(6)**.

3.2.4. ^{1}H NMR spectrum

The ^{1}H NMR spectrum of the Zn(II) complex was recorded in DMSO at room temperature **(**Fig. 10) A singlet at 11.710 ppm can be assigned to N–H proton. A singlet at 9.384 ppm can be assigned to N–H proton adjacent to azomethine group. A singlet at 7.872 ppm can be assigned to OH proton. Aromatic protons gave a multiplet peak in the region 6.763–7.461 ppm. ^{4}N–CH_3 protons absorbed at 3.793 ppm. Singlet at 3.838 ppm may be assigned to methoxy protons. In addition to this, CH_3 protons of acetyl group absorbed at 3.793 ppm.

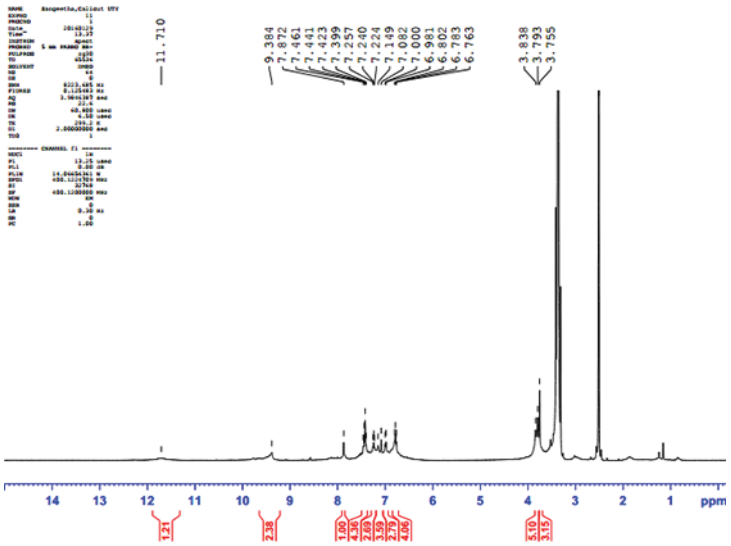

Fig. 10. ^{1}H NMR spectrum of the Zn(II) complex.

3.2.5. Thermal studies

For [ZnHLCH$_3$COO], two stages of decomposition occurred in the temperature range 260°C–390°C which may be due to the partial decomposition of the ligand moiety. The residual mass of 15.4% was observed at 750°C and may be due to the formation of zinc sulfide (calc. 15.9%). TG-DTG curve of [Zn(HL)CH$_3$COO] **(7)** is shown in Fig.11.

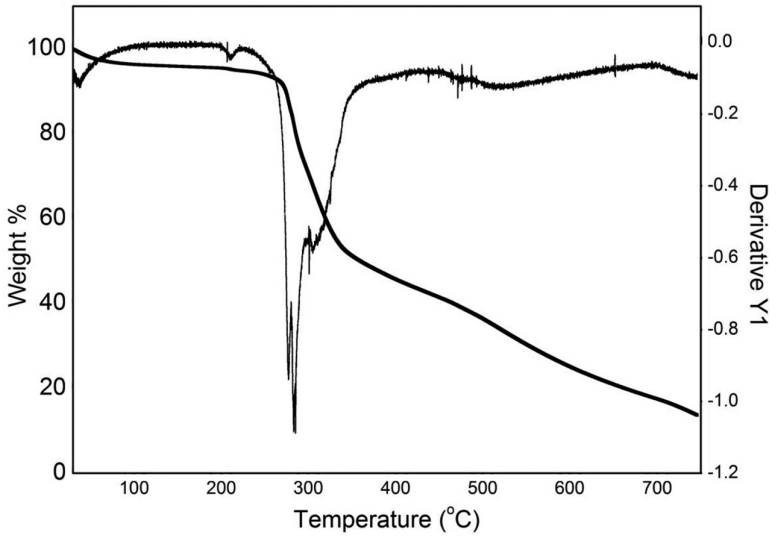

Fig. 11. TG-DTG curve of [Zn(HL)CH$_3$COO] **(7)**.

4. Conclusions

The synthesis and characterisation of Mn(II), Co(II), Ni(II), Cu(II), Zn(II) and Cd(II) complexes of 2-{2-[(4-hydroxy-3-methoxyphenyl)methylidene]hydrazinecarbonothioyl}-N-methyl-N-phenylhydrazine-1-carbothioamide (H_2L) have been discussed. Based on the magnetic moments and spectral data, the Co(II), Zn(II) and Cd(II) complexes are assigned a tetrahedral geometry. Cu(II) complexes are assigned square-planar geometry. The Mn(II) and Ni(II) complexes are assigned octahedral geometry. According to IR and ^{1}H NMR spectral data, H_2L was found to function as monobasic tridentate ligand (HL^-) (Figs. 12–15).

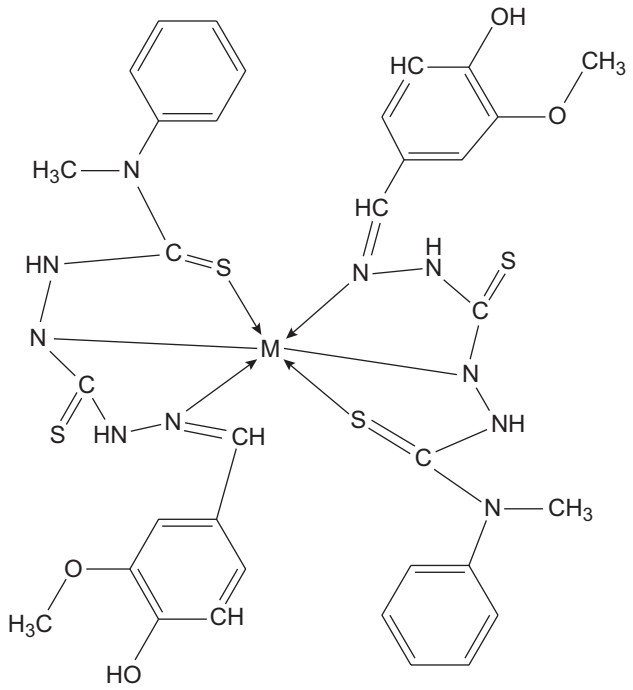

Fig. 12. Proposed structure of the complexes [ML_2], where M = Mn(II), Ni(II) **(1)** and **(4).**

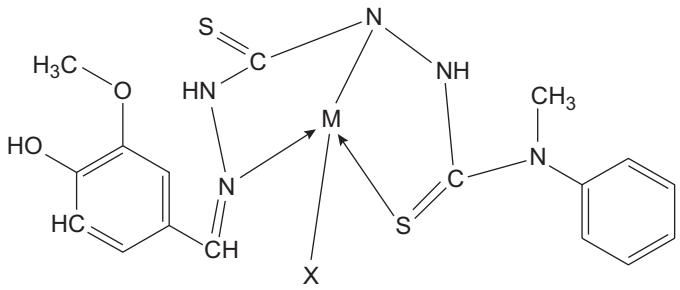

Fig. 13. Proposed structure of the complexes [MLX], where M = Co(II), Zn(II) and Cd(II); X = CH_3COO^-, **(2)**, **(7)** and **(8)**.

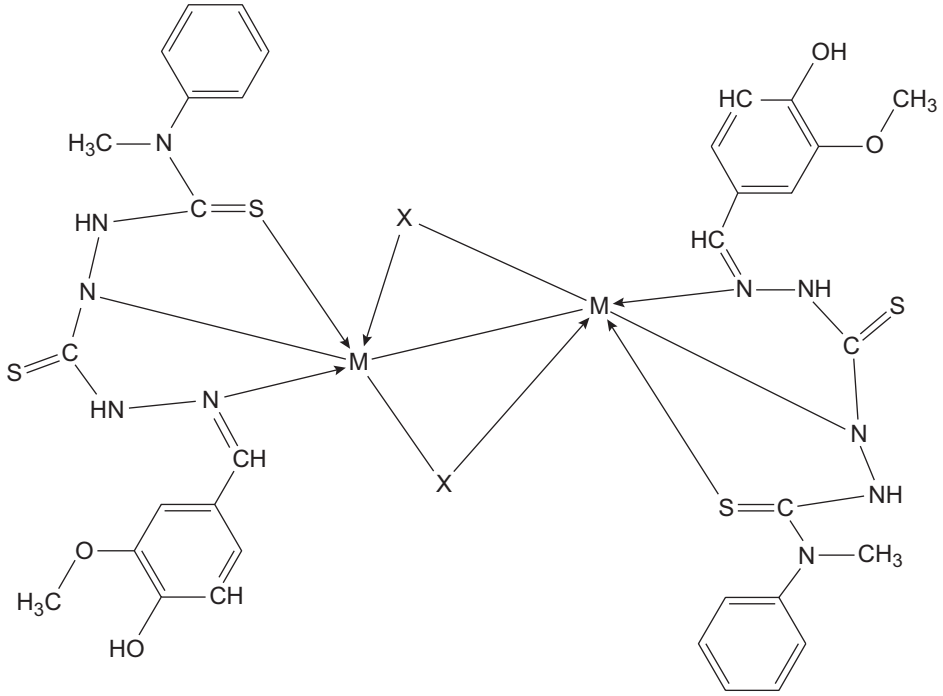

Fig. 14. Proposed structure of the complex $[MLX_2]$, where M = Ni(II); X = CH_3COO^- **(3).**

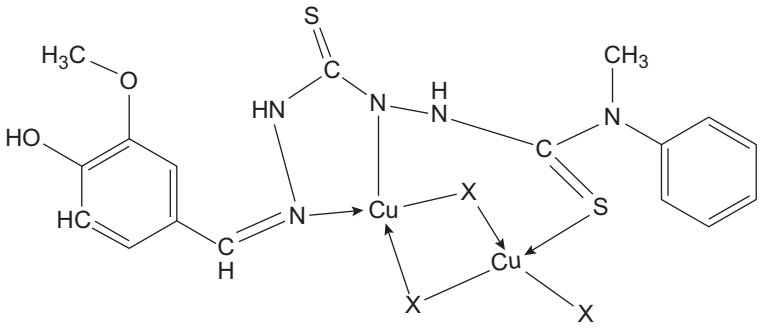

Fig. 15. Proposed structure $[Cu_2LX_3]$; where X = CH_3COO^-, Cl^- **(5)** and **(6).**

References

1. R. Schlapp, W. G. Penny, Phys. Rev., 42 (1932) 666.
2. S. M. Devi, A. M. Singh, Int. J. Res. Chem. Environ., 2 (2012) 290.
3. D. Sutton, Electronic Spectra of Transition Metal Complexes. McGraw Hill, London, 1968.
4. O. Maddock, A. Sharpe, R. L. Martin, Proc. Roy. Austral. Chem. Inst., 38 (1971) 33.
5. J. Kuncheria., Ph.D Thesis, University of Calicut, 1992.
6. K. Nakamoto, Infrared and Raman Spectra of Inorganic and Coordination Compounds, 3rd ed., John Wiley and Sons, New York city, New York, 1978.

CHAPTER VII

NOVEL LIGAND DERIVED FROM 3, 4-DIMETHOXYBENZALDEHYDE AND N(4)-METHYL-N(4)-PHENYLTHIOSEMICARBAZIDE AND ITS TRANSITION METAL COMPLEXES

1. Introduction

The compound 3, 4 dimethoxybenzaldehyde (Fig. 1) is commonly used as a flavourant and odorant. It is used as an intermediate in the production of some pharmaceutical drugs like Prazosin, Tiapamil, Verazide and so on.

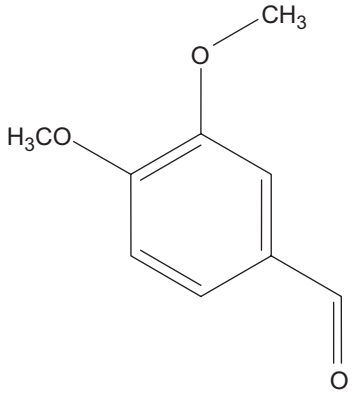

Fig. 1. 3,4 Dimethoxybenzaldehyde.

A Schiff's base from 3,4-dimethoxybenzaldehyde and p-aminobenzoic acid was synthesized by novel supersonic speed gas impacting method by Cai *et al.*[1] Synthesis, characterisation, antibacterial and antifungal activities of a Schiff's base, 1-(3,4-dihydroxybenzalidene)-thiosemicarbazide and its Ni(II) and Fe(II) complexes have been reported.[2] Synthesis and characterisation of three Zn(II) complexes, $[Zn(3,4\text{-}MBTSC)_2Cl_2]$, $[Zn(3,4\text{-}MBTSC)_2Br_2]$ and $[Zn(3,4\text{-}MBTSC)_2I_2]$ of 3,4-dimethoxybenzaldehyde thiosemicarbazone (3,4-MBTSC) were reported by Khalaji *et al*[3] This chapter portrays the synthesis and characterisation of a novel ligand derived from 3,4 dimethoxybenzaldehyde and N(4)-methyl-N(4)-phenylthiosemicarbazide and its complexes. The structure of the ligand, 2-{2-[(3,4-dimethoxyphenyl)methylidene]hydrazinecarbonothioyl}-N-methyl-N-phenylhydrazine-1-carbothioamide, (H_2L) is shown as Fig. 2.

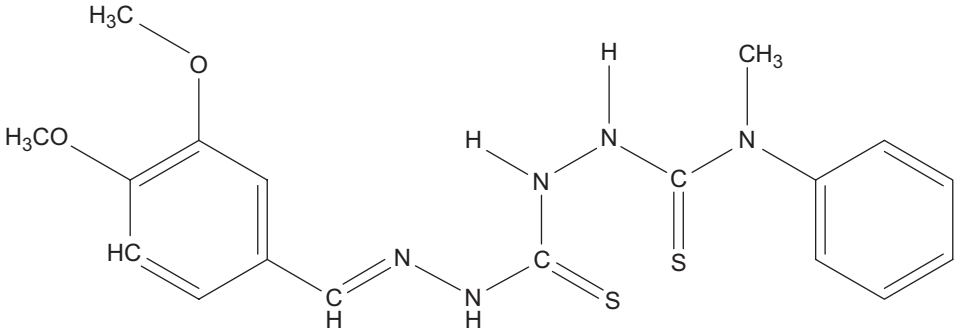

Fig. 2. 2-{2-[(3,4-dimethoxyphenyl)methylidene]hydrazinecarbonothioyl}-N-methyl-N-phenylhydrazine-1-carbothioamide (3,4 VMPTSC)(H_2L) (IUPAC name of the compound).

2. Experimental

2.1. Materials and method

3,4 Dimethoxybenzaldehyde (Merck), glacial acetic acid and commercially available metal salts were used without further purification. The solvents were purified and dried by using standard procedure. The melting points of the ligand and the complexes were recorded on a melting point apparatus. The ligand was further characterised by partial elemental analyses, Fourier-transform infrared (FT-IR), FT-Raman, electronic, ^{1}H NMR spectra and single-crystal X-ray diffraction (XRD) studies. The complexes were characterised using partial elemental analyses, FT-IR and electronic spectra. ^{1}H NMR spectrum of Zn(II) complex was recorded. Magnetic susceptibilities of the complexes at room temperature were measured. The details regarding the techniques are given in Chapter II.

2.2. Synthesis

Synthesis of the precursor, N(4)-methyl-N(4)-phenylthiosemicarbazide (MPTSC) is discussed in Chapter II.

2.2.1. 2-{2-[(3,4-dimethoxyphenyl)methylidene]hydrazinecarbonothioyl}-N-methyl-N-phenylhydrazine-1-carbothioamide (H_2L)

H_2L was prepared by dropwise addition of the 70% hot ethanolic solution of 3,4 dimethoxybenzaldehyde (0.164 g, 1 mmol) into the boiling 70% ethanolic solution of N(4)-methyl-N(4)-phenylthiosemicarbazide (MPTSC) (0.364 g, 2 mmol) taken in a flat-bottomed flask. A few drops of glacial acetic acid were added, stirred and refluxed at 60°C–80°C for 1 hour. A yellow-coloured precipitate obtained was filtered and washed with water, followed by ethanol and dried. The melting point and solubility of the compound in different solvents were noted. The reaction pathway in the synthesis of the ligand H_2L is shown in Scheme 1.

2.2.2. Metal complexes

A hot ethanolic solution of metal acetate/chloride/nitrate (1 mmol) was added dropwise to a hot ethanolic H_2L solution (1 mmol). After the complete addition, a pinch of sodium acetate trihydrate was added. It was then refluxed for 3 hours, and then cooled to room temperature. The solid formed was collected, washed with water followed by ethanol and dried.

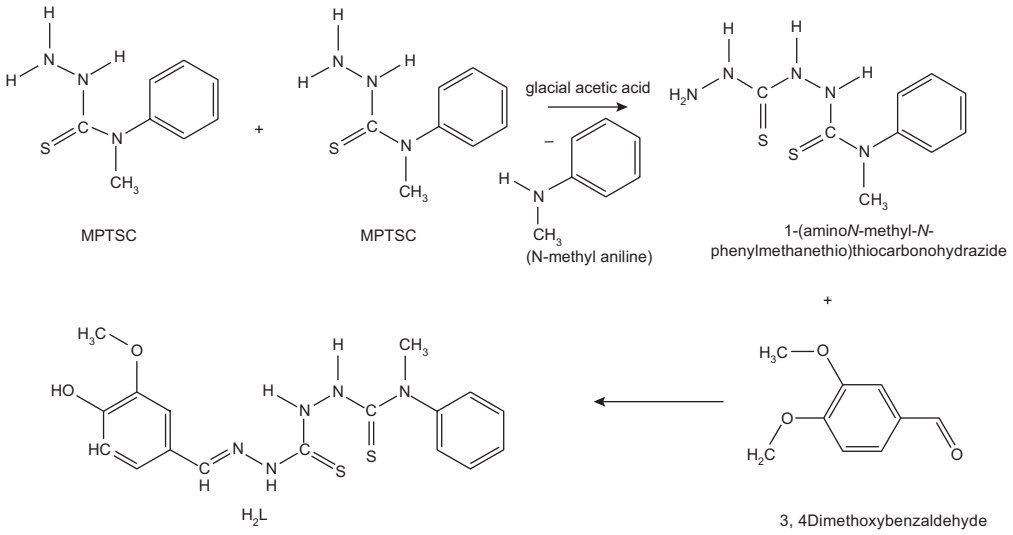

Scheme 1. The reaction pathway of the ligand H_2L.

3. Results and discussion

3.1. Characterisation of the ligand

3.1.1. Microanalytical data

The ligand H_2L is light yellow in colour and melted at 185°C. The suggested formula for the ligand is $C_{18}H_{21}N_5O_2S_2$. CHNS percentages of the ligand are in agreement with the suggested molecular formulae (Table 1). The ligand is soluble in common solvents like methanol, ethanol, and so on.

Table 1. Analytical data of the ligand (H_2L)

Compound	Molecular Weight	Melting Point	Colour	Yield	Elemental Analysis Found(calculated)			
					C	H	N	S
$C_{18}H_{21}N_5O_2S_2$	403	185	Yellow	80	53.7 (53.6)	5.0 (5.2)	17.6 (17.4)	8.0 (7.9)

3.1.2. Single-crystal XRD studies of ligand (H_2L)

Single crystals of H_2L suitable for X-ray analysis were obtained by the slow evaporation of its solution in 1:1:1 (v/v) mixture of methanol: DMF: dichloromethane. A crystal with dimension, 0.420 × 0.350 × 0.250 mm^3 was selected for collecting the data. H_2L crystallizes with four molecules per asymmetric unit into monoclinic crystal system with a space group of *P 21/c* (Fig. 3).

X-ray crystallographic data for H_2L were collected at 293(2) K on a Bruker AXS Kappa Apex2 CMOS diffractometer. Direct methods were performed to solve the structures and refined by least-square on F^2 using SHELXL-2014/7.[4] All non-hydrogen atoms were refined anisotropically. All hydrogen atoms, except those attached to nitrogen were geometrically fixed at calculated positions. The crystallographic tools, PLATON[5] for Windows, DIAMOND 3.2d[6], and MERCURY 3.5.1[7] were used for structure analysis and presentation of the results. The structure was finally refined to the conventional *R*-value, $R_1 = 0.0476$.

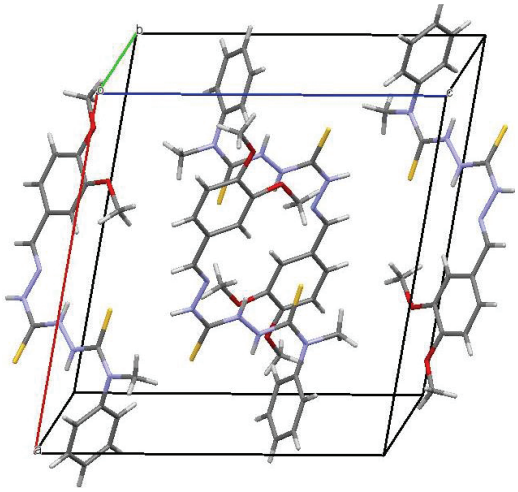

Fig. 3. Packing diagram of compound H_2L in the unit cell.

Crystal data and structure refinement parameters are given in Table 2. Ortep diagram of H_2L with the atom numbering scheme are shown in Fig. 4. Selected bond lengths and bond angles are listed in Table 3. It was found that the molecules in the unit cell are arranged in face-to-face manner, which are the repeating units of the packing in the crystal lattice. Molecules packed into molecular columns along b direction are shown in Fig. 5. Table 4 shows hydrogen bonding interaction parameters of H_2L.

Table 2. Crystal data and structure refinement for H_2L

Identification code	H_2L		
Empirical formula	$C_{18}\ H_{21}\ N_5\ O_2\ S_2$	Absorption coefficient	0.28
Formula weight	403.52	F(000)	848
Temperature (K)	273(2)	Crystal size(mm^3)	0.420 × 0.350 × 0.250
Wavelength (Å)	0.71073	Theta range for data collection	2.628°–24.989°.
Crystal system	Monoclinic	Index ranges	$-16 \le h \le 6$, $-10 \le k \le 7$, $-6 \le l \le 17$
Space group	*P 21/c*	Reflections collected	2786
Unit cell dimensions		Independent reflections	1964 [*R*(int) = 0.0328]
a (Å)	15.683(4)	Completeness to theta = 25.242°	95.10%
α (°)590	Absorption correction	Semi-empirical from equivalents	
b (Å)	9.2382(15)	Max. and min. Transmission	0.91 and 0.84
b (°)	101.979(8	Refinement method	Full-matrix least-squares on F^2
c (Å)	14.564(3)	Data/restraints/parameters	1964/0/248
g (°)	90	Goodness-of-fit on F^2	1.422
Volume ($Å^3$)	2064.0(8)	Final *R* indices [$I > 2\text{sigma}(I)$]	$R_1 = 0.0476$, $wR_2 = 0.0371$
Z	4	*R* indices (all data)	$R_1 = 0.0983$, $wR_2 = 0.0417$
Density (calculated) mg/m^3	1.299	Extinction coefficient	0.0050(2)
Absorption coefficient	0.28	Largest diff. peak and hole (e.$Å^{-3}$)	0.122 and −0.121

The bond lengths, C(8)–S(1) and C(9)–S(2) are found to be 1.679(7) and 1.663(7) Å, respectively, which is in agreement with C=S bond length (1.71 Å). This shows that the compound is in thione form in the solid state. The bond lengths, N(5)–C(7), N(4)–C(8), N(3)–C(8), N(2)–C(9), N(1)–C(9), N(3)–N(2) and N(5)–N(4) are 1.245(8), 1.315(7), 1.333(4), 1.368(5), 1.357(9), 1.365(4) and 1.410(8) Å, respectively. They are found to be at midway between the analogous single [C–N, 1.47; N–N, 1.45 Å] and double bonds [C=N, 1.28 Å; N=N, 1.25 Å].[8,9] The bond lengths, C(3)–O(1) and C(18)–O(1) of the ligand are 1.382(10) and 1.394(8) Å, respectively.

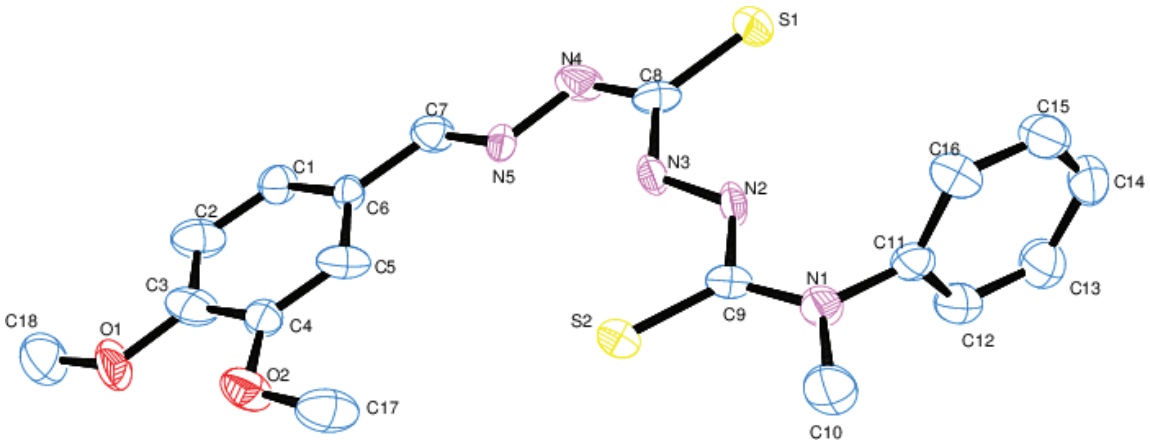

Fig. 4. Ortep diagram of the molecule with atom numbering scheme (omitting H atoms).

Table 3. Selected bond lengths [Å] and bond angles [°] of H_2L

Bond Length [Å]		**Bond Length [Å]**		**Bond Angle [°]**	
S(2)–C(9)	1.663(7)	C(12)–H(12)	0.93	C(6)–C(1)–C(2)	122.2(5)
S(1)–C(8)	1.679(7)	C(15)–C(14)	1.379(7)	C(6)–C(1)–H(1)	118.9
O(2)–C(4)	1.369(4)	C(15)–H(15)	0.93	C(2)–C(1)–H(1)	118.9
O(2)–C(17)	1.426(5)	C(10)–H(10A)	0.96	N(5)–C(7)–C(6)	121.1(5)
N(5)–C(7)	1.245(8)	C(10)–H(10B)	0.96	N(5)–C(7)–H(7)	119.4
N(5)–N(4)	1.410(8)	C(10)–H(10C)	0.96	C(6)–C(7)–H(7)	119.4
N(4)–C(8)	1.315(7)	C(14)–C(13)	1.396(7)	C(4)–C(3)–O(1)	116.1(5)
N(4)–H(4)	0.86	C(13)–H(13)	0.93	C(4)–C(3)–C(2)	121.6(7)
O(1)–C(3)	1.382(10)	C(17)–H(17A)	0.96	C(15)–C(16)–C(11)	119.3(7)
O(1)–C(18)	1.394(8)	C(17)–H(17B)	0.96	C(15)–C(16)–H(16)	120.4
N(3)–C(8)	1.333(4)	C(17)–H(17C)	0.96	C(11)–C(16)–H(16)	120.4
N(3)–N(2)	1.365(4)	C(18)–H(18A)	0.96	N(4)–C(8)–N(3)	114.3(6)
N(3)–H(3)	0.86	C(18)–H(18B)	0.96	N(4)–C(8)–S(1)	122.4(4)
N(2)–C(9)	1.368(5)	C(18)–H(18C)	0.96	N(3)–C(8)–S(1)	123.4(4)
N(2)–H(2)	0.86	Bond angles (°)		N(1)–C(9)–N(2)	113.6(6)
N(1)–C(9)	1.357(9)	N(2)–N(3)–H(3)	119.8	O(1)–C(3)–C(2)	122.3(8)
N(1)–C(11)	1.427(11)	N(3)–N(2)–C(9)	121.3(5)	N(1)–C(9)–S(2)	126.8(4)
N(1)–C(10)	1.481(4)	N(3)–N(2)–H(2)	119.4	N(2)–C(9)–S(2)	119.6(5)
C(4)–C(5)	1.363(10)	C(9)–N(2)–H(2)	119.4	C(1)–C(2)–C(3)	117.2(7)

C(4)–C(3)	1.377(9)	C(9)–N(1)–C(11)	122.3(4)	C(1)–C(2)–H(2A)	121.4
C(6)–C(1)	1.352(8)	C(9)–N(1)–C(10)	119.8(6)	C(3)–C(2)–H(2A)	121.4
C(6)–C(5)	1.431(5)	C(11)–N(1)–C(10)	117.8(6)	C(13)–C(12)–C(11)	120.7(6)
C(6)–C(7)	1.477(10)	C(5)–C(4)–C(3)	120.3(5)	C(13)–C(12)–H(12)	119.6
C(5)–H(5)	0.93	O(2)–C(4)–C(3)	114.8(6)	C(11)–C(12)–H(12)	119.6
C(11)–C(12)	1.368(9)	C(1)–C(6)–C(5)	119.5(6)	C(16)–C(15)–C(14)	121.6(5)
C(11)–C(16)	1.390(6)	C(1)–C(6)–C(7)	122.3(5)	C(16)–C(15)–H(15)	119.2
C(1)–C(2)	1.394(11)	C(5)–C(6)–C(7)	118.2(6)	C(14)–C(15)–H(15)	119.2
C(1)–H(1)	0.93	C(4)–C(5)–C(6)	119.2(6)	N(1)–C(10)–H(10A)	109.5
C(7)–H(7)	0.93	C(4)–C(5)–H(5)	120.4	N(1)–C(10)–H(10B)	109.5
C(3)–C(2)	1.402(5)	C(6)–C(5)–H(5)	120.4	H(10A)–C(10)–H(10B)	109.5
C(16)–C(15)	1.367(12)	C(12)–C(11)–C(16)	119.8(7)	N(1)–C(10)–H(10C)	109.5
C(16)–H(16)	0.93	C(12)–C(11)–N(1)	119.9(5)	H(10A)–C(10)–H(10C)	109.5
C(2)–H(2A)	0.93	C(16)–C(11)–N(1)	120.3(6)	H(10B)–C(10)–H(10C)	109.5
C(12)–C(13)	1.365(14)			C(15)–C(14)–C(13)	118.3(7)

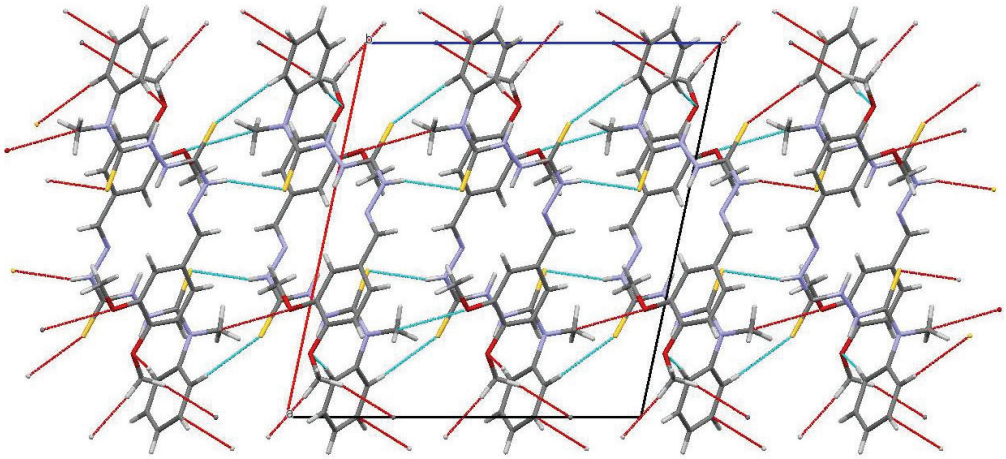

Fig. 5. Molecules packed into molecular columns along *b*-axis.

Table 4. Hydrogen bonding interaction parameters of H_2L

D-H···A	**d(D-H)**	**d(H···A)**	**d(D···A)**	**<(DHA)**
N(4)-H(4)···.S(2) [a]	0.86	2.60	3.431(3)	161
C(16)-H(16)···O(1)[b]	0.93	2.53	3.415(4)	160

[a]Symmetry transformations used to generate equivalent atoms: x, $1/2 - y$, $-1/2 + z$
[b]Symmetry transformations used to generate equivalent atoms:$1 - x$, $1 - y$, $1 - z$

The bond angles, N(4)–C(8)–N(3), N(4)–C(8)–S(1), N(3)–C(8)–S(1), N(1)–C(9)–N(2), N(1)–C(9)–S(2) and N(2)–C(9)–S(2) are 114.3(6), 122.4(4), 123.4(4), 113.6(6), 126.8(4) and 119.6(5)°, respectively, which show deviation of the molecule from planarity.

The torsion angle of 175.9(4)° for N(2)–N(3)–C(8)–N(4) represents an *E*-conformation with respect to C(8)–N(3) bond and is in *Z*-conformation with respect to N(2)–N(3–)–C(8)–S(1) with an angle −3.7(6)°. The N(3)–N(2)–C(9)–S(2) is in *Z* conformation with respect to N(2)–C(9) with torsion angle of −1.8(6)°.

The least square planes comprising, C(7)–N(5)–N(4)–C(8)–S(1) (**1**) and N(1)–C(9)–S(2)–N(2)–N(3) (**2**) form a dihedral angle 10.115(94)°**.** The planes C(6)–C(7)–C(9)–N(2)–N(3) (**3**) and C(11)–N(1)–C(9)–N(2)–N(3) (**4**) form a dihedral angle of 13.796(188)°. The mean plane (111) forms an angle 9.63(97)° with plane (**1**) and with plane (**3**) 10.504(103)°. The planes (**2**) and (**4**) deviated from mean plane with dihedral angles, 19.714(53)° and 24.297(170)°, respectively. The phenyl rings of the ligand C(1)–C(2)–C(3)–C(4)–C(5)–C(6) and C(11)–C(12)–C(13)–C(14)–C(15)–C(16) are twisted from the molecular plane with an angle of 80.533(128)°.

3.1.3. Spectroscopic analysis

(a) Electronic spectrum

The solid-state electronic absorption spectrum of the ligand was recorded in the range 200–900 nm (Fig. 6). The compound registered charge-transfer bands at 263, 322, 393 and 622 nm. The former two bands may be attributed to the π–π* transitions of the azomethine chromophore and the benzene ring (intra-ligand charge transfer). The latter bands may be due to the n–π* transition.

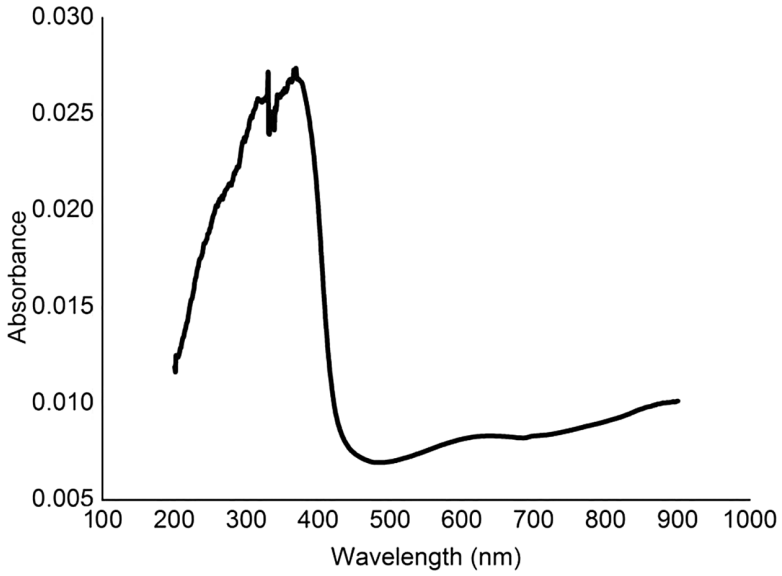

Fig. 6. Electronic spectrum of the ligand.

(b) Vibrational spectra

The FT-IR spectrum of the compound was recorded in the region 4000–400 cm^{-1} and is presented in Fig.7. The ligand, H_2L showed a doublet at 3293–3143 cm^{-1} due to N–H stretching vibration. This splitting may be due to the interacting molecules in the unit cell. A sharp band at 1602 cm^{-1} in the ligand is assigned to ν(C=N). The ν(S–H) band is absent at 2560 cm^{-1} in the IR spectrum, indicating the existence of thione tautomer of the ligand in the solid state.[10] The bands at 1269 and 767 cm^{-1} in the ligand may be assigned to ν(NH–C=S) and *ν*(C=S), respectively.

The FT-Raman spectrum of the compound was recorded in the region 4000–400 cm^{-1} and is presented in Fig. 8. In Raman spectrum, the ligand H_2L showed a doublet at

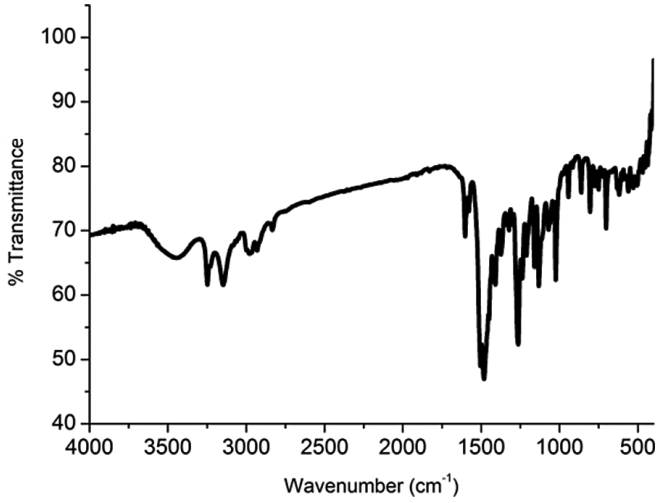

Fig. 7. FT-IR spectrum of the ligand.

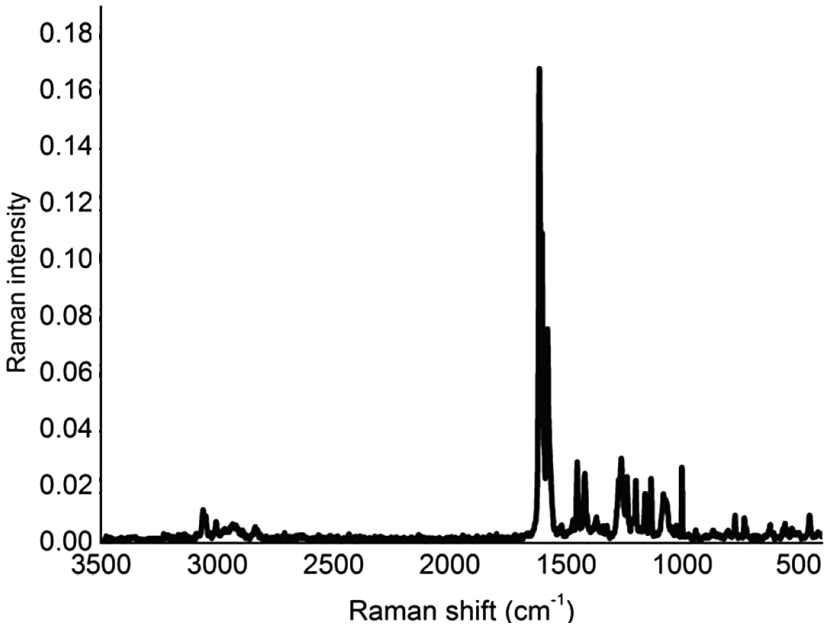

Fig. 8. FT-Raman spectrum of the ligand.

3058 cm^{-1} due to N–H stretching vibration. The bands observed at 1613 and 1582 cm^{-1} are assigned to ν(C=N). The bands at 1266 and 770 cm^{-1} in the ligand may be assigned to ν(NH–C=S) and ν(C=S), respectively.

(c) ^{1}H NMR spectrum

The ^{1}H NMR spectrum of the ligand is recorded in $CDCl_3$ (Fig. 9). In the ^{1}H NMR spectrum of the ligand, two doublets at 10.883–10.900 and 8.868–8.838 ppm are assigned for adjacent N–H protons. A singlet at 8.80 ppm could be assigned to N–H proton adjacent to azomethine group. Aromatic protons show a multiplet peak in the region 6.74–7.66 ppm. Singlets at 3.924 and 3.968 ppm are assigned to methoxy protons. N–CH_3 protons absorb at 3.700 ppm.

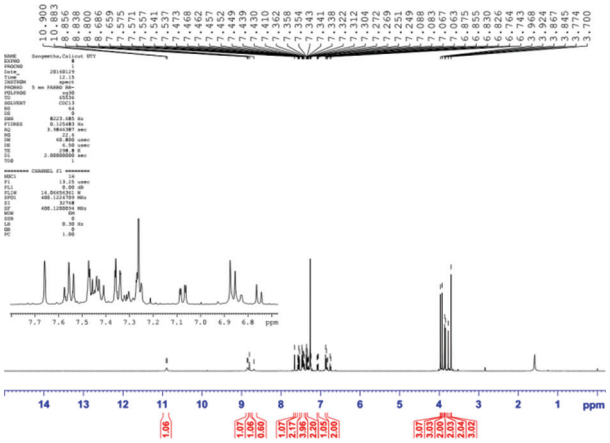

Fig. 9. ^{1}HNMR spectrum of the ligand.

3.2. Characterisation of metal complexes

3.2.1. Formulae and general properties of the complexes

All the complexes were found to be stable at room temperature. The analytical data of the complexes are presented in Table 5 and are consistent with the proposed empirical formulae.

Table 5. Molecular formulae, colour, partial elemental analyses and magnetic moments of the complexes

No.	Compound	Molecular Weight	Melting Point	Colour	Yield	Elemental Analysis Found(calculated)					μ in BM
						C	H	N	S	M	
	$C_{18}H_{21}N_5O_2S_2$	403	185	Yellow	80	53.7 (53.6)	5.0 (5.2)	17.6 (17.4)	8.0 (7.9)	–	–
1	$[Mn(H_2L)_2(CH_3COO)_2]$	979	205	Brown	70	48.8 (49.0)	4.5 (4.9)	14.5 (14.3)	6.6 (6.5)	5.5 (5.6)	3.1
2	$[Co(H_2L)_2(CH_3COO)_2]$	983	220	Brown	70	48.9 (48.8)	4.6 (4.9)	14.3 (14.2)	6.6 (6.5)	6.2 (6.0)	3.1
3	$[Co(HL)Cl_2H_2O]$	551	250	Green	80	39.4 (39.2)	3.6 (3.8)	12.9 (12.7)	11.8 (11.6)	10.8 (10.7)	D
4	$[Ni(HL)_2]$	865	215	Yellowish green.	80	49.8 (49.9)	4.4 (4.6)	16.1 (16.2)	7.2 (7.4)	6.5 (6.7)	2.7
5	$[Cu_2(HL)(CH_3COO)_3]$	707	200	Black	80	43.66 (40.7)	4.5 (4.1)	9.9 (9.9)	8.4 (9.1)	18.0 (17.9)	1.2
6	$[Cu_2(HL)Cl_3]$	637	220	Green	80	31.9 (33.9)	2.4 (3.1)	10.6 (10.9)	9.0 (10.0)	18.8 19.9	D
7	$[Cu_2(HL)(NO_3)_3]$	716	210	Green	80	30.0 (30.1)	2.5 (2.8)	16.5 (15.6)	8.4 (8.9)	15.8 (17.7)	D
8	$[(Cu(HL)OHH_2O)_2]$	1041	240	Green	80	41.1 (41.5)	4.5 (4.8)	12.7 (13.4)	11.3 (12.2)	11.9 (12.2)	D
9	$[Zn(HL)CH_3COO]$	586	270	Yellow	70	45.5 45.5	3.4 4.4	11.7 13.4	7.3 12.1	11.7 12.4	D
10	[Cd(HL)OH]	532	>270	Yellow	75	40.0 (40.6)	3.9 (3.9)	13.0 (13.1)	11.5 (12.0)	23.8 (21.1)	D

3.2.2. Electronic spectra and magnetic moments

The electronic spectra of complexes were recorded in solid state and their probable assignments are given in Table 6.

Table 6. Electronic spectral bands and their assignments

Complex No:	Compound	Band nm	cm^{-1}	Assignments
	$C_{18}H_{21}N_5O_2S_2$	263	38022	$\pi\rightarrow\pi^*$
		322	30959	$n\rightarrow\pi^*$
		393	25445	$n\rightarrow\pi^*$
		626	15974	*C–T*
1	$[Mn(H_2L)_2(CH_3COO)_2]$	309	32362	$n\rightarrow\pi^*$
		430	23255	*C*–T
		723	13831	$T_{2g}\rightarrow E_g$
2	$[Co(H_2L)_2(CH_3COO)_2]$	280	35714	$\pi\rightarrow\pi^*$
		413	24213	*C–T*
		604–760, 682sh	16556–13157, 14662sh	$^4T_{1g}(F) \rightarrow {}^4T_{2g}(F)$, $^4T_{1g}(F) \rightarrow {}^4A_{2g}(F)$
3	$[Co(HL)Cl_2H_2O]$	316	31645	$n\rightarrow\pi^*$
		387	25839	*C–T*
		725	13793	$^1A_{1g} \rightarrow {}^1T_{2g}$, $^1A_{1g}\rightarrow {}^1T_{1g}$
4	$[Ni(HL)_2]$	264	37878	$\pi\rightarrow\pi^*$
		423	23640	$^3A_{2g}(F) \rightarrow {}^3T_{1g}(P)$
		687	14556	$^3A_{2g}(F)\rightarrow {}^3T_{1g}(F)$
		895	11173	$^3A_{2g}(F)\rightarrow {}^3T_{2g}(F)$
5	$[Cu_2L(CH_3COO)_3]$	275	36363	$\pi\rightarrow\pi^*$
		306	32679	$n\rightarrow\pi^*$
		349	26385	*C–T*
		411	24330	$^2B_{1g} \rightarrow {}^2A_{2g}$
		685–751	14589–13315	$^2B_{1g}\rightarrow {}^2E_g$
		885	11,249	$^2B_{1g}\rightarrow {}^2A_{1g}$
6	$[Cu_2LCl_3]$	261, 287	38341, 34843	$\pi\rightarrow\pi^*$
		330, 352	30303, 22213	$n\rightarrow\pi^*$
		402	24875	*C–T*
		700	14285	$^2B_{1g} \rightarrow {}^2A_{2g}$
		854	11709	$^2B_{1g}\rightarrow {}^2E_g$
		885	11299	$^2B_{1g}\rightarrow {}^2A_{1g}$
7	$[Cu_2L(NO_3)_3]$	287	34843	$\pi\rightarrow\pi^*$
		352	28409	$n\rightarrow\pi^*$
		690	14492	$^2B_{1g} \rightarrow {}^2A_{2g}$
		850	11764	$^2B_{1g}\rightarrow {}^2E_g$
8	$[Cu(HL)OH\ H_2O)_2]$			
		311	32514	$n\rightarrow\pi^*$
		387	25839	*C–T*

		725	13793	$T_{2g} \rightarrow E_g$
9	[Zn(HL)CH_3COO]	260	38341	$\pi \rightarrow \pi^*$
		328	30487	$n \rightarrow \pi^*$
		630	15873	*C–T*
10	[Cd(HL)OH]	267	37457	$\pi \rightarrow \pi^*$
		313	31494	$n - \pi^*$
		405	24691	*C–T*
		635	15748	*C–T*

In the high-spin, octa hedrally coordinated Mn(II) complex, the lowest configuration $(t_{2g})^3(e_g)^2$ gives rise to the ground state, $^6A_{1g}$. But for the low-spin octahedral complexes, the ground state is $^2T_{2g}$. High-spin Mn(II) ions in octahedral and tetrahedral geometries have a spin-only value of 5.92 BM at room temperature. But the low-spin octahedral complexes with $^2T_{2g}$ ground term can have orbital contribution and the experimental magnetic moment values are found close to 2.50 BM. The observed magnetic moment value of Mn(II) complex is found to be 3.1 BM corresponding to low-spin octahedral geometry.

Usually, Co(II) complexes exist in octahedral, tetrahedral and square-planar geometries. If the ligand has several donor atoms, five coordinate geometry is possible for Co(II) complexes. Co^{2+}(d^7 system) gives rise to the ground state, ^3F and the excited states ^3P, ^1G, ^1D and ^1S. The transitions from the ground state to the three singlet states (^1G, ^1D, ^1S) are spin forbidden. The two remaining states, ^3F and ^3P can have spin permitted transitions. The F state splits into $A_{2g}+T_{1g}+T_{2g}$ and P state is transformed into a T_{1g} state. Hence, three peaks should appear in the spectrum corresponding to $^4T_{1g}(F) \rightarrow {}^4T_{2g}(F)$, $^4T_{1g}(F) \rightarrow {}^4A_{2g}(F)$, and $^4T_{1g}(F) \rightarrow {}^4T_{1g}(P)$ transitions. In this case, a broad d–d spectral band is formed in the region 604–760 nm with a shoulder at 682 nm, indicating its octahedral geometry. Octahedral, tetrahedral and square-planar Co(II) complexes show magnetic moments of 4.7–5.2, 4.3–4.8 and 2.2–2.9 BM, respectively.[11] The magnetic moment value of the Co(II) complex herein is 3.1 BM.[12] Such low magnetic moment values for Co(II) complexes with S and N chelating agents were reported previously.[13] The anomalous value of magnetic moment may be due to the anti-ferromagnetic spin–spin interaction between Co–Co metal centres or due to high-spin–low-spin equilibrium.[14]

Co(III) ion has a d^6 configuration, giving an electronic arrangement $(t_{2g})^6(e_g)^0$ and the ground state is $^1A_{1g.}$ In this study, a broad band at 723 nm is observed for complex (**3)** and may be due to $^1A_{1g} \rightarrow {}^1T_{2g}$ and $^1A_{1g} \rightarrow {}^1T_{1g}$ transitions. In [Co(HL)Cl_2 H_2O], cobalt is in +III oxidation state and is in low spin octahedral configuration showing a diamagnetic behaviour.

Octahedral complexes of Ni(II) ion with d^8 configuration have a ground state $^3A_{2g.}$ The three spin-allowed transitions are, $^3A_{2g}(F) \rightarrow {}^3T_{2g}(F)$, $^3A_{2g}(F) \rightarrow {}^3T_{1g}(F)$ and $^3A_{2g}(F) \rightarrow {}^3T_{1g}(P)$ in the range 8000–11000, 15000–19000 and 25000–29000 cm^{-1}, respectively. In this case, the peaks at 423, 687 and 895 nm are due to $^3A_{2g}(F) \rightarrow {}^3T_{1g}(P)$, $^3A_{2g}(F) \rightarrow {}^3T_{1g}(F)$ and $^3A_{2g}(F) \rightarrow {}^3T_{2g}(F)$ transitions, respectively. The magnetic moment of nickel complex herein is 2.7 BM proposing octahedral geometry.

For square-planar copper complexes with a $dx^2\_y^2$ ground state, three spin-allowed transitions are expected.[15] [$^2B_{1g} \rightarrow {}^2A_{2g}$ ($d_{x^2-y^2} \rightarrow d_{z^2}$), $^2B_{1g} \rightarrow {}^2B_{2g}$ ($d_{x^2-y^2} \rightarrow d_{xy}$) and $^2B_{1g} \rightarrow {}^2E_g$ ($d_{x^2-y^2} \rightarrow d_{xz,yz}$)]. The complex **[**$Cu_2L(CH_3COO)_3$**]** (**5**) showed three bands 411, 740 and 885 nm. This may be due to $^2B_{1g} \rightarrow {}^2A_{2g}$, $^2B_{1g} \rightarrow {}^2E_g$ and $^2B_{1g} \rightarrow {}^2A_{1g}$ transitions, respectively.

The complex Cu_2LCl_3 (**6**) showed three bands at 700, 854 and 885 nm due to $^2B_{1g} \rightarrow {}^2A_{2g}$, $^2B_{1g} \rightarrow {}^2E_g$, and $^2B_{1g} \rightarrow {}^2A_{1g}$ transitions, respectively. The broad band observed at 725 nm in the electronic spectrum of the Cu(II) complex **(8)** is assigned to $^2E_g \rightarrow {}^2T_{2g}$ transition. This is in agreement with the distorted octahedral geometry of the complex.

All Cu(II) complexes, except complex (5) were diamagnetic. Magnetic moments of binuclear Cu(II) complexes were found in the range of 1.15–1.40 BM. In this case, the observed magnetic moment is 1.21 BM. This low magnetic moment may be attributed to the presence of a strong anti-ferromagnetic spin–spin interaction between metal centres.[16] Low magnetic moment or diamagnetism of complexes strongly supports their existence as dimers in the solid state.[17]

Cd(II) and Zn(II) complexes showed bands at 630 nm due to charge-transfer transition. As expected zinc and cadmium complexes were diamagnetic. Representative electronic spectra of the complexes (**1**), (**2**), (**4**) and (**5**) are presented in Fig. 10.

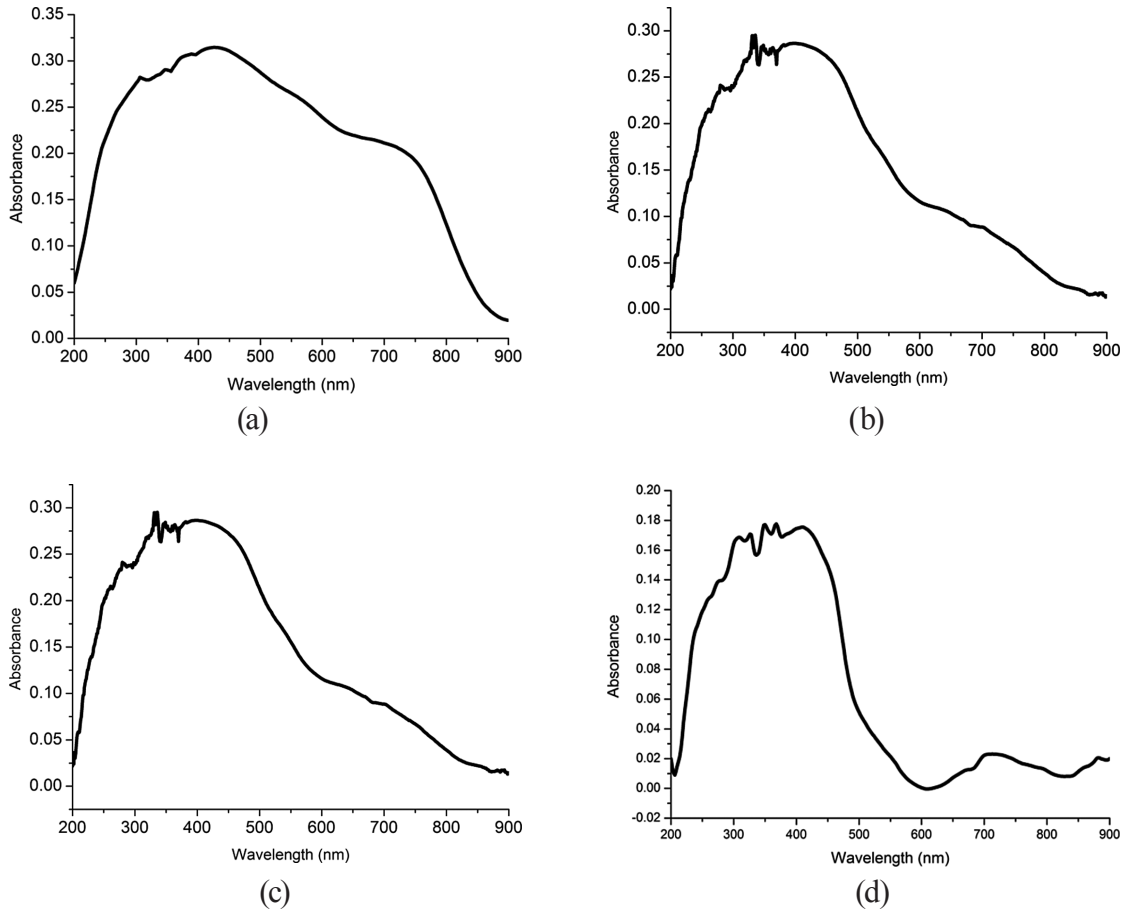

Fig. 10. Electronic spectra of the complexes (a) [$Mn(H_2L)(CH_3COO)_2$] (**1**), (b) [$Co(H_2L)_2(CH_3COO)_2$] **(2),** (c) [$Ni(HL)_2$] **(4)** and (d) [$Cu_2(L)(CH_3COO)_3$] **(5).**

3.2.3. Vibrational spectra

The IR spectral assignments of the ligand and the complexes are depicted in Table 7. The band observed at 1602 cm^{-1} in the ligand spectrum due to *ν*(C=N) is shifted to lower wavenumbers in the spectra of the complexes. However, the band observed at 1126 cm^{-1}, due to N–N stretching mode is shifted to higher wavenumbers in the spectra of metal complexes. Moreover, the IR spectra of all the complexes revealed new bands in the region, 400–470 nm assigned to *ν*(M–N). These observations indicate the involvement of azomethine nitrogen in coordination.

Broad bands in the region 3500–3100 cm^{-1} in the complexes (**3**) and (**8**) suggest that water is coordinated to central metal ions in these complexes. The inclusion of water molecules in the coordination spheres of these metal complexes are also supported by the strong bands at ~850–940nm. In addition to this, *ν*(M–O) bands were observed at 520–620 cm^{-1} in certain complexes. The *ν*(M–O) band may be either due to coordinated acetate, nitrate or hydroxyl anions or coordinated water molecules.

The complex (**1**) showed bands at 1720 and 1655 cm^{-1} possibly due to the ν_{as}(COO) of the two unidentate acetate groups.[18] The ν_{s}(COO) was observed at 1511 cm^{-1}. The complex (**2**) showed bands at 1677 and 1504 cm^{-1} due to ν_{as}(COO) and ν_{s}(COO) of unidentate acetate group. Here the separation between ν_{as}(COO) and ν_{s}(COO) is greater than 144 cm^{-1}, which confirmed the coordination of acetate group.[19] In the case of $[Cu_2(HL)(CH_3COO)_3]$ **(5)**, the bands at 1677 and 1345 cm^{-1} may be due to the bridged

Table 7. IR spectral assignments

No:	Compound	ν(O-H)/ ν(N-H)/ Coordinated H_2O	ν(C=N)	ν(C–O)	ν(NH–C=S)	ν(N–N)	ν(C=S)	ν(M–N)	ν(M–O)
	$C_{18}H_{21}N_5O_2S_2$	3444 3247	1602	1415	1266	1126	770	–	–
1	$[Mn(H_2L)(CH_3COO)_2]$	3412 3279	1596	1345	1265	1137	764	440	545
2	$[Co(H_2L)_2(CH_3COO)_2]$	3438	1592	1345	1265	1132	760	417	549
3	$[Co(HL)Cl_2\ H_2O]$	3438	1602	1344	1259	1137	756	439	-
4	$[Ni(HL)_2]$	3435	1596	1344	1271	1135	765	437	539
5	$[Cu_2(L)(CH_3COO)_3]$	3435	1592	1345	1267	1132	758	463	-
6	$[Cu_2(H_2L)Cl_3]$	3435	1595	1342	1268	1132	758	420	-
7	$[Cu_2(HL)(NO_3)_3]$	3435	1597	1342	1270	1139	760	419	613
8	$[CuHLOH\ H_2O)_2]$	3438	1594	1343	1263	1133	765	433	620
9	$[Zn(HL)CH_3COO]$	3439	1592	1341	1267	1136	758	440	620
10	[Cd(HL)OH]	3447	1602	1363 1336	1267	1106	760	447	556

acetate groups. Additional bands at 1511 and 1456 cm^{-1} may be due to the presence of unidentate acetate group. Representative IR spectra of the complexes **(3)**, **(4)** and (**5**) are presented in Fig. 11.

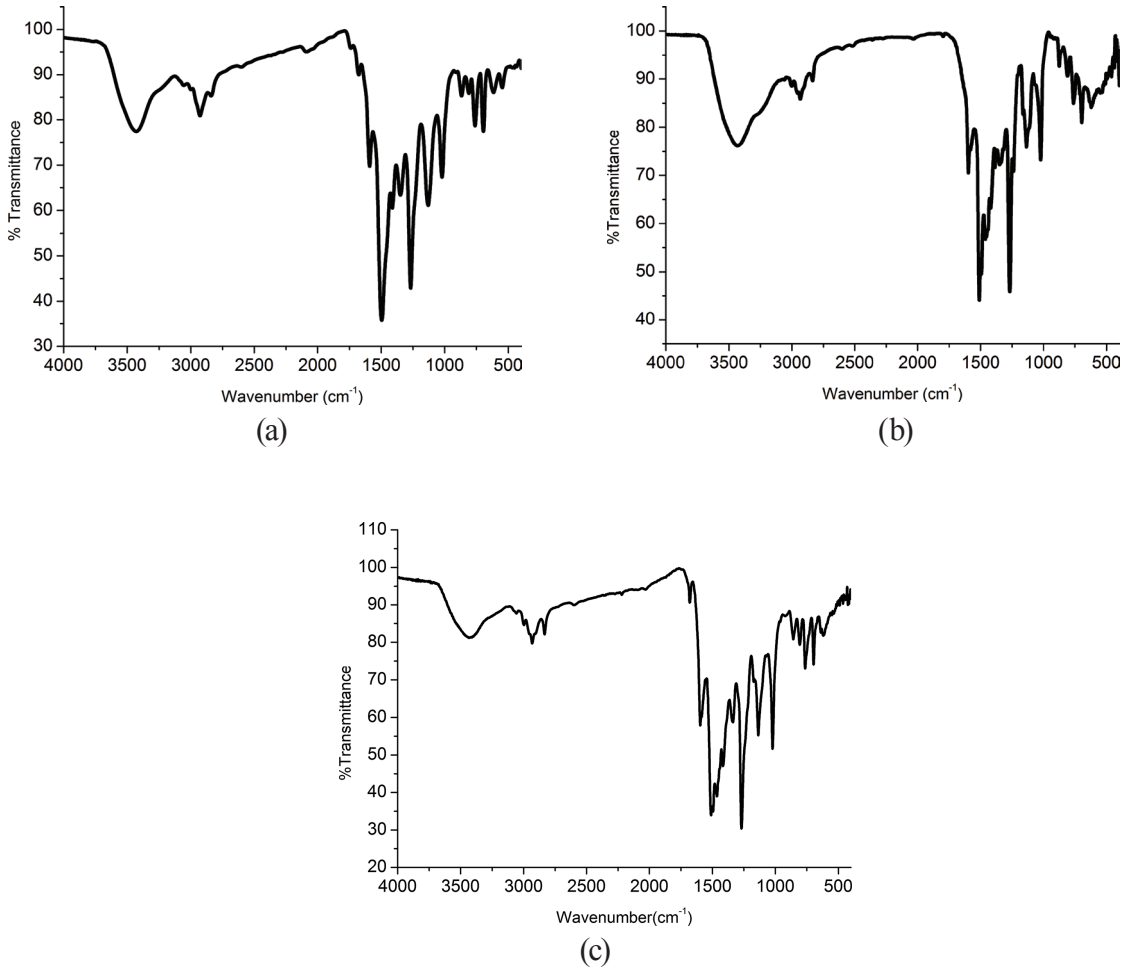

Fig. 11. IR spectra of the complexes (a) $[Co(HL)Cl_2H_2O]$ (**3**), (b) $[Ni(HL)_2]$ (**4**) and (c) $[Cu_2 (L)(CH_3COO)_3]$ (**5**).

3.2.4. ^{1}H NMR spectrum

The ^{1}H NMR spectrum of the Zn(II) complex was recorded in DMSO at room temperature (Fig. 12). Singlets at 3.100–3.478 and 3.499–3.761 ppm are assigned to methoxy protons and $^4N–CH_3$ protons, respectively. Singlets at 6.712 and 6.996 ppm are assigned to azomethine protons. The spectrum also showed several signals in the range 7.817–7.084 ppm, assigned to the different types of aromatic protons in the molecule. Peaks observed in the range, 1.252–1.575 ppm can be assigned to CH_3 protons of acetate group. Singlet observed at 2.841 ppm may be due to DMSO protons.

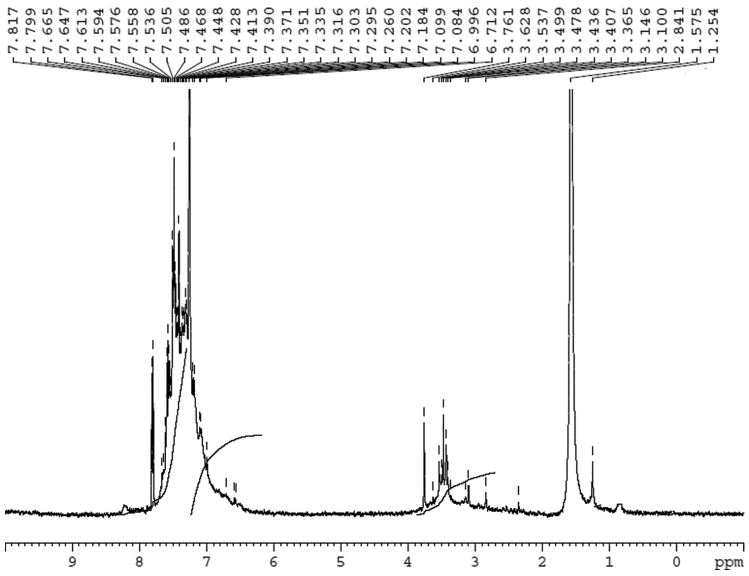

Fig. 12. ^{1}H NMR spectrum of the Zn(II) complex.

4. Conclusions

In the present investigation, we were able to obtain single crystals of the ligand, 2-{2-[(3,4-dimethoxyphenyl)methylidene]hydrazinecarbonothioyl}-N-methyl-N-phenyl-hydrazine-1-carbothioamide. Based on elemental analyses, spectral and magnetic studies, the following geometries are assigned to the complexes (Figs. 13–19).

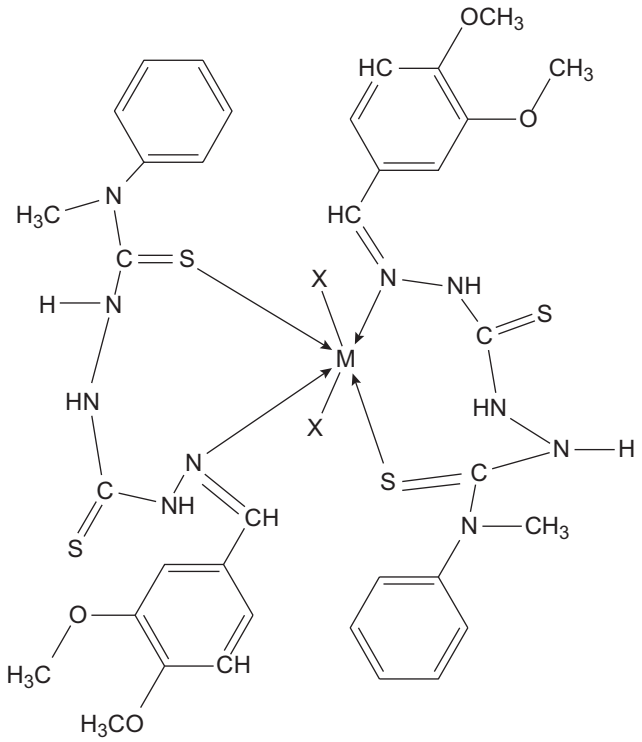

Fig. 13. Proposed structure of complexes, $[M(HL)_2X_2]$, where M = Mn(II) or Co(II); X = CH_3COO^- **(1)** and **(2)**.

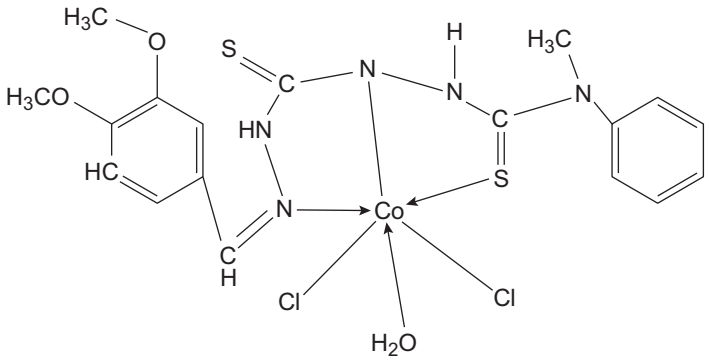

Fig. 14. Proposed structure of complex $[Co(HL)Cl_2 H_2O]$ **(3).**

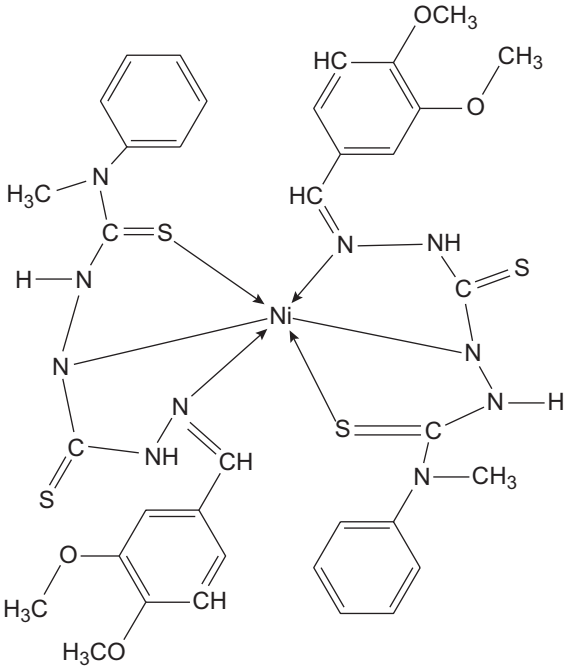

Fig. 15. Proposed structure of $[Ni(HL)_2]$ **(4)**.

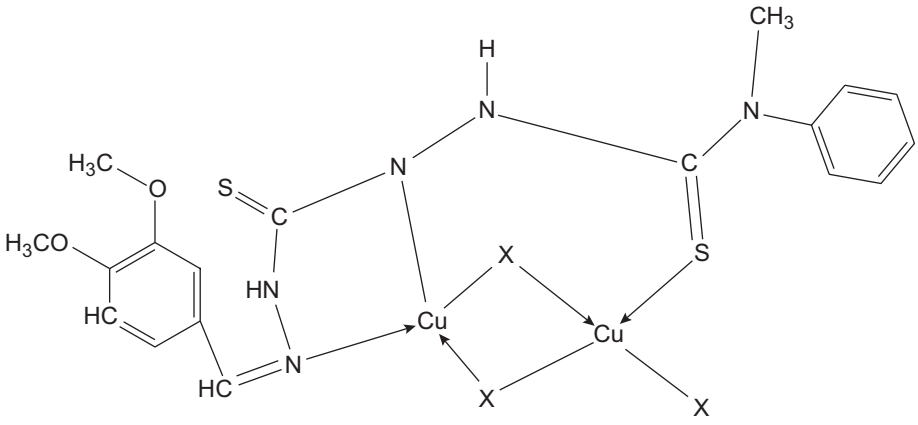

Fig. 16. Proposed structure of $[Cu_2(HL)X_3]$, where $X = CH_3COO^-$ **(5)**.

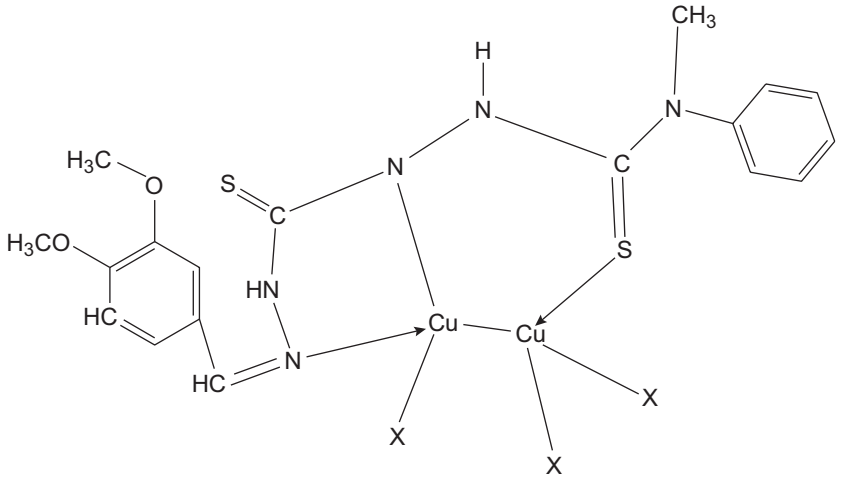

Fig. 17. Proposed structure of $[Cu_2LX_3]$, where X = Cl^- or NO_3^- **(6), (7)**.

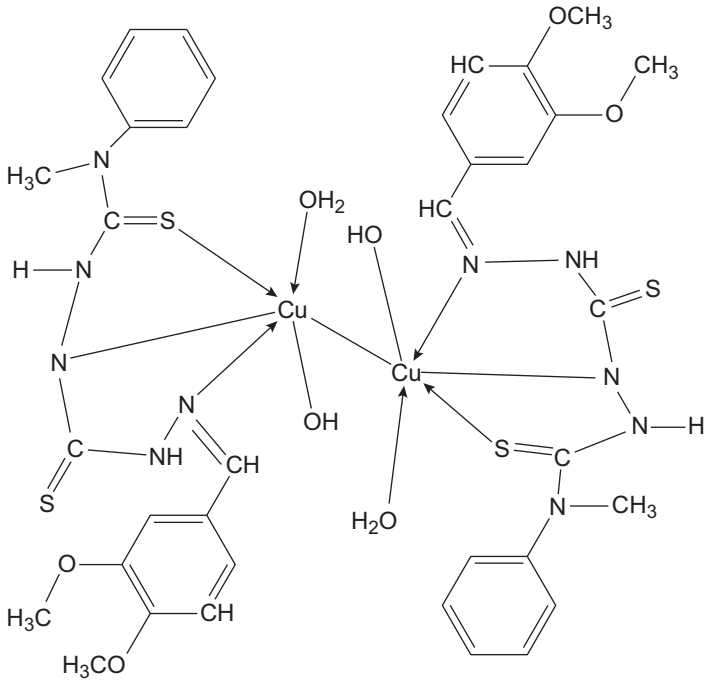

Fig. 18. Proposed structure of $[CuHLOH\ H_2O)]_2$ **(8).**

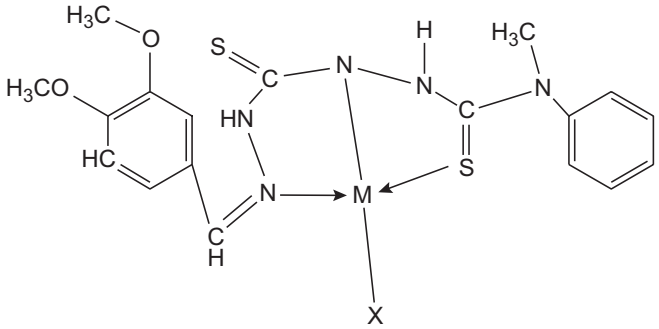

Fig. 19. Proposed structure of [MLX], where M = Zn(II) or Cd(II); X = CH_3COO^- or OH^-**(9)** and **(10)**.

References

1. Y-H Cai, W. Luo, J. Chem., (2014), Article ID 218376, 5 pages. doi:10.1155/2014/218376.
2. X. Zhu, C. Wang, Z. Lu, Y. Dang, Transition Met. Chem., 22 (1997) 9.
3. A. D. Khalaji, G. Grivani, M. Rezaei, K. Fejfarova, M. Dusek, Phosphorus, Sulfur Silicon and the Relat. Elem., 188 (2013) 1119.
4. G. M. Sheldrick, SHELXL-2014/7: Program for the Solution of Crystal Structures, University of Göttingen, Göttingen, Germany, 2014.
5. A. L. Spek, PLATON, A Multipurpose Crystallographic Tool, Utrecht University, Utrecht, the Netherlands (1999).
6. Diamond-Crystal and Molecular Structure Visualization Crystal Impact – Dr. H. Putz & Dr. K. Brandenburg GbR, Kreuzherrenstr. 102, 53227 Bonn, Germany.
7. C. Macrae, P. R. Edington, P. McCabe, E. Pidcock, G. P. P. Sheilds, R. Taylor, M. Towler, J. Van de Streek, J. Appl. Cryst., 39 (2006) 453.
8. G. J. Palenik, D. F. Rendle, W. S. Cru1er, Acta Cryst., B30 (1974) 2390.
9. K. O. Ferraz, S. M. S. V. Wardell, J. L. Wardell, S. R. W. Louro, H. Beraldo, Spectrochim. Acta A 73 (2009) 140.
10. R. M. Silverstein, G. C. Bassler, C. Morril, Spectroscopic Identification of Organic Compounds, 4th ed., John Wiley & Sons, New York city, New York 1981.
11. B. N. Figgis, Introduction to Ligand Field, John Wiley & Sons, New York City, New York, 1966.
12. F. A. Cotton, Progress in Inorganic Chemistry, Interscience publishers, John Wiley and Sons, New York City, New York; London, 1967.
13. P. S. K. Chia, S. E. Livingstone, Aust. J. Chem., 22 (1969) 1825 and references therein; R. Roy, P. Paul and K. Nag, Transition Met. Chem., 9 (1984) 152.
14. B. N. Figgis, J. Lewis., Progress in Inorganic Chemistry. Vol. 6, Albert Cotton. F. (ed.), Interscience, New York City, New York, 1964.
15. B. Harikumar, M. R. P. Kurup, T. N. Jayaprakash, Transition Met. Chem., 22 (1997) 507; (b) P. Bindu, M.R.P. Kurup, Transition Met. Chem., 22 (1997) 578.
16. D. Sutton, Electronic Spectra of Transition Metal Complexes. McGraw Hill, London, 1968.
17. O. Maddock, A. Sharpe, R. L. Martin, Proc. Roy. Austral. Chem. Inst., 38 (1971) 33.
18. N. R. Sangeetha, S. Pal, Polyhedron., 19 (2000) 1593.
19. K. Nakamoto, Infrared and Raman spectra of Inorganic and Coordination compounds, 5th ed., John Wiley & Sons, New York City, New York, 1997.

CHAPTER VIII

IN-SILICO SCREENING FOR THE NON-LINEAR OPTICAL PROPERTY OF LIGANDS

1. Introduction

The foremost endeavour of quantum chemistry is to apply the quantum mechanics in physical models and experiments of chemical systems. Quantum chemists usually use mathematical methods accomplished by computer programs to find out the energies and structures of molecules. Computational chemistry simulates chemical structures and reactions numerically based on fundamental laws of physics. For chemists, it opens a new frame to study chemical phenomena by running calculations on computers rather than by studying the reactions and compounds experimentally. Schrödinger equation is the basis of all quantum chemical models.

The main idea of density functional theory (DFT) is to explain an interacting system of fermions through its density and not through its many body wave function.[1] The convergence of traditional quantum chemical methodology and DFT were recognized by the announcement of Nobel Prize in chemistry in 1998 to John Pople and Walter Kohn. Nowadays, DFT has been considered as a cost-effective approach for the computation of molecular structure, vibration frequencies and energies of chemical reactions. Literature survey revealed that the DFT has a great accuracy in reproducing the experimental values in terms of geometry, dipole moment, vibrational frequencies, thermodynamic properties, and so on. Several studies have shown that the molecular structures and vibration frequencies calculated by DFT methods are more reliable than those obtained by other quantum chemical methods.[2]

2. Applications of DFT method

2.1. Geometry optimization

It is the name for the process to find the configuration of minimum energy of a molecule. A minimum energy structure will have no imaginary frequencies. A sensible starting point for geometry optimization is to use experimental data, that is, the X-ray diffraction data of the molecules, whenever possible. The gas phase structures of the compounds were optimized by using DFT method proposed by Hohenberg and Kohn.[3]

2.2. GAUSSVIEW–GUI for GAUSSIAN 09 program

It is an affordable, full-featured graphical user interface for GAUSSIAN 09 program.[4] With the help of Gaussview,[5] one can prepare input for submission to Gaussian and to examine graphically the output that Gaussian produces. Gaussview can graphically display the results of a variety of Gaussian calculations, such as molecular orbitals, atomic charges, surfaces from the electron density, electrostatic potential, NMR shielding density and other properties. Surfaces may be displayed in solid, translucent and wire mesh modes. Surfaces can be coloured by a separate property. Animation of the normal modes of vibrational frequencies, animation of the steps in geometry optimizations, potential energy surface scans, intrinsic reaction coordinate (IRC) paths can also be generated using Gaussview.

2.3. HOMO–LUMO

To elucidate several types of reactions and for understanding the most reactive position in conjugated systems, molecular orbitals and their properties like energy are utilized.[6] Red and green colours in the picture represent the positive and negative values for the wave function. The charge exchange inside the molecule can be identified by evaluating the HOMO–LUMO energy gap which is a sign of its biological activity.[7] The HOMO–LUMO energy gap is also an identification factor of stability index.[8] The small energy gaps normally indicate a high chemical reactivity and low kinetic stability. Such molecules are termed as delicate ones.[9]

2.4. Global descriptors

According to the Koopmans' theorem, the HOMO and LUMO orbital energies are related to gas-phase vertical ionization energies (I) and vertical electron affinities (A) of the isomers through the equations, $A = -E_{LUMO}$, $I = -E_{HOMO}$.[10] Electron affinity indicates the potential of a ligand to accept precisely one electron from a donor. By using HOMO and LUMO energy values, global descriptors such as chemical hardness, $[\eta = (I - A)/2]$, chemical softness, $[\zeta = 1/2\eta]$, chemical potential, $[\mu = (E_{LUMO} + E_{HOMO})/2]$ and the global electrophilicity index, $[\omega = \mu^2/2\eta]$, were also calculated.[11] Physically, chemical potential μ describes the escaping tendency of electrons from an equilibrium system.[12] Electrophilicity index measures the property or capacity of a species to accept electrons.[13] It is a measure of the stabilization in energy after a system accepts additional amount of electronic charge from the environment.[14,15]

2.5. Molecular electrostatic potential

Molecular electrostatic potential (MEP) at a point in the space around a molecule gives an indication of the net electrostatic effect produced at that point by a total charge distribution of the atom or molecule. The electrophilic and nucleophilic sites in a molecule can easily be identified with the help of MEP map which in turn determines the chemical reactivity of a compound and is responsible for non-covalent interactions.[16] The distinct values of the electrostatic potential at the surface are represented by different colours: red represents the regions of most negative electrostatic potential, blue represents the regions of most positive electrostatic potential and green represents the regions of zero potential.

The ascending order of potential is red < orange < yellow < green < blue. It is also very useful to correlate the molecular structure with physico-chemical property.

2.6. Natural bond orbital analysis

It gives a profound insight into the intra- and intermolecular orbital interactions in the molecules between filled donor and empty acceptor natural bond orbitals (NBOs), which also provides a convenient basis for investigating charge-transfer or conjugative interaction in molecular systems.[17,18] Second-order perturbation energy gives clear information regarding the origin of stabilization of a molecule by analyzing the interactions between occupied Lewis NBO (bond pair or lone pair) as donor and an unoccupied non-Lewis NBO (anti-bonding or Rydberg) as acceptor.[19] NBO analysis allows us to understand which orbital interactions are primarily involved in the stability of the observed conformer. Since the occupancies of filled NBOs are highly condensed, the delocalizing interactions can be further treated by the second-order perturbation energies ($E^{(2)}$):

$$E(2) = -q_i F_{ij}/\epsilon_i - \epsilon_j$$

where q_i is the population of donor orbital or donor orbital occupancy; ϵ_i, ϵ_j are orbital energies of donor and acceptor NBOs, respectively, and F_{ij} is the off-diagonal Fock or Kohn–Sham matrix element between i and j NBOs.[18]

2.7. Calculation of polarizability and hyperpolarizability to screen non-linear optical property

Non-linear optics deals with the interaction of applied electromagnetic fields in various materials to generate new electromagnetic fields, altered in wave number, phase or other physical properties. Non-linear optical (NLO) materials have diverse applications in telecommunication, signal processing, optical interconnection, optical computing, sensor protection, optical switching and various other photonic technologies. Organic crystals are mainly employed for optical applications owing to their high conversion efficiency, transparency in the UV–Vis region, large optical susceptibilities and inherent ultrafast response time. Currently, organic NLO materials are an important substitute to inorganic materials due to their low cost and flexible molecular structures. Intramolecular charge-transfer (ICT) from the donor to acceptor group through a single-double bond conjugated path can induce large variations in both molecular dipole moment and polarizability. The NLO property of a molecule originates from the non-centrosymmetric alignment of NLO chromophore. When a beam of light is imposed on a material, the oscillation of charges on each atom of that material takes place. The amount of charge displaced in a linear material is proportional to the magnitude of the electric field with same frequency as the incident light. For small fields, the displacement of charge from the equilibrium, mean polarization (P), will be directly proportional to the applied field, E

$$P = \alpha E$$

where α is the linear polarizability.

In an NLO material, the displacement of charges from its equilibrium position will be a non-linear function of the electric field. If the electric field is of high intensity, the polarizability of all materials will deviate from linear regime.[20]
For non-linear polarization,

$$P = P_0 + \chi^1 E + \chi^2 E^2 + \chi^3 E^3 + \ldots$$

The total dipole moment of a chemical system that arises while applying electric field can be calculated by considering four components and is given in the equation:

$$\mu = \mu_0 + \alpha \, \mathrm{F} + \tfrac{1}{2} \beta \, \mathrm{F}^2 + 1/6 \, \gamma^3 + \ldots$$

where μ_0 is the permanent dipole moment, α is polarizability, β is the first-order polarizability and γ is the second-order polarizability. The first-order hyperpolarizability is a third rank tensor that can be described by a $3 \times 3 \times 3$ matrix. However, according to Kleinman symmetry, the 27 components of the 3D matrix can be reduced to 10 components for a molecule with no symmetry.[21] It can be given in the lower tetrahedral format. It is obvious that the lower part of the $3 \times 3 \times 3$ matrices is tetrahedral. The components of β are defined as the coefficients in the Taylor series expansion of the energy in the external electric field.[22,23] For the calculation of the terms, μ, α, $\Delta\alpha$ and β_o are defined as follows:

$$\alpha_{\text{total}} = 1/3(\alpha_{xx} + \alpha_{yy} + \alpha_{zz})$$

$$\Delta\alpha = 1/2^{1/2}[(\alpha_{xx} - \alpha_{yy})^2 + (\alpha_{yy} - \alpha_{zz})^2 + (\alpha_{zz} - \alpha_{xx})^2 + 6\alpha^2_{xz} + 6\alpha^2_{xy} + 6\alpha^2_{yz}]^{1/2}$$

$$\beta_{\text{total}} = [(\beta_{xxx} + \beta_{xzz} + \beta_{xyy})^2 + (\beta_{yyy} + \beta_{xxy} + \beta_{yzz})^2 + (\beta_{zzz} + \beta_{xxz} + \beta_{yyz})^2]^{1/2}$$

$$\mu_{\text{total}} = (\mu_x^2 + \mu_y^2 + \mu_z^2)^{1/2}$$

Since the values of the polarizabilities (α) and first-order hyperpolarizability (β) of GAUSSIAN-09W output are reported in atomic units (a.u.), the calculated values have been converted into electrostatic units (esu) (1 a.u. = 0.1482×10^{-24} esu for α; 1 a.u. = 8.6393×10^{-33} cm^5/esu for β).[24] Urea is one of the prototypical molecules used in the study of the NLO properties of molecular systems. Therefore, it is used frequently as a threshold value for comparative purposes. The μ, α and β_{total} of urea are 1.3732 Debye, 3.8312 Å^3 and 0.37289×10^{-30} cm^5/esu obtained by B3LYP/6-31+G(d,p) method.[25,26]

3. Computational details

All theoretical computations were done by using GAUSSIAN 09 software package and GAUSS-VIEW 5.0.9 visualization program. In this study, the compounds were optimized by using DFT with Beck's three parameter[27] for exchange interaction and Lee–Yang–Parr[28] to consider correlation functional (B3LYP) with the 6-31+G(d,p) basis sets. The starting geometries

of molecules were taken from the X-ray refinement data or by drawing structures using Gauss view program. In order to know more about the compounds, HOMO–LUMO energy gap, global reactivity descriptors, the MEP map and NBO analysis were computed using the same method. In order to explore NLO properties, the total static dipole moment (μ), the linear polarizability (α), the anisotropy of polarizability ($\Delta\alpha$) and the mean first-order hyperpolarizability (β_{total}) were calculated using the abovementioned method.

4. Results and discussion

The following novel ligands synthesized by us were selected for computational studies:

1. N-Methyl-2-((3-methyl-5-oxo-1-phenyl-4,5-dihydro-1H-pyrazol-4-yl)(phenyl) methylene)-N-phenylhydrazinecarbothioamide (H_2L1)
2. 2-[2-(Diphenylmethylidene)hydrazine]-N-methyl-N-phenylhydrazine-1-carbothioamide (H_2L2)
3. 3-Formylchromone N(4)-methyl-N(4)-phenylthiosemicarbazone (HL3)
4. 2-{2-[(4-Hydroxy-3-methoxyphenyl)methylidene]hydrazinecarbonothioyl}-N-methyl-N-phenylhydrazine-1-carbothioamide (H_2L4)
5. 2-{2-[(3,4-Dimethoxyphenyl)methylidene]hydrazinecarbonothioyl}-N-methyl-N-phenylhydrazine-1-carbothioamide (H_2L5)

4.1. N-Methyl-2-((3-methyl-5-oxo-1-phenyl-4,5-dihydro-1H-pyrazol-4-yl) (phenyl)methylene)-N-phenylhydrazinecarbothioamide (H_2L1)

4.1.1. Optimized structure, MEP and HOMO–LUMO analysis of H_2L1

Starting geometry of the molecule was taken from X-ray refinement data. The optimized molecular structure, HOMO-, LUMO- and MEP plots of H_2L1 have been generated at B3LYP/6-31+G(d,p) using the GAUSS-VIEW 5.0.9 program and are shown in Fig. 1. The optimized geometry shows an energy –1713.7165 a.u. On the basis of frontier molecular orbital approach, the HOMO, HOMO-1, LUMO and LUMO+1 orbitals are mainly responsible for electronic transitions. Here, transitions originating from the highest occupied molecular orbital (HOMO) to the lowest unoccupied molecular orbital (LUMO) is $n \rightarrow \pi^*$ type. The transitions from HOMO-1→LUMO is characterised as $\pi \rightarrow \pi^*$ type. Theoretically, HOMO–LUMO energy gap is found to be 3.865 eV, and experimentally it was 3.87 eV. By using HOMO and LUMO energy values, global descriptors such as chemical hardness, chemical softness, chemical potential and the global electrophilicity index were also calculated and is presented in Table 1. It is also observed that the chemical potential of the compound is negative and shows the stability of the compound. They do not decompose spontaneously into the elements from which they are made up of.[29] In the MEP map of our molecule, the most negative region is positioned on the O, N and S atoms linked with carbon through double bonds, which can be considered as potential sites for electrophilic attack. However, the maximum positive region is located on the H atom attached to nitrogen. This also shows a possible site for nucleophilic attack. MEP map of the molecule elucidates ICT in the molecule.

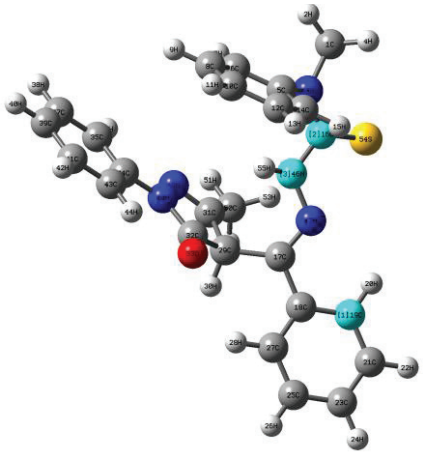

Optimized molecule

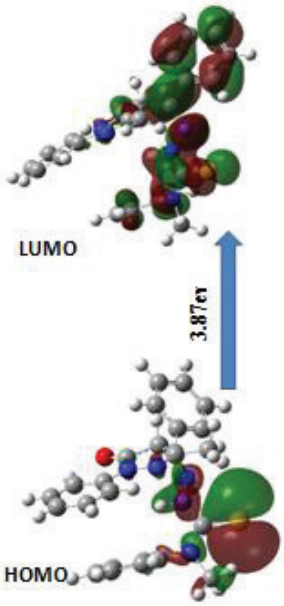

HOMO-LUMO orbitals, corresponding energy gap

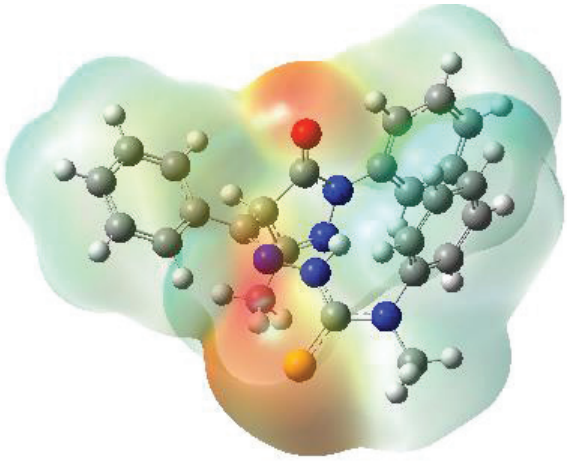

MEP surface

Fig. 1. The optimized molecular structure, HOMO-, LUMO- and MEP plots of H_2L1.

Table 1. Calculation of global descriptors

Global Descriptive Parameters			
Homo	–5.71	Softness ζ	0.259
Lumo	–1.84	Chemical potential μ	–3.78
Vertical ionization energy I	5.71	Electronegativity	3.78
Vertical electron affinity A	1.84	Global electrophilic index ω	3.69
Hardness η	1.93		

4.1.2. NBO analysis

Several donor–acceptor interactions have been observed among the strongly occupied NBOs of the compound (Table 2). The most important delocalization sites are seen in the π system and in the lone pairs of the oxygen, sulphur and nitrogen atoms. The larger the $E^{(2)}$ value, the more intense is the interaction between electron donors and electron acceptors, that is, more the donating tendency from electron donors to electron acceptors, greater the extent of conjugation of the whole system.

The most important interaction energy, related to the resonance in the molecule, is electron donation from LP(1) C(35) to the anti-bonding acceptor π*C(34)–N(48) with enormous stabilization energy of 412.75 kcal mol^{-1}. Further, LP(1) C(35) conjugates with π*C(37)–C(39) leading to a stabilization energy of 63.82 kcal mol^{-1}. LP(1) N(45) and LP(1) N(46) stabilize the thiosemicarbazide moiety *via* conjugation with σ*C(16)–S(54) leading to the stabilization energies of 79.89 and 49.01 kcal mol^{-1}, respectively. Intramolecular O···H–N hydrogen bond interactions are shown in the NBO analysis by the interaction between the O lone pair and N–H anti-bonding orbital [LP(1) O(33) → σ* N(46)–H(55) and LP(2) O(33) → σ* N(46)–H(55)] leading to interaction energies of 10.83 and 19.4 kcal mol^{-1}, respectively. LP(2) O(33) NBO further conjugates with σ*C(32)–N(48) resulting an energy of 24.74 kcal mol^{-1}.

From Table 2, several ICT interactions are observed which are formed by the orbital overlap between bonding (π) and anti-bonding (π*) orbitals. They result in the stabilization of the system. The movement of π-electron cloud from donor to acceptor makes the molecule more polarized and it must be responsible for the NLO properties of the molecule. NBO analysis together with HOMO–LUMO energy gap and MEP map of the molecule elucidate ICT in the molecule.

4.1.3. Polarizability and hyperpolarizability

The calculated dipole moment (μ), polarizability (α) and the mean first-order hyperpolarizability (β_{total}) for the compound, H_2L1 are 3.2829 D, 28.0639 Å^3 and 0.783748 × 10^{-30} cm^5/esu, respectively, are also summarized in Table 3. Theoretically, the linear polarizability (α) of the compound is nine times higher than that of urea. It is also found that the compound shows twofold higher value of first-order hyperpolarizability (β) and the dipole moment (μ) than urea.

4.2. 2-[2-(Diphenylmethylidene)hydrazine]-N-methyl-N-phenylhydrazine-1-carbothioamide (H_2L2)

4.2.1. Optimized structure, MEP and HOMO–LUMO analysis of H_2L2

Starting geometry of the molecule was drawn using GAUSS-VIEW 5.0.9 program. The optimized geometry shows energy –1921.1254 a.u. The optimized molecular structure, HOMO-, LUMO- and MEP plots of H_2L2 have been generated at B3LYP/6-31+G(d,p) using the GAUSS-VIEW 5.0.9 program and are shown in Fig. 2. Theoretically, HOMO–LUMO energy gap was found to be 4.24 eV. By using HOMO and LUMO energy values, global descriptors such as chemical hardness, chemical softness, chemical potential and the global electrophilicity index were also calculated and is presented in Table 4. It is also observed that the chemical potential of the compound is negative which shows the stability of the compound. In MEP, red regions mainly extend over the sulphur atoms linked to

Table 2. Major donor–acceptor interactions of the compound and their second-order perturbation energies (kcal/mol)

Donor NBO (*i*)	Acceptor NBO (*j*)	$E^{(2)}$ kcal/mol	*Ej – Ei* a.u.	*Fij* a.u.	Donor NBO (*i*)	Acceptor NBO (*j*)	$E^{(2)}$ kcal/mol	*E*j-Ei a.u.	*F*ij a.u.
πC(5)–C(6)	π*C(8)–C(10)	20.31	0.3	0.07	πC(34)–N(48)	π*C(32)–O(33)	42.76	0.31	0.106
πC(5)–C(6)	π*C(12)–C(14)	20.44	0.3	0.07	πC(37)–C(39)	LP(1) C35	46.86	0.14	0.09
πC(8)–C(10)	π*C(5)–C(6)	21.27	0.29	0.07	πC(37)–C(39)	π*C(41)–C(43)	22.38	0.29	0.072
πC(8)–C(10)	π*C(12)–C(14)	20.58	0.29	0.07	πC(41)–C(43)	π*C(34)–N(48)	37.27	0.19	0.089
πC(12)–C(14)	π*C(5)–C(6)	22.43	0.29	0.072	πC(41)–(43)	π*C(37)–C(39)	21.01	0.29	0.07
πC(12)–C(14)	π*C(8)–C(10)	20.36	0.29	0.069	LP(1) O(33)	σ*N(46)–H(55)	10.83	1.23	0.104
πC(18)–C(19)	π*C(21)–C(23)	19.58	0.29	0.068	LP(2) O(33)	σ*C(29)–C(32)	12.69	0.74	0.088
πC(18)–C(19)	π*C(25)–C(27)	20.87	0.28	0.069	LP(2) O(33)	σ*C(32)–N(48)	24.74	0.73	0.122
πC(21)–C(23)	π*C(18)–C(19)	20.31	0.29	0.069	LP(2) O(33)	σ*N(46)–H(55)	19.4	0.82	0.114
πC(21)–C(23)	π*C(25)–C(27)	21.71	0.28	0.07	LP(2) S(54)	σ*C(16)–N(45)	11.27	0.65	0.078
πC(25)–C(27)	π*C(18)–C(19)	20.15	0.3	0.069	LP(2) S(54)	σ*C(16)–N(46)	12.83	0.62	0.081
πC(25)–C(27)	π*C(21)–C(23)	20.43	0.29	0.069	π*C(17)–N(47)	π*C(18)–C(19)	11.03	0.04	0.033
σC(29)–H(30)	π*C(17)–N(47)	17.5	0.54	0.087	π*C(25)–C(27)	π*C(18)–C(19)	250.06	0.01	0.082
σC(29)–H(30)	π*C(31)–N(49)	17.54	0.53	0.086	π*C(34)–N(48)	π*C(31)–N(49)	14.79	0.04	0.03
σC(29)–H(30)	π*C(32)–O(33)	22.53	0.51	0.101	π*C(34)–N(48)	π*C(32)–O(33)	134.1	0.02	0.059
πC(34)–N(48)	π*C(31)–N(49)	14.24	0.33	0.062	π*C(34)–N(48)	π*C(41)–C(43)	83.04	0.09	0.1

Table 3. Calculated electric dipole moment, polarizability and first-order hyperpolarizability of the compound

Polarizability	**Hyperpolarizability**
$\alpha_{XX} = -176.1604$	$\beta_{XXX} = -6.8175$
$\alpha_{XY} = 15.7388$	$\beta_{XYY} = 17.8458$
$\alpha_{YY} = -201.6986$	$\beta_{XZZ} = 27.4541$
$\alpha_{XZ} = 0.0255$	$\beta_{YYY} = -14.5805$
$\alpha_{ZZ} = -191.0043$	$\beta_{XXY} = -55.7806$
$\alpha_{YZ} = -5.9678$	$\beta_{YZZ} = 5.2974$
$\alpha_{total} = 28.0639 Å^3$	$\beta_{ZZZ} = -3.9677$
$\Delta\alpha = 49.70691 Å^3$	$\beta_{XXZ} = -26.8267$
$\mu = 3.2829$ Debye	$\beta_{YYZ} = -19.3684$
	$\beta_{total} = 0.783748 \times 10^{-30}$ cm^5/esu

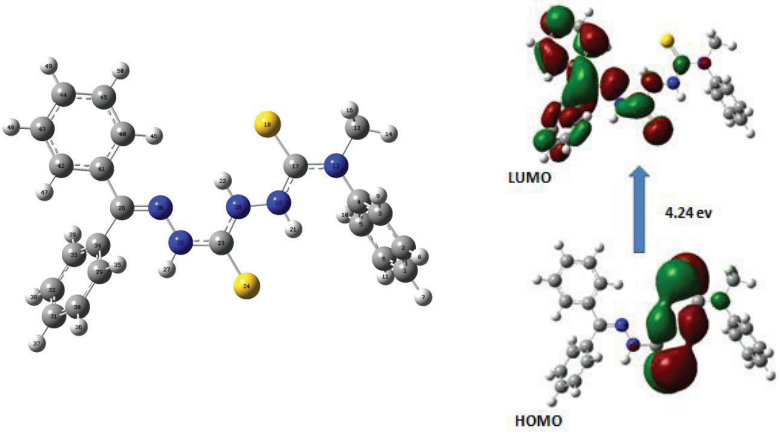

Optimized molecule HOMO-LUMO orbitals, corresponding energy gap

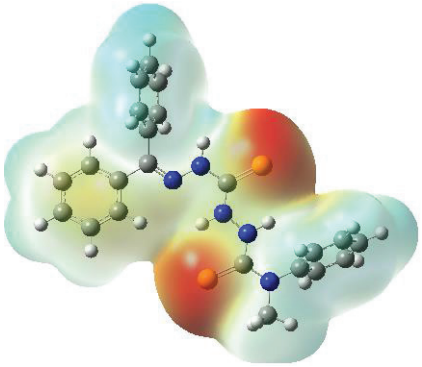

MEP surface

Fig. 2. The optimized molecular structure, HOMO-, LUMO- and MEP plots of H_2L2.

Table 4. Calculation of global descriptors

Global Descriptive Parameters			
Homo	–5.7880	Softness ζ	0.5248
Lumo	–1.6349	Chemical potential μ	–3.6680
Vertical ionization energy I	5.7880	Electronegativity	–3.6680
Vertical electron affinity A	–1.6349	Global electrophilic index ω	3.1733
Hardness η	1.9055		

carbon through double bonds, predicting that they are susceptible sites for electrophilic attack. The blue regions of the molecule are found to be spread over the hydrogen atoms. This indicates that these sites may involve in nucleophilic processes.

4.2.2. NBO analysis

Several donor–acceptor interactions have been observed among the strongly occupied NBOs of the compound (Table 5). The most important delocalization sites are seen in the π system and in the lone pairs (n) of the oxygen, sulphur and nitrogen atoms. The electron donation from LP(1) N(25) to the anti-bonding π^* N(26)–C(28) stabilizes the molecule with an energy of 30.82 kcal mol^{-1}. Further, LP(2) S(18) conjugates with σ^*N(12)–C(17) leading to a stabilization energy of 10.87 kcal mol^{-1}. The interactions πC(29)–C(34) → π^*C(30)–C(31)/π^*C(32)–C(33) and πC(30)–C(31) → π^*C(32)–C(33) are responsible for the extended conjugation of benzene ring and stabilize the molecule with

Table 5. Major donor–acceptor interactions of the compound and their second-order perturbation energies (kcal/mol)

Donor NBO (*i*)	**Acceptor NBO (*j*)**	$E^{(2)}$ **kcal/mol**	***E*(*j*)–*E*(*i*) a.u.**	***F*(*i*,*j*) a.u.**
πC(1)–C(6)	π^*C(2)–C(3)	20.49	0.28	0.068
πC(1)–C(6)	π^*C(4)–C(5)	21.83	0.27	0.069
πC(2)–C(3)	π^*C(1)–C(6)	19.81	0.28	0.067
πC(2)–C(3)	π^*C(4)–C(5)	21.04	0.27	0.068
πC(4)–C(5)	π^*C(1)–C(6)	18.76	0.29	0.066
πC(4)–C(5)	π^*C(2)–C(3)	19.81	0.29	0.068
πC(29)–C(34)	π^*C(30)–C(31)	19.43	0.29	0.067
πC(29)–C(34)	π^*C(32)–C(33)	19.41	0.29	0.067
πC(30)–C(31)	π^*C(32)–C(33)	19.89	0.28	0.067
LP(2) S(18)	σ^*N(12)–C(17)	10.87	0.65	0.076
LP(2) S(18)	σ^*N(12)–C(17)	10.87	0.65	0.076
LP(2) S(18)	σ^*N(20)–H(22)	6.84	0.62	0.06
LP(2) S(24)	σ^*N(19)–H(21)	5.74	0.62	0.055
LP(2) S(24)	σ^*N(20)–C(23)	9.64	0.67	0.074
LP(2) S(24)	σ^*C(23)–N(25)	10.24	0.63	0.073
LP(2) S(24)	σ^*C(23)–N(25)	10.24	10.24	0.073
LP(1) N(26)	σ^*N(25)–H(27)	9.45	0.82	0.08
LP(1) N(26)	σ^*C(28)–C(34)	10.83	0.83	0.085

a maximum energy ~19.89 kcal/mol. LP(2) S(18) conjugates with σ*N(12)–C(17) and σ*N(20)–H(22) with stabilization energies 10.87 and 6.84 kcal/mol, respectively. In this case, we have observed several ICT interactions resulted from the orbital overlap between bonding (π) and anti-bonding (π*) orbitals. These movements of π-electron cloud from donor to acceptor make the molecule more polarized and it must be responsible for its NLO properties.

4.2.3. Polarizability and hyperpolarizability

The calculated dipole moment (μ), polarizability (α) and the mean first hyperpolarizability (β_{total}) for the compound, H_2L2 are 2.6576 Debye, 24.8058 Å3 and 0.363 cm^5/esu, respectively, are also summarized in Table 6. Theoretically, the linear polarizability (α) of the compound is nine times higher than that of urea. It is also found that the compound shows comparable value of first-order hyperpolarizability (β_{total}) to that of urea. The dipole moment of the molecule is twice that of urea.

Table 6. Calculated electric dipole moment, polarizability and first-order hyperpolarizability of the compound

Polarizability	Hyperpolarizability
α_{XX} = 148.3006	β_{XXX} = –23.0405
α_{XY} = –2.0194	β_{XYY} = 51.0368
α_{YY} = 173.8425	β_{XZZ} = –11.6842
α_{XZ} = –2.9088	β_{YYY} = 28.9689
α_{ZZ} = 179.999	β_{XXY} =12.8631
α_{YZ} = 7.5779	β_{YZZ} = –2.0286
α_{total} = 24.8058 Å^3	β_{ZZZ} = 1.6134
$\Delta\alpha$ = 32.51816 Å^3	β_{XXZ} = –16.485
μ = 2.6576 Debye	β_{YYZ} = –13.0981
	β_{total} = 0.363 × 10^{-30} cm^5/esu

4.3. Formylchromone N(4)-methyl-N(4)-phenylthio-semicarbazone(HL3)

4.3.1. Optimized structure, MEP and HOMO–LUMO analysis of HL3

Starting geometry of the molecule was drawn using GAUSS-VIEW 5.0.9 program. The optimized geometry shows an energy –1407.8536 a.u. The optimized molecular structure HOMO-, LUMO- and MEP plots of HL3 have been generated at B3LYP/6-31+G(d,p) using the GAUSS-VIEW 5.0.9 program and are shown in Fig. 3. Theoretically, HOMO–LUMO energy gap is found to be 3.29 eV. By using HOMO and LUMO energy values, global descriptors such as chemical hardness, chemical softness, chemical potential and the global electrophilicity index were also calculated and is presented in Table 7. It is also observed that the chemical potential of the compound is negative, showing its stability. In MEP, red regions mainly extend over the oxygen and sulphur atoms predicting them as susceptible sites for electrophilic attack. The blue regions of the molecule mainly spread over the hydrogen atoms. This indicates that these sites may be involved in nucleophilic processes.

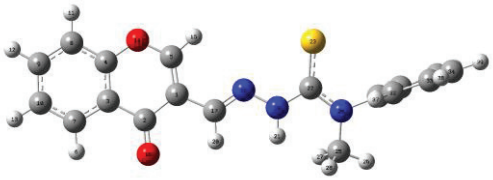

Optimized molecule

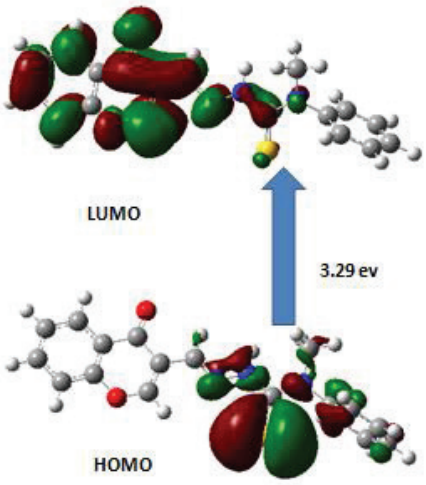

HOMO-LUMO orbitals, corresponding energy gap

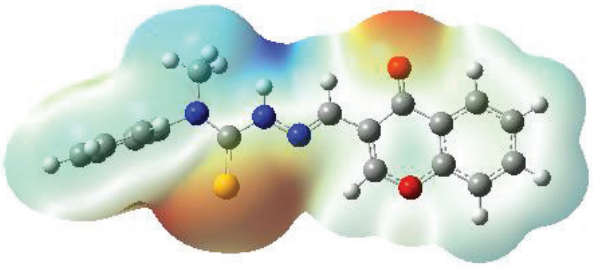

MEP surface

Fig. 3. The optimized molecular structure, HOMO-, LUMO- and MEP plots of HL3.

Table 7. Calculation of global descriptors

Global Descriptive Parameters			
Homo	–5.4089	Softness ζ	0.6078
Lumo	–2.1187	Chemical potential μ	–3.7638
Vertical ionization energy I	5.4089	Electronegativity	3.7638
Vertical electron affinity A	2.1187	Global electrophilic index ω	4.3056
Hardness η	1.6451		

4.3.2. NBO analysis

Several donor–acceptor interactions have been observed among the strongly occupied NBOs of the compound (Table 8). The interactions πC(29)–C(34) $\rightarrow$ π *C(30)–C(31)/π * C(32)–C(33) and π C(32)–C(33) $\rightarrow$ π*C(30)–C(31) are responsible for the extended

conjugation of benzene ring and stabilize the molecule with a maximum energy, ~21.07 kcal/mol. πC(1)–C(5) and πC(3)–C(4) conjugate with π*C(2)–O(16) with a maximum energy, 23.62 kcal/mol. LP(2) O(14) conjugates with π*C(1)–C(5) leading to a stabilization energy of 33.48 kcal mol^{-1}. LP(2) O(16) NBO conjugates with σ*C(1)–C(2) and σ*C(2)–C(3) and the resulting energies are 19.54 and 20.08 kcal mol^{-1}, respectively. LP(1) N(19) stabilizes *via* conjugation with σ*C(22)–S(23) leading a stabilization energy of 58.01 kcal mol^{-1}. The interactions πC(2)–O(16)→π*C(1)–C(5) and πC(17)–N(18)→π*C(1)–C(5) stabilize the system with energies 5.28 and 8.71 kcal mol^{-1}, respectively. LP(1) N(18) conjugates with σ*C(17)–H(20), σ*N(19)–H(21) π*C(17)–N(18), σ*N(19)–C(22) and σ*C(22)–N(24) with stabilization energies 10.61, 8.36, 27.9, 13.49 and 11.88 kcal mol^{-1}, respectively. The movement of π-electron cloud from donor to acceptor makes the molecule more polarized and it must be responsible for its NLO properties.

Table 8. Major donor–acceptor interactions of the compound and their second-order perturbation energies (kcal/mol)

Donor NBO (*i*)	**Acceptor NBO (*j*)**	**$E^{(2)}$ kcal/mol**	**$E(j)$–$E(i)$ a.u.**	**$F(i,j)$ a.u.**
πC(1)–C(5)	π*C(2)–O(16)	23.62	0.3	0.077
πC(3)–C(4)	π*C(2)–O(16)	21.78	0.29	0.072
πC(7)–C(10)	π*C(8)–C(9)	21.24	0.28	0.069
πC(8)–C(9)	π*C(3)–C(4)	21.76	0.28	0.071
πC(29)–C(34)	π*C(30)–C(31)	20.64	0.28	0.068
πC(29)–C(34)	π*C(32)–C(33)	19.89	0.28	0.067
πC(32)–C(33)	π*C(30)–C(31)	21.07	0.28	0.068
LP(2) O(14)	π*C(1)–C(5)	33.48	0.37	0.101
LP(2) O(16)	σ*C(1)–C(2)	19.54	0.71	0.107
LP(2) O(16)	σ*C(2)–C(3)	20.08	0.71	0.108
LP(1) N(19)	σ*C(22)–S(23)	58.01	0.23	0.107
πC(2)–O(16)	π*C(1)–C(5)	5.28	0.38	0.042
πC(2)–O(16)	π*C(3)–C(4)	4.78	0.37	0.042
πC(3)–C(4)	π*C(7)–C(10)	18.2	0.3	0.068
πC(3)–C(4)	π*C(8)–C(9)	16.02	0.29	0.062
πC(7)–C(10)	π*C(3)–C(4)	17.95	0.27	0.064
πC(8)–C(9)	π*C(7)–C(10)	16.1	0.29	0.062
πC(17)–N(18)	π*C(1)–C(5)	8.71	0.35	0.051
LP(1) N(18)	σ*C(17)–H(20)	10.61	0.82	0.084
LP(1) N(18)	σ*N(19)–H(21)	8.36	0.77	0.072
LP(1) N(19)	π*C(17)–N(18)	27.9	0.29	0.083
LP(2) S(23)	σ*N(19)–C(22)	13.49	0.59	0.081
LP(2) S(23)	σ*C(22)–N(24)	11.88	0.61	0.077

4.3.3. Polarizability and hyperpolarizability

The calculated dipole moment (μ), polarizability (α) and the mean first hyperpolarizability (β_{total}) for the compound HL3 are 4.6184 Debye, 20.5995 Å^3, and 2.027 cm^5/esu, respectively, are summarized in Table 9. Theoretically, the linear polarizability (α) of the compound is seven times higher than that of urea. It is also found that the compound shows 5.44 times higher value of first-order hyperpolarizability and four times higher dipole moment than urea.

Table 9. Calculated electric dipole moment, polarizability and first-order hyperpolarizability of the compound

Polarizability	Hyperpolarizability
$\alpha_{XX} = 123.3269$	$\beta_{XXX} = -242.201$
$\alpha_{XY} = -15.8475$	$\beta_{XYY} = 16.5671$
$\alpha_{YY} = 144.7186$	$\beta_{XZZ} = 26.9125$
$\alpha_{XZ} = -5.2107$	$\beta_{YYY} = 17.1051$
$\alpha_{ZZ} = 148.9494$	$\beta_{XXY} = 60.5281$
$\alpha_{YZ} = 7.0254$	$\beta_{YZZ} = -5.638$
$\alpha_{total} = 20.5995$	$\beta_{ZZZ} = -0.3415$
$\Delta\alpha = 39.35684$ Å^3	$\beta_{XXZ} = -84.708$
$\mu = 4.6184$ Debye	$\beta_{YYZ} = -16.709$
	$\beta_{total} = 2.027 \times 10^{-30}$ cm^5/esu

4.4. 2-{2-[(4-Hydroxy-3-methoxyphenyl)methylidene] hydrazinecarbonothioyl}-N-methyl-N-phenylhydrazine-1-carbothioamide (H_2L4)

4.4.1. Optimized structure, MEP and HOMO–LUMO analysis of H_2L4

Starting geometry of the molecule was drawn using GAUSS-VIEW 5.0.9 program. The optimized molecular structure HOMO-, LUMO- and MEP plots of H_2L4 have been generated at B3LYP/6-31+G(d,p) using the GAUSS-VIEW 5.0.9 program and are shown in Fig. 4. The optimized geometry shows an energy –1879.803 a.u. Theoretically, HOMO–LUMO energy gap is found to be 4.08 eV. Global descriptors such as chemical hardness, chemical softness, chemical potential and the global electrophilicity index were also calculated using HOMO and LUMO energy values and are presented in Table 10. It is also observed that the chemical potential of the compound is negative, showing the stability of the compound. In MEP, red regions mainly extend over the oxygen and sulfur atoms linked to carbon through double bond, predicting them to be susceptible site for electrophilic attack. The blue regions of the molecule mainly spread over the hydrogen atoms. This indicates that these sites can be involved in nucleophilic processes.

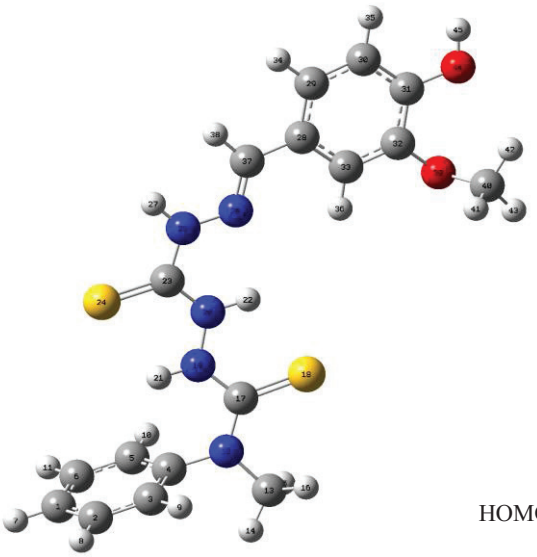

Optimized molecule

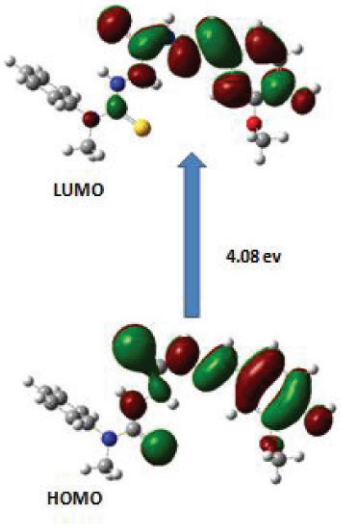

HOMO-LUMO orbitals, corresponding energy gap

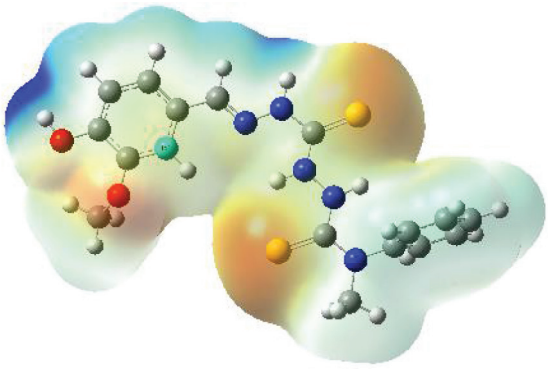

MEP surface

Fig. 4. The optimized molecular structure, HOMO-, LUMO- and MEP plots of H_2L4.

Table 10. Calculation of global descriptors

Global Descriptive Parameters			
Homo	–5.5453	Softness ζ	0.4899
Lumo	–1.4629	Chemical potential μ	–3.5041
Vertical ionization energy I	5.5453	Electronegativity	3.5041
Vertical electron affinity A	1.4629	Global electrophilic index ω	3.0077
Hardness η	2.0411		

4.4.2. NBO analysis

Several donor–acceptor interactions have been observed among the strongly occupied NBOs of the compound (Table 11). The interactions among πC(1)–C(6) → π*C(2)–C(3)/π*C(4)–C(5), πC(2)–C(3) → π*C(1)–C(6)/π*C(4)–C(5) and πC(4)–C(5) → π*C(2)–C(3) are responsible for the extended conjugation of benzene ring and stabilize the molecule with a maximum energy of ~21.07 kcal/mol. The other interactions such as πC(28)–C(29) → π*N(26)–C(37)/π*C(30)–C(31)/π*C(32)–C(33), πC(30)–C(31) → π*C(28)–C(29) and πC(32)–C(33) → π*C(28)–C(29)/π*C(30)–C(31) are responsible for the extended conjugation of 3-hydroxy-4-methoxybenzene ring and stabilize the molecule with a maximum energy ~21.85 kcal/mol. Further, LP(2) O(44) conjugates with anti-bonding, π*C(30)–C(31) with a stabilization energy of 29.14 kcal/mol. The movement of π-electron cloud from donor to acceptor makes the molecule more polarized and it must be responsible for its NLO properties.

Table 11. Major donor–acceptor interactions of the compound and their second-order perturbation energies (kcal/mol)

Donor NBO (*i*)	Acceptor NBO (*j*)	$E^{(2)}$ kcal/mol	$E(j)–E(i)$ a.u.	$F(i,j)$ a.u.
πC(1)–C(6)	π*C(2)–C(3)	20.42	0.28	0.068
πC(1)–C(6)	π*C(4)–C(5)	22.06	0.27	0.069
πC(2)–C(3)	π*C(1)–C(6)	19.98	0.28	0.068
πC(2)–C(3)	π*C(4)–C(5)	21.07	0.27	0.068
πC(4)–C(5)	π*C(2)–C(3)	20.04	0.29	0.068
πC(4)–C(5)	π*C(1)–C(6)	18.7	0.29	0.066
πC(28)–C(29)	π*N26–C(37)	21.85	0.26	0.069
πC(28)–C(29)	π*C(30)–C(31)	18.52	0.27	0.064
πC(28)–C(29)	π*C(32)–C(33)	19.67	0.29	0.068
πC(30)–C(31)	π*C(28)–C(29)	20.89	0.3	0.072
πC(32)–C(33)	π*C(28)–C(29)	17.62	0.29	0.065
πC(32)–C(33)	π*C(30)–C(31)	21.19	0.28	0.07
LP(2) O(44)	π*C(30)–C(31)	29.14	0.35	0.096

4.4.3. Polarizability and hyperpolarizability

The calculated dipole moment (μ), polarizability (α) and the mean first-order hyperpolarizability (β_{total}) for the compound, H2L4 are 2.8586 D, 21.4993Å^3 and 2.866 cm^5/esu, respectively, and are summarized in Table 12. Theoretically, the linear polarizability of the compound is seven times higher than that of urea. It is also found that the compound shows 7.7 times higher value of first-order hyperpolarizability and two times the dipole moment than urea. The largest β_{xxx} value indicates charge delocalization along the bond axis and the involvement of σ orbitals in ICT process.

Table 12. Calculated electric dipole moment, polarizability and first-order hyperpolarizability of the compound

Polarizability	Hyperpolarizability
$\alpha_{XX} = 110.6858$	$\beta_{XXX} = 310.0444$
$\alpha_{XY} = 8.4827$	$\beta_{XYY} = 17.9493$
$\alpha_{YY} = 163.6227$	$\beta_{XZZ} = -12.6565$
$\alpha_{XZ} = 2.5520$	$\beta_{YYY} = -52.8289$
$\alpha_{ZZ} = 160.9015$	$\beta_{XXY} = -7.4362$
$\alpha_{YZ} = -10.5813$	$\beta_{YZZ} = -7.5303$
$\alpha_{total} = 21.4993 Å^3$	$\beta_{ZZZ} = -4.6331$
$\Delta\alpha = 56.89435$	$\beta_{XXZ} = -55.5444$
$\mu = 2.856$ Debye	$\beta_{YYZ} = -17.3907$
	$\beta_{total} = 2.866 \times 10^{-30}$ cm^5/esu

4.5. 2-{2-[(3,4-Dimethoxyphenyl)methylidene]hydrazinecarbonothioyl}-N-methyl-N-phenylhydrazine-1-carbothioamide (H_2L5)

4.5.1. Optimized structure, MEP and HOMO–LUMO analysis of H_2L5

The geometry of H_2L5 has been optimized using X-ray diffraction data as initial point at B3LYP level of theory with 6-31+G(d,p) basis sets. The optimized geometry shows an energy –1919.1088 a.u. The optimized molecular structure, HOMO-, LUMO- and MEP plots of H_2L5 have been generated at B3LYP/6-31+G(d,p) using the GAUSS-VIEW 5.0.9 program and are shown in Fig. 5. Theoretically, HOMO–LUMO energy gap is found to be 3.90 eV. By using HOMO and LUMO energy values, global descriptors such as chemical hardness, chemical softness, chemical potential and the global electrophilicity index were also calculated and are presented in Table 13. It is also observed that the chemical potential of the compound is negative showing the stability of the compound. In MEP, red regions mainly extend over the oxygen and sulphur atoms predicting them as susceptible sites for electrophilic attack. The blue regions of the molecule mainly spread over the hydrogen atoms. This indicates that these sites can involve in nucleophilic processes.

4.5.2. NBO analysis

Several donor–acceptor interactions have been observed among the strongly occupied NBOs of the compound (Table 14). The interactions πC(13)–C(15) → π*C(14)–C(18) and πC(13)–C(15) → π*C(22)–C(27) are responsible for the extended conjugation of benzene ring and stabilize the molecule with a maximum energy ~18.13 kcal/mol. LP(1) N(5) conjugates with π*N(4)–C(20) leading to a stabilization energy of 28.01 kcal/mol. The electron donation from LP(2) O(7) to anti-bonding π*C(22)–C(27) stabilizes the molecule with an energy of 31.87 kcal/mol. LP(2) S(1) conjugates with σ*N(8)–H(9), σ*N(10)–C(26),

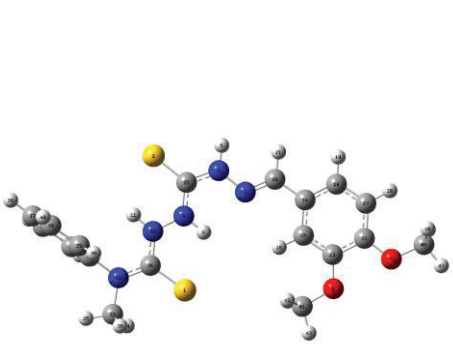

Optimized molecule

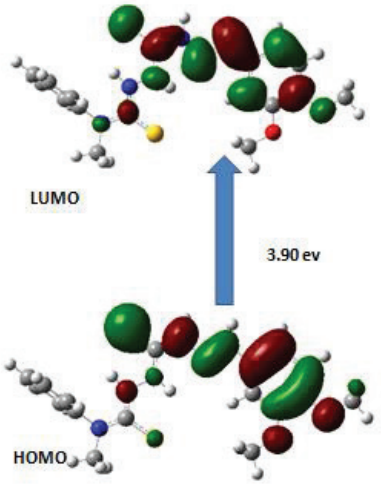

HOMO-LUMO orbitals, corresponding energy gap

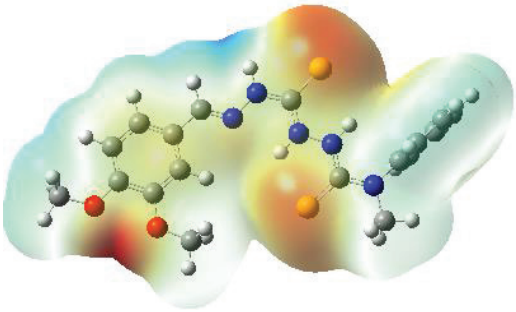

MEP surface

Fig. 5. The optimized molecular structure, HOMO-, LUMO- and MEP plots of H_2L5.

Table 13. Calculation of global descriptors

Global Descriptive Parameters			
Homo	–5.6263	Softness ζ	0.5125
Lumo	–1.7236	Chemical potential μ	–3.6749
Vertical ionization energy I	–5.6263	Electronegativity	3.6749
Vertical electron affinity A	1.7236	Global electrophilic index ω	3.4605
Hardness η	1.9513		

σ*N(12)–C(26) and σ*C(33)–H(35) with stabilization energies 7.5, 9.14, 11.32 and 1.01 kcal/mol, respectively. The movement of π-electron cloud from donor to acceptor makes the molecule more polarized and it must be responsible for the NLO properties of the molecule.

Table 14. Major donor–acceptor interactions of the compound and their second-order perturbation energies (kcal/mol)

Donor NBO (*i*)	Acceptor NBO (*j*)	$E^{(2)}$ kcal/mol	$E(j)-E(i)$ a.u.	$F(i,j)$ a.u.
πC(13)–C(15)	π*C(14)–C(18)	18.13	0.29	0.067
πC(13)–C(15)	π*C(22)–C(27)	17.41	0.28	0.064
πC(14)–C(18)	π*C(13)–C(15)	17.5	0.28	0.063
πC(14)–C(18)	π*C(22)–C(27)	17.96	0.27	0.063
πC(14)–C(18)	π*N(4)–C(20)	22.28	0.25	0.069
πC(17)–C (23)	π*C(29)–C(39)	19.85	0.29	0.068
πC(17)–C(23)	π*C(31)–C(37)	18.33	0.29	0.065
πC(22)–C(27)	π*C(13)–C(15)	16.03	0.29	0.062
πC(22)–C(27)	π*C(14)–C(18)	19.37	0.3	0.069
LP(1) N(5)	π*N(4)–C(20)	28.01	0.28	0.081
LP(2) O(7)	π*C(22)–C(27)	31.87	0.34	0.097
LP(2) S(1)	π*(1)–N(8)–H(9)	7.5	0.6	0.061
LP(2) S(1)	π*(1)–N(10)–C(26)	9.14	0.65	0.07
LP(2) S(1)	π*(1)–N(12)–C(26)	11.32	0.64	0.078
LP(2) S(1)	π*(1)–C(33)–H(35)	1.01	0.64	0.024

4.5.3. Polarizability and hyperpolarizability

The calculated dipole moment (μ), polarizability (α) and the mean first hyperpolarizability (β_{total}) for the compound H_2L5 are 3.2934 Debye, 23.0806 Å^3, 1.489 cm^5/esu, respectively, and are also summarized in Table 15. Theoretically, the linear polarizability of the compound is eight times higher than that of urea. It is also found that the compound shows four times higher value of first-order hyperpolarizability (β). The largest β_{xxx} value indicates charge delocalization along the bond axis and the involvement of σ orbitals in ICT process.[31] Higher the dipole moment, stronger is the intermolecular interaction. The small

Table 15. Calculated electric dipole moment, polarizability and first-order hyperpolarizability of the compound

Polarizability	Hyperpolarizability
$\alpha_{XX} = 120.9182$	$\beta_{XXX} = 130.4061$
$\alpha_{XY} = 25.0038$	$\beta_{XYY} = 53.5658$
$\alpha_{YY} = 173.577$	$\beta_{XZZ} = 17.5237$
$\alpha_{XZ} = 0.8259$	$\beta_{YYY} = -38.8044$
$\alpha_{ZZ} = 172.7232$	$\beta_{XXY} = 32.8514$
$\alpha_{YZ} = 2.5559$	$\beta_{YZZ} = -13.1573$
$\alpha_{total} = 23.0806$	$\beta_{ZZZ} = -8.8381$
$\Delta\alpha = 68.01421$ Å^3	$\beta_{XXZ} = 43.4677$
$\mu = 3.2934$ Debye	$\beta_{YYZ} = 5.942$
	$\beta_{total} = 1.489 \times 10^{-30}$ cm^5/esu

frontier orbital energy gap and high dipole moment of the compound may increase its NLO activity.

5. Conclusions

Geometries of all the compounds were optimized using DFT employing 6-31+G(d,p) basis set. Global reactivity descriptor parameters were calculated and analyzed through HOMO–LUMO analysis. The MEP map shows that the negative potential sites are on the electronegative atoms as well as the positive potential sites are around the hydrogen atoms. NBO analysis together with HOMO–LUMO energy gap and MEP map of the molecule elucidates ICT in the molecules. It is responsible for the non-linearity and hence the stability of the molecules. The compounds showed higher value of linear polarizability and the dipole moment than urea. The theoretical calculation of hyperpolarizability (β) component is very useful as it clearly indicates the direction of charge delocalization. The first-order hyperpolarizabilities (β_{total}) of all the compounds are higher than urea. Based on the total static dipole moment (μ), the linear polarizability (α), the anisotropy of polarizability ($\Delta\alpha$) and the mean first-order hyperpolarizability (β_{total}), 2-{2-[(4-hydroxy-3-methoxyphenyl) methylidene]hydrazinecarbonothioyl}-N-methyl-N-phenylhydrazine-1-carbothioamide (H_2L4) is most suitable for further studies as NLO material.

References

1. R. G. Parr, W. Yang, Density-Functional Theory of Atoms and Molecules, Oxford University Press, Oxford, 1989.
2. W. Kohn, L. J. Sham, Phys. Rev., 140 (1965), A1133.
3. P. Hohenberg, W. Kohn, Phys. Rev., 136 (1964) B846.
4. M. J. Frisch, G. W. Trucks, H. B. Schlegel, G. E. Scuseria, M. A. Robb, J. R. Cheeseman, G. Scalmani, V. Barone, B. Mennucci, G. A. Petersson, H. Nakatsuji, M. Caricato, X. Li, H. P. Hratchian, A. F. Izmaylov, J. Bloino, G. Zheng, J. L. Sonnenberg, M. Hada, M. Ehara, K. Toyota, R. Fukuda, J. Hasegawa, M. Ishida, T. Nakajima, Y. Honda, O. Kitao, H. Nakai, T. Vreven, J.A. Montgomery, Jr., J. E. Peralta, F. Ogliaro, M. Bearpark, J. J. Heyd, E. Brothers, K. N. Kudin, V. N. Staroverov, R. Kobayashi, J. Normand, K. Raghavachari, A. Rendell, J. C. Burant, S. S. Iyengar, J. Tomasi, M. Cossi, N. Rega, J. M. Millam, M. Klene, J. E. Knox, J. B. Cross, V. Bakken, C. Adamo, J. Jaramillo, R. Gomperts, R. E. Stratmann, O. Yazyev, A. J. Austin, R. Cammi, C. Pomelli, J. W. Ochterski, R. L. Martin, K. Morokuma, V. G. Zakrzewski, G. A. Voth, P. Salvador, J. J. Dannenberg, S. Dapprich, A. D. Daniels, Ö. Farkas, J. B. Foresman, J. V. Ortiz, J. Cioslowski, D. J. Fox, Gaussian 09, Revision A.1, Gaussian, Inc., Wallingford, Connecticut, 2009.
5. A. Frisch, H. P. Hratchian, R. D. Dennington, II, T. A. Keith, J. Millam, A. B. Nielsen, A. J. Holder, J. Hiscocks, GaussView Version 5.0.8, Gaussian, Inc., Wallingford, Connecticut, 2009.
6. N. Choudhary, S. Bee, A. Gupta, P. Tandon, Comput. Theor. Chem., 1016 (2013) 8.
7. E. Kavitha, N. Sundaraganesan, S. Sebastian, J. Pure Ap. Phy., 48 (2010) 20.
8. A. A. R. Despaigne, J. G. Da Silva, A. C. M. Do Carmo, F. Sives, O. E. Piro, E. E. Castellano, H. Beraldo, Polyhedron, 28 (2009) 3797.
9. Orbitals IFF. Organic Chemical Reactions, John Wiley and Sons, New York City, New York, 1976.
10. A. Vektariene, G. Vektaris, J. Svoboda, Arkivoc, 7 (2009) 311.
11. R. G. Pearson, Proc. Natl. Acad. Sci., 83 (1986) 8440.
12. P. K. Chattaraj, B. Maiti, J. Am. Chem. Soc., 125 (2003) 2705.
13. R. G. Parr, L. Szentpaly, S. Liu, J. Am. Chem Soc., 121 (1999) 1922.
14. T. Koopmans, Physica., 1 (1933) 104.
15. S. Liu, J. Chem. Sci., 117 (2005) 477.
16. E. Scrocco, J. Tomasi, in: P. Lowdin (Ed.), Advances in Quantum Chemistry, Academic Press, New York City, New York, 1978.
17. E. Scrocco, J. Tomasi, Topics in Current Chemistry, Vol. 42, Springer-Verlag, Berlin, 1973.
18. A. E. Reed, R. B. Weinhold, F. Weinhold, J. Chem. Phys., 83 (1985) 735.
19. A. Reed, L. A. Curtiss, F. Weinhold, Chem. Rev., 88 (1988) 899.
20. P. Günter, Nonlinear Optical Effects and Materials, Springer Series in Optical Sciences: Springer Verlag, 2000.
21. Y. P. Tian, W. T. Yu, C. Y. Zhao, M. H. Jiang, Z. G. Cai, H. K. Fun, Polyhedron, 21 (2002) 1217.
22. R. Zhang, B. Du, G. Sun, Y. Sun, Spectrochim. Acta A Mol. Biomol. Spectrosc., 75 (2010) 1115.
23. C. Albayrak, M. Odabas¸ Oglu, A. Ozek, O. Büyükgüng, Spectrochim. Acta A, 85 (2012) 85.
24. M. Adant, L. Dupuis, L. Bredas, Int. J. Quantum Chem., 56 (2004) 497.
25. H. Tanak, Y. Köysal, Ş. Işık, H. Yaman, V. Ahsen, Bull. Korean Chem. Soc., 32 (2011) 2673.
26. J. Prashanth, G. Ramesh, J. L. Naik, J. K. Ojha, B. V. Reddy, G. Ramana Rao, Opt. Photon. J., 5 (2015) 91.

27. A. D. Becke, J. Chem. Phys., 98 (1993) 5648.
28. C. Lee, W. Yang, R. G. Parr, Phys. Rev. B., 37 (1988) 785.
29. Y. S. Mary, K. Raju, C. Y. Panicker, A. A. Al-Saadi, T. Thiemann, C. Van Alsenoy, Spectrochim. Acta A Mol. Biomol. Spectrosc., 128 (2014) 638.
30. V. Deepha, R. Praveena, K. Sadasivam, J. Mol. Struct., 1082 (2015) 131.
31. H. N. Mishra, PhD thesis, University of Lucknow, 2013.

CHAPTER IX

IN-SILICO SCREENING OF LIGANDS FOR THEIR ANTICANCER ACTIVITY USING MOLECULAR DOCKING STUDIES

1. Introduction

Cancer therapies target cell cycle-based mechanism which imitates the body's natural process in order to prevent the growth of cancer cells. This approach can limit damages to normal cells and the associated side effects caused by usual chemotherapeutic agents. It has been unambiguously proved that the genome contains information in two forms: genetic and epigenetic. The genetic information provides the scheme of assembling of all the proteins necessary to create a living organism, while the epigenetic information directs when, where, and how the genetic information must be used. Epigenetics has just moved to the forefront of studies describing various processes such as transcriptional regulation, chromatin structure, genome integrity and tumorigenesis.[1]

1.1 Role of histone deacetylases in human cancer

Inhibition of histone deacetylases (HDAC) enzymes is emerging as an innovative and important approach for the treatment of cancer. HDAC inhibitor interacts with chromosomes in the cancer cell and stops their growth.

Acetylation levels are the outcome of the activities of histone acetyltransferase (HAT) and HDAC. They have a critical role in the regulation of gene expression. HATs induce histone acetylation. It is coupled with gene transcription. HDAC induces histone hypoacetylation. It is associated with gene silencing. Altered appearance and mutations of genes that encode HDACs have been correlated to tumour growth. These changes induce the abnormal transcription of genes which regulates the important cellular functions such as cell proliferation, cell-cycle regulation and apoptosis.[2] HDACs are expressed in colon, breast,[3] lung cancers, hepato-cellular carcinoma, gastric cancer,[4] pancreatic tumour tissue, metastatic melanoma, acute myeloid leukemia (AML), acute lymphocytic leukemia (ALL) as well as in childhood tumors of the nervous system, such as neuroblastoma.[5–8] As a result, HDACs have become one of the most potential therapeutic targets for cancer treatment.

Four families of human HDACs have been described and categorized into four classes. Class I includes HDAC 1–3 and 8; class II includes HDAC 4–7, 9 and 10; class III includes sirtuins 1–7; and class IV includes HDAC 11. The HDACs belonging to classes I, II and IV have Zn^{2+} as a cofactor and class III enzymes are characterised for being NADP-dependent.[9,10]

1.2. Role of histone deacetylase 8 in oncogenesis

Histone deacetylase 8 (HDAC8) is a class I HDAC. It is concerned as a therapeutic target in various diseases, including cancer, X-linked intellectual disability and parasitic infections.[11,12] This enzyme also deacetylates non-histone proteins. This enzyme is a major 'epigenetic player' and it is linked to uncontrolled expression or interaction with transcription factors important for tumourigenesis. In the parasite *Schistosoma mansoni* and in viral infections, HDAC8 is a novel target to suppress infection. The current challenge is to develop potent selective inhibitors that would solely target HDAC8 with less adverse effects.

1.3. Role of DNA methyltransferases in human cancer

Contemporary works have revealed how DNA methylation and chromatin structure are correlated at the molecular level and how methylation plays a direct role in tumourigenesis and genetic disease. A great deal of information is available concerning the cellular methylation mechanism.

DNA methyltransferases are the main components of larger complexes which are actively involved in transcriptional control and chromatin structure modulation. These findings enhance our perceptive about the roles of DNA methylation in novel therapies to prevent or repair these defects. Variation in DNA methylation process can cause changes in gene transcription patterns and can also promote mutational events.[13,14] Abnormal DNA methylation patterns also play an essential role in the development of cancer. Cancer cells show an overall decrease in the level of genomic cytosine methylation, mainly in centromeric satellite and other repeated sequences.[15] This genome hypomethylation is believed to be linked to genome instability resulting in a variety of chromosomal defects and tumorigenesis.[16] In addition to the loss of methylation at satellite sequences, cancer cells acquire methylation in normally un-methylated promoter regions. In many cancer types, one can see tumour suppressor genes epigenetically silenced by hypermethylation.[17]

Azacytidine (Vidaza; Celgene) and Decitabine (5 aza 2′ deoxycytidine) (Dacogen; SuperGen) are the two DNMT inhibitors (azanucleosides) currently approved by the US Food and Drug Administration (FDA).[18] These two types of drugs are the first molecules that have been characterised as the archetypal DNMT inhibitors and the only epidrugs that have been approved for the treatment of patients with AML and myelodysplastic syndrome (MDS).[8] Azacytidine has also been approved by the FDA and the European Medicines Agency (EMA) for the use against chronic myelomonocytic leukemia (CMML).[19] Even though several new inhibitors of DNMT have been identified, none of them can substitute azacytidine and decitabine.

1.4. Role of ribonucleotide reductase subunit, R2 in human cancer

Ribonucleotide reductase (RR), a distinct enzyme which is responsible for reducing ribonucleotides to deoxyribonucleotides, the building blocks required for DNA replication and repair. Dysregulated RR activity is allied with genomic instability, malignant transformation and cancer development. The use of RR inhibitors, either as a single agent or combined with other therapies, has proven to be a promising approach for treating solid tumors and hematological malignancies.

RR subunit, R2 regulates catalytic action of the enzyme to provide DNA synthesis *via* reduction. It has been constantly investigated as anticancer drug target for design and discovery of its inhibitors. RR plays an important role in determining cell fate and increased expression. Activity of human RR has been associated with many types of cancer. Failure to control the levels and balance of dNTPs can lead to mutagenesis, carcinogenesis and even cell death. After the occurrence of transformation, cancer cells require increased RR activity to meet the demand for dNTPs that are needed to support their rapid proliferation. However, accumulating evidences also indicate that RR subunits play biological roles in promoting cancer development that are distinct from their role in forming the active RR holoenzyme to supply dNTPs.

RRM2 has been proposed as an oncoprotein. It not only can cooperate with a variety of oncogenes to promote cellular transformation but also can enhance the invasive potential of cancer cells. Discovering novel RR inhibitors is a challenge for improving cancer therapies in the future. Investigation of RR expression and action in clinical samples will provide a logical platform for modified cancer therapy using RR inhibitors.

1.5. Molecular docking studies

Molecular docking is a well-known computational technique which predicts the interaction energy between two molecules. Docking is frequently used to predict the binding affinity and to identify the bound conformation of ligands with the protein targets. It can provide information regarding the intermolecular interactions between the ligands and the targets.[20] This in turn can be used for the development of novel drugs.[21] Considerable efforts have been made to improve the methods used to predict docking, due to their significance in the biological and pharmaceutical fields.

This chapter portrays the molecular docking studies of the ligands synthesized by us with different enzyme targets.

2. Materials and methods

Molecular docking studies were performed using the Glide program. Glide means Grid-Based Ligand Docking With Energetics. The Maestro (version 10.4) was used as graphical user interface. It was used to set up and execute the docking protocol and also for analysis of the docking results. The three-dimensional structures of all the proteins were retrieved from the Protein Data Bank (PDB). The ligands under study were docked into the binding sites of the proteins. PyMOL was used for the three-dimensional visualization of proteins to superimpose the structures and for the characterisation of ligand–protein interactions. PyMOL supports different macromolecular structural representations such as ribbon structure, wired structure, ball and sick model, surface model, cartoon model and so on. The selection of the best pose was done based on the interaction energy between the ligand and the protein. The results were analyzed by a statistical scoring function which converts interacting energy into numerical values called as the glide score.

Docking methodology consists of four basic steps:

1. Preparation of protein
2. Ligand preparation
3. Receptor grid generation
4. Ligand docking

2.1. Preparation of protein

Protein preparation was done by protein preparation wizard. The PDB structure file consists of different metal ions, hetero atoms, cofactors, water molecules, co-crystallized ligands and so on. Therefore, the PDB structure files as such are not suitable for molecular modelling calculations. Schrodinger contains all the tools to prepare appropriate protein for its calculations. The appropriate protein structure is refined through optimization and minimization[22] during protein preparation. Minimization process is coordinated by a defined RMSD of 0.30 Å and force fields OPLS 2005.[23] Protein preparation wizard prepares accurate protein structure for docking. The different procedures used for protein preparation include pre-processing, review, modification, refinement and minimization.

2.2. Ligand preparation

The ligand preparation was done by ligand preparation wizard, which is also known as LigPrep. The ligands were prepared using LigPrep with parameter force field, OPLS 2005 in Schrodinger. This is used for the conversion of 2D molecules to 3D structures. The steps involved in the process are convert to the structure format (sd format), select the structures, add hydrogen atoms, remove unwanted molecules, neutralize charged groups, generate ionization states, generate tautomers, filter the structures, generate alternative chiralities, generate low-energy ring conformations, remove problematic structures, optimize the geometries and finally convert the output file. Many of these steps are optional and are controlled by selecting options in the LigPrep panel or by specifying command-line options. Prepared ligands are saved with maegz extension or in maestro format and all the ligands are available in the project table. Now, the ligands are ready for the docking process. We can export the project table as csv format and keep the details of ligands.

2.3. Receptor grid generation

The prepared protein was loaded into maestro environment and the active site was defined using Glide grid generation wizard. For grid generation, we want to specify the active site residue. Certain proteins may have metal ions or may possess one or more ligands. These already existing ligands or metal ions can be selected as active site residues. If no ligand or metal ion is present, then active site amino acids are used for grid generation. Grid centre was defined for the active site and box sizes were set to 15 Å.

Receptor grid should be generated by using Receptor Grid Generation feature of maestro. The van der Waals radius scaling involves a scaling factor as 1.0 and partial charge cut off as 0.25. The shapes and properties of receptor molecule were represented on a grid.

The prepared protein structure was used for receptor grid generation. It determines the position and size of the active site. Receptor grid generation was selected from the application menu and it includes three fields such as receptor, site and constraints. Receptor section defines the respective target molecule and picks the ligand molecule. Several constraints can be applied in grid generation, which are positional constraint, H-bond constraint, metal constraint and hydrophobic constraint. The generated grid was used for docking.

2.4. Ligand docking

This was carried out using Glide dock. Ligands were kept flexible, while the protein was rigid and docking started with extra precision mode (XP mode). The docking calculation generated a few poses for each ligand. The selection of the best pose was done based on the interaction energy between the ligand and the protein. The least negative XP g-score (negative value) indicates the best binding score for the ligand with protein.

3. Results and discussion

Crystal structures of HDAC8 (PDB ID: 1T69), DNA methyltransferase (PDB ID: 2QRV) and RR M2 subunit (PDB ID: 2UW2) (Fig. 1) were downloaded from PDB.

The following novel ligands synthesized by us were selected for performing molecular docking studies:

1. N-Methyl-2-((3-methyl-5-oxo-1-phenyl-4,5-dihydro-1H-pyrazol-4-yl)(phenyl) methylene)-N-phenylhydrazinecarbothioamide (H_2L1)
2. 2-[2-(Diphenylmethylidene)hydrazine]-N-methyl-N-phenylhydrazine-1-carbothioamide (H_2L2)
3. 3-Formylchromone N(4)-methyl-N(4)-phenylthiosemicarbazone (HL3)
4. 2-{2-[(4-Hydroxy-3-methoxyphenyl)methylidene]hydrazinecarbonothioyl}-N-methyl-N-phenylhydrazine-1-carbothioamide (H_2L4)
5. 2-{2-[(3,4-Dimethoxyphenyl)methylidene]hydrazinecarbonothioyl}-N-methyl-N-phenylhydrazine-1-carbothioamide (H_2L5)

The compounds were characterised by spectroscopic analysis (electronic, FT-IR, FT-Raman and ^{1}H NMR). The compounds **1** and **5** were further characterised by single-crystal XRD and others by powder XRD. The details of identification of selected compounds are presented in the earlier chapters of the thesis (Chapters III–VII). For interpreting the docking results, mainly four parameters were considered: Glide score, Glide energy, H-bonds and non-bonded interactions (van der Waals and electrostatic). Based on these, the binding affinity of the ligand towards the receptor has been discussed. The result demonstrates that all the compounds could effectively be docked into the same binding site of each protein. Details of binding affinity of each ligand towards different receptors are discussed in detail below.

1. **N-Methyl-2-((3-methyl-5-oxo-1-phenyl-4,5-dihydro-1H-pyrazol-4-yl)(phenyl) methylene)-N-phenylhydrazinecarbothioamide (H_2L1)**

   The amino acid residues in the active site of RR M2 subunit are Glu 232, Gly 233, Le 234, Phe 236, Ser 237, Val 327, Arg 330, Leu 331, Glu 334, Asp 271, Glu 260, Cys 270, Leu 268, Gly 267, Glu 266, Arg 264, Phe 244, Met 350 and Ser 263.

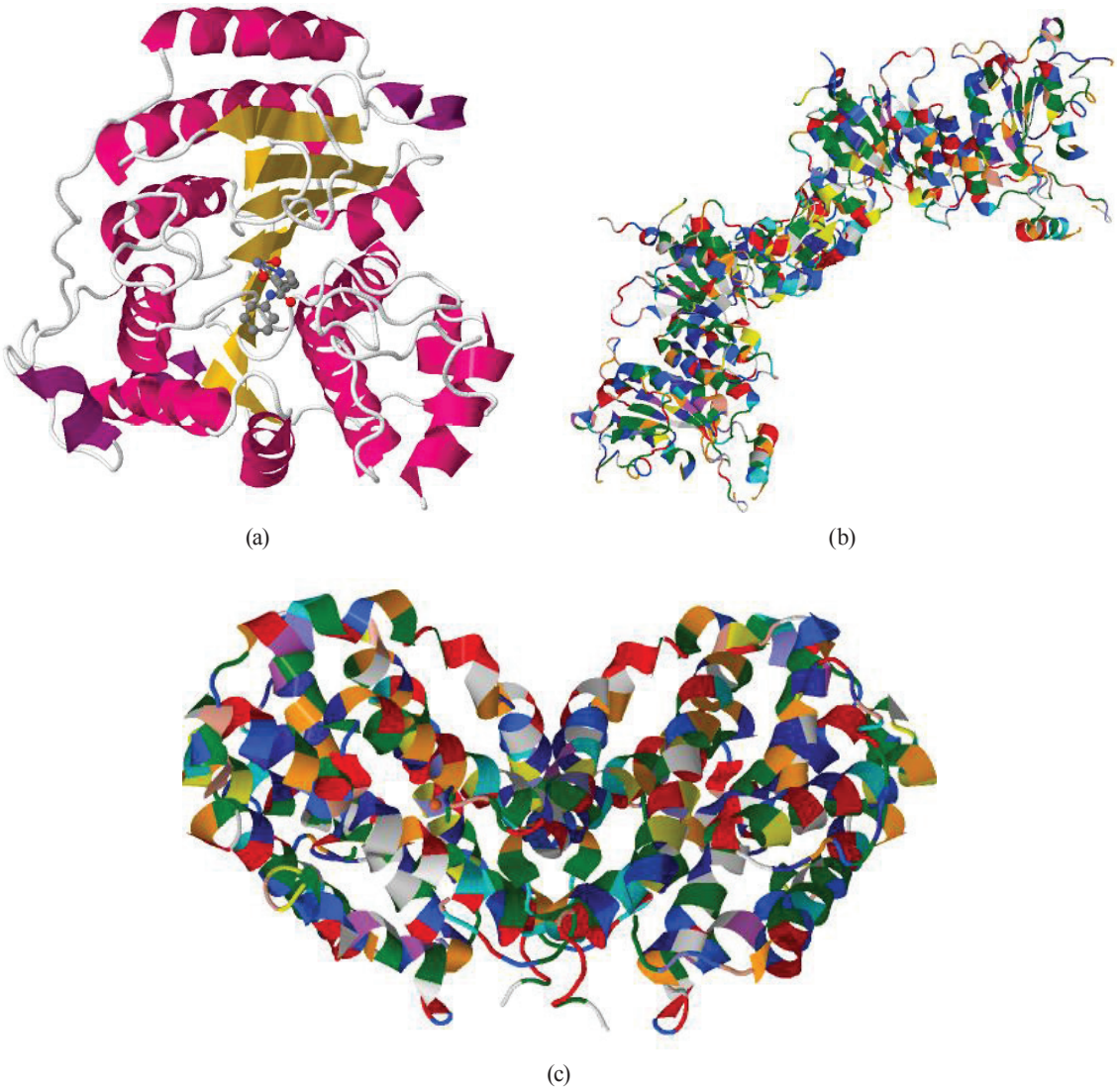

Fig. 1. Crystal structures of (a) HDAC8 (PDB ID: 1T69) with SAHA, (b) DNA methyltransferase (PDB ID: 2QRV) and (c) RR R2 subunit (PDB ID: 2UW2).

The compound was docked deeply into the active site region making interactions with the residues Asp 271 and Ser 263. The compound formed three hydrogen bonded contacts through Ser 263 and Asp 271 with the NH functionality and Ser 263 with the SH group. Certain very prominent interactions between the compound and the active site residues Gly 703, Ar 887, Glu 660 and Phe 636 of DNA methyltransferases were observed. The other residues that were found in the locality of this docked ligand were Leu 635, Phe 636, Asp 637, Gly 638, Le 639, Ala 640, Thr 641, Gly 642, Glu 752, Trp 889, Ser 888, Arg 887, Ser 665, Cys 662, Gly 660, Ser 659, Gly 703, Ser 704, Pro 705, Cys 706, Cys 662, Val 661, Glu 660, Asp 682, Val 683, Arg 684 and Leu 726. The amino acid residues in the active site of HDAC8 were Arg 37, Le 34, Lys 33, Tyr 306, Gly 305, Gly 304, Gly 303, Asp 178, He 180, Gly 151, Phe 152, Cys 153, Asp 101, Asp 267, Phe 206, Phe 208, His 143, Gly 206, Met 274 and Trp 141. H_2L1 binds in the pockets defined by Asp 101 and Gly 206 of HDAC8. It is found that H_2L1 is able to bind all the selected targets (Fig. 1). The

docking results for the inhibitory compound, H_2L1 are reported in Table 1. Fig. 2 shows the docked pose of the inhibitor, H_2L1 inside the binding pockets of the proteins (a) PDB ID: 2UW2, (b) PDB ID: 2QRV and (c) PDB ID: 1T69.

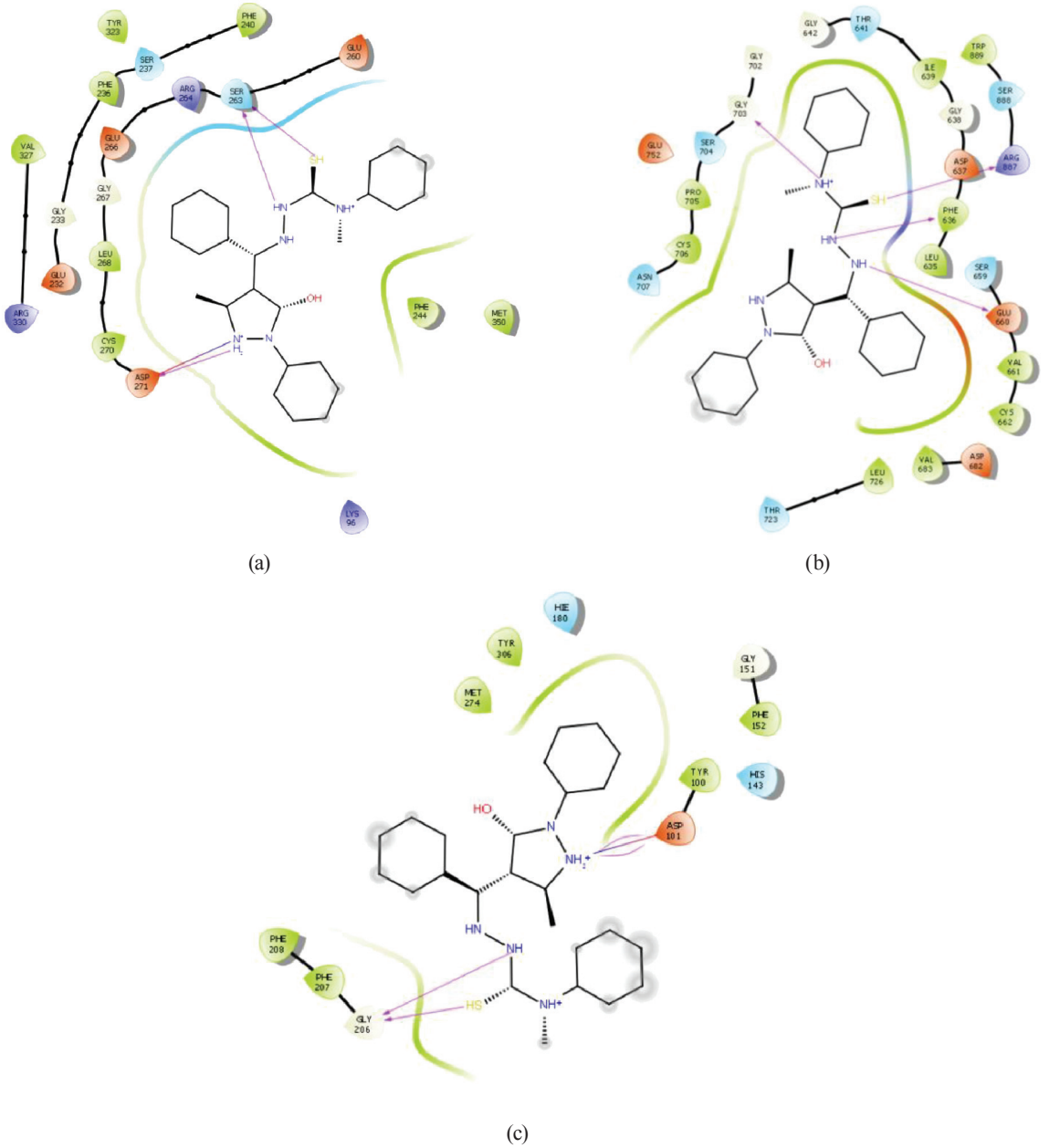

(a) (b)

(c)

Fig. 2. Docked pose of the inhibitor, H_2L1 inside the binding pockets of proteins. (a) PDB ID: 2UW2, (b) PDB ID: 2QRV and (c) PDB ID: 1T69.

Table 1. Glide score and Glide energy of H_2L1

Protein	Glide Score	Glide Energy
Ribonucleoside diphosphate reductase M2 subunit (PDB ID: 2UW2)	−7.047803	−47.1708
DNA methyltransferase (PDB ID: 2QRV)	−4.32107	−18.399939
Histone deacetylase 8 (PDB ID: 1T69	−5.034831	−31.793303

2. **2-[2-(Diphenylmethylidene)hydrazine]-N-methyl-N-phenylhydrazine-1-carbothioamide (H_2L2)**

The compound, H_2L2 binds in the pocket defined by Asp 271 and Ser 263 of RR M2 subunit. It binds in the pocket defined by Val 661 and Glu 663 of DNA methyltransferase. It binds in the pocket defined by Asp 271 of HDAC8. The docking results for H_2L2 are reported in Table 2. Fig. 3 shows the docked pose of the inhibitor, H_2L2 inside the binding pockets of the proteins (a) PDB ID: 2QRV and (b) PDB ID: 1T69.

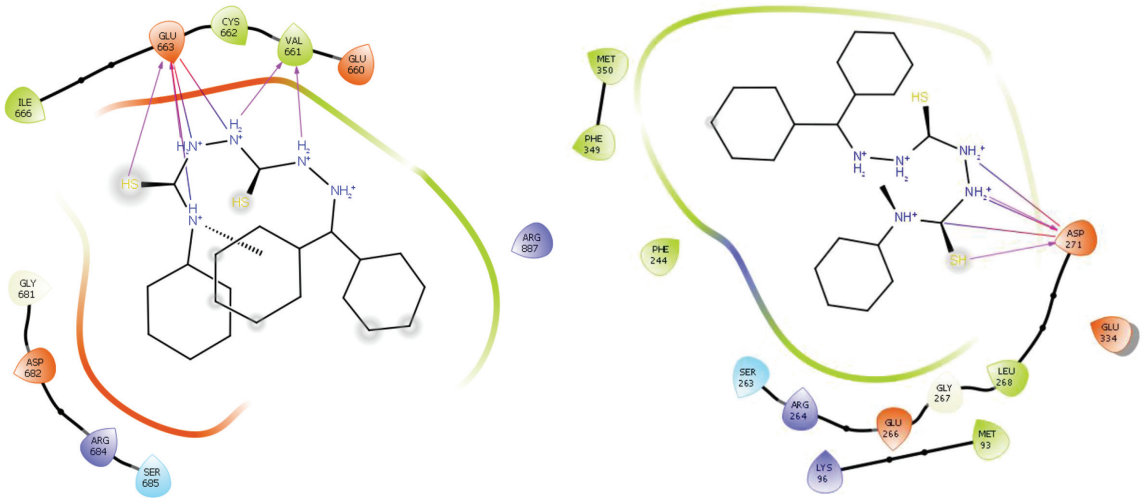

(a) (b)

Fig. 3. Docked pose of the inhibitor, H_2L2 inside the binding pockets of proteins. (a) PDB ID: 2QRV and (b) PDB ID: 1T69.

Table 2. Glide score and Glide energy of H_2L2

Protein	Glide Score	Glide Energy
Ribonucleoside diphosphate reductase M2 subunit (PDB ID: 2UW2)	–5.13638	–47.9122
DNA methyltransferase (PDB ID: 2QRV)	–3.11166	–44.3094
Histone deacetylase 8 (PDB ID: 1T69	–3.03165	–35.7943

3. **3-Formylchromone N(4)-methyl-N(4)-phenylthiosemicarbazone(HL3)**

The compound docked deeply into the active site region of ribonucleoside diphosphate reductase M2 subunit, making three hydrogen bonding interactions with the residues Arg 330, Glu 334, Asp 271 and Ser 263. The compound docked deeply into the active site region of DNA methyltransferase, making interactions with the residues Glu 660, Phe 636, Gly 703, Trp 889 and Ser 263. It docked deeply into the active site region of HDAC8, making hydrogen bonded interactions with the residues His 143, He 180, Asp 178, Asp 101, Gly 151 and Ser 263. The docking results for HL3 are reported in Table 3. Fig. 4 shows the docked pose of the inhibitor HL3 inside the binding pockets of the proteins (a) PDB ID: 2UW2, (b) PDB ID: 2QRV and (c) PDB ID: 1T69.

Table 3. Glide score and Glide energy of HL3

Protein	Glide Score	Glide Energy
Ribonucleoside diphosphate reductase M2 subunit (PDB ID: 2UW2)	−6.438	−43.039
DNA methyltransferase (PDB ID: 2QRV)	−6.222	−45.642
Histone deacetylase 8 (PDB ID: 1T69)	−8.148	−34.238

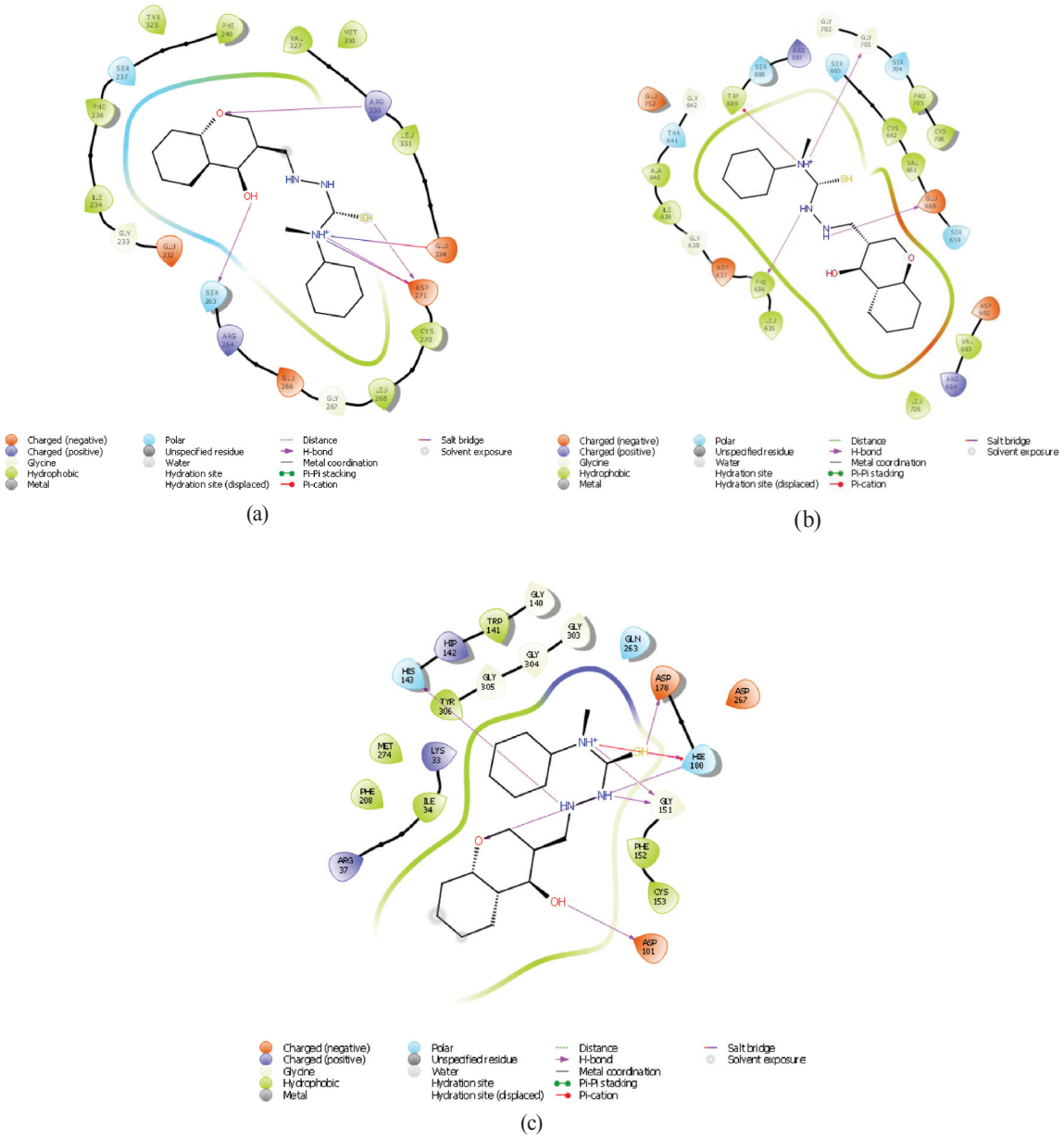

Fig. 4. Docked pose of the inhibitor, HL3 inside the binding pockets of proteins. (a) PDB ID: 2UW2, (b) PDB ID: 2QRV and (c) PDB ID: 1T69.

4. **2-{2-[(4-Hydroxy-3-methoxyphenyl)methylidene]hydrazinecarbonothioyl}-N-methyl- N-phenylhydrazine-1-carbothioamide (H_2L4)**

The compound H_2L4 bound in the pocket defined by Asp 271, Ser 237 and Tyr 323 of RR. H_2L4 stabilized within the active site of DNA methyltransferase through hydrogen bonding interactions with Arg 887, Val 661 and Glu 663 residues. It bound in the pocket defined by Asp 101, Phe 208, Gly 206 of HDAC8. The docking results for the inhibitory compound H_2L4 are reported in Table 4. Fig. 5 shows the docked pose of the inhibitor H_2L4 inside the binding pocket of protein (PDB ID: 2UW2).

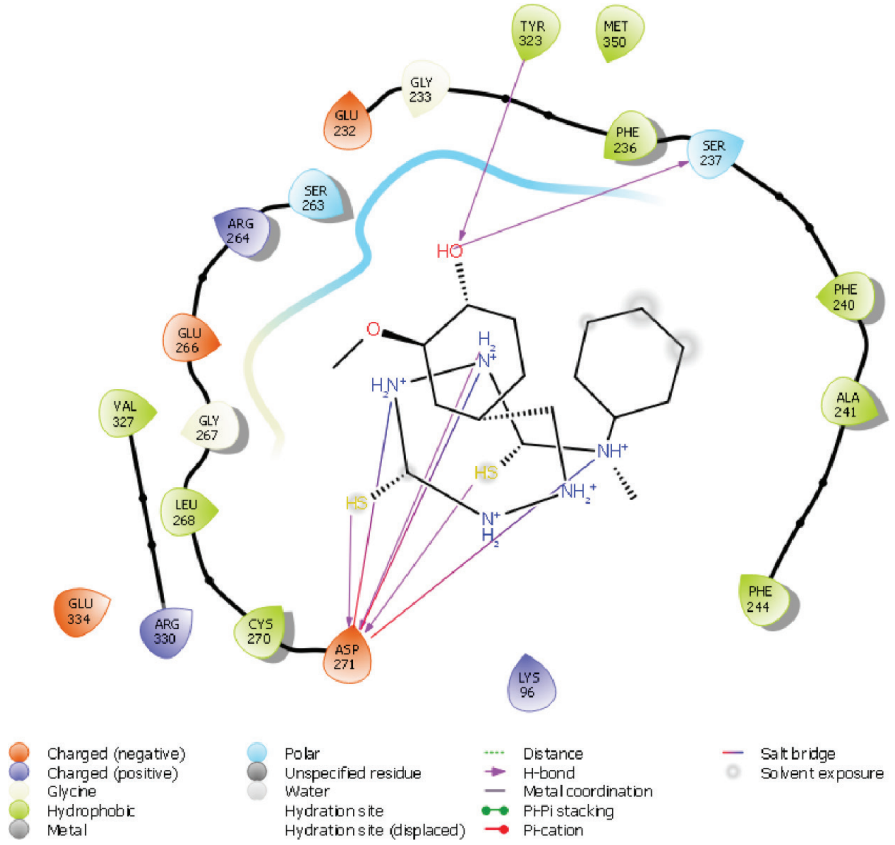

Fig. 5. Docked pose of the inhibitor, H_2L4 inside the binding pocket of protein (PDB ID: 2UW2).

Table 4. Glide score and Glide energy of H_2L4

Protein	Glide Score	Glide Energy
Ribonucleoside diphosphate reductase M2 subunit (PDB ID: 2UW2)	−8.13072	−56.5909
DNA methyltransferase (PDB ID: 2QRV)	−3.99925	−45.9494
Histone deacetylase 8 (PDB ID: 1T69)	−4.18525	−38.1185

5. 2-{2-[(3,4-Dimethoxyphenyl)methylidene]hydrazinecarbonothioyl}-N-methyl-N-phenylhydrazine-1-carbothioamide (H_2L5)

The compound stabilized within the active site of RR through four prominent hydrogen bonding interactions: first between the oxygen atom of methoxy group and Arg330 residue, second and third interactions between NH group and Asp 271, while fourth interactions between NH group and Ser 263 residue. The compound H_2L5 stabilized within the active site of DNA methyltransferase through two prominent hydrogen bonding interactions. The first between the NH group and Asn 707 residue while the second between SH and Asn 707 residue. H_2L5 bound in the pocket defined by Asp 708, Asn 707 of DNA methyltransferase. It bound in the pocket defined by Asp 101, Phe 208 of HDAC8. The docking results for the inhibitory compound H_2L5 are reported in Table 5. Fig. 6 shows the docked poses of the inhibitor, H_2L5 inside the binding pockets of the proteins (a) PDB ID: 2UW2 and (b) PDB ID: 1T69.

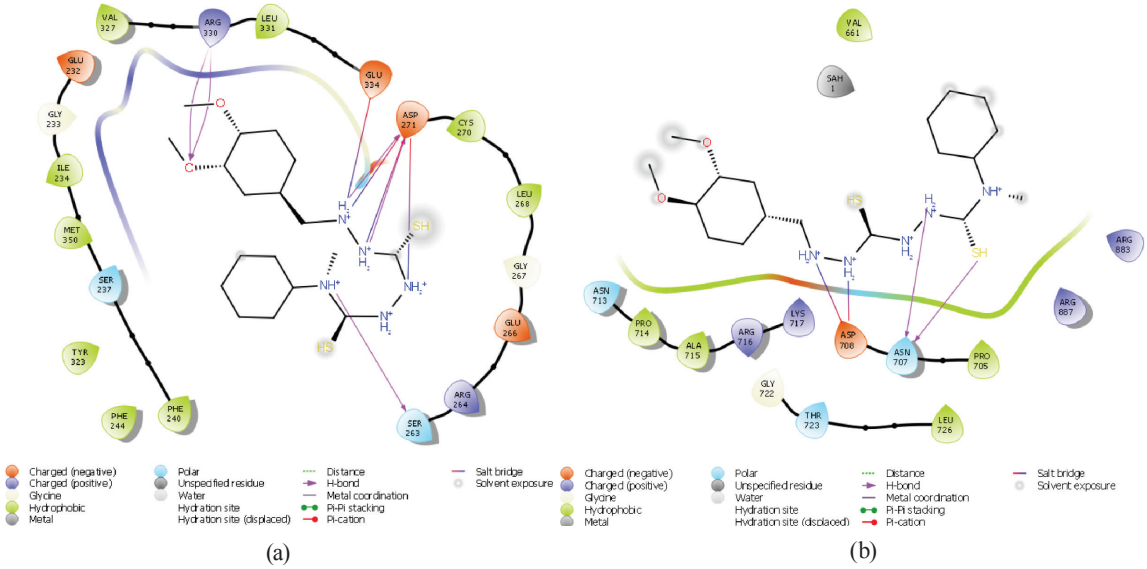

Fig. 6. Docked pose of the inhibitor, H_2L5 inside the binding pockets of proteins. (a) PDB ID: 2UW2 and (b) PDB ID: 1T69.

Table 5. Glide score and glide energy of H_2L5

Protein	Glide Score	Glide Energy
Ribonucleoside diphosphate reductase M2 subunit (PDB ID: 2UW2)	−6.46082	−43.6959
DNA methyltransferase (PDB ID: 2QRV)	−3.99925	−3.11166
Histone deacetylase 8 (PDB ID: 1T69	−3.60968	−36.5944

4. Conclusions

The results of this study can be helpful for the design and development of new compounds having enhanced inhibitory activity against several types of cancer. These compounds will be hopeful candidates for anticancer studies. The molecular docking studies revealed that all these compounds have affinity towards the active site of RR M2 subunit with Glide score ranging from −5.13638 to −8.13072. They can further be explored as selective RR inhibitors. It is also found that the compound 3-formylchromone N(4)-methyl-N(4)-phenylthiosemicarbazone (HL3) has affinity towards all the selected target with good binding score and is a good candidate for anticancer studies. This can further be validated in wet lab studies.

References

1. D. Keith Robertson, Oncogene, 20 (2001) 3139.
2. S. Minucci, P. G. Pelicci, Nat. Rev. Cancer, 6 (2006) 38.
3. Z. Zhang, H. Yamashita, T. Toyama, H. Sugiura, Y. Ando, K. Mita, M. Hamaguchi, Y. Hara, S. Kobayashi, H. Iwase, Breast Cancer Res. Treat., 94 (2005) 11.
4. J. H. Choi, H. J. Kwon, B. I. Yoon, J. H. Kim, S. U. Han, H. J. Joo, D. Y. Kim, Jpn. J. Cancer Res., 92 (2001) 1300.
5. M. Nakagawa, Y. Oda, T. Eguchi, S. Aishima, T. Yao, F. Hosoi, Y. Basaki, M. Ono, M. Kuwano, M. Tanaka, M. Tsuneyoshi, Oncol. Rep., 18(4) (2007) 769.
6. J. Wu, C. Du, Z. Lv, C. Ding, J. Cheng, H. Xie, L. Zhou, Z. S. Dig. Dis. Sci., 58(12) (2013) 3545.
7. S. Song, Y. Wang, P. Xu, G. Zhang, Int. J. Oncol., 47(5) (2015) 1819.
8. J. S. Wilmott, A. J. Colebatch, H. Kakavand, P. Shang, M. S. Carlino, J. F. Thompson, G. V. Long, R. A. Scolyer, P. Hersey, Mod. Pathol., 28(7) (2015) 884.
9. S. Minucci, P. G. Pelicci, Nat. Rev. Cancer, 6 (2006) 38.
10. I. V. Gregoretti, Y. M. Lee, H. V. Goodson, J. Mol. Biol., 338 (2004) 17.
11. S. Balasubramanian, J. Ramos, W. Luo, M. Sirisawad, E. Verner, J. J. Buggy, Leukemia, 22(5) (2008) 1026.
12. M. Marek, S. Kannan, A. -T. Hauser, M. Moraes Mourão, S. Caby, V. Cura, D. A. Stolfa, K. Schmidtkunz, PLoS Pathog., 9(9) (2013) e1003645. doi:10.1371/journal.ppat.1003645
13. A. Bird, Genes Dev., 16 (2002) 6.
14. P. A. Jones, S. B. Baylin, Nat. Rev. Genet., 3 (2002) 415; K. D. Robertson, Nat. Rev. Genet., 6 (2005) 597.
15. M. Ehrlich, Oncogene, 21 (2002) 5400.
16. A. Eden, F. Gaudet, A. Waghmare, R. Jaenisch, Science, 300 (2003) 455.
17. S. Baylin, T. H. Bestor, Cancer Cell, 1 (2002) 299.
18. A. Gnyszka, Z. Jastrzębski, S. Flis, Anticancer Res., 33 (2013) 2989.
19. C. Gros, J. Fahy, L. Halby, I. Dufau, A. Erdmann, J. M. Gregoire, F. Ausseil, S. Vispé, P. B. Arimondo, Biochimie, 94 (2012) 2280.
20. K. C. Chou, Curr. Med. Chem., 11 (2004) 2105.
21. Q. S. Du, R. B. Huang, S. Q. Wang, K. C. Chou, 5 (2010) 9388.
22. J. J. Blessy, D. J. S. Sharmila, J. Biomol. Struct. Dyn., 33(5) (2015) 1126.
23. G. A. Kaminski, R. A. Friesner, J. Tirado-Rives, W. L. Jorgensen, J. Phys. Chem. B, 105 (2001) 6474.

CHAPTER X
ANTIMICROBIAL STUDIES

1. Introduction

Nowadays, there is an increasing interest in research to develop new antimicrobial agents from different sources to combat microbial resistance. The foundation of modern chemotherapy has mainly been due to the efforts of Dr. Paul Ehrlich (1910) who found Salvarsan, an arsenic derivative effective against syphilis. Paul Ehrlich used the term chemotherapy for curing infectious diseases without causing any injury to the host tissue, using known chemotherapeutic agents such as antibacterial, antiprotozoal, antiviral, antineoplastic, antitubercular and antifungal agents. Later in 1935, Domagk was credited with the discovery of sulfonamidochrysoidine—the first commercially available antibiotic.[1]

Antimicrobial drugs may either kill microorganisms completely or simply prevent their growth. There are various ways in which these agents may exhibit their antimicrobial activity. They may inhibit cell-wall synthesis, protein synthesis, nucleic acid synthesis, enzymatic activity, folate metabolism, or may damage cytoplasmic membrane.[2]

In order to evaluate or screen *in vitro* antimicrobial activity of a compound, various laboratory methods can be used. The methods used for evaluation are the following: turbidometric method, agar-streak dilution method, serial dilution method, agar diffusion method. The techniques used in agar diffusion methods are agar cup method, agar ditch method and paper disc method.[3] We have used the agar paper disc diffusion method to evaluate the antibacterial activity.[4] This method yields a zone of inhibition in millimeters (mm).[4] It indicates the amount of antimicrobial agents that is needed to inhibit the growth of specific microorganisms. It is carried out in petri plates. The agar disc diffusion method is not appropriate to determine the minimum inhibitory concentration (MIC), as it is impossible to quantify the amount of the antimicrobial agent which has diffused into the agar medium.

The most important conditions to be satisfied for screening the antimicrobial activity of a compound are listed below:

1. The test organisms and substance to be evaluated should be in intimate contact.
2. Necessary conditions should be provided for the growth of the microorganisms.
3. Conditions should be same throughout the study.
4. Aseptic/sterile environment should be maintained.

Nowadays, it is found that most of the microbes are resistant towards the available antibiotics. So, there is a crucial need for the development of new and useful antimicrobial agents. Therefore, designing antimicrobial agents which are distinct from those of the classical antibiotics becomes one of the main objectives of our current study. Our literature survey revealed that Schiff's bases exhibit immense biological activities.[5,6] This chapter portrays the antimicrobial screening of five ligands and their selected metal complexes synthesized

by us. For the sake of convenience, the antimicrobial studies are discussed in two subsections, A and B and the ligands synthesized by us were named as follows:

1. N-Methyl-2-((3-methyl-5-oxo-1-phenyl-4,5-dihydro-1H-pyrazol-4-yl)(phenyl) methylene)-N-phenylhydrazinecarbothioamide (H_2L1).
2. 2-[2-(Diphenylmethylidene)hydrazine]-N-methyl-N-phenylhydrazine-1-carbothioamide (H_2L2).
3. 3-Formylchromone N(4)-methyl-N(4)-phenylthiosemicarbazone (HL3).
4. 2-{2-[(4-Hydroxy-3-methoxyphenyl)methylidene]hydrazinecarbonothioyl}-N-methyl-N-phenylhydrazine-1-carbothioamide (H_2L4).
5. 2-{2-[(3,4-Dimethoxyphenyl)methylidene]hydrazinecarbonothioyl}-N-methyl-N-phenylhydrazine-1-carbothioamide (H_2L5).

SECTION A

A. Antibacterial studies of ligands and selected metal complexes

The synthesized compounds were tested *in vitro* for their antibacterial activity against Gram-positive and Gram-negative organisms by Kirby–Bauer agar disc diffusion method.[7]

2. Materials and methods

2.1. Bacterial strains

The bacterial strains used were *Staphylococcus aureus*, *Enterococcus faecalis, Bacillus subtili*, *Escherichia coli*, *Pseudomonas aeruginosa* and *Klebsiella pneumonia*. These strains were obtained from Medical college, Kannur. Mueller–Hinton agar medium was used in this method.

2.2. Preparation of Mueller–Hinton agar

1. Beef infusion: 300 g
2. Acid hydrolysate of casein: 17.5 g
3. Starch: 1.5 g
4. Agar: 17 g
5. Distilled water: 1 L

2.3. Kirby–Bauer agar disc diffusion method

Stock solutions with 2 mg/mL concentration of the test compounds were prepared in 1% DMSO. The stock solution was suitably diluted with sterilized distilled water to get solutions of concentrations of 200, 20 and 2 ppm. Nutrient agar medium, 25 mL was poured in each petriplate. After solidification, 0.1 mL of test bacteria was spread over the medium using a spreader. Filter paper discs, approximately 6 mm in diameter were soaked with 10 µl of the test solution. It was allowed to dry and placed in the previously prepared agar

plates. Each disc was pressed down to ensure complete contact with the agar surface. They were distributed evenly so that they are not closer than 24 mm (centre-to-centre) from each other. These petriplates were kept in the refrigerator for 24 hours for pre-diffusion. The agar plates were then incubated at 37ºC. After 16–18 hours of incubation, each plate was examined. The activity results were calculated as a mean of triplicates. The zone of inhibition was carefully measured in millimeters. A paper disc treated with DMSO served as negative control. Kanamycin and methicillin are used as standard drugs.

3. Results and discussion

The preliminary antibacterial screening results revealed that the metal complexes showed significant activities compared to the ligands. All of the selected compounds showed good activities against *S. aureus* and *K. pneumonia*. However, most of them showed no activity against *B. subtili* even at higher concentrations. Another observation was that all copper complexes exhibited higher inhibition towards most of the bacterial strains. The results of antibacterial studies by agar disc diffusion method are tabulated in Table 1 and shown in Figs. 1–3.

Table 1. Preliminary *in vitro* antibacterial screening studies of the ligands and their selected complexes

Sl No.	Compound	Diameter of Zone of Inhibition(mm)					
		Staphylo-coccus aureus	*Entero-coccus faecalis*	*Bacillus subtili*	*Escheri-chia coli*	*Pseudo-monas aeruginosa*	*Klebsiella pneumonia*
1	H_2L1	7	–	–	8	8	10
2	$[Cu(HL1)_2]H_2O$	10	10	–	7	10	15
3	[Cu(HL1)Cl]	7	8	–	7	7	18
4	$[Cu(HL1)NO_3]$	8	7	–	7	10	18
5	$[CuHL1)_2(OH)_2]5H_2O$	14	8	–	–	–	8
6	$[Zn(HL1)_2]$	7	10	–	8	8	11
7	$[Zn(HL1)_2(NO_3)_2]4H_2O$	10	10	–	7	7	10
8	H_2L2	10	–	–	9	7	15
9	$[Mn(HL2)_2]H_2O$	13	8	–	10	7	18
10	$[Co(H_2L2)_2]Cl_2$	11	7	–	11	8	19
11	$[Co(H_2L2)_2](NO_3)_2$	10	7	–	10	7	15
12	$Ni(H_2L2)(CH_3COO)_2$	10	8	7	10	10	13
13	$[Cu(HL2)NO_3]_2\ 2H_2O$	18	8	7	11	8	22
14	$[(Cu(HL2)(H_2O)_2)SO_4]$	18	8	7	10	10	20
15	$[Zn(H_2L2)(CH_3COO)_2]\ 2H_2O$	18	7	8	11	8	21
16	HL3	5	10	5	12	15	8
17	$[Cu(L3)_2]$	8	14	8	18	17	20
18	$[CuL3Cl]\ H_2O$	8	10	8	18	15	9
19	$[Zn(L3)CH_3COO]2H_2O$	8	13	7	13	17	10
20	$[Co(L3)OH]\ 4H_2O$	10	10	6	10	18	9
21	H_2L4	5	9	4	–	–	14
22	$[Cu_2\ L4(CH_3COO)_3]$	9	9	5	–	–	20

Sl No.	Compound	Diameter of Zone of Inhibition(mm)					
		Staphylo-coccus aureus	*Entero-coccus faecalis*	*Bacillus subtili*	*Escheri-chia coli*	*Pseudo-monas aeruginosa*	*Klebsiella pneumonia*
23	$[Cu_2(HL4)Cl_3]$	9	9	5	–	–	12
24	$[Zn(HL4)CH_3COO]$	10	9	8	–	8	12
25	H_2L5	4	4	–	–	–	10
26	$[Cu_2(L5)(CH_3COO)_3]$	6	8	–	–	–	12
27	$[Cu_2(H_2L5)Cl_3]$	6	8	–	–	–	12
28	$[Zn(HL5)CH_3COO]$	8	6	6	–	6	10
	Kanamycin	12	9	12	12	10	20
	Methicillin	10	8	10	15	12	25
	DMSO		–	–	–	–	–

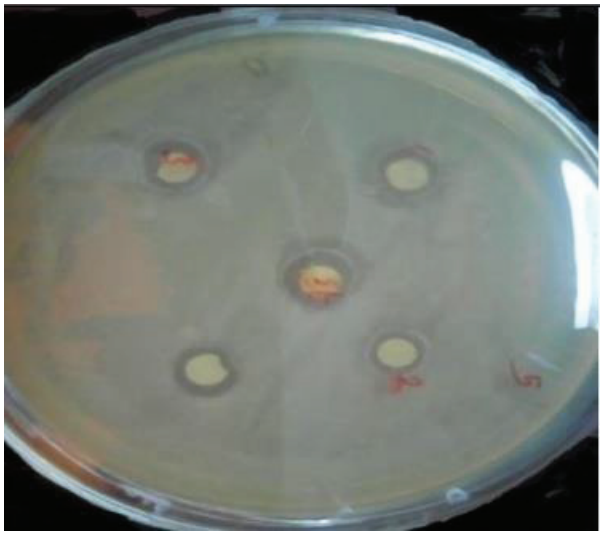

Fig. 1. Zone of inhibition for Enterococcus faecalis (6).

Fig. 2. Zone of inhibition for *Pseudomonas aeruginosa* (18).

Fig. 3. Zone of inhibition *for Klebsiella pneumonia* (17).

SECTION B

B. Antifungal studies of ligands and selected complexes

The antifungal activities of the ligands and complexes were tested for their effect on the growth of microbial cultures.

2. Materials and methods

The fungal strains used were *Aspergillus niger, Alternaria alternata*, *Colletotrichum gloeosporioides* and *Sclerotium rolfsii.* These strains were obtained from Department of Botany, the Zamorin's Guruvayurappan College, Calicut. Potato-Dextrose agar medium was used in this method.[8]

2.1. Preparation of Potato dextrose agar medium

Potato: 200 g
Dextrose: 20g
Agar-agar: 20g
Distilled water: 1000 mL

2.2. Procedure

Potato dextrose agar medium was prepared by using potato, dextrose, agar-agar and distilled water. Appropriate quantities of the compounds in DMSO were added to potato dextrose agar medium in order to get concentrations of 20, 40 and 60 ppm of compound in the medium. The medium was poured into a set of three petriplates under aseptic conditions in a laminar flow hood. When the medium in the plates solidified, mycelial discs of 5 mm in diameter cut from the periphery of the 48 hours old culture were aseptically inoculated upside down in the centre of the petriplates. These treated petriplates were incubated at room temperature until fungal growth in the control petriplates was almost complete. The

mycelial growth of fungi (mm) in each petriplates was measured diametrically and growth inhibition (*I*) was calculated by using the formula:

$$\text{Percentage inhibition} = C - T/C \times 100$$

where *C* and *T* are the diameters of the fungal colony in the control and the test plates, respectively.

3. Results and discussion

The results of antifungal activities are tabulated in Tables 2 -6 and shown in Figs. 4 -7. The studies revealed that metal complexes inhibit the growth of all the four fungal strains more than the ligands even at very low concentration. The higher activity of metal chelates may be attributed to their increased lipophilic nature due to chelation. Out of the four fungal strains, ligands and complexes show very high activity against *S. rolfsii*. 3-Formylchromone N(4)-methyl-N(4)-phenylthiosemicarbazone (HL3) and its complexes showed greater activity towards all the fungal strains and may be due to the existence of chromone ring in these compounds. It was also observed that the activity of 2-{2-[(3,4- Dimethoxyphenyl) methylidene]hydrazinecarbonothioyl}-N-methyl-N-phenylhydrazine-1-carbothioamide (H2L5) and its complexes was less than that 2-{2-[(4-Hydroxy-3-methoxyphenyl)methylidene] hydrazinecarbonothioyl}-N-methyl-N-phenylhydrazine-1-carbothioamide (H2L4) and its complexes. This may be due to the presence of additional methoxy group in H2L5.

Table 2. Preliminary *in vitro* antifungal screening studies of H_2L1 and its complexes

Fungi	**Percentage of Inhibition**																	
	H_2L1			**$[Cu(HL1)_2]$**			**[Cu(HL1)Cl]**			**$[Cu(HL1)NO_3]$**			**$[(CuHL1)_2(OH)_2]5H_2O$**			**$[Zn(HL1)_2]$**		
Conc. (ppm)	**20**	**40**	**60**	**20**	**40**	**60**	**20**	**40**	**60**	**20**	**40**	**60**	**20**	**40**	**60**	**20**	**40**	**60**
A. niger	38	49	48	58	62	80	44	63	85	46	58	80	38	55	75	64	60	72
A. alternata	30	38	42	40	56	77	49	71	78	47	65	80	60	74	85	64	62	65
C. gloeosporioides	36	37	38	62	60	60	70	85	85	64	75	80	37	48	73	40	62	83
S. rolfsii	35	55	40	68	88	95	76	85	95	70	85	95	72	87	95	75	88	92

Table 3. Preliminary *in vitro* antifungal screening studies of H_2L2 and its complexes

Fungi	**Percentage of Inhibition**														
	H_2L2			**$Mn(HL2)_2H_2O$**			**$[Cu(HL2)NO_3]_2 2H_2O$**			**$[(Cu(HL2)H_2O)_2SO_4]$**			**$Zn(H_2L2)(CH_3COO)_2 2H_2O$**		
Conc. (ppm)	**20**	**40**	**60**	**20**	**40**	**60**	**20**	**40**	**60**	**20**	**40**	**60**	**20**	**40**	**60**
A. niger	40	45	47	60	62	64	75	75	85	73	75	85	70	73	76
A. alternata	40	43	43	42	55	62	60	68	70	56	66	76	60	62	72
C. gloeosporioides	20	25	27	34	35	45	26	27	38	26	27	29	50	52	54
S. rolfsii	55	65	70	67	75	82	80	85	90	81	88	90	67	77	80

Table 4. Preliminary *in vitro* antifungal screening studies of HL3 and its complexes

Fungi	**Percentage of Inhibition**														
	HL3			**$[Cu(L3)_2]$**			**$[CuL3Cl]H_2O$**			**$[Zn(L3)CH_3COO]2H_2O$**			**$[Co(L3)OH]4H_2O$**		
Conc. (ppm)	**20**	**40**	**60**	**20**	**40**	**60**	**20**	**40**	**60**	**20**	**40**	**60**	**20**	**40**	**60**
A. niger	53	65	70	65	75	84	68	70	82	65	72	78	65	65	71
A. alternata	48	55	70	58	70	84	56	69	85	62	74	86	50	64	74
C. gloeosporioides	45	68	70	60	64	80	55	75	82	60	78	86	48	68	74
S. rolfsii	67	70	74	70	85	96	68	87	96	67	84	95	65	68	78

Table 5. Preliminary *in vitro* antifungal screening studies of H_2L4 and its complexes

Fungi	**Percentage of Inhibition**											
	H_2L4			**$[Cu_2(HL)(CH_3COO)_3]$**			**$[Cu_2(HL)Cl_3]$**			**$[Zn(HL)CH_3COO]$**		
Conc. (ppm)	**20**	**40**	**60**	**20**	**40**	**60**	**20**	**40**	**60**	**20**	**40**	**60**
A. niger	50	67	65	65	79	85	68	70	82	55	62	90
A. alternata	38	45	50	58	70	70	56	69	75	62	74	84
C. gloeosporioides	35	50	58	60	64	70	55	75	82	60	73	89
S. rolfsii	57	76	80	68	74	85	65	80	86	69	78	86

Table 6. Preliminary *in vitro* antifungal screening studies of H_2L5 and its complexes

Fungi	**Percentage of Inhibition**											
	H_2L5			**$[Cu_2(HL5)(CH_3COO)_3]$**			**$[Cu_2(HL5)Cl_3]$**			**$[Zn(HL5)CH_3COO]$**		
Conc. (ppm)	**20**	**40**	**60**	**20**	**40**	**60**	**20**	**40**	**60**	**20**	**40**	**60**
A. niger	45	58	60	60	65	75	55	67	77	50	59	79
A. alternata	35	38	45	50	60	70	53	59	69	50	64	80
C. gloeosporioides	25	50	59	50	53	68	48	63	75	58	65	80
S. rolfsii	50	68	70	56	65	69	60	75	82	61	76	80

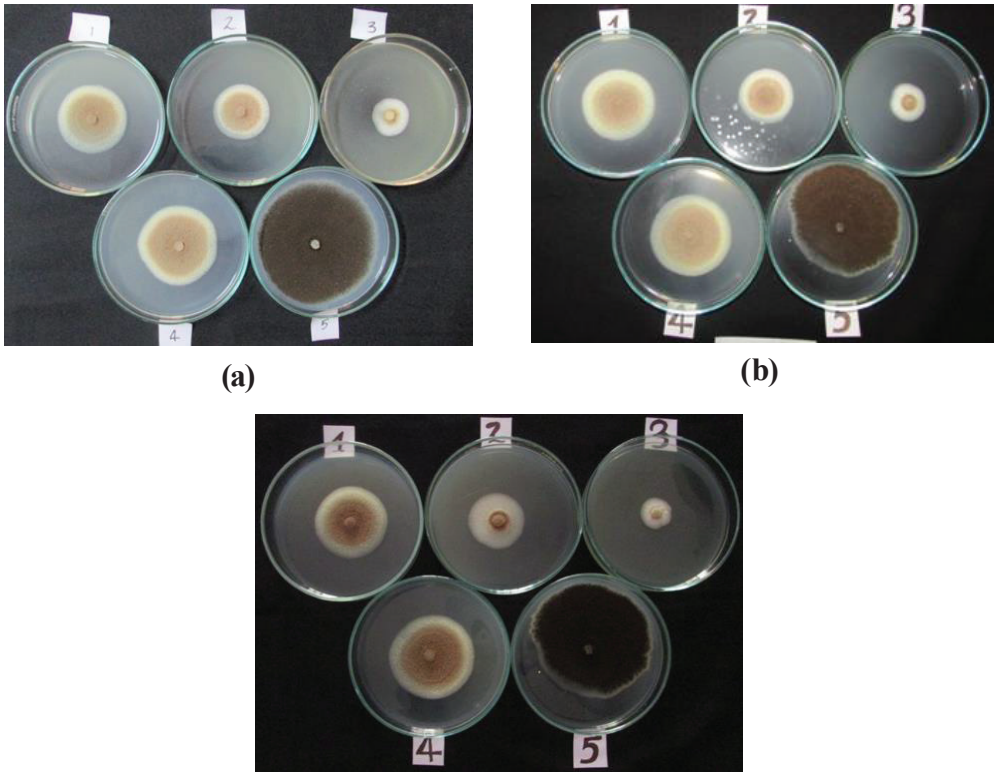

(a) **(b)**

(c)

Fig. 4. *In vitro* antifungal activity of compounds against *Aspergillus niger.* (a) ligand, (b) and (c) complexes.

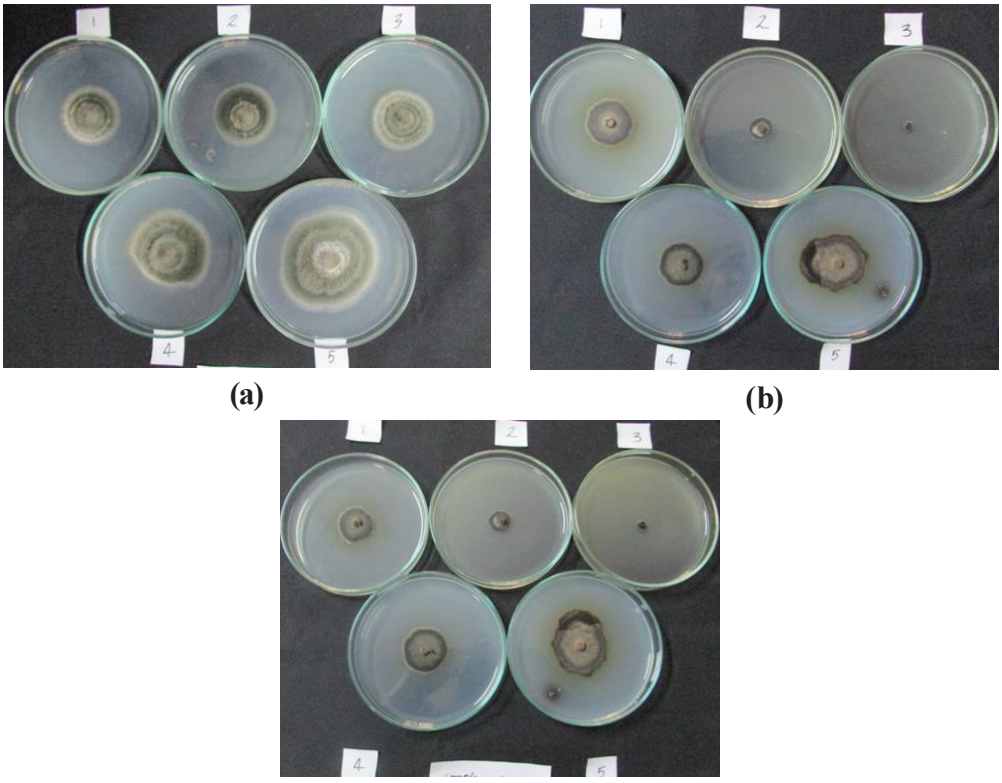

(a) **(b)**

(c)

Fig. 5. *In vitro* antifungal activity of compounds against *Alternaria alternata.* (a) ligand, (b) and (c) complexes.

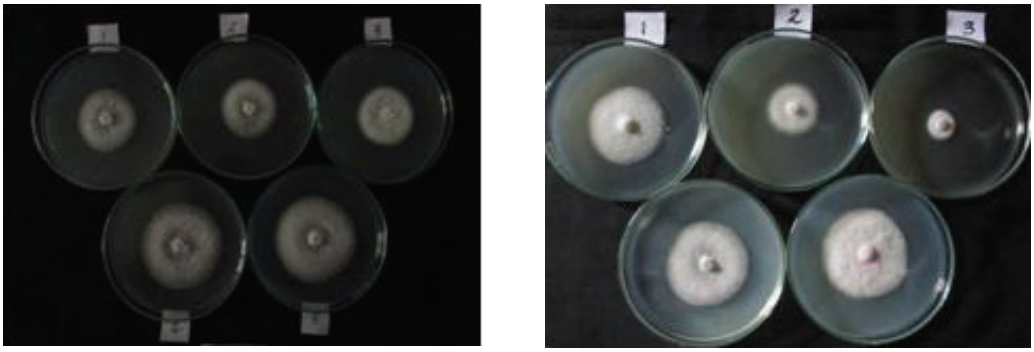

(a) (b)

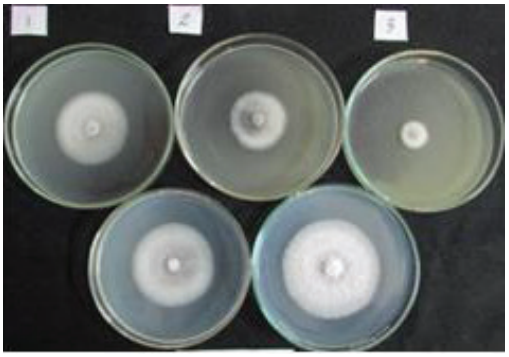

(c)

Fig. 6. *In vitro* antifungal activity of compounds against *Colletotrichum gloeosporioides.* (a) ligand, (b) and (c) complexes.

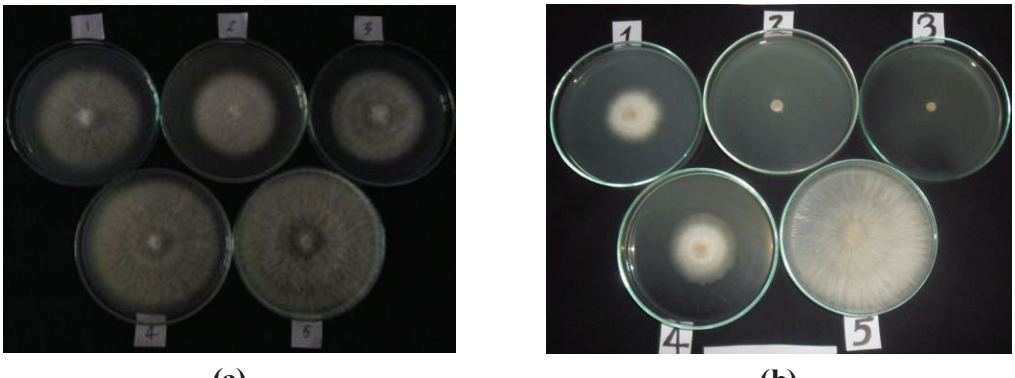

(a) (b)

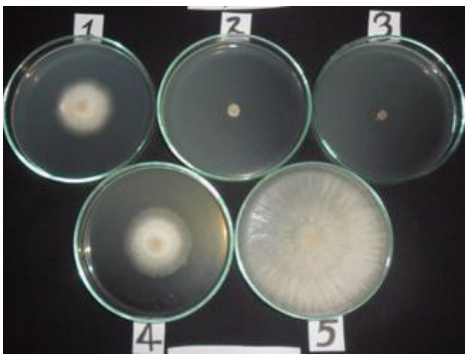

(c)

Fig. 7. *In vitro* antifungal activity of compounds against *Sclerotium rolfsii.* (a) ligand, (b) and (c) complexes.

4. Conclusions

The observations in this study revealed selective activities of the compounds against microbes. At this phase, it is hard to find a simple explanation for antimicrobial activities of these compounds and further studies will be needed to clarify these observations.

References

1. G. Domagk. Dtsch. Med. Wschr., 61 (1935) 250.
2. L. D. Gebbharadt, J. G. Bachtold, Proc. Soc. Exptl. Biol. Med., 88 (1955) 103.
3. M. Balouiri, M. Sadiki, S. K. Ibnsouda, J. Pharm. Anal., 6 (2016) 71–79.
4. N.G. Heatley, Biochem. J. 38 (1944) 61–65.
5. P. Bindu, M. R. P. Kurup, T. R. Satyakeerthy, Polyhedron., 18 (1999) 321.
6. M. Sheikhy, A. R. Jalilian, A. Novinrooz, F. J. Motamedi-Sedeh. J. Biomed. Sci. Eng. 5(2012) 39.
7. A. W. Bauer, W. M. Kirby, J. C. Sherries, M. Tuck, Am. J. Clin. Pathol., 45 (1966) 493.
8. H. L. Singh, Inorg. Chem: An Indian J., 2 (2007) 135.

Appendix

Journal of Molecular Structure 1150 (2017) 135–145

Contents lists available at ScienceDirect

Journal of Molecular Structure

journal homepage: http://www.elsevier.com/locate/molstruc

Insight into the theoretical and experimental studies of 1-phenyl-3-methyl-4-benzoyl-5-pyrazolone *N*(4)-methyl-*N*(4)-phenylthiosemicarbazone - A potential NLO material

K.G. Sangeetha [a, *], K.K. Aravindakshan [a], K.P. Safna Hussan [b]

[a] Department of Chemistry, University of Calicut, 673635, Kerala, India
[b] Department of Physics, University of Calicut, 673635, Kerala, India

ARTICLE INFO

Article history:
Received 17 April 2017
Received in revised form
18 August 2017
Accepted 22 August 2017
Available online 26 August 2017

Keywords:
Thiosemicarbazones
DFT
NBO
NLO
Docking

ABSTRACT

The synthesis, geometrical parameters, spectroscopic studies, optimised molecular structure, vibrational analysis, Mullikan population analysis, MEP, NBO, frontier molecular orbitals and NLO effects of 1-phenyl-3-methyl-4-benzoyl-5-pyrazolone *N*-(4)-methyl-*N*-(4)-phenylthiosemicarbazone, $C_{25}H_{23}N_5OS$ (L_1) have been communicated in this paper. A combined experimental and theoretical approach was used to explore the structure and properties of the compound. For computational studies, Gaussian 09 program was used. Starting geometry of molecule was taken from X-ray refinement data and has been optimized by using DFT (B3LYP) method with the 6-31+G (d, p) basis sets. NBO analysis gave insight into the strongly delocalized structure, responsible for the nonlinearity and hence the stability of the molecule. Frontier molecular orbitals have been defined to forecast the global reactivity descriptors of L_1. The computed first-order hyperpolarizability (β) of the compound is 2 times higher than that of urea and this account for its nonlinear optical property. Simultaneously, a molecular docking study of the compound was performed using GLIDE Program. For this, three biological enzymes, histone deacetylase, ribonucleotide reductase and DNA methyl transferase, were selected as receptor molecules.

1. Introduction

Thiosemicarbazide and thiosemicarbazones reveal manifold pharmacological properties such as antiviral [1,2], antibacterial [3,4], antiparasitic [5,6], antitumor [7,8] and anticonvulsant [9,10]. They are agents that obstruct the development of microbes and parasites. The presence of sulphur atom plays a key role in the biological activities of thiosemicarbazones and generally provides a higher activity compared to semicarbazones. Moreover, these properties are enhanced when these molecules are N(4)-substituted [11]. Pyrazolones exhibit promising antiproliferative activity against human myelogenous leukaemia HL-60 cells [12].

Literature survey revealed that the DFT has a great accuracy in reproducing the experimental values in terms of geometry, dipole moment, vibrational frequencies, thermodynamic properties, etc. [13,14]. The compound was optimized by using DFT (B3LYP) method with 6-31+G (d, p) basis sets, using Gaussian 09 [15] program. In order to explore non-linear optical properties, the total static dipole moment μ, the linear polarizability α, the anisotropy of polarizability Δα and the mean first order hyperpolarizability β_o were calculated by using the above mentioned method [16,17].

Currently, the use of computers to predict the binding of small molecules to known target structures is a vital factor in the drug discovery process [18]. Docking is often used to predict the binding modes of small molecules to their targeted proteins. Inhibition of histone deacetylase-, ribonucleotide reductase- and DNA methyl transferase enzymes are emerging as an innovative and significant approach for the treatment of cancer [19–21]. Therefore, molecular docking was conducted to investigate the biological behaviour through the determination of the probable binding mode by inserting the compound into the active sites of three protein targets-histone deacetylase8, ribonucleotide reductase and DNA methyl transferase.

In this paper, we report the experimental and theoretical studies of 1-phenyl-3-methyl-4-benzoyl-5-pyrazolone N (4)-methyl-N (4)-phenylthiosemicarbazone.

* Corresponding author.
E-mail addresses: sangtkg@gmail.com (K.G. Sangeetha), aravindkuttamath@yahoo.com (K.K. Aravindakshan), safnahussain2@gmail.com (K.P. Safna Hussan).

http://dx.doi.org/10.1016/j.molstruc.2017.08.078
0022-2860/

2. Experimental details

Carbon disulphide (Merck), *N*-methyl aniline (SRL), hydrazine hydrate (98%) (Glaxo fine Chemicals), ethylacetoacetate (Merck), phenylhydrazine, benzoyl chloride and calcium hydroxide were used as received. The solvents were purified and dried by using standard procedures. N(4)-methyl-N(4)-phenylthiosemicarbazide was prepared by taking up and modifying a procedure reported by Scovill [22]. 1- Phenyl- 3-methyl- 4-benzoyl- 5- pyrazolone was prepared by using Jenson's method [23].

The compound (L_1) was prepared by stirring a hot methanolic mixture of 1- phenyl-3-methyl- 4-benzoyl-5-pyrazolone (PMBP) (750 mg, 2.76 mmol) and N(4)-methyl-N(4)-phenyl-thiosemicarbazide (4MPTSC) (500 mg, 2.76 mmol) on a magnetic stirrer. The solution was then refluxed at 60–80 °C for 30 min. The compound obtained was filtered, washed with methanol and dried.

The compound was characterized by using partial elemental analyses, vibrational spectrum, electronic spectrum, ^{1}H NMR spectrum and single crystal X-ray diffraction. Elemental analyses (C, H, N and S) were performed on Vario EL III elemental analyzer. Infrared (IR) spectrum was recorded on a Jasco-FT-IR-4100 model spectrometer using KBr pellets. Raman spectrum was recorded on MultiRAM spectrometer, range 3600 to 50 cm^{-1} with a laser excitation wavelength of 1064 nm. The electronic spectrum was recorded on a model JascoV-550 UV–Vis spectrometer. NMR spectrum was recorded on a 400 MHz BrukerAvance111 FT NMR spectrometer. X-ray crystallographic data were collected at 296 (2) K on a Bruker Model Kappa Apex II diffractometer with graphite monochromatic Mo Kα (λ = 0.71073 Å) radiation.

2.1. X-ray crystallography

Yellow crystals suitable for X-ray analysis were grown from a solution 1:1 (v/v) mixture of methanol and DMSO. A crystal with an approximate dimension of 0.35 × 0.30 × 0.30 mm^3 was selected for collecting the data. L_1 crystallizes with a molecule per asymmetric unit into triclinic crystal system with a space group of *P-1*. Direct methods were used to solve the structure and refined by least-square on F^2 using SHELXL-97 [24]. All non-hydrogen atoms were refined anisotropically. All hydrogen atoms, except those attached to nitrogen were geometrically fixed at calculated positions. Those on the nitrogen atoms were refined from Fourier maps. The crystallographic tools, PLATON [25], ORTEP [26] and MERCURY [27] were used for structure analysis and presentation of the results. The structures were finally refined to the conventional *R*-value, 0.0561.

3. Computational details

In order to ascertain more about the structure-activity relationship of the molecule, we have performed density functional theory (DFT) studies [28]. The geometric structure of the compound were wholly optimized at the Becke's three-parameter hybrid exchange functional and the Lee-Yang-Parr non-local correlation functional (B3LYP) [29,30] level in the ground state. Visualization of HOMO and LUMO calculations has been done by GaussView 5.0.9 program [31]. Vibrational frequencies of the molecule were computed by applying the above mentioned method. ^{1}H NMR chemical shifts were calculated using the GIAO approach in vacuum and in chloroform. The chemical shift values are expressed in ppm relative to TMS as an internal standard. A comparison of the experimental and theoretical spectra was very helpful in making suitable assignments and understanding of vibrational behaviour of the molecule. In addition, the molecular electrostatic potential map, NBO analysis and NLO properties of the compound were calculated using 631+G (d,p) basis set and (B3LYP) method. Starting geometry of the molecule was taken from X-ray refinement data and compared the data with theoretical results.

3.1. Molecular docking methodology

Molecular docking of the compound into the 3D crystal structure of histone deacetylase8 (PDB ID: 1T69), DNA methyl transferase (PDB ID: 2QRV) and ribonucleotide reductase M-2 subunit (PDB ID: 2UW2) have been performed using GLIDE Dock Program. Protein structure was refined using protein preparation wizard which employs under restrained minimization and heavy atoms were restrained using Impref minimization [32], which can done by OPLS 2005 force field [33]. The ligands were subjected to ligand preparation using the ligand preparation wizard (Lprep) of Schrodinger software in the Maestro interface (9.0). Grid center is defined for the active site and box sizes are set to 15 Å. Glide score and glide energy were analyzed using XP visualize. The selection of the best pose was done based on the interaction energy between the ligand and the protein. The results were analyzed by a statistical scoring function which converts interacting energy into numerical values called as the glide score.

4. Results and discussion

The compound L_1 is yellow in colour having a melting point 163 °C. The suggested formula for the compound is $C_{25}H_{23}N_5OS$. CHNS percentages are in agreement with the suggested molecular formulae. Elemental Analysis found (Calcd.) (%): C: 68.04 (68.18) H: 5.00 (5.15) N: 15.9 (15.88) S: 6.27 (6.21). The compound is completely soluble in $CHCl_3$ but partially soluble in DMSO, DMF, ethanol and methanol.

Crystal data and structure refinement parameters are given in Table 1. Fig. 1 is the ORTEP diagram of L_1 with the atom numbering scheme, Fig. 2 is the optimised geometry of molecule along with the atom numbering scheme and Fig. 3 is the supramolecular chain stabilised by van der Waals interaction along the axis b.

It is found that the molecules in a unit cell were arranged in inverted manner, which are the repeating units of the packing in the crystal lattice. An interesting attribute of the crystal packing is the formation of a supramolecular chain mediated by intermolecular C–H···O and H···C interactions.

Comparison of optimized geometrical parameters such as bond length, bond angles, torsion angles with the experimental data are listed in Table 2. The experimental bond distances, C (9)–N (3), C (8)–N (1), C (8)–N (2) and N (2)–N (3) are 1.328 (3) Å, 1.352 (3) Å, 1.368 (3) Å, 1.391 (2)Å, respectively. The corresponding computational values are, 1.2899, 1.3721, 1.3837 and 1.3787 Å. They are found to be at the midway between the analogous single [C–N, 1.47 Å N–N, 1.45 Å] and double bond lengths [C=N, 1.28 Å N=N, 1.25 Å] [34]. The experimental C (8)–S (1) bond length is 1.669 (2) and theoretical value is 1.6737 Å. They are closer to C=S bond length [1.61 Å] than to C–S bond length [1.81 Å] [35]. It supports the existence of sulphur in the thione form. The bond length C (18)–O (1) is 1.256 (2) Å and the DFT calculations give a value of 1.2216 Å. They are corresponding to C=O double bond, indicating that the compound in the keto-form in the crystalline state. The calculated C–C, C–H and N–H bond length values calculated agree well with the experimental ones. All the other bond lengths posses bond equalization due to partial double bond and single bond characteristics. This indicates that there is a significant electron delocalization around the pyrazolone ring and the thiosemicarbazide moiety [36].

A torsion angle value of 2.1 corresponding to S (1)–C (8)–N (2)–N (3) moiety confirms the syn-periplanar configuration of the S1

Table 1
Crystal data and structure refinement for L_1.

Parameters	L_1	Parameters	L_1
Empirical formula	C_{25} H_{23} N_5 O S	Completeness to theta	28.31 97.6%
Formula weight	441.54	Max. and min. Transmission	0.9503 and 0.9424
Temperature (K)	296 (2)	Absorption correction	Semi-empirical from Equivalents
Wavelength	0.71073	Refinement method	Full-matrix least-squares on F^2
Crystal system, space group	Triclinic, *P-1*	Data/restraints/parameters	5465/0/295
Unit cell dimensions	a (Å) = 7.8930 (4) α(°) = 96.175 (3)	Goodness-of-fit on F^2	0.956
	b (Å) = 11.2019 (5) β(°) = 100.922 (3)	Final R indices [I > 2sigma(I)]	R1 = 0.0561, w*R*2 = 0.1647
	c (Å) = 13.0211 (7) γ(°) = 91.005 (3)	R indices (all data)	R1 = 0.0848, w*R*2 = 0.2003
Volume (A^3)	1123.02 (10)	Largest diff. peak and hole ($e.A^{-3}$)	0.442 and −0.362
Z, Calculated density (mg/m^3)	2, 1.303		
Absorption coefficient (mm^{-1})	0.172		
F (000)	462		
Crystal size (mm^3)	0.35 × 0.30 x 0.30		
Theta range for data collection	1.60 to 28.31		
Limiting indices	−10 ≤ h<=10, −14 ≤ k<=14, −11 ≤ l<=17		
Reflections collected/unique	8957/5465 [R (int) = 0.0174]		

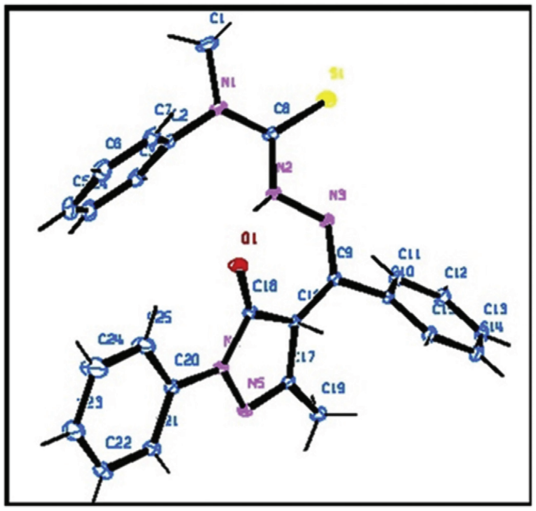

Fig. 1. ORTEP diagram of molecule, with ellipsoids drawn at the 60% probability level.

atom with respect to azomethine nitrogen atom N3. The terminal nitrogen atoms, N (1) and N (3) of the thiosemicarbazide fragment are in an antiperiplanar conformation with respect to the C (8)–N (2) with a torsion angle of −179.1 (2). Similarly, the nitrogen atoms, N (1) and N (2) of the thiosemicarbazide fragment are in an antiperiplanar conformation with respect to the C (8)–N (3) with a torsion angle of −179.1 (3). In addition, the thiosemicarbazide moiety is not exactly coplanar to pyrazolone ring, since C (16)–C (9)–N (3) and C (8)–N (3)–N (2) and C (9)–N (3)–N (2) angles are 124.95, 115 and 123, respectively. According to the B3LYP calculations these values are 124.45, 119 and 117, respectively. The root mean square deviation of the theoretical and observed geometrical parameters were calculated and are found to be 0.0555 Å for bond lengths and 4.182° for bond angles. These variations may be due to the difference in the molecular states of compound in the experimental and computational method [37]. The theoretical data are calculated in gas phase without considering molecular interactions, but the experimental data are collected in the solid state where the interactions such as van der Waals, hydrogen bonds and crystal packing forces make slight changes in the structure. In the crystalline structure, we can see intramolecular hydrogen bonding existing between pyrazolone oxygen and *N*–H of thiosemicarbazide moiety.

5. Vibrational analysis

The experimental and generated IR spectra are shown in Fig. 4.

Each molecule of the compound under investigation possesses 55 atoms and 159 normal modes of vibrations. It has C_1 point group symmetry. All the vibrations are active in both Raman and infrared absorptions. The FT-IR spectrum of the compound shows distinguishable stretching vibrational bands due to N–H, N–N, C=O, C=N, C=S, aromatic ring and methyl groups.

The vibrations due to N–H stretching usually absorb in the region 3450–3250 cm^{-1} [38]. The DFT computation predicts N–H stretching vibrational mode at 3524 cm^{-1}. In FT-IR and FT-Raman spectra, a broad band is observed at 3411 cm^{-1} [39]. It indicates the presence of hydrogen bonded tautomeric keto-imine or imine-ol form (O…H–N form or the O–H…N form) of the compound in the solid state [40]. Based on the information obtained from single crystal XRD studies, the presence of O–H…N form in the compound is ruled out.

DFT calculation predicts C=O stretching vibrational mode at 1768 cm^{-1} which is in accordance with the literature values. However, in FT-IR and FT-Raman spectra, the band for (C=O) of pyrazol-5-one moiety is at 1597 and 1594 cm^{-1}, respectively. This is at a lower wavenumbers than that is usually found for carbonyls and indicates its involvement in hydrogen bonding with N–H of the thiosemicarbazone moiety. The compound does not show any band between 2000 and 2500 cm^{-1} suggesting that in the solid state it is not in the thiol form [41].

The aromatic and aliphatic C–H vibrations generally absorb in the region 2850–3100 cm^{-1} [42]. In the present investigation, the experimental aromatic and aliphatic C–H stretching bands appear at 2924–3150 cm^{-1} in FT-IR and at 2926-3057 cm^{-1} in FT-Raman as weak bands while the theoretical C–H vibrations are assigned in the region 3257–3037 cm^{-1} (B3LYP). These are in accordance with the literature values and experimental data.

In aromatic compounds, the C–H in-plane bending vibrations appear in the range of 1000–1300 cm^{-1}. Out-of-plane vibrations appear in the range 750–1000 cm^{-1} [43]. In the present study, these bands are observed in the range 695–1283 cm^{-1} in the FT-IR

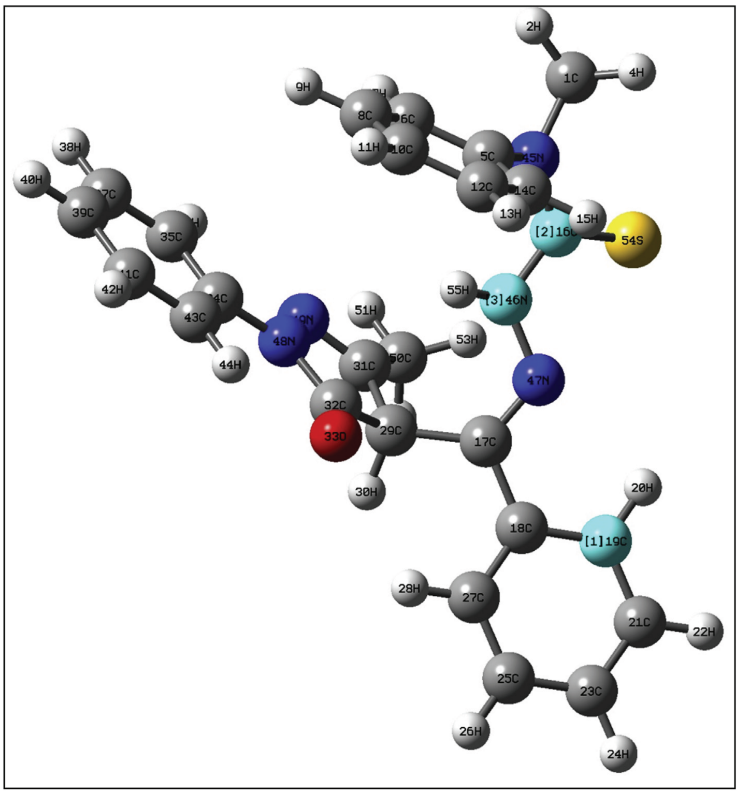

Fig. 2. Optimized geometry of the molecule.

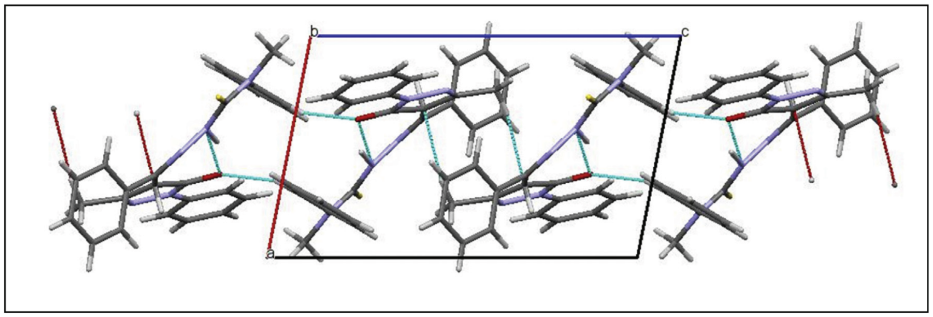

Fig. 3. Supramolecular chain stabilized by van der Waals forces along the axis b.

and FT-Raman spectra. The harmonic vibrations in the range 675–1366 cm^{-1}(B3LYP) are assigned to C–H in-plane and out-of-plane bending vibrations. Most of these bending vibrations are not pure but contain a significant contribution from other stretching modes, having weak to medium intensities.

The C–C ring stretching vibrations appear in the range 1200–1650 cm^{-1} [44]. The identification of vibrations in this range is very difficult because of the mixing of C=N band which is usually observed in this range. In the present work, the very strong bands observed at 1478, 1534 cm^{-1} in the FT-IR and 1482, 1532 cm^{-1} in FT-Raman are assigned to the C–C stretching vibrations. The theoretically calculated values, 1479, 1482, 1531, 1534, 1628 cm^{-1} show excellent agreement with the experimental data.

The C=N stretching modes of thiosemicarbazone appear in the region 1600–1630 cm^{-1} [45]. The harmonic vibrations in the range 1619–1662 cm^{-1} (B3LYP) are assigned to C=N stretching. In FT-IR and FT-Raman, this band is observed at 1626, 1629 cm^{-1}, respectively. The C–N stretching vibration is moderately to strongly active

Table 2
Geometrical parameters of L_1 - Bond lengths (Å), Bond angles (°) and Dihedral angles (°).

Bond length (Å)	XRD	DFT	Bond angle (°)	XRD	DFT	Dihedral angle (°)	XRD	Dihedral angle (°)	DFT
(N1–C45)	1.466 (3)	1.468	A (45,16,54)	124.81 (17)	124.36	D (47,17,18,19)	−56.2 (3)	D (47,17,18,27)	152.643
(C1–H2)	0.96	1.091	A (46,16,54)	122.06 (16)	121.42	D (47,17,18,27)	126.1 (2)	D (47,17,29,32)	−76.461
(C5–C6)	1.374 (4)	1.401	A (17,18,19)	120.29 (18)	119.84	D (47,17,29,32)	−21.9 (3)	D (46,16,45,5)	25.07
(C5–C14)	1.373 (3)	1.402	A (18,19,21)	120.0 (2)	120.34	D (46,16,45,5)	−3.0 (3)	D (54,16,45,5)	−159.13
(N5–C45)	1.431 (3)	1.441	A (33,32,48)	125.15 (18)	127.922	D (54,16,45,5)	175.74 (18)	D (46,16,45,1)	−169.57
(C6–C8)	1.371 (4)	1.399	A (29,32,33)	129.98 (19)	127.24	D (46,16,45,1)	178.5 (3)	D (54,16,45,1)	6.2293
(C6–H7)	0.93	1.086	A (5,45,16)	122.23 (18)	121.94	D (54,16,45,1)	−2.7 (4)	D (14,5,45,1)	−103.07
(C8–C10)	1.369 (5)	1.398	A (1,45,16)	121.3 (2)	119.71	D (14,5,45,1)	104.6 (3)	D (6,5,45,1)	75.0547
(C12–C14)	1.376 (5)	1.396	A (1,45,5)	116.5 (2)	116.8	D (6,5,45,1)	102.1 (3)	D (45,16,46,47)	−153.8
(C9–C11)	1.369 (4)	1.398	A (16,46,47)	115.03 (17)	119.47	D (45,16,46,47)	−179.08 (19)	D (54,16,46,47)	30.2853
(C16–N45)	1.352 (3)	1.371	A (17,47,46)	123.52 (17)	117.31	D (54,16,46,47)	2.1 (3)	D (29,17,47,46)	7.3866
(N16–C46)	1.368 (3)	1.384				D (29,17,47,46)	−13.0 (3)	D (18,17,47,46)	−176.33
(C16–S54)	1.669 (2)	1.674				D (18,17,47,46)	166.62 (18)	D (16,46,47,17)	−157.04
(C17,N47)	1.328 (3)	1.2899				D (16,46,47,17)	−168.74 (19)	D (33,32,48,49)	178.662
(C17–C29)	1.403 (3)	1.5252				D (33,32,48,49)	−178.3 (2)	D (33,32,48,34)	−2.7395
(C17–C18)	1.485 (3)	1.4849				D (33,32,48,34)	−1.8 (4)		
(C18–C19)	1.379 (3)	1.4078							
(C18–C27)	1.388 (3)	1.4048							
(C19–C21)	1.386 (3)	1.3926							
(C21–C23)	1.376 (4)	1.4							
(C23–C25)	1.373 (4)	1.396							
(C25–C27)	1.378 (3)	1.3971							
(C29–C31)	1.438 (3)	1.5143							
(C29–C32)	1.436 (3)	1.536							
(C31–C49)	1.303 (3)	1.288							
(C31–C50)	1.487 (3)	1.49							
(C32–O33)	1.256 (2)	1.222							
(C32–N48)	1.368 (3)	1.388							
(N34–C48)	1.423 (3)	1.421							
(N46–N47)	1.391 (2)	1.379							
(N46–H55)	0.99 (3)	1.016							
(N48–N49)	1.397 (2)	1.407							
(C50–H51)	0.96	1.092							

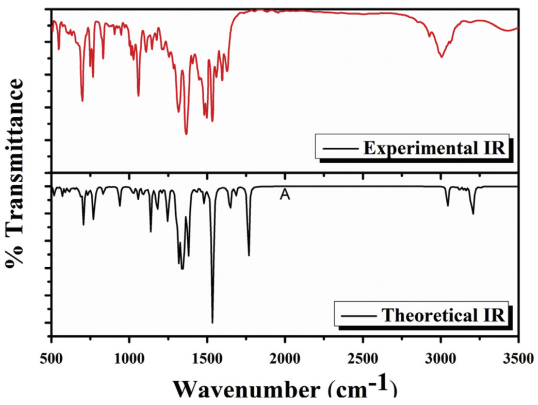

Fig. 4. Experimental and Theoretical IR spectra.

in the range 1220–1330 cm^{-1}. In DFT (B3LYP) calculations, the harmonic vibrations in the range 1237–1350 cm^{-1} are assigned to C–N stretching. Experimentally, the sharp band at 1316 and 1313 cm^{-1} in FT-IR and FT-Raman, respectively, are assigned to C–N stretching vibration.

Crane et al. [46] reported N–N stretching mode at 1115 cm^{-1}. In the present case, the bands observed at 1024 and 1106 cm^{-1} in FT-IR spectrum and 1167 and 1147 cm^{-1} in FT-Raman are assigned to *N*–N stretching vibrations. This also shows good agreement with predicted DFT calculation in the range 1029–1181 cm^{-1}. In this study, we observed the C=S stretching mode at 1362,1250 and 831 cm^{-1} in FT-IR and at 1247, 1367 cm^{-1} in FT-Raman spectra. The theoretically computed C=S stretching vibrations occurred at 1376, 1248 and 840 cm^{-1}.

6. Nuclear magnetic resonance spectra

The ^1H NMR spectra of the compound was recorded in $CDCl_3$ (Fig. 5.). ^1H chemical shifts are calculated with the GIAO approach in chloroform.

A sharp singlet, which integrates as one hydrogen, at $\delta = 14.479$ ppm in the spectrum may be due to the presence of NH proton. A sharp singlet at 11.176 ppm corresponds to OH proton. The downfield shift of NH and OH proton signals is assigned to its intramolecular hydrogen bonding interactions leading to a decrease in the electron density around the proton. Absence of a singlet peak corresponding to –CH proton substantiates the existence of imine-ol tautomer of the compound in solution. However, in the solid state, the compound is in its keto-imine form. The peak corresponding to OH is absent in DFT model, as the keto form obtained from single crystal XRD is used for this calculation. In DFT, the NH peak is observed at 7.4359 ppm. In DFT, the CH proton shows a singlet at 5.148 ppm. Aromatic protons give multiplet peaks in the region, 7.159–7.662 ppm. The peak observed at 3.179 ppm may be due to $^4N–CH_3$. Methyl protons in the substituted pyrazolone show peaks at 1.5 ppm. The DFT computation predicts $^4N–CH_3$ peak in the range 3.1–4.2 ppm and methyl protons of the substituted pyrazolone show peak in the range 2.1–2.5 ppm. The slight discrepancies observed in the experimental and theoretical spectra may be due to the existence of imine-ol tautomer and intra-molecular hydrogen bonding in the compound.

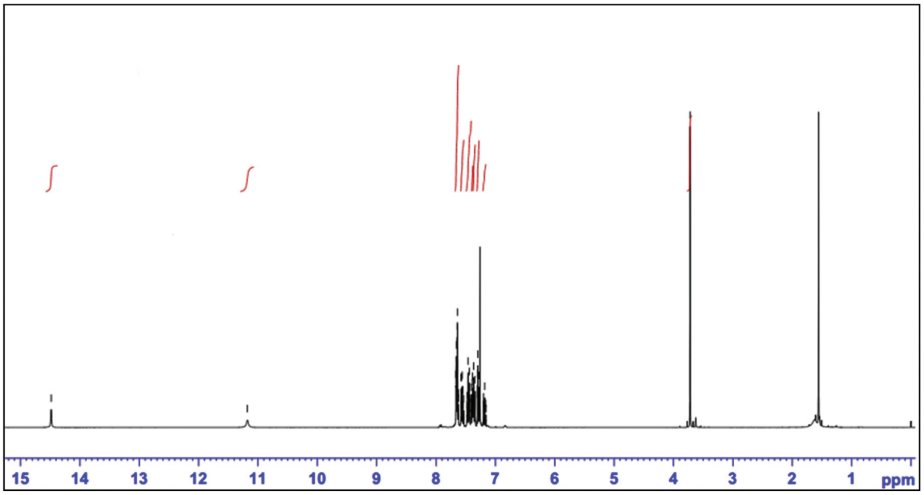

Fig. 5. Experimental ^{1}H NMR spectra of the compound.

7. Electronic spectrum

The maximum absorption wavelength (λ_{max}), oscillator strength (f), excitation energy (E_{ex}) and combination of electronic transitions of the molecule were calculated in chloroform by TD-DFT method at B3LYP/6-31+G level and compared the values with electronic absorption spectrum of the compound in chloroform in the range of 200–900 nm. Experimental UV–Vis absorptions were at 256, 318, 357 and 415 nm. The absorption bands observed below 350 nm may be attributed to the π-π* transitions of the azomethine chromophore and the benzene ring (intra-ligand charge - transfer). Those found above 350 nm may be due to n-π* transitions. It is very interesting to note that a single broad absorption in the theoretical spectrum ranging from 275 to 410 nm is observed as three singlets at 322.46 (f = 0.0374), 334.35 (f = 0.3483), and 386.12 nm (f = 0.0038) in the Gaussian output file. Thus, the observed single absorption may be a superimposed Gaussian peak of the revealed three singlets. Fig. 6 depicts theoretical and experimental spectra of the compound in chloroform.

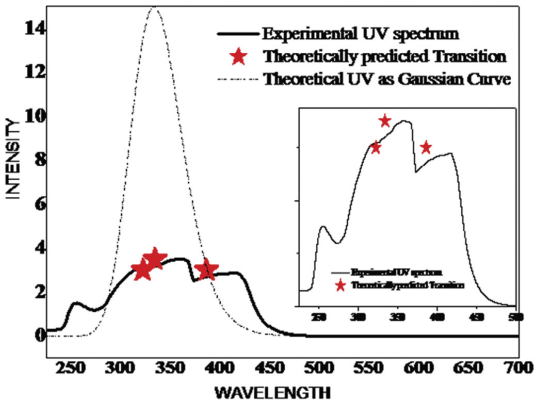

Fig. 6. Theoretical and Experimental electronic spectra in chloroform.

8. Frontier orbital approach

On the basis of frontier molecular orbital approach, the HOMO, HOMO-1, LUMO, LUMO+1 orbitals are mainly responsible for electronic transitions. Here, transitions originating from the highest occupied molecular orbital (HOMO) to the lowest unoccupied molecular orbital (LUMO) is n→ π* type. The transitions from HOMO-1→LUMO is characterized as π→ π* type. Fig. 7 shows the isosurfaces of the frontier molecular orbital on which charge density is localized. Theoretically, HOMO-LUMO energy gap is found to be 3.865ev, and experimentally it was 3.87ev. By evaluating the HOMO-LUMO energy gap, we can firmly state that intra-molecular charge exchange (ICT) is taking place between donor and acceptor moieties of the molecule, which is a good sign of its biological activity [47]. The HOMO-LUMO energy gap is also an identification factor of stability index [48]. The small energy gap shows high chemical reactivity and low kinetic stability of the compound [49].

9. Computation of global reactivity descriptors

According to the Koopmans' theorem [50], through equations $A = -E_{LUMO}$, $I = -E_{HOMO}$, the HOMO and LUMO orbital energies are related to gas phase vertical ionization energies (I) and vertical electron affinities (A) of the isomers. Electron affinity indicates the potential of a compound to accept precisely one electron from a donor. By using HOMO and LUMO energy values, global descriptors such as chemical hardness $\eta = (I - A)/2$, chemical softness $\zeta = 1/2\eta$, chemical potential $\mu = (E_{LUMO} + E_{HOMO})/2$ and the global electrophilicity index $\omega = \mu^2/2\ \eta$ can also be calculated. Calculated global descriptors are shown in the Table 3. Physically, chemical potential μ describes the escaping tendency of electrons from an equilibrium system [51]. Electrophilicity index is a measure of the stabilization in energy after a system accepts additional amount of electronic charge from the environment. When two molecules react, which one will act as an electrophile (nucleophile) will depend upon higher (lower) value of electrophilicity index [52].

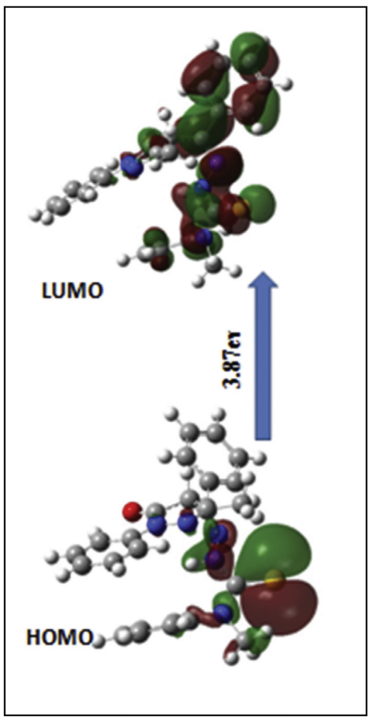

Fig. 7. showing the isosurfaces of the frontier molecular orbitals.

Table 3
Calculation of Global descriptors.

Global Descriptive Parameters			
Homo	−5.71	Softness ζ	0.259
Lumo	−1.84	Chemical potential μ	−3.78
Vertical Ionisation energy I	5.71	Electronegativity	3.78
Vertical Electron affinity A	1.84	Globalelectrophilic index ω	3.69
Hardness η	1.93		

10. Mulliken population analysis

Mulliken atomic charges for the compound were calculated at the B3LYP/6-31+G (d,p) level in gas-phase and are presented in Table S1(supporting information). Mulliken population analysis is basis set dependent and is used to determine the electron density of each atom [53]. Mulliken atomic charges show that all the hydrogen atoms in the molecule have positive charge density and negative charge density for the oxygen, nitrogen and sulphur atoms. It has also been observed that some carbon atoms are positive, while some others show negative charge density. The negative charge density of oxygen appears as −0.3618 esu, which is significantly larger than those of the other atoms bearing negative charges. This shows that oxygen can acts as donor site for traditional hydrogen bonding [54]. From single crystal XRD data, it is clear that the crystal packing is stabilized by intramolecular (N–H––O) hydrogen bonding. This type of charge allocation generates a total dipole moment of 3.2829 Debye.

11. Molecular electrostatic potential map (MEP)

The electrophilic and nucleophilic sites in a molecule can easily be identified with the help of molecular electrostatic potential map (MEP) which in turn determines the chemical reactivity of a compound which is responsible for non-covalent interactions [55]. For this reason, the MEP has been calculated for the compound at the B3LYP/6-31+G (d,p) level (Fig. 8). The ascending order of potential at the surface is represented by different colours, red < orange < yellow < green < blue. Red represents regions of most negative electrostatic potential, blue represents regions of most positive electrostatic potential and green represents regions of zero potential. In the MEP map of our molecule, the most negative region is positioned on the O, N and S atoms which can be considered as potential site for electrophilic attack. However, the maximum positive region is located on the H atom attached to nitrogen. This also shows a possible site for nucleophilic attack. Based on the MEP map, intra- and intermolecular interactions observed in the solid state can be accounted.

12. Natural bond orbital analysis (NBO)

It gives a profound insight into the intra and intermolecular orbital interactions in the molecules between filled donor and empty acceptor NBOs. It also provides a convenient basis for investigating charge transfer or conjugative interactions in molecular systems [56]. Second order perturbation energy will give clear information regarding the origin of stabilization of the molecule by analyzing the interactions between an occupied Lewis NBO (bond pair or lone pair) as donor and an unoccupied non-Lewis NBO (antibonding or Rydberg) as acceptor [57]. In order to elucidate the intramolecular, rehybridization and delocalization of electron density within the molecule, NBO analysis has been performed on the molecule at the DFT/B3LYP/6-31G (d,p) level. From the NBO analysis, it is found that the π-bond is characterized by p-orbital only i.e. contribution from s-orbital is zero. All the other bonds present are sigma bonds and have an occupancy value close to 1.9. NBO analysis allowed us to understand which orbital interactions are primarily involved in the stability of the observed conformer. Since the occupancies of filled NBOs are highly condensed, the delocalizing interactions can be further treated by the second-perturbation energies $E^{(2)}$,

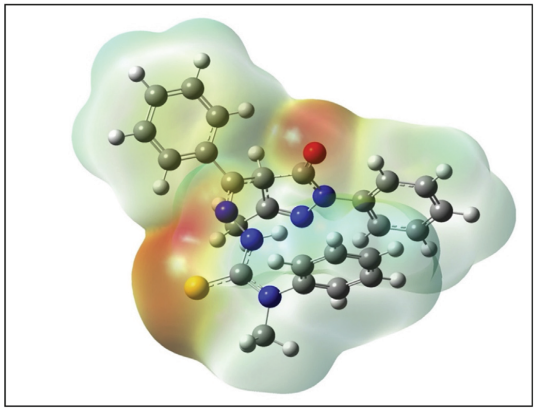

Fig. 8. Molecular electrostatic potential map.

$E^{(2)} = -\ q_i\ F_{ij}\ /\varepsilon_i - \varepsilon_j$

where q_i is the population of donor orbital or donor orbital occupancy; ε_i, ε_j are orbital energies of donor and acceptor NBO orbitals, respectively and F_{ij} is the off-diagonal Fock or Kohn–Sham matrix element between i and j NBO orbitals [58].

Several donor–acceptor interactions have been observed among the strongly occupied NBOs of the compound (Table 4). The most important delocalization sites are seen in the π system and in the lone pairs (n) of the oxygen, sulphur and nitrogen atoms. The larger the $E^{(2)}$ value, the more intense is the interaction between electron donors and electron acceptors, *i.e.* more the donating tendency from electron donors to electron acceptors, greater the extent of conjugation of the whole system.

The most important interaction energy, related to the resonance in the molecule, is electron donation from LP (1) C (35) to the antibonding acceptor π* C (34)–N (48) with enormous stabilization energy of 412.75 kcal mol^{-1}. Further, LP (1) C (35) conjugate with π *C (37)–C (39) leading to a stabilization energy of 63.82 kcal mol^{-1}. LP (1) N (45) and LP (1) N (46) stabilize thiosemicarbazide moeity *via* conjugation with σ*C (16)–S (54) leading to the stabilization energies of 79.89 and 49.01 kcal mol^{-1}, respectively. Intramolecular O...H–N hydrogen bond interactions are shown in the NBO analysis by the interaction between the O lone pair and N–H antibonding orbital [LP (1) O (33) → σ * N (46)–H (55), LP (2) O (33) → σ * N (46)–H (55)] leading to an interaction energy of 10.83 and 19.4 $kcalmol^{-1}$. LP (2) O (33) NBO further conjugates with σ *C (32)-N (48) resulting to an energy of 24.74 kcal mol^{-1}.

From the Table 4, several ICT interactions are observed which are formed by the orbital overlap between bonding (π) and antibonding (π*) orbitals. They result in the stabilization of the system. The movement of p-electron cloud from donor to acceptor makes the molecule more polarized and it must be responsible for the NLO properties of the molecule. NBO analysis together with HOMO-LUMO energy gap and molecular electrostatic potential map of the molecule elucidates intra-molecular charge-transfer in the molecule.

13. Non linear optical property (NLO)

Organic molecules containing conjugated π electrons are characterized by large values of molecular first-order hyperpolarizability as analyzed by means of vibrational spectroscopy [59]. They can manipulate photonic signals as is important for nonlinear optics.

In order to explore NLO properties of the title compound, the total static dipole moment μ, the linear polarizability α, the anisotropy of polarizability Δα and the mean first order hyperpolarizability β_o are calculated by using the B3LYP method with 6-31+G (d,p) level in the gas phase of the compound based on the finite-field approach. The first-order hyperpolarizability is a third rank tensor that can be described by a 3 × 3 × 3 matrix. The 27 components of the 3D matrix can be reduced to 10 components due to Kleinman symmetry [60]. It can be given in the lower tetrahedral format. It is obvious that the lower part of the 3 × 3 × 3 matrices is tetrahedral. The components of β are the coefficients in the Taylor series expansion of the energy in the external electric field. For the calculation of μ, α, Δα and β_o are defined as follows [61]. The calculated data are given in Table 5.

$$\alpha_{total} = 1/3(\alpha_{xx}+\alpha_{yy}+\alpha_{zz})$$

$$\Delta\alpha = 1/2^{1/2}[(\alpha_{xx}\text{-}\alpha_{yy})^2 + (\alpha yy\text{-}\alpha_{zz})^2 + (\alpha_{zz}\text{-}\alpha_{xx})^2 + 6\alpha^2_{xz} + 6\alpha^2_{xy} + 6\alpha^2_{yz}]^{½}$$

$$\beta_o = [(\beta_{xxx}+\beta_{xzz}+\beta_{xyy})^2 + (\beta_{yyy}+\beta_{yxx}+\beta_{yzz})^2 + (\beta_{zzz}+\beta_{zxx}+\beta^2_{zyy})]^{1/2}$$

$$\mu_{total} = (\mu_x^2+\mu_y^2+\mu_z^2)^{1/2}$$

Since the polarizability and hyperpolarizability are reported in atomic units (a.u.), the calculated values have been converted by using 1a.u is 0.1482 $Å^3$ for α and 1a.u is 8.6393 × 10^{-30} for β. Urea is one of the reference materials, used for comparative purpose to study the NLO properties of organic compounds. The calculated dipole moment (μ), polarizability (α) and the mean first hyperpolarizability (β) for the compound are 3.2829 D, 28.0639 $Å^3$ and

Table 5
Calculated electric dipole moment, polarizability and first hyperpolarizability of the compound.

Polarisability	Hyperpolarisability
$\alpha_{XX} = -176.1604$	$\beta_{XXX} = -6.8175$
$\alpha_{XY} = 15.7388$	$\beta_{XYY} = 17.8458$
$\alpha_{YY} = -201.6986$	$\beta_{XZZ} = 27.4541$
$\alpha_{XZ} = 0.0255$	$\beta_{YYY} = -14.5805$
$\alpha_{ZZ} = -191.0043$	$\beta_{XXY} = -55.7806$
$\alpha_{YZ} = -5.9678$	$\beta_{YZZ} = 5.2974$
$\alpha_{total} = 28.0639\ Å^3$	$\beta_{ZZZ} = -3.9677$
$\Delta\alpha = 49.70691\ Å^3$	$\beta_{XXZ} = -26.8267$
μ = 3.2829Debye	$\beta_{YYZ} = -19.3684$
	$\beta_{total} = 7.83748 \times 10^{-31} cm^5 e.s.u$

Table 4
Major donor–acceptor interactions of title compound and their second-order perturbation energies (kcal/mol).

Donor NBO (i)	Acceptor NBO (j)	$E^{(2)}$ kcal/mol	$E_j - E_i$ a.u.	F_{ij} a.u.	Donor NBO (i)	Acceptor NBO (j)	$E^{(2)}$ kcal/mol	$E_j - E_i$ a.u.	F_{ij} a.u.
π C 5 - C 6	π* C 8 - C 10	20.31	0.3	0.07	π C 34 - N 48	π* C 32 - O 33	42.76	0.31	0.106
πC 5 - C 6	π*C 12 - C 14	20.44	0.3	0.07	π C 37 - C 39	LP (1) C 35	46.86	0.14	0.09
πC 8 - C 10	π* C 5 - C 6	21.27	0.29	0.07	πC 37 - C 39	π* C 41 - C 43	22.38	0.29	0.072
π C 8 - C 10	π* C 12 - C 14	20.58	0.29	0.07	π C 41 - C 43	π*C 34 - N 48	37.27	0.19	0.089
πC 12 - C 14	π*C 5 - C 6	22.43	0.29	0.072	πC 41 - C 43	π*C 37 - C 39	21.01	0.29	0.07
π C 12 - C 14	π* C 8 - C 10	20.36	0.29	0.069	LP (1) O 33	RY*(1) C 32	11.62	1.62	0.123
π C 18 - C 19	π* C 21 - C 23	19.58	0.29	0.068	LP (1) O 33	σ* N 46 - H 55	10.83	1.23	0.104
π C 18 - C 19	π* C 25 - C 27	20.87	0.28	0.069	LP (2) O 33	σ* C 29 - C 32	12.69	0.74	0.088
πC 21 - C 23	π* C 18 - C 19	20.31	0.29	0.069	LP (2) O 33	σ* C 32 - N 48	24.74	0.73	0.122
π C 21 - C 23	π* C 25 - C 27	21.71	0.28	0.07	LP (2) O 33	σ*N 46 - H 55	19.4	0.82	0.114
π C 25 - C 27	π* C 18 - C 19	20.15	0.3	0.069	LP (2) S 54	σ* C 16 - N 45	11.27	0.65	0.078
π C 25 - C 27	π* C 21 - C 23	20.43	0.29	0.069	LP (2) S 54	σ* C 16 - N 46	12.83	0.62	0.081
σC 29 - H 30	π*C 17 - N 47	17.5	0.54	0.087	π* C 17 - N 47	π* C 18 - C 19	11.03	0.04	0.033
σC 29 - H 30	π* C 31 - N 49	17.54	0.53	0.086	π*C 25 - C 27	π* C 18 - C 19	250.06	0.01	0.082
σC 29 - H 30	π*C 32 - O 33	22.53	0.51	0.101	π* C 34 - N 48	π*C 31 - N 49	14.79	0.04	0.03
π C 34 - N 48	π*C 31 - N 49	14.24	0.33	0.062	π* C 34 - N 48	π* C 32 - O 33	134.1	0.02	0.059
					π*C 34 - N 48	π* C 41 - C 43	83.04	0.09	0.1

0.783748 × 10^{-30}cm^{5}e.s.u., respectively, as compared with those of urea, 1.3732 D, 3.8312 Å^3 and 0.37289 × 10^{-30} cm.^{5}e.s.u., respectively, for B3LYP/631+G (d,p). Theoretically, the first-order hyperpolarizability (β) of our compound is 2 times higher than that of urea. It is also found that the compound shows two-fold higher value of linear polarizability (α) and the dipole moment than urea. These results indicate that the present compound possess good non-linear optical properties and can be used in future studies in this area.

14. Molecular docking

Cancer therapies target cell cycle-based mechanism which imitates the body's natural process to prevent the growth of cancer cells. This approach can limit the damage to normal cells and the associated side effects caused by usual chemotherapeutic agents. The motivation behind the selection of histone deacetylase8 (HDAC8), ribonucleotide reductase (RR2) and DNA methyl transferase (DMT), as anticancer targets in the present investigation is due to their involvement in different cell growth and metabolism such as biosynthesis of DNA, gene silencing, transcriptional control and chromatin structure modulation.

The ligand under study was docked into the binding sites of the proteins. The docking calculation generated few poses for the ligand. The selection of the best pose was done based on the interaction energy between the ligand and the protein. The least negative XP g-score (negative value) indicates the best binding score for the ligand with protein. Docking simulation of the compound within the active site of the receptors has been analyzed (Fig. 9). The anticancer activity of the compound was measured based on the glide score, glide energy and protein-ligand binding characteristics. The glide score and glide energy are shown in Table 6.

The amino acid residues in the active site of ribonucleotide reductase are Glu 232, Gly 233, Le 234, Phe 236, Ser 237, Val 327, Arg 330, Leu 331, Glu 334, Asp 231, Cys 270, Leu 268, Gly 267, Glu 266, Arg 264 and Ser 263. The compound was docked deeply into the active site region making interactions with the residues Asp 271 and Ser 263. Some very prominent interactions between the compound and the active site residues Val 661 and Glu 663 of DNA methyl transferases were observed. The other residues that were found in the locality of this docked ligand were Leu 635, Phe 636, Asp 637, Gly 638, Le 639, Ala 640, Thr 641, Gly 642, Glu 752, Trp 889, Ser 888, Arg 887, Ser 665, Cys 662, Gly 660, Ser 659, Gly 703, Ser 704, Pro 705, Cys 706, Cys 662, Val 661, Glu 660 Asp 682, Val 683, Arg 684 and Leu 726. The amino acid residues in the active site of Histone deacetylase8 are Arg-37, Le-34, Lys-33, Tyr-306, Gly-305, Gly-304, Gly-303, Asp-178, He-180, Gly-151, Phe-152, Cys-153, Asp-101, Asp-267, Phe-208, His-143 and Trp-141. The compound L_1 binds in the pockets defined by Tyr-306, Lys-33 of histone deacetylase8. It is found that the compound is able to bind all the selected targets. Hence, the compound is a promising candidate for anticancer studies. It can be validated in wet lab studies for its proper function.

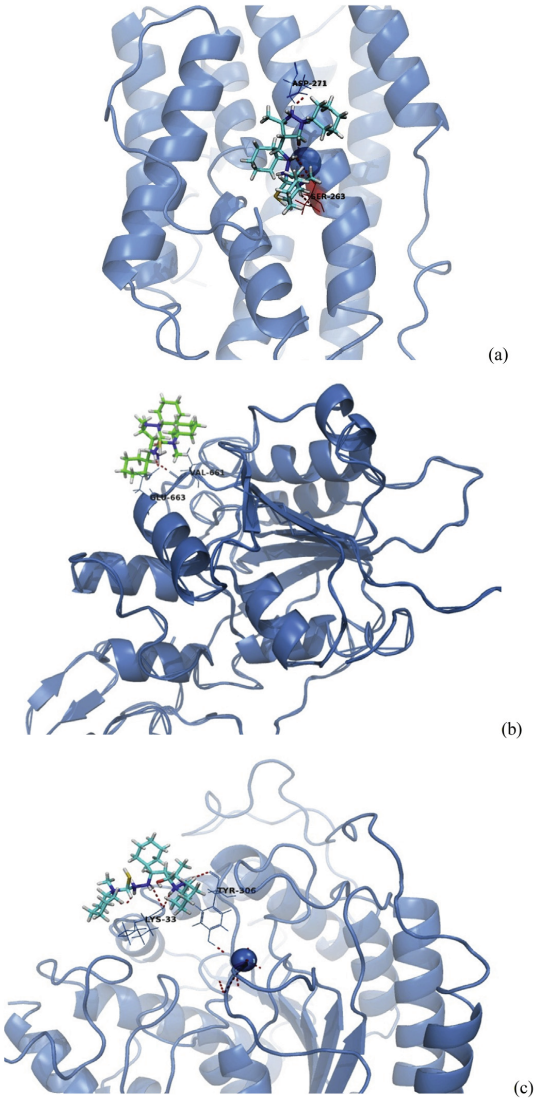

Fig. 9. Docked pose of the inhibitor inside the binding pockets of proteins (a) (PDB ID: 2UW2) (b) (PDB ID: 2QRV) (c) (PDB ID: 1T69) depicted in ribbon style, black letters shows the amino acids involved in the bonding and compounds are shown in capped stick model.

15. Conclusions

The single crystal of 1-phenyl-3-methyl-4-benzoyl-5-pyrazolone N (4)-methyl-N (4)-phenylthiosemicarbazone was grown by slow evaporation of a 1:1 DMSO-methanol solution at room temperature. The red shift of the C=O stretching band in the infrared spectrum from the computed one indicates the weakening of the C=O bond. It may be due to the presence of hydrogen bond vibrations in the crystal leading to strong perturbation of the infrared band. The experimental and theoretical UV–Vis spectral analysis provide information about the excitation energy, oscillator strength and predict mainly the n→ π*, π → π* type electronic transitions which are intra-molecular charge-transfer type. Slight differences between the theoretical and experimental electronic spectral data may due to the participation of the carbonyl group in intra-molecular hydrogen bonding and the tautomerism existing in the molecule. Further, small HOMO–LUMO energy gap accounts for the possibility of charge-transfer in the compound. NBO analysis also gives insight to the strongly delocalized structure, responsible for the nonlinearity and hence the stability of the molecule.

Table 6
Glide score and Glide energy of compound L_1.

Protein	Glide score	Glide energy
Ribonucleoside diphosphate reductase M2subunit (**RR2**) (PDB ID: 2UW2)	−4.386865	−48.885156
DNA Methyl transferase (**DMT**) (PDB ID: 2QRV)	−2.35165	−37.04767
Histone deacetylase 8 (**HDAC8**) (PDB ID: 1T69)	−3.108071	−31.370547

Theoretically, the linear polarizability (α) of the compound is 9 times higher than that of urea. It is also found that the compound shows two-fold higher value of first order hyperpolarizability(β) and the dipole moment than urea. These results indicate that the compound is suitable for further studies as non-linear optical material. The docking score and -energy draw us to the conclusion that the investigated compound might exhibit anticancer activity. However, *in vitro* and *in vivo* analyses need to be done to validate the computational predictions.

Acknowledgements

The authors are grateful to SAIF, Cochin University of Science and Technology, Kochi, Kerala, India for elemental analyses and NMR spectral analysis. We are thankful to SAIF Cochin, India for providing single crystal XRD result. We are also thankful to Department of Biotechnology and Microbiology, School of Life sciences, Kannur university Kerala, India for providing software for molecular docking studies. The University Grants Commission (UGC) India is also gratefully acknowledged for financial support.

Appendix A. Supplementary data

Supplementary data related to this article can be found at http://dx.doi.org/10.1016/j.molstruc.2017.08.078.

References

[1] D.X. West, S.B. Padhyé, P.B. Sonawane, R.C. Chikate, Copper(II) complexes of tridentate (O, N,S) thiosemicarbazones, Asian J. Chem. Rev. 4 (1990) 125.
[2] E. De Clercq, Vaccinia virus inhibitors as a paradigm for the chemotherapy of poxvirus infections, Clin. Microb. Rev. 14 (2) (2001) 382.
[3] D.K. San, R.J. Butcher, S. Chandhuri, N. Saha, Spectroscopic, structural and antibacterial properties of copper(II) complexes with bio-relevant 5-methyl-3-formylpyrazole N(4)-benzyl-N(4)-methylthiosemicarbazone, Mol. Cell. Biochem. 253 (2003) 21.
[4] A. Perez-Rebolledo, G.M. de Lima, L.N. Gambi, N.L. Speziali, D.F. Maia, C.B. Pinheiro, Ardisson, M.E. Cortes, H. Beraldo, Tin(IV) complexes of 2-benzoylpyridine N(4)-phenyl-thiosemicarbazone: spectral characterization, structural studies and antifungal activity, Appl. Organomet. Chem. 17 (2003) 945.
[5] N. Fujii, J.P. Mallari, E.J. Hansell, Z. Mackey, P. Doyle, Y.M. Zhou, J. Gut, P.J. Rosenthal, J.H. McKerrow, R.K. Guy, Discovery of potent thiosemicarbazone inhibitors of rhodesain and cruzain, Bioorg. Chem. 15 (1) (2005) 121.
[6] D.C. Greenbaum, Z. Machey, E. Hansell, P. Doyle, J. Gut, C.R. Caffrrey, J. Lehrman, P.J. Rosenthal, J.H. McKerrow, K. Chibale, Synthesis and structure-activity relationships of parasiticidal thiosemicarbazone cysteine protease inhibitors against Plasmodium falciparum, Trypanosoma brucei, and Trypanosoma cruzi, J. Med. Chem. 47 (12) (2004) 3212.
[7] X. Du, C. Guo, E. Hansell, S.P. Doyle, C.R. Caffrey, T.P. Holler, J.H. McKerrow, F.E. Cohen, Synthesis and structure–activity relationship study of potent trypanocidal thiosemicarbazone inhibitors of the trypanosomal cysteine protease cruzain, J. Med. Chem. 45 (2002) 2695.
[8] Z. Afrasiabi, E. Sinn, J.N. Chen, Y.F. Ma, A.L. Rheingold, L.N. Zakharov, N. Rath, S. Padhye, Appended 1,2-naphthoquinones as anticancer agents 1; Synthesis, Structural, Spectral and antitumor activities of ortho-naphthaquinone thiosemicarbazone and its transition metal, Inorg. Biochem. Acta 357 (2004) 271.
[9] P. Yogeeswari, D. Sriram, L.R.J.S. Jit, S.S. Kumar, J.P. Stables, Anticonvulsant and neurotoxicity evaluation of some 6-chlorobenzothiazolyl-2-thiosemicarbazones, Eur. J. Med. Chem. 37 (2002) 231.
[10] A. Pérez-Rebolledo, L.R. Teixeira, A.A. Batista, A.S. Mangrich, G. Aguirre, H. Cerecetto, M. Gonzalez, P. Hernandez, A.M. Ferreira, N.L. Speziali, H. Beraldo, 4-nitroacetophenone-derived thiosemicarbazones and their copper(II) complexes with significant in vitro anti-trypanosomal activity, Eur. J. Med. Chem. 43 (2008) 939.
[11] R.K. Mahajan, I. Kaur, T.S. Lobana, A mercury(II) ion-selective electrode based on neutral salicylaldehyde thiosemicarbazone, Talanta 59 (2003) 101.
[12] Elena Pahontu Felicia Julea, Tudor Rosu, Victor Purcarea, Yurie Chumakov, Petru Petrenco, Aurelian Gulea, Antibacterial, antifungal and in vitro anti-leukaemia activity of metal complexes with thiosemicarbazones, J. Cell. Mol. Med. 19 (2015) 865.
[13] V. Narayan, H.N. Mishra, O. Prasad, L. Sinha, Electronic structure, electric moments and vibrational analysis of 5- nitro 2- furaldehyde semicarbazone: a D.F.T. study, Comput. Theor. Chem. 973 (2011) 20.
[14] A.A. El-Emam, A.M.S. Al-Tamimi, K.A. Al-Rashood, H.N. Misra, V. Narayan, O. Prasad, L. Sinha, Monomeric and Dimeric structures, electronic properties and vibrational spectra of azelaic acid by HF and B3LYP methods, J. Mol. Struct. 1022 (2012) 49.
[15] M.J. Frisch, G.W. Trucks, H.B. Schlegel, G.E. Scuseria, M.A. Robb, J.R. Cheeseman, G. Scalmani, V. Barone, B. Mennucci, G.A. Petersson, H. Nakatsuji, M. Caricato, X. Li, H.P. Hratchian, A.F. Izmaylov, J. Bloino, G. Zheng, J.L. Sonnenberg, M. Hada, M. Ehara, K. Toyota, R. Fukuda, J. Hasegawa, M. Ishida, T. Nakajima, Y. Honda, O. Kitao, H. Nakai, T. Vreven, J.A. Montgomery Jr., J.E. Peralta, F. Ogliaro, M. Bearpark, J.J. Heyd, E. Brothers, K.N. Kudin, V.N. Staroverov, T. Keith, R. Kobayashi, J. Normand, K. Raghavachari, A. Rendell, J.C. Burant, S.S. Iyengar, J. Tomasi, M. Cossi, N. Rega, J.M. Millam, M. Klene, J.E. Knox, J.B. Cross, V. Bakken, C. Adamo, J. Jaramillo, R. Gomperts, R.E. Stratmann, O. Yazyev, A.J. Austin, R. Cammi, C. Pomelli, J.W. Ochterski, R.L. Martin, K. Morokuma, V.G. Zakrzewski, G.A. Voth, P. Salvador, J.J. Dannenberg, S. Dapprich, A.D. Daniels, O. Farkas, J.B. F. Gaussian 09, Revision D.01, Gaussian, Inc, Wallingford CT, 2013.
[16] R.G. Parr, W. Yang, Density Functional Theory of Atoms and Molecules, New York, Oxford, 1989.
[17] V. Krishnakumar, N. Prabavathi, S. Muthunatesan, Structure and vibrational frequencies of 1-naphthaldehyde based on density functional theory calculations, Spectrochim. Acta A 69 (2008) 528.
[18] B.K. Schoichet, Virtual screening of chemical libraries, Nature 43 (2004) 862.
[19] S. Balasubramanian, J. Ramos, W. Luo, M. Sirisawad, E. Verner, J.J. Buggy, A novel histone deacetylase 8 (HDAC8)-specific inhibitor PCI-34051 induces apoptosis in T- cell lymphomas, Leukemia 22 (5) (2008) 1026.
[20] G. Nocentini, W.E. Maerner, S.M. Silence, Ribonucleotide reductase inhibitors: new strategies for cancer, Polymeric photorefractive materials, Chem. Rev. 94 (1994) 127.
[21] M. Ehrlich, DNA methylation in cancer: too much, but also too little, Oncogene 21 (2002) 5400.
[22] J.P. Scovill, D.L. Klayman, C.F. Franchino, 2-Acetylpyridine thiosemicarbazones. 4. Complexes with transition metals as antimalarial and antileukemic agents, J. Med. Chem. 25 (1982) 1261.
[23] B.S. Jensen, The synthesis of 1-phenyl-3-methyl-4-acyl-pyrazol-5ones, Acta Chem. Scand. 13 (1959) 1668.
[24] G.H. Sheldrick, SHELXL 97. Program for Crystal Structure Refinement, University of Göttingen, Göttingen, Germany, 1997.
[25] A.L. Speck, PLATON a Multipurpose Crystallographic Tool, Utrecht University, Utrecht, The Netherlands (, 1999.
[26] L.J. Farrugia, WinGX and ORTEP for windows: an update, J. Appl. Cryst. 45 (2012) 849.
[27] C.F. Macrae, P.R. Edington, P. McCabe, E. Pidcock, G.P. Sheilds, R. Taylor, M. Towler, J. Van de Streek, Mercury: visualization and analysis of crystal structures, J. Appl. Cryst. 39 (2006) 453.
[28] S.A. Khan, A.M. Asiri, K. Sharma, Synthesis of steroidal thiazolidinones as antibacterial agents based on the in vitro and quantum chemistry calculation, Med. Chem. Res. 22 (2013) 1998.
[29] A.P. Scott, L. Radom, Harmonic vibrational Frequencies: an evaluation of Hartree–Fock, Mølller–Plesset, quadratic configuration interaction, density functional theory, and semiempirical scale factors, J. Phys. Chem. 100 (1996) 16502.
[30] A. Ricca, C.W. Bauschlicher Jr., Successive H_2O binding energies for $Fe(H_2O)n+$, J. Phys. Chem. 99 (1995) 9003.
[31] R.D. Dennington, T.A. Keith, J.M. Millam, GaussView 5.0. 8, Gaussian Inc, 2008.
[32] J.J. Blessy, D.J.S. Sharmila, Molecular simulation of N acetylneuraminic acid analogs and molecular dynamics studies of cholera toxin-Neu5Gc complex, J. Biomol. Struct. Dyn. 33 (5) (2015) 1126.
[33] G.A. Kaminski, R.A. Friesner, J. Tirado-Rives, W.L. Jorgensen, Evaluation and reparametrization of the OPLS-AA force field for proteins via comparison with accurate quantum chemical calculations on peptides, J. Phys. Chem. B 105 (2001) 6474.
[34] K.O. Ferraz, S.M.S.V. Wardell, J.L. Wardell, S.R.W. Louro, H. Beraldo, Copper(II) complexes with 2-pyridineformamide-derived thiosemicarbazones: spectral studies and toxicity against Artemia salina, Spectrochim. Acta. A 73 (2009)

140.
[35] V. Suni, M.R.P. Kurup, M. Nethaji, Structural and spectral perspectives of a novel thiosemicarbazone synthesized from di-2-pyridyl ketone and 4-phenyl-3-thiosemicarbazide, Spectrochim. Acta A 63 (2006) 174.
[36] E.M. Jouad, M. Allain, M.A. Khan, G.M. Bouet, Structural and spectral studies of thiosemicarbazones derived 3-furadehyde and 3-(2-furyl)prop-2-enal, J. Mol. Struct. 604 (2002) 205.
[37] Ç. Yüksektepe, N. Çalişkan, M. Genç, S. Servi, Synthesis, crystal structure, HF and DFT calculations of 1-(2-chlorobenzyl)-N-(1-(2-chlorobenzyl)-4,5-dihydro-1H-imidazol-2-yl)-1H-benzimidazol-2-amine, Crystallogr. Rep. 55 (2010) 1188.
[38] M. Silverstein, G.C. Bassler, C. Morril, Spectroscopic Identification of Organic Compounds, John Wiley, Newyork, 1981.
[39] D.X. West, N.M. Kozub, G. Bain, Copper(II) complexes of 2-formyl-, 2-acetyl- and 2-benzoyl-pyridine N(4)-phenyl-, N(4)-o-methoxyphenyl-, N(4)-p-methoxy-phenyl- and N(4)-p-nitrophenylthiosemicarbazones, Transit. Met. Chem. 21 (1996) 213.
[40] V. Selvarani, B. Annaraj, M.A. Neelakantan, S. Sundaramoorthy, D. Velmurugan, Synthesis and crystal structure of hydroxyacetophenone Schiff bases containing propargyl moiety: solvent effects on UV–visible spectra, Spectrochim. Acta, Part A 91 (2012) 329.
[41] M. Belicchi Ferrari, S. Capacchi, G. Pelosi, G. Reffo, P. Tarasconi, R. Albertini, S. Pinelli, P. Lunghi, Synthesis, structural characterization and biological activity of helicin thiosemicarbazone monohydrate and a copper (II) complex of salicylaldehyde thiosemicarbazone, Inorg. Chim. Acta 286 (1999) 134.
[42] Y. Sun, Y. Wang, Z. Liu, C. Huang, C. Yu, Structural, proton-transfer, thermodynamic and nonlinear optical studies of (E)-2-((2-hydroxyphenyl)iminiomethyl)phenolate, Spectrochim. Acta A 96 (2012) 42.
[43] G. Varsányi, Assignment for Vibrational Spectra of Seven Hundred Benzene Derivatives, Akadémiai Kiadó, Budapest, 1974.
[44] A. Srivastava, Rashmi Mishra, Sudhir Kumar Kapil Dev, Poonam Tandon, Rakesh Maurya, Molecular structure, spectral investigation (1 H NMR, 13C NMR, UV–Visible, FT-IR, FT-Raman), NBO, intramolecular hydrogen bonding, chemical reactivity and first hyperpolarizability analysis of formononetin [7-hydroxy-3(4-methoxyphenyl)chromone]: a quantum chemical study, J. Mol. Struct. 1084 (2015) 55.
[45] M. Yildiz, H. Unver, D. Erdener, A. Kiraz, N.O. Iskeleli, Synthesis, spectroscopic studies and crystal structure of (E)-2-(2, 4-dihydroxybenzylidene) thiosemicarbazone and (E)-2-[(1H-indol-3-yl)methylene], J. Mol. Struct. 919 (2009) 227.
[46] L.G. Crane, D. Wang, L.M. Sears, B. Heyns, K. Carron, SERS surfaces modified with a 4-(2-pyridylazo)resorcinol disulfide derivative: detection of copper, lead, and cadmium, Anal. Chem. 67 (1995) 360.
[47] E. Kavitha, N. Sundaraganesan, S. Sebastian, Molecular structure, vibrational spectroscopic and HOMO, LUMO studies of 4-nitroaniline by density functional method, Indian J. Pure Appl. Phy. 48 (2010) 20.
[48] A.A.R. Despaigne, J.G. Da Silva, A.C.M. Do Carmo, F. Sives, O.E. Piro, E.E. Castellano, H. Beraldo, Copper (II) and zinc (II) complexes with 2-formylpyridine-derived hydrazones, Polyhedron 28 (2009) 3797.
[49] I.F.F. Orbitals, Organic Chemical Reactions, John Wiley and Sons, New York, 1976.
[50] Tjalling Koopmans, Über die Zuordnung von Wellenfunktionen und Eigenwerten zu den einzelnen Elektronen eines Atoms, Physica 1 (1934) 104. Elsevier.
[51] P.K. Chattaraj, B. Maiti, HSAB principle applied to the time evolution of chemical reactions, J. Am. Chem. Soc. 125 (2003) 2705.
[52] R.K. Singh, A.K. Singh, Synthesis, molecular structure, spectral analysis, natural bond order and intramolecular interactions of 2-acetylpyridine thiosemicarbazone: a combined DFT and AIM approach, J. Mol. Struct. 1094 (2015) 61.
[53] E.R. Davidson, S. Chakravorty, A test of the Hirshfeld definition of atomic charges and moments, Theor. Chim. Acta 83 (1992) 319.
[54] B.S. Kusmariya, A.P. Mishra, Experimental, theoretical and docking studies of 2-hydroxy Schiff base type compounds derived from 2-amino-4-chlorobenzenethiol, J. Mol. Struct. 1101 (2015) 176.
[55] E. Scrocco, J. Tomasi, in: P. Lowdin (Ed.), Advances in Quantum Chemistry, Academic Press, New York, 1978.
[56] E. Scrocco, J. Tomasi, Topics in Current Chemistry, vol. 42, Springer-Verlag, Berlin, 1973.
[57] A. Reed, L.A. Curtiss, F. Weinhold, Intermolecular interactions from a natural bond orbital, donor-acceptor viewpoint, Chem. Rev. 88 (1988) 899.
[58] M. Del zoppo, C. Castiglioni, G. Zerbi, A novel approach to estimate N.L.O. Response in organic conjugated molecules from vibrational spectra: molecules with large.BETA. values, Non-Linear Opt. 9 (1995) 73.
[59] D.A. Kleinman, Nonlinear dielectric polarization in optical media, Phys. Rev. 126 (1962) 1977.
[60] Y.P. Tian, W.T. Yu, C.Y. Zhao, M.H. Jiang, Z.G. Cai, H.K. Fun, Structural characterization and second-order nonlinear optical properties of zinc halide thiosemicarbazone complexes, Polyhedron 21 (2002) 1217.
[61] R. Zhang, B. Du, G. Sun, Y. Sun, Experimental and theoretical studies on o-, m- and p-chlorobenzylideneaminoantipyrines, Spectrochim. Acta Part A Mol. Biomol. Spectrosc. 75 (2010) 1115.

Inorganica Chimica Acta 469 (2018) 25–31

Contents lists available at ScienceDirect

Inorganica Chimica Acta

journal homepage: www.elsevier.com/locate/ica

Research paper

Synthesis, structural and spectroscopic studies of 1-phenyl-3-methyl-4-benzoyl-5-pyrazolone N(4)-methyl-N(4)-phenyl thiosemicarbazone and its cadmium(II) complex

K.G. Sangeetha *, K.K. Aravindakshan

Department of Chemistry, University of Calicut, 673635 Kerala, India

ARTICLE INFO

Article history:
Received 14 April 2017
Received in revised form 21 August 2017
Accepted 22 August 2017
Available online 23 August 2017

Keywords:
Single crystal
Pyrazolone
Cadmium(II) complex
Electronic spectra
Thiosemicarbazones

ABSTRACT

Synthesis, spectral and single crystal XRD studies of a novel ligand 1-phenyl-3-methyl-4-benzoyl-5-pyrazolone N(4)-methyl-N(4)-phenylthiosemicarbazone and its cadmium(II) complex have been communicated in this work. The ligand crystallizes in triclinic system with space group *P*-1, *a*(Å) = 7.8930(4), *b*(Å) = 11.2019(5), *c*(Å) = 13.0211(7); *α*(°) = 96.175(3), *β*(°) = 100.922(3)°, *γ*(°) = 91.005(3)°, *V*(Å^3) = 1123.02(10), *r*(mg/m^3) = 1.306 and *Z* = 2. Cadmium(II) complex crystallizes in the monoclinic crystal system with space group $P2_1/c$, unit cell dimensions *a*(Å) = 9.6939(5), *b*(Å) = 22.5183(11), *c*(Å) = 21.2054(10); *α*(°) = 90, *β*(°) = 99.960(2), *γ* (°) = 90, *V*(Å^3) = 4559.2(4) and *Z* = 4. The packing of the molecules in the crystal lattice is stabilized by intermolecular hydrogen bonds. Spectroscopic data along with crystal structure, confirmed the involvement of azomethine nitrogen, thione sulphur and enolic oxygen of pyrazolone moiety in coordination with the metal ion.

1. Introduction

Thiosemicarbazones and their metal complexes have gained considerable attention in many research areas because of their unique chemical and biological properties [1,2]. The flexibility of their structures in terms of coordination and their ability to behave as neutral as well as anionic ligands increased our interest in this area [3,4]. They can exist in *E* form (*trans*-) and *Z* form (*cis*-) [5]. Generally, they coordinate to the metal ions in *Z*-form which is attributed to the chelate effect on complexation. When an extra coordination functionality is present near to the donor centres of thiosemicarbazones, they act as tridentate ligands.

Nowadays, coordination chemistry of cadmium(II) has been studied substantially because of the fatal environmental impact of cadmium. The mobilization and immobilization of cadmium in the surroundings, in organisms, and in some practical processes have been shown to depend significantly on the complexation of the metal center by chelating nitrogen donor ligands. Furthermore, chelating sulphur donors are under investigation as antidotes in cadmium(II) poisoning [6,7]. Now, many research groups are focusing on the fabrication of novel luminescent cadmium complexes as emitters and electron transporters in OLED [8–11].

In addition, cadmium complexes appear to be more fascinating from a structural point of view because of the ability of the cation to vary both coordination numbers and geometries. It is found that Cd(II) forms 4-coordinate and tetrahedral complexes with monodentate ligands, while with bidentate chelating ligands it forms 6-coordinate and octahedral complexes [12,13]. Crystal structures of cadmium halide complexes of 2-pyridineformamide N(4)-thiosemicarbazone are reported by Alfonso Castineiras *et al.* [14]. Here cadmium(II) is pentacoordinated with tridentate thiosemicarbazone and two halide ions as ligands.

Growth of single crystals and their characterisation for device fabrication have assumed immense thrust due to their importance in both academic- as well as applied research fields. Here, we report the synthesis and characterization of a novel ligand, 1-phenyl-3-methyl-4-benzoyl-5-pyrazolone N(4)-methyl-N(4)-phenylthiosemicarbazone and its Cd(II) complex using infrared-, electronic- and ^{1}H NMR spectral- and single crystal X-ray diffraction analyses.

2. Experimental

2.1. Materials and methods

Elemental analyses (C, H, N and S) were performed on Vario EL III elemental analyzer. Infrared (IR) spectra were recorded on a

* Corresponding author.
E-mail addresses: sangtkg@gmail.com (K.G. Sangeetha), aravindkuttamath@yahoo.com (K.K. Aravindakshan).

http://dx.doi.org/10.1016/j.ica.2017.08.046
0020-1693/

Jasco-FT-IR-4100 model spectrometer using KBr pellets. The electronic spectra were recorded on JascoV-550 UV–Vis model spectrometer. NMR was recorded on 400 MHz Bruker Avance III FT NMR spectrometer. Carbon disulphide (Merck), *N*-methyl aniline (SRL), hydrazine hydrate 98% (Glaxo fine chemicals), ethylacetoacetate (Merck), phenyl hydrazine, benzoyl chloride, cadmium acetate (Merck), etc were used as received. The solvents were purified and dried by using standard procedures.

2.2. Synthesis of ligand [H_2L] (**1**)

N(4)-Methyl-N(4)-phenylthiosemicarbazide was prepared by taking up and modifying the procedure reported by Scovill [15]. 1-Phenyl-3-methyl-4-benzoyl-5-pyrazolone was prepared by using Jenson's method [16,17]. The ligand was prepared by stirring the hot methanolic solution of 1-phenyl-3-methyl-4-benzoyl-5-pyrazolone (PMBP) (750 mg, 2.76 mmol) and N(4)-methyl-N(4)-phenylthiosemicarbazide (MPTSC) (500 mg, 2.76 mmol) on a magnetic stirrer, followed by refluxing at 60-80 °C for 30 min. The ligand formed was filtered and washed with methanol and dried over anhydrous $CaCl_2$.

Yield: 80%, m.p (163 °C), IR(KBr) ν_{max}/cm^{-1}: 3411(NH), 1626 (C═O), 1024, 1106(*N-N*), 1362, 766(C═S), UV(solid) λ_{max}/ nm: 256, 318, 362–415, 379 sh, ^{1}H NMR ($CDCl_3$) δ 14.479(s, 1H, ^{3}NH), δ 11.176(s, 1H, OH), δ 7.159–7.662(m, 15H, Ar), δ 3.179(s, 3H, ^{1}N-CH_3), δ 1.5(s, 3H, C-CH_3). Anal Calc. for $C_{25}H_{23}N_5OS$, Found: C: 68.18; H: 5.15; N: 15.88; S: 7.21, calculated: C: 68.04; H: 5.00; N: 15.90; S: 7.27%.

2.3. Synthesis of cadmium complex [$Cd(HL)_2$] (**2**)

H_2L (0.441 g, 1 mmol) was dissolved in few drops of chloroform and excess of methanol. To this solution, a hot methanolic solution of $Cd(OAc)_2{\cdot}2H_2O$ (0.266 g, 1 mmol) was added dropwise. The solution mixture was refluxed for 2–3 h at 60 °C. The product formed was filtered, washed with methanol and finally with ether and dried over anhydrous $CaCl_2$.

Yield: 70%, m.p (230 °C), IR (KBr) ν_{max}/cm^{-1}: 3439(N—H), 1597 (C═O), 1571(C═N), 1126 (*N-N*), 1348, 762(C═S), 659 (M—N), (M—O) 465. UV(solid) λ_{max}/nm 256, 321, 703. ^{1}H NMR ($CDCl_3$) δ 7.126–8.13 (m, 30H, Ar), δ 6.675 (s, 2H, NH) δ 1.2–1.29 (s, 6H, CH_3) δ 3.4–3.64 (s, 6H, ^{4}N-CH_3). Anal Calc. for $C_{50}H_{44}N_{10}O_2S_2Cd$ Found C: 60.30; H: 4.42; N: 14.06; S: 6.43; Cd: 11.2 calculated: C: 60.80; H: 4.49; N: 14.56; S: 6.83; Cd: 11.6%.

2.4. X-ray diffraction studies

X-ray crystallographic data of ligand were collected at 296(2)K on a Bruker Model Kappa Apex II diffractometer at SAIF, STIC, Cochin with graphite monochromatic Mo Kα (λ = 0.71073 Å) radiation. X-ray crystallographic data of Cd(II) complex were collected at 293(2) K on a Bruker Model Kappa Apex II diffractometer at SAIF IIT, Madras. Direct methods were performed to solve the structures and refined by least-square on F^2 using SHELXL-97 [18] for H_2L and SHELXL-2014/7 [19] for Cd(II) complex. All non-hydrogen atoms were refined anisotropically. All hydrogen atoms, except those attached to nitrogen were geometrically fixed at calculated positions. The crystallographic tools, PLATON for Windows [20], DIAMOND 3.2d [21] and MERCURY 3.5.1 [22] were used for structure analysis and presentation of the results. Crystallographic restraints (SADI and SIMU) were used in the initial refinement of disordered S(2) in the structure of cadmium(II) complex. The structure of H_2L was finally refined to the conventional *R*-value *R1* = 0.0540 and structure of Cd(II) complex was refined to the *R*-value *R1* = 0.0308.

3. Results and discussion

The ligand crystallised as dark yellow solid with a melting point of 163 °C, while the complex was golden yellow with a melting point of 230 °C. They were found to be stable at room temperature. CHNS percentages were in agreement with the suggested molecular formulae and were in accordance with their crystal structure. The ligand and the complex are partially soluble in most of the common polar solvents and are completely soluble in $CHCl_3$.

One of the starting compounds, 1-phenyl-3-methyl-4-benzoyl-5-pyrazolone (PMBP) used for the preparation of ligand can undergo keto-enol tautomerism in solution (I & II). During the synthesis of the ligand, it may be the enolic form of PMBP (II) that reacts with N(4)-methyl-N(4)-phenylthiosemicarbazide (MPTSC) (III) forming the product. As a result, the ligand formed can be a mixture of keto-imine/enol-imine tautomer (IV & V) in solution. On crystallisation, as a result of delocalisation of electrons due to extended conjugation, the compound undergoes rearrangement and tends to exist in a stable conformer (VI). However, during complexation, in the presence of metal ions in solution, the ligand can exist in enol-imine tautomer (IV) and coordinates through enolic oxygen after deprotonation. The possibility of thione- thiol tautomerism and coordination of the ligand through S^- is ruled out because of the presence of NH—C═S bond in the crystal structure of the Cd(II) complex.

The ligand (H_2L) can act as dianionic, monoanionic or neutral tridentate/bidentate/monodentate one. But in the present case, it is monoanionic and coordinates through azomethine nitrogen, thione sulphur and enolic oxygen of pyrazolone moiety after deprotonation. The reaction pathway in the formation of the ligand, 1-phenyl-3-methyl-4-benzoyl-5-pyrazolone N(4)-methyl-N(4)-phenylthiosemicarbazone (H_2L) can be represented as follows: Scheme 1.

3.1. Comparison of crystal structure of H_2L (**1**) and its complex [$Cd(HL)_2$] (**2**)

Single crystals of H_2L of X-ray diffraction quality were grown from its 1:1 methanol-DMSO solution by slow evaporation at room temperature in air. A crystal with dimensions of $0.350 \times 0.300 \times 0.300$ mm^3 was selected for collecting the data of the ligand. H_2L crystallizes with one molecule per asymmetric unit into triclinic crystal system with a space group of *P*-1. The molecular structure of the compound **1** with atom numbering scheme is depicted in Fig. 1. Fig. 2, demonstrates the hydrogen bond interaction of **1** along c* axis.

It is found that the molecules in the unit cell are arranged in inverted face to face manner, which is the repeating unit of the packing in the crystal lattice. The bond distances, C(9)—N(3), C(8)—N(1), C(8)—N(2) and N(2)—N(3) are 1.327(2) A°, 1.349(3) A°, 1.368(2) A°, 1.384(2) A°, respectively. The ligand exists in the thione form with a C(8)—S(1) bond length of 1.671 (2) Å. The bond length C(18)—O(1) is 1.258(2) Å which is in accordance with the C═O bond. All the bond lengths posses bond equalization due to partial double bond and single bond characteristics. The terminal nitrogen atoms N(1) and N(3) of the thiosemicarbazide fragment are in an antiperiplanar conformation with respect to the C(8)—N(2), with a torsion angle of −179.16(18)°. The bond angles of C(16)—C(9)—N(3), C(8)—N(3)—N(2) and C(9)—N(3)—N(2) are 124.68(16), 115.50(16) and 124.21(16)°, respectively, which is an evidence for the deviation from coplanarity of thiosemicarbazide and pyrazolone moieties.

Single crystals of cadmium (II) complex were grown from its chloroform solution.

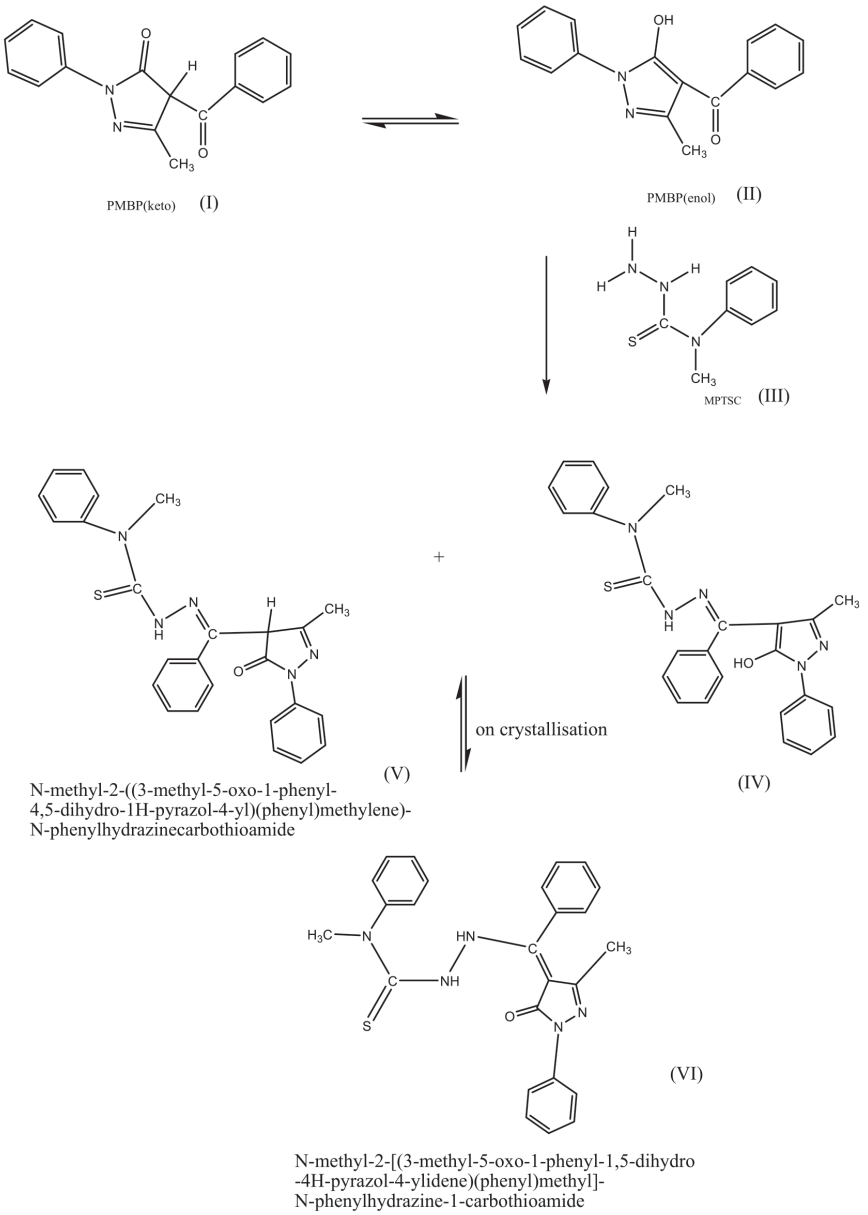

Scheme 1. The reaction pathway of 1-phenyl-3-methyl-4-benzoyl-5-pyrazolone N(4)-methyl-N(4)-phenylthiosemicarbazone (H_2L).

A crystal with dimensions $0.300 \times 0.250 \times 0.200\ mm^3$ was selected for collecting the data of the cadmium(II) complex. The compound crystallized with one molecule per asymmetric unit into monoclinic crystal system with a space group of $P2_1/c$. The molecular structure of the compound **2** with atom numbering scheme is presented in Fig. 3. Crystal data and structure refinement parameters of **1** and **2** are given in Table 1. The important hydrogen bonding interaction parameters of **1** and **2** are listed in Table 2. Selected bond lengths, bond angles and torsion angles are summarized in Table 3.

An interesting attribute of the crystal packing in the case of ligand and complex was the formation of a supramolecular chain mediated by intermolecular C—H···O hydrogen bond [23]. The crystal structure **2** is further stabilized by intermolecular C—H. . .. . .S interactions. In the unit cell of **2**, molecules are arranged in a face to face manner, which are the repeating units of the packing in the

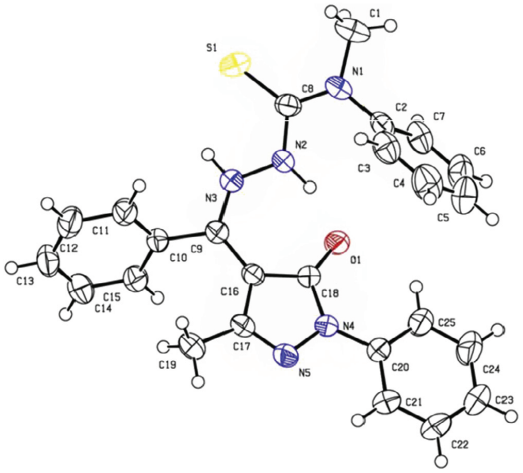

Fig. 1. The molecular structure of the compound **1** with atom numbering scheme.

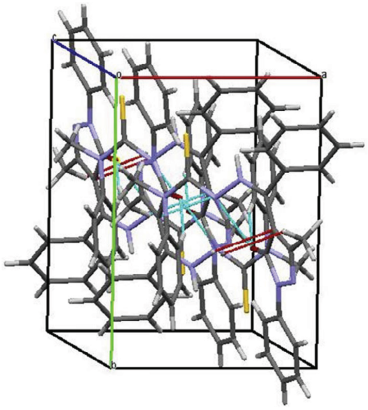

Fig. 2. Hydrogen bond interactions of **1** along c* axis.

crystal lattice. Fig. 4. shows the packing diagram along with hydrogen bonding interaction of **2** along b axis.

On complex formation, significant changes occur in the geometrical parameters of the ligand **1**. It is clear from the Table 2 that the bond length C(9)—N(3) in the complex is compressed to 1.306(3) Å from 1.326(2) Å. Coordination lengthens the C(9)—C(16) bond from 1.401(3) to 1.429(3) Å in the complex. It is also found that the C(8)—N(2) bond in the complex is compressed to 1.333(3) from 1.368(2) Å. This supports the extensive π delocalization along the thiosemicarbazone chain and the involvement of azomethine nitrogen in coordination. It is also confirmed by the existence of S(1) and N(3) in Z configuration with respect to C(8)—N(2) bond with a torsion angle of −5.10(4) Å.

Coordination lengthens the C(8)—S(1) bond from 1.671(2) Å to 1.692(3) Å but is intermediate between C=S bond length [1.60 Å] and C—S bond length [1.81 Å] [24]. The bond lengths, Cd—S(1) 2.6029(8) Å and Cd—–S(2) 2.573(9) Å corroborates the coordination through the thione form.

From the above observations, we confirm that the ligand is coordinated through the azomethine nitrogen [Cd—N(3) = 2.369 (2) Å], [Cd—N(8) = 2.384(2) Å], thione sulphur [Cd—S(1) = 2.6029 (8) Å], [Cd—S(2) = 2.573(9) Å] and pyrazolone oxygen [Cd—O(1) = 2.297(2) Å], [Cd—O(2) = 2.368(2) Å] of the ligand. These bond lengths are comparable to those reported for similar cadmium(II) complexes [25].

The coordination results in the formation of two 5 membered [Cd—N(3)—N(2)—S(1)—C(8)], [Cd—N(7)—N(8)—C(33)—S(2)] and two 6 membered [Cd—O(1)—C(18)—C(16)—C(9)—N(3)], [Cd—O (2)—C(36)—C(35)—C(34)—N(8)] metallocycles in the complex. Ring puckering analyses and least-square plane calculations showed that the 5 membered ring comprising of atoms Cd(1), N(3), N(2), C(8) and S(1) adopts an envelope conformation on Cd(l).

The least square planes comprising of [Cd, N(3), N(2), S(1), C(8)] (plane 1) and [Cd, N(7), N(8), S(2), C(33)] (plane 2) with a dihedral angle of 38.206(64)° show a Z conformation existing between these planes. The least square planes involving [Cd, O(1), C(18), C (16), C(9), N(3)] (plane 3), [Cd, O(2), C(36), C(35), C(34), N(8)] (plane 4) with a dihedral angle 81.185 (43)° show a puckered arrangement. The dihedral angles formed by the least square, (plane 1) and (plane 4), (plane 2) and (plane 4), (plane 2) and (plane 3), (plane 1) and (plane 3) are 64.830(44)°, 36.820(81)°, 72.323(54)°, 39.130(4)°, respectively. These evidences suggested a distorted octahedral coordination geometry for the complex,

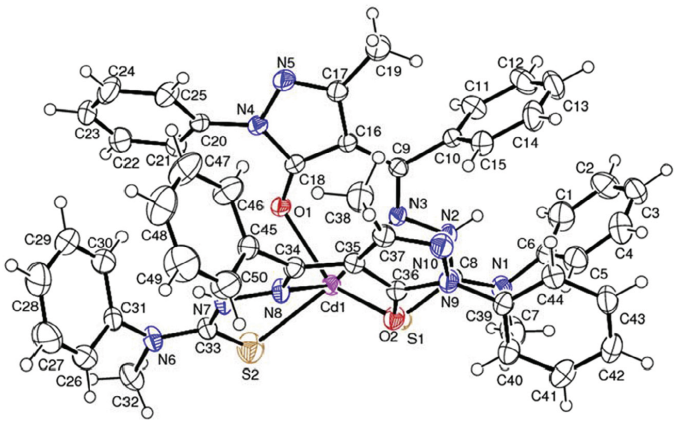

Fig. 3. The molecular structure of the compound **2** with atom numbering scheme.

Table 1
Crystal data and structure refinement parameters of $Cd(HL)_2$.

Identification code	H_2L	$Cd(HL)_2$
Empirical formula	C_{25} H_{23} N_5 O S	C_{50} H_{44} Cd N_{10} O_2 S_2
Formula weight	441.54	993.47
Temperature (K)	296(2)	293(2)
Wavelength (Å)	0.71073	0.71073
Crystal system	Triclinic	Monoclinic
Space group	*P*-1	*P* $2_1/c$
Unit cell dimensions		
a (Å)	7.8930(4)	9.6939(5)
b (Å)	11.2019(5)	22.5183(11)
c(Å)	13.0211(7)	21.2054(10)
α(°)	96.175(3)	90
β(°)	100.922(3)	99.960(2)
γ(°)	91.005(3)	90
Volume ($Å^3$)	1123.02(10)	4559.2(4)
Z	2	4
ρ(calculated)(mg/m^3)	1.306	1.447
Absorption coefficient (mm^{-1})	0.172	0.624
F(0 0 0)	464	2040
Crystal size(mm^3)	0.350 × 0.300 × 0.300	0.300 × 0.250 × 0.200
Theta range for data collection	1.60–28.31°	2.055–24.999°.
Index ranges	$-10\leq h\leq 10$, $-14\leq k\leq 14$, $-11\leq l\leq 17$	$-11\leq h\leq 11$, $-26\leq k\leq 26$, $-25\leq l\leq 25$
Reflections collected	8957	66073
Independent reflections	5465 [R(int) = 0.0174]	8034[R(int) = 0.0346]
Completeness to theta	28.31° 97.6%	24.99° 100%
Refinement method	Full-matrix least-squares on F^2	Full-matrix least-squares on F^2
Data/ restraints/parameters	5465/0/299	8034/10/604
Goodness-of-fit on F^2	0.981	1.084
Final R indices [I > 2sigma(I)]	R1 = 0.0540, w*R*2 = 0.1461	R1 = 0.0308, w*R*2 = 0.0748
R indices (all data)	R1 = 0.0828, w*R*2 = 0.1790	R1 = 0.0411, w*R*2 = 0.0829
Largest diff. peak and hole ($e.A^{-3}$)	0.381 and -0.365	0.445 and -0.390

with the Cd atom lying in an approximate plane with the O(1)—O(2)—N(1)—N(8)—S(1)—S(2) atoms. It is also found that the two ligands coordinated in a *fac*-configuration and the orientation of the two monoanionic ligands are *cis to* each other.

3.2. Spectroscopic analysis

The band observed at 1626 cm^{-1} in the spectrum ligand may be due to ν(C═O) of pyrazolone moiety. This is at a lower wave number than that usually found for carbonyls and indicates its involvement in hydrogen bonding with N—H of the thiosemicarbazide moiety. This band is absent in the spectrum of the cadmium(II) complex, suggesting the enolization and deprotonation of the —C—O—H group and coordination through the enolic oxygen. The ν(M—O) observed at 659 cm^{-1} corroborates the coordination of oxygen of pyrazolone moiety.

Several bands are observed in the ligand in the region 1560–700 cm^{-1} may be due to vibrations involving interactions between C═S and C—N stretchings [26]. Presence of band at 1571 cm^{-1} in the complex indicates the azomethine stretching vibration. The shift of the centre of the broad band due to the NH stretching from 3411 cm^{-1} in the ligand to 3437 cm^{-1} in the complex substantiates the involvement of azomethine nitrogen in the complex formation [27]. The ν(*N-N*) band at 1106 cm^{-1} has undergone a shift to higher wavenumber in the spectrum of the complex indicating the coordination of azomethine nitrogen. This blue shift is due to the decrease in the repulsion between the lone pairs on the two nitrogen atoms. The ν(M-N) stretching frequency observed at 465 cm^{-1} corroborates the coordination of azomethine nitrogen. Absence of a band in the region 2500–2800 cm^{-1} substantiates that the ligand is in the thione form even after coordination with cadmium. The thioamide bands which are partly due to ν(C═S) found at lower frequencies (1348, 762 cm^{-1}) in the spectrum of the complex also supports the above assignments.

The electronic spectra of the ligand and the cadmium(II) complex in chloroform were recorded. The electronic spectrum of ligand registered three charge-transfer bands at 256, 318 and 362–415 nm with a shoulder at 379 nm. The first two bands can be attributed, respectively, to the π-π∗ and n- π∗ transitions of the azomethine chromophore and the benzene ring. These bands are found unshifted in the spectrum of the complex. A broad band observed between 360 and 415 nm can be attributed to the strong intramolecular hydrogen bonding in the ligand. It may be due to the promotion of lone pair electrons on the nitrogen to an antibonding π-orbital of imine group. In the complex, this band has undergone a slight blue shift and appears as a narrow band at 395 nm and the splitting of band was not observed. It may be due to the involvement of azomethine chromophore in coordination and due to the absence of hydrogen bonding in the complex. A weak band observed at 703 nm can be due to the ligand to metal charge- transfer transition.

The ^1H NMR spectra of the ligand and the complex were recorded in $CDCl_3$. In the solution state, the ligand is in imine-ol form and is evident from the NMR spectrum. Intramolecular hydrogen bonding de-shielded the N—H proton to δ = 14.479 ppm and O—H proton to 11.176 ppm in the ligand.

Table 2
Hydrogen bonding interaction parameters of **1** and **2.**

D—H…A	d(D—H)	d(H…A)	d(D…A)	<(DHA)
*H_2L (**1**)*				
N(3)—H(3N)……S(1)	0.89(2)	2.29(2)	2.8517(18)	121.20(19)
N(2)—H(2N)……O(1)	0.98(2)	1.61(2)	2.558(2)	162(2)
C(7)—H(7)……O(1) #1	0.93	2.42	3.324(3)	163
C(21)—H(21)……N(5)	0.93	2.42	2.767(3)	102
C(25)—H(25)……O(1)	0.93	2.24	2.873(3)	125
Symmetry transformations used to generate equivalent atoms: #1 1 − x, 1 − y, −z				
*$Cd(HL)_2$ (**2**)*				
C(21)—H(21)…O(1)	0.93	2.47	2.982(3)	115.2
C(26)—H(26)…O(2)#1	0.93	2.52	3.354(4)	150
C(32)—H(32 B)…S(1)#2	0.96	2.92	3.648(4)	133.4
C(40)—H(40)…O(2)	0.93	2.32	2.902(3)	120
Symmetry transformations used to generate equivalent atoms: #1 − x + 1, −y,−z + 2 #2 −x, −y, −z + 2				

Table 3
Selected bond lengths (Å), bond angles and torsion angles (°) of H_2L (**1**) and $Cd(HL)_2$ (**2**).

bond length (Å)	H_2L	$Cd(HL)_2$	bond angle (°)	H_2L	$Cd(HL)_2$	torsion angle (°)	$Cd(HL)_2$
C(1)—N(1)	1.469(4)		N(2)—C(8)—N(1)	113.40(2)		S(1)—C(8)—N(2)—N(3)	−5.10(4)
C(8)—N(1)	1.350(3)	1.349(3)	N(1)—C(8)—S(1)	124.60(2)	121.50(2)	C(8)—N(2)—N(3)— C(9)	−172.50(3)
C(8)—N(2)	1.368(3)	1.333(3)	N(2)—C(8)—S(1)	121.90(1)	123.60(2)	N(2)—N(3)—C(9)—C(16)	177.40(2)
C(33)—N(7)		1.340(4)	N(3)—C(9)—C(16)	124.7(2)	119.20(2)	C(35)—C(36)—O(2)—Cd(1)	37.40(4)
C(8)—S(1)	1.671(2)	1.692(3)	C(8)—N(2)—N(3)	115.5(2)	122.10(2)	C(16)—C(18)—O(1)—Cd(1)	33.00(4)
C(33)—S(2)		1.698(8)	C(9)—N(3)—N(2)	124.2(2)	115.30(2)	N(4)—C(18)—O(1)—Cd(1)	−147.30(2)
C(33—S(2′)		1.695(5)	C(8)—N(1)—C(2)	122.0(2)			
C(9)—N(3)	1.327(3)	1.306(3)	C(8)—N(1)—C(1)	121.20(2)		N(9)—C(36)—O(2)—Cd(1)	−142.90(2)
C(34)—N(8)		1.300(3)	C(2)—N(1)—C(1)	116.80(2)		N(1)—C(8)—S(1)—Cd(1)	166.50(2)
C(9)—C(16)	1.401(3)	1.429(3)	O(1)—C(18)—C(16)	129.8(2)	132.10(2)	N(6)—C(33)—S(2)—Cd(1)	161.70(2)
C(34)—C(35)		1.434(4)				N(7)—C(33)—S(2)—Cd(1)	−16.40(9)
C(9)—C(10)	1.483(3)	1.494(3)	O(1)—C(18)—N(4)	125.1(2)	123.50(2)	N(2)—C(8)—S(1)—Cd(1)	−16.20(3)
C(17)—N(5)	1.304(2)	1.308(3)				N(3)—Cd(1)—S(2′)	165.90(2)
C(17)—C(19)	1.491(3)	1.492(4)	C(10)—C(11)—C(12)	120.0		N(3)—Cd(1)—S(2)	164.30(4)
C(18)—O(1)	1.257(3)	1.254(3)	C(11)—C(10)—C(9)	120.4(2)		N(8)—Cd(1)—S(2)	74.80(2)
C(36)—O(2)		1.261(3)	C(10)—C(9)—N(3)		120.30(2)	N(8)—Cd(1)—S(2′)	74.09(15)
C(18)—N(4)	1.367(3)	1.378(3)	O(1)—Cd(1)—O(2)		130.69(6)	O(2)—Cd(1)—S(2′)	113.70(2)
C(20)—N(4)	1.420(2)	1.411(3)	O(1)—Cd(1)—S(2)		94.10(3)		
			O(1)—Cd(1)—S(2′)		95.50(2)		
N(2)—N(3)	1.384(2)	1.385(3)	O(1)—Cd(1)—N(3)		76.90(7)		
N(7)—N(8)		1.384(3)	O(2)—Cd(1)—N(3)		79.92(7)		
N(4)—N(5)	1.399(2)	1.391(3)	O(1)—Cd(1)—N(8)		79.11(7)		
N(3)—Cd(1)		2.369(2)	O(2)—Cd(1)—N(8)		72.55(7)		
N(2)—H(2 N)	0.97(2)	0.88(2)	C(18)—O(1)—Cd(1)		119.73(16)		
N(7)—H(7)		0.88(2)	C(36)—O(2)—Cd(1)		119.73(16)		
N(8)—Cd(1)		2.384(2)	C(33)—S(2)—Cd(1)		97.90(3)		
N(3)—Cd(1)		2.369(2)	C(33)—S(2′)—Cd(1)		97.33(18)		
O(1)—Cd(1)		2.297(2)	S(2)—Cd(1)—S(1)		101.88(18)		
O(2)—Cd(1)		2.368(2)	S(2′)—Cd(1)—S(1)		101.77(10)		
S(1)—Cd(1)		2.6029(8)	N(6)—C(33)—S(2)		121.10(3)		
Cd(1)—S(2)		2.573(9)	N(6)—C(33)—S(2′)		121.30(3)		
Cd(1)—S(2′)		2.593(4)					
C(7)—N(1)		1.456(4)	N(7)—C(33)—S(2′)		123.3(2)		
N(9)—N(10)		1.395(3)	N(7)—C(33)—S(2)		123.5(3)		

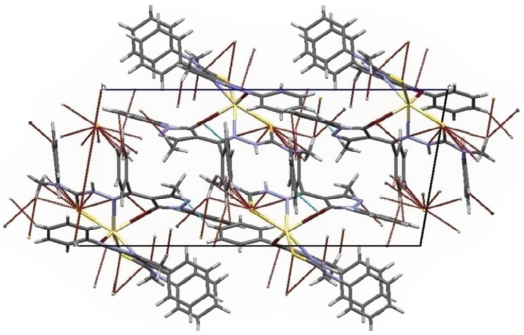

Fig. 4. Hydrogen bond interactions of $Cd(HL)_2$ along b axis.

Absence of peak at 11.176 ppm, corresponding to the O—H, proton in the complex indicates that the ligand has undergone deprotonation during complex formation. The appearance of a new signal at 6.675 ppm, corresponding to NH protons, in the complex corroborates the involvement of sulphur in coordination in the thione form. Aromatic protons show multiplet signals in the range 7.159–7.662 ppm in the ligand spectrum and at 7.126–8.13 ppm in the complex spectrum. N—CH_3 protons in the ligand and complex show peaks at 3.179 and 3.4–3.64 ppm, respectively. A singlet at 1.5 ppm in the ligand and the peaks at 1.2–1.3 ppm in the complex correspond to the methyl protons of the substituted pyrazolone. A slight shift of these signals in the complex compared to the ligand spectrum can be attributed to the distortion in the chemical environment during complex formation.

4. Conclusion

In summary, the focus of the present work was on the synthesis, spectral and single crystal XRD studies of 1-phenyl-3-methyl-4-benzoyl-pyrazolone N(4)-methyl-N(4)-phenyl thiosemicarbazone and its cadmium(II) complex. It has been found that cadmium metal ion gets coordinated through oxygen, azomethine nitrogen and thione sulphur. Crystal data and the spectral analyses ratify the above observation. In this study, it is also observed that the crystal packing in the ligand and complex was stabilised by the formation of a supramolecular chain mediated by intermolecular C—H···O hydrogen bond.

Acknowledgements

The authors are grateful to SAIF, Cochin University of Science and Technology, Kochi, Kerala, India for elemental analyses and ^{1}H NMR spectral analysis. We are thankful to SAIF IIT, Madras, SAIF Cochin, India for providing single crystal XRD results. The University Grants Commission (UGC), India is also gratefully acknowledged for financial support.

Appendix A. Supplementary data

Supplementary data associated with this article can be found, in the online version, at http://dx.doi.org/10.1016/j.ica.2017.08.046.

References

[1] C.C. García, B.N. Brousse, M.J. Carlucci, A.G. Moglioni, M.M. Alho, G.Y. Moltrasio, N.B. D'Accorso, E.B. Damonte, Antivir. Chem. Chemother. 14 (2003) 99.
[2] Z. Afrasiabi, E. Sinn, J.N. Chen, Y.F. Ma, A.L. Rheingold, L.N. Zakharov, N. Rath, S. Padhye, Inorg. Chim. Acta 357 (2004) 271.
[3] P. Domiano, G.G. Fava, M. Nardelli, P. Sagarabotto, Acta Crystallogr. B 25 (1969) 343;
G.D. Andreetti, G. Fava, M. Nardelli, P. Sagarabotto, Acta Crystallogr. B 26 (1970) 1005.
[4] N.V. Gebeleu, M.D. Revenko, V.M. Leovats, Russ. J. Inorg. Chem. 22 (1977) 1009.
[5] D.X. West, G.A. Bain, R.J. Butcher, J.P. Jasinki, Y. Li, R.Y. Pozdniakiv, J. Valdez-Martinez, R.A. Toscano, S.H. Ortega, Polyhedron 15 (1996) 665.
[6] J.S. Casas, A. Sanchez, J. Bravo, S. Garcia-Fontan, E.E. Castellano, M.M. Jones, Inorg Chim. Acta 158 (1989) 119.
[7] M.A. Romero-Molina, M.D. Gutierrez-Valere, R. Lopez-Garzon, J.M. Salas-Peregrin, M.I. Arriortua, F.J. Zuniga, Inorg. Chim. Acta 136 (1987) 8.
[8] Y. Hamada, T. Sano, H. Fujii, Y. Nishio, H. Takahashi, K. Shibata, Jpn. J. Appl. Phys. 35 (1996) 1339.
[9] Q. Wu, J.A. Lavigne, S. Wang, Inorg. Chem. 39 (2000) 5248.
[10] N. Donze, P. Pechy, M. Gratzel, M. Schaer, L. Zuppiroli, Chem. Phys. Lett. 315 (1999).
[11] S.F. Liu, Q. Wu, H.L. Schmider, H. Aziz, N.X. Hu, Z. Popovic, S. Wang, J. Am. Chem. Soc. 122 (2000) 3671.
[12] M.A. Ali, A.H. Mirza, M. Nazimuddin, H. Rahman, R.J. Butcher, Transition Met. Chem. 27 (2002) 268.
[13] Vanessa Senna Nogueira, Leandro Bresolin, Christian Näther, Inke Jess, Adriano Bof de Oliveira, Acta Crystallogr. E 71 (2015) 234.
[14] Alfonso Castineiras, Isabel Garcia, Elena Bermejo, Douglas X. West, Polyhedron 19 (2000) 1873.
[15] J.P. Scovill, D.L. Klayman, C.F. Franchino, J. Med. Chem. 25 (1982) 1261.
[16] B.S. Jensen, Acta Chem. Scand. 13 (1959) 1668.
[17] B.A. Uzoukwu, Synth. React. Inorg. Met. Org. Chem. 23 (1993) 1087.
[18] G.H. Sheldrick, SHELXL 97. Program for Crystal Structure Refinement, University of Göttingen, Göttingen, Germany, 1997.
[19] G.M. Sheldrick, SHELXL-2014/7: Program for the Solution of Crystal Structures, University of Göttingen, Göttingen, Germany, 2014.
[20] A.L. Spek, PLATON, A Multipurpose Crystallographic Tool, Utrecht University, Utrecht, The Netherlands, 1999.
[21] Diamond-Crystal and Molecular Structure Visualization Crystal Impact - Dr. H. Putz, Dr. K. Brandenburg GbR, Kreuzherrenstr. 102, 53227 Bonn, Germany.
[22] C.F. Macrae, P.R. Edington, P. McCabe, E. Pidcock, G.P. Sheilds, R. Taylor, M. Towler, J. Van de Streek, J. Appl. Cryst. 39 (2006) 453.
[23] R.P. John, A. Sreekanth, M.R.P. Kurup, A. Usman, I.A. Razak, H.-K. Fun, Spectrochim. Acta A 59 (2003) 1349.
[24] S. Renjusha, M.R.P. Kurup, Polyhedron 27 (2008) 3294.
[25] Z.-F. Chen, Y.-Z. Tang, H. Liang, H.-K. Fun, K.-B. Yu, J. Coord. Chem. 59 (2006) 207.
[26] D.X. West, A.M. Stark, G.A. Bain, A.E. Liberta, Transition Met. Chem. 21 (1996) 289.
[27] K. Nakamoto, Infrared and Raman Spectra of Inorganic and Coordination Compounds, Wiley, New York, NY, USA, 1978.

Inorganica Chimica Acta 469 (2018) 387–396

Contents lists available at ScienceDirect

Inorganica Chimica Acta

journal homepage: www.elsevier.com/locate/ica

Research paper

Novel ligands, benzophenone N(4)-methyl-N(4)-phenylthiosemicarbazone, 1-(amino-*N*-methylphenylmethanethio)(diphenylmethylene)thiocarbonohydrazide and the transition metal complexes of the latter

K.G. Sangeetha *, K.K. Aravindakshan

Department of Chemistry, University of Calicut, 673635 Kerala, India

ARTICLE INFO

Article history:
Received 26 May 2017
Received in revised form 2 September 2017
Accepted 26 September 2017
Available online 28 September 2017

Keywords:
Thiosemicarbazone
Single crystal
Benzophenone
Thioketo-thioenol equilibrium

ABSTRACT

Two Schiff base ligands, benzophenone N(4)-methyl-N(4)-phenylthiosemicarbazone (HL), 1-(amino-*N*-methyl-*N*-phenylmethanethio)(diphenylmethylene)thiocarbonohydrazide (H_2L') were synthesized. They were characterized by elemental analyses and spectral [Electronic, FT-IR, FT-Raman and ^{1}H NMR] studies. The structure of HL was determined by single-crystal X-ray diffraction studies. The complexes of Co(II), Ni(II), Cu(II) and Zn(II) of H_2L' were synthesized. They were characterized by the elemental analyses, magnetic susceptibility, IR, electronic, NMR and thermal (TGA) studies. The crystal structure of Ni $(HL')_2{\cdot}1.5H_2O$ was determined by single-crystal X-ray diffraction.

1. Introduction

Benzophenone derivatives are very important due to their versatile physicochemical properties such as electrochemical, spectroscopic, metal complexation, adsorptive and crystallographic properties [1,2]. They have the ability to absorb a broad range of UV radiation (200–350 nm). The benzophenone derivatives like 2-hydroxy-4-methoxybenzophenone are used as raw material in the manufacturing of sunscreen creams [3]. These creams are useful in various medical treatments to shun photosensitization, phototoxicity or allergic reactions of patients [4].

Topical studies have shown that benzophenone thiosemicarbazone exhibit inhibitory effects on parasites including *Trypanosoma brucei* and *Plasmodium falciparum* [5]. Schiff bases derived from benzophenone have been extensively studied for their cytotoxic activities against human oral squarnous carcinoma cells HSC-2 and normal human gingival fibroblasts (HGF). Antibiotic activities of these compounds against methicillin-resistant staphylococcus aureus and vancomycin-resistant Enterococcus faecium and protein kinase C inhibitor have been studied [6].

The main group- as well as transition metal complexes of thiosemicarbazones are of current importance by virtue of their interesting structural characteristics and diverse biological applications [7,8]. Benzophenone thiosemicarbazone containing π-electron conjugation system could act as one of the potential semi-organic optical materials. The flexible applications of benzophenone in different areas encouraged us to synthesize its N(4)-disubstituted thiosemicarbazone containing NS donor atoms. The metal ions used in this investigation are Co(II), Ni(II), Cu(II) and Zn(II), a few typical transition metal ions, the coordination compounds of which have immense structural, biological and industrial importance [9,10]. In this communication, we report the synthesis and characterisation of two compounds (HL) and (H_2L') derived from benzophenone and N(4)-methyl-N(4)-phenylthiosemicarbazide. In addition to this, crystal structure of (HL), synthesis and characterisation of transition metal complexes of (H_2L') and crystal structure of nickel complex are reported here.

2. Experimental details

All the chemicals used in the present study are of A.R grade. Metal salts were purchased from E. Merck and used as received.

2.1. Physical measurements

Elemental analyses (C, H, N and S) were performed on Vario EL III elemental analyzer. Infrared (IR) spectra were recorded on a

* Corresponding author.
E-mail addresses: sangtkg@gmail.com (K.G. Sangeetha), aravindkuttamath@yahoo.com (K.K. Aravindakshan).

https://doi.org/10.1016/j.ica.2017.09.057
0020-1693/

Jasco-FT-IR-4100 model spectrometer using KBr pellets. The electronic spectra were recorded on JascoV-550 UV–Vis spectrometer. ^{1}H NMR spectra were recorded on 400 MHz Bruker NMR spectrometer. Magnetic susceptibility values of the complexes at room temperature were measured using Sherwood Scientific Magnetic Susceptibility Balance. TG/DTG was recorded on TGA Q50 V20.13 Build 39 model thermo gravimetric analyzer fitted with a thermal analysis controller in nitrogen atmosphere with a heating rate of 10 °C/min.

2.2. X-ray crystal determination

X-ray crystallographic data were collected at 296(2) K for HL and at 273(2) K for $Ni(HL')_2 \cdot 1.5H_2O$ on a Bruker Model Kappa Apex II diffractometer with graphite monochromatic Mo Kα (λ = 0.71073 Å) radiation. Direct methods were performed to solve the structure and refined by least-square on F^2 using SHELXL-97 for HL and SHELXL-2014/7 for nickel(II) complex. All non-hydrogen atoms were refined anisotropically. All hydrogen atoms, except those attached to nitrogen were geometrically fixed at calculated positions. The crystallographic tools, PLATON for Windows [11], DIAMOND 3.2d, and MERCURY 3.5.1 [12] were used for structure analysis and presentation of the results. The structure was finally refined to the conventional *R*-value 0.0611 for HL and 0.0641 for Ni(II) complex.

2.3. Synthesis of ligands

(a) Synthesis of Benzophenone N(4)-methyl-N(4)-phenylthiosemicarbazone (HL)
N(4)-Methyl-N(4)-phenylthiosemicarbazide (MPTSC) was prepared by modifying the procedure reported by Scovill [13]. The compound was prepared by dropwise addition of a hot methanolic solution of benzophenone (.345 g, 1 mmol) into the boiling methanolic solution of N(4)-methyl-N(4)-phenylthiosemicarbazide (.182 g, 1 mmol) (MPTSC) taken in a round bottom flask. The reaction mixture was refluxed for 2 h. The volume of the solution was reduced and kept for overnight. The Schiff base compound obtained was filtered, washed with methanol, water and dried over anhydrous $CaCl_2$ (Fig. 1).

(b) Synthesis of 1-(aminophenylmethanethio)(diphenylmethylene)thiocarbonohydrazide (BP-MPTSC) (H_2L')
1-(AminoN-methyl-*N*-phenylmethanethio)(diphenylmethylene) thiocarbonohydrazide (H_2L') is prepared by dropwise addition of a hot methanolic solution of benzophenone (0.345 g, 1 mmol) to a boiling methanolic solution of MPTSC (0.364 g, 2 mmol) taken in a round bottom flask, 2 drops of glacial acetic acid was added to the reaction mixture and refluxed at 60–80 °C for 30 min. The solution was chilled and kept overnight. The cream coloured Schiff base ligand obtained was filtered and washed with methanol and dried (Fig. 2).

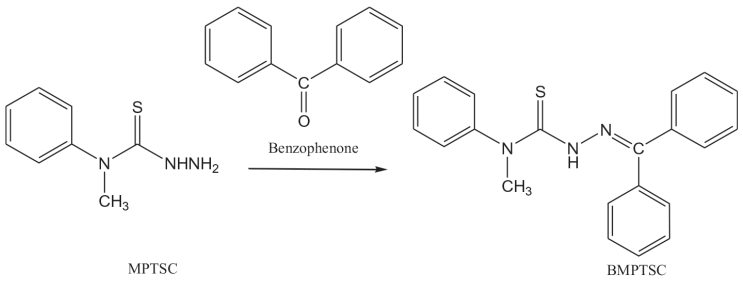

Fig. 1. The formation of Benzophenone N(4)-methyl-N(4)-phenyl thiosemicarbazone (BMPTSC) (HL).

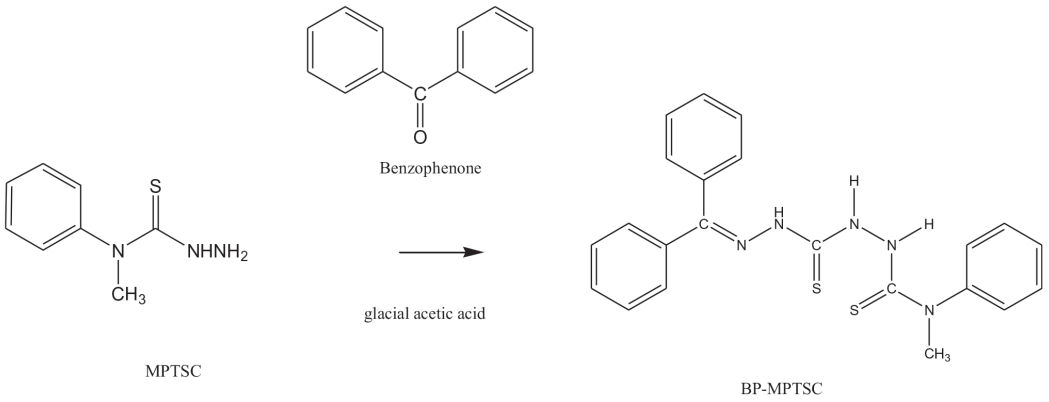

Fig. 2. The formation of 1-(AminoN-methyl-*N*-phenylmethanethio) (diphenylmethylene)thiocarbonohydrazide (BP-MPTSC) (H_2L').

2.4. Synthesis of metal complexes of ligand H_2L'

A hot methanolic solution of H_2L' is added dropwise to hot methanolic/hot water solution of metal acetate/sulphate/chloride/nitrate solution in 1:1 molar ratio. After complete addition, a pinch of sodium acetate was added, refluxed for 3 h and then cooled to room temperature. The precipitate formed was filtered, washed with water followed by methanol.

3. Results and discussion

In the present investigation, we were able to obtain single crystals of benzophenone N(4)-methyl-N(4)-phenylthiosemicarbazone by refluxing equimolar quantities of benzophenone and N(4)-methyl-N(4)-phenyl thiosemicarbazide. However, the yield of the product was low. Therefore, we decided to modify the procedure for increasing the yield and also to enhance the speed of the reaction. In the modified procedure, we added two drops of glacial acetic acid to the reaction mixture and chilled the resultant solution. We were able to obtain a faster reaction rate and a better yield. Anticipating that the ligand thus obtained was benzophenone N(4)-methyl-N(4)-phenylthiosemicarbazone (HL), we prepared its complexes. However, the elemental analytical- and NMR spectral data of the ligand (H_2L') and complexes were not in agreement with the crystal data of expected ligand. We were able to synthesise and study the single crystals of nickel(II) complex (**2**) of the ligand. This prompted us to investigate more about the unexpected structure of H_2L'. Further, data obtained from elemental analysis and NMR spectrum helped us to confirm the ligand structure. The formation of H_2L' might have taken place through the following hidden steps (Scheme 1). As *N*-methyl aniline is a better leaving group, its substitution with other group has been already reported [14]. To the best of our knowledge the structure of the ligand obtained (H_2L') has not been reported so far.

3.1. Characterisation of the ligands (HL and H_2L')

The ligands are characterized on the basis of elemental analysis, electronic, IR, Raman and ^{1}H NMR spectra.

Benzophenone N(4)-methyl-N(4)-phenylthiosemicarbazone, Yield 65%, mp 153 °C. Found C, 73.5; H, 5.3; N, 12.1; S, 9.2. $C_{21}H_{19}N_3S$ calculated: C, 73.0; H, 5.5; N, 12.2; S, 9.3% .UV (solid), λ_{max}/nm: 257, 319, 352 and 419 nm. IR (KBr) ν_{max}/cm^{-1}: ν(NH) 3255–3169, ν(C=N) + ν(C=C) 1561–1594, ν(NH—C=S) 1332, ν(*N*—*N*) 1111, 1063, ν(C=S) 770. FT-Raman (ν_{max}/cm^{-1}): ν(NH)

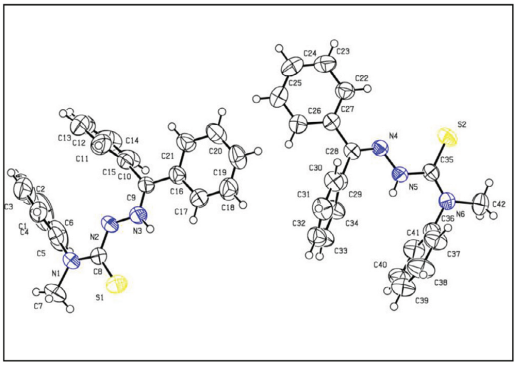

Fig. 3. The molecular structure of HL with the atom numbering scheme.

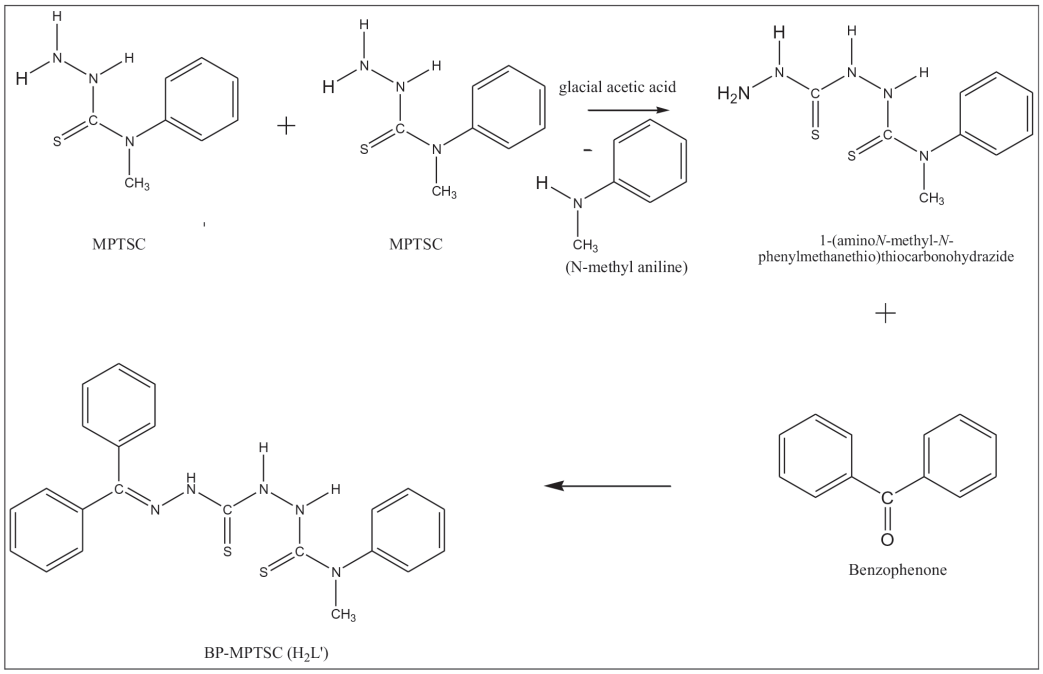

Scheme 1. The formation of 1-(amino-*N*-methyl-*N*-phenylmethanethio) (diphenylmethylene)thiocarbonohydrazide (BP-MPTSC) (H2L′).

Table 1
Crystal data and structure refinement for HL and $[Ni(HL')_2]\cdot 1.5H_2O$.

Identification code	HL	$Ni(HL')_2\cdot 1.5H_2O$
Empirical formula	$C_{21}H_{19}N_3S$	$C_{44}H_{36}C_{10}N_{10}NiS_4O_{1.5}$
Formula weight	345.45	907.78
Temperature (K)	296(2)	273(2)
Wavelength (Å)	0.71073	0.71073
Crystal system	Triclinic	Triclinic
Space group	*P*-1	*P*-1
Unit cell dimensions		
a (Å)	10.0166(6)	11.0784(9)
b (Å)	10.0685(5)	13.3220(7)
c (Å)	19.2274(11)	16.3160(9)
α (°)	103.794(3)	75.823(2)
β (°)	90.656(2)	74.2340(10)
γ (°)	96.566(3)	84.270(2)
Volume (A^3)	1869.34(18)	2245.4(3)
Z	4	2
$P_{calculated}$ (mg/m^3)	1.227	1.343
Absorption coefficient (mm^{-1})	0.181	0.664
F(0 0 0)	728	940
Crystal size (mm^3)	0.35 × 0.30 × 0.20	0.630 × 0.560 × 0.510
Theta range for data collection (°)	1.09–28.37	1.818–24.999
Limiting indices	$-13 \le h \le 13$–$8 \le k \le 13$–$25 \le l \le 23$	$-13 \le h \le 13$, $-14 \le k \le 15$, $-19 \le l \le 19$
Reflections collected/unique	15,549/9040 [R(int) = 0.0252]	13,992/7315 [R(int) = 0.0582]
Completeness to theta = 28.37	96.70%	95.50%
Absorption correction	Semi-empirical from equivalents	Semi-empirical from equivalents
Max. and min. transmission	0.9648 and 0.9395	0.71 and 0.62
Refinement method	Full-matrix least-squares on F^2	Full-matrix least-squares on F^2
Data/restraints/parameters	9040/0/453	7315/0/544
Goodness-of-fit on F^2	1.022	0.963
Final R indices [I > 2sigma(I)]	R1 = 0.0611 w*R2* = 0.1543	R1 = 0.0641, w*R2* = 0.1511
R indices (all data)	R1 = 0.1360, w*R2* = 0.1954	R1 = 0.1192, w*R2* = 0.1794
Largest diff. peak and hole (e A^{-3})	0.388 and −0.389	1.296 and −0.270

3064, *ν*(C=N) 1583, *ν* (C=S), 1334, 1143. ^{1}H NMR: ($CDCl_3$) *δ* 7.036–7.48 (15H, m), *δ* 7.02 (1H, s), 3.79 (3H, s).

1-(AminoN-methyl-*N*-phenylmethanethio)(diphenyl-methylene)thiocarbonohydrazide, Yield 85%, mp 160 °C. Found C, 62.8; H, 5.2; N, 16.5; S, 15.0. $C_{22}H_{21}N_5S_2$ calculated: C, 63.0; H, 5.0; N, 16.7; S, 15.2%. UV (solid), λ_{max}/nm: 256, 344, 574 nm. IR (KBr) ν_{max}/cm^{-1}: *ν*(NH) 3250–3153, *ν*(C=N) + *ν*(C=C) 1583, *ν*(NH—C=S) 1323, *ν*(*N—N*) 1060, *ν*(C=S) 771. FT-Raman (ν_{max}/cm^{-1}): *ν*(NH) 3071, *ν*(C=N) 1589, *ν* (C=S) 1296 and 1111. ^{1}H NMR: ($CDCl_3$) *δ* 11.02–10.96 (1H, d), 8.84–8.82 (1H, d), *δ* 8.44 (1H, s), *δ* 7.6–7.252 (15H, m), 3.718 (3H, s)

3.1.1. Crystal structure of $C_{21}H_{19}N_3S$ (**HL**)

A crystal with dimensions, 0.35 × 0.30 × 0.20 mm was selected for collecting the data. HL crystallizes with two molecules per asymmetric unit into triclinic crystal system with a space group of *P*-1. The molecular structure of HL with the atom numbering scheme is given in Fig. 3. Crystal data and structure refinement for HL are given in Table 1. Hydrogen bonding interaction parameters of HL are shown in Table 2. Selected bond lengths and bond angles are listed in Table 3. Packing diagram, showing intermolecular interactions of HL along b axis is shown as Fig. 4.

The bond lengths, C(9)—N(3), C(8)—N(1), C(8)—N(2), N(3)—N(2) are 1.285(3) Å, 1.339(4), 1.388(4), 1.371(3), respectively. They are found to be midway between the analogous single [C—N; 1.47 Å, *N—N*; 1.45 Å] and double bonds [C=N; 1.28 Å, N=N; 1.25 Å] [15–17]. The C(9)—N(3) bond length 1.285(3) Å is close to C=N bond length. This confirms the presence of azomethine bond in the compound which is evidenced from the IR data [15]. C(8)—S(1) bond length is found to be 1.655 (2) Å which is close to C=S bond length of 1.61 Å than to C—S single bond length of 1.81 Å [18]. This substantiates the existence of HL in thione form in solid state.

Table 3
Selected bond lengths, bond angles and torsion angles of HL [Å and °].

C(8)—N(1)	1.339(4)	C(9)—N(3)—H(3 N)	121.60
C(8)—N(2)	1.388(4)	N(2)—N(3)—H(3 N)	121.60
C(8)—S(1)	1.655(4)	C(9)—N(3)—N(2)—C(8)	177.0(3)
C(9)—N(3)	1.285(3)	N(1)—C(8)—N(2)—N(3)	177.1(3)
N(3)—N(2)	1.371(3)	S(1)—C(8)—N(2)—N(3)	3.7(5)
N(3)—H(3 N)	0.86	N(2)—C(8)—N(1)—C(6)	0.5(5)
N(1)—C(8)—S(1)	124.50(3)	S(1)—C(8)—N(1)—C(6)	179.7(3)
N(2)—C(8)—S(1)	123.30(3)	N(2)—C(8)—N(1)—C(7)	179.2(4)
N(1)—C(8)—N(2)	112.20(3)	S(1)—C(8)—N(1)—C(7)	0.0(5)
C(9)—N(3)—N(2)	116.80(2)		

Table 2
Hydrogen bonding interaction parameters of HL [Å and °].

D—H...A	d(D—H)	d(H...A)	d(D...A)	∠(DHA)
N(3)—H(3N)...*S*(1)	0.86	2.66	3.004(2)	105
C(39)—H(39)...*S*(2) #1	0.93	2.87	3.644(3)	141
C(25)—H(25)...*S*(1) #2	0.93	2.83	3.569(3)	138
C(34)—H(34)...*S*(2) #3	0.93	2.73	3.657(3)	172
C(42)—H(42A)...*S*(2)	0.96	2.54	3.051	114
Symmetry transformations used to generate equivalent atoms:				
#1 −1 + x, y, z, #2 1 + x, y, z, #3 1 − x, 1 − y, 2 − z				

A torsion angle of 3.7(5)° corresponding to S(1)—C(8)—N(2)—N (3) moiety confirms the syn or *Z* configuration of S(1) atom with respect to azomethine nitrogen atom N(3). N(1) lies trans to N(3) corresponding to N(1)—C(8)—N(2)—N(3) with a torsion angle of —177.0(3)°. Atom C(9) lies trans to C(8) corresponding to C(9)—N(3)—N(2)—C(8) with a torsion angle of 177.0(2)°.

The mean plane of the phenyl rings [C(1), C(2), C(3), C(4), C(5), C(6)] and [C(10), C(11), C(12), C(13), C(14), C(15)] forms a dihedral angle of 17.60(115)°. This indicates a *Z* conformation between these planes. The mean plane of the phenyl rings [C(10), C(11), C(12), C(13), C(14), C(15)] and [C(16), C(17), C(18), C(19), C(20), C(21)] of benzophenone moiety forms a dihedral angle 76.177(138)°. It indicates that the phenyl rings of benzophenone moiety are substantially out of plane with each other. The mean plane deviation calculation shows that the central thiosemicarbazone bridge C(9)—N(3)—N(2)—C(8)—S(1) itself is nearly planar with a maximum mean plane deviation of 0.0045 Å for S(1) and C(9)—N(3)—N(2)—C(8)—(N1) with a maximum deviation of 0.0158 Å for N(1). In the crystal lattice, two dimensional packing of the molecules is stabilized by non-conventional intermolecular hydrogen bonding interactions.

3.2. Characterisation of metal complexes

3.2.1. Microanalytical data

On the basis of elemental analyses and spectral studies, the compounds were assigned empirical formulae as represented in Table 4. In the complexes **1** and **3** H_2L' acts as neutral bidendate ligand whereas in the complexes **2**, **4**, **5** and **6**, it acts as a monoanionic tridentate one (HL′).

3.2.2. Electronic spectra and magnetic moments

The electronic spectra of complexes of Co(II), Ni(II), Cu(II) and Zn(II) were recorded in solid state and their probable assignments are given in Table 5.

The ground state in tetrahedral Co(II) ion is $^4A_2$. The possible transitions are $^4A_2 \rightarrow {}^4T_2$, $^4A_2 \rightarrow {}^4T_1$ (F), $^4A_2 \rightarrow {}^4T_1$ (P). The first transition, $^4A_2 \rightarrow {}^4T_2$ is not usually observed since it occurs in the region 3000–5000 cm^{-1}. $^4A_2 \rightarrow {}^4T_1$ (P) transition appears as intense broad band in the visible region. In the present case, a band in the region 15,748–14,598 cm^{-1} (635–687 nm) may due to $^4A_2 \rightarrow {}^4T_1$ (P) absorption [19]. However, the other transitions were not observed as it is out of the range of the used spectrophotometer.

Tetrahedral Co(II) complexes show magnetic moment corresponding to the spin only value (3.88 B.M.) for three unpaired electrons. In the present investigation, the observed magnetic moment of the cobalt complex is 3.73 B.M which indicates its tetrahedral geometry.

Octahedral nickel(II) ion with d^8 configuration has $^3A_{2g}$ ground state. The three, spin-allowed transitions are $^3A_{2g}$ (F) → $^3T_{2g}$ (F), $^3A_{2g}$ (F) → $^3T_{1g}$ (F) and $^3A_{2g}$ (F) → $^3T_{1g}$ (P) which absorbs in the range 8000–11,000, 15,000–19,000 and 25,000–29,000 cm^{-1}, respectively. The broad bands observed at 14,556 (687 nm) and

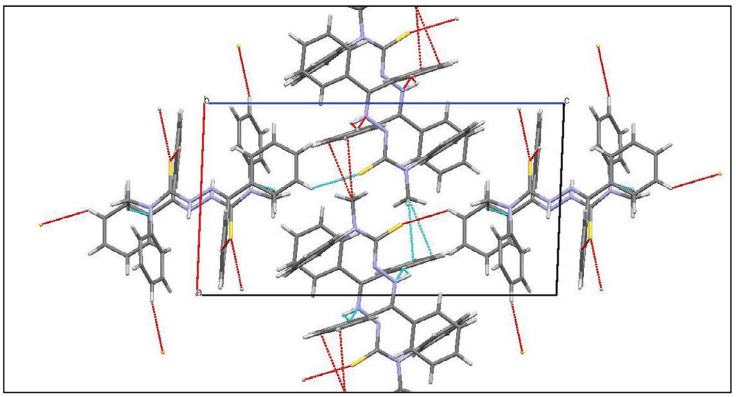

Fig. 4. Packing diagram showing intermolecular interactions of HL along b axis.

Table 4
Molecular formula, colour, partial elemental analyses and magnetic moments of the complexes.

Compound No.	Compound	Molecular weight	Colour	Yield	Melting point	Found (Calculated)					μ in B.M
						C	H	N	S	M	
	$C_{22}H_{21}N_5S_2$ (**H_2L'**)	419	Cream	85	155	62.8 (63.0)	5.2 (5.0)	16.5 (16.7)	15.0 (15.2)	–	D
1	$[Co(H_2L')(CH_3COO)_2]\cdot 2H_2O$	631.9	Green	80	225	49.3 (49.4)	4.6 (4.7)	11.2 (11.1)	10.2 (10.1)	9.1 (9.3)	3.7
2	$[Ni(HL')_2]\cdot 1.5H_2O$	921	Brown crystals	65	220	56.6 (56.8)	4.4 (4.6)	15.1 (15.2)	13.6 (13.8)	6.4 (6.4)	3.0
3	$[Ni(H_2L')_2]SO_4$	993	Brown	65	200	53.5 (53.5)	4.1 (4.2)	14.1 (14.1)	15.9 (16.1)	6.1 (5.9)	3.2
4	$[CuHL']_2$	965	Black	80	220	54.7 (54.7)	3.8 (3.9)	14.6 (14.5)	13.4 (13.3)	13 (13.1)	1.48
5	$[Cu(HL')Cl]_2\cdot 4H_2O$	1180	Green	80	160	44.9 (44.7)	3.9 (4.1)	12.1 (11.8)	10.7 (10.8)	10.5 (10.7)	D
6	$[Zn(HL')_2]$	903	Light yellow	70	199	58.8 (58.5)	4.6 (4.7)	15.6 (15.5)	14.2 (14.2)	7.4 (7.2)	D

Table 5
Electronic spectral band assignments in nm and cm^{-1}.

Compound No.	Compound	λ nm	λ cm^{-1}	Assignments
	$C_{22}H_{21}N_5S_2$ (H_2L')	254	39370.07	$\pi \rightarrow \pi^*$
		344	29069.76	$n \rightarrow \pi^*$
1	$[Co(H_2L')(CH_3COO)_2]\cdot 2H_2O$	423br	23640.6	C-T
		634br	15772.8	$^4A_2 \rightarrow {}^4T_1$ (P)
		687	14,556	$^4A_2\ ^4 \rightarrow T_1$ (P)
2	$[Ni(HL')_2]\cdot 1.5H_2O$	416	24038.4	$3A_{2\ g}(F) \rightarrow 3T_{1\ g}(P)$
		687br	14,556	$3A_{2\ g}(F) \rightarrow 3T_{2\ g}(F)$
3	$[Ni(H_2L')_2]\cdot SO_4$	308	32467.5	$n \rightarrow \pi^*$
		678	14749.2	$3T_1(F) \rightarrow 3T_1(P)$
4	$[Cu(HL')]_2$	252	39682.53	$\pi \rightarrow \pi^*$
		311	32154.3	$\pi \rightarrow \pi^*$
		349	28,653	$n \rightarrow \pi^*$
		428	23,364	C-T
5	$[Cu(HL')Cl]_2\cdot 4H_2O$	261	38314.7	$\pi \rightarrow \pi^*$
		328	30487.8	$n \rightarrow \pi^*$
		402	24,875	C-T
6	$[Zn(HL')_2]$	250	40,000	$\pi \rightarrow \pi^*$
		308	32,467	$n \rightarrow \pi^*$

Table 6
IR spectral assignments.

Compound	ν(N—H)/OH	ν(C—H)	ν(C=N)	Phenyl/CN—NH	ν(NH—CS)	ν(C=S)	ν(N—N)	νC=S	ν(M—N)
$C_{22}H_{21}N_5S_2$	3444	3165	1583	1468	1332	1269	1060	771	–
	3249	2920							
$[Co(H_2L')CH_3COO)_2]\cdot 2H_2O$	3414	3046	1599	1492	1405	1231	1045	696	478
		2924							
$[Ni(HL')_2]\cdot 1.5H_2O$	3363	3057	1555	1488	1361	1223	1065	696	469
	3133	2920							
$[Ni(H_2L')_2]SO_4$	3438	3059	1586	1492	1352	1230	1060	696	468
	3138	2920							
$[Cu(HL')]_2$	3430	3057	1596	1492	1386	1277	1051	696	473
		2923							
$[Cu(HL')Cl]_2\cdot 4H_2O$	3439	3057	1552	1489	1381	1277	1071	696	440
	3260	2924							
$[Zn(HL')_2]$	3413	3057	1586	1489	1368	1218	1058	696	445
	3317	2924	1545	1422					

24038.4 cm^{-1} (416 nm) in complex is due to $^3A_{2g}$ (F) → $^3T_{1g}$ (F) and $^3A_{2g}$ (F) → $^3T_{1g}$ (P) transitions.

The magnetic moments of octahedral Ni(II) complexes fall in the range 2.90–3.30 B.M. which is due to spin orbit coupling or higher states, mixing with the ground states [20]. In the present investigation the observed magnetic moment of the nickel complex (**2**) is 3.0 B.M which indicates octahedral coordination.

For tetrahedral nickel(II) complexes, two broad bands are observed in the visible region. One at 15,000 cm^{-1} due to $^3T_1(F) \rightarrow {}^3T_1(P)$ transition and another at 8000 cm^{-1} due to $^3T_1(F) \rightarrow {}^3A_2(F)$ transitions. The ground state for regular tetrahedral Ni(II) is $^3T_1(F)$. In the present study, complex (**3**) shows a band at 678 nm (14,749 cm^{-1}) is due to $^3T_1(F) \rightarrow {}^3T_1(P)$ transition. However, the other transition is not observed as it is out of the range of the used spectrophotometer.

Tetrahedral Ni(II) complexes are expected to have orbital contributions to the magnetic moment due to the orbital degeneracy. The spin–orbit coupling also allows the $^3T_2(F)$ term to mix with the ground state. Normally, they show magnetic moment in the range 3.6–4.10 B.M. In certain cases effective magnetic moment is found to be as low as 3.20 B.M [21]. This may be due to the distortions and inequalities in the field of coordinated ligands which give only small orbital contribution. In the present case, the observed magnetic moment of complex (**3**) is 3.2 B.M.

The tetrahedral and pseudo-tetrahedral copper(II) complexes usually show transitions in the range 7000–10,000 cm^{-1} and the energy of these bands are very low compared to square planar or distorted octahedral complexes. Square planar or distorted octahedral complexes normally show absorptions in the region 10,000–20,000 cm^{-1}. If this region is blank we can infer a tetrahedral geometry for such Cu(II) complexes. In the present investigation, no bands are observed in the region above mentioned. This confirms the tetrahedral geometry for the copper complexes (**4**) and (**5**). The compound (**4**) shows a magnetic moment 1.48 B.M. The

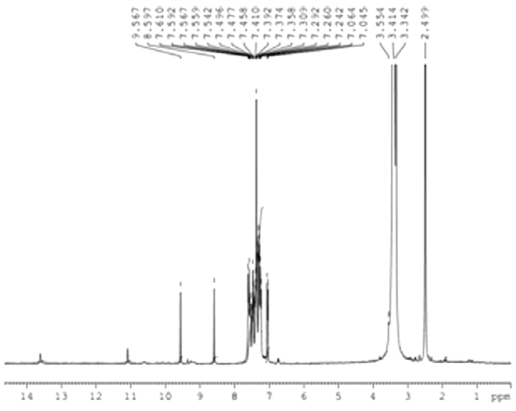

Fig. 5. NMR spectrum of $[Zn(HL')_2]$ (**6**).

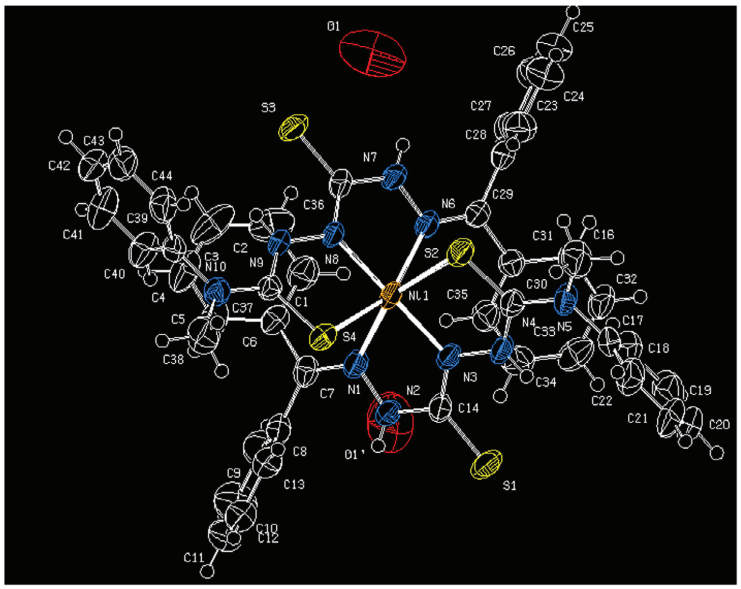

Fig. 6. *ORTEP* diagram for compound $[Ni(HL')_2]\cdot 1.5H_2O$ with atom numbering scheme.

compound **5** is diamagnetic, which strongly supports its existence as a dimer in the solid state [22]. The low magnetic moment value of copper complex (**4**) is in accordance with that of dimers having antiferro or ferromagnetic interactions [23]. No absorptions are observed in the visible region for Zn(II) complex as they are in d^{10} configuration and diamagnetic in nature.

3.2.3. Vibrational spectra

The IR spectral assignments are depicted in the Table 6. In the complexes, N—H region shows a slight shift in the centres of the bands to a lower frequency. The band at 1583 cm^{-1} in the free ligand is assigned to *ν*(C=N) stretching. However, in the complexes this band is shifted to higher (2–27 cm^{-1}) or lower (5 cm^{-1}) wave

Table 7
Selected bond lengths (Å), bond angles and torsion angles (°).

C(14)—N(3)	1.312(7)	N(3)—C(14)—N(2)—N(1)	12.6(6)	C(15)—S(2)—Ni(1)	95.5(2)
C(14)—N(2)	1.371(7)	S(1)—C(14)—N(2)—N(1)	−166.8(3)	N(1)—Ni(1)—S(2)	155.92(12)
C(14)—S(1)	1.696(5)	N(2)—C(14)—N(3)—Ni(1)	6.1(6)	N(6)—Ni(1)—S(2)	83.45(12)
C(15)—N(4)	1.339(7)	S(1)—C(14)—N(3)—N(4)	2.4(6)	S(4)—Ni(1)—S(2)	100.67(6)
C(15)—N(5)	1.343(7)	S(1)—C(14)—N(3)—Ni(1)	−174.6(2)	N(7)—N(6)—Ni(1)—N(3)	−166.2(3)
C(15)—S(2)	1.704(5)	S(2)—C(15)—N(4)—N(3)	0.9(6)	N(7)—N(6)—Ni(1)—N(8)	17.2(3)
C(36)—N(8)	1.302(6)	S(2)—C(15)—N(4)—H(4 A)	−174(3)	N(7)—N(6)—Ni(1)—S(2)	−86.2(3)
C(36)—N(7)	1.393(7)	N(4)—C(15)—S(2)—Ni(1)	−6.0(4)	N(7)—N(6)—Ni(1)—S(4)	15.4(4)
C(36)—S(3)	1.694(5)	N(5)—C(15)—S(2)—Ni(1)	174.2(4)	Ni(1)—N(8)—N(9)—C(37)	10.3(5)
C(37)—N(9)	1.335(6)	Ni(1)—N(1)—N(2)—C(14)	−20.5(5)	N(1)—Ni(1)—S(2)	155.92(12)
C(37)—N(10)	1.352(6)	C(7)—N(1)—Ni(1)—N(3)	167.3(4)	C(36)—N(8)—Ni(1)—N(1)	−110.4(3)
C(37)—S(4)	1.707(5)	C(7)—N(1)—Ni(1)—N(6)	−91.0(4)	C(36)—N(8)—Ni(1)—N(3)	−63(2)
N(1)—N(2)	1.394(6)	C(7)—N(1)—Ni(1)—N(8)	−16.0(4)	C(36)—N(8)—Ni(1)—N(6)	−13.2(3)
N(1)—Ni(1)	2.328(5)	C(7)—N(1)—Ni(1)—S(2)	171.6(3)	C(36)—N(8)—Ni(1)—S(2)	66.5(3)
N(3)—N(4)	1.375(6)	C(7)—N(1)—Ni(1)—S(4)	65.4(4)	C(36)—N(8)—Ni(1)—S(40	166.1(3)
N(3)—Ni(1)	1.959(4)	N(2)—N(1)—Ni(1)—N(3)	16.5(3)	N(9)—N(8)—Ni(1)—N(1)	73.1(3)
N(6)—N(7)	1.378(6)	N(2)—N(1)—Ni(1)—N(6)	118.3(3)	N(9)—N(8)—Ni(1)—N(3)	120(2)
N(6)—Ni(1)	2.394(4)	N(2)—N(1)—Ni(1)—N(8)	−166.7(3)	N(9)—N(8)—Ni(1)—N(6)	170.2(3)
N(8)—N(9)	1.390(6)	N(2)—N(1)—Ni(1)—S(2)	20.8(4)	N(9)—N(8)—Ni(1)—S(2)	−110.0(3)
N(8)—Ni(1)	1.948(4)	N(2)—N(1)—Ni(1)—S(4)	−85.3(3)	N(9)—N(8)—Ni(1)—S(4)	−10.5(3)
Ni(1)—S(4)	2.4194(17)	Ni(1)—N(3)—N(4)—C(15)	7.1(6)	C(15)—S(2)—Ni(1)—N(1)	2.5(3)
Ni(1)—S(2)	2.4318(17)	C(14)—N(3)—Ni(1)—N(1)	−13.2(3)	C(15)—S(2)—Ni(1)—N(3)	6.7(2)
C(29)—N(6)	1.297(7)	C(14)—N(3)—Ni(1)—N(6)	−110.3(4)	C(15)—S(2)—Ni(1)—N(6)	−98.5(2)
N(1)—Ni(1)—N(6)	100.44(16)	C(14)—N(3)—Ni(1)—N(8)	−61(2)	C(15)—S(2)—Ni(1)—N(8)	−170.0(2)
N(8)—Ni(1)—S(4)	82.67(13)	C(14)—N(3)—Ni(1)—S(2)	168.5(4)	C(15)—S(2)—Ni(1)—S(4)	105.5(2)
N(3)—Ni(1)—S(4)	100.08(15)	C(14)—N(3)-Ni(1)—S(4)	69.1(4)	C(37)—S(4)—Ni(1)—N(1)	-96.0(2)
N(1)—Ni(1)—S(4)	85.54(12)	N(4)—N(3)—Ni(1)—N(1)	169.9(4)	C(37)—S(4)—Ni(1)—N(3)	−169.1(2)
N(6)—Ni(1)—S(4)	155.83(11)	C(29)—N(6)—Ni(1)—S(2)	61.7(4)	C(37)—S(4)—Ni(1)—N(6)	9.3(3)
N(8)—Ni(1)—S(2)	100.75(14)	C(29)—N(6)—Ni(1)—S(4)	163.4(3)	C(37)—S(4)—Ni(1)—N(8)	7.7(2)
N(3)—Ni(1)—S(2)	81.84(14)	N(7)—N(6)—Ni(1)—N(1)	117.7(3)	C(37)—S(4)—Ni(1)—S(2)	107.3(2)

Table 8
Hydrogen bonding interaction parameters [Å and °]

D—H...A	d(D—H)	d(H...A)	d(D...A)	∠(DHA)
N(4)—H(4A)...S(1)	0.84(4)	2.47(4)	2.9(5)	113(3)
N(7)—H(7A)...O(1)	0.85(3)	2.47(3)	3.32(7)	150(3)
N(9)—H(9A)...S(3)	0.85(4)	2.39(4)	2.896(4)	119(3)
C(38)—H(38a)...S(4)	0.96	2.68	3.05 (6)	103
C(43)—H(43)...S(2)#1	0.93	2.82	3.49(7)	130
Symmetry transformations used to generate equivalent atoms:				
#1 1 – x, 1 – y, 1 – z				

numbers indicating the participation of azomethine nitrogen in coordination [24]. Since there are more than one N—H, C=N, C=S groups, we couldn't clearly explain the shifts of these bands in all the complexes. Appearance of new bands in the spectra of complexes in the region 440–478 cm^{-1} is assigned to (M—N) stretching vibration [25–27]. The bands appearing in the regions 1490–1440 cm^{-1}, 1100–1064 cm^{-1} and 805–740 cm^{-1} are due to usual modes of phenyl ring vibration [28]. The ligand can exhibit thione-thiol tautomerism since it contains two thioamido —NH—C=S functional group. The ν(S—H) band (2560 cm^{-1}) is absent in the IR spectrum of ligand, but ν(N—H) band is present at 3260–3057 cm^{-1}, indicating that in solid state, the ligand remains as the thione tautomer [29,20,30]. The appearance of broad bands around 3400 cm^{-1} in the spectra of complexes may be due to ν(OH) of the water molecules [31–33]. The bands near 1340 and 771 cm^{-1} in the free ligand may be assigned to

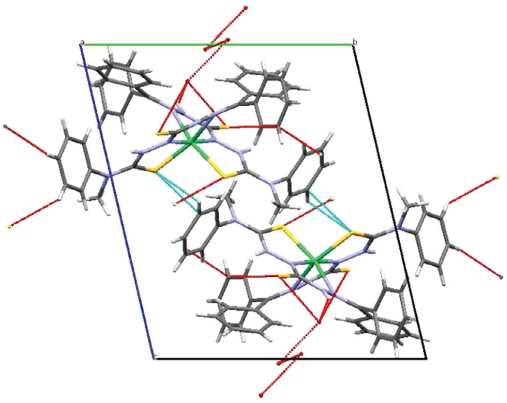

Fig. 7. Packing diagram of $Ni(HL')_2 \cdot 1.5H_2O$ along the a axis showing intermolecular interactions.

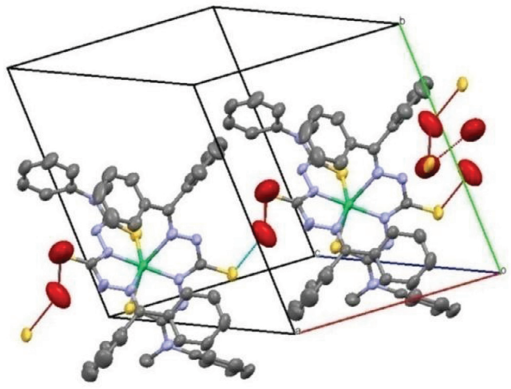

Fig. 8. Supramolecular chain of $[Ni(HL')_2] \cdot 1.5H_2O$ interlinked with water molecule (omitting H atoms).

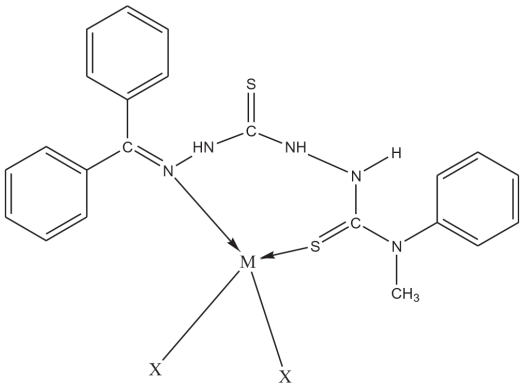

Fig. 9. Proposed structure of complex, $[M(H_2L')X_2]$, where M = Co(II), X = CH_3COO (**1**).

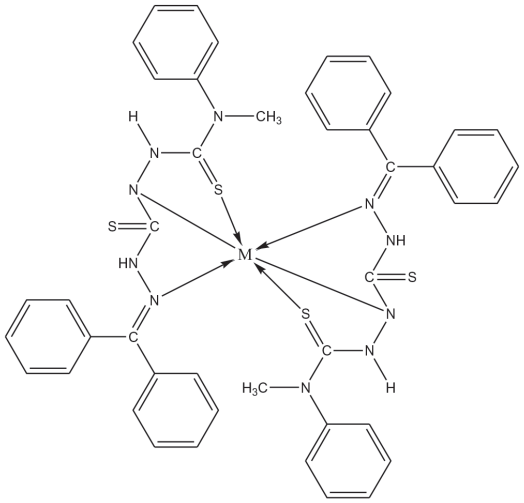

Fig. 10. Proposed structure of complex, $[M(HL')_2]$, where M = Ni(II) (**3**).

ν(NH—C═S) and ν(C═S) vibrations. These bands are seen to be shifted to lower or higher wave numbers in the spectra of the complexes indicating the involvement of sulphur in coordination. We can thus conclude that ligand can act as bidentate/tridentate one coordinating through azomethine nitrogen, hydrazine nitrogen and thione/thiolato sulfur.

3.2.3.1. Coordination of anions. The ν_{as}(COO—) and ν_s(COO—) stretching frequencies of the free acetate ions are observed at 1560 and 1416 cm^{-1}, respectively [34]. In the present study for the complex (**1**), ν_{as}(COO—) and ν_s(COO—) are found at 1632 and 1405 cm^{-1} [35]. As expected, the energy of separation between these two are greater than 144 cm^{-1} [36]. This is in favour of unidentate coordination of acetate group in complex (**1**).

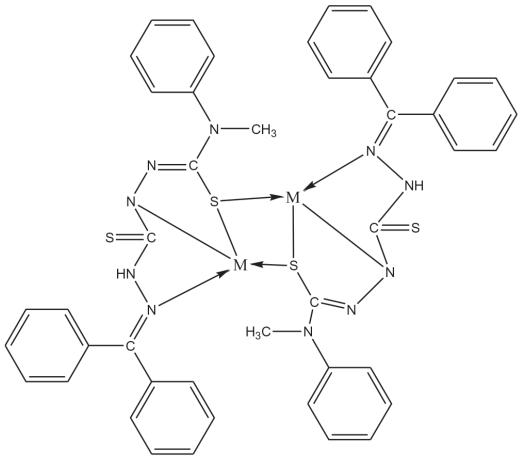

Fig. 11. Proposed structure of complex, $[M(HL')]_2$, where M = Cu(II) (**4**).

3.2.4. NMR spectrum of $[Zn(HL')_2]$

The NMR spectrum of $[Zn(HL')_2]$ in DMSO is presented in Fig. 5. A singlet at 9.567 ppm is attributed to N—H proton. Singlet peak at 8.59 ppm may be assigned to N—H proton adjacent to azomethine group. Aromatic protons show multiplets in the range 7.04–7.61 ppm. Singlet peak in the range 3.34–3.55 ppm is attributed to N—CH_3 protons.

3.2.5. Thermal studies

The thermal decomposition of $[Ni(HL')_2]\cdot 1.5H_2O$ occurs in two stages. It is evident from DTG peaks at 200 and 290 °C. The first stage is at 150–230 °C and demonstrates a mass-loss of 2%, corresponding to the loss of a water molecule (calc. 1.96%). The second stage occurs at 250–400 °C, with a mass loss of 61%. The residual mass of 11.8% is observed at 750 °C and may be due to the formation of nickel sulphide (calc. 11.6%).

For $[Cu(HL')_2]$, two stage decomposition occurs in the temperature range 260–390 °C which may be due to the partial decomposition of ligand moiety. A residual mass of 15% was observed at 750 °C which may be due to the formation of Cu_2S (calc. 14.8%).

For $[Zn(HL')_2]$, the decomposition occurs in three stages in the temperature range 240–410 °C which may be due to the decomposition of the ligand moiety. The residual mass of 9.3% is observed at 750 °C which may be due to the formation of ZnO (calc. 9.0%).

3.2.6. Crystal structure of nickel complex

Single crystals of $Ni(HL')_2\cdot 1.5H_2O$ (**2**) suitable for X-ray analysis were obtained from its solution in 1:1 (v/v) mixture of methanol and DMF. A crystal with dimensions of $0.630 \times 0.560 \times 0.510\ mm^3$ was selected for collecting the data.

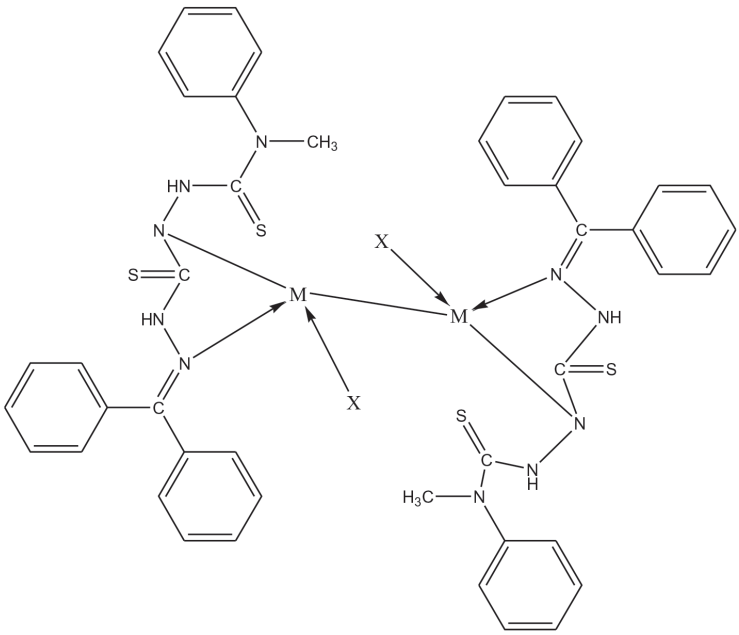

Fig. 12. Proposed structure of complex $[M(HL')X]_2$, where M = Cu(II) (**5**).

$[Ni(HL')_2]\cdot 1.5H_2O$ crystallized with one molecule per asymmetric unit into triclinic crystal system with a space group of *P*-1. *ORTEP* diagram for compound $[Ni(HL')_2]\cdot 1.5H_2O$ with atom numbering scheme is depicted in Fig. 6. Crystal data and structure refinement parameters of complex are given in Table 1. Selected bond lengths and bond angles are summarized in Table 7. The important hydrogen bonding interaction parameters are listed in Table 8.

The single crystal X-ray diffraction studies disclose the occurrence of 6-coordinate nickel(II) complex with a distorted octahedral geometry. One half of the molecule of the complex is related to the other half by a two-fold axis passing through Ni(II) atom. It is coordinated through the azomethine N, hydrazine N and the thione S atoms of two deprotonated ligands in a meridonal fashion. The metal center is shared by four fused five membered chelate rings. The adjacent molecules are arranged in an offset manner within the unit cell when viewed along the **c** axis.

An interesting attribute of the crystal packing is the formation of a supramolecular chain linked by water molecule. Fig. 7. shows packing diagram of $Ni(HL')_2\cdot 1.5H_2O$ along the a axis showing intermolecular interactions. Fig. 8. shows supramolecular chain interlinked with water molecule along **c** axis(omitting H atoms). In the crystal, the molecules are interconnected by N—H...S and N—H...O interactions, forming a three dimensional network.

The bond lengths, C(14)—N(3), C(29)—N(6) bonds to 1.312(7) and 1.297(7) Å respectively, are shorter, when compared to C—N bonds which are not involved in coordination. Comparatively shorter bond lengths, N(3)—Ni(1) 1.959; N(6)—Ni(1) 2.394; N(8)—Ni(1) 1.948; Ni(1)—S(4) 2.4194; N(8)—Ni(1) 1.948 Å indicate strong coordination of the ligand with Ni(II).

The bite angles, N(6)—Ni(1)—S(4) (155.83°), N(1)—Ni(1)—S(2) (155.92°), N(8)—Ni(1)—S(4) (82.67°), N(6)—Ni(1)—S(2) 83.45(12), N(8)—Ni(1)—S(2) (100.75°), S(4)—Ni(1)—S(2) (100.67°) and N(3)—Ni(1)—S(2) (81.84°) are somewhat far from a perfect octahedron indicating significant distortion in the geometry.

4. Conclusions

The two dimensional packing of Benzophenone N(4)-methyl-N(4)-phenylthiosemicarbazone (HL) is stabilized by non-conventional intermolecular hydrogen bonding interactions. From crystal data and IR data, it is clear that in the solid state, the compound is in thione form. From the UV–Vis spectrum, it is clear that the crystal is transparent in the region between 420 and 900 nm. Hence, this compound can be used for photonic and optoelectronic applications in future studies. The ligand, 1-(aminoN-methyl-*N*-phenylmethanethio)(diphenylmethylene)thiocarbonohydrazide (H_2L') acts as monoanionic tridentate one in **2**, **4**, **5** and **6**, and as neutral bidentate one in **1** and **3** complexes. The complexes **1**, **3**, **4** and **5** have a tetrahedral geometry and **2** and **6** have an octahedral geometry. The single crystal X-ray diffraction studies of complex **2** revealed the occurrence of 6-coordinate distorted octahedral geometry and are also proposed for complex **6**. Based on the elemental analyses, spectral, magnetic and thermal investigations, following tentative structures were assigned for the complexes (Figs. 9–12).

Acknowledgements

The authors are grateful to SAIF, Cochin University of Science and Technology, Kochi, Kerala, India for elemental analyses and single crystal XRD result. The authors are also grateful to School of Pure and Applied Physics, M G University, Kottayam, for single crystal XRD result of nickel(II) complex. One of the authors (K. G) is thankful to the University Grants Commission, Bangalore, for financial assistance in the form of a FDP fellowship.

Appendix A. Supplementary data

Crystallographic data for the structure reported in this article have been deposited with the Cambridge Crystallographic Centre CCDC No: 1481064, 1551080. Copies of the data can be obtained free of charge from The Director, CCDC, 12 Union Road, Cambridge CB2 1EZ, UK; fax (+44) 1223-336-033 or e-mail: deposit@ccdc.cam.ac.uk. Supplementary data associated with this article can be found, in the online version, at https://doi.org/10.1016/j.ica.2017.09.057.

References

[1] S.E. Blanco, J.J. Silber, F.H. Ferretti, J. Mol. Struct. (Theochem). 582 (2002) 91.
[2] A.A. Osowole, R. Kempe, R. Schobert, Int. Res. J. Pure Appl. Chem. 2 (2) (2012) 105.
[3] P. Jandera, M. Skavrada, L. Andel, D. Komers, G. Guiochon, J. Chromatogr. 908A (2001) 3.
[4] A.K. Kadry, C.S. Okereke, M.S. Abdel-Rahman, M.A. Friedman, R.A. Davis, J. Appl. Toxicol. 15 (1995) 97.
[5] R. Siles, S. Chen, M. Zhou, K.G. Pinney, M.L. Trawick, Bioorg. Med. Chem. Lett. 16 (16) (2006) 4405.
[6] A.A. Jarrahpour, M. Zarei, Molbank 374 (2004) 243.
[7] Nan. Zhang, Yanxue. Tai, Mingxue. Li, Pengtao. Ma, Junwei. Zhao, Jingyang Niu, Dalton Trans. 43 (2014) 5182.
[8] Yan-Xue Tai, Yu-Mei Ji, Yan-Li Lu, Mi-Xue Li, Yuan-Yuan Wu, Qiu-Xia Han, Synth. Met. 219 (2016) 109.
[9] D.L. Klayman, J.F. Bartosevich, T.S. Griffin, C.J. Mason, J.P. Scovill, J. Med. Chem. 22 (1979) 855;
B. Le Guennic, S. Petit, G. Chastanet, G. Pilet, D. Luneau, N. BenAmor, V. Robert, Inorg. Chem. 47 (2008) 572.
[10] M. Wang, L.-F. Wang, Y.-Z. Li, Q.-X. Li, Z.-D. Xu, D.-M. Qu, Transit. Met. Chem. 26 (2001) 307;
J. Yoon, E.I. Solomon, Coord. Chem. Rev. 251 (2007) 379.
[11] A.L. Speck, PLATON, Utrechi University, Utrecht, The Netherlands, A Multipurpose Crystallographic Tool, 1999.
[12] C.F. Macrae, P.R. Edington, P. McCabe, E. Pidcock, G.P. Sheilds, R. Taylor, M. Towler, J. Van de Streek, J. Appl. Crystallogr. 39 (2006) 453.
[13] J.P. Scovill, D.L. Klayman, C.F. Franchino, J. Med. Chem. 25 (1982) 1261.
[14] J.P. Scovill, Phosphorus, Sulfur Silicon Relat. Elem. 60 (1991) 25.
[15] G.J. Palenik, D.F. Rcndle, W.S. Cruler, Acta Crystallogr. 830 (1974) 2390.
[16] K.O. Ferraz, S.M.S.V. Wardell, J.L. Wardell, S.R.W. Louro, H. Beraldo, Spectrochim. Acta, Part A 73 (2009) 140.
[17] H. Arslan, U. Florke, N. Kulcu, G. Binzet, Spectrochim. Acta, Part A 68 (2007) 1347.
[18] V. Suni, M.R.P. Kurup, M. Nethaji, Spectrochim. Acta 63A (2006) 174.
[19] B.P. Singh, Int. Pharm. Res. Dev. 4 (3) (2012) 51.
[20] A.B.P. Lever, Inorganic Electronic Spectroscopy, second ed., Elsevier, Amsterdam, 1984.
[21] L. Sacconi, Transition Metal Chemistry, in: R.L. Carlin (Ed.), 4 (1968) 199.
[22] D. Sutton, Electronic Spectra of transition metal complexes, MC Graw Hill, Landon, 1968.
[23] O. Maddock, A. Sharpe, R.L. Martin, Proc. R. Austr. Chem. Inst. 38 (1971) 33.
[24] G.G. Mohamed, M.M. Omar, A.M.M. Hindy, Spectrochim. Acta, Part A 62 (2005) 1140.
[25] M.M. Omar, G.G. Mohamed, A.M.M. Hindy, J. Therm. Anal. Calorim. 86 (2006).
[26] G.G. Mohamed, M.M. Omar, A.M. Hindy, Turk. J. Chem. 30 (2006) 3.
[27] Mohammad Shakira, Ambreen Abbasia, Asad U. Khanb, Shahper N. Khan, Spectrochim. Acta, Part A 78 (2011) 29.
[28] A.H. Al-Amiery, K. Al-Majedy, H.A. Razzaq, J. Al-Nahrain Univ. 14 (1) (2011) 7.
[29] M.H. Moustafa, A.A. Elnaeem, O.A. Abbas, Ass. Univ. Bull. Environ. Res. 14 (2) (2011) 27.
[30] K. Krishnankutty, M.B. Ummathur, D.K. Babu, J. Serb. Chem. Soc. 75 (5) (2010) 639.
[31] A.P. Mishra, D.K. Mishra, Int. J. Pharm. Biol. Sci. 2 (2011) 430.
[32] R.M. Issa, A.M. Khedr, H.F. Rizk, Spectrochim. Acta, Part A 62 (2005) 621.
[33] M.H. Habibi, M. Montazerozohori, A. Lalegani, R.W. Harrington, W. Clegg, J. Fluor. Chem. 127 (2006) 769.
[34] Joshi Kuncheria., Ph.D Thesis, University of Calicut, 1992.
[35] N.F. Curtis, J. Chem. Soc. A (1968) 1579.
[36] K. Nakamoto, Infrared and Raman Spectra of Inorganic and Coordination Compounds, third ed., John Wiely and Sons, NY, 1978.

wjpmr, 2017,3(9), 238-245

SJIF Impact Factor: 4.103

WORLD JOURNAL OF PHARMACEUTICAL AND MEDICAL RESEARCH
www.wjpmr.com

Research Article
ISSN 2455-3301
WJPMR

EXPLORING THE COORDINATION CAPABILITIES, THERMAL AND ANTIMICROBIAL STUDIES OF 1-PHENYL-3-METHYL-4-BENZOYL-5-PYRAZOLONE N (4)- METHYL- N(4)-PHENYLTHIOSEMICARBAZONE

K. G. Sangeetha* and K. K. Aravindakshan

Department of Chemistry, University of Calicut, 673635, Kerala, India.

***Corresponding Author: K. G. Sangeetha**
Department of Chemistry, University of Calicut, 673635, Kerala, India.

Article Received on 09/08/2017 **Article Revised on 29/08/2017** **Article Accepted on 19/09/2017**

ABSTRACT

Transition metal complexes of an ONS donor ligand, 1-phenyl-3-methyl-4-benzoyl-5-pyrazolone, N(4)-methyl-N(4)-phenylthiosemicarbazone (H_2L) were synthesised. The metal complexes were characterized by elemental analyses, magnetic susceptibility measurements, electronic, vibrational and ^{1}H-NMR spectra. ESR spectrum of the copper(II) complex was recorded. Thermal stabilities of the complexes were also ascertained. The preliminary *in vitro* antimicrobial screening of the ligand, copper and zinc complexes were also performed. For this studies, four fungal strains, three Gram (-ve) and three Gram (+ve) bacteria were used. Complexes showed better microbial inhibition activity than the ligand.

KEYWORDS: N(4)-Methyl-N(4)-phenylthiosemicarbazide, 1-phenyl-3-methyl-4-benzoyl-5- pyrazolone, complexes, magnetic susceptibility.

INTRODUCTION

Thiosemicarbazones are considered as one of the most vital scaffolds and are embedded in many biologically active compounds. They belong to the family of thiourea derivatives. Parent aldehyde or ketone moiety in the compound has a substantial role towards its biological property. Metal complexes of thiosemicarbazones show more activity than the free ligands.[1] A mesmerizing feature of thiosemicarbazones is that, they generally exist in the thioketo form in the solid state, while in solution state, they display a thioketo- thioenol tautomerism. In thioketo form they act as a neutral bidentate ligands and the enol form they deprotonate and act as monoanionic bidentate ligand towards metal ions. They can exist in *E* form (*trans*-) and Z form (cis-).[2] In *E* form they will act as monodentate ligands by coordinating through the sulphur atom alone. If the sulfur centre is substituted, the bonding may occur through the hydrazine nitrogen and the amide nitrogen atoms. Generally, the compound is in the *Z*-form while coordinating to the metal ions and is attributed to the chelate effect on complexation. When an extra coordination site is present near to the donating centres, they will coordinate in a tridentate manner.

Studies showed that the substitutions at the terminal positions of thiosemicarbazones have much improved their anticancer activity.[3] Biological properties are enhanced when these molecules are substituted at the 4th nitrogen. The presence of phenyl group at N(4) position of isatin-β thiosemicarbazones derivatives exposed increased cytotoxicity against the parental KB-3-1 cell lines and the P-glycoprotein-expressing cell line KB-V1.[4,5]

Pyrazolone derivatives are used as starting materials for the synthesis of biologically active compounds and for the construction of condensed heterocyclic systems.[6] They are found to exhibit keto-enol tautomerism. Yuting Zhong *et al.*[7] reported the crystal structure and photoisomerism of 1-phenyl-3-methyl-4-(4-fluorobenzal)-5-pyrazolone 4-methylthiosemicarbazone in the solid state. However, pyrazolone-based thiosemicarbazone chemistry is less extensive.

For a last few decades, we have been in constant hunt of the synthesis and structural characterization of a variety of Schiff bases with the aim to correlate their structure with chelating ability and biological activity.[8,9] It is found that most of the microbes are resistant towards the available antibiotics. So there is a crucial need for the development of new and useful antimicrobial agents. Therefore, designing antimicrobial agents which are distinct from those of the classical antibiotics becomes one of the main aims of our current study.

So we focused on the synthesis of thiosemicarbazones with disubstitution at N(4) position (methyl and phenyl groups). The current study describes the syntheses of 1-phenyl-3-methyl-4-benzoyl-5-pyrazolone N(4)-methyl-

N(4)-phenylthiosemicarbazone (H_2L), their nine transition metal complexes and their spectral, thermal and *in vitro* antimicrobial properties.

EXPERIMENTAL

Materials

N(4)-Methyl-N(4)-phenylthiosemicarbazide was prepared according to the reported procedure.[10] 1-Phenyl-3-methyl-4-benzoyl-5-pyrazolone was prepared by using Jenson's method.[11]. Commercially available metal salts were used without further purification. The solvents were purified and dried according to the standard procedures.

Preparation

Preparation of 1-phenyl-3-methyl-4-benzoyl-5-pyrazolone N (4)-methyl-N (4)-Phenylthiosemicarbazone

The ligand was prepared by stirring the hot methanolic solution of 1- phenyl-3-methyl-4-benzoyl-5-pyrazolone (PMBP) (750mg, 2.76mmol) and N (4)-methyl-N (4)-

Phenylthiosemicarbazide (MPTSC) (500mg, 2.76mmol) on a magnetic stirrer, followed by refluxing at 60-80°C for 30 minutes. The ligand formed was filtered and washed with methanol and dried over anhydrous $CaCl_2$. The suggested empirical formula for the ligand is $C_{25}H_{23}N_5OS$.

General procedure for the preparation of metal complexes

Ligand (H_2L) (1mmol) was dissolved in two or three drops of chloroform and excess of hot methanol. To this solution, metal salt (1mmol) dissolved in hot water/ hot methanol was added dropwise and refluxed for 3-4 h. The precipitate formed was filtered. It was then washed with water followed by methanol and dried over $CaCl_2$ in a desiccator.

Physicochemical techniques

Elemental analyses were performed on EURO VECTOR CHNS analyser Model No: EA 3000. Electronic spectra were recorded on JascoV-550 UV-Vis spectrometer. Infrared (IR) spectra were recorded on a Jasco-FT-IR-4100 model spectrometer using KBr pellets. NMR was recorded on 400MHz BrukerAvance111 FT NMR spectrometer. The magnetic susceptibilities of the complexes at room temperature were measured using Sherwood Scientific Magnetic Susceptibility Balance. Diamagnetic corrections were made using Pascal's constants for all atoms and bonds. TG was recorded on TGA Q50 V20.13 Build 39 model thermo gravimetric analyzer fitted with a thermal analysis controller. DSC of the ligand was recorded on a Perkin Elmer DSC apparatus 4000 series. The ESR spectrum of copper complex was recorded on FA200 ESR instrument calibrated with Mn^{2+} marker. The melting points of the ligand and complexes were determined using a melting point apparatus.

Procedure for antimicrobial studies

Antibacterial studies

The synthetized compounds were tested *in vitro* for their antibacterial activity against Gram positive and Gram-negative organisms by Kirby–Bauer agar diffusion method.[12] Mueller–Hinton agar medium was used in this method. The bacterial strains used were *Staphylococcus aureus* (MTCC 3160), *Enterococcus faecalis, Bacillus subtili* (MTCC-619), *E.coli* (MTCC 4296), *pseudomonas aeruginosa* (MTCC 2488) and *Klebsiella Pneumonia*. Muller Hinton Agar plates were prepared and the test microorganisms were inoculated by the spread plate method. Filter paper discs, approximately 6 mm in diameter, were soaked with 10µl of the test substance. It is allowed to dry and placed in the previously prepared agar plates. Each disc was pressed down to ensure complete contact with the agar surface and distributed evenly so that they are no closer than 24 mm (center to center) from each other. The agar plates were then incubated at 37ºC. After 16 to 18 hours of incubation, each plate was examined. The activity was measured by calculating the diameter of the inhibition zone (in mm). Standard antibiotics, Kanamycin and Ampicillin (10 µg/disc), were used as the positive control. DMSO was used as a negative control under the same conditions for each organism and no activity was found. The activity results were calculated as a mean of triplicates. Dilution susceptibility testing methods were used to determine the minimal concentration of antimicrobial needed to inhibit or kill the microorganism. The test compounds were diluted to get a series of concentrations from 2000 ppm to 0.315 ppm in seven test tubes. The microorganism suspension of 500µl was added to the broth dilutions. In control 1, added culture and broth and in control 2 added the compound and broth. These were incubated for 18 hours at 37ºC. MIC of each sample was taken as the lowest concentration that did not give any visible bacterial growth.

Antifungal studies

The antifungal activities of the ligand and complexes were tested against *Alternaria alternata* MTCC 2724, *Aspergillus* niger (MTCC282), *Colletotrichum gloeosporioides* (MTCC 3439), *Candida Albicans* ((MTCC 227) using Potato-Dextrose agar medium(PDA).[13] This is having the composition, potato 200g, dextrose 20 g, agar–agar 20 g and distilled water 1000 ml. To the molten PDA medium, requisite amount of the ligand was added after being dissolved in DMSO to get certain concentrations (20 to 60 ppm). The amended medium then was poured into sterile Petri plates and allowed to solidify. After solidification, 5mm diameter mycelia discs were taken from the actively growing 48hrs old culture by using a sterile cork borer and placed on the medium with the help of inoculum's needle. For the control, the discs were inoculated on PDA medium without the ligand. These Petri plates were placed in an incubator at room temperature. Triplicates were used in each case. The diametrical growth of the fungus was recorded in each Petri plate and average

growth of the fungal colony after 72 h and the percentage inhibition was calculated by the equation: Percentage inhibition = C-T x 100/C, where *C* and *T* are the diameters of the fungal colony in the control and the test plates, respectively.

RESULTS AND DISCUSSION

Formulae and general properties of the ligand

The empirical formula, melting point, colour, partial elemental analyses and magnetic moments of the ligand and its metal complexes are depicted in Table 1.

The ligand and all the complexes were found to be stable at room temperature. The colour of all the complexes indicate the presence of sulfur-to-metal charge-transfer transitions.[14] In complexes, the ligand coordinates in dianionic(L^{2-}), monoanionic (HL^-) or neutral (HL_2) form. Elemental analyses values were in good harmony with the proposed empirical formula.

Table 1: The empirical formula, melting point, colour, partial elemental analyses, and magnetic moments of the ligand and its metal complexes.

Complex No:	Compound	M.W	M.P	Colour	Yield	Elemental Analysis Found(calculated)					μ in BM
						C	H	N	S	M	
	$C_{25}H_{23}N_5OS$	442	163	Yellow	80	68.2 (68.0)	5.2 (5.0)	15.9 (15.9)	7.2 (7.3)	–	–
1	$[NiHLCH_3COO]$	559	225	brown	70	53.5 (53.6)	4.0 (4.2)	12.5 (12.5)	6.0 (5.7)	10.3 (10.5)	D
2	$[Ni(HL)_2]H_2O$	960	204	light green	70	62.4 (62.5)	4.8 (4.6)	14.8 (14.6)	7.0 (6.7)	5.8 (5.8)	2.7
3	$[Cu(HL)_2]H_2O$	965	203	green	80	62.2 (62.2)	4.6 (4.8)	14.5 (14.5)	6.8 (6.6)	6.8 (6.6)	2.1
4	[Cu(HL)Cl]	541	230	dark green	80	55.7 (55.5)	3.7 (4.0)	12.8 (12.9)	5.8 (5.9)	11.9 (11.7)	1.7
5	$[Cu(HL)NO_3]$	568	215	green	80	52.8 (52.8)	3.7 (3.9)	12.0 (12.3)	5.8 (5.6)	10.9 (11.1)	1.7
6	$[(CuHL)_2(OH)_2]$ $5H_2O$	1135	195	green	70	53.0 (52.7)	4.7 (4.9)	12.1 (12.3)	5.8 (5.6)	10.9 (11.1)	D
7	$[Zn(HL)_2]$	948	190	yellow	80	63.3 (63.4)	4.6 (4.6)	14.6 (14.8)	7.0 (6.8)	6.9 (6.9)	D
8	$[(ZnHL)_2(NO_3)_2]$ $2H_2O$	1174	130	yellow	80	51.0 (51.1)	4.0 (4.0)	14.0 (14.3)	5.3 (5.4)	11.2 (11.1)	D
9	$[(ZnHL)_2(OH)_2]$ $2H_2O$	1138	178	yellow	70	52.7 (52.7)	4.6 (4.9)	12.2 (12.3)	5.7 (5.6)	11.4 (11.5)	D

Electronic spectra and magnetic moment

The electronic spectrum of ligand registered bands at 259, 321 and 425 nm in the solid state. The complexes have bands in the range 250-260 and 320-360 nm, which are due to $\pi \rightarrow \pi^*$ and $n \rightarrow \pi^*$ transitions. Additonal bands were observed in the range 350-390 nm in the spectra of complexes. These may be due to sulphur to metal charge-transfer transitions.

Ni (II) complex (1) showed a single broad band at 509 nm could be assigned to $^1A_{1g} \rightarrow {}^1B_{1g}$ transition. This is consistent with square planar geometry.[15] For the complex (2), broad bands at 873 nm, due to $^3A_{2g} \rightarrow {}^3T_{2g}(F)$ and 590 nm, due to $^3A_{2g} \rightarrow {}^3T_{1g}(F)$ transitions were observed. The broad band between 330-410 nm may be assigned for charge-transfer as well as to the $^3A_{2g}$ (F) $\rightarrow {}^3T_{1g}$ (P) transitions and is consistent with the octahedral geometry.

The broad band observed at 532 nm in the complex (3) is assigned to $^2E_g \rightarrow {}^2T_{2g}$ transition. This is in agreement with the octahedral geometry of this complex.

The coordinated anions, X-Cu (II) charge-transfer was observed at 400-500 nm. For the complex 4, the Cl-Cu (II) charge-transfer band was found at 488 nm. In the complex (5), the O-Cu (II) charge-transfer band was observed at 419 nm. Complexes (4), (5) and (6) have broad d-d combination bands in the range 666-588 cm^{-1} and appear as a shoulder on the intraligand and charge transfer bands. In accordance with previous observation, such an attribute is expected for a square planar Cu (II) complex.

As expected zinc complexes shows band almost similar to the ligand. The electronic spectral data of the ligand and the complexes are shown in Table 2.

[NiHLCH$_3$COO] (1) is diamagnetic with square planar geometry. The magnetic moment of complex (2) is 2.7 B.M. and supports its octahedral geometry. The complex (3) shows magnetic moment value 2.1 B.M. supporting its distorted octahedral structure. The magnetic moment values of the complexes (4) and (5) are found to be 1.70 B.M., respectively, and support their square planar structure. The copper (II) complex, (6) is found to be diamagnetic which is in accordance with the dimeric nature. This may be due to the strong antiferromagnetic interaction between the adjacent copper(II) ions. The zinc(II) complexes are found to be diamagnetic.

Table 2: Electronic spectral data of the ligand and complexes (nm).

Complex No:	Compound	Intraligand and CT bands(nm)	d-d bands (nm)
	H_2L	256 ,321, 425	-
1	[Ni(HL)CH$_3$COO]	338	509
2	[Ni(HL)$_2$] H$_2$O	254, 283, 340	330-410, 590, 873
3	[Cu(HL)$_2$.H$_2$O	260, 343, 386	533
4	[Cu(HL)Cl]	259,302,334, 353, 489	646
5	[Cu(HL)NO$_3$]	260, 328, 419	600, 889
6	[(CuHL)$_2$(OH)$_2$] 5H$_2$O	252,305,327, 431	598
7	[Zn(HL)$_2$]	259, 409	-
8	[(ZnHL)$_2$(NO$_3$)$_2$] 2H$_2$O	354, 416	-
9	[(ZnHL)$_2$(OH)$_2$] 2H$_2$O	263,	350, 414

FT-IR Spectra

The IR spectral data of the ligand and the complexes are shown in Table 3. The vibrations belonging to N-H stretching usually occur in the region 3450–3250 cm^{-1}.[16] The ligand shows a broad band at 3411 cm^{-1} due to ν(NH). The increase in the wavenumber of the centre of this broad band may be due to the involvement of azomethine nitrogen during the complex formation. The band due to ν(C=O) at 1626 cm^{-1} shifts to higher wavenumber on coordination with metals. The ν(N-N) band at 1106 cm^{-1} undergoes a shift to higher wavenumber in the spectra of the complexes compared to that of the ligand substantiate the involvement of azomethine nitrogen in coordination .[17] This blue shift may be due to the decrease in the repulsion between the lone pairs on the two nitrogen atoms. The ν(M-N) vibration are observed around 440-485 cm^{-1}. All these findings confirm the participation of azomethine nitrogen in coordination.

In the present case, Ni(HL)CH$_3$COO (1) shows band at 1519 cm^{-1} and 1430 cm^{-1} which may be due to the unidentate coordinated acetate group. Since thiols can cause spin pairing more effectively than thioethers, coordination occurs through the thiolato sulphur atom after deprotonation in this Ni(II) complex. The spectrum of nitrate complex of copper has strong bands at 1440, 1350, 1022 cm^{-1} due to $\nu_{as}(NO_2)$, $\nu_s(NO_2)$ and ν(NO), respectively, indicating the unidentate coordination of the nitrate ion to the Cu(II) ion. The separation of the two highest frequency bands is 90 cm^{-1}. The broad absorption band centred at 3400 cm^{-1} in the IR spectra of certain metal complexes has also been assigned to lattice water molecule.

Table 3: IR spectral assignments.

No:	COMPOUND	N-H/OH	C=O	CN-NH	C-O	C=S	N-N	M-O	M-N
H_2L	$C_{25}H_{23}N_5OS$	3411	1626	1478	-	1362, 831	1106	-	-
1	[NiHLCH$_3$COO]	3437		1486		1349, 850	1117	-	433
2	[Ni(HL)$_2$].H$_2$O	3440	1603	1489	1437	1348, 850	1107	660	472
3	[Cu(HL)$_2$].H$_2$O	3435	1599	1485	1439	1354, 842	1128	661	462
4	[Cu(HL)Cl]	3445	1591	1486	1416	1351	1129	663	441
5	[Cu(HL)NO$_3$]	3442	1592	1485	1441 1419	1372, 854	1129	662	448
6	[(CuHL)$_2$(OH)$_2$]5H$_2$O	3443	1598	1486		1366, 838	1128	661	453
7	[Zn(HL)$_2$]	3438	1602	1482	1434	1346, 851	1126	659	433
8	[(ZnHL)$_2$(NO$_3$)$_2$] 2H$_2$O	3438	1599	1486	1437	1348, 848	1129	-	450
9	[(ZnHL)$_2$(OH)$_2$] 2H$_2$O	3425	1602	1485	1436	1346, 849	1108	659	444

^{1}H-NMR Spectrum

The ^{1}H NMR spectrum of the zinc complexes are recorded in $CDCl_3$ (figure.1). Two singlets observed in the ligand spectrum at 14.476 ppm due to NH proton and 11.176 ppm due to OH proton were absent in zinc(II) complex. The absence of peak at 11.176 ppm is due to the deprotonation of O-H proton during complexation. Aromatic protons exhibit multiplet signals in the range 7.13-8.13 ppm. A new peak at 6.675 ppm due to N-H proton is observed. It is an evidence for the participation of thione sulphur in complexation. N-CH_3 protons in the complex show peaks at 3.4-3.64 ppm. Singlet peaks at 1.2-1.3 ppm in the complex correspond to the methyl protons in the substituted pyrazolone. Both CHNS data and NMR data are in agreement with the formulae $M(HL)_2$ for zinc(II) complex (7).

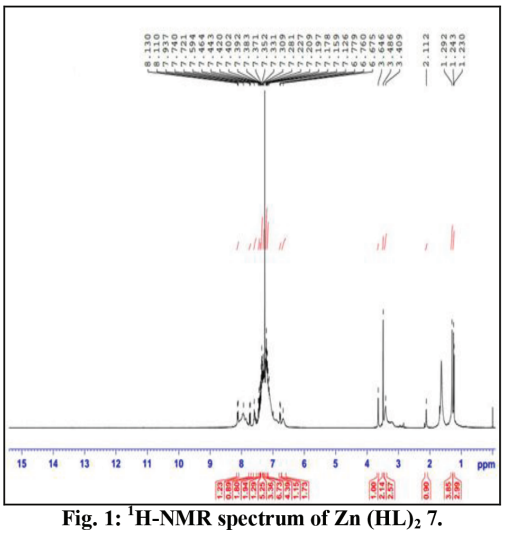

Fig. 1: ^{1}H-NMR spectrum of Zn $(HL)_2$ 7.

ESR spectrum

The ESR spectrum of copper(II) complex (3) were recorded in frozen DMF solution at 77 K in the X-band with 100 kHz field modulation and *g* factors were assigned in comparison with the standard marker Mn^{2+}. The Cu(II) ion has an effective spin of *S*=3/2. It is associated with a spin angular momentum *ms*= ±1/2, leading to a doubly degenerate spin state in the absence of magnetic field. The degeneracy is lifted between these states in a magnetic field. The energy difference between them is given by $E = h\nu = g\beta B$, where *h* is the Planck's constant, *v* is the frequency, *g* is the Lande's splitting factor equals to 2.0023 (for a free electron), β is the Bohr magneton and *B* is the magnetic field. The solution spectrum of the complex (3) at 77 K in DMF was axial and showed four hyperfine lines characteristic of a monomeric Cu(II) complexes corresponding to -3/2, -1/2, 1/2 and 3/2 which arise from the coupling of the odd electron with copper nuclei(I=3/2). The spectrum also gave three superhyperfine lines in the perpendicular region which arose from the coupling of the electron spin with nuclear spin of nitrogen atom which is coplanar. It indicates that in this complex azomethine nitrogen atom has coordinated to the metal centre. Since there is no half field signal, we can confirm the monomeric nature of complex (3).

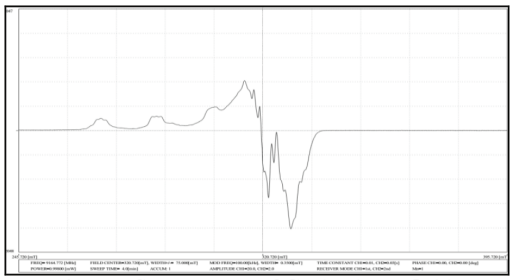

Fig. 2: ESR spectrum of Cu $(HL)_2.H_2O$ (3).

Thermal studies

The thermal studies of the ligand and metal complexes were carried out using the thermogravimetric technique (TG-DTG) in order to provide more insight into their structure of the complexes.

For the ligand H_2L, two stages of decomposition were observed and is evident from DTG peaks at 163°C and 273°C. The first stage of decomposition of the ligand occured at 140-170 °C, and second stage due to complete decomposition of ligand at 170-750 °C. The absence of any thermal change before this temperature demonstrates their high thermal stability. DSC plot supports the TG-DTG analysis giving temperature maxima at 163°C and at 273°C. The TG/DTG/DSC study reveals the purity of the compound and no decomposition is observed up to the melting point.

Ni(HL)CH_3COO (1) showed four decomposition stages. It is evident from DTG peaks at 225, 302, 310 and 321°C. Here the decomposition starts after the melting point of the compound at 225°C. The first stage is at 202–274°C and demonstrates a mass loss of 5 %, corresponding to the loss of CO (calc.5 %). The second stage occurs at 274–507 °C, with a mass loss of 39.8 %. The residual mass left behind at 745°C was 55.35 %.

$Ni(HL)_2.H_2O$ (2) has four decomposition stages are observed. It is evident from DTG peaks at 71, 204, 231 and 309°C. Initial mass loss corresponds to the loss of one lattice held water molecule. Here also the decomposition starts after the melting point of the compound at 204°C. The first stage is at 184–210°C and demonstrates a mass loss of 3.3 %. The second stage occurs at 254–649°C, with a mass loss of 70.5%. A residual mass of 17.7 % was left which may be due to the formation of a mixture of oxide and sulphide of nickel.

For $Cu(HL)_2.H_2O$ (3), an initial mass loss of 2% corresponds to loss of one water molecule in temperature range 150-170°C. The next steps of decomposition occur in the temperature range 180-250°C and 230-350°C. These steps are shown by DTG peaks at 161°C, 203°C

and 307°C. A residual mass of 23% was left which may be due to the formation of a mixture of copper oxide and copper sulphide (calc. 24.7 %).

For Cu(HL)Cl (4), a two staged decomposition occurred and is evident from DTG peaks at 231 and 300°C. The first stage is at 220–240°C, and demonstrates a mass loss of 6.5 %, corresponding to the loss of HCl (calc. 6.7%). The second stage occurs at 245–500 °C, with a mass loss of 56.9%. The residual mass left behind at 745°C was 28.6%. This may be due to the formation of Cu_2S (29.4%).

For $[Cu(HL)NO_3]$ (5), two stages of decomposition occur and is evident from DTG peaks at 214°C and 297 °C. The first stage is at 190-223°C, and demonstrates a mass loss of 6%, corresponding to the loss of NO (calc.5.3 %). The second stage occurs at 240-550°C, with a mass loss of 61%. The residual mass of 27.5 % was observed at 750°C which may be due to the formation of copper sulphide (calc.28 %).

For $[(CuHL)_2(OH)_2].5H_2O$ (6), DTG peaks are observed at 196 and 302°C indicating its two step decomposition. The first stage is at 183-216°C, and demonstrates a mass loss of 6 %. The second stage occurs at 240-467°C, with a mass loss of 47.2%. The residual mass of 34.81% was observed at 750°C which may be due to the formation of Cu_2S (calc. 34.2 %). Antimicrobial studies

The preliminary *in vitro* antibacterial screening studies of H_2L and its complexes are given in Table 4. However, the correct biochemical mechanism of such compound is not yet completely understood. The mode of action of antimicrobials may involve various targets in the microorganisms.[18]

1. By interefering during the synthesis of cellular walls, causes damage which leads to altered cell permeability characteristics or disordered lipoprotein arrangements, eventually resulting in cell death.
2. By the deactivation of a variety of cellular enzymes that play a crucial role in the metabolic pathways of these microorganisms.
3. Denaturation of cellular proteins, causing the normal cellular processes to be impaired.
4. A hydrogen bond formation through the azomethine group with the active centres of various cellular constituents, resulting in interference with normal cellular processes.

Cu $(HL)_2.H_2O$ (3) exhibited high activity towards *Staphylococcus aureus* in comparison with the standard drugs. It is observed that most of the compounds are particularly effective on *Enterococcus faecalis, pseudomonas aeruginosa* and *Klebsiella pneumonia*. They exhibited no activity against *Bacillus subtili even* at higher concentration. These observations can be assumed as selective activity. MIC value of all the complexes was found to be 0.315µg/ml.

The data in Table 5 show that the copper chloride and copper nitrate complexes are active against the fungi, *Aspergillus niger* and *Colletrotrichum gleosporides*. The percentage of inhibition is found to be 85% at 60ppm. Cu $(HL)_2.H_2O$ shows 70% inhibition towards Candida Albicans at 40 ppm. Zinc (II) complex (7) shows promising antifungal activity towards all the fungi under study whereas $[(CuHL)_2(OH)_2].5H_2O$ shows less activity against all fungi.

Table 4: Preliminary in vitro antibacterial screening studies of H_2L and its complexes.

Compound	Diametre of Zone of Inhibition(mm)					
	Staphylococcus aureus	***Enterococcus faecalis***	***Bacillus subtili***	***E.coli***	***pseudomonas aeruginosa***	***Klebsiella pneumonia***
H_2L	7	-	-	8	8	10
$Cu(HL)_2\ H_2O$	10	10	-	7	10	15
Cu(HL)Cl	7	8	-	7	7	18
$Cu(HL)NO_3$	8	7	-	7	10	18
$[(CuHL)_2(OH)_2].5H_2O$	14	8	-	-	-	8
$Zn(HL)_2$	7	10	-	8	8	11
$[(ZnHL)_2(NO_3)_2]\ 2H_2O$	-	10	-	7	7	-
Kanomycin	12	9	12	12	10	20
Methicillin	10	8	10	15	12	25
DMSO	-	-	-	-	-	-

Table 5: Preliminary in vitro antifungal screening studies of H_2L and its complexes.

Fungi	Percentage of inhibition																	
	H_2L			$Cu(HL)_2$			$Cu(HL)Cl$			$Cu(HL)NO_3$			$[(CuHL)_2(OH)_2].5H_2O$			$Zn(HL)_2$		
Conc:ppm	20	40	60	20	40	60	20	40	60	20	40	60	20	40	60	20	40	60
Aspergillus niger	38	49	48	58	60	58	44	63	85	46	48	50	33	35	35	64	60	62
Alternaria alternata	30	38	41	40	56	57	49	51	48	47	56	50	30	37	32	64	62	65
Candida Albicans	30	36	42	56	70	71	59	59	58	32	35	45	28	30	30	63	70	70
Colletrotrichum gleosporides	56	57	58	62	60	60	70	85	85	77	85	80	25	28	33	84	82	83

CONCLUSION

From the study, coordination capabilities of thiosemicarbazones are found to be unpredictable and are very interesting. We observed that with different salts of same metal, same ligand has coordinated in different modes. Nickel acetate yielded diamagnetic square planar complex with formula $M(HL)CH_3COO$ whereas nickel chloride gave paramagnetic octahedral complex, $M(HL)_2.H_2O$. Out of the four copper(II) complexes of H_2L, two have the general formula [MHLX] where X=Cl, NO_3. By using copper(II) acetate and zinc(II) acetate, H_2L yielded the complexes with general formula $[M(HL)_2]$ where M=Cu(II), Zn(II). This Cu(II) complex is diamagnetic and strongly supports its existence as a dimer in the solid state. The preliminary antimicrobial screening results revealed that the complexes showed a significant activity compared to the ligand, H_2L. The observations in our study understood a selective activity of the compounds towards microbes. At this phase, it is hard to find a simple explanation for the antimicrobial activity of the compounds and further studies will be needed to clarify these observations. The proposed structures of the complexes are given in FIGs 3, 4, 5.

As a continuation of our work on the synthesis of biologically active compounds, docking studies and *in vivo* biological activities are conducted on various transition metal complexes.

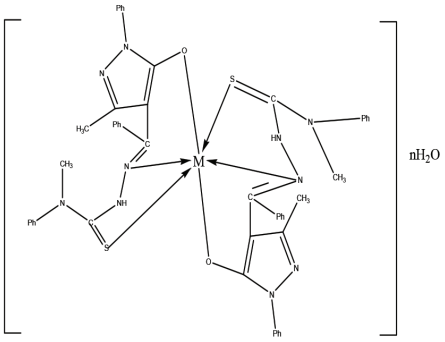

Fig. 3: Proposed structure of complex M $(HL)_2$ nH_2O (2, 3, 7).
where M = Ni(II), Cu(II), Zn(II)

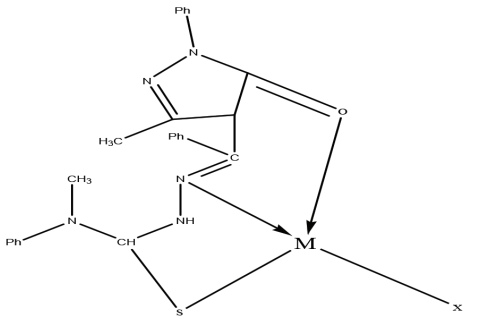

Fig. 4: Proposed structure of complex M (HL) CH_3COO.
Where M=Ni, X=CH_3COO^-

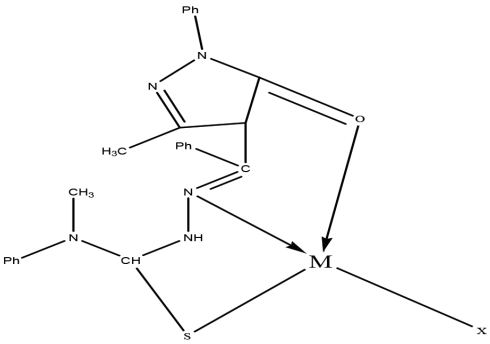

Fig. 5: Proposed structure of complex M(HL)X (4, 5).
Where M = Cu (II), X = Cl^-, NO_3^-.

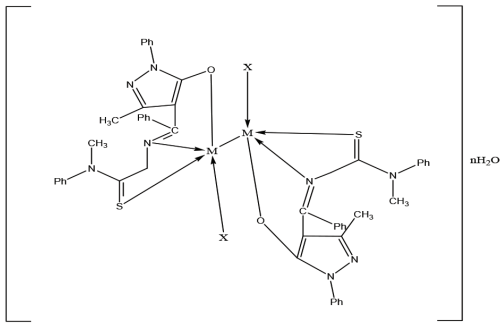

Fig. 6: Proposed structure of complex $(ML)_2$ X_2 (6, 8 and 9).
Where M = Zn (II), Cu(II).

ACKNOWLEDGMENTS

The authors are grateful to KFRI, Peechi, Thrissur, Kerala, India for elemental analyses. We are thankful to SAIF Cochin, Kerala, India for providing NMR results. We are also thankful to SAIF IIT Madras, India for providing EPR result. We are also thankful to Department of Botany, The Zamorin's Guruvayurappan college, Calicut and Department of Biotechnology and Microbiology, School of life sciences, Thalassery Campus for providing laboratory facility to do antimicrobial studies. The University Grants Commission (UGC) India is also gratefully acknowledged for financial support.

REFERENCES

1. Bindu, P.; Kurup, M.R.P.; Satyakeerty, T.R. EPR, cyclic voltammetric and biological activities of copper (II) complexes of salicylaldehyde N (4)-substituted thiosemicarbazone and heterocyclic bases. *Polyhedron,* 1999; 18: 321–331.
2. D. X. West, G.A. Bain, R.J. Butcher, J.P. Jasinki, Y. Li, R.Y. Pozdniakiv, J .Valdez-Martinez, R.A. Toscano, S.H. Ortega, Structural studies of three isomeric forms of heterocyclic N (4)-substituted thiosemicarbazones and two nickel (II) complexes *Polyhedron,* 1996; 15: 665-674.
3. C. R. Kowol, R. Berger, R. Eichinger, A. Roller, M. A. Jakupec, P. P. Schmidt, V. B. Arion, B. K. Keppler, Gallium (III) and iron (III) complexes of alpha-N- heterocyclic thiosemicarbazones: synthesis, characterization, cytotoxicity, and interaction with ribonucleotide reductase. *.J. Med. Chem,* 2007; 50: 1254–1265.
4. Hall, M. D.; Brimacombe, K. R.; Varonka, M. S.; Pluchino, K. M.; Monda, J. K.; Li, J.; Walsh, M. J.; Boxer, M. B.; Warren, T. H.; Fales, H. M.; Gottesman, M. M. Synthesis and Structure–Activity Evaluation of Isatin-β-thiosemicarbazones with Improved Selective Activity toward Multidrug-Resistant Cells Expressing P-Glycoprotein *J. Med. Chem,* 2011; 54: 5878–5889.
5. Mouayed A. Hussein, Muhammad Adnan Iqbal, Muhammad Asif, Rosenani A. Haque, Mohammed B. Khadeer Ahamed, Amin M. S. Abdul Majid, Teoh Siang Guan, Asynthesis, Crystal Structures and in Vitro Anticancer Studies of New Thiosemicarbazone Derivatives, Phosphorus, Sulfur Silicon Relat. Elem., 2015; 190: 1498-1508.
6. S. Gelin, B. Chantegrel, A.I. Nadi, Synthesis of 4-(acylacetyl)-1-phenyl-2-pyrazolin- 5-ones from 3-acyl- 2H-pyran-2, 4(3H)-diones. Their synthetic applications to functionalized 4-oxopyrano [2, 3-c] pyrazole derivatives *J. Org.Chem.,* 1983; 48: 4078–4082.
7. Yuting Zhong, Lang Liu, Guangfei Liu, Dongling Wu, Jixi Guo, Dianzeng Jia Crystal structure and photoisomerism of 1-phenyl-3-methyl-4-(4-fluorobenzal)-5-pyrazolone 4-methylthiosemicarbazone in the solid state *J. Mol. Struct.*, 2008; 889: 259–264.
8. S. Jayasree, K.K. Aravindakshan Structural and antitumour studies of metal complexes with thiosemicarbazones of β-diketoesters, *Polyhedron,* 1993; 10: 1187-1192.
9. S. Jayasree, KK Aravindakshan - Synthesis, characterization and antitumour studies of metal chelates of acetoacetanilide thiosemicarbazone *Transition Met, Chem*, 1993; 18(1): 85-88.
10. J. P. Scovill, D.L. Klayman, C. F. Franchino, 2-Acetylpyridine thiosemicarbazones. 4. Complexes with transition metals as antimalarial and antileukemic agents, J. Med. Chem, 1982; 25: 1261-1264.
11. B.S. Jensen, The Synthesis of 1-phenyl-3-methyl-4-acyl-pyrazol-5ones, Acta Chem. Scand, 1959; 13: 1668-1670.
12. A.W. Bauer, W.M. Kirby, J.C. Sherris, M. Turck Antibiotic susceptibility testing by a standardized single disk method. Am J Clin Pathol, 1966; 45(4): 493–496.
13. H.L. Singh, A.V. Varshney, Synthetic, structural, and biochemical studies of organotin (IV) with Schiff bases having nitrogen and sulphur donor ligands. Bioinorg. Chem. Appl., 2006; 7: 2006-2013.
14. D.X. West, J.S. Ives, G.A. Bain, A.E. Liberta, J. Valdes-Martinez, K.H. Ebert, S. H- Ortega, Copper(II) and nickel (II) complexes of 2, 3-butanedione bis(N(3)-substituted thiosemicarbazones) *Polyhedron,* 1997; 16: 1895–1905.
15. B. Gray, C.J. Ballhausen, A Molecular Orbital Theory for Square Planar Metal Complexes *J. Am. Chem. Soc.,* 1963; 85: 260-265.
16. M. Silverstein, G. C. Bassler, C. Morril, Spectroscopic Identification of Organic Compounds, John Wiley, Newyork, 1981.
17. S. Renjusha, M.R.P. Kurup, Structural and spectral studies on manganese (II) complexes of di-2-pyridyl ketone N (4) - methyl and N (4)-ethyl thiosemicarbazones, *Polyhedron,* 2008; 27: 3294-3298.
18. R. S. Joseyphus, M.S. Nair, Antibacterial and antifungal studies on some Schiff base complexes of zinc (II). *Mycology,* 2008; 36: 93–98.